THE INSECT CENTRAL COMPLEX – FROM SENSORY CODING TO DIRECTING MOVEMENT

EDITED BY: Stanley Heinze and Keram Pfeiffer
PUBLISHED IN: Frontiers in Behavioral Neuroscience

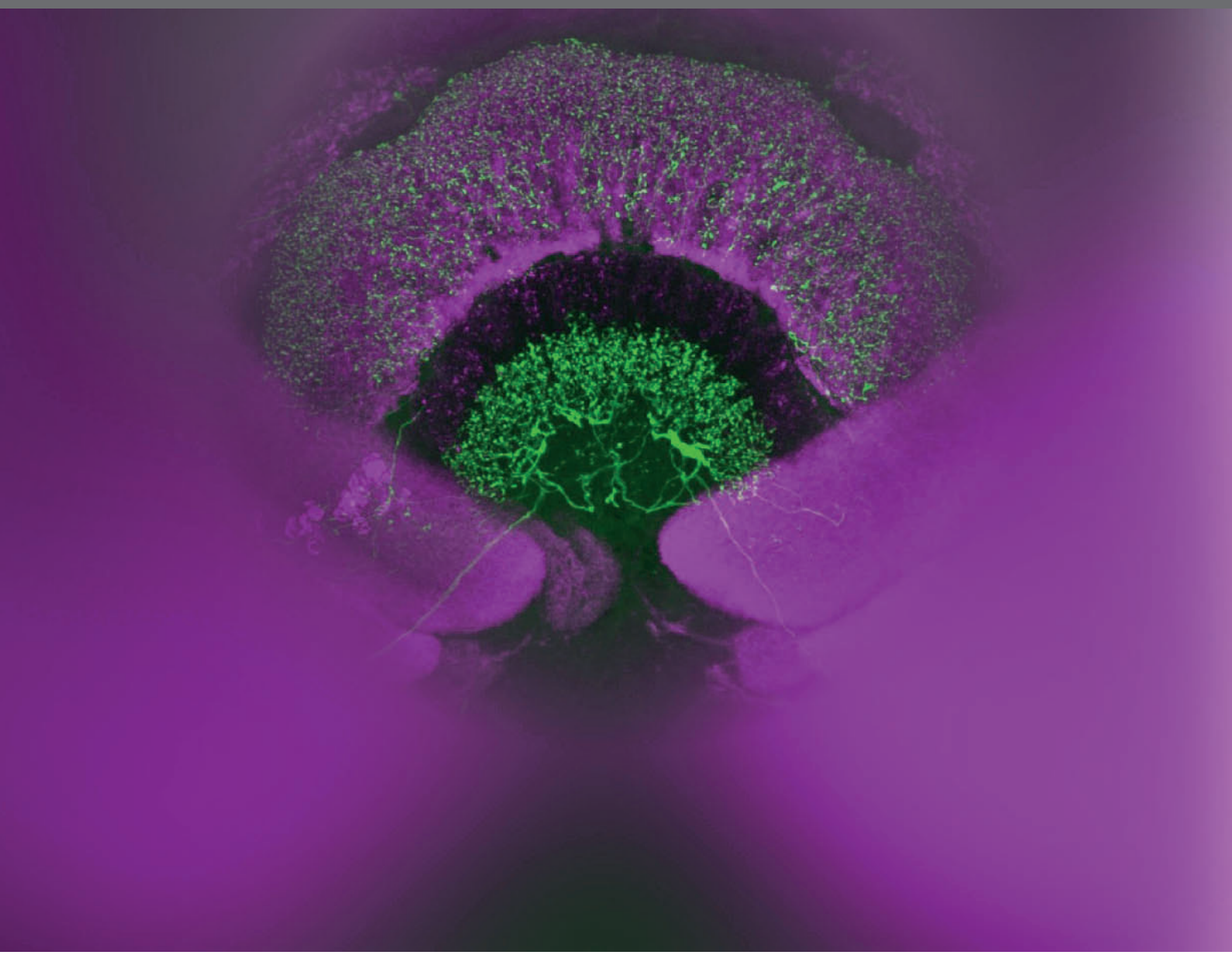

frontiers Research Topics

ISSN 1664-8714
ISBN 978-2-88945-578-2
DOI 10.3389/978-2-88945-578-2

About Frontiers

Frontiers is more than just an open-access publisher of scholarly articles: it is a pioneering approach to the world of academia, radically improving the way scholarly research is managed. The grand vision of Frontiers is a world where all people have an equal opportunity to seek, share and generate knowledge. Frontiers provides immediate and permanent online open access to all its publications, but this alone is not enough to realize our grand goals.

Frontiers Journal Series

The Frontiers Journal Series is a multi-tier and interdisciplinary set of open-access, online journals, promising a paradigm shift from the current review, selection and dissemination processes in academic publishing. All Frontiers journals are driven by researchers for researchers; therefore, they constitute a service to the scholarly community. At the same time, the Frontiers Journal Series operates on a revolutionary invention, the tiered publishing system, initially addressing specific communities of scholars, and gradually climbing up to broader public understanding, thus serving the interests of the lay society, too.

Dedication to Quality

Each Frontiers article is a landmark of the highest quality, thanks to genuinely collaborative interactions between authors and review editors, who include some of the world's best academicians. Research must be certified by peers before entering a stream of knowledge that may eventually reach the public - and shape society; therefore, Frontiers only applies the most rigorous and unbiased reviews.
Frontiers revolutionizes research publishing by freely delivering the most outstanding research, evaluated with no bias from both the academic and social point of view. By applying the most advanced information technologies, Frontiers is catapulting scholarly publishing into a new generation.

What are Frontiers Research Topics?

Frontiers Research Topics are very popular trademarks of the Frontiers Journals Series: they are collections of at least ten articles, all centered on a particular subject. With their unique mix of varied contributions from Original Research to Review Articles, Frontiers Research Topics unify the most influential researchers, the latest key findings and historical advances in a hot research area! Find out more on how to host your own Frontiers Research Topic or contribute to one as an author by contacting the Frontiers Editorial Office: researchtopics@frontiersin.org

THE INSECT CENTRAL COMPLEX – FROM SENSORY CODING TO DIRECTING MOVEMENT

Topic Editors:
Stanley Heinze, Lund University, Sweden
Keram Pfeiffer, University of Würzburg, Germany

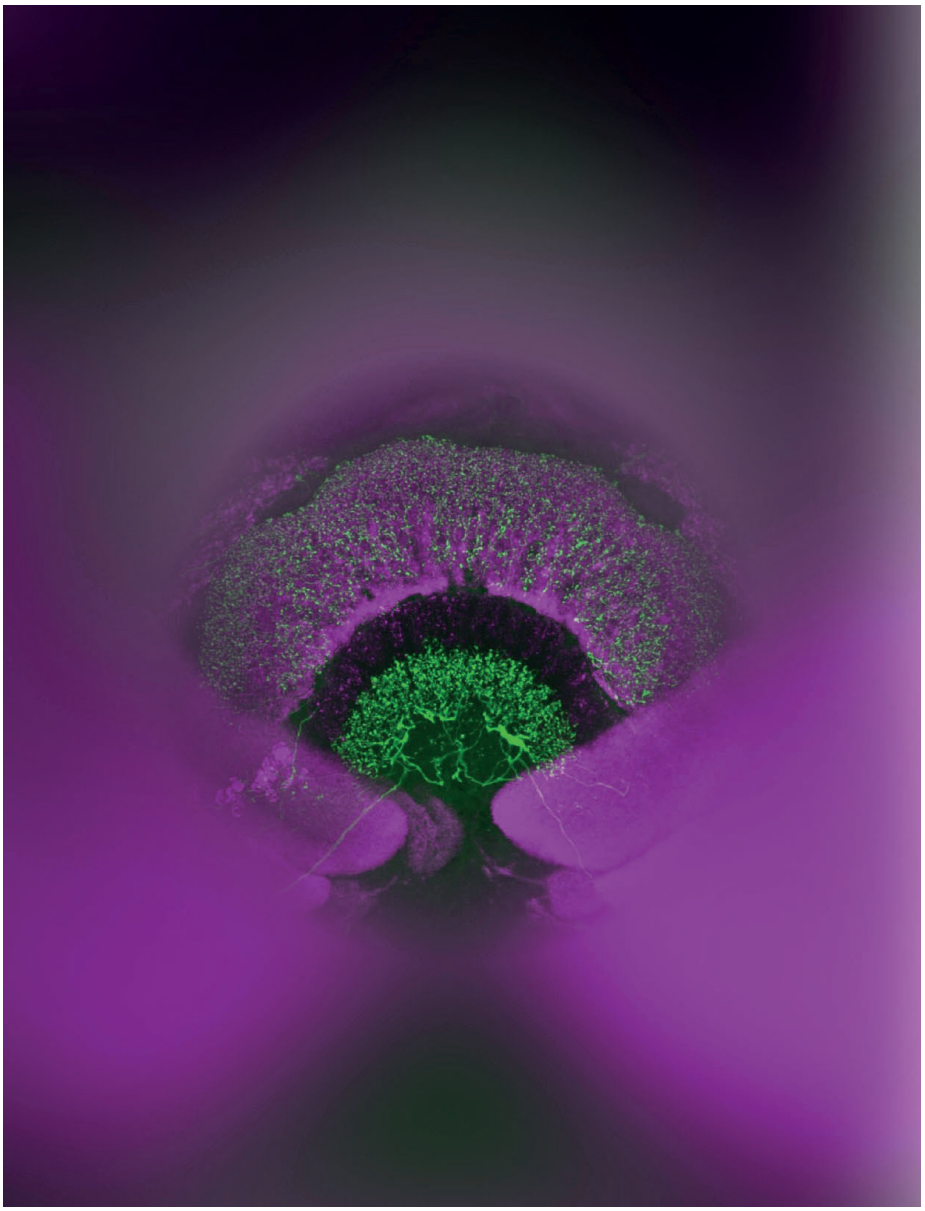

Confocal image of the central complex of the tropical sweatbee Megalopta genalis. Magenta: anti-synapsin immunolabelling; green: anti-serotonin immunolabelling.
Image: Stanley Heinze.

Citation: Heinze, S., Pfeiffer, K., eds (2018). The Insect Central Complex – From Sensory Coding to Directing Movement. Lausanne: Frontiers Media.
doi: 10.3389/978-2-88945-578-2

Table of Contents

SECTION 5

SENSORY MOTOR INTEGRATION AS ONE MAIN FUNCTION OF THE CENTRAL COMPLEX

frontiers in Behavioral Neuroscience

EDITORIAL
published: 30 July 2018
doi: 10.3389/fnbeh.2018.00156

Editorial: The Insect Central Complex—From Sensory Coding to Directing Movement

Stanley Heinze[1]* *and Keram Pfeiffer*[2]

[1] Department of Biology, Lund University, Lund, Sweden, [2] Behavioral Physiology and Sociobiology (Zoology II), Biozentrum, University of Würzburg, Würzburg, Germany

Keywords: central complex, action selection, sensory integration, insects, brain, motor control, neuroanatomy

Editorial on the Research Topic

The Insect Central Complex—From Sensory Coding to Directing Movement

Structure and function of any nervous system are intimately linked. The function of the brain and its components cannot be understood without knowing their morphological characteristics, whereas the anatomical outline of the brain only gains relevance through functional insights. This is true on many levels, from entire brains, to circuits and individual neurons. Evolution has yielded elaborate, ordered arrangements of neurons in brains as diverse as those of mammals and flies, e.g., arrays of neurons with regularly intercalating branches, multilayered brain areas, or parallel sensory pathways. Those regularly occurring motifs of anatomical arrangements are promising access points for gaining insights into the fundamental computations supported by those structures and thus can lead the way to understanding brains in general.

One such region of almost crystalline regularity is the insect central complex (CX), a midline spanning conglomerate of four brain areas that is conserved across all insects (Pfeiffer and Homberg, 2014). It consists of 16–18 vertical columns that are intersected by horizontal layers, formed by repeating arrays of columnar neurons and layer-specific tangential neurons. While many types of columnar neuron provide highly specific, cross-hemispheric connections between the individual components of the CX, the tangential neurons provide input from other brain areas. Output is carried by very few types of columnar neuron and converges in premotor command centers. While input and output to this region have been characterized in some detail, the intrinsic computations carried out by this highly complex, yet ordered entanglement of neurons are largely unknown.

The function of the CX has been tackled from many angles, revealing three main roles: motor control, sensory integration, and a range of functions that can be summarized under the term "higher functions," such as control of sleep, attention, spatial and object memory (Pfeiffer and Homberg, 2014). All those functions lie at the heart of neural control of behavior, and action-selection based on sensory information, previous experience and internal state have been proposed as a unifying function for the CX. Given that those functions are arguably among the most fundamental tasks carried out by all brains, understanding the CX could lead to fundamental insights into essential computations that underlie how brains control behavior across animals.

This Research Topic thus examines the CX from various angles. As already mentioned, the CX is highly conserved across insects. The first paper by Thoen et al. expands this view by characterizing a CX in mantis shrimps, sophisticated marine crustaceans that are otherwise renown for their exceptional color vision. While other crustacean brains lack many features of the insect CX, the authors find almost perfect resemblance between insects and the studied mantis shrimps, leading to interesting implications about the origin of this brain area, the functional necessity of its intrinsic organization and its relation to behavior.

OPEN ACCESS

Edited and reviewed by:
Nuno Sousa,
Instituto de Pesquisa em Ciências da Vida e da Saúde (ICVS), Portugal

***Correspondence:**
Stanley Heinze
stanley.heinze@biol.lu.se

Received: *25 June 2018*
Accepted: *05 July 2018*
Published: *30 July 2018*

Citation:
Heinze S and Pfeiffer K (2018) Editorial: The Insect Central Complex—From Sensory Coding to Directing Movement. Front. Behav. Neurosci. 12:156. doi: 10.3389/fnbeh.2018.00156

Second, the origin of the regular CX-neuroarchitecture as well as its complex expression patterns of neurochemical substances during embryonic development is reviewed in the paper by Boyan and Liu. Given the intricate structure-function relation in the CX-circuits, understanding how the neurochemical architecture is established at the same time as the neuroanatomical architecture, together resulting in an ordered topology of neurons with distinct projection patterns and molecular identities, is key for systematically narrowing down functional roles for each cell type and has implications for the evolutionary origin of those neuron types. The latter is crucial for cross-species comparisons, which often implicitly assume that the CX is identical across species separated by hundreds of millions of years of evolution.

The second part of the Research Topic explores the relation between the gross morphology of the CX components and behavioral characteristics of the species. As sensory processing in the context of navigation and orientation is probably the best described CX-function (e.g., Heinze and Homberg, 2007; Seelig and Jayaraman, 2015; Stone et al., 2017), both papers examine navigation behaviors. Firstly, de Vries et al. compare the volume of the CX alongside functionally related brain regions between a migratory and a non-migratory moth species. In line with the idea that the basic computations carried out by this region of the brain are crucial for all insects, no large-scale differences were found that reflect the different behavioral strategies of those insects. Differences that explain these distinct behaviors therefore have to result from differences in circuit architecture that do not lead to alterations in neuropil volumes. Differently, Grob et al. compare ants before and after their first learning walks, a characteristic behavior that enables these insects to learn the arrangements of landmarks around the nest entrance for returning to home after foraging. Exposure to a natural pattern of skylight polarization during this behavior was crucial for volume increases in the CX and in the mushroom body; changes that therefore correlate with the ability of foraging ants to navigate precisely.

As mentioned before, the CX also is involved in spatial learning (e.g., Ofstad et al., 2011). While this aspect has previously been explored exclusively in flies, Plath et al. provide first insights into possible roles of the bee CX in spatial learning of color cues. The authors find an interesting division of labor between the mushroom body and the CX by pharmacologically silencing each region during the learning assay. The CX appeared to be crucial in mediating the goal directed behavioral response to the learned stimulus, while the mushroom body carried out the actual cue association.

To gain a deep understanding of how CX-neurons are involved in guiding the mentioned behaviors, the detailed outline of the neural circuits have to be illuminated. Two papers, Held et al. and Homberg and Müller, investigate the ultrastructure of neural elements in key parts of the CX in bees and locusts, respectively. Held et al. confirm that the detailed organization of input pathways involved in compass sensing is conserved between bees and locusts, whereas Homberg and Müller identify complex local interactions within the ellipsoid body (lower division of the central body) in locusts, providing an interesting dataset for comparison to similar information in flies.

By combining all known information, both anatomical and physiological, the next two papers explore possible functional implications of circuit architecture. Fiore et al. examine the local connectome of the *Drosophila* ellipsoid body. Their models result in potential roles of this neuropil in driving goal directed behaviors. Second, Kakaria and de Bivort condense all known connections of the *Drosophila* CX into a spiking model and reveal that this is sufficient to yield an array of head direction cells in the protocerebral bridge, as was recently observed experimentally (Seelig and Jayaraman, 2015). Adding to this, Givon et al. present a novel, web-based tool that allows to visualize activity in CX models to efficiently evaluate the functional consequences of altered connections, e.g., in mutants, or to test hypotheses about CX-function *in silico*.

Finally, the review by Varga et al. covers recent insights into the function of the cockroach CX, linking sensory integration and motor control in exquisite detail. The authors further explore the resemblance of functional concepts between vertebrate brains and the insect CX, alluding to the possibility that, indeed, we can gain fundamental insights into general brain function by studying the tiny brains of insects.

AUTHOR CONTRIBUTIONS

SH wrote the initial draft. KP reviewed and edited the manuscript.

REFERENCES

Heinze, S., and Homberg, U. (2007). Maplike representation of celestial E-vector orientations in the brain of an insect. *Science* 315, 995–997. doi: 10.1126/science.1135531

Ofstad, T. A., Zuker, C. S., and Reiser, M. B. (2011). Visual place learning in *Drosophila melanogaster*. *Nature* 474, 204–207. doi: 10.1038/nature 10131

Pfeiffer, K., and Homberg, U. (2014). Organization and functional roles of the central complex in the insect brain. *Annu. Rev. Entomol.* 59, 165–184. doi: 10.1146/annurev-ento-011613-162031

Seelig, J. D., and Jayaraman, V. (2015). Neural dynamics for landmark orientation and angular path integration. *Nature* 521, 186–191. doi: 10.1038/nature 14446

Stone, T., Webb, B., Adden, A., Weddig, N. B., Honkanen, A., Templin, R., et al. (2017). An anatomically constrained model for path integration in the bee brain. *Curr. Biol.* 27, 3069.e11–3085.e11. doi: 10.1016/j.cub.2017.08.052

Conflict of Interest Statement: The authors declare that the research was conducted in the absence of any commercial or financial relationships that could be construed as a potential conflict of interest.

frontiers in Behavioral Neuroscience

ORIGINAL RESEARCH
published: 07 February 2017
doi: 10.3389/fnbeh.2017.00012

Insect-Like Organization of the Stomatopod Central Complex: Functional and Phylogenetic Implications

Hanne H. Thoen[1], Justin Marshall[1], Gabriella H. Wolff[2] and Nicholas J. Strausfeld[3]**

[1]*Sensory Neurobiology Group, Queensland Brain Institute, University of Queensland, St. Lucia, Brisbane, QLD, Australia,* [2]*Department of Biology, University of Washington, Seattle, WA, USA,* [3]*Department of Neuroscience, School of Mind, Brain and Behavior, University of Arizona, Tucson, AZ, USA*

One approach to investigating functional attributes of the central complex is to relate its various elaborations to pancrustacean phylogeny, to taxon-specific behavioral repertoires and ecological settings. Here we review morphological similarities between the central complex of stomatopod crustaceans and the central complex of dicondylic insects. We discuss whether their central complexes possess comparable functional properties, despite the phyletic distance separating these taxa, with mantis shrimp (Stomatopoda) belonging to the basal branch of Eumalacostraca. Stomatopods possess the most elaborate visual receptor system in nature and display a fascinating behavioral repertoire, including refined appendicular dexterity such as independently moving eyestalks. They are also unparalleled in their ability to maneuver during both swimming and substrate locomotion. Like other pancrustaceans, stomatopods possess a set of midline neuropils, called the central complex, which in dicondylic insects have been shown to mediate the selection of motor actions for a range of behaviors. As in dicondylic insects, the stomatopod central complex comprises a modular protocerebral bridge (PB) supplying decussating axons to a scalloped fan-shaped body (FB) and its accompanying ellipsoid body (EB), which is linked to a set of paired noduli and other recognized satellite regions. We consider the functional implications of these attributes in the context of stomatopod behaviors, particularly of their eyestalks that can move independently or conjointly depending on the visual scene.

Keywords: central complex, stomatopod, crustaceans, insects, eye movements, evolution

OPEN ACCESS

Edited by:
Stanley Heinze,
Lund University, Sweden

Reviewed by:
Vivek Jayaraman,
Howard Hughes Medical Institute, USA
Michael Bok,
University of Maryland, Baltimore County, USA

****Correspondence:***
Hanne H. Thoen
h.thoen@uq.edu.au
Nicholas J. Strausfeld
flybrain@neurobio.arizona.edu

Received: *17 November 2016*
Accepted: *13 January 2017*
Published: *07 February 2017*

Citation:
Thoen HH, Marshall J, Wolff GH and Strausfeld NJ (2017) Insect-Like Organization of the Stomatopod Central Complex: Functional and Phylogenetic Implications. Front. Behav. Neurosci. 11:12. doi: 10.3389/fnbeh.2017.00012

INTRODUCTION

Stomatopod Vision and Midbrain Organization

Mantis shrimp (Stomatopods) are a group of stemward eumalacostracans that separated from other malacostracan lineages about 400 million years ago (Schram, 1969). They possess one of the most elaborate visual systems known, at least at the receptor level (Marshall, 1988; Cronin and Marshall, 1989a,b; Marshall et al., 2007). An equatorial system of photoreceptors (called the midband) can detect up to 12 different spectral channels (Marshall et al., 1991b, 1996; Cronin et al., 1994), as well as both linear (Marshall et al., 1991a, 1999; Kleinlogel and Marshall, 2006) and circular polarized light (Chiou et al., 2008; Gagnon et al., 2015). The midband

divides the eye into three different regions: the midband itself, and the dorsal and ventral hemispheres, some combination of which must also mediate luminance and spatial vision tasks. The retina, together with the nested optic neuropils and numerous discrete neuropils comprising the lateral protocerebrum (LP) are contained within the distally expanded mobile eyestalk. The optic neuropils and LP are further connected to the midbrain by axon bundles that project to it through the eyestalks (**Figure 1**).

One unique feature of stomatopods is that they are able to move their eyestalks independently and asymmetrically (Land et al., 1990) using coordinated actions of eight independent muscles (Jones, 1994). These movements include slow "scanning" movements and fast "saccadic" movements (Land et al., 1990; Marshall et al., 2014) as well as object tracking and optomotor stabilizations (Cronin et al., 1988, 1991) mediated by pitch, yaw and roll rotations of the eye. Some of these movements are thought to be involved in optimizing visual perception of certain modalities such as polarized light (Daly et al., 2016) and are possibly also involved in their putative interval-decoding color vision system where the perceived color corresponds to the peak sensitivity of the most responsive photoreceptor (Thoen et al., 2014; Zaidi et al., 2014). Another unique feature is that each eye has the potential for stereopsis due to the overlapping visual fields of the convex upper and lower eye halves (Marshall and Land, 1993). Observing the independent eye movements of stomatopods gives the strong impression of a crustacean equipped with two independent brains that occasionally function in unison (for example see Bok, 2012).

Stomatopods can switch from asymmetric to more coordinated eye movements, which appear to be triggered by threshold-sized objects (such as potential prey, predators, competitors or mates) detected by one or both eyes. This switch and subsequent actions are likely to be mediated by circuits that are supplied by inputs from both eyestalks. Hundreds of axons extend from each LP, many of which distribute to lateralized neuropils in the mid-brain. However, as demonstrated by dye fills (see below) certain axons converge at a system of midline neuropils known as the central complex (CX). In dicondylic insects the CX is implicated in the selection and execution of motor actions (Martin et al., 2015), and all species thus far examined have the same ground pattern organization (Williams, 1975; Strausfeld, 1976; Hanesch et al., 1989). Homologous but divergent centers are found in Myriapoda, Chelicerata and Onychophora (Loesel et al., 2002; Strausfeld et al., 2016). Comparable midline neuropils found in vertebrates (Strausfeld and Hirth, 2013), polychaete annelids (Heuer et al., 2010) and polyclad flatworms (Wolff and Strausfeld, 2015) suggest an ancient Precambrian origin for this center.

Stomatopoda is prominent amongst crustacean orders in that its central complex is organized much like that of homologous centers in dicondylic insects. Furthermore, many stomatopod species display highly coordinated appendicular actions, in addition to independent and conjoint movements of the eyestalks. We have consequently begun a wide-ranging investigation of the stomatopod CX in terms of its functional organization and control properties, comparing these with the CX of dicondylic insects. Here we discuss the first phase

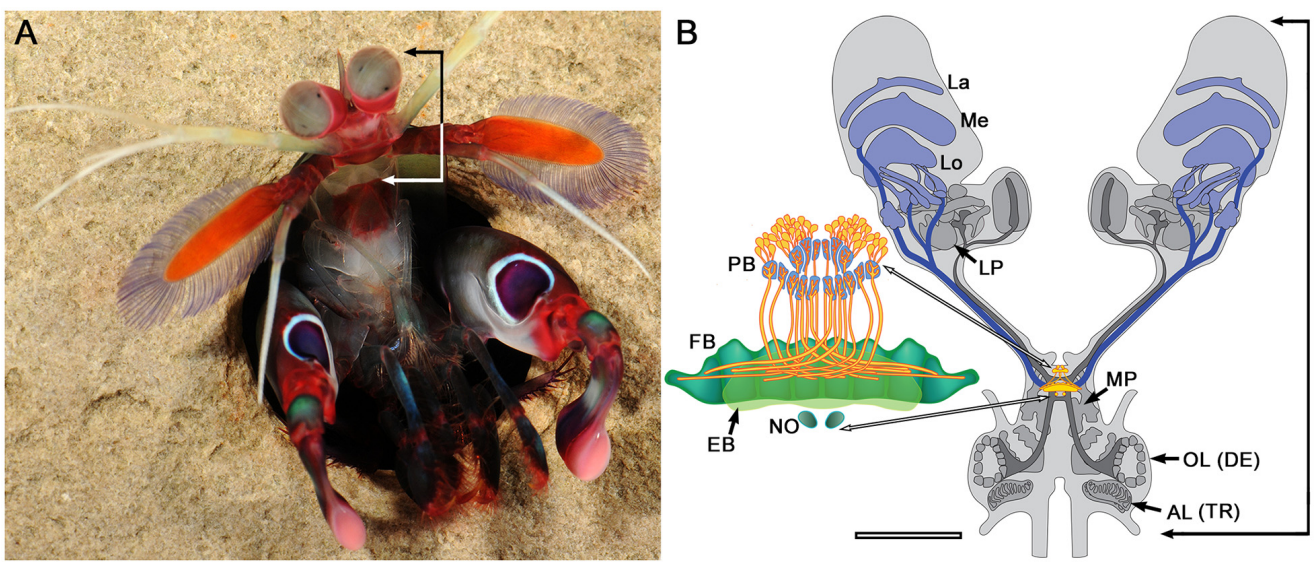

FIGURE 1 | Stomatopod crustacean, brain and central complex. (A) *Gonodactylus smithii*, with raised eyes and frontal "head" region (bracketed). Image: Roy Caldwell. **(B)** Schematic of brain (based on sections of *Neogonodactylus oerstedii*) showing the fused neuromeres of tritocerebrum (indicated by the antennal lobes, AL (TR)), deutocerebrum (indicated by the antennular olfactory lobes, OL (DE)) and the medial protocerebrum (MP), the latter containing the central complex (enlarged showing protocerebral bridge, PB; fan-shaped and ellipsoid bodies, FB, EB; noduli, NO). Neuropils within the eyestalks comprise the lateral protocerebrum (LP) and optic lobes (La, Me, Lo). Ascending axon bundles (dark gray) from the OL extend to the lateral protocerebra; descending axon bundles (dark blue) extend from the optic lobes, and optic glomeruli to reach the midbrain and central complex. Scale bar for a small example of this species is 2 mm.

of this study showing that the stomatopod CX possesses structural characters that show multiple correspondences to structures in the CX of Dicondylia. We further explore the functional implications of these correspondences and suggest likely roles of the CX in relation to the stomatopods behavioral repertoire.

MATERIALS AND METHODS

Animals

Between 4 and 50 Stomatopods of the species *Pseudosquilla ciliata, Gonodactylus smithii* and *Haptosquilla trispinosa* were obtained from designated areas overseen by the Lizard Island Research Station, Australia (GBRMPA Permit no. G12/35005.1, Fisheries Act no. 140763). Seventy two *Neogonodactylus oerstedii* were collected in the Florida Keys, USA. Twelve specimens of *Ligia exotica* were collected from a beach near Qingdao Pier, Qingdao, China.

Reduced Silver Staining

Using Bodian's (1936) original method, tissue was fixed in AAF (16 ml 80% ethanol, 1 ml glacial acetic acid, 3 ml 37% formaldehyde), before being dehydrated in ascending alcohols, cleared in terpineol and embedded in Paraplast Plus (Sherwood Medical, St. Louis, MO, USA). The 12 μm serial sections were mounted on slides using albumin, then deparaffinized, rehydrated and incubated in a solution of 2.5 g Protargol (Roques, Paris, France) and 5 g copper in 250 ml double-distilled water at 60°C overnight. The sections were next washed briefly in distilled water, processed through a solution of 1% hydroquinone and 5% sodium sulfite (5 min), 1% gold chloride (9 min), 2% oxalic acid (5 min) and 5% sodium thiosulfate (5 min). Sections were dehydrated before being mounted in Entellan (Merck, Darmstadt, Germany) under coverslips.

Immunocytochemistry

A range of different antibodies was employed to visualize structures in the stomatopod central complex (**Table 1**). A monoclonal antibody against synapsin (3C11, "SYNORF1"), a protein associated with synaptic vesicles in *Drosophila* (kindly provided by E. Buchner, University of Würzburg, Germany) was used at a concentration of 1:50. It has consistently been used to label brain structure in all major malacostracan subgroups, including stomatopods (Sullivan and Beltz, 2004) and recognizes at least four synapsin isoforms (70, 74, 80 and 143 kDa; Klagges et al., 1996). An antibody against serotonin (5HT, Immunostar, Hudson, WI, USA) has been previously used to label neurons in several crustacean species, including the stomatopod *Neogonodactylus oerstedii* (Derby et al., 2003) and was used at a concentration of 1:1000. A monoclonal antiserum against α-tubulin (12G10) was used at a concentration of 1:100 and was developed by Drs. J. Frankel and E. M. Nelsen. This antiserum was obtained from the Developmental Studies Hybridoma Bank developed under the auspices of the NICHD and maintained by the Department of Biology, University of Iowa (Iowa City, IA, USA). Anti-DC0, a generous gift of Dr. D. Kalderon (Columbia University, New York, NY, USA) was used at a concentration of 1:250 and recognizes the catalytic subunit of cAMP dependent protein kinase A across all arthropods investigated thus far (Wolff and Strausfeld, 2015). Antisera against FMRFamide were generously provided by Dr. E. Marder (Brandeis University, Waltham, MA, USA) and used at a concentration of 1:100. Anti-NPF antisera were generously donated by Dr. P. Shen (University of Georgia) and used at a concentration of 1:1000. Anti-GABA (Sigma-Aldrich, A2052) was used at a concentration of 1:200. Finally, cell nuclei were labeled using a blue-fluorescent DNA-stain (DAPI, Molecular Probes, D1306) or a green fluorescent nucleic acid stain (SYTO 13, Molecular Probes, S7575).

Procedure

Animals were cold anesthetized, decapitated and dissected out in cold (4°C) fixative (4% paraformaldehyde and 10% sucrose in phosphate-buffered saline, pH 7.4 (PBS, Sigma, St. Louis, MO, USA)). Brains fixed for the synapsin and serotonergic staining was left in fixative overnight (4°C), while brains fixed for the remaining antibodies were fixed in a microwave at 18°C for two cycles of 2 min with power and 2 min under vacuum before being placed in fresh fixative overnight at 4°C. The next day the brains were washed 3× 10 min in PBS and embedded in 5% LMP agarose (LMP, A9414, Sigma Aldrich; for the synapsin and serotonergic staining) or albumin gelatin (for the remaining antibodies) before being cut at 60–150 μm thick sections using a Leica vibratome. Sections were next washed 6 × 20 min in 0.1 M PBS containing 0.5% Triton X-100 before being preincubated in 0.1 M PBS with 0.2% Triton

TABLE 1 | Antibody data.

Antibody	Immunogen	Supplier	Host
Synapsin "SYNORF 1"	A glutathione S–transferase-fusion protein including a portion of a *Drosophila* synapsin homolog	DSHB, # 3C11	Mouse (monoclonal)
Alpha-tubulin	Alpha-tubulin from a mixture of *Tetrahymena thermophila* and *Tetrahymena pyriformis*	DSHB, #12G10	Mouse (monocolonal)
Serotonin (5HT)	Serotonin coupled to bovine serum albumin (BSA) with paraformaldehyde	Immunostar, Hudson, WI 20080	Rabbit, (polyclonal)
FMRFamide (671)	FMRFamide conjugated to succinylated thyroglobulin	Dr. E. Marder	Rabbit (polyclonal)
Neuropeptide F	A peptide with 36 residues synthesized based on the deduced sequence of *Drosophila* NPF and amidated at the C-terminus	Dr. P. Shen	Rabbit (polyclonal)
GABA	GABA coupled to BSA	Sigma-Aldrich, # A2052	Rabbit (polyclonal)
DC0	Purified DC0, the major catalytic subunit of *Drosophila* c-AMP-dependent protein kinase A	Dr. D. Kalderon	Rabbit (polyclonal)

X-100 and 5% Normal Goat Serum (NGS, Life-Technologies, Carlsbad, CA, USA 50-062Z) for 1 h at room temperature. Sections were then incubated with the respective antibodies at the concentrations listed above in either 0.1 M PBS with 0.2% Triton X-100 and 2% NGS for 3 days at 4°C (synapsin and serotonin) or with 0.1 M PBS with 0.5% Triton X-100 and 5% NGS overnight on a shaker in room temperature (for the remaining antibodies).

Sections were next rinsed for 5× 10 min in 0.1 M PBS before two different procedures were carried out. For the synapsin and serotonergic staining: incubation in 0.1 M PBS with 1% NGS containing Alexa Fluor 647 goat anti-mouse (1:250 Molecular Probes, A21236) and Alexa Fluor 568 goat anti-rabbit (1:250 Molecular Probes, A11011) for 2 h in room temperature. After rinsing in 0.1 M PBS 2 × 10 min, sections were incubated with 300 μM DAPI (Molecular probes, D1306) for 5 min, rinsed again in 0.1 M PBS for 10 min before being mounted on slides in 80% glycerol. For the remaining antibodies: 1000 μL aliquots of PBS-TX were placed in tubes with 0.25% secondary Cy2-, Cy3-, or Cy5-conjugated IgGs (Jackson ImmunoResearch, West Grove, PA, USA) and centrifuged at 13,000 rpm for 15 min at 4°C. The top 900-μL of this solution was added to each well. The well plate was left on a shaker to gently agitate the sections overnight at room temperature. Tissue sections were then washed in PBS six times over 3 h, embedded on glass slides in a medium of 25% polyvinyl alcohol, 25% glycerol and 50% PBS, and then imaged on the confocal microscope. Where applicable, sections were incubated in the fluorescent nuclear stain Syto-13 at a concentration of 1:4000 prior to embedding on glass slides.

Whole Mount Immunocytology

Some brains were processed as whole mounts, rather than being sectioned, using the same fixation procedure as described above. After fixation, the brains were washed for 6× 10 min in 0.1 M PBS before being pre-incubated in 0.1 M PBS with 0.1% Triton X-100 and 2% NGS for 3 h in room temperature. The brains were then incubated for 6 days at 4°C in SYNORF1 diluted with 0.1 M PBS with 0.2# Triton X-100 and 2% NGS. The brains were then washed 5× 20 min in 0.1 M PBS before being incubated for 4 days in 1:250 Alexa Fluor 647 goat anti-mouse (Molecular Probes, A21236) in 0.1 M PBS with 1% NGS at 4°C. The brains were then washed in 0.1 M PBS for 3× 20 min, dehydrated in ascending series of ethanol, cleared in methyl salicylate and mounted in Permount using spacer rings to avoid tissue compression.

Mass Filling of Neurons

Mass fills of neurons were carried out using the method of Ehmer and Gronenberg (2002). Briefly, crystals of dextran conjugated with either Texas Red (D-3328) or Fluorescein (D-3306 Molecular probes, Life Technologies) were made into a paste on a glass slide using water from condensation built up from ice placed beneath the slide. A small droplet of paste was applied to the tip of a glass electrode and inserted into either the LP or central complex. Dye was allowed to spread for about 6 h before the animal was euthanized, nervous tissue exposed and placed in fixative (4% paraformaldehyde) overnight. Dissected tissue was embedded in 5% agarose (LMP, A9414, Sigma Aldrich), vibratome sectioned at 100 or 150 μm, mounted and coverslipped using 80% glycerol.

Image Acquisition and Processing

Sections and whole mounts labeled with antibodies against serotonin and synapsin were imaged using an LSM 710 inverted point-scanning laser confocal microscope (ARC LIEF grant no. LE130100078) with the 10× (0.45) air objective at 1024 × 1024 resolution and 0.5–1 μm depth. Sections labeled with antibodies against alpha-tubulin, FMRFamide, Neuropeptide F, GABA or DC0 were imaged using an LSM 5 Pascal confocal microscope (Zeiss, Oberkochen, Germany) with the 10× (0.45) air objective or 20× /0.5 plan Neofluar objective at 1024 × 1024 resolution and 0.5–1 μm depth. Maximum projection images were made using the *z*-project plugin in the open source software Fiji (Schindelin et al., 2012). 3D-reconstructions of the synapsin-stained tissue were created using the TrakEM-2 plugin in Fiji and visualized using the 3D-viewer. Light microscopy images of serially sectioned Bodian-stained brains were acquired using a 40× plan-apochromatic objective, employing step focusing at 1 μm increments to obtain stacks used for reconstruction. Images were adjusted for brightness, contrast, and threshold using Adobe Photoshop CC.

Reconstructions

Reconstructions of central complexes and their satellite neuropils are derived from aligned serial sections stained by the Bodian method, in which neuropils, large axons and axon bundles are delineated. Regions in successive sections are montaged for clarity, as in the case of the noduli and lateral accessory lobes (LAL; **Figure 2**). Additional data for reconstructions are derived from selective neuron labeling using antibodies listed in **Table 1**.

RESULTS

Before describing central complex organization in stomatopods, it is useful to briefly review here the occurrence and known attributes of these centers in insects and neuronal arrangements in the CX of crustaceans generally.

An Outline of the Insect Central Complex

The class Insecta consists of two clades: Monocondylia and Dicondylia, the first represented by wingless Archaeognatha dating back 420 million years to the Devonian period (Labandeira et al., 1988). The second clade includes all other insects. The archaeognathan central complex is notable for its simplicity and its similarity to that of many malacostracans, with the exception of stomatopods. The archaeognathan CX consists of a bilayered spindle-shaped central body (CB) supplied by an incomplete decussation of axons from small, paired centers

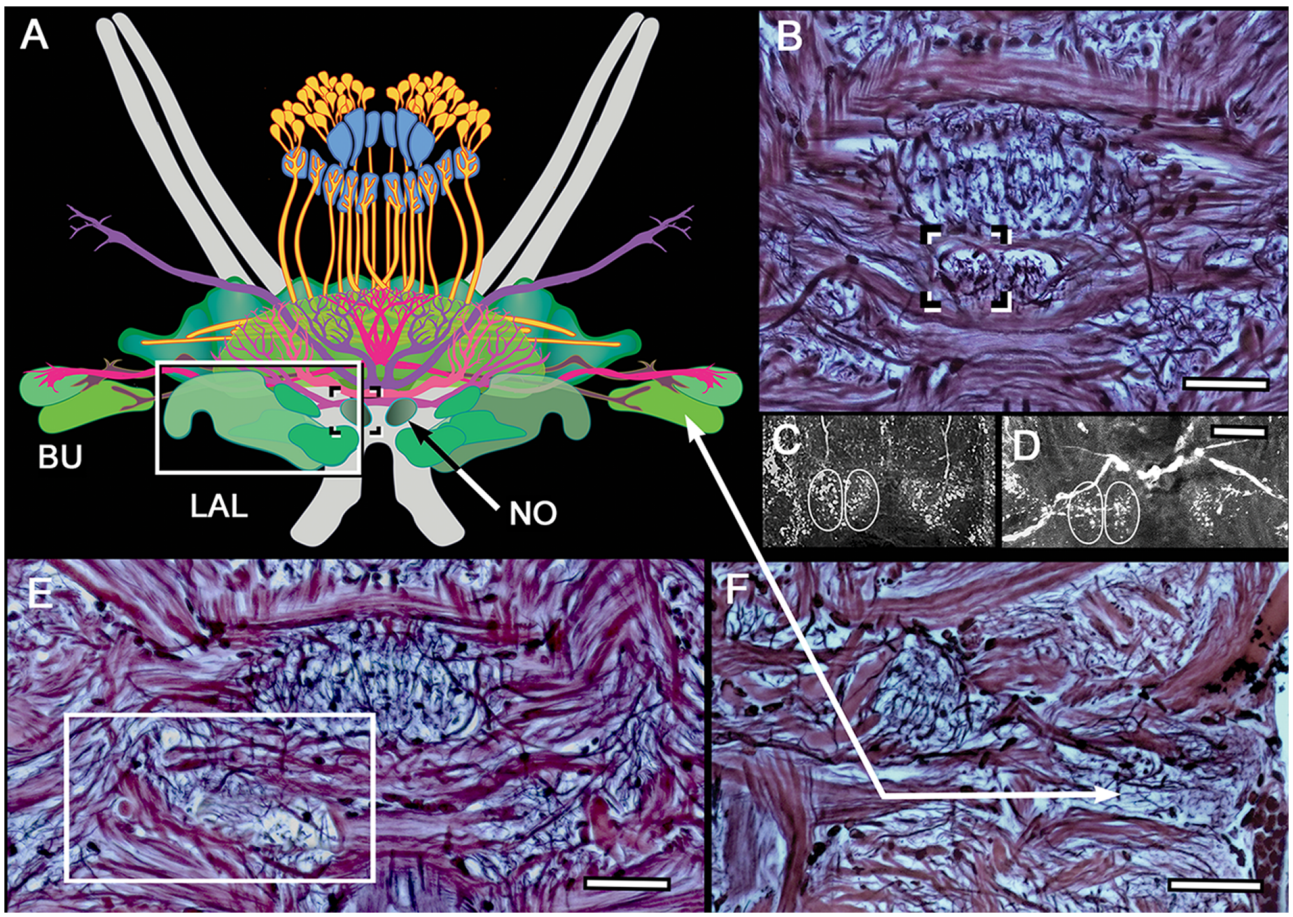

FIGURE 2 | Noduli and lateral accessory lobe (LAL) neuropils. (A) Overview of the two lateral bulbs (Bu), paired noduli (No) and LAL. **(B)** The noduli (one boxed) are prominent and have been resolved in all species so far examined. Unlike in insects, each nodulus appears to have two side-by-side domains, as revealed by FMRF and 5HT immunocytology of *N. oerstedii* **(C)** and *H. trispinosa* **(D)**. **(E)** Bodian staining resolves the LAL as a multi-lobed neuropil, one of which (boxed) is shown here. **(F)** Bodian staining of the lateral bulbs distinguishes their large dendritic trees and different staining densities. Scale bars: **(B–F)** 50 μm.

situated at the extreme rostromedial margins of the protocerebral lobes. These are referred to as the protocerebral bridge (PB) because the two centers are linked by axons that extend across the protocerebrum's midline (Strausfeld, 2012). Neurons link the CB to flanking neuropils that may correspond to the LAL recognized in Dicondylia. There are, however, no associated ball-like centers, which in Dicondylia are referred to as the "noduli."

The central complex in dicondylic insects consists of four delineated neuropils (Williams, 1975; Strausfeld, 1976, 1999; Homberg, 1985, 2008; Mobbs, 1985). The PB is usually a long and narrow bilateral neuropil extending between the most rostro-ventral medial lobes of the protocerebrum. Fully decussating axons project from the PB to a scallop-shaped multilayered neuropil called the fan-shaped body (FB) linked by through-going axons to the deeper ellipsoid body (EB), a name coined for its toroidal appearance in *Drosophila* (Power, 1943), although it is derived from an ancestrally shallow arch-like geometry typical of most Dicondylia. In pterygote (winged) insects, paired ball-like noduli ventral to the CB are reciprocally connected to the FB and EB. The dicondylic CX is subdivided into modules that repeat across the midline (Ito et al., 2014). Its PB is divided into 16–18 modules (8–9 on each side of the midline) that supply the FB through four pairs of fiber bundles termed the *w*-, *x*-, *y*-, and *z*-tracts (Williams, 1975). The modules each side of the midline are mapped point-for-point across the entire extent of the FB thereby dividing it into eight modules (four in each half) that are horizontally stratified by tangentially arranged terminals and dendrites. The noduli do not show any columnar organization, but consist of several stacked subunits. The FB and EB are flanked by the LAL that are partitioned into at least three domains, each receiving the terminals of modular neurons originating from cell bodies above the PB. The LAL is further linked to neuropils, into which premotor descending neurons extend axon collaterals. Thus, relays from the CX to the LAL, and thence to subsequent stations, are thought to gate the downstream activity of descending neurons supplying segmentally arranged sensory-motor circuits in thoracic ganglia (Namiki and Kanzaki, 2016).

In addition to the LAL, a satellite system associated with the EB referred to as the lateral complex, consists of three centers: the bulb, gall and wedge (Iwano et al., 2010; Ito et al., 2014). The CX, LAL and its satellites receive indirect afferents from higher order protocerebral neuropils, including indirect channels from the iconic mushroom bodies via relays to local interneurons in the superior medial protocerebrum (MP; Wolff and Strausfeld, 2016). From there, afferent neurons terminate across layers of the FB (Phillips-Portillo and Strausfeld, 2012; Strausfeld, 2012). With few exceptions, visual inputs to the CX are indirect, relayed to it via the lateral complex (Pfeiffer and Homberg, 2015; Held et al., 2016) and LP (Liu et al., 2006). Exceptions are connections between the PB of the locust *Schistocerca gregaria* and its anterior optic tubercle, an optic glomerulus receiving afferents from the medulla and lobula, and from the optic glomerular complex to the PB in muscomorphous Diptera (Phillips-Portillo, 2012) and from a corresponding region of the LP in *Drosophila melanogaster* (Lin et al., 2013). A direct projection into the CX, extending directly from the optic lobes, has been documented in Orthoptera (Honegger and Schürmann, 1975).

Roles Ascribed to the Insect Central Complex

Properties of the dicondylic CX have been much debated in recent years, with the emergence of two potentially related views of its role in behaviors. One is that because the distribution of celestial e-vectors are so precisely represented in modules of the PB and other levels of the CX, the primary role of the CX is to mediate compass-like celestial navigation (Heinze and Homberg, 2007; Homberg et al., 2011; Pfeiffer and Homberg, 2015). The other is that the CX processes a dynamic representation of information about an insect's orientation with respect to broader features of its visual surrounding relevant for path integration (Neuser et al., 2008; Triphan et al., 2010; Webb and Wystrach, 2016). While there is thus far no conclusive behavioral experimental evidence to support the CX as mediating path integration, there is compelling behavioral and optogenetic support for the CX's role in visual action selection and landmark orientation by walking flies (Seelig and Jayaraman, 2013, 2015), as well as visual place memory (Liu et al., 2006; Neuser et al., 2008; Ofstad et al., 2011). Other functions suggested to rely on the central complex are the control of song production (Kunst et al., 2011); the control of appendicular movements requiring asymmetric actions (Bausenwein et al., 1986; Strauss and Heisenberg, 1993; Ilius et al., 2007); and the selection of behavioral actions and motor commands (Huber, 1959, 1960; Ridgel et al., 2007; Bender et al., 2010; Ritzmann et al., 2012; Guo and Ritzmann, 2013; Martin et al., 2015). The recognition of such a variety of functional roles are in part a consequence of the species studied and what each offers in terms of experimental access and the application of a palette of sensory stimuli. One emerging consensus is that the CX receives direct and highly synthesized inputs involving most sensory modalities, and that these inputs provide information from which the CX determines what motor actions are appropriate for current environmental conditions (Strausfeld and Hirth, 2013; Fiore et al., 2015).

There is agreement that modular organization of the PB and its extensions into the FB reflect a representation of the multisensory surround and thus spatially segmented sensory information. In locusts, for example, the PB carries a topographical representation of zenithal e-vector orientations (Heinze and Homberg, 2007). In cockroaches, the locations of haptic mechanosensory stimuli are represented across the PB (Ritzmann et al., 2008) as are the representation of directional motion in flies (Phillips-Portillo, 2012). It is likely that acoustic and other mechanical stimuli are characterized as representations in overlaying sensory space.

There is, however, a second important correlate of modularity; not in the PB but in the FB where the more defined its modular subunits, the more these indicate the ability of the species to execute highly coordinated appendicular actions: tasks such as climbing or obstacle avoidance that require asymmetric but coordinated multijoint actions (Strausfeld and Hirth, 2013).

Overview of the Stomatopod Brain

Stomatopods have bulbous eyestalks that contain the four nested optic lobe neuropils serving the compound eye together with the neuropils of the LP (**Figure 1**). The LP is elaborate, comprising neuropils that are obvious homologs of those in other eumalacostracans in addition to centers that appear to be unique to Stomatopoda. Optic glomeruli are numerous. Preliminary observations show these connected by many discrete tracts to other regions of the LP. Several axon bundles extend through the eyestalks that connect lateral protocerebral neuropils, in addition to the medulla and lobula, to the midbrain. A substantial volume of each eyestalk is also occupied by the olfactory globular tract, which originates in the deutocerebrum's olfactory lobes (OL) and extends out to the lateral protocerebra (**Figure 1**). The central brain comprises the fused trito-, deuto- and the medial regions of protocerebral ganglia. The central complex is situated towards the rostrum and consists of a well-defined PB, its projections to the "CB" (the FB and the EB), paired noduli, lateral accessary lobes and an accessory complex (**Figures 1**, **2**). These combined features typify the central complex of dicondylic insects, but within Crustacea, appear to be unique to stomatopods.

The Stomatopod Central Complex

The stomatopod central complex features a prominent PB that supplies decussating axons to a two component CB: a broad tapering upper division (here named the FB) and a narrower lower division (the EB) that provides axons to a pair of defined noduli (**Figure 1**). Lateral to and some distance from the CB are two clearly defined neuropils connected by axons to the EB. The disposition and connections of these neuropils correspond to the dicondylic lateral and medial bulbs and are distinct from the paired LAL that lie ventral to the EB (**Figure 2**).

The architecture of the stomatopod PB (**Figure 3**) appears to be more elaborate than in other crustaceans and, possibly, in Dicondylia. Located at the extreme rostral margin of the brain, it extends as one continuous neuropil linking both protocerebral hemispheres. This part of the bridge is composed of 6–8 modules on either side of the midline, each of which provides bundled axons that project to the CB. The bridge has a further heterolateral extension from its dorsal side that carries a system of decussating axons between the two protocerebral hemispheres. Synapsin labeling reveals two protruding branches originating from the front of the bridge that extend a short distance rostrally before bending towards the dorsal surface of the protocerebral lobes. These branches are of a similar thickness to the bridge itself, and both Bodian and synapsin-labeled preparations show these to be connected to the bridge (**Figure 3**). Axons extending from each side of the PB cross each other above their entry into the CB and then extend laterally to overlap each other in the FB itself. Anti-5HT immunolabeling separately distinguishes the upper and lower neuropils of the FB (**Figure 4**) and also resolves a third layer with fiber bundles extending laterally on the proximal side of the EB. Other antibodies, such as anti-DC0 (**Figure 5**), reveal the correspondence of the FB and EB to the same named centers in Dicondylia. Anti-5HT, -Neuropeptide F and -FMRF all reveal the FB as comprising eight modules, four each side of the midline (**Figures 4**, **5**). Anti-5HT labeling also resolves large fan-shaped tangentials with small branches in both the FB and EB, and large axons extending from the lateral and medial bulb (**Figure 4**). Neuropeptide F shows some labeling of the decussating neurons from the PB (**Figure 5**). Antisera against GABA show labeling of an arch-like territory in the EB, whereas DC0 mainly resolves the EB. However, we consider the results of GABA immunocytology still incomplete using the present antiserum as it strongly labels numerous neuronal perikarya but resolves very few processes. **Figure 2** illustrates the paired noduli attached to the ventral-proximal side of the EB. The noduli appear ovoid, comprising two adjacent synaptic territories.

Although much of the internal organization of the stomatopod CX is at present unknown, there is compelling evidence that efferents from the LP, including its visual neuropils, converge in CX neuropils. Injections of tracer dyes into lateral protocerebral neuropils fill numerous axons that project through the eyestalks into the midbrain. While many of these terminate in lateral neuropils, a number of others converge at the CX providing it with terminal arborizations (**Figures 6**, **7**). Certain of these are clearly constrained within modules of the FB (**Figure 6D**); others extend diffusely across the width of the EB (**Figure 7D**). Terminals arranged across the PB (**Figure 7A**) are reminiscent of optic lobe inputs to the PB identified in Diptera (Phillips-Portillo, 2012; Lin et al., 2013).

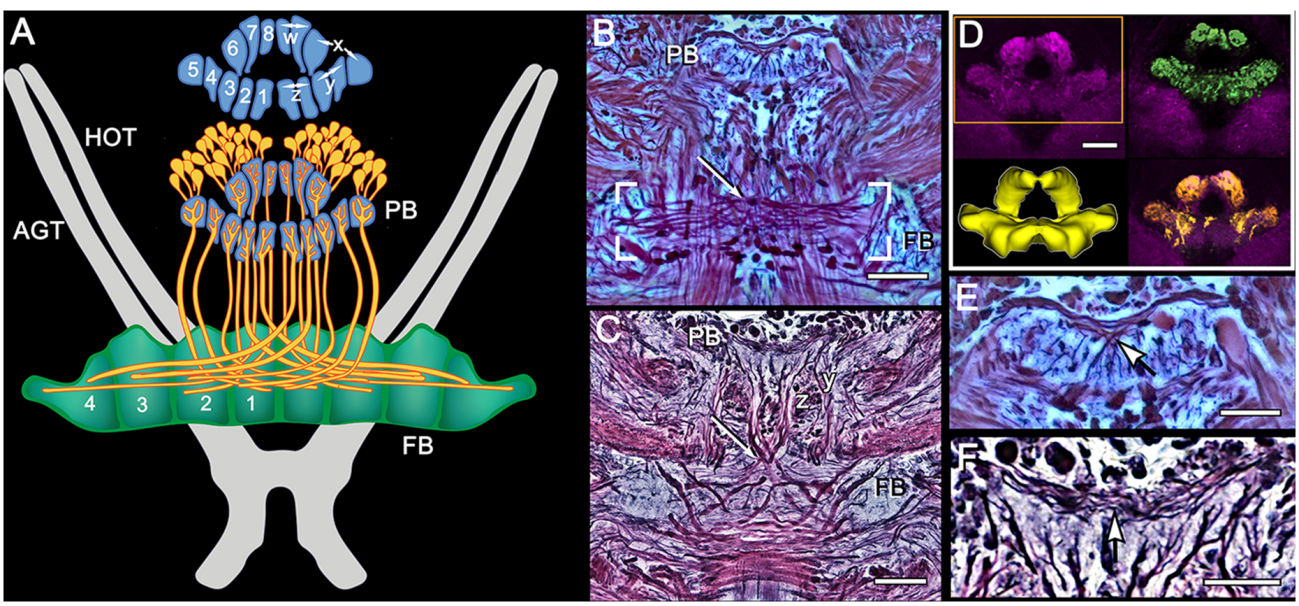

FIGURE 3 | Modular organization of the PB and projections to the FB. (A) Reconstruction from Bodian serial sections (*Pseudosquilla ciliata*) and synapsin immunocytology (*Gonodactylus smithii*) resolve eight modules of the PB. Each module is numbered 1–8. Pairs of modules relate to the *w, x, y, z* ground pattern of axon projections originally described for the insect CX. Each PB module provides bundled axons (each schematized as a single fiber) that map all eight modules from each side of the bridge across the entire FB, itself divided into eight modules. **(B)** Bodian stained decussation (box) and PB in *P. ciliata*. Region of decussation arrowed. **(C)** Bodian-stained decussation (arrowed) in *G. smithii* where the *y* and *z* bundles are clearly resolved. **(D)** Anti-synapsin labeled PBs of *G. smithii*. The box indicates the volume used for the reconstruction lower left. The top- and bottom-right panels show feature extractions revealing tangential processes extending across the bridge (green profiles) and some of the modular dendritic arrays of modular neurons supplying the FB (yellow profiles). **(E,F)** Enlargements showing tangential processes extending across the bridge. As in other pancrustaceans, these characteristically invert their top-down order at the midline (arrowed). Scale bars: **(B–D)** 50 μm: **(E,F)** 25 μm.

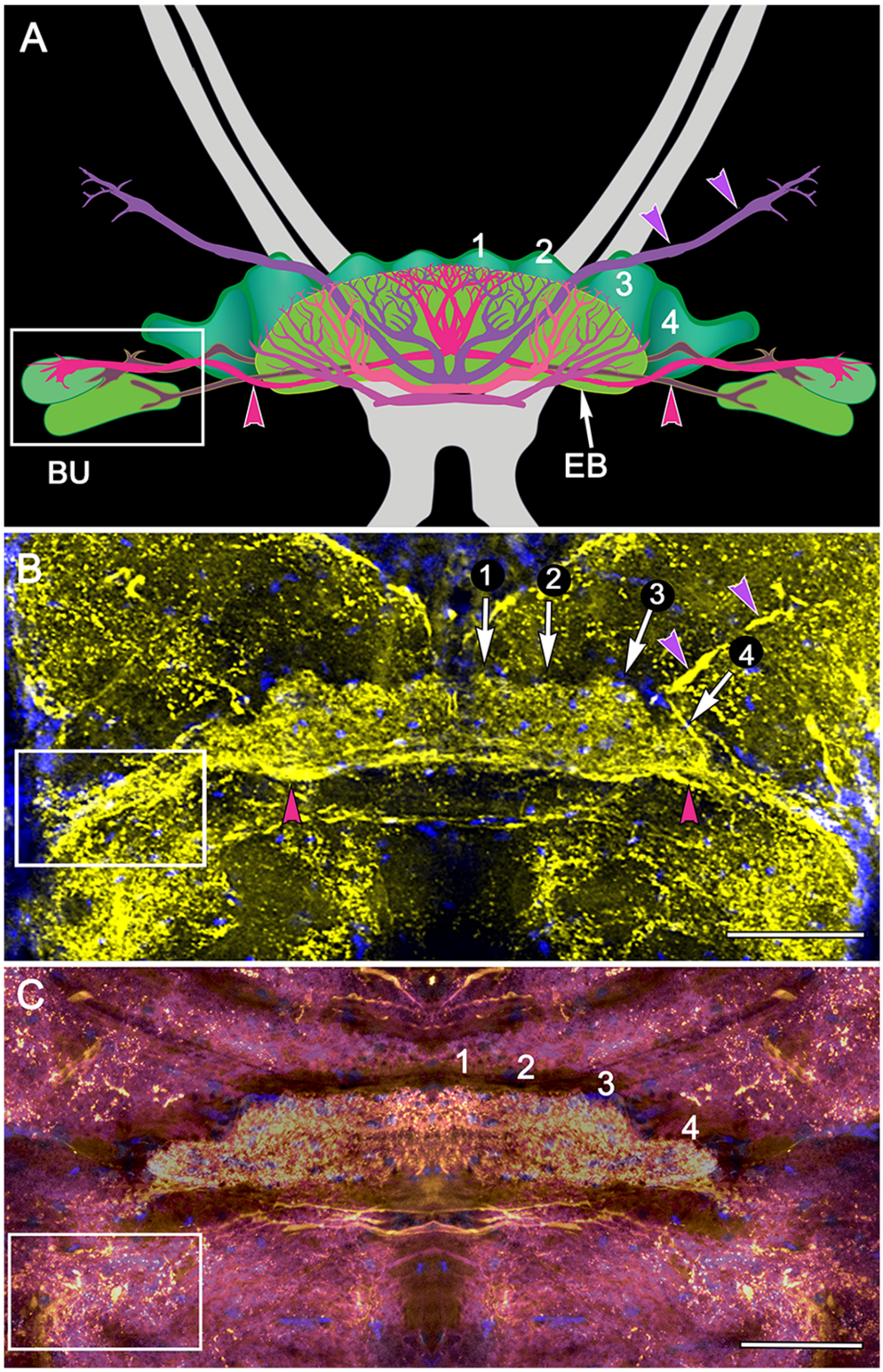

FIGURE 4 | Organization of modules and fan-shaped neurons. (A) Reconstruction of the FB and EB of *P. ciliata*, and some of its largest fan-shaped neurons. These originate from the lateral bulbs (Bu) and anterolateral protocerebral neuropils. **(B,C)** Serotonin immunolabeling resolved the modular organization of the FB (1–4) as well as major axons, some of which correspond to those identified in *P. ciliata*. Of interest are minor differences of serotonergic labeling in these two species (*H. trispinosa* in **B**, *G. smithii* in **C**), particularly the density of labeling and the stratification of the FB, which in *G. smithii* clearly resolves three layers. The boxed areas indicate the neuropil of the bulbs. Scale bars: **(B,C)** 100 μm.

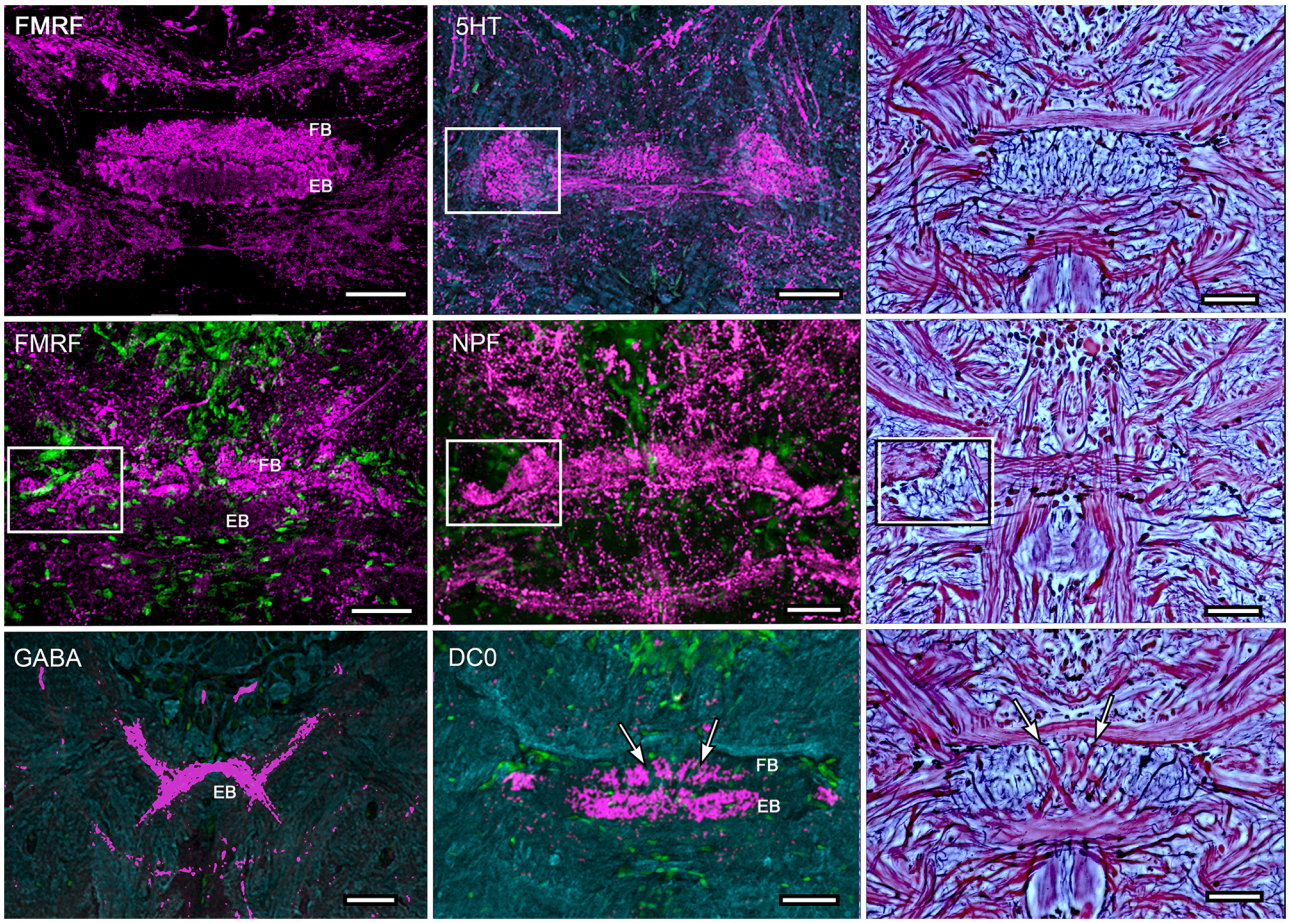

FIGURE 5 | Immunocytological partitions of the fan-shaped and ellipsoid bodies in *Neogonodactylus oerstedii*. Antibodies raised against FMRFamide resolve the EB (upper left) and the upper layer of the modular FB (middle left). In contrast, anti-5HT labels modules through the depth of the FB. Anti-NPF also selectively resolves modules in the FB. In contrast anti-GABA thus far resolves an arch-like territory in the most ventral area of the EB that appears to be supplied by axons entering it from the anterior protocerebrum. Anti-DC0 labels the EB, as it does in *Coenobita clypeatus* and dicondylic insects (Wolff et al., 2012). Bodian-stained CXs (right hand column) show corresponding cytoarchitectures in *P. ciliata*. Abbreviations as for other figures. Corresponding areas shown boxed, corresponding axon trajectories indicated by arrows. Scale bars, 50 μm.

DISCUSSION

The Central Complex of Crustaceans Other than Stomatopoda

With the exception of antennal and antennular movements, and apart from actions by gnathal appendages in feeding, asymmetric appendicular actions may be less common in crustaceans (Marshall and Diebel, 1995). For example, even though male crabs show asymmetric movements of one claw such actions are stereotypic, ritualized signals rather than independent adaptive reactions. Minor elaborations of the CX, such as an additional synaptic layer in the male fiddler crab, denote such sexually dimorphic arrangements (Loesel, unpublished observations), but other than in the CX of stomatopods and possibly in the CX of fast running littoral isopods (**Figures 8A–F**, see below), there is no clear evidence for a more defined modularity.

CX organization in eumalacostracan crustaceans, as mentioned, generally appears less elaborate when compared with dicondylic insects. In most eumalacostracans, as exemplified by the crayfish *Cherax destructor* (Utting et al., 2000), the PB provides incomplete decussation of axons into a wide spindle-shaped bilayered CB (**Figures 8G,H**). Although a satellite region comparable to the LAL has been resolved as receiving inputs from the CB, noduli have not yet been documented for any crustacean other than Stomatopoda (see below). As mentioned above, the archaeognathan CX is similarly spindle-shaped, its arrangement suggesting that Archaeognatha is more stemward than is any dicondylic species, an affinity also suggested by the lack of a blood-brain barrier between the archaeognathan circulatory system and retina, implying that this group also shares an important feature of its retinal physiology with marine crustaceans (Shaw and Varney, 1999).

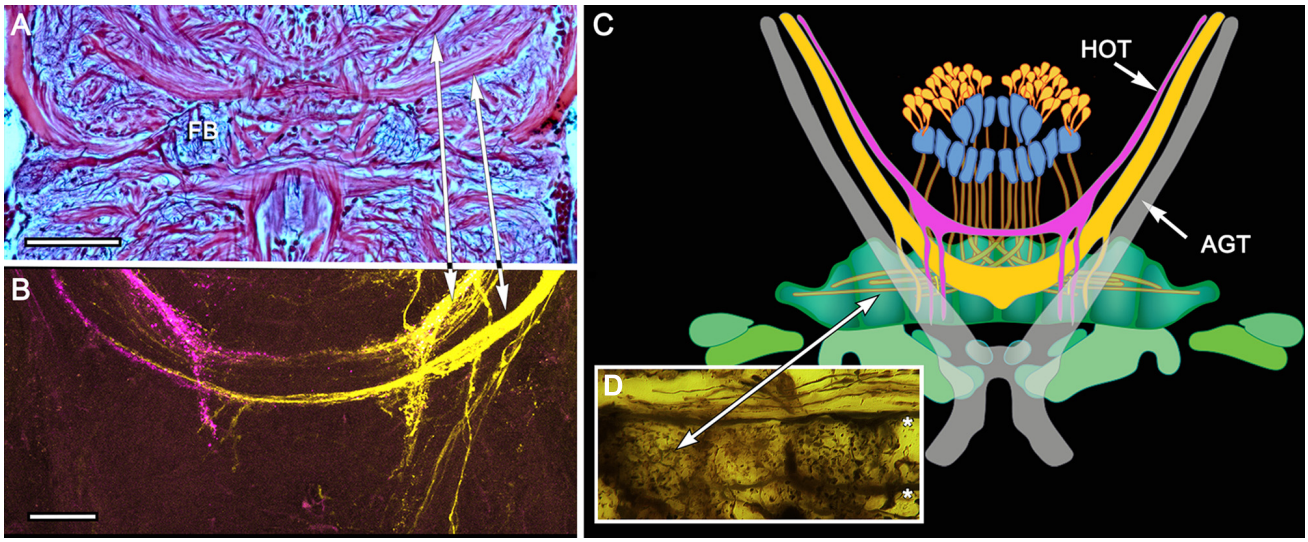

FIGURE 6 | Eyestalk convergence at the central complex. (A) Silver stained brain of *P. ciliata* reveals numerous heterolateral fiber projections to the central complex amongst which are tracts originating from the eyestalks (arrowed). **(B)** Dye tracing in *Haptosquilla trispinosa* resolves tracts as providing processes mainly to the FB, showing that most but not all fibers appear to terminate there. **(C)** Summary figure showing FB in relation to the antennal glomerular tract (AGT), carrying olfactory neuron relays, and the two main tributaries of the heterolateral optic tracts (HOT). **(D)** Golgi impregnation showing eyestalk axons (above asterisks) extending across the CX, providing discrete terminal processes clustered in the FB modules. Scale bars: **(A)** 50 μm; **(B)** 100 μm.

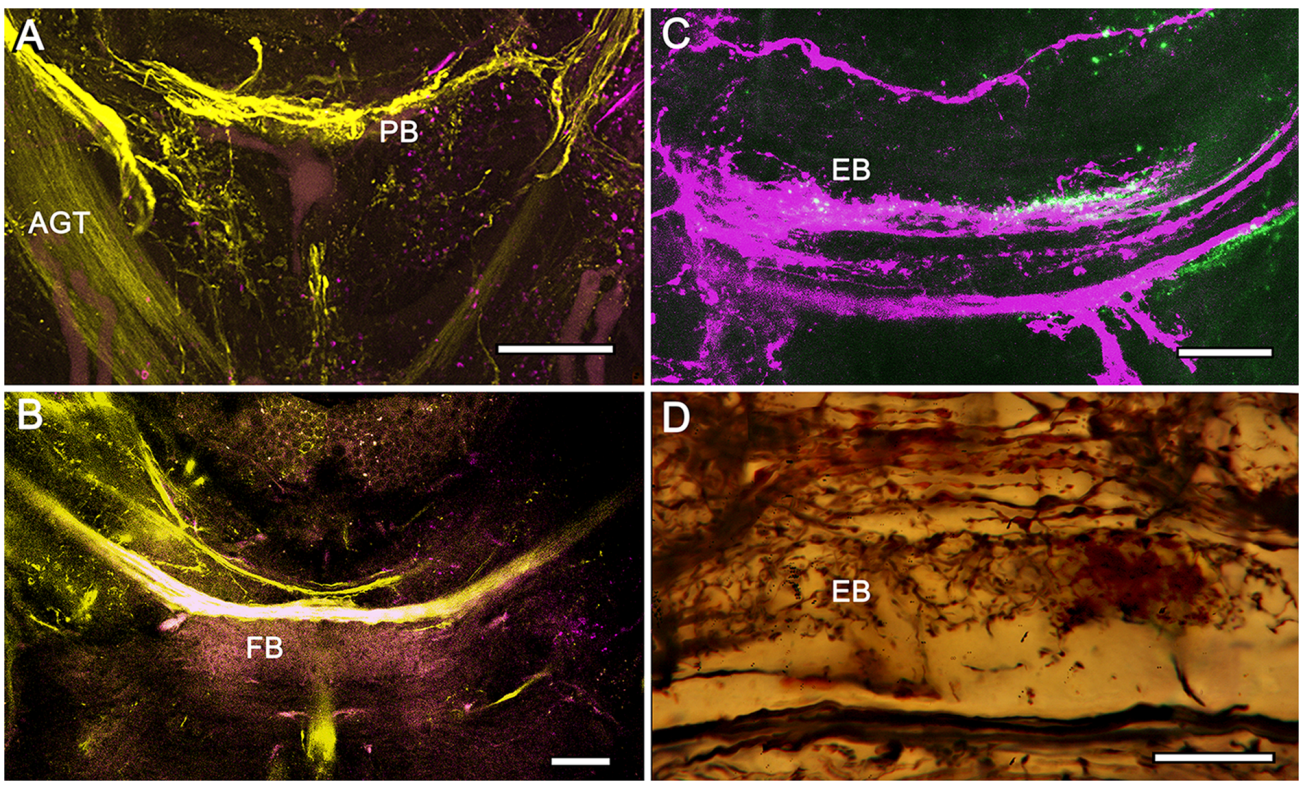

FIGURE 7 | Eyestalk convergence at the central complex. (A) Dextran-fluorescein fills into the LP retrogradely label axons in the AGT and anterogradely filled axons extending to lateral midbrain regions as well as the midline PB. **(B)** Large heterolateral axons from the LP supplying the FB, their upper margins delineating FB modules. **(C)** Dextran-Texas Red fills reveal heterolateral inputs to the EB. **(D)** Detail of the EB showing heterolateral terminals of eyestalk axons. Scale bars: **(A,B)** 50 μm; **(C,D)** 25 μm.

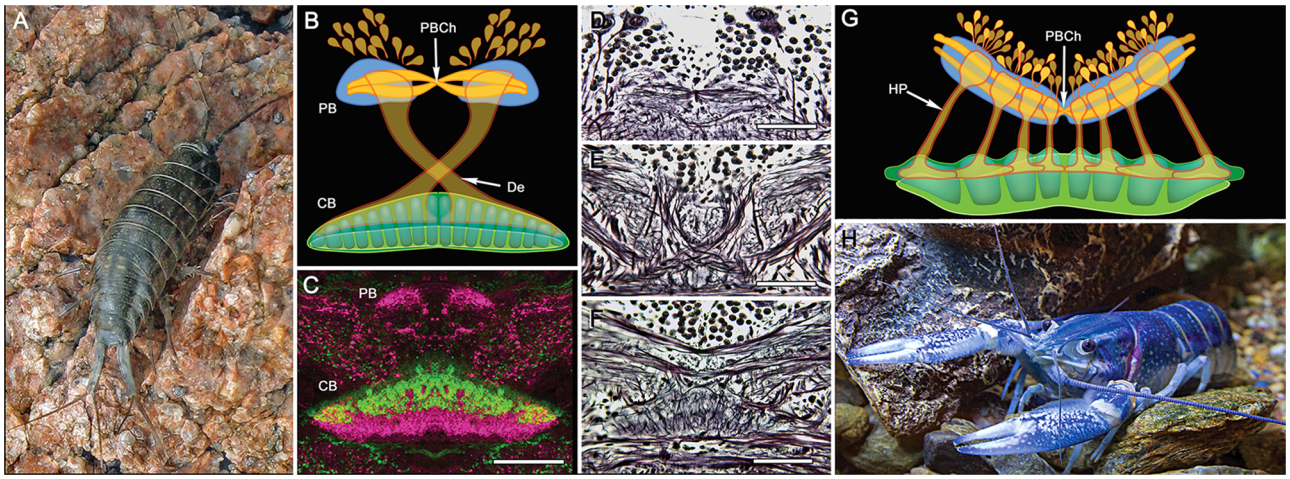

FIGURE 8 | PB and central body (CB) connections in two other eumalacostracans. (A) The littoral isopod *Ligia exotica*. **(B)** Reconstruction of the PB and bistratified CB showing the incomplete decussation of axons from each side of the PB to the opposite site of the CB. Like other pancrustaceans, transverse fibers spanning the PB undergo a chiasma-like cross over at the mid-line (PBCh). **(C)** In many eumalacostracans, the CX lacks noduli and an obvious EB homolog. Instead, the composite CB is clearly divided into two levels each with different immunocytological properties: here affinities to allatostatin (green) and tachykinin (magenta) (image: Rudi Loesel). Bodian stained brain reveals the PBCh **(D)**, the contralateral projections of *w, x, y, z*, bundles **(E)** and the bistratified architecture of the CB **(F)**. **(G)** Homolateral projections (HP) of the *w, x, y, z* projections between the PB and CB in the fossorial crayfish *Cherax destructor* **(H)** (after Utting et al., 2000). Scale bars: **(C–F)** 100 μm.

The Insect-Like Central Complex of Stomatopods

In Malacostraca (and Remipedia; Fanenbruck et al., 2004) the PB is a single span of neuropil extending between the two protocerebral lobes (Sandeman et al., 1988, 1992; Utting et al., 2000; Harzsch and Hansson, 2008), whereas in stomatopods it is distinguished by two extended swellings from each side that meet again at the brain's mid-line (**Figure 3**). That this attribute is so far unknown in any other pancrustacean suggests its apomorphic nature. Given that the PB in Dicondylia carries representations of the sensory surround (Heinze and Homberg, 2007; Ritzmann et al., 2008), the functional implications of the organization of the stomatopod bridge will certainly be of future interest. The division of the stomatopod PB into an 8 + 8 modular arrangement suggests that modules may together carry discrete representations of the sensory surround, as demonstrated for Orthoptera, Lepidoptera and Dictyoptera (Heinze and Homberg, 2007; Ritzmann et al., 2008; Heinze and Reppert, 2011).

Another insect-like feature is the manner in which axons extending from the PB decussate into the FB. In decapod malacostracans, exemplified by the crayfish *Cherax destructor* (**Figure 8**), parallel projections homologous to the *w, x, y, z* bundles of Dicondylia extend ipsilaterally from the PB to the outer layer of the CB to there bifurcate and extend laterally: subunits of the PB are thus represented as overlapping elements within defined domains the CB neuropil (Utting et al., 2000). In stomatopods, on the other hand, axon projections from the PB decussate distal to the FB, as do the *w*-, *x*-, *y*-, and *z*-bundles described for the dicondylic brain (Williams, 1975; Boyan et al., 2015), and then overlap each other within the FB itself such that each half of the PB appears to be represented across the whole of the FB.

The stomatopod CB is prominently divided into a distinct upper and lower neuropil, corresponding to the FB and EB found in insects, and as in the insect EB the lower neuropil is correspondingly labeled by anti-DC0 (**Figure 5**). As in the insect FB, the upper neuropil resolves 4 distinct modules on each side of the midline, again corresponding to the dicondylic arrangement (**Figure 4**). As in dicondylic insects, prominent tangential neurons in the lower neuropil (the EB) providing large terminal branches are connected by axons to the lateral and median bulb. In *Drosophila* these centers have been shown to encode visual motion information from different segments of each monocular visual field (Seelig and Jayaraman, 2013) and to supply axons to the EB.

The discovery that paired noduli-like neuropils are part of the stomatopod central complex is surprising. These structures, as yet unidentified in any other crustacean, have been suggested as one of the more recently evolved additions to the dicondylic central complex, the proposition being that they may be associated with flight due to their presence in pterygote insects (Homberg, 2008) but not in apterygote Zygentoma (Loesel et al., 2002). They are, however, equally prominent in pterygote species that have an evolved loss of wings, such as the dermapteran *Anisolabis maritima* (Loesel et al., 2002). The presence of noduli in Stomatopoda, which may be unique within crustaceans, allows speculation about their possible association with locomotion. Of all crustaceans, stomatopods may be amongst the most accomplished swimmers, and move with a speed, agility and accuracy not seen in other crustaceans. Are noduli perhaps involved in facilitating such agility? An

intriguing finding by Buchanan et al. (2015) is that in *Drosophila*, one synaptic domain in the noduli is involved in the control of handedness during walking. A preference of left vs. right during locomotion may be an important criterion in achieving maneuverability.

One obvious exception to the claim that most eumalacostracans have relatively simple central complexes is Isopoda, particularly in littoral species. *Ligia exotica* (**Figure 8**) is a fast running eumalacostracan, the CX of which is equipped with a prominent PB and a deep bilayered CB. Its PB consists of two bilateral neuropils connected across the brain's midline by a system of heterolaterally decussating fibers like those observed in the stomatopod PB. In *L. exotica*, the PB supplies axons to the CB (Strausfeld, 1998, 2012) in a manner reminiscent of the CX of a dicondylic insect; except that in the isopod, axons from one side of the bridge appear to innervate the opposite side of the CB, rather than its entire heterolateral extent (**Figure 8**).

Evolutionary Considerations and Correspondences with Dicondylia

Comparisons across the rather small sample so far investigated suggest that there may be more divergence of CX organization amongst crustacean species than amongst insects, and that organization of CXs in certain basal malacostracans, such as Leptostraca (Strausfeld, 2012; Kenning et al., 2013), might be closest to the ancestral ground pattern. This would be plausible if the most derived crustacean CXs belong to Stomatopoda. Indeed, their dicondylic-like organization (**Figure 9** inset) suggests no closer phylogenetic relationship between Stomatopoda and Hexapoda than currently resolved by molecular phylogenetics (**Figure 9**), which show Eumalacostraca as phyletically distant from the clade comprising Hexapoda and Remipedia (Oakley et al., 2012). But are the dicondylic-like aspects of the stomatopod CX the result of independently evolved convergent elaborations of an ancestral ground pattern? Or might correspondences of the CXs of Dicondylia and Stomatopoda suggest that those lineages alone conserved a far more elaborate ancestral ground pattern than suggested by Leptostraca or any other crustacean? That cerebral organization found in extant eumalacostracans and insects is known to have existed in stem arthropods in the early Cambrian (Ma et al., 2012) admits the possibility that an elaborate central complex may also be as ancient (Strausfeld et al., 2016). Simpler CX arrangements in crown taxa would then reflect an evolutionary history of central complex simplification and in some lineages, such as Cephalocarida, even complete loss.

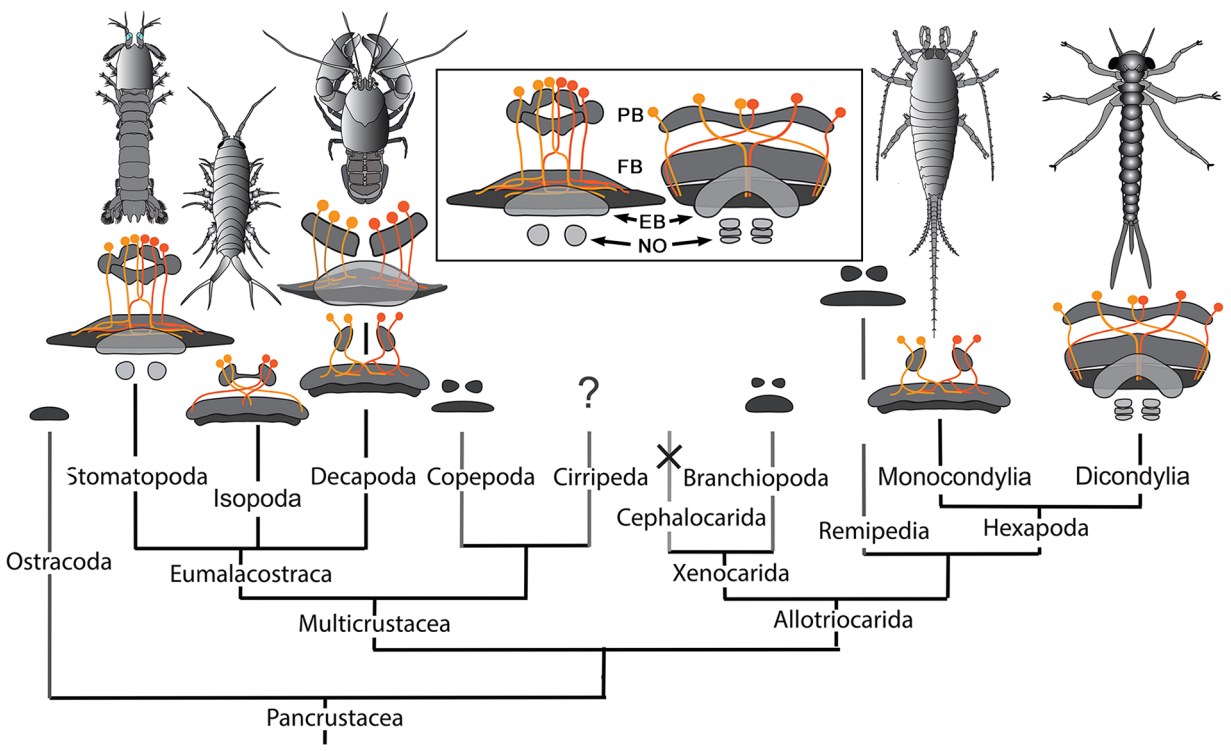

FIGURE 9 | Central complexes and pancrustacean phylogeny (Oakley et al., 2012). CX organization in the phyletically distant Stomatopoda and Dicondylia (here represented by an odonate naiad) show close correspondence of their PB, FB, EB, and noduli (NO), and the representation of the PB in the FB by decussating axons (inset). Other CXs in eumalacostracans show simpler arrangements. Decapoda have either homolateral PB-CB projections (as in *C. destructor*) or partially decussating projections, as in Caridea and Dendrobranchiata (examples of species not shown here) that are almost identical to those of monocondylic insects (Strausfeld, 2012). Central complex neuropils, though not their detailed morphologies, have been identified in Branchiopoda (Strausfeld, 2012), Copepoda (Andrew et al., 2012), Remipedia (Fanenbruck et al., 2004), and possibly in Ostracoda. Their presence in cirripede larvae has not been established. There is no evidence for a central complex in Cephalocarida (Stegner and Richter, 2011) where it is assumed to have undergone reduction and loss.

What are the distinctive characters of malacostracan CXs that sets them apart, and which may impact considerations about functional commonalities? The proposition that CXs may be computationally equivalent in mediating compass headings and path integration (Webb and Wystrach, 2016) still requires reflection on the diversity of CX arrangements across pancrustaceans. In dicondylic insects, for example, major inputs to layers of the FB originate from the medial lobes of the protocerebrum, a complex neuropil that is supplied by, if not all, then the majority of output neurons from the mushroom body lobes (Li and Strausfeld, 1997, 1999; Phillips-Portillo and Strausfeld, 2012; Wolff and Strausfeld, 2016). If eumalacostracans generally do not possess these iconic centers then such circuits might be entirely absent. Indeed, the lack of prominent multistratified FBs in crustaceans (and in archaeognathans, which lack mushroom bodies) suggests a major functional difference from their dicondylic counterparts, stomatopods again being the exception. In Dicondylia, the multiple strata that define the FB reflect the elaboration and identities of its inputs, particularly from the protocerebral lobes, as well as arrangements of numerous species of peptidergic neurons (Herbert et al., 2010; Kahsai and Winther, 2011) certain of which are implicated in the modulation of locomotory activity (Kahsai et al., 2010).

Of the many divergent CX arrangements across Dicondylia, one is particularly notable. This relates to the representation of appendicular control. In Dicondylia, modular organization of the CX's FB and EB appear to directly bear on appendicular versatility, such as required for directional change during walking, obstacle avoidance, climbing and even predation. The precision of modular organization in the FB, allowing the recognition of 4 + 4 discrete modules on each side of the midline, relates to the amount of overlap between dendrites and collaterals belonging to neurons in adjacent modules, there being the least overlap in those species with the most refined appendicular dexterity (Strausfeld and Hirth, 2013). Surveys across eumalacostracan central complexes have not resolved comparable distinctions. The exception is in fossorial crayfish, in which the CB is divided into 4 + 4 modules (Utting et al., 2000), littoral isopods, where the foliated CB comprises 8 + 8 modules, and stomatopods where immunocytology clearly identifies eight subdivisions across the FB (**Figure 4**).

Differences of organization amongst homologous neurons reflect specific differences of synaptic arrangements within homologous circuits. Such differences may provide important avenues towards interpreting the significance of CX neuroanatomy with respect to motor repertoires and the ecological constraints in which they are elicited. It is not just in insects that divergent modifications of the ancestral ground pattern may reveal functional attributes. For example, despite the relative few detailed studies of eumalacostracan brains, it is notable that both the morphology of the PB, and the organization of the *w, x, y, z* fibers from it, can differ substantially. The relatively simple unistratified PB of the crayfish *Cherax destructor* (Utting et al., 2000) occupies a span broader than that of the more elaborate stomatopod PB. However, in *C. destructor* the *w, x, y, z* tracts do not decussate as they do in Stomatopoda and Dicondylia (**Figures 3**, **8**) but project directly into the CB beneath. In littoral isopods, such as *Ligia exotica*, *w, x, y, z* tracts project from each half of the PB into the contralateral half of the CB rather than distributing across the whole of CB (**Figure 8**). Such differences of representation in the PB would suggest important differences of homologous computational circuits and it is of considerable interest that in Dicondylia only some classes of neurons from the PB do indeed decussate. As described from *Drosophila* and *Schistocerca*, certain modular neurons from each of half the PB map across the whole FB, as in Stomatopoda. These contrast with a class of PB neurons in Dicondylia, the axons of which extend directly to the FB without any decussation, only to undergo heterolateral projection from the FB into the LAL (Hanesch et al., 1989; Heinze and Homberg, 2008).

The Central Complex and Efferent Sensory-Motor Convergence

In conclusion, our still preliminary studies of the stomatopod central complex suggest numerous similarities with CXs of dicondylic insects (for a summary of shared features see **Table 2**). Across eumalacostracans, and mostly likely in other crustacean groups as well, antennules, antennae and gnathal appendages can all show lateralized as well as bilateral coordination. For example, fossorial decapods dig burrows and walk about; littoral isopods run rapidly, and even jump across gaps. Nevertheless, certain appendicular actions of stomatopods do stand apart. One is cleaning actions by the maxillipeds in maintaining debris-free retinal surfaces. Another is the range of actions executed by the large antennal plates or scales that appear to play a crucial role in swimming, possibly serving a dual function in mechanosensory input. And lastly, one of the most interesting actions is the extraordinary range of independent movements carried out by the eyestalks.

As introduced at the beginning of this article, the highly modular arrangement of the stomatopod FB combined with refined appendicular dexterity lends support to the proposition that the CX, as a recipient of inputs from both eyestalks (**Figures 6**, **7**), is a likely candidate for the control of their conjoint movements. Although no studies on insect CXs show a role in action selection by head appendages, the anatomical and physiological organization of crustacean eyestalks conform to a sensory and motor ground pattern typifying jointed appendages, such as the legs. Eumalacostracan eyestalks usually comprise three articles, albeit fused: proximal, medial and distal segments, the last surmounted by the eye. Eyestalks are equipped with muscles providing coordinated rotational and translator movements in response to visual and gravitational stimuli (Mellon, 1977). Thus, as do legs, eyestalks perform discrete behavioral actions in response to specific multisensory stimuli. In stomatopods, the two eyestalks can switch from independent movements to conjoint scans of potential prey using saccadic movements for acquisitive vision (Marshall et al., 2014). Such responses are comparable to visually-driven leg movements of

TABLE 2 | Summary of central complex features found across groups of crustaceans, monocondylic and dicondylic insects.

	Stomatopoda	"Other" crustaceans	"Dexterous" dicondylic insects	"Non-dexterous" dicondylic insects	Monocondylic insect (Archaeognatha)
Protocerebral bridge (PB)	Prominent	Varied: in some species small inconspicuous and lateralized.	Prominent	Prominent	Small, lateralized
Complete decussation of axons from PB	Yes	"Incomplete" decussation: PB represent mainly in contralateral half of FB. (see **Figure 8**); or, homolateral PB-CB projection.	Yes: each side of the PB represented across entire FB	Yes, each side of the PB represented across entire FB	"Incomplete" decussation: PB represent mainly in contralateral half of FB.
Central body bilayered or multi component	Central body (CB) divided into two discrete stratified neuropils, the FB and EB	At least two layers resolvable with certain antibodies	Central body divided into two discrete stratified neuropils, the FB and EB	Central body divided into two discrete stratified neuropils, the FB and EB	At least two layers resolvable with certain antibodies
Central body shape	Broad tapering upper division, narrower lower division	Usually spindle-shaped	Fan-shaped upper level, arched- to ellipsoid shaped body lower level	Fan-shaped upper level, arched- to ellipsoid- shaped body lower level	Spindle-shaped
Prominent modules in the fan-shaped body	Yes	Rarely	Yes	No	No
Noduli present	Yes	None identified	Yes	Yes	None identified

FIGURE 10 | Behavioral actions in stomatopods. Stomatopods frequently compete over burrows in coral reef substrate. *Haptosquilla trispinosa* (shown here) also meet for potential mating and both activities may be hazardous, hence the approach of the intruder/suitor using the telson as armor. During these encounters, sensory structures such as the antennae, antennules, antennal scales and eyes (for clearer view, see **Figure 2**) are pointed in a forward position and actively gather information through both independent and conjoint movements. Image: Roy Caldwell.

mantispid Neuroptera during prey tracking (Kral et al., 2000). The appendicular nature of the eyestalk was well known to 19th Century zoologists who demonstrated that an articulated appendage is regenerated in lieu of an amputated eyestalk (Milne-Edwards, 1864). And in insects, suppressing genes that determine the development of a compound eye results in the default development of an articulated appendage in place of the eye (Kumar and Moses, 2001).

In addition to their appendicular nature, neuroanatomical evidence shows that the two eyestalks provide numerous efferent axons that converge at the stomatopod CX. The existence of these pathways (**Figures 6**, **7**), combined with the highly modular arrangement of the stomatopod FB, strengthens the proposition that this locus of efferent convergence may be pivotal to eyestalk action selection. Furthermore, preliminary electrophysiological recordings using sharp extracellular electrodes coated with fluorescent dye demonstrate that it is neurons in the stomatopod CX that vigorously respond to visual movements, being activated immediately prior to movements of the two eyes (N. Lessios, unpublished data).

Doubtlessly there are other behaviors that are under control of action-selecting circuits. **Figure 10** shows an example of an encounter between two stomatopods, manifesting some of a range of behavioral actions. However, whereas these are not unique to this group of eumalacostracans, independent eye movements are unparalleled except in two other taxa both of which are vertebrates. One is chameleons, in which each eye functions independently of the other and, as the authors suggest, each half of the brain is likely associated with homolateral oculomotor and visual processing (Tauber and Atkin, 1967). The other is the sandlance *Limnichthyes fasciatus*, a teleost that like the chameleon and stomatopod employs ballistic strikes to capture prey (Fritsches and Marshall, 1999). The ability of the stomatopod to switch from independent optokinetic nystagmus and visual pursuit to tight collaboration of the two eyes during fixation and targeting provides a fascinating behavior that demands the identification of neural circuits mediating its orchestration. Thus far, neuroanatomical observations suggest that the CX might be the most likely candidate.

ETHICS STATEMENT

This study was carried out in accordance with the recommendations of the Australian Code of Practice for the Care and Use of Animals for Scientific Purposes, National Health and Medical Research Council. The protocol was approved by the University of Queensland Animal Ethics Committee (AEC).

AUTHOR CONTRIBUTIONS

NJS, HHT, GHW and JM designed the study, NJS, HHT and GHW collected the data; NJS and HHT made the figures; NJS, HHT, GHW and JM wrote the manuscript.

FUNDING

This work was supported by a grant from the U.S. Air Force Research Laboratory (FA86511010001) and the Center for Insect Science, University of Arizona to NJS, grants to JM from the Asian Office of Aerospace Research and Development (AOARD-12-4063) and the Australian Research Council (FL140100197), and a grant to HHT from the Lizard Island Research Foundation, a Doctoral Fellowship (2013) from the Lizard Island Research Station, a facility of the Australian Museum.

REFERENCES

Andrew, D. R., Brown, S. M., and Strausfeld, N. J. (2012). The minute brain of the copepod *Tigriopus californicus* supports a complex ancestral ground pattern of the tetraconate cerebral nervous systems. *J. Comp. Neurol.* 520, 3446–3470. doi: 10.1002/cne.23099

Bausenwein, B., Wolf, R., and Heisenberg, M. (1986). Genetic dissection of optomotor behavior in *Drosophila melanogaster* studies on wild-type and the mutant optomotor-blind H31. *J. Neurogenet.* 3, 87–109. doi: 10.3109/01677068609106897

Bender, J. A., Pollack, A. J., and Ritzmann, R. E. (2010). Neural activity in the central complex of the insect brain is linked to locomotor changes. *Curr. Biol.* 20, 921–926. doi: 10.1016/j.cub.2010.03.054

Bodian, D. (1936). A new method for staining nerve fibers and nerve endings in mounted paraffin sections. *Anat. Rec.* 65, 89–97. doi: 10.1002/ar.10906 50110

Bok, M. J. (2012). Available online at: https://www.youtube.com/watch?v=ZhlAYDvAeFk

Boyan, G., Williams, L., and Liu, Y. (2015). Conserved patterns of axogenesis in the panarthropod brain. *Arthropod Struct. Dev.* 44, 101–112. doi: 10.1016/j.asd.2014.11.003

Buchanan, S. M., Kain, J. S., and de Bivort, B. L. (2015). Neuronal control of locomotor handedness in *Drosophila*. *Proc. Natl. Acad. Sci. U S A* 112, 6700–6705. doi: 10.1073/pnas.1500804112

Chiou, T. H., Kleinlogel, S., Cronin, T., Caldwell, R., Loeffler, B., Siddiqi, A., et al. (2008). Circular polarization vision in a stomatopod crustacean. *Curr. Biol.* 18, 429–434. doi: 10.1016/j.cub.2008.02.066

Cronin, T. W., and Marshall, N. J. (1989a). Multiple spectral classes of photoreceptors in the retinas of gonodactyloid stomatopod crustaceans. *J. Comp. Physiol. A* 166, 261–275. doi: 10.1007/bf00193471

Cronin, T. W., and Marshall, N. J. (1989b). A retina with at least ten spectral types of photoreceptors in a mantis shrimp. *Nature* 339, 137–140. doi: 10.1038/339137a0

Cronin, T. W., Marshall, N. J., and Land, M. F. (1991). Optokinesis in gonodactyloid mantis shrimps (Crustacea; Stomatopoda; Gonodactylidae). *J. Comp. Physiol. A* 168, 233–240. doi: 10.1007/bf00218415

Cronin, T. W., Marshall, N. J., Quinn, C. A., and King, C. A. (1994). Ultraviolet photoreception in mantis shrimp. *Vision Res.* 34, 1443–1452. doi: 10.1016/0042-6989(94)90145-7

Cronin, T. W., Nair, J. N., Doyle, R. D., and Caldwell, R. L. (1988). Ocular tracking of rapidly moving visual targets by stomatopod crustaceans. *J. Exp. Biol.* 138, 155–179.

Daly, I. M., How, M. J., Partridge, J. C., Temple, S. E., Marshall, N. J., Cronin, T. W., et al. (2016). Dynamic polarization vision in mantis shrimps. *Nat. Commun.* 7:12140. doi: 10.1038/ncomms12140

Derby, C. D., Fortier, J. K., Harrison, P. J. H., and Cate, H. S. (2003). The peripheral and central antennular pathway of the Caribbean stomatopod crustacean *Neogonodactylus oerstedii*. *Arthropod Struct. Dev.* 32, 175–188. doi: 10.1016/s1467-8039(03)00048-3

Ehmer, B., and Gronenberg, W. (2002). Segregation of visual input to the mushroom bodies in the honeybee (*Apis mellifera*). *J. Comp. Neurol.* 451, 362–373. doi: 10.1002/cne.10355

Fanenbruck, M., Harzsch, S., and Wägele, J. W. (2004). The brain of the Remipedia (Crustacea) and an alternative hypothesis on their phylogenetic relationships.

Proc. Natl. Acad. Sci. U S A 101, 3868–3873. doi: 10.1073/pnas.0306212101

Fiore, V. G., Dolan, R. J., Strausfeld, N. J., and Hirth, F. (2015). Evolutionarily conserved mechanisms for the selection and maintenance of behavioural activity. *Philos. Trans. R. Soc. Lond. B Biol. Sci.* 370:20150053. doi: 10.1098/rstb.2015.0053

Fritsches, K. A., and Marshall, J. (1999). A new category of eye movements in a small fish. *Curr. Biol.* 9, R272–R273. doi: 10.1016/s0960-9822(99)80176-6

Gagnon, Y. L., Templin, R. M., How, M. J., and Marshall, N. J. (2015). Circularly polarized light as a communication signal in mantis shrimps. *Curr. Biol.* 25, 3074–3078. doi: 10.1016/j.cub.2015.10.047

Guo, P. Y., and Ritzmann, R. E. (2013). Neural activity in the central complex of the cockroach brain is linked to turning behaviors. *J. Exp. Biol.* 216, 992–1002. doi: 10.1242/jeb.080473

Hanesch, U., Fischbach, K.-F., and Heisenberg, M. (1989). Neuronal architecture of the central complex in *Drosophila Melanogaster*. *Cell Tissue Res.* 257, 343–366. doi: 10.1007/Bf00261838

Harzsch, S., and Hansson, B. S. (2008). Brain architecture in the terrestrial hermit crab *Coenobita clypeatus* (Anomura, Coenobitidae), a crustacean with a good aerial sense of smell. *BMC Neurosci.* 9:58. doi: 10.1186/1471-2202-9-58

Heinze, S., and Homberg, U. (2007). Maplike representation of celestial E-vector orientations in the brain of an insect. *Science* 315, 995–997. doi: 10.1126/science.1135531

Heinze, S., and Homberg, U. (2008). Neuroarchitecture of the central complex of the desert locust: intrinsic and columnar neurons. *J. Comp. Neurol.* 511, 454–478. doi: 10.1002/cne.21842

Heinze, S., and Reppert, S. M. (2011). Sun compass integration of skylight cues in migratory monarch butterflies. *Neuron* 69, 345–358. doi: 10.1016/j.neuron.2010.12.025

Held, M., Berz, A., Hensgen, R., Muenz, T. S., Scholl, C., Rössler, W., et al. (2016). Microglomerular synaptic complexes in the sky-compass network of the honeybee connect parallel pathways from the anterior optic tubercle to the central complex. *Front. Behav. Neurosci.* 10:186. doi: 10.3389/fnbeh.2016.00186

Herbert, Z., Rauser, S., Williams, L., Kapan, N., Güntner, M., Walch, A., et al. (2010). Developmental expression of neuromodulators in the central complex of the grasshopper *Schistocerca gregaria*. *J. Morphol.* 271, 1509–1526. doi: 10.1002/jmor.10895

Heuer, C. M., Müller, C. H., Todt, C., and Loesel, R. (2010). Comparative neuroanatomy suggests repeated reduction of neuroarchitectural complexity in Annelida. *Front. Zool.* 7:13. doi: 10.1186/1742-9994-7-13

Homberg, U. (1985). Interneurones of the central complex in the bee brain (*Apis-Mellifera, L*). *J. Insect Physiol.* 31, 251–264. doi: 10.1016/0022-1910(85)90127-1

Homberg, U. (2008). Evolution of the central complex in the arthropod brain with respect to the visual system. *Arthropod Struct. Dev.* 37, 347–362. doi: 10.1016/j.asd.2008.01.008

Homberg, U., Heinze, S., Pfeiffer, K., Kinoshita, M., and el Jundi, B. (2011). Central neural coding of sky polarization in insects. *Philos. Trans. R. Soc. Lond. B Biol. Sci.* 366, 680–687. doi: 10.1098/rstb.2010.0199

Honegger, H. W., and Schürmann, F. W. (1975). Cobalt sulphide staining of optic fibres in the brain of the cricket, *Gryllus campestris*. *Cell Tissue Res.* 159, 213–225. doi: 10.1007/bf00219157

Huber, F. (1959). Auslösung von Bewegungsmustern durch elektrische Reizung des Oberschlundganglions bei Orthopteren (Saltatoriab: Gryllidae, Acridiidae). *Verh. Dtsch. Zool. Ges.* 1959, 248–269.

Huber, F. (1960). Untersuchungen über die Funktion des Zentralnervensystems und insbesondere des Gehirnes bei der Fortbewegung und der Lauterzeugung der Grillen. *Vergl. Physiol.* 44, 60–132. doi: 10.1007/BF00297863

Ilius, M., Wolf, R., and Heisenberg, M. (2007). The central complex of *Drosophila melanogaster* is involved in flight control: studies on mutants and mosaics of the gene ellipsoid body open. *J. Neurogenet.* 21, 321–338. doi: 10.1080/01677060701693503

Ito, K., Shinomiya, K., Ito, M., Armstrong, J. D., Boyan, G., Hartenstein, V., et al. (2014). A systematic nomenclature for the insect brain. *Neuron* 81, 755–765. doi: 10.1016/j.neuron.2013.12.017

Iwano, M., Hill, E. S., Mori, A., Mishima, T., Mishima, T., Ito, K., et al. (2010). Neurons associated with the flip-flop activity in the lateral accessory lobe and ventral protocerebrum of the silkworm moth brain. *J. Comp. Neurol.* 518, 366–388. doi: 10.1002/cne.22224

Jones, J. (1994). Architecture and composition of the muscles that drive stomatopod eye-movements. *J. Exp. Biol.* 188, 317–331.

Kahsai, L., Martin, J. R., and Winther, Å. M. E. (2010). Neuropeptides in the *Drosophila* central complex in modulation of locomotor behavior. *J. Exp. Biol.* 213, 2256–2265. doi: 10.1242/jeb.043190

Kahsai, L., and Winther, Å. M. E. (2011). Chemical neuroanatomy of the *Drosophila* central complex: distribution of multiple neuropeptides in relation to neurotransmitters. *J. Comp. Neurol.* 519, 290–315. doi: 10.1002/cne.22520

Kenning, M., Müller, C., Wirkner, C. S., and Harzsch, S. (2013). The Malacostraca (Crustacea) from a neurophylogenetic perspective: new insights from brain architecture in *Nebalia herbstii* Leach, 1814 (Leptostraca, Phyllocarida). *Zool. Anz.* 252, 319–336. doi: 10.1016/j.jcz.2012.09.003

Klagges, B. R. E., Heimbeck, G., Godenschwege, T. A., Hofbauer, A., Pflugfelder, G. O., Reifegerste, R., et al. (1996). Invertebrate synapsins: a single gene codes for several isoforms in *Drosophila*. *J. Neurosci.* 16, 3154–3165.

Kleinlogel, S., and Marshall, N. J. (2006). Electrophysiological evidence for linear polarization sensitivity in the compound eyes of the stomatopod crustacean *Gonodactylus chiragra*. *J. Exp. Biol.* 209, 4262–4272. doi: 10.1242/jeb.02499

Kral, K., Vernik, M., and Devetak, D. (2000). The visually controlled prey-capture behaviour of the European mantispid *Mantispa styriaca*. *J. Exp. Biol.* 203, 2117–2123.

Kumar, J. P., and Moses, K. (2001). EGF receptor and notch signaling act upstream of Eyeless/Pax6 to control eye specification. *Cell* 104, 687–697. doi: 10.1016/s0092-8674(01)00265-3

Kunst, M., Pförtner, R., Aschenbrenner, K., and Heinrich, R. (2011). Neurochemical architecture of the central complex related to its function in the control of grasshopper acoustic communication. *PLoS One* 6:e25613. doi: 10.1371/journal.pone.0025613

Labandeira, C. C., Beall, B. S., and Hueber, F. M. (1988). Early insect diversification–evidence from a lower devonian bristletail from Quebec. *Science* 242, 913–916. doi: 10.1126/science.242.4880.913

Land, M. F., Marshall, J. N., Brownless, D., and Cronin, T. W. (1990). The eye-movements of the mantis shrimp *Odontodactylus-Scyllarus* (Crustacea, Stomatopoda). *J. Comp. Physiol. A Neuroethol. Sens. Neural Behav. Physiol.* 167, 155–166. doi: 10.1007/bf00188107

Li, Y., and Strausfeld, N. J. (1997). Morphology and sensory modality of mushroom body extrinsic neurons in the brain of the cockroach, *Periplaneta americana*. *J. Comp. Neurol.* 387, 631–650. doi: 10.1002/(SICI)1096-9861(19971103)387:4<631::AID-CNE9>3.3.CO;2-Z

Li, Y., and Strausfeld, N. J. (1999). Multimodal efferent and recurrent neurons in the medial lobes of cockroach mushroom bodies. *J. Comp. Neurol.* 409, 647–663. doi: 10.1002/(SICI)1096-9861(19990712)409:4<647::AID-CNE9>3.0.CO;2-3

Lin, C. Y., Chuang, C. C., Hua, T. E., Chen, C. C., Dickson, B. J., Greenspan, R. J., et al. (2013). A comprehensive wiring diagram of the protocerebral bridge for visual information processing in the *Drosophila* brain. *Cell Rep.* 3, 1739–1753. doi: 10.1016/j.celrep.2013.04.022

Liu, G., Seiler, H., Wen, A., Zars, T., Ito, K., Wolf, R., et al. (2006). Distinct memory traces for two visual features in the *Drosophila* brain. *Nature* 439, 551–556. doi: 10.1038/nature04381

Loesel, R., Nässel, D. R., and Strausfeld, N. J. (2002). Common design in a unique midline neuropil in the brains of arthropods. *Arthropod Struct. Dev.* 31, 77–91. doi: 10.1016/s1467-8039(02)00017-8

Ma, X., Hou, X., Edgecombe, G. D., and Strausfeld, N. J. (2012). Complex brain and optic lobes in an early Cambrian arthropod. *Nature* 490, 258–261. doi: 10.1038/nature11495

Marshall, N. J. (1988). A unique colour and polarization vision system in mantis shrimps. *Nature* 333, 557–560. doi: 10.1038/333557a0

Marshall, J., Cronin, T. W., and Kleinlogel, S. (2007). Stomatopod eye structure and function: a review. *Arthropod Struct. Dev.* 36, 420–448. doi: 10.1016/j.asd.2007.01.006

Marshall, J., Cronin, T. W., Shashar, N., and Land, M. (1999). Behavioural evidence for polarisation vision in stomatopods reveals a potential channel for communication. *Curr. Biol.* 9, 755–758. doi: 10.1016/s0960-9822(99)80336-4

Marshall, N. J., and Diebel, C. (1995). 'Deep-sea spiders' that walk through the water. *J. Exp. Biol.* 198, 1371–1379.

Marshall, N. J., Jones, J. P., and Cronin, T. W. (1996). Behavioural evidence for colour vision in stomatopod crustaceans. *J. Comp. Physiol. A Neuroethol. Sens. Neural Behav. Physiol.* 179, 473–481. doi: 10.1007/bf00192314

Marshall, N. J., and Land, M. F. (1993). Some optical-features of the eyes of stomatopods. 2. ommatidial design, sensitivity and habitat. *J. Comp. Physiol. A Neuroethol. Sens. Neural Behav. Physiol.* 173, 583–594. doi: 10.1007/bf00197766

Marshall, N. J., Land, M. F., and Cronin, T. W. (2014). Shrimps that pay attention: saccadic eye movements in stomatopod crustaceans. *Philos. Trans. R. Soc. Lond. B Biol. Sci.* 369:20130042. doi: 10.1098/rstb.2013.0042

Marshall, N. J., Land, M. F., King, C. A., and Cronin, T. W. (1991a). The compound eyes of mantis shrimps (Crustacea, Hoplocarida, Stomatopoda). I. Compound eye structure: the detection of polarized light. *Philos. Trans. R. Soc. Lond. B Biol. Sci.* 334, 33–56. doi: 10.1098/rstb.1991.0096

Marshall, N. J., Land, M. F., King, C. A., and Cronin, T. W. (1991b). The compound eyes of mantis shrimps (Crustacea, Hoplocarida, Stomatopoda). II. Colour pigments in the eyes of stomatopod crustaceans: polychromatic vision by serial and lateral filtering. *Philos. Trans. R. Soc. Lond. B Biol. Sci.* 334, 57–84. doi: 10.1098/rstb.1991.0097

Martin, J. P., Guo, P., Mu, L., Harley, C. M., and Ritzmann, R. E. (2015). Central complex control of movement in the freely walking cockroach. *Curr. Biol.* 25, 2795–2803. doi: 10.1016/j.cub.2015.09.044

Mellon, D. (1977). Anatomy and motor-nerve distribution of eye-muscles in crayfish. *J. Comp. Physiol. A Neuroethol. Sens. Neural Behav. Physiol.* 121, 349–366. doi: 10.1007/bf00613014

Milne-Edwards, A. (1864). Sur un cas de transformation du pedoncle oculaire en une antenne, observe chez une Langouste. *Comptes Rendus Academie Sci.* 59, 710–712.

Mobbs, P. G. (1985). "Brain structure," in *Comprehensive Insect Physiology Biochemistry and Pharmacology, Nervous System: Structure and Motor Function*, (Vol. 5) eds G. A. Kerkut and L. I. Gilbert (Oxford: Pergamon), 299–370.

Namiki, S., and Kanzaki, R. (2016). Comparative neuroanatomy of the lateral accessory lobe in the insect brain. *Front. Physiol.* 7:244. doi: 10.3389/fphys.2016.00244

Neuser, K., Triphan, T., Mronz, M., Poeck, B., and Strauss, R. (2008). Analysis of a spatial orientation memory in *Drosophila*. *Nature* 453, 1244–1247. doi: 10.1038/nature07003

Oakley, T. H., Wolfe, J. M., Lindgren, A. R., and Zaharoff, A. K. (2012). Phylotranscriptomics to bring the understudied into the fold: monophyletic ostracoda, fossil placement and pancrustacean phylogeny. *Mol. Biol. Evol.* 30, 215–233. doi: 10.1093/molbev/mss216

Ofstad, T. A., Zuker, C. S., and Reiser, M. B. (2011). Visual place learning in *Drosophila melanogaster*. *Nature* 474, 204–207. doi: 10.1038/nature10131

Pfeiffer, K., and Homberg, U. (2015). Organization and functional roles of the central complex in the insect brain. *Ann. Rev. Entomol.* 59, 165–184. doi: 10.1146/annurev-ento-011613-162031

Phillips-Portillo, J. (2012). The central complex of the flesh fly, *Neobellieria bullata*: recordings and morphologies of protocerebral inputs and small-field neurons. *J. Comp. Neurol.* 520, 3088–3104. doi: 10.1002/cne.23134

Phillips-Portillo, J., and Strausfeld, N. J. (2012). Representation of the brain's superior protocerebrum of the flesh fly, *Neobellieria bullata*, in the central body. *J. Comp. Neurol.* 520, 3070–3087. doi: 10.1002/cne.23094

Power, M. E. (1943). The brain of *Drosophila melanogaster*. *J. Morphol.* 72, 517–559. doi: 10.1002/jmor.1050720306

Ridgel, A. L., Alexander, B. E., and Ritzmann, R. E. (2007). Descending control of turning behavior in the cockroach, *Blaberus discoidalis*. *J. Comp. Physiol. A Neuroethol. Sens. Neural Behav. Physiol.* 193, 385–402. doi: 10.1007/s00359-006-0193-7

Ritzmann, R. E., Harley, C. M., Daltorio, K. A., Tietz, B. R., Pollack, A. J., Bender, J. A., et al. (2012). Deciding which way to go: how do insects alter movements to negotiate barriers? *Front. Neurosci.* 6:97. doi: 10.3389/fnins.2012.00097

Ritzmann, R. E., Ridgel, A. L., and Pollack, A. J. (2008). Multi-unit recording of antennal mechano-sensitive units in the central complex of the cockroach, *Blaberus discoidalis*. *J. Comp. Physiol. A Neuroethol. Sens. Neural Behav. Physiol.* 194, 341–360. doi: 10.1007/s00359-007-0310-2

Sandeman, D. C., Sandeman, R. E., and Aitken, A. R. (1988). Atlas of serotonin-containing neurons in the optic lobes and brain of the crayfish, *Cherax destructor*. *J. Comp. Neurol.* 269, 465–478. doi: 10.1002/cne.902690402

Sandeman, D., Sandeman, R., Derby, C., and Schmidt, M. (1992). Morphology of the brain of crayfish, crabs and spiny lobsters–a common nomenclature for homologous structures. *Biol. Bull.* 183, 304–326. doi: 10.2307/1542217

Schindelin, J., Arganda-Carreras, I., Frise, E., Kaynig, V., Longair, M., Pietzsch, T., et al. (2012). Fiji: an open-source platform for biological-image analysis. *Nat. Methods* 9, 676–682. doi: 10.1038/nmeth.2019

Schram, F. R. (1969). Polyphyly in the eumalacostraca? *Crustaceana* 16, 243–250. doi: 10.1163/156854069x00286

Seelig, J. D., and Jayaraman, V. (2013). Feature detection and orientation tuning in the *Drosophila* central complex. *Nature* 503, 262–266. doi: 10.1038/nature12601

Seelig, J. D., and Jayaraman, V. (2015). Neural dynamics for landmark orientation and angular path integration. *Nature* 521, 186–191. doi: 10.1038/nature14446

Shaw, S. R., and Varney, L. P. (1999). Primitive, crustacean-like state of blood-brain barrier in the eye of the apterygote insect *Petrobius* (Archaeognatha) determined from uptake of fluorescent tracers. *J. Neurobiol.* 41, 452–470. doi: 10.1002/(SICI)1097-4695(199912)41:4<452::AID-NEU2>3.3.CO;2-X

Stegner, M. E., and Richter, S. (2011). Morphology of the brain in *Hutchinsoniella macracantha* (Cephalocarida, Crustacea). *Arthropod Struct. Dev.* 40, 221–243. doi: 10.1016/j.asd.2011.04.001

Strausfeld, N. J. (1976). *Atlas of An Insect Brain.* Heidelberg, New York, NY: Springer-Verlag Berlin.

Strausfeld, N. J. (1998). Crustacean–Insect relationships: the use of brain characters to derive phylogeny amongst segmented invertebrates. *Brain Behav. Evol.* 52, 186–206. doi: 10.1159/000006563

Strausfeld, N. J. (1999). A brain region in insects that supervises walking. *Prog. Brain Res.* 123, 273–284. doi: 10.1016/s0079-6123(08)62863-0

Strausfeld, N. J. (2012). *Arthropod Brains: Evolution, Functional Elegance and Historical Significance.* Cambridge, MA: Belknap Press of Harvard University Press.

Strausfeld, N. J., and Hirth, F. (2013). Deep homology of arthropod central complex and vertebrate basal ganglia. *Science* 340, 157–161. doi: 10.1126/science.1231828

Strausfeld, N. J., Ma, X., and Edgecombe, G. D. (2016). Fossils and the evolution of the arthropod brain. *Curr. Biol.* 26, R989–R1000. doi: 10.1016/j.cub.2016.09.012

Strauss, R., and Heisenberg, M. (1993). A higher control center of locomotor behavior in the *Drosophila* brain. *J. Neurosci.* 13, 1852–1861.

Sullivan, J. M., and Beltz, B. S. (2004). Evolutionary changes in the olfactory projection neuron pathways of eumalacostracan crustaceans. *J. Comp. Neurol.* 470, 25–38. doi: 10.1002/cne.11026

Tauber, E. S., and Atkin, A. (1967). Disconjugate eye movement patterns during optokinetic stimulation of the African chameleon, *Chameleo melleri*. *Nature* 214, 1008–1010. doi: 10.1038/2141008b0

Thoen, H. H., How, M. J., Chiou, T. H., and Marshall, J. (2014). A different form of color vision in mantis shrimp. *Science* 343, 411–413. doi: 10.1126/science.1245824

Triphan, T., Poeck, B., Neuser, K., and Strauss, R. (2010). Visual targeting of motor actions in climbing *Drosophila*. *Curr. Biol.* 20, 663–668. doi: 10.1016/j.cub.2010.02.055

Utting, M., Agricola, H. J., Sandeman, R., and Sandeman, D. (2000). Central complex in the brain of crayfish and its possible homology with that of insects. *J. Comp. Neurol.* 416, 245–261. doi: 10.1002/(SICI)1096-9861(20000110)416:2<245::AID-CNE9>3.3.CO;2-1

Webb, B., and Wystrach, A. (2016). Neural mechanisms of insect navigation. *Curr. Opin. Insect Sci.* 15, 27–39. doi: 10.1016/j.cois.2016.02.011

Williams, J. (1975). Anatomical studies of the insect central nervous system: a ground-plan of the midbrain and an introduction to the central complex in the locust, *Schistocerca gregaria* (Orthoptera). *J. Zool.* 176, 67–86. doi: 10.1111/j.1469-7998.1975.tb03188.x

Wolff, G., Harzsch, S., Hansson, B. S., Brown, S., and Strausfeld, N. (2012). Neuronal organization of the hemiellipsoid body of the land hermit crab, *Coenobita clypeatus*: correspondence with the mushroom body ground pattern. *J. Comp. Neurol.* 520, 2824–2846. doi: 10.1002/cne.23059

Wolff, G. H., and Strausfeld, N. J. (2015). Genealogical correspondence of mushroom bodies across invertebrate phyla. *Curr. Biol.* 25, 38–44. doi: 10.1016/j.cub.2014.10.049

Wolff, G. H., and Strausfeld, N. (2016). "The insect brain: a commentated primer," in *Structure and Evolution of Invertebrate Nervous Systems*, eds A. Schmidt-Rhaesa, S. Harzsch and G. Purschke (Oxford: Oxford University Press), 597–639.

Zaidi, Q., Marshall, J., Thoen, H., and Conway, B. R. (2014). Evolution of neural computations: mantis shrimp and human color decoding. *Iperception* 5, 492–496. doi: 10.1068/i0662sas

Conflict of Interest Statement: The authors declare that the research was conducted in the absence of any commercial or financial relationships that could be construed as a potential conflict of interest.

The reviewer MB and handling Editor declared their shared affiliation, and the handling Editor states that the process nevertheless met the standards of a fair and objective review.

frontiers in Behavioral Neuroscience

REVIEW
published: 31 August 2016
doi: 10.3389/fnbeh.2016.00167

Development of the Neurochemical Architecture of the Central Complex

George S. Boyan and Yu Liu*

Developmental Neurobiology Group, Department of Biology II, Ludwig-Maximilians-Universität, Munich, Germany

The central complex represents one of the most conspicuous neuroarchitectures to be found in the insect brain and regulates a wide repertoire of behaviors including locomotion, stridulation, spatial orientation and spatial memory. In this review article, we show that in the grasshopper, a model insect system, the intricate wiring of the fan-shaped body (FB) begins early in embryogenesis when axons from the first progeny of four protocerebral stem cells (called W, X, Y, Z, respectively) in each brain hemisphere establish a set of tracts to the primary commissural system. Decussation of subsets of commissural neurons at stereotypic locations across the brain midline then establishes a columnar neuroarchitecture in the FB which is completed during embryogenesis. Examination of the expression patterns of various neurochemicals in the central complex including neuropeptides, a neurotransmitter and the gas nitric oxide (NO), show that these appear progressively and in a substance-specific manner during embryogenesis. Each neuroactive substance is expressed by neurons located at stereotypic locations in a given central complex lineage, confirming that the stem cells are biochemically multipotent. The organization of axons expressing the various neurochemicals within the central complex is topologically related to the location, and hence birthdate, of the neurons within the lineages. The neurochemical expression patterns within the FB are layered, and so reflect the temporal topology present in the lineages. This principle relates the neuroanatomical to the neurochemical architecture of the central complex and so may provide insights into the development of adaptive behaviors.

Keywords: insect, brain, central complex, development, neurochemicals

OPEN ACCESS

Edited by:
Stanley Heinze,
Lund University, Sweden

Reviewed by:
Uwe Homberg,
University of Marburg, Germany
Amir Ayali,
Tel Aviv University, Israel

****Correspondence:***
George S. Boyan
george.boyan@lmu.de

Received: *21 June 2016*
Accepted: *16 August 2016*
Published: *31 August 2016*

Citation:
Boyan GS and Liu Y (2016) Development of the Neurochemical Architecture of the Central Complex. Front. Behav. Neurosci. 10:167. doi: 10.3389/fnbeh.2016.00167

INTRODUCTION

Modular brain structures such as the insect mushroom bodies (MB) and central complex provide an ideal substrate for studies aiming to understand the developmental/genetic basis of neuronal function and behavior (Wegerhoff and Breidbach, 1992; Ito et al., 1997; Mizunami et al., 1997; Tettamanti et al., 1997; Meinertzhagen et al., 1998; Strausfeld, 1999; Farris and Sinakevitch, 2003; Ito and Awasaki, 2008). Located in the brain midline, the insect central complex comprises five major modules: the protocerebral bridge (PB), fan-shaped body (FB; or upper division of the central body), ellipsoid body (EB; or lower division of the central body), noduli (N) and lateral accessory lobes (LAL), and represents one of the most distinctive neuroarchitectures to be found among arthropods (Williams, 1975; Strauss et al., 1992; Strauss and Heisenberg, 1993; Renn et al., 1999; Heinze and Homberg, 2008; El Jundi et al., 2010; Young and Armstrong, 2010a,b; Boyan and Reichert, 2011; Ito et al., 2014;

Pfeiffer and Homberg, 2014; Boyan et al., 2015; Koniszewski et al., 2016). The roles that these different modules play in organizing motor activity, in orientation, and in visual pattern memory and storage, have been demonstrated by both mutant analyses and lesioning studies (Huber, 1960; Ilius et al., 1994; Strauss, 2002; Liu et al., 2006; Neuser et al., 2008; Pan et al., 2009; Harley and Ritzmann, 2010).

In insects, the most conspicuous central complex module is the FB whose neuroarchitecture is characterized by layers of dendritic arbors accompanying a stereotypic columnar organization, both formed by the axonal projections of clusters of neurons located in the pars intercerebralis (PI) region of each protocerebral hemisphere (see Strausfeld, 2012). It has been proposed that the degree to which the insect central complex is elaborated in a given species is correlated with its lifestyle (Strausfeld, 2012; Koniszewski et al., 2016). Developmental studies have revealed that the intricate columnar wiring of the FB is established quite rapidly, but at stages which also vary with the lifestyle of the insect. In the grasshopper, it develops fully during embryogenesis (Boyan et al., 2008b, 2015), while in beetles, modules are added sequentially during larval development (Wegerhoff and Breidbach, 1992), and in flies, early-born neurons only become wired into the central complex during the pupal to adult transition (Renn et al., 1999; Young and Armstrong, 2010a,b; Riebli et al., 2013; Wolff et al., 2015). Despite this temporal diversity, the developmental mechanisms involved appear to be conserved and involve a process known as fascicle switching in which the axons of commissural neurons systematically decussate at stereotypic locations across the brain midline and in so doing generate the columnar neuroarchitecture required for adaptive behavior (see Boyan and Reichert, 2011; Boyan et al., 2015).

Paralleling this anatomical development is the development of the neurochemical architecture of the central complex. This is less well understood, but critical for understanding the role central complex circuits play in behavior. In the grasshopper, expression of neuroactive substances commences at a time when the neural stem cells (neuroblasts) are still present, allowing the participating neurons to be ontogenetically identified according to their lineage of origin (Boyan and Liu, 2014). This feature has led to central complex neuroblasts being shown to be multipotent in that they generate lineages in which a range of neuroactive substances are expressed (Boyan et al., 2010a). In *Drosophila*, by contrast, expression of such substances has only been documented in cell clusters of the adult brain (Kahsai and Winther, 2011) where no central complex neuroblasts remain (Ito and Awasaki, 2008), therefore making ontogenetic analyses more speculative.

In this review article, we use the grasshopper as a model system for central complex development. We focus on the FB and relate its neuroarchitecture to stereotypic patterns of axogenesis involving subsets of neurons from identified neuroblasts. We then show that neuroactive substances essential for the synaptic interactions within this system appear progressively during development according to a temporal topology that relates the position of neurons within a lineage to their age and axonal projection pattern. Temporal topology relates the structural to the biochemical neuroarchitecture of the FB and so may provide insights into the development of adaptive behavior.

DISCUSSION

Neuroarchitecture, Neuronal Classes and Behavior

The central complex comprises a set of five neuropilar modules—PB, FB (or upper division of the central body in the grasshopper), EB (or lower division of the central body in the grasshopper), noduli (N), LAL—of which the unpaired FB with its columns and stratified layers is the most prominent (**Figures 1A,B**; and see Williams, 1975; Heinze and Homberg, 2008; Strausfeld, 2012; Pfeiffer and Homberg, 2014). Four major neuronal types have been identified in the central complex of the grasshopper based on their projection patterns in and to its various modules (for details, see Heinze and Homberg, 2008; Pfeiffer and Homberg, 2014). Briefly, these are: (1) *Columnar neurons*, which connect single columns of the PB and/or the FB with the LAL or the noduli. Columnar axons project from the PB to the FB via the four fiber pathways known as the *w, x, y, z* tracts (**Figure 1B**; Williams, 1975; Strausfeld, 1976; Hanesch et al., 1989; Williams and Boyan, 2008). Within the FB, these axons form nine columnar bundles which will be considered in this review with respect to the developmental expression of various neurochemicals. (2) *Tangential neurons*, which innervate single layers of the FB, EB or PB and also interconnect the central complex with other brain regions (Strausfeld, 1976; Homberg, 1991; Müller et al., 1997). (3) *Pontine neurons*, which are intrinsic elements that connect specific columns and layers within the FB (Homberg, 1985; Hanesch et al., 1989). (4) *Amacrine neurons*, which are intrinsic to the FB. The one example recorded to date has a soma in the PI, a neurite in a *z* tract, and arborizations in a lateral hemisphere of the FB.

The insect central complex has been described as a multisensory neuropil processing visual, mechanosensory and olfactory signals on the one hand, while also serving as a premotor center, controlling walking, flight, acoustic communication and courtship on the other hand (see Strausfeld, 2012; Pfeiffer and Homberg, 2014). In *Drosophila*, specific subcompartments of the EB are involved in different aspects of spatial and landmark learning, orientation, and flight control (Ilius et al., 1994; Martin et al., 1999; Liu et al., 2006; Neuser et al., 2008; Pan et al., 2009; Triphan et al., 2010), while in the cockroach the FB regulates locomotory activity for negotiating barriers (Bender et al., 2010; Harley and Ritzmann, 2010). Of all the central complex modules in the grasshopper brain, the FB offers perhaps the clearest correlation between identified neuronal morphology, general neuroarchitecture, and information processing subserving behavior. This involves a particular form of visual information processing, namely sky polarization, which is fundamental to general navigation behavior in insects (see Wehner, 1989; Homberg et al., 2011;

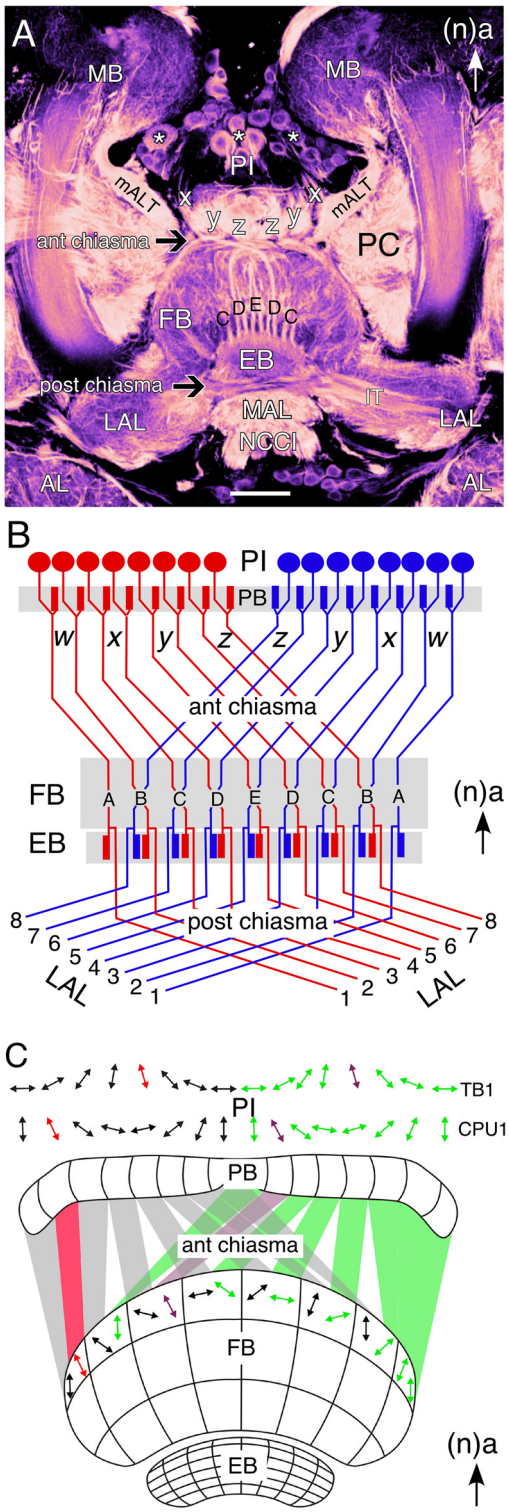

FIGURE 1 | Wiring of the central complex subserves information processing. (A) Confocal image of a brain slice in an adult grasshopper (*Schistocerca gregaria*) following 8 B7 immunolabeling reveals the neuroarchitecture of the central complex between the bilateral mushroom bodies (MB) in the central brain. Neurons (white stars) of the pars

(*Continued*)

FIGURE 1 | Continued

intercerebralis (PI) direct axons via the *w, x, y, z* tracts into a chiasmal system (black arrow) anterior to the fan-shaped body (FB). These fibers then form columnar bundles (of which C, D, E, D, C are visible) in the FB and project further to the ellipsoid body (EB) and via a posterior chiasmal system (black arrow) laterally in the isthmus tract (IT) to the lateral accessory lobes (LAL). Note that the FB is also termed the upper division of the central body, and the EB the lower division of the central body (see Müller et al., 1997; Heinze and Homberg, 2008). White arrow points to anterior (a) according to the neuraxis (n) and is repeated for emphasis in all panels. **(B)** Wiring diagram (not to scale) illustrates the essential plan of axon projections from neurons of the PI via the protocerebral bridge (PB) into the *w, x, y, z* tract system of the left (red) and right (blue) protocerebral hemispheres and hence via the anterior chiasmal system to form nine columns (A–E) in the FB and EB of the central brain. Axons subsequently exit the EB posteriorly and project via a posterior chiasmal system to the bilateral LALs. **(C)** Schematic (not to scale) illustrates the preferred polarization sensitivities (double arrows) of tangential (TB1) and columnar (CPU1) neurons in the PI of the grasshopper and the way these sensitivities are projected via the anterior chiasmal system to be represented within the columnar neuroarchitecture of the FB (CBU; see panel **B**). Other abbreviations: mALT, medial antennal lobe tract; AL, antennal lobe; MAL, median accessory lobe; NCCI, nervus corporis cardiaci I; PC, protocerebrum. Scale bar in **(A)** represents 100 μm. Panel **(A)** modified from Boyan et al. (2015) with permission; panel **(B)** modified from Williams (1975) with permission; panel **(C)** personal communication courtesy of U. Homberg.

Weir and Dickinson, 2012). Electrophysiological recordings from identified tangential (TB1) and columnar (CPU1) neurons in the PI region reveal preferred polarization sensitivities representing a sky chart segmented into eight channels per brain hemisphere (**Figure 1C**). A comparison of preferred polarization sensitivities in the PI with those in an upper layer of the FB indicates a transformation en route which reflects the wiring plan for fibers entering the FB through the chiasmal system of *w, x, y, z* tracts (see **Figure 1B**, and see Williams, 1975).

Development of the Central Complex

Organization of Neural Stem Cells

Topologically, the central complex belongs to the protocerebral neuromere of the brain (see Strausfeld, 2012). In the grasshopper, the brain is generated by approximately 100 bilaterally symmetrical pairs of neural stem cells called neuroblasts (**Figure 2A**), each of which is individually specified by molecular, positional and temporal cues (Zacharias et al., 1993; Reichert and Boyan, 1997; Urbach and Technau, 2003; Williams et al., 2005; Boyan and Reichert, 2011). Four of the neuroblasts (termed W, X, Y, Z) in each hemisphere play a key role in FB development in that their progeny establish the basic columnar organization of its neuropil. Genetic analysis reveals that a similar set of neuroblasts is found in each hemisphere of the developing brain of *Drosophila* (Izergina et al., 2009), and that these lineages contain the numerous columnar or small-field neurons that project to, innervate and interconnect the PB, FB, EB and noduli of the central complex (Ito and Awasaki, 2008; Izergina et al., 2009; Bayraktar et al., 2010; Young and Armstrong, 2010a,b; Riebli et al., 2013).

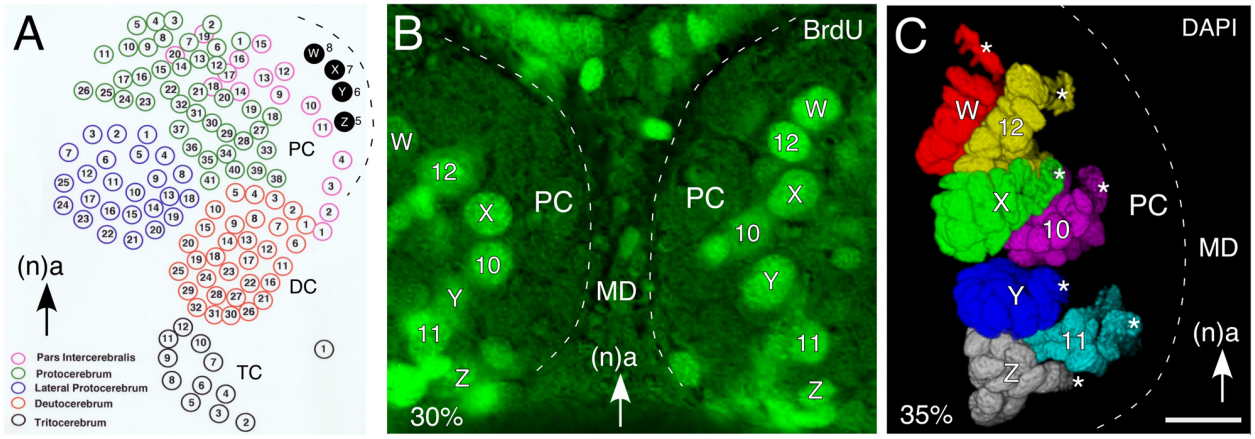

FIGURE 2 | Organization of neural stem cells (neuroblasts) in the early embryonic brain of the grasshopper. (A) Schematic (not to scale) summarizes location of identified neuroblasts in the protocerebrum (PC), deutocerebrum (DC) and tritocerebrum (TC) of the left hemisphere of the grasshopper brain prior to mid-embryogenesis. Of these, W, X, Y, Z neuroblasts (shaded black) generate progeny contributing to the columnar organization of the FB of the central complex. Arrow points to anterior (a) according to the neuraxis (n) and is repeated for emphasis in all panels. **(B)** Fluorescent photomicrograph (false color) of a brain slice following bromodeoxyuridine (BrdU) incorporation at 30% of embryogenesis showing the bilaterally symmetrical distribution of identified mitotically active neuroblasts such as W, X, Y, Z in the median PC of each brain hemisphere. **(C)** 3D reconstruction based on *z*-stacks of confocal images following nuclear staining with DAPI at 35% of embryogenesis reveals the lineages associated with identified neuroblasts (white stars). Lineages appear in false colors. Other abbreviations: MD, median domain. Scale bar in **(C)** represents 35 μm in **(B,C)**. Panel **(A)** modified from Zacharias et al. (1993) with permission.

Since a neuroblast occupies a stereotypic location in the neuroepithelium (**Figure 2B**; Bate, 1976; Doe and Goodman, 1985a,b; Zacharias et al., 1993), and the lineages maintain their topological position in the CNS (**Figure 2C**), it is possible to profile such cell clusters temporally, biochemically and physiologically (Goodman et al., 1979, 1980).

Modular Organization of Lineages and Projections

Examination of the cortical organization of the PI region of the brain reveals four discrete clusters of neurons (W, X, Y, Z) associated with the central complex (**Figure 3A**). This association is confirmed by the fact that axons from each of the clusters form a discrete tract (*w, x, y, z*) in which they remain, and then project to a small subset of commissural fascicles (AC III, VIII, IX) of the FB (Boyan et al., 1993; Boyan and Williams, 1997). The neuroblasts, their neuronal lineages, and the tracts they generate, can therefore be considered to represent individual modules or clonal units, consistent with the mechanism building association centers of the insect (Ito et al., 1997; Lee and Luo, 2001; Ito and Awasaki, 2008) and the vertebrate (Leise, 1990) brain. As in the ventral nerve cord, the progeny of a given lineage are generated according to a temporal order, and maintain their position according to birthdate within the cluster, so that the lineage acquires a temporal topology. Reconstruction of a central complex lineage after neuron-specific labeling confirms that early-born, mature, neurons at the tip of a lineage are already generating the initial tract while later-born, immature neurons nearer the neuroblast are yet to express the label (**Figure 3B**). Further, axon tracing reveals that there is a clear correlation between cell body location within such a lineage and the topology of axon projections into the associated tract en route to the primordial FB (**Figure 3C**).

Establishing a Neuroarchitecture

Developmental studies reveal that in both the grasshopper (**Figures 4A–C**) and *Drosophila* (**Figure 4D**), the intricate neuroarchitecture of the mature FB arises in a stepwise manner. Conserved cellular and molecular mechanisms, which may even extend to vertebrates (Arendt and Nübler-Jung, 1996; Tomer et al., 2010), establish an initial orthogonal axonal scaffold in the brain (**Figures 4A,Ci,Di**; see Reichert and Boyan, 1997). At these early stages, commissural axons remain tightly bundled within their fascicles. Significantly, the pioneers of the *w, x, y, z* tract system utilize the existing axonal scaffold previously founded by the commissural pioneers in order to navigate the brain midline (Williams and Boyan, 2008). As these *w, x, y, z* tract pioneers remain committed to their commissural fascicles, axonal reorganization must involve cells from each lineage which are either born later, or generate axons later.

The subsequent transformation of this initial orthogonal ground plan into the mature chiasmal/columnar neuroarchitecture involves a topographic decussation of axons (also known as "fascicle switching") across the cerebral midline. Homologous clusters of later-born neurons from each protocerebral hemisphere redirect their axonal growth cones from an anterior to a posterior commissural subsystem (dorsal to ventral according to body axis) at stereotypic locations to generate the columnar neuropil of the mature FB (**Figures 4B,Cii–iv,Dii,iii**; Boyan et al., 2008b; Ito and Awasaki, 2008; Young and Armstrong, 2010a,b; Riebli et al., 2013). The points at which de- and re-fasciculation occur ultimately hinge the columnar system of fiber bundles within the FB. In both systems the columns subsequently thicken as progressively more axons decussate, and the gap between the

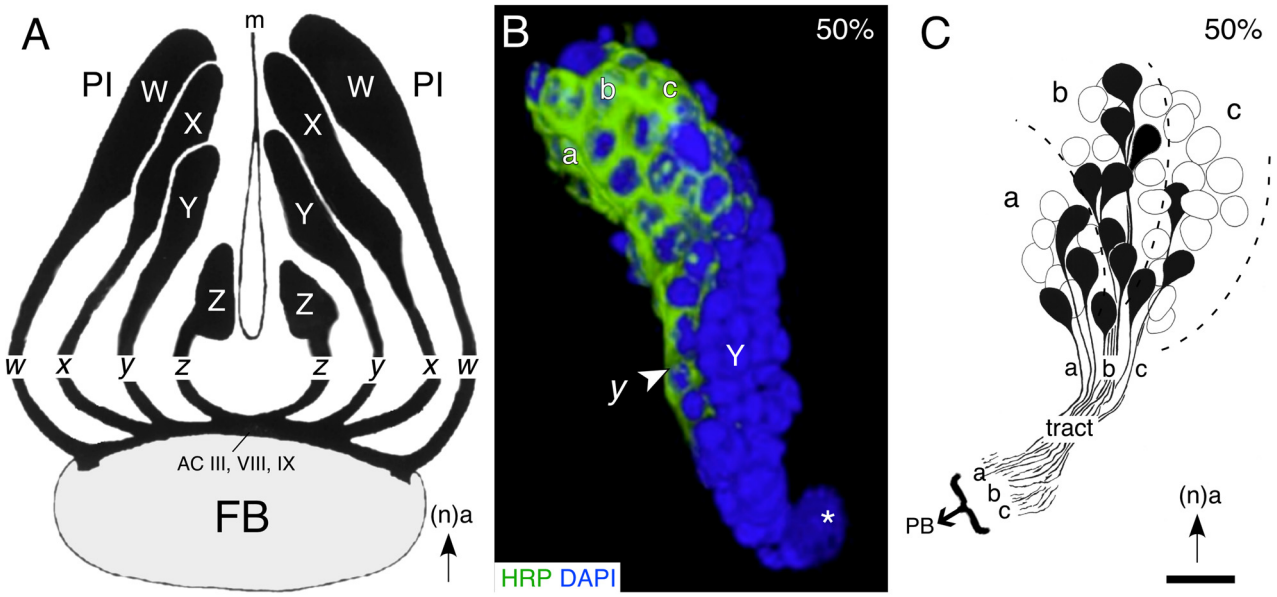

FIGURE 3 | Lineages of embryonic progeny and organization of projections into tracts of the central complex. (A) Reconstruction based on serial brain sections shows the outlines of the W, X, Y, Z lineages of progeny and the associated tracts of axons projecting to identify commissural fascicles (ACIII, VIII and IX) of the embryonic (100%) FB. Arrow points to anterior (a) according to the neuraxis (n). **(B)** 3D reconstruction of a representative central complex lineage (Y) at 50% of embryogenesis based on *z*-stacks of confocal images following double labeling with the neuron-specific label HRP (green) and the nuclear stain DAPI (blue). Location of the Y neuroblast (white star), the initial *y* tract (white arrowhead), and subclusters (a, b, c) of mature (HRP-positive) neurons within the lineage, are indicated. Arrow indicates anterior (a) and applies to all panels. **(C)** Drawing from serial sections shows the soma locations and axon projections of individual cells from the a, b, c subcluster of cells at the tip of a representative central complex lineage (Z) at 50% of embryogenesis. Axon projections within the tract are topologically ordered according to the location of the somata within the lineage. Scale bar represents 15 μm in **(B)**, 25 μm in **(C)**. Panel **(A)** modified from Boyan and Williams (1997) with permission; panel **(B)** modified from Liu and Boyan (2013) with permission; panel **(C)** modified from Williams et al. (2005) with permission.

commissural subsystems widens as the dendritic arbors from other innervating neurons expand. This leads to the staves assuming a progressively more orthogonal orientation (Boyan et al., 2008b, 2015). In the grasshopper, the neuroarchitecture of the chiasmal system at 70% of embryogenesis already resembles that of the adult (see **Figure 1A**).

Since the decussation follows topographically—axons from medial lineages (e.g., Z) project furthest across the midline while those from more lateral lineages (e.g., W) project the least—the data argue for there being a signal gradient, or a specific label, distributed along the medio-lateral axis that instructs neurons at specific locations (and therefore ages) within the lineage as to where to make their axons decussate (see Boyan et al., 2015). The pattern of axogenesis is also remarkably similar across species despite the fact that in *Drosophila* the columns are generated postembryonically from secondary neuron populations and not from primary embryonic populations as in the grasshopper, again arguing for a conserved molecular signal.

Neuroactive Substances and Neuroarchitecture

Developmental Expression Patterns

Association centers in the insect brain such as the central complex possess a conspicuous cellular neuroarchitecture: that of the FB for instance, that has been shown to comprise not only two systems of columnar tracts, but also multiple layers involving projections from pontine cells of the PI and tangential fibers from cells elsewhere in the protocerebrum (PC; Williams, 1975; Strausfeld, 1976, 2012; Müller et al., 1997; Heinze and Homberg, 2008; El Jundi et al., 2010). This neuroarchitecture is paralleled by a neurochemical architecture as revealed, for example, in the axonal projections of subsets of neurons from the PI expressing serotonin (5HT) and allatostatin (AST) in the adult (**Figure 5A**), or by diaphorase (NADPHd) staining as a marker for nitric oxide (NO) already at 85% of embryogenesis (**Figures 5Bi,ii**). This congruence of anatomical and neurochemical architecture can also be demonstrated using a range of other molecules (Homberg, 2002; Herbert et al., 2010; Pfeiffer and Homberg, 2014; Beetz et al., 2015) whose contributions to adult behaviors are steadily being revealed (Seidel and Bicker, 1996, 2002; Homberg, 2002; Nässel, 2002; Winther et al., 2006; Kahsai and Winther, 2011; Kunst et al., 2011). The question at the center of this study is when and how these stereotypic neurochemical projection patterns arise during embrygenesis. Clearly the central complex has adult characteristics well before hatching (see Boyan et al., 2015) and we need to look earlier for the origins of its neurochemical architecture.

Neuronal networks in the grasshopper have been shown to be activated by neurochemicals prior to the appearance of the

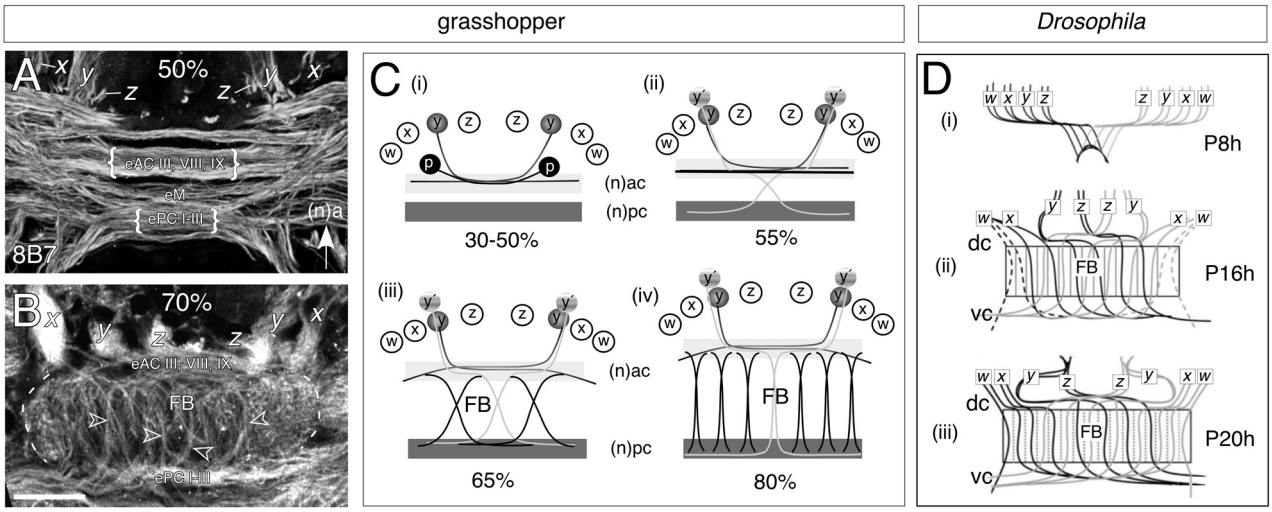

FIGURE 4 | Decussation of commissural axons from W, X, Y, Z lineages generates the columnar neuroarchitecture of the FB in the grasshopper (A,B) and *Drosophila* (C). (A) Confocal image of a brain slice after 8B7 immunolabeling at 50% of embryogenesis shows axons from *x, y, z* tracts projecting into a commissural system of axons organized into parallel fascicles. Decussation of axons has not yet occurred but will involve fibers from embryonic anterior commissures (eAC) III, VIII, IX, the median commissure (eM), and embryonic posterior commissures (ePC) I-III (nomenclature from Boyan et al., 1993). Arrow indicates anterior (a) according to the neuraxis (n) and applies to panels **(A–C). (B)** Confocal image of a brain slice after 8B7 immunolabeling at 70% of embrogenesis shows axons from the *x, y, z* tracts entering eAC III, VIII and IX and then decussating to ePC I-III thus generating the initial fiber columns (open white arrowheads) of the FB. **(C)** Schematics (not to scale) illustrating the process of decussation to form the columns of the FB. The Y lineage here is representative for the general process. **(Ci)** Between 30% and 50% of embryogenesis, pioneer axons *(y)* from the Y lineage in each brain hemisphere fasciculate with the pioneers *(p)* of the anterior commissures but remain within their original fascicles as they cross the midline. **(Cii)** At approximately 55% of embryogenesis, later born neurons *(y')* from the Y lineage follow the pioneers into the commissural system, but then decussate to enter the posterior commissural (pc) system. **(Ciii)** At 65% of embryogenesis, the process of decussation is repeated by axons from the other central complex lineages (W, X, Z). Decussation of bilaterally homologous axons occurs at stereotypic locations across the midbrain so that their crossing points mark the location of future columns. **(Civ)** At 80% of embryogenesis, the midbrain neuropil exapnds as dendritic arborizations increase (not shown) forcing the ac and pc commissural fascicles apart and making the columnar fiber bundles more orthogonal. The neuroarchitecture of the FB at these ages already resembles that of the adult brain (see **Figure 1A**). **(D)** Projection patterns (not to scale) of small-field neurons as summarized from anti-Echinoid labeling show that decussation in *Drosophila* during pupal development follows the same pattern as that in the embryonic grasshopper. Time is given in hours after puparium formation (Ph). Neurons originating from the right brain hemisphere (gray) are superimposed on the neurons from the left hemisphere (black). **(Di)** By P8 h double fiber bundles which we interpret as being equivalent to the *w, x, y, z* tracts of the grasshopper have projected to the midline and decussate to initiate the columnar organization of the primordial FB. **(Dii)** By P16h axons are decussating at specific locations across the midline thereby generating columns of the FB. **(Diii)** By P20 h, fibers project topographically, through the FB, to posterior neuropils (not shown). Commissures in *Drosophila* are named according to the body axis. Scale bar in **(B)** represents 35 μm in **(A,B)**. Panel **(A)** modified from Boyan et al. (2015) with permission; panel **(B)** modified from Boyan et al. (2008b) with permission; panel **(C)** modified from Young and Armstrong (2010b) with permission.

adult behavior (Stevenson and Kutsch, 1986) and in the central complex, their expression begins during embryogenesis at a time when the mother neuroblasts are still present (Herbert et al., 2010; Boyan and Liu, 2014). This is a considerable advantage because if the original neuronal population can be age-profiled (see **Figures 3B,C**), expression can be traced to the temporal topology of a lineage so that a biochemical "fingerprint" of the central complex at different embryonic ages can be generated. This may, in turn, provide an insight into the developmental origins of central complex-related behaviors.

Here we consider a small range of neuroactive substances with respect to their development in the central complex of the grasshopper. These fall into three groups: (a) the neuropeptides, locustatachykinin (LTK), leucokinin-1 (LK-1), AST, periviscerokinin/pyrokinin (PVK/PK), FLRFamide (FLRF); (b) a classical transmitter, 5HT; and (c) a gas, NO. While by no means exhaustive, we suggest that the embryonic expression patterns of this subset of substances (**Figure 6**; and for greater detail, see Herbert et al., 2010) nevertheless reflect the major trends in neurochemical and neuroanatomical organization of the developing central complex.

Locustatachykinin (LTK)

Locustachykinins have a variety of effects in physiological and pathological events (as neurohormones and neuromodulators) which may vary substantially depending on the activation of different receptor subtypes (see Severini et al., 2002). A relatively early expression of tachykinins has been reported for a range of insect nervous systems (Nässel and Winther, 2002; Nässel, 2002) and there is some evidence that members of the tachykinin family can act as neurotrophic factors (Satake et al., 2003), perhaps comparable to their role in the development of vertebrate respiratory networks (Wong-Riley and Liu, 2005).

Vitzthum and Homberg (1998) distinguish six distinct types of LTK-immunoreactive neurons with ramifications in the central complex of the adult grasshopper: four columnar neuron groups (LTC I-IV), and two tangential neuron groups (LTT I-II).

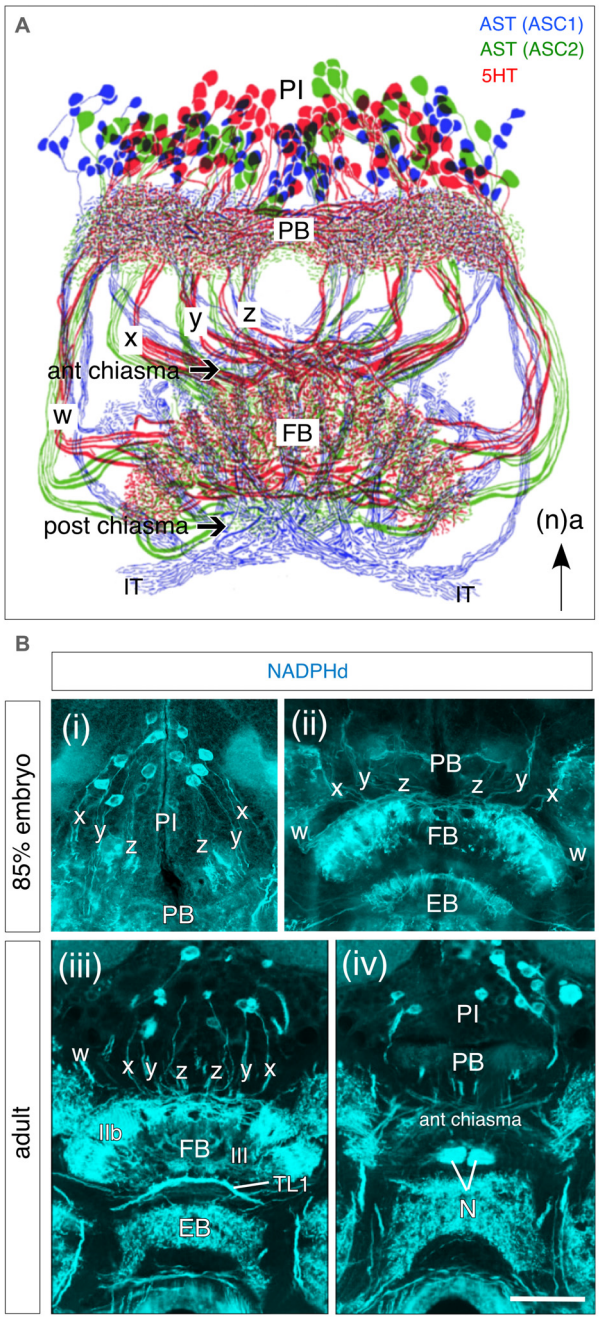

FIGURE 5 | Neurochemical architecture of the central complex based on projections from progeny of W, X, Y, Z lineages. (A) Reconstruction reveals a highly conserved pattern of projections from bilateral populations of columnar cells in the PI to the FB via the *w, x, y, z* tracts following immunolabeling against serotonin (5HT, red), and allatostatin (AST; ASC1 subpopulation, blue; ASC2 subpopulation, green). Axons form columnar fiber bundles within the FB and then project via the IT to the LAL (not shown). Arrow indicates anterior (a) according to the neuraxis (n) and applies to all panels. **(B)** Frontal sections through the brain of an 85% embryonic **(Bi,ii)** and adult **(Biii,iv)** grasshopper following diaphorase (NADPHd) staining reveal nitric oxide (NO)-positive cell bodies from pontine and columnar neurons in the PI with projections into the *w, x, y, z* tracts and then to the FB via the PB.

(*Continued*)

FIGURE 5 | Continued

(iii) Note staining of columnar neurites in layer III of the adult FB. Axonal fibers of tangential TL1 neurons are visible between the FB and EB. **(iv)** Neurites from columnar neurons project from the PB into the anterior chiasma (according to neuraxis) and then to the noduli (N). Scale bar in **(Biv)** represents 1mm in **(A)**, 25 μm in **(Bi,ii)**, and 115 μm in **(Biii,iv)**. Panel **(A)** modified from Homberg (1991) and Vitzthum et al. (1996) both with permission; panels **(Bi,ii)** modified from Herbert et al. (2010) with permission; panels **(Biii,iv)** modified from Kurylas et al. (2005) with permission.

The LTC I cells are located anteriorly (according to the neuraxis) in the PI, project into the columnar tracts of the FB, and give rise to arborizations in the PB, EB and the lateral bulb (LBU). LTC II neurons are also located anterior to the PB and project via the columnar tracts to arborize in the PB and LBU. The columnar LTC III cell group is composed of eight large and 16 small neurons anterior to the PB with arborizations also in layers I and II of the FB. LTC IV neurons project into the posterior (ventral in Heinze and Homberg, 2008) groove and arborize in layers I and IIa of the FB. The tangential LTT I neurons located in the inferior median PC project to the LAL and ramify in the LBU. They then project through the isthmus tract (IT) to the EB. LTT II are posterior PI neurons which richly arborize in the PB, terminating in the posterior median PC of the contralateral brain.

In the developing central complex, LTK immunoreactivity is already detected at 50% of embryogenesis in tangential neurons of the LALs (**Figure 6B**). These neurons have their terminals in the area of the developing EB, posterior to the future FB. The pattern is consistent with these fibers belonging to the tangential LTT I neurons described by Vitzthum and Homberg (1998) in adults. At 60% of development, an additional tangential projection system belonging to the LTT II group begins to express LTK. The stained structures observed in the LALs colocalize to the adult LBU and the IT. At this stage there is also a relatively weak LTK immunostaining in the PB. LTK immunoreactivity in columnar neurons is first observed at 70% of embryogenesis (**Figure 6A**). Strong immunoreactivity is present in the PB, the *w, x, y, z* tracts, and the EB. LTK-positive arborizations are present in the anterior part of layer Ib of the FB, consistent with these being from the LTC I, II neurons of the adult. At 85% of embryogenesis, LTK immunoreactivity is seen in arborizations within the FB, and appears in the median accessory lobe (MAL), and in the posterior part of the noduli. This immunoreactivity subsequently becomes more intense (especially in the EB), but the overall pattern does not change. In early postembryonic stages, immunoreactive arborizations originating from the LTC III columnar cell group appear in layers I and II of the FB, and there is also expression in the posterior groove indicating LTK expression in LTC IV neurons. The immunoreactive pattern at this stage already resembles that of the adult (see Vitzthum and Homberg, 1998).

Allatostatin (AST)

The ASTs, termed schistostatins (Schoofs et al., 1998), have previously been identified in the adult central complex

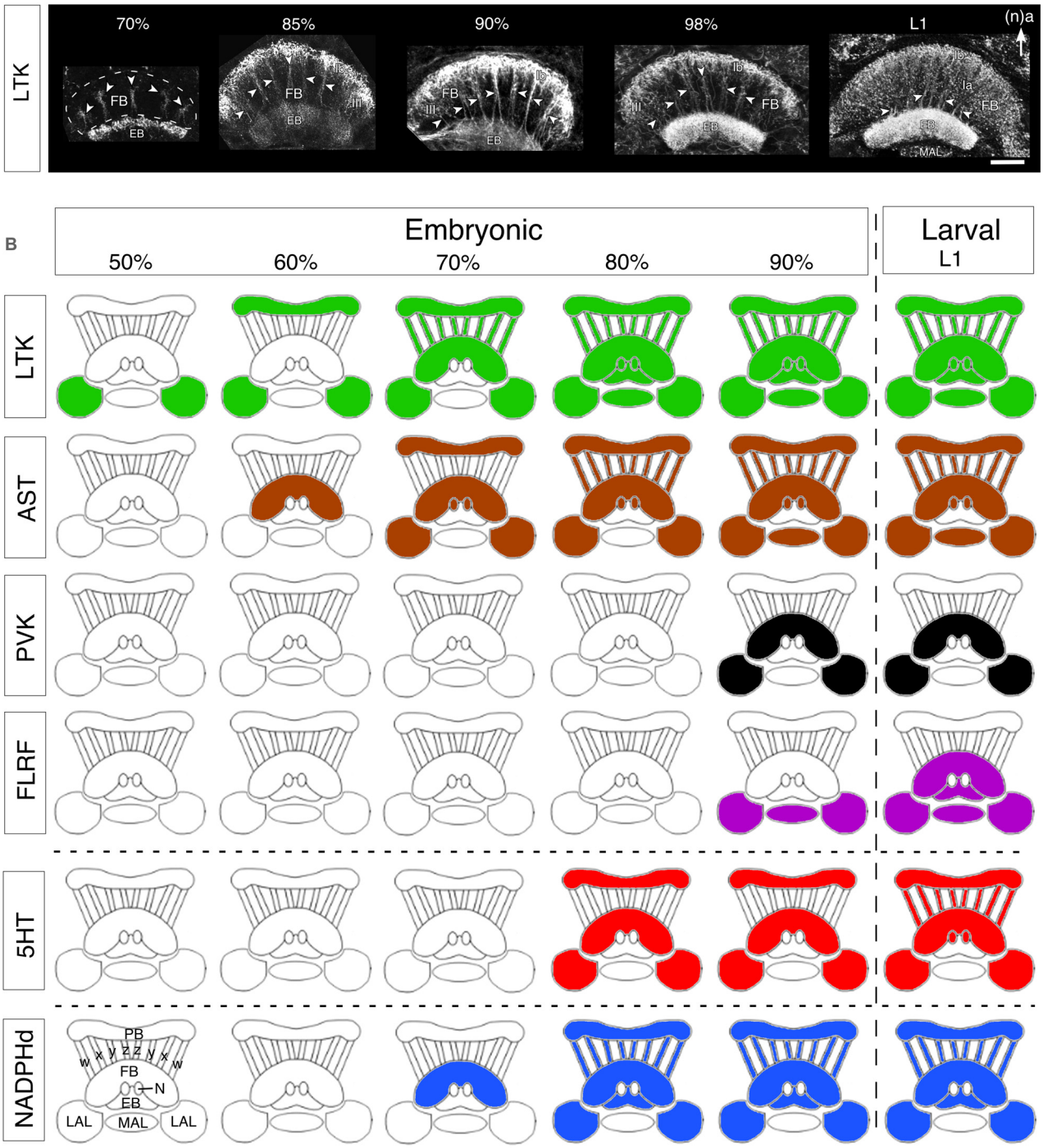

FIGURE 6 | Developmental expression of neurochemicals in the central complex. (A) Confocal images of Locustatachykinin (LTK) immunolabeling in the FB and EB through successive embryonic (%) and postembryonic (larval stage 1, L1) stages. At 70% of embryogenesis, LTK labeling is present in the initial fiber columns (white arrowheads in all panels), region III of the FB, and an upper layer of the EB. At 85%, LTK labeling has expanded to include the Ib layer of the FB and most of the EB. At 90% of embryogenesis, the intensity of LTK labeling increases in layer Ib, fiber columns, and region III of the FB. The doublet structure of fiber columns (white arrowheads) is clearly revealed (see **Figure 1B**). Toward the end of embryogenesis (98%), LTK labeling in the EB increases to levels found postembryonically (L1). At L1, LTK labeling in neuropilar subregion Ia of the FB increases significantly reflecting the expanded dendritic arborizations there. Arrow indicates anterior (a) according to the neuraxis (n) and applies to all panels. Other abbreviations: MAL, median accessory lobe. **(B)** Schematics (not to scale) reveal

(*Continued*)

FIGURE 6 | Continued
stepwise expression of neurochemicals in the central complex over successive embryonic (%) up to the first postembryonic (L1) stages. Colors indicate the presence of immunoreactivity. Hatching from the egg is indicated by the vertical dashed line. Data are grouped into representative neuropeptides (LTK, AST, perivisceroKinins and pyrokinins (PVK, PK), FLRFamide), a classical transmitter (5HT, 5HT), and the synthesizing enzyme (NADPHd) for the endogenous messenger NO. Modules of the CX are shown in outline and represent, as labeled at bottom left: PB, protocerebral bridge; *w, x, y, z* tracts; FB, fan-shaped body; N, noduli; EB, ellipsoid body; LAL, lateral accessory lobes; MAL, median accessory lobe. Scale bar in **(A)** represents 50 μm. Panels **(A,B)** modified from Herbert et al. (2010) with permission.

(Vitzthum et al., 1996) and are pleiotropic in function. As neurohormones they inhibit juvenile hormone (JH) synthesis by the corpora allata, while as inhibitory substances they are also involved in the modulation of muscle contraction, and the maturation of neural circuits (Rankin et al., 1998; Dircksen et al., 1999; Kreissl et al., 1999). JH has been shown to regulate aggregation behavior and olfactory processing in *Schistocerca gregaria* (Ignell et al., 2001). The expression of ASTs in the brain could therefore be consistent with a role in the maturation of synaptic pathways for locomotion, stridulation, and antennal-based behaviors known to involve the central complex (Bender et al., 2010; Harley and Ritzmann, 2010; Kunst et al., 2011).

AST expression in the central complex first appears in tangential projection neurons at the 60–65% stage (**Figure 6B**). Based on their morphology and location, these first AST-immunoreactive fibers are likely to be projections of AST one neurons (see **Figure 5A**). There is no AST immunoreactivity in the PB, *w, x, y, z* tracts or LALs at this stage. After 70%, further AST-immunoreactive tangential projections appear in the FB, with strong immunoreactivity in the PB, but still not in the columnar *w, x, y* and *z* tracts, suggesting that these PB projections belong to type IV tangential projection neurons with cell bodies located dorso-laterally of the PB (see Vitzthum et al., 1996). AST-immunoreactive horizontal fibers branching off in layers Ib and IIb are consistent with their being the AST three neurons described by Vitzthum et al. (1996). The AST two projection system is also labeled in the IT, and in layer IIB and the columnar system of the FB (see **Figure 5A**). From 80% onward all four AST tangential projection systems are immunoreactive, as are the columnar neurons and their processes in the PB, the *w, x, y* and *z* tracts, the noduli, and the LALs. Based on their labeling in layers Ia, Ib of the FB, it is likely that the ASC one neurons are the first to express AST in the columnar system. During further development, additional labeling appears in the MAL and in branches within the FB consistent with AST expression in the columnar ASC one neurons. The density of the AST-immunoreactive arborizations subsequently increases so that the pattern in first instars is essentially the same as in the adult.

Perivisceroкinins and pyrokinins (PVK and PK)

PVKs and PKs are the major neuroactive components of the neurosecretory organs of the abdominal ganglia, and are also present in interneurons of the CNS (such as the columnar neurons in the cockroach central complex) in several insect species (Eckert et al., 1999) In the adult grasshopper, Herbert et al. (2010) report PVK/PK immunoreactivity in the tangential system, in the LAL and in all CB layers. Columns of the ascending tangential system of the FB also show immunoreactivity. Two immunoreactive cell groups located in the inferior PC project axons through the LALs into the FB. The first group projects via the ipsilateral LALs into layer Ib of the FB, the second group projects through the ipsilateral LAL into the contralateral LAL and into the FB.

PVKs appear relatively late in embryogenesis (90%) in the cell group projecting via the LAL into layer Ib of the FB (**Figure 6B**). However, strong PVK/PK staining is seen earlier (80%) in the lateral PC and in neurosecretory pathways. Staining is absent in the columnar PI neurons, in PB fibers, in the EB and in the noduli. The immunoreactive pattern in early postembryonic stages already resembles that of the adult (Clynen et al., 2009; Herbert et al., 2010). While effects on neurogenesis or neuronal differentiation are not known, PVKs are known to have myomodulatory and diuretic effects (Predel and Wegener, 2006), so that their postembryonic appearance could conceivably be associated with olfactory inputs regulating the transition from a yolk to a vegetative diet after hatching.

FLRFamide

FLRFamide-like peptides are expressed primarily in tangential projection neurons of the adult central complex. These neurons project into the accessory lobes and then via the IT into the EB and layer I of the FB (Homberg et al., 1999). FLRFamide-like immunoreactivity in the central complex appears only relatively late (90%) during embryogenesis and then in fibers of the LALs and MAL (**Figure 6B**). Other cerebral regions, however, show intensive FLRFamide-like immunoreactivity already at 65% of embryogenesis. In the first instar, weak staining is present in tangential fibers which follow columnar tracts of the FB and EB and becomes stronger during subsequent instars. As a neurohormone, FLRFamide is released by the corpora cardiaca-corpora allata system and regulates the heartbeat, influences the contraction of leg muscles (Robb and Evans, 1990) and has myoinhibitory effect on the locust oviduct (Peeff et al., 1994). These functions are more likely to be associated with aggregation and approaching sexual maturity in free-living (postembryonic) developmental stages, but a specific role with respect to the central complex is yet to be determined.

Serotonin (5HT)

5HT immunoreactivity has been extensively described in the central complex of adult *Schistocerca* (see Homberg, 1991, 2002; Herbert et al., 2010). Several serotonergic small-field neurons (S1 cells) of the PI project via the PB and the columnar *w*, *x*, *y* and *z* tracts into layer III of the FB, and to the noduli (see **Figure 5A**). Five other large-field neuron pairs/groups constitute the tangential serotonergic projection system of the central complex: the S2 cells project to the PB and the posterior optic tubercules; the S3 neurons of the inferior PC run through the LAL and the IT into layer Ia of the FB; the S4 neuron pair in the fronto-median PC gives rise to varicose branches in layer Ib

of the FB; the S5 neuron pair in the posterior PI innervates layer Ia of the FB and the S6 pair projects into the contralateral LALs where their terminals arborize extensively.

In the grasshopper, appreciable 5HT immunoreactivity appears in the central complex only after 75% of embryogenesis, but then intensifies significantly during further development (**Figure 6B**). 5HT appears first (75–80%) in tangential projections in a manner similar to that of members of LTK and AST peptide families, and can be first detected in the columnar system shortly before hatching. At the 80% stage, tangential projection neurons (the future S2-S6 group) begin to express 5HT in their projections to the PB (S2), and via the LALs into the FB (S5). Serotonergic fibers are also present throughout the FB indicating that 5HT is present in the S3, S4 and S6 groups. All these serotonergic tangential projection neurons are immunoreactive simultaneously. By contrast, 5HT immunoreactivity is yet to be detected in the columnar *w*, *x*, *y* and *z* tracts and in PI neurons. In the late embryo (90–95%), the staining intensity rises in the tangential projection neurons as the neuropilar volume of the central complex expands due to increasing fiber density from additional ingrowing neurons. 5HT immunoreactivity in the columnar system can be first detected at 99%, shortly before hatching, and the overall pattern is then very similar to that of the L1 and adult stages, although the full complement of S1 immunoreactive cells (∼60 cells after Homberg, 1991) is not evident yet.

In adult insects, 5HT which is involved in regulating circadian rhythms (Saifulla and Tomioka, 2002; Yuan et al., 2005), plays a role in odor-dependent behaviors (Kloppenburg et al., 1999), is necessary for spatial learning and memory (Sitaraman et al., 2008; Zars, 2009), modulates aggression (Edwards and Kravitz, 1997; Diereck and Greenspan, 2007; Johnson et al., 2009) and in the grasshopper, raised serotonergic levels which mediate the phase change from solitary to gregarious (Rogers et al., 2004)—all behaviors in which the brain, and with it the central complex, is likely to be involved. Neuroactive substances are known to be hierarchically organized (Gammie and Truman, 1997) and developmentally, 5HT has been considered to function as a general coordinator of neurogenesis, axogenesis and cellular and biochemical differentiation (Turlejski, 1996; Gaspar et al., 2003; Richards et al., 2003; Vitalis et al., 2007; Filla et al., 2009). Serotonergic neurons have been shown to require chemical signals in order to become functionally active (Condron, 1999) including 5HT itself (Sykes and Condron, 2005) suggesting that feedback as well as feedforward networks are active in the developing grasshopper nervous system.

Nitric oxide (NADPHd)

NADPHd activity is present in the adult MB and central complex (O'Shea et al., 1998; Kurylas et al., 2005; Siegl et al., 2009) and NO has been linked to cell proliferation, retinal patterning, axogenesis, synaptogenesis and neuronal maturation in developing insect nervous systems (Kuzin et al., 1996; Truman et al., 1996a,b; Ball and Truman, 1998; Gibbs and Truman, 1998; Seidel and Bicker, 2000). A detailed analysis of NO (NADPHd) immunolabeling associated with the central complex of the adult grasshopper is presented in the study by Kurylas et al. (2005). Six neuron types (about 170 neurons) involving tangential, pontine and columnar projection systems were identified: (a) *columnar neurons*. About 50 neurons from the posterior PI (according to the body axis) contribute to the columnar NO system of the FB. Their fibers run first to the PB, and then via the *w*, *x*, *y* and *z* tracts into layer III of the FB and further to the noduli. (b) *tangential neurons*. The single pair neurons of the first tangential system (TL1, see **Figure 5Biii**) are located in the ventromedian PC. Their neurites ramify in the LBUs and enter the EB via the IT. The second tangential neuron group (TL2) is located in the median PC, the projections are similar to those of the TL1, but they enter the EB more ventrally. The third tangential neuron group (TL3) has arborization fields in the posterior optic tubercle and in the PB. Their somata (about 20) are located posteriorly to the PB. The fourth tangential neuron group (TL4) is composed of six bilateral pairs of neurons which run along the w tract to the LALs. Terminal arborizations are also found in layer II of the FB. The fifth tangential arborization system is localized in posterior commissure I, in layer II of the FB, and in the anterior lip. (c) *Pontine neurons*. These neurons (45 somata in the anterior PI) project through the PB to the FB via the anterior chiasm (according to neuraxis, see **Figures 5Biii,iv**) and contribute to the columns of layer I and layer IIb in the FB. They also interconnect the columns of these layers.

During development, NADPHd activity first appears at about 70% of embryogenesis in layer IIb of the FB (consistent with the cells of the pontine system being involved), in the EB and in the LAL. At 75%, NADPHd activity appears in columnar neurons in the PI, in the PB, in the columnar y and z tracts, in layer III of the FB, expands via the ITs to the TL2 tangential system and into the posterior groove. (for ventral groove see Kurylas et al., 2005). At 85% of embryogenesis, the staining in the *w, x, y, z* columnar system, in layer III of the FB, in the EB, in the noduli and in the IT intensifies further so that there is a clear resemblance to that of the adult (see **Figures 5Bi–iv**).

A distinguishing characteristic of the NO system in the developing central complex is that while NADPHd activity in the tangential systems increases in a stepwise manner as more fibers innervate the region, that in the columnar system of the FB appears abruptly and simultaneously in all its elements, suggestive of a temporally coordinated mechanism for establishing this neurochemical architecture (Williams et al., 2005; Herbert et al., 2010).

Interim summary

Several consistent features characterize the developmental expression pattern of neurochemicals in the central complex. First, all the substances tested are expressed in the modules of the embryonic central complex according to a substance-specific temporal pattern, and not synchronously. For some (e.g., 5HT), specific modules (noduli, *w, x, y, z* tracts) only become immunoreactive after hatching, while others (e.g., LTK, AST, NO) appear to have completed their developmental plan during embryogenesis. Second, if we consider individual neuropilar modules, then immunoreactivity appears very early in the LAL and/or the FB, and somewhat later in the PB and *w, x, y, z* tracts. Third, some neuropeptides are expressed earlier (LTK,

50%; AST, 60%) than the NO-synthesizing enzyme diaphorase (70%) or the classical transmitter 5HT (80%). If we focus on just the columnar system, we observe a similar pattern: LTK-related peptides are the first neuroactive substances to appear (70%), followed by AST and diaphorase (NO) at 75–80%, and 5HT only postembryonically. Finally, immunoreactivity does not appear in an all-or-nothing manner during development—there is a clear stepwise increase in signal strength for each neurochemical during development (e.g., LTK, **Figure 6A**). We can show this (see **Figure 7D** below) to be due to an increase in the proportion of immunoreactive cells from a given lineage expressing the relevant neurochemical.

Biochemical Profiling of Central Complex Lineages

Given that the pattern according to which individual neuroactive substances appear during development is critical for the adaptive functioning of the adult nervous system (see Nässel, 2002), knowledge about whether this neurochemical architecture can be related to the lineages of central complex neurons could provide valuable insights into the behavioral role the central complex plays at various critical stages such as hatching, molting, and pupation. Insect lineages of the ventral nerve cord possess an internal temporal topology (see Goodman and Doe, 1994) and this aspect has proven instrumental in integrating neuronal ontogeny and physiology (Goodman et al., 1979, 1980; Taghert and Goodman, 1984; Thompson and Siegler, 1991). It therefore seems relevant to ascertain whether the discrete biochemical layering of the FB neuropil is due to a biochemical zoning within the lineages of neurons, thus reflecting their ages, and suggesting there is a temporal dimension to the biochemical expression pattern associated with central complex neuropils.

Reconstructions have revealed the Y and Z lineages, as representative of central complex lineages, to be bilaterally symmetrical and since they retain their internal organization up to hatching and beyond, they are resolvable to the level of single, identifiable, presumably homologous cells (Boyan et al., 2010a). As a result, the lineages can be shown to possess a temporal topology according to which location within the lineage accords to the birth date of a given cell. This, in turn, allows a lineage to be age-profiled with respect to the expression of various neurochemicals (**Figure 6**; Boyan et al., 2008a, 2010a), and compare this with the expression patterns of these same substances in the central complex.

The results of such an analysis (**Figure 7A**) reveal first, that all different neuroactive substances indeed co-localize to the same lineage, implying that the neuroblasts responsible for each lineage are biochemically multipotent. Second, the lineages are almost identically zoned with respect to where neurons expressing these substances are located, suggestive of a common developmental program. LK-1- (a cephalotropin which acts as

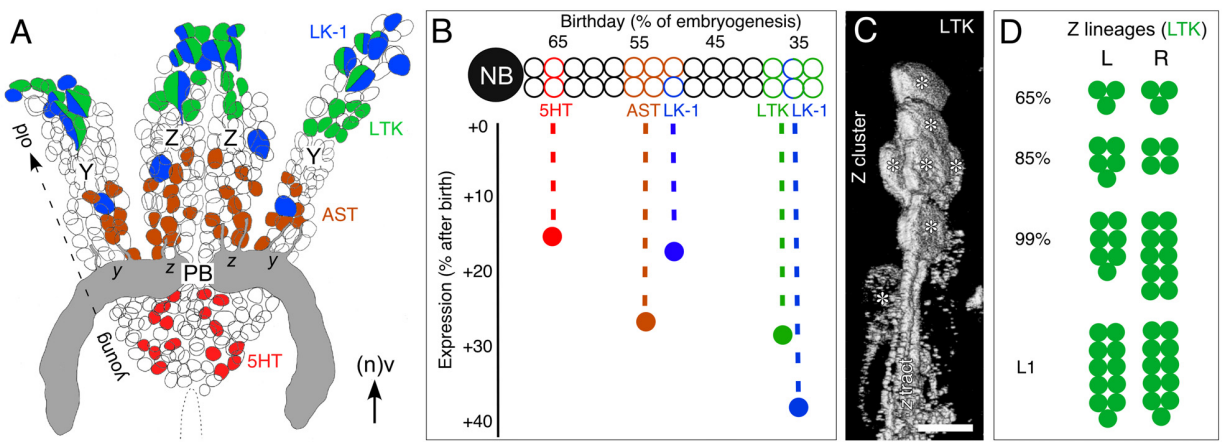

FIGURE 7 | Topology of neurons expressing various neurochemicals in central complex lineages. (A) Reconstruction from serial sections following immunolabeling summarizes the location of neurons expressing the neurochemicals 5HT (red), AST (brown), LTK (green) and leukokinin (LK-1, blue) within the bilateral Z and Y lineages at 100% of embryogenesis. Some neurons co-express neurochemicals LK-1 and LTK. Neurons expressing the various neurochemicals are found at stereotypic locations (also representing age) within their lineage: the youngest (latest born) cells are at the base and the oldest at the tip. Neurons direct axons via tract doublets (see **Figure 1C**) to the PB (gray). Neuroblasts are no longer present at this age (see Boyan and Liu, 2014). Arrow indicates anterior (a) according to the neuraxis (n). **(B)** Schematic illustrates the temporal expression of neurochemicals 5HT (red), AST (brown), LTK (green) and LK-1 (blue) from a representative central complex lineage. Neurons occupy stereotypic locations within the lineage reflecting their birth date. Vertical axis shows the time after birth when neurochemical expression appears. LK-1 cells at the tip of the lineage are born early in embryogenesis but lie immunohistochemically dormant for almost 40% of embryogenesis. 5HT cells at the base of the lineage are born late but express their neurochemical relatively soon thereafter. The data predict there should be a stepwise appearance of neurochemicals within the central complex neuropil. **(C)** 3D image from confocal *z*-stacks following immunolabeling at 80% of embryogenesis shows a cluster of LTK-positive cells (white asterisks) at the tip of the Z lineage along with their projections forming the *z* tract. **(D)** Number of LTK-immunoreactive cells in the left (L) and right (R) Z lineages at various stages of development collated from three preparations in which both Z lineages were completely visualized. LTK-immunoreactive cells make up 2% of the Z lineage at 65% of embryogenesis, 3% at 85%, 5% at 99% and 8% at L1. Scale bar in **(A)** represents 15 μm in **(C)**, 30 μm in **(A)**. Panels **(A,B,D)** modified from Boyan et al. (2010a) with permission.

a circulating hormone modulating visceral muscle contractions and diuresis (Cook et al., 1989; Hayes et al., 1989)) and LTK-expressing cells are clustered apically in each lineage. These cells represent the first-born (oldest) cells of each neuroblast. At the single-cell level, neuroactive substances are also seen to co-localize in some instances. This is not unique as co-expression of neuropeptides has been extensively documented in insect nervous systems (e.g., Taghert and Truman, 1982a,b; Thompson et al., 1995; Duve et al., 2000; Nässel and Winther, 2002), including the central complex (Homberg et al., 1999), although co-localization does not necessarily imply co-release (Marder, 1999).

There is also a prominent second LK-1 expression zone comprising a single large, putatively homologous, cell at an equivalent location midway along each lineage. This younger cell is the evidence to show that the Y and Z neuroblasts have, at the same developmental stage, simultaneously orchestrated a cell division yielding this single LK-1 expressing cell. AST-expressing cells, on the other hand, appear in a continuous zone straddling the central region of each lineage and so are generated by several cell cycles. Serotonergic cells are located only in the basal region of their lineage and so represent the youngest cells of the lineage generated by the last series of divisions of the neuroblast. The clear zoning of expression is the evidence to show that, as in *Drosophila* (Taghert and Goodman, 1984), successive neuroblast divisions generate biochemically distinct cells. The mechanism may involve the neuroblast expressing a transcription factor specific to a given mitotic division or series of divisions thereby providing successive daughter cells with a unique identity (Pearson and Doe, 2003).

All the neuroblasts generating the neurons of the central complex undergo apoptosis between 70% and 75% of embryogenesis (Boyan and Liu, 2014), which means that the central complex of an hemimetabolous insect such as the grasshopper is structurally complete at hatching. Biochemically, however, this is obviously not the case. The brain neurons expressing the various neurochemicals discussed here are all born during embryogenesis, but then remain biochemically dormant for varying periods (**Figure 7B**). This dormant period is stereotypic for each substance and can last for over 40% of embryogenesis. LTK-expressing cells at the apical tip of the lineage, for example, are born early in embryogenesis (*ca.* 35%), but subsequently lie immunocytochemically dormant for almost 30% of embryogenesis. LK-1-expressing cells also found at the apical tip of the lineage are born over the same time window,

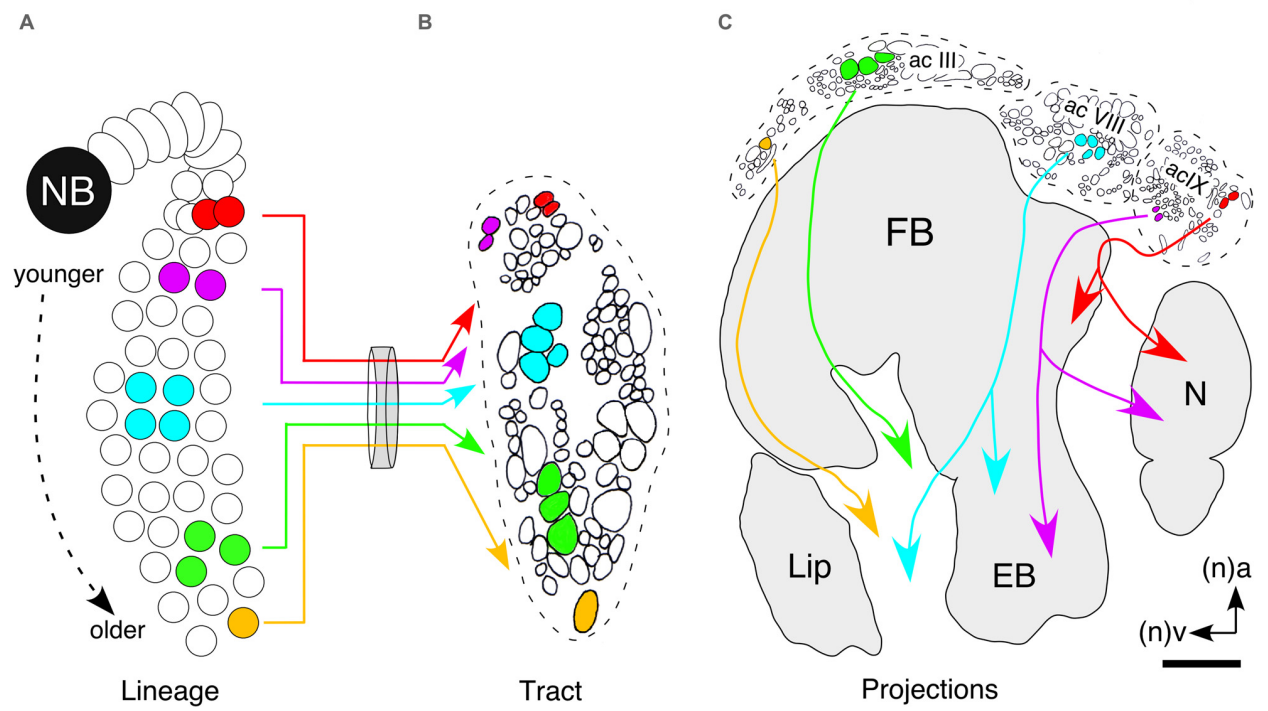

FIGURE 8 | Hypothesis as to how neuronal topology in a lineage can translate into the topology of columnar projections in the FB. (A) Neurons occupy stereotypic locations according to birthdate as in this hypothetical lineage of the central complex. Colors are intended to indicate the expression of different, non-specified, neurochemicals. **(B)** Cross-section of the tract shows that axon projections are topologically ordered according to the location of the somata within the lineage. **(C)** Axon position within a tract translates directly into location in commissural fascicles (AC III, VIII, IX) of the central complex. Axons from these fascicles decussate and so generate a columnar neuroarchitecture in the developing FB. In this way the temporal and biochemical topology of the lineage is reflected in the neurochemical architecture of the central complex itself. Arrows indicate anterior (a) and ventral (v) according to the neuraxis (n). Scale bar in **(C)** represents 15 μm in **(B)**. Panel **(B)** modified from Williams et al. (2005); panel **(C)** modified from a personal communication courtesy of Williams.

but only express the neurochemical about 40% later, i.e., well after the LTK-expressing cells. Serotonergic cells at the base of the lineage are among the last born in the lineage (*ca*. 65% of embryogenesis) but express the neurotransmitter relatively soon thereafter (at 80%).

We reported (in "Developmental Expression Patterns" Section) that immunoreactivity does not appear in an all-or-nothing manner in the FB during development—there is a clear stepwise increase in signal strength for each neurochemical during development. At least in the case of the columnar system, this is most probably due to an increase in the proportion of immunoreactive cells from a given cell cluster of the PI expressing the relevant neurochemical (**Figures 7C,D**). The cell cluster itself cannot increase in size after 75% because all the proliferative cells responsible for these central complex lineages, including the neuroblasts, ganglion mother cells, and intermediate progenitors, are no longer mitotically active by then (Boyan et al., 2010b; Boyan and Liu, 2014).

Lineage Topology Translates into Neuroarchitecture

The temporal and biochemical profile of a lineage, coupled with the known times when neurochemicals are expressed in the central complex, allows us to generate a time-line with which to resolve the ontogeny of biochemical expression in the central complex. A concept for how this temporal and biochemical topology might translate into the neurochemical architecture of the central complex can now be formulated.

Neurons occupy stereotypic locations according to birthdate as in the hypothetical lineage of the central complex (**Figure 8A**). A cross-section of the tract shows that axon projections are topologically ordered according to the location of the somata within the lineage (**Figure 8B**) and that axon position within a tract translates directly into location in commissural fascicles (AC III, VIII, IX) of the central complex (**Figure 8C**). Subsets of axons from these fascicles decussate and so generate a columnar neuroarchitecture in the developing FB. In this way, the temporal and biochemical topology of the lineage translates into the neurochemical architecture of the central complex itself.

If our hypothesis that discrete expression zones within the W, X, Y, Z lineages translate into a biochemical neuroarchitecture is correct, then a zoning of neurochemical projection systems might manifest itself as a layered expression pattern in the FB. Indeed, double immunolabeling experiments reveal no co-expression of 5HT on the one hand, and the neuropeptides (Dip)-AST I, FLRFamide, LK-1, PVK/PK and LTK on the other, in arborizations within the same subregions of the FB in either the developing grasshopper (**Figures 9A–C**; Herbert et al., 2010) or in the case of 5HT and tachykinin, in adult *Drosophila* (**Figure 9D**; Kahsai and Winther, 2011). Since 5HT and LTK, for example, are expressed by neurons of different ages (see **Figure 6**), the cellular neuroarchitecture of the FB based on histology (**Figure 10B**) can now be analyzed via its neurochemical architecture from a temporal perspective (**Figure 10C**). Late in embryogenesis, ventral commissures, ventral regions

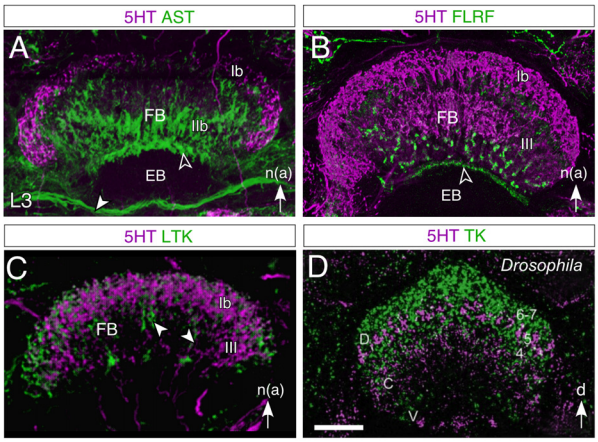

FIGURE 9 | Layered expression of neurochemicals in the FB of the central complex in the larval (L3) grasshopper (A–C) and adult *Drosophila* (D). All panels show confocal images following double immunolabeling as follows: **(A)** 5HT/AST, **(B)** 5HT/FLRF, **(C)** 5HT/LTK, **(D)** 5HT/TK. 5HT labeling is magenta throughout. In both species, 5HT is observed not to co-localize to any great degree (lack of white in the image) with the other neurochemicals tested. In the grasshopper, AST labeling **(A)** appears in tangential fibers of region IIb, in an anterior strip (open white arrowhead) of the EB, and in the IT (white arrowhead) between the EB and the MAL (not shown), while 5HT appears as a crescent in region Ib and in the columnar system of the FB; FLRF labeling **(B)** appears in a subregion of III, and in a narrow strip (open white arrowhead) of the EB; LTK labeling **(C)** is present in the Ib and III regions as well as in the columnar system (white arrowheads) but does not colocalize to 5HT. Nomenclature of neuropilar regions is from Vitzthum and Homberg (1998). In *Drosophila* **(D)**, 5HT labeling is present as a thin crescent in layer 5 of the dorsal (D) FB where there may be some minimal co-localization to tachykinin (TK), as well as in central (C) and ventral (V) regions, where there is no co-localization. Abbreviations: (Dip)-Allatostatin I (AST); Phe-Leu-Arg-Phe-NH2 (FLRF); LTK; Tachykinin (TK); 5HT (5HT). White arrow in **(A–C)** points to anterior according to the neuraxis (n). Scale bar in **(D)** represents 35 μm in **(A)**, 65 μm in **(B)**, 95 μm in **(C)**, 25 μm in **(D)**. Panels **(A,B)** modified from Herbert et al. (2010), panel **(C)** modified from Boyan et al. (2010a), panel **(D)** modified from Kahsai and Winther (2011).

of the PB and noduli, are predominantly serotonergic suggesting the axon processes here are from younger cells. The embryonic EB and columnar projections in the FB, by contrast, are almost exclusively LTK-positive, and therefore comprise axons from older cells. This matches the order in which the neuroarchitecture of central complex modules is established (Boyan and Williams, 1997; Williams et al., 2005).

CONCLUSIONS AND OUTLOOK

The insect central complex has been shown to orchestrate locomotor and stridulatory behaviors (Strauss, 2002; Kunst et al., 2011), but insect behaviors are not all expressed synchronously during development. They appear sequentially due to induction via steroid hormones (Zitnan et al., 1999), a successive maturation of the neurochemicals themselves (Predel et al., 2003) and the neural circuits responsible (Levine, 1984; Stevenson and Kutsch, 1986; Truman et al., 1996a,b; Wegerhoff et al., 1996). In the holometabolous grasshopper,

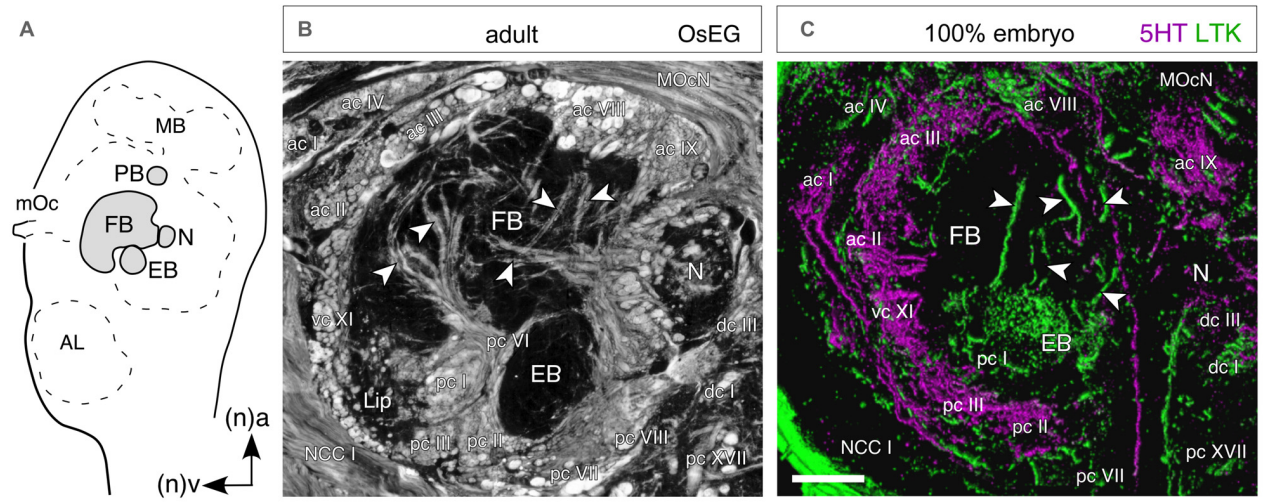

FIGURE 10 | Temporal topology of neurochemical expression reflects architecture of the central complex. (A) Schematic (not to scale) shows the location of central complex modules in the brain as seen in sagittal view. Abbreviations: MB, mushroom body; mOc, median ocellus; FB, fan-shaped body; N, nodulus; EB, ellipsoid body; AL, antennal lobe. Arrows point to anterior (a) and ventral (v) according to the neuraxis (n). Axes apply to all panels. **(B)** Histological (sagittal) section of the central complex in the adult brain following osmium ethyl gallate staining reveals axon profiles in anterior (ac), posterior (pc), ventral (vc) and dorsal (dc) commissures circumscribing the FB, EB, N and ventral lip. Other fiber tracts seen are the median ocellar nerve (MocN) and nervus corporis cardiaci I (NCC I). **(C)** Confocal image of a parasagittal section through the central complex at 100% of embryogenesis following 5HT (magenta) and LTK (green) double labeling. There is no co-expression (absence of white) in the commissural and columnar (white arrowheads) neuroarchitecture of the central complex. Since 5HT and LTK are expressed by neurons of different ages (see **Figure 7**), the co-labeling provides a temporal insight into the neuroarchitecture of the central complex. Scale bar in **(C)** represents 40 μm in **(B)**, 100 μm in **(C)**. Modified from Boyan et al. (2010a).

neural circuits mediating respiratory and skeletal muscle activity must mature during the embryonic phase of development, prior to hatching, and in advance of those regulating, for example, feeding, stridulation or reproduction in the free-living phase (see Chapman, 1982). The temporal differentiation of neurochemicals in the central nervous system reflects this sequence (Goodman et al., 1979; O'Shea and Adams, 1986; Stern et al., 2007).

Clonal analyses of brain neuroarchitecture have been undertaken in larvae and adult *Drosophila* (Ito et al., 1997; Ito and Awasaki, 2008). While these lineages are organized such that cell location accords to birthdate (Lai et al., 2008; Izergina et al., 2009; Riebli et al., 2013) neurochemicals only appear at the adult stage after the central complex neuroarchitecture is established (see Kahsai and Winther, 2011). The mechanisms generating this neuroarchitecture reside at the molecular level with the specification of neurogenesis in the neuroblasts (Doe, 2008) and the guidance cues regulating axogenesis in their progeny (see Dickson, 2002), arguing against a causal role for expressed neuropeptides in the establishment of the central complex. The neuropeptides, monoamines and endogenous messengers expressed in the central complex are also found in other regions of the brain of embryonic insects (Romeuf and Rémy, 1984; Westbrook and Bollenbacher, 1990; Wegerhoff et al., 1996; Bicker, 2001; Seidel and Bicker, 2002). In the case of the grasshopper, however, we can show that these neuroactive substances are expressed in the embryonic central complex at a time when the specific subset of identified neuroblasts responsible for the establishment of its characteristic neuroarchitecture are still present, along with their primary lineages. By linking the neurochemical expression patterns in the developing central complex to the stereotypic location of neurons in these identified lineages, we can relate lineage topology to a developmental plan for establishing the cellular neuroarchitecture of at least one central complex module—the FB.

It is clear that any functional interpretation of the developmental role of specific neurochemicals must be made with caution since neuroactive substances can have different physiological effects in the embryonic nervous system than in the adult, and receptors can be expressed before some of the neuroactive substances themselves are present in the circuit (Roeder, 2002; Rehm et al., 2008). Further, neurochemicals reported for the ventral nerve cord in the adult (e.g., O'Shea and Adams, 1986) or embryonic (e.g., Keshishian and O'Shea, 1985) grasshopper need not play the equivalent role in the development of the central complex in the brain. Since most of the substances examined here are expressed in subsets of tangential and columnar neurons, and some additionally in pontine neurons, our current level of resolution does not allow us to relate a given temporal expression pattern to the functional morphology of individual neuron types. This may eventually prove possible for certain columnar (CPU1, 2) or tangential (TB1a, TB1d) neurons with regionalized morphologies spanning different modules (see Heinze and Homberg, 2008; Pfeiffer and Homberg, 2014; Beetz et al., 2015) if these neurons were to

also regionalize their developmental expression of a given neurochemical.

Several other caveats with respect to the data presented in this study must be considered. The first is whether the restricted range of neurochemicals examined in this review is sufficiently representative to draw any major conclusions. Major neurotransmitter systems (glutaminergic, GABergic, dopaminergic and cholinergic), all with clear expression profiles in the adult central complex and established functional roles in behavior (see Homberg, 2002; Kunst et al., 2011; Pfeiffer and Homberg, 2014), are missing. Second, how representative are the W, X, Y, Z lineages for the development of the neurochemical architecture of the central complex *in toto*? We report the expression patterns only up to the first larval stage of development. This is an obvious gap in our knowledge database, and although we see no major neuroarchitectural differences between the central complex of the hemimetabolous grasshopper immediately after hatching and in the adult at the level of resolution available to us (see Boyan et al., 2015), this need not apply at the neurochemical level. Despite the fact that the behavior of the first larval instar has similarities (feeding, locomotion) to that of the adult, there are many differences (reproductive, flight, phase/aggregation; see Chapman, 1982) and these may have their roots at the neurochemical level, even though neural circuits for some behaviors are present at hatching (Stevenson and Kutsch, 1986). For instance, our studies reveal no co-localization of serotonergic and peptidergic cells in embryonic W, X, Y Z lineages (**Figure 7**), and no cells co-expressing 5HT and neuropeptides in the FB or noduli during embryogenesis (**Figures 6**, **9**, **10**). This is clearly not the case in the adult where 5HT and AST are co-localized both in columnar neurons innervating the noduli (Vitzthum et al., 1996; Homberg, 2002) and in clusters of TB neurons projecting into the tract linking the posterior optic tubercle and the PB (Beetz et al., 2015). The lineages of these co-expressing TB neurons have yet to be determined, but as far as the columnar neurons from the W, X, Y, Z lineages are concerned, two possible explanations can be offered: either distinct populations of neurons from the same lineage, but with different biochemical profiles, differentially innervate the FB and noduli, or at least some neurons have changed their biochemical profile during larval development. Axon tracing has yet to clarify the former, but the latter possibility has a precedence in changing peptide co-expression levels during metamorphosis of holometabolous insects (see Honegger et al., 2011) where major structural changes in the central brain (see Wegerhoff and Breidbach, 1992; Renn et al., 1999; Young and Armstrong, 2010a,b; Riebli et al., 2013; Wolff et al., 2015), accompany a neurochemical profile that only reaches maturity at adulthood (Kahsai and Winther, 2011). Nevertheless, our hope is that the temporal sequence of neurochemical expression we uncover in the central complex of the grasshopper also reflects the synaptic maturation of its circuitry, and so may ultimately provide an insight into the way the behaviors it regulates develop.

AUTHOR CONTRIBUTIONS

GSB and YL helped with conception, with the text, the figures, and critically reviewed the manuscript.

ACKNOWLEDGMENTS

We thank Dr. Leslie Williams for sharing with us his concept of the temporal topology of axonal projection patterns. Financial support was provided by the Deutsche Forschungsgemeinschaft (Grant number BO 1434/3-5).

REFERENCES

Arendt, D., and Nübler-Jung, K. (1996). Common ground plans in early development in mice and flies. *Bioessays* 18, 255–259. doi: 10.1002/bies.950180314

Ball, E. E., and Truman, J. W. (1998). Developing grasshopper neurons show variable levels of guanylyl cyclase activity on arrival at their targets. *J. Comp. Neurol.* 394, 1–13. doi: 10.1002/(SICI)1096-9861(19980427)394:1<1::AID-CNE1>3.0.CO;2-4

Bate, C. M. (1976). Embryogenesis of an insect nervous system. I. A map of the thoracic and abdominal neuroblasts in *Locusta migratoria*. *J. Embryol. Exp. Morphol.* 35, 107–123.

Bayraktar, O. A., Boone, J. Q., Drummond, M. L., and Doe, C. Q. (2010). *Drosophila* type II neuroblast lineages keep Prospero levels low to generate large clones that contribute to the adult brain central complex. *Neural Dev.* 5:26. doi: 10.1186/1749-8104-5-26

Beetz, M. J., El Jundi, B., Heinze, S., and Homberg, U. (2015). Topographic organization and possible function of the posterior optic tubercles in the brain of the desert locust *Schistocerca gregaria*. *J. Comp. Neurol.* 523, 1589–1607. doi: 10.1002/cne.23736

Bender, J. A., Pollack, A. J., and Ritzmann, R. E. (2010). Neural activity in the central complex of the insect brain is linked to locomotor changes. *Curr. Biol.* 20, 921–926. doi: 10.1016/j.cub.2010.03.054

Bicker, G. (2001). Sources and targets of nitric oxide signalling in insect nervous systems. *Cell Tissue Res.* 303, 137–146. doi: 10.1007/s004410000321

Boyan, G., and Liu, Y. (2014). Timelines in the insect brain: fates of identified neural stem cells generating the central complex in the grasshopper *Schistocerca gregaria*. *Dev. Genes Evol.* 224, 37–51. doi: 10.1007/s00427-013-0462-8

Boyan, G. S., and Reichert, H. (2011). Mechanisms for complexity in the brain: generating the insect central complex. *Trends Neurosci.* 34, 247–257. doi: 10.1016/j.tins.2011.02.002

Boyan, G. S., and Williams, J. L. D (1997). Embryonic development of the pars intercerebralis/central complex of the grasshopper. *Dev. Genes Evol.* 207, 317–329. doi: 10.1007/s004270050119

Boyan, G. S., Williams, J. L. D., and Herbert, Z. (2008a). An ontogenetic anaysis of locustatachykinin-like expression in the central complex of the grasshopper *Schistocerca gregaria*. *Arthropod Struct. Dev.* 37, 480–491. doi: 10.1016/j.asd.2008.04.002

Boyan, G. S., Williams, J. L. D., and Herbert, Z. (2008b). Fascicle switching generates a chiasmal neuroarchitecture in the embryonic central body of the grasshopper *Schistocerca gregaria*. *Arthropod Struct. Dev.* 37, 539–544. doi: 10.1016/j.asd.2008.07.005

Boyan, G., Williams, L., and Herbert, Z. (2010a). Multipotent neuroblasts generate a biochemical neuroarchitecture in the central complex of the grasshopper *Schistocerca gregaria*. *Cell Tissue Res.* 340, 13–28. doi: 10.1007/s00441-009-0922-7

Boyan, G. S., Williams, L., Legl, A., and Herbert, Z. (2010b). Proliferative cell types in embryonic lineages of the central complex of the grasshopper *Schistocerca gregaria*. *Cell Tissue Res.* 341, 259–277. doi: 10.1007/s00441-010-0992-6

Boyan, G., Williams, L., and Liu, Y. (2015). Conserved patterns of axogenesis in the panarthropod brain. *Arthropod Struct. Dev.* 44, 101–112. doi: 10.1016/j.asd.2014.11.003

Boyan, G. S., Williams, J. L. D., and Meier, T. (1993). Organization of the commissural fibers in the adult brain of the locust. *J. Comp. Neurol.* 332, 358–377. doi: 10.1002/cne.903320308

Chapman, R. F. (1982). *The Insects: Structure and Function.* London: Hodder and Stoughton.

Clynen, E., Husson, S. J., and Schoofs, L. (2009). Identification of new members of the (short) neuropeptide F family in locusts and *Caenorhabditis elegans*. *Ann. N Y Acad. Sci.* 1163, 60–74. doi: 10.1111/j.1749-6632.2008.03624.x

Condron, B. G. (1999). Serotonergic neurons transiently require a midline-derived FGF signal. *Neuron* 24, 531–540. doi: 10.1016/s0896-6273(00)81110-1

Cook, B. J., Holman, G. M., Wagner, R. M., and Nachman, R. J. (1989). Pharmacological actions of a new class of neuropeptides, the leucokinins I-IV, on the visceral muscles of *Leucophaea maderae*. *Comp. Biochem. Physiol. C* 93, 257–262. doi: 10.1016/0742-8413(89)90230-2

Dickson, B. J. (2002). Molecular mechanisms of axon guidance. *Science* 298, 1959–1964. doi: 10.1126/science.1072165

Diereck, H. A., and Greenspan, R. J. (2007). Serotonin and neuropeptide F have opposite modulatory effects on fly aggression. *Nat. Genet.* 39, 678–682. doi: 10.1038/ng2029

Dircksen, H., Skiebe, P., Abel, B., Agricola, H., Buchner, K., Muren, J. E., et al. (1999). Structure, distribution and biological activity of novel members of the allatostatin family in the crayfish *Orconectes limosus*. *Peptides* 20, 695–712. doi: 10.1016/s0196-9781(99)00052-2

Doe, C. Q. (2008). Neural stem cells: balancing self-renewal with differentiation. *Development* 135, 1575–1587. doi: 10.1242/dev.014977

Doe, C. Q., and Goodman, C. S. (1985a). Early events in insect neurogenesis. I. Development and segmental differences in the pattern of neuronal precursor cells. *Dev. Biol.* 111, 193–205. doi: 10.1016/0012-1606(85)90445-2

Doe, C. Q., and Goodman, C. S. (1985b). Early events in insect neurogenesis. II. The role of cell interactions and cell lineage in the determination of neuronal precursor cells. *Dev. Biol.* 111, 206–219. doi: 10.1016/0012-1606(85)90446-4

Duve, H., Audsley, N., Weaver, R. J., and Thorpe, A. (2000). Triple co-localisation of two types of allatostatin and an allatotropin in the frontal ganglion of the lepidopteran *Lacanobia oleracea* (Noctuidae): innervation and action on the foregut. *Cell Tissue Res.* 300, 153–163. doi: 10.1007/s004410050056

Eckert, M., Predel, R., and Gundel, M. (1999). Periviscerokinin-like immunoreactivity in the nervous system of the American cockroach. *Cell Tissue Res.* 295, 159–170. doi: 10.1007/s004410051222

Edwards, D. H., and Kravitz, E. A. (1997). Serotonin, social status and aggression. *Curr. Opin. Neurobiol.* 7, 812–819. doi: 10.1016/s0959-4388(97)80140-7

El Jundi, B., Heinze, S., Lenschow, C., Kurylas, A., Rohlfing, T., and Homberg, U. (2010). The locust standard brain: a 3D standard of the central complex as a platform for neural network analysis. *Front. Syst. Neurosci.* 3:21. doi: 10.3389/neuro.06.021.2009

Farris, S. M., and Sinakevitch, I. (2003). Development and evolution of the insect mushroom bodies: towards the understanding of conserved developmental mechanisms in a higher brain center. *Arthropod Struct. Dev.* 32, 79–101. doi: 10.1016/s1467-8039(03)00009-4

Filla, A., Hiripi, L., and Elekes, K. (2009). Role of aminergic (serotonin and dopamine) systems in the embryogenesis and different embryonic behaviors of the pond snail, *Lymnaea stagnalis*. *Comp. Biochem. Physiol. C Toxicol. Pharmacol.* 149, 73–82. doi: 10.1016/j.cbpc.2008.07.004

Gammie, S. C., and Truman, J. W. (1997). Neuropeptide hirarchies and the activation of sequential motor behaviors in the hawkmoth *Manduca sexta*. *J. Neurosci.* 17, 4389–4397.

Gaspar, P., Cases, O., and Maroteaux, L. (2003). The developmental role of serotonin: news from mouse molecular genetics. *Nat. Rev. Neurosci.* 4, 1002–1012. doi: 10.1038/nrn1256

Gibbs, S. M., and Truman, J. W. (1998). Nitric oxide and cyclic GMP regulate retinal patterning in the optic lobe of *Drosophila*. *Neuron* 20, 83–93. doi: 10.1016/s0896-6273(00)80436-5

Goodman, C. S., and Doe, C. Q. (1994). "Embryonic development of the *Drosophila* central nervous system," in *The Development of Drosophila* (Vol. 1), eds M. Bate and A. Martinez-Arias (New York, NY: Cold Spring Harbor Press), 1131–1206.

Goodman, C. S., O'Shea, M., McCaman, R., and Spitzer, N. C. (1979). Embryonic development of identified neurons: temporal pattern of morphological and biochemical differentiation. *Science* 204, 1219–1222. doi: 10.1126/science.36661

Goodman, C. S., Pearson, K. G., and Spitzer, N. C. (1980). Electrical excitability: a spectrum of properties in the progeny of a single embryonic neuroblast. *Proc. Natl. Acad. Sci. U S A* 77, 1676–1680. doi: 10.1073/pnas.77.3.1676

Hanesch, U., Fischbach, K.-F., and Heisenberg, M. (1989). Neuronal architecture of the central complex in *Drosophila melanogaster*. *Cell Tissue Res.* 257, 343–366. doi: 10.1007/BF00261838

Harley, C. M., and Ritzmann, R. E. (2010). Electrolytic lesions within central complex neuropils of the cockroach brain affect negotiation of barriers. *J. Exp. Biol.* 213, 2851–2864. doi: 10.1242/jeb.042499

Hayes, T. K., Pannabecker, T. L., Hinckley, D. J., Holman, G. M., Nachman, R. J., Petzel, D. H., et al. (1989). Leucokinins, a new family of ion stimulators and inhibitors in insect Malphigian tubules. *Life Sci.* 44, 1259–1266. doi: 10.1016/0024-3205(89)90362-7

Heinze, S., and Homberg, U. (2008). Neuroarchitecture of the central complex of the desert locust: intrinsic and columnar neurons. *J. Comp. Neurol.* 511, 454–478. doi: 10.1002/cne.21842

Herbert, Z., Rauser, S., Williams, L., Kapan, N., Güntner, M., Walch, A., et al. (2010). Developmental expression of neuromodulators in the central complex of the grasshopper *Schistocerca gregaria*. *J. Morphol.* 271, 1509–1526. doi: 10.1002/jmor.10895

Homberg, U. (1991). Neuroarchitecture of the central complex in the brain of the locust *Schistocerca gregaria and S. americana* as revealed by serotonin immunocytochemistry. *J. Comp. Neurol.* 303, 245–254. doi: 10.1002/cne.903030207

Homberg, U. (1985). Interneurons of the central complex in the bee brain *(Apis mellifera, L.)*. *J. Insect Physiol.* 31, 251–264. doi: 10.1016/0022-1910(85)90127-1

Homberg, U. (2002). Neurotransmitters and neuropeptides in the brain of the locust. *Microsc. Res. Tech.* 56, 189–209. doi: 10.1002/jemt.10024

Homberg, U., Heinze, S., Pfeiffer, K., Kinoshita, M., and El Jundi, B. (2011). Central neural coding of sky polarization in insects. *Philos. Trans. R. Soc. Lond. B Biol. Sci.* 366, 680–687. doi: 10.1098/rstb.2010.0199

Homberg, U., Vitzthum, H., Müller, M., and Binkle, U. (1999). Immunocytochemistry of GABA in the central complex of the locust *Schistocerca gregaria*: identification of immunoreactive neurons and colocalization with neuropeptides. *J. Comp. Neurol.* 409, 495–507. doi: 10.1002/(SICI)1096-9861(19990705)409:3<495::AID-CNE12>3.0.CO;2-F

Honegger, H.-W., Estévez-Lao, T. Y., and Hillyer, J. F. (2011). Bursicon-expressing neurons undergo apoptosis after adult ecdysis in the mosquito *Anopheles gambiae*. *J. Insect Physiol.* 57, 1017–1022. doi: 10.1016/j.jinsphys.2011.04.019

Huber, F. (1960). Untersuchungen über die Funktion des Zentralnervensystems und insbesondere des Gehirnes bei der Fortbewegung und der Lauterzeugung der Grillen. *Z. Vgl. Physiol.* 44, 60–132. doi: 10.1007/bf00297863

Ignell, R., Couillaud, F., and Anton, S. (2001). Juvenile-hormone-mediated plasticity of aggregation behaviour and olfactory processing in adult desert locusts. *J. Exp. Biol.* 204, 249–259.

Ilius, M., Wolf, R., and Heisenberg, M. (1994). The central complex of *Drosophila melanogaster* is involved in flight control: studies on mutants and mosaics of the gene ellipsoid body open. *J. Neurogenet.* 9, 189–206. doi: 10.3109/01677069409167279

Ito, K., and Awasaki, T. (2008). "Clonal unit architecture of the adult fly brain," in *Brain Development in Drosophila Melanogaster*, ed. G. M. Technau (New York, NY: Springer), 137–158.

Ito, K., Awano, W., Suzuki, K., Hiromi, Y., and Yamamoto, D. (1997). The *Drosophila* mushroom body is a quadruple structure of clonal units each of which contains a virtually identical set of neurones and glial cells. *Development* 124, 761–771.

Ito, K., Shinomiya, K., Ito, M., Armstrong, J. D., Boyan, G., Hartenstein, V., et al. (2014). A systematic nomenclature for the insect brain. *Neuron* 81, 755–765. doi: 10.1016/j.neuron.2013.12.017

Izergina, N., Balmer, J., Bello, B., and Reichert, H. (2009). Postembryonic development of transit amplifying neuroblast lineages in the *Drosophila* brain. *Neural Dev.* 4:44. doi: 10.1186/1749-8104-4-44

Johnson, O., Becnel, J., and Nichols, C. D. (2009). Serotonin 5-HT (2) and 5-HT (IA)-like receptors differentially modulate aggressive behaviors in *Drosophila melanogaster*. *Neuroscience* 158, 1292–1300. doi: 10.1016/j.neuroscience.2008.10.055

Kahsai, L., and Winther, A. M. E. (2011). Chemical neuroanatomy of the *Drosophila* central complex: distribution of multiple neuropeptides in relation to neurotransmitters. *J. Comp. Neurol.* 519, 290–315. doi: 10.1002/cne.22520

Keshishian, H., and O'Shea, M. (1985). The acquisition and expression of a peptidergic phenotype in the grasshopper embryo. *J. Neurosci.* 5, 1005–1015.

Kloppenburg, P., Ferns, D., and Mercer, A. R. (1999). Serotonin enhances central olfactory neuron responses to female sex pheromone in the male sphinx moth *Manduca sexta*. *J. Neurosci.* 19, 8172–8181.

Koniszewski, N. D. B., Kollmann, M., Bigham, M., Farnworth, M., He, B., Büscher, M., et al. (2016). The insect central complex as model for heterochronic brain development—background, concepts and tools. *Dev. Genes Evol.* 226, 209–219. doi: 10.1007/s00427-016-0542-7

Kreissl, S., Weiss, T., Djokaj, S., Balezinam, O., and Rathmayer, W. (1999). Allatostatin modulates skeletal muscle performance in crustaceans through pre- and postsynaptic effects. *Eur. J. Neurosci.* 11, 2519–2530. doi: 10.1046/j.1460-9568.1999.00674.x

Kunst, M., Pförtner, R., Aschenbrenner, K., and Heinrich, R. (2011). Neurochemical architecture of the central complex related to its function in the control of grasshopper acoustic communication. *PLoS One* 6:e25613. doi: 10.1371/journal.pone.0025613

Kurylas, A. E., Ott, S. R., Schachtner, J., Elphick, M. R., Williams, L., and Homberg, U. (2005). Localization of nitric oxide synthase in the central complex and surrounding midbrain neuropils of the locust *Schistocerca gregaria*. *J. Comp. Neurol.* 484, 206–223. doi: 10.1002/cne.20467

Kuzin, B., Roberts, I., Peunova, N., and Enikolopov, G. (1996). Nitric oxide regulates cell proliferation during *Drosophila* development. *Cell* 87, 639–649. doi: 10.1016/s0092-8674(00)81384-7

Lai, S. L., Awasaki, T., Ito, K., and Lee, T. (2008). Clonal analysis of *Drosophila* antennal lobe neurons: diverse neuronal architectures in the lateral neuroblast lineage. *Development* 135, 2883–2893. doi: 10.1242/dev.024380

Lee, T., and Luo, L. (2001). Mosaic analysis with a repressible cell marker (MARCM) for *Drosophila* neural development. *Trends Neurosci.* 24, 251–254. doi: 10.1016/s0166-2236(00)01791-4

Leise, E. M. (1990). Modular construction of nervous systems: a basic principle of design for invertebrates and vertebrates. *Brain Res. Brain Res. Rev.* 15, 1–23. doi: 10.1016/0165-0173(90)90009-d

Levine, R. B. (1984). Changes in neuronal circuits during insect metamorphosis. *J. Exp. Biol.* 112, 27–44.

Liu, Y., and Boyan, G. (2013). Glia associated with central complex lineages in the embryonic brain of the grasshopper *Schistocerca gregaria*. *Dev. Genes Evol.* 223, 213–223. doi: 10.1007/s00427-013-0439-7

Liu, G., Seiler, H., Wen, A., Zars, T., Ito, K., Wolf, M., et al. (2006). Distinct memory traces for two visual features in the *Drosophila* brain. *Nature* 439, 551–556. doi: 10.1038/nature04381

Marder, E. (1999). Neural signalling: does colocalisation imply co-transmission? *Curr. Biol.* 9, R809–R811. doi: 10.1016/s0960-9822(99)80496-5

Martin, J. R., Raabe, T., and Heisenberg, M. (1999). Central complex substructures are required for the maintenance of locomotor activity in *Drosophila melanogaster*. *J. Comp. Physiol. A* 185, 277–288. doi: 10.1007/s003590050387

Meinertzhagen, I. A., Emsley, J. G., and Sun, X. J. (1998). Developmental anatomy of the *Drosophila* brain: neuroanatomy is gene expression. *J. Comp. Neurol.* 402, 1–9. doi: 10.1002/(SICI)1096-9861(19981207)402:1<1::AID-CNE1>3.0.CO;2-Q

Mizunami, M., Iwasaki, M., Nishikawa, M., and Okada, R. (1997). Modular structures in the mushroom body of the cockroach. *Neurosci. Lett.* 229, 153–156. doi: 10.1016/s0304-3940(97)00438-2

Müller, M., Homberg, U., and Kühn, A. (1997). Neuroarchitecture of the lower division of the central body in the brain of the locust (*Schistocerca gregaria*). *Cell Tissue Res.* 288, 159–176. doi: 10.1007/s004410050803

Nässel, D. R. (2002). Neuropeptides in the nervous system of *Drosophila* and other insects: multiple roles as neuromodulators and neurohormones. *Prog. Neurobiol.* 68, 1–84. doi: 10.1016/s0301-0082(02)00057-6

Nässel, D. R., and Winther, A. M. (2002). Neuronal co-localization of different isoforms of tachykinin-related peptides (LemTRPs) in the cockroach brain. *Cell Tissue Res.* 308, 225–239. doi: 10.1007/s00441-002-0538-7

Neuser, K., Triphan, T., Mronz, M., Poeck, B., and Strauss, R. (2008). Analysis of a spatial orientation memory in *Drosophila*. *Nature* 453, 1244–1247. doi: 10.1038/nature07003

O'Shea, M., and Adams, M. (1986). Proctolin: from "gut factor" to model neuropeptide. *Adv. Insect Physiol.* 19, 1–28. doi: 10.1016/s0065-2806(08)60099-5

O'Shea, M., Colbert, R., Williams, L., and Dunn, S. (1998). Nitric oxide compartments in the mushroom bodies of the locust brain. *Neuroreport* 9, 333–336. doi: 10.1097/00001756-199801260-00028

Pan, Y., Zhou, Y., Guo, C., Gong, H., Gong, Z., and Liu, L. (2009). Differential roles of the fan-shaped body and the ellipsoid body in *Drosophila* visual pattern memory. *Learn. Mem.* 16, 289–295. doi: 10.1101/lm.1331809

Pearson, B. J., and Doe, C. Q. (2003). Regulation of neuroblast competence in *Drosophila*. *Nature* 425, 624–628. doi: 10.1038/nature01910

Peeff, N. M., Orchard, I., and Lange, A. B. (1994). Isolation, sequence and bioactivity of PDVDHVFLRFamide and ADVGHVFLRFamide peptides from the locust central nervous system. *Peptides* 15, 387–392. doi: 10.1016/0196-9781(94)90193-7

Pfeiffer, K., and Homberg, U. (2014). Organization and functional roles of the central complex in the insect brain. *Annu. Rev. Entomol.* 59, 165–184. doi: 10.1146/annurev-ento-011613-162031

Predel, R., Herbert, Z., and Eckert, M. (2003). Neuropeptides in perisympathetic organs of *Manduca sexta*: specific composition and changes during the development. *Peptides* 24, 1457–1464. doi: 10.1016/j.peptides.2003.07.020

Predel, R., and Wegener, C. (2006). Biology of the CAPA peptides in insects. *Cell Mol. Life Sci.* 63, 2477–2490. doi: 10.1007/s00018-006-6187-3

Rankin, S. M., Stay, B., Chan, K., and Jackson, E. S. (1998). Cockroach allatostatin-immunoreactive neurons and effects of cockroach allatostatin in earwigs. *Arch. Insect Biochem. Physiol.* 38, 155–165. doi: 10.1002/(SICI)1520-6327(1998)38:4<155::AID-ARCH1>3.0.CO;2-Q

Rehm, K. J., Deeg, K. E., and Marder, E. (2008). Developmental regulation of neuromodulator function in the stomatogastric ganglion of the lobster, *Homarus americanus*. *J. Neurosci.* 28, 9828–9839. doi: 10.1523/JNEUROSCI.2328-08.2008

Reichert, H., and Boyan, G. S. (1997). Building a brain: insights from insects. *Trends Neurosci.* 20, 258–264. doi: 10.1016/s0166-2236(96)01034-x

Renn, S. C. N., Armstrong, J. D., Yang, M., Wang, Z., An, X., Kaiser, K., et al. (1999). Genetic analysis of the *Drosophila* ellipsoid body neuropil: organization and development of the central complex. *J. Neurobiol.* 41, 189–207. doi: 10.1002/(SICI)1097-4695(19991105)41:2<189::AID-NEU3>3.0.CO;2-Q

Richards, K. S., Simon, D. J., Pulver, S. R., Beltz, B. S., and Marder, E. (2003). Serotonin in the developing stomatogastric system of the lobster, *Homarus americanus*. *J. Neurobiol.* 54, 380–392. doi: 10.1002/neu.10136

Riebli, N., Viktorin, G., and Reichert, H. (2013). Early-born neurons in type II neuroblast lineages establish a larval primordium and integrate into adult circuitry during central complex development in *Drosophila*. *Neural Dev.* 8:6. doi: 10.1186/1749-8104-8-6

Robb, S., and Evans, P. D. (1990). FMRFamide-like peptides in the locust: distribution, partial characterization and bioactivity. *J. Exp. Biol.* 149, 335–360.

Roeder, T. (2002). Biochemistry and molecular biology of receptors for biogenic amines in locusts. *Microsc. Res. Tech.* 56, 237–247. doi: 10.1002/jemt.10027

Rogers, S. M., Matheson, T., Sasaki, K., Kendrick, K., Simpson, S. J., and Burrows, M. (2004). Substantial changes in central nervous system neurotransmitters and neuromodulators accompany phase change in the locust. *J. Exp. Biol.* 207, 3603–3617. doi: 10.1242/jeb.01183

Romeuf, M., and Rémy, C. (1984). Early immunohistochemical detection of somatostatin-like and methionine-enkephalin-like neuropeptides in the brain of the migratory locust embryo. *Cell Tissue Res.* 236, 289–292. doi: 10.1007/bf00214229

Saifulla, A. S. M., and Tomioka, K. (2002). Serotonin sets the day state in the neurons that control coupling between the optic lobe circadian pacemakers in the cricket *Gryllus bimaculatus*. *J. Exp. Biol.* 205, 1305–1314.

Satake, H., Kawada, T., Nomoto, K., and Minakata, H. (2003). Insight into tachykinin-related peptides, their receptors and invertebrate tachykinins: a review. *Zoolog. Sci.* 20, 533–549. doi: 10.2108/zsj.20.533

Schoofs, L., Janssen, I., Veelaert, D., Vanden Broeck, J., Tobe, S. S., and De Loof, A. (1998). Ecdysiostatins and allatostatins in *Schistocerca gregaria*. *Proc. Ann. N Y Acad. Sci.* 15, 301–305. doi: 10.1111/j.1749-6632.1998.tb10780.x

Seidel, C., and Bicker, G. (1996). The developmental expression of serotonin-immunoreactivity in the brain of the pupal honeybee. *Tissue Cell* 28, 663–672. doi: 10.1016/s0040-8166(96)80070-x

Seidel, C., and Bicker, G. (2000). Nitric oxide and cGMP influence axogenesis of antennal pioneer neurons. *Development* 127, 4541–4549.

Seidel, C., and Bicker, G. (2002). Developmental expression of nitric oxide/cyclic GMP signaling pathways in the brain of the embryonic grasshopper. *Brain Res. Dev. Brain Res.* 138, 71–79. doi: 10.1016/s0165-3806(02)00466-2

Severini, C., Improta, G., Falconieri-Erspamer, G., Salvadori, S., and Erspamer, V. (2002). The tachykinin peptide family. *Pharmacol. Rev.* 54, 285–322. doi: 10.1124/pr.54.2.285

Siegl, T., Schachtner, J., Holstein, G. R., and Homberg, U. (2009). NO/cGMP signalling: L-citrulline and cGMP immunostaining in the central complex of the desert locust *Schistocerca gregaria*. *Cell Tissue Res.* 337, 327–340. doi: 10.1007/s00441-009-0820-z

Sitaraman, D., Zars, M., Laferriere, H., Chen, Y. C., Sable-Smith, A., Kitamoto, T., et al. (2008). Serotonin is necessary for place memory in *Drosophila*. *Proc. Natl. Acad. Sci. U S A* 105, 5579–5584. doi: 10.1073/pnas.0710168105

Stern, M., Knipp, S., and Bicker, G. (2007). Embryonic differentiation of 5HT-containing neurons in the enteric nervous system of the locust (*Locusta migratoria*). *J. Comp. Neurol.* 501, 38–51. doi: 10.1002/cne.21235

Stevenson, P. A., and Kutsch, W. (1986). Basic circuitry of an adult-specific motor program completed with embryogenesis. *Naturwissenschaften* 73, 741–743. doi: 10.1007/bf00399248

Strausfeld, N. J. (1976). *Atlas of an Insect Brain.* Berlin, Heidelberg, New York, NY: Springer.

Strausfeld, N. J. (1999). A brain region in insects that supervises walking. *Prog. Brain Res.* 123, 273–284. doi: 10.1016/s0079-6123(08)62863-0

Strausfeld, N. J. (2012). *Arthropod Brains*. Cambridge, MA: Harvard Univ. Press.

Strauss, R. (2002). The central complex and the genetic dissection of locomotor behaviour. *Curr. Opin. Neurobiol.* 12, 633–638. doi: 10.1016/s0959-4388(02)00385-9

Strauss, R., Hanesch, U., Kinkelin, M., Wolf, R., and Heisenberg, M. (1992). *No-bridge of Drosophila melanogaster*: portrait of a structural brain mutant of the central complex. *J. Neurogenet.* 8, 125–155. doi: 10.3109/01677069209083444

Strauss, R., and Heisenberg, M. (1993). A higher control center of locomotor behavior in the *Drosophila* brain. *J. Neurosci.* 13, 1852–1861.

Sykes, P. A., and Condron, B. G. (2005). Development and sensitivity to serotonin of *Drosophila* serotonergic varicosities in the central nervous system. *Dev. Biol.* 286, 207–216. doi: 10.1016/j.ydbio.2005.07.025

Taghert, P. H., and Goodman, C. S. (1984). Cell determination and differentiation of identified serotonin-immunoreactive neurons in the grasshopper embryo. *J. Neurosci.* 4, 989–1000.

Taghert, P. H., and Truman, J. W. (1982a). The distribution and molecular characteristics of the tanning hormone, bursicon, in the tobacco hornmoth, *Manduca sexta*. *J. Exp. Biol.* 98, 373–383.

Taghert, P. H., and Truman, J. W. (1982b). Identification of the bursicon-containing neurons in abdominal ganglia of the tobacco hornworm moth, *Manduca sexta*. *J. Exp. Biol.* 98, 385–401.

Tettamanti, M., Armstrong, J. D., Endo, K., Yang, M. Y., Furukubo-Tokunaga, K., Kaiser, K., et al. (1997). Early development of the *Drosophila* mushroom bodies, brain centres for associative learning and memory. *Dev. Genes Evol.* 207, 242–252. doi: 10.1007/s004270050112

Thompson, K. S. J., Rayne, R. C., Gibbon, C. R., May, S. T., Patel, M., Coast, G. M., et al. (1995). Cellular colocalization of diuretic peptides in locusts: a potent control mechanism. *Peptides* 16, 95–104. doi: 10.1016/0196-9781(94)00158-3

Thompson, K. S. J., and Siegler, M. V. S. (1991). Anatomy and physiology of spiking local and intersegmental interneurons in the median neuroblast lineage of the grasshopper. *J. Comp. Neurol.* 305, 659–675. doi: 10.1002/cne.903050409

Tomer, R., Denes, A. S., Tessmar-Raible, K., and Arendt, D. (2010). Profiling by image registration reveals common origin of Annelid mushroom bodies and vertebrate pallium. *Cell* 142, 800–809. doi: 10.1016/j.cell.2010.07.043

Triphan, T., Poeck, B., Neuser, K., and Strauss, R. (2010). Visual targeting of motor actions in climbing *Drosophila*. *Curr. Biol.* 20, 663–668. doi: 10.1016/j.cub.2010.02.055

Truman, J. W., De Vente, J., and Ball, E. E. (1996a). Nitric oxide-sensitive guanylate cyclase activity is asociated with the maturational phase of neuronal development in insects. *Development* 122, 3949–3958.

Truman, J. W., Ewer, J., and Ball, E. E. (1996b). Dynamics of cyclic GMP levels in identified neurones during ecdysis behaviour in the locust *Locusta migratoria*. *J. Exp. Biol.* 199, 749–758.

Turlejski, K. (1996). Evolutionary ancient roles of serotonin: long-lasting regulation of activity and development. *Acta Neurobiol. Expt. (Wars)* 56, 619–636.

Urbach, R., and Technau, G. M. (2003). Early steps in building the insect brain: neuroblast formation and segmental patterning in the developing brain of different insect species. *Arthropod Struct. Dev.* 32, 103–123. doi: 10.1016/s1467-8039(03)00042-2

Vitalis, T., Cases, O., Passemard, S., Callebert, J., and Parnavelas, J. G. (2007). Embryonic depletion of serotonin affects cortical development. *Eur. J. Neurosci.* 26, 331–344. doi: 10.1111/j.1460-9568.2007.05661.x

Vitzthum, H., and Homberg, U. (1998). Immunocytochemical demonstration of locustatachykinin-related peptides in the central complex of the locust brain. *J. Comp. Neurol.* 390, 455–469. doi: 10.1002/(SICI)1096-9861(19980126)390:4<455::AID-CNE1>3.0.CO;2-#

Vitzthum, H., Homberg, U., and Agricola, H. (1996). Distribution of Dip-allatostatin I-like immunoreactivity in the brain of the locust *Schistocerca gregaria* with detailed analysis of immunostaining in the central complex. *J. Comp. Neurol.* 369, 419–437. doi: 10.1002/(SICI)1096-9861(19960603)369:3<419::AID-CNE7>3.0.CO;2-8

Wegerhoff, R., and Breidbach, O. (1992). Structure and development of the larval central complex in a holometabolous insect, the beetle *Tenebrio molitor*. *Cell Tissue Res.* 268, 341–358. doi: 10.1007/bf00318803

Wegerhoff, R., Breidbach, O., and Lobemeier, M. (1996). Development of locustatachykinin immunopositive neurons in the central complex of the beetle *Tenebrio molitor*. *J. Comp. Neurol.* 375, 157–166. doi: 10.1002/(SICI)1096-9861(19961104)375:1<157::AID-CNE10>3.0.CO;2-S

Wehner, R. (1989). Neurobiology of polarization vision. *Trends Neurosci.* 12, 353–359. doi: 10.1016/0166-2236(89)90043-x

Weir, P. T., and Dickinson, M. H. (2012). Flying *Drosophila* orient to sky polarization. *Curr. Biol.* 22, 21–27. doi: 10.1016/j.cub.2011.11.026

Westbrook, A. L., and Bollenbacher, W. E. (1990). The development of identified neurosecretory cells in the tobacco hornworm, *Manduca sexta*. *Dev. Biol.* 140, 291–299. doi: 10.1016/0012-1606(90)90079-x

Williams, J. L. D. (1975). Anatomical studies of the insect central nervous system: a ground-plan of the midbrain and an introduction to the central complex in the locust, *Schistocerca gregaria* (Orthoptera). *J. Zool. Lond.* 176, 67–86.doi: 10.1111/j.1469-7998.1975.tb03188.x

Williams, J. L., and Boyan, G. S. (2008). Building the central complex of the grasshopper *Schistocerca gregaria*: axons pioneering the w, x, y, z tracts project onto the primary commissural fascicle of the brain. *Arthr. Struct. Dev.* 37, 129–140. doi: 10.1016/j.asd.2007.05.005

Williams, J. L. D., Güntner, M., and Boyan, G. S. (2005). Building the central complex of the grasshopper *Schistocerca gregaria*: temporal topology organizes the neuroarchitecture of the w, x, y, z tracts. *Arthr. Struct. Dev.* 34, 97–110. doi: 10.1016/j.asd.2004.11.001

Winther, A. M., Acebes, A., and Ferrus, A. (2006). Tachykinin-related peptides modulate odor perception and locomotor activity in Drosophila. *Mol. Cell. Neurosci.* 31, 399–406. doi: 10.1016/j.mcn.2005.10.010

Wolff, T., Iyer, N. A., and Rubin, G. M. (2015). Neuroarchitecture and neuroanatomy of the *Drosophila* central complex: a GAL4-based dissection of protocerebral bridge neurons and circuits. *J. Comp. Neurol.* 523, 997–1037. doi: 10.1002/cne.23705

Wong-Riley, M. T., and Liu, Q. (2005). Neurochemical development of brain stem nuclei involved in the control of respiration. *Respir. Physiol. Neurobiol.* 149, 83–98. doi: 10.1016/j.resp.2005.01.011

Young, J. M., and Armstrong, J. D. (2010a). Structure of the adult central complex in *Drosophila*: organization of distinct neuronal subsets. *J. Comp. Neurol.* 518, 1500–1524. doi: 10.1002/cne.22284

Young, J. M., and Armstrong, J. D. (2010b). Building the central complex in *Drosophila*: the generation and development of distinct subsets. *J. Comp. Neurol.* 518, 1525–1541. doi: 10.1002/cne.22285

Yuan, Q., Lin, F., Zheng, X., and Sehgal, A. (2005). Serotonin modulates circadian entrainment in *Drosophila*. *Neuron* 47, 115–127. doi: 10.1016/j.neuron.2005.break05.027

Zacharias, D., Williams, J. L. D., Meier, T., and Reichert, H. (1993). Neurogenesis in the insect brain: cellular identification and molecular characterization of brain neuroblasts in the grasshopper embryo. *Development* 118, 941–955.

Zars, T. (2009). Spatial orientation in *Drosophila*. *J. Neurogenet.* 23, 104–110. doi: 10.1080/01677060802441364

Zitnan, D., Ross, L. S., Zitnanova, I., Hermesman, J. L., Gill, S. S., and Adams, M. (1999). Steroid induction of peptide hormone gene leads to orchestration of a defined behavioral sequence. *Neuron* 23, 523–535. doi: 10.1016/s0896-6273(00)80805-3

Conflict of Interest Statement: The authors declare that the research was conducted in the absence of any commercial or financial relationships that could be construed as a potential conflict of interest.

frontiers in Behavioral Neuroscience

ORIGINAL RESEARCH
published: 04 September 2017
doi: 10.3389/fnbeh.2017.00158

Comparison of Navigation-Related Brain Regions in Migratory versus Non-Migratory Noctuid Moths

*Liv de Vries[1], Keram Pfeiffer[2], Björn Trebels[2], Andrea K. Adden[1], Ken Green[3], Eric Warrant[1] and Stanley Heinze[1]**

[1]Lund Vision Group, Department of Biology, Lund University, Lund, Sweden, [2]Department of Biology, Marburg University, Marburg, Germany, [3]New South Wales National Parks and Wildlife Service, Jindabyne, NSW, Australia

Brain structure and function are tightly correlated across all animals. While these relations are ultimately manifestations of differently wired neurons, many changes in neural circuit architecture lead to larger-scale alterations visible already at the level of brain regions. Locating such differences has served as a beacon for identifying brain areas that are strongly associated with the ecological needs of a species—thus guiding the way towards more detailed investigations of how brains underlie species-specific behaviors. Particularly in relation to sensory requirements, volume-differences in neural tissue between closely related species reflect evolutionary investments that correspond to sensory abilities. Likewise, memory-demands imposed by lifestyle have revealed similar adaptations in regions associated with learning. Whether this is also the case for species that differ in their navigational strategy is currently unknown. While the brain regions associated with navigational control in insects have been identified (central complex (CX), lateral complex (LX) and anterior optic tubercles (AOTU)), it remains unknown in what way evolutionary investments have been made to accommodate particularly demanding navigational strategies. We have thus generated average-shape atlases of navigation-related brain regions of a migratory and a non-migratory noctuid moth and used volumetric analysis to identify differences. We further compared the results to identical data from Monarch butterflies. Whereas we found differences in the size of the nodular unit of the AOTU, the LX and the protocerebral bridge (PB) between the two moths, these did not unambiguously reflect migratory behavior across all three species. We conclude that navigational strategy, at least in the case of long-distance migration in lepidopteran insects, is not easily deductible from overall neuropil anatomy. This suggests that the adaptations needed to ensure successful migratory behavior are found in the detailed wiring characteristics of the neural circuits underlying navigation—differences that are only accessible through detailed physiological and ultrastructural investigations. The presented results aid this task in two ways. First, the identified differences in neuropil volumes serve as promising initial targets for electrophysiology. Second, the new standard atlases provide an anatomical reference frame for embedding all functional data obtained from the brains of the Bogong and the Turnip moth.

Keywords: central complex, Bogong moth, standard brain, 3D-neuroanatomy, migration, navigation, insect brain

OPEN ACCESS

Edited by:
Martin Giurfa, UMR5169 Centre de Recherches sur la Cognition Animale (CRCA), France

Reviewed by:
Theo Mota, Universidade Federal de Minas Gerais, Brazil
Stephen Hugh Montgomery, University College London, United Kingdom
Daniel Tomsic, University of Buenos Aires, Argentina

****Correspondence:***
Stanley Heinze
stanley.heinze@biol.lu.se

Received: *05 May 2017*
Accepted: *15 August 2017*
Published: *04 September 2017*

Citation:
de Vries L, Pfeiffer K, Trebels B, Adden AK, Green K, Warrant E and Heinze S (2017) Comparison of Navigation-Related Brain Regions in Migratory versus Non-Migratory Noctuid Moths. Front. Behav. Neurosci. 11:158. doi: 10.3389/fnbeh.2017.00158

INTRODUCTION

Every brain is optimized to generate the behavior required for an animal's survival. As neural tissue is energetically extremely costly, brains have evolved to extract required sensory information in the most economical way, while at the same time guiding behaviors as efficiently as possible (Laughlin, 2001; Niven and Laughlin, 2008). Through evolution, neural circuits have thus been adapted to match each species' ecological niche, i.e., the combination of behavioral strategy and sensory environment. Uncovering the ways these adaptations have been achieved in different animals will provide major insights into the functional outline of brains in general. While circuit adaptations to sensory requirements have been documented in several species (e.g., el Jundi et al., 2015; Stöckl et al., 2016b), the questions of how behavioral strategies are manifested in the neuroarchitecture of brains remains largely unanswered.

As neural circuits consist of thousands of neurons and span multiple brain regions, it is difficult to examine them directly and in full detail across many animals, even when focusing on the comparably simple brains of insects. In order to pinpoint promising regions of the brain in which species show differential investment in neural tissue, volumes of brain regions have served as a beacon (e.g., Gronenberg and Hölldobler, 1999; Kondoh et al., 2003; Ott and Rogers, 2010; O'Donnell et al., 2013). Volumetric analysis between closely related species inhabiting different environments has indeed revealed that the sensory abilities of an animal are reflected in the amount of neural tissue devoted to the processing of the dominant sensory cues which drive its behavior (Gronenberg and Hölldobler, 1999; Stöckl et al., 2016a; Immonen et al., 2017). For instance, nocturnal hawkmoths invest more in olfactory brain areas in comparison to diurnal hawkmoths, which invest more heavily in visual processing (Stöckl et al., 2016a). Such tradeoffs between enlarging important brain regions at the expense of regions not needed to the same degree are found even in higher order brain areas as long as they could be linked to processing information from a single sensory modality (Gronenberg and Hölldobler, 1999; Gronenberg et al., 2008; Stöckl et al., 2016a). Besides the finding that differences in neuropil volumes can indicate innate functional differences between species, volume changes due to plasticity within species can also hint at underlying functions. For instance, foraging bees have significantly larger mushroom bodies compared to non-foraging nursing bees of the same age (Farris et al., 2001; Fahrbach, 2006; Riveros and Gronenberg, 2010), a change that in honeybees can be attributed to the greater demands imposed on long-term memory while foraging in a rich visual environment (Gronenberg and Couvillon, 2010). This finding was confirmed in butterflies, where wild-caught individuals possessed a massively enlarged mushroom body compared to individuals raised in captivity (Montgomery et al., 2016). Recently, the overall volumetric changes in honeybee mushroom bodies were linked to distinct changes in the fine-structure of specific synapses (Groh et al., 2012), suggesting direct functional relevance for memory processes. Whereas not all small-scale structural changes translate into larger volume differences (Hourcade et al., 2010), this example shows that volumetric analysis of brain areas can indeed deliver a meaningful starting point for highlighting regions of interest for closer examination. Although such links have been revealed in sensory information processing and memory circuits, it has remained unclear whether similar effects can be found with respect to behavioral control mechanisms, e.g., navigational strategies. Are specific, elaborate navigation behaviors reflected in the structure of the brain regions that control them?

To address this question, we have investigated the brains of two species of closely related, nocturnal moths, the Australian Bogong moth (*Agrotis infusa*) and the Turnip moth (*A. segetum*). The Bogong moth is a long-distance migrant (Heinze and Warrant, 2016; Warrant et al., 2016), while the Turnip moth is an opportunistic, agricultural pest species without clear seasonal migrations (Esbjerg and Sigsgaard, 2014). Although short distance seasonal movements (40–60 km) matching prevailing winds have been reported for this species in China (Guo et al., 2015), Turnip moths do not show reproductive diapause, a hallmark of most truly migratory insects (oogenesis-flight syndrome; Dingle, 1972; Zhan et al., 2011; Guo et al., 2015). In contrast, the Bogong moth's migrations are reminiscent of the famous Monarch butterfly, a species that performs spectacular yearly migrations across North America, albeit during the day (Merlin et al., 2012; Guerra and Reppert, 2015; Reppert et al., 2016). Each spring an estimated 2 billion moths migrate over 1000 km from their breeding grounds in various regions of southeast Australia to the alpine regions of the Australian Alps, where they locate specific caves for spending the summer (Warrant et al., 2016). In the cool and constant climate of these alpine caves they enter a dormant state (called aestivation) for 3–4 months, after which, at the beginning of the autumn, they carry out the long return trip to their breeding grounds to mate, reproduce and die (Warrant et al., 2016). Unlike diurnal migrants, these moths cannot use the sun and other sun-derived sky-compass cues during their nocturnal migratory flights, but instead rely on an unknown combination of nocturnal visual and, possibly, magnetic-field based compass cues (Heinze and Warrant, 2016; Warrant et al., 2016).

The regions of the insect brain that have been generally implicated in processing compass stimuli and controlling migratory behavior have collectively been called the "compass neuropils" in the Monarch butterfly (Heinze et al., 2013) and comprise the central complex (CX), the lateral complex (LX) and the anterior optic tubercles (AOTU; Heinze and Reppert, 2012; Heinze et al., 2013; Pfeiffer and Homberg, 2014). These regions are highly conserved across all insects (Homberg, 2008; Ito et al., 2014; Immonen et al., 2017) and likely play a major role in all orientation behaviors, carrying out multiple computational steps from sensory integration to generation of premotor commands (Heinze and Homberg, 2007; Seelig and Jayaraman, 2013, 2015; Martin et al., 2015; Namiki and Kanzaki, 2016a,b).

In the work presented here, we generated an average-shape atlas of these regions and used volumetric analysis

to identify potential differences in their layout between the migratory and non-migratory moths. We further compared the results to identical data from Monarch butterflies (Heinze et al., 2013). Whereas we found differences in the size of the nodular unit of the AOTU, the PB, as well as in parts of the LX between the two moths, these did not reflect migratory behavior across all three species. We conclude that the phylogenetic relationship is clearly the biggest predictor of brain anatomy and that navigational strategy, at least in the case of long-distance migration in lepidopteran insects, is not easily deductible from anatomical features at the level of neuropils.

MATERIALS AND METHODS

Animals

Australian Bogong moths (*Agrotis infusa*) were collected either in early January or in late October (2013–2015) from caves near the peak of South Ramshead mountain, in Kosciuszko National Park, NSW, Australia. The moths had already undergone their forward spring migration and were in an aestivating state when captured. They were brought to Lund, Sweden and kept in the aestivating state in an artificial cave environment, set to temperatures of 6°C at night and 10°C during the day under long-day conditions (16 h, dim illumination:8 h, dark). Diluted honey solution (10 g honey, 10 g sucrose, in 1 l of water) was provided as food *ad libitum*. The animals used were dissected within 5 months of capture.

Turnip moths (*Agrotis segetum*) were bred in captivity at Lund University at 21°C (13 h, light:11 h, dark). The moths used were from populations from the years 2013 to 2016. Twelve moths of each species were used for reconstruction and standardization. Both female and male individuals of Bogong moths were used, while for Turnip moths we used only male individuals.

Raw data from Monarch butterflies was published by Heinze et al. (2013) and was reanalyzed in the current article to enable direct comparisons to the moth species.

Immunocytochemistry

The moth brains were dissected out of the head capsule in fixative (1% formaldehyde/zinc-chloride in Hepes-buffered saline (HBS; Ott, 2008)) and fixed overnight at 4°C. The brains were then subjected to rinses (8 × 20 min) in HBS, during which tracheae and the retinae were removed. The Bogong moth brains were then bleached with 10% H_2O_2 in Tris/HCl buffer for 6 h (Stöckl and Heinze, 2015) while *A. segetum* brains were bleached in 1% H_2O_2 in Tris/HCl buffer, exchanged every hour for 6 h. Following a wash in Tris/HCl buffer (3 × 10 min) the brains were incubated in a fresh mixture of methanol and dimethylsulfoxide solution (DMSO, 80:20; Bogong moths: 70 min, Turnip moths: 85 min; Ott, 2008). After an additional Tris/HCl buffer wash (3 × 10 min) the brains were pre-incubated with 5% normal goat serum (NGS) in 0.01 M phosphate-buffered saline (PBS), containing 0.3% TritonX-100 (PBT), overnight at 4°C. For visualization of neuropils, they were subsequently incubated with mouse derived primary antibodies against the presynaptic vesicle protein synapsin (Klagges et al., 1996; 1:25 in 0.01 M PBT containing 1% NGS for 5–6 days in 4°C). Following extensive washing in PBT (8 × 20 min) the brains were incubated with Cy5-conjugated secondary antibody (goat anti-mouse; 1:300 in 0.01 M PBT with 1% NGS for 5 days in 4°C). After rinsing in 0.01 M PBT (6 × 30 min) and 0.1 M PBS (2 × 30 min) the samples were dehydrated with an ascending ethanol series (50%, 70%, 90%, 95%, 2 × 100%, 15 min each). Thereafter, the preparations were transferred to a fresh mixture of methyl salicylate and ethanol (1:1) for 15 min, followed by pure methyl salicylate for a minimum of 60 min. Finally, the brains were embedded in Permount between two coverslips, using a stack of plastic spacers to avoid compression.

Intracellular Dye Injections

Neurons were injected with neurobiotin in the context of intracellular recordings (performed according to standard methods, for details see e.g., Heinze and Reppert, 2011). We used glass microelectrodes of 50–150 MΩ resistance that were filled with 4% Neurobiotin solution (in 1 M KCl), backed up with 1 M KCl. After impaling a cell, a positive current (1–3 nA, for 1–3 min) was applied to the electrode in order to iontophoretically eject neurobiotin molecules from the electrode tip. The brain was dissected out of the head capsule, and fixed in neurobiotin fixative (4% paraformaldehyde, 0.25% glutaraldehyde, 2% saturated picric acid, in 0.01 M PBS) overnight at 4°C. Brains were then rinsed 4 × 15 min with 0.1 M PBS and incubated with Cy3-conjugated streptavidin (1:1000, in 0.01 M PBT) for 3 days at 4°C. Brains were then washed 4 × 20 min in PBT and 2 × 20 min in PBS, after which they were dehydrated in an ethanol series of increasing concentrations, cleared in methyl salicylate, and mounted between two coverslips using Permount (details identical as for immunohistochemistry).

Image Acquisition

We imaged the labeled samples using a confocal laser scanning microscope (Zeiss LSM 510) equipped with a 25× long distance objective (LD LCI Plan-Apochromat 25×/0.8 Imm Corr DIC; Zeiss) with either the 633 nm laser line (Cy5-labels) or with the 561 nm laser line (Cy3-labels). To cover the entire region of interest, 2–3 contiguous image-stacks had to be acquired per brain. To minimize photo-bleaching and to maximize scanning efficiency, anti-synapsin-labeled samples were imaged at a resolution close to the final desired voxel-size of 1 × 1 × 1 μm: 512 × 512 pixels per stack in *x-y* direction (voxel-size: 0.99 × 0.99 μm) and 1.03 μm in *z* direction, using bidirectional scanning. Injected neurons were imaged at a voxel size of 0.29 × 0.29 × 0.89 μm using the same objective.

Image Processing and 3D Reconstruction

The image stacks for each sample were aligned, merged and resampled to a voxel size of 1 × 1 × 1 μm using the software Fiji or Amira 5.3. These image data were then used as raw data for semi-manual image segmentation. Hereby we first created a label field, in Amira 5.3, in which voxels were assigned a

neuropil identity. Neuropil boundaries of key optical sections were labeled in every spatial plane (*x-y, x-z, y-z*), generating a scaffold for each neuropil of interest. The scaffolds were automatically completed to contain all voxels that belong to each neuropil by the "wrap" function in Amira. Finally, a triangulated surface model was generated from the segmented label-fields. The neuropils included were upper and lower divisions of the central body (CBU, CBL), the noduli (NO), the protocerebral bridge (PB), the lateral accessory lobe (LAL), the gall (GA), the bulb (BU), the upper unit of the AOTU (AOTU-UU), the lower unit of the AOTU (AOTU-LU) and the nodular unit of the AOTU (AOTU-NU). The color code introduced for these neuropils by Heinze et al. (2013) was used as a template.

Neurons were traced manually in 3D using the skeletonize plug-in for Amira 5.3 (Schmitt et al., 2004; Evers et al., 2005). First, confocal image stacks containing a labeled neuron were aligned into a common frame of reference. Second, the skeleton of the neuron was traced by manually selecting key points along the neuron's path as well as selecting all branch points. The resulting straight neuron segments were fitted to the brightness information of the image stack to obtain realistic midline curvature and diameter for each branch.

Standardization

For standardization we reconstructed the neuropils of interest from twelve individuals for each species. We chose the computational morphometry toolkit (CMTK) as standardization method, implemented by the iterative shape averaging (ISA) protocol (Rohlfing et al., 2001; el Jundi and Heinze, in press), given that this method has been used successfully for many species, including the "compass neuropils" of the Monarch butterfly (Brandt et al., 2005; Kurylas et al., 2008; Kvello et al., 2009; Wei et al., 2010). In the ISA protocol gray values are used as the basis for image comparison. As the compass neuropils were scanned from the center of the brain, the edges of the individual image stacks visible in the merged overall image stack contained the highest contrast, however did not correspond to any brain structure. These boundaries thus had to be eliminated to prevent the algorithm to align the boundaries of the image stacks, rather than the internal brain structures. Following the method introduced by el Jundi et al. (2009a) and Heinze et al. (2013), we therefore removed all image information located further than 25 voxels away from the labeled neuropil boundaries. This generated a "cut-out" image stack with consistent outer borders. These image stacks provided the raw material for the ISA protocol. Before the actual registration process, a reference brain was chosen, which in terms of shape and volume represented the population average of the 12 reconstructed individual brains most closely. This is crucial since the reference brain strongly influences the volume of the final result of the ISA protocol. In general terms, the ISA protocol is a two-step procedure, in which an affine registration is followed by an elastic registration, which is iterated multiple times. In the first step, the reference brain is used as a template to which all remaining brains are aligned through affine registration. The affine registration was carried out twice, first with 6 degrees of freedom (rotation and translation along the three cardinal axes), then with 9 degrees of freedom, i.e., additional scaling along all three cardinal axes. This initial procedure compensated for difference in rotation, size and position between the individual image stacks. The registered brains were then averaged and the resulting coarse average brain was used as the reference for the elastic registration. This process adjusts shape differences between brains by introducing local deformations to maximize image similarity. This process is repeated five times, each round using the previously generated averaged image stack as the new template. This leads to the final average image stack. The set of registration parameters obtained from each individual brain were then applied to the label field data from the same brain, yielding a set of 12 registered label fields. Using the shape based averaging method (Rohlfing and Maurer, 2007), a standardized surface reconstruction was calculated. All computations required to run the ISA protocol were performed on the MaRC2 HPC Linux cluster based at the IT-facilities of the University of Marburg, Germany. Using 64 cores (AMD 6276 at 2.3 GHz) and approximately 4 GB of shared memory, the ISA protocol took approximately 5 days to complete. The atlases are available for download as well as for interactive use at the InsectBrainDatabase (Bogong moth: https://www.insectbraindb.org/species/2/; Turnip moth: www.insectbraindb.org/species/21/).

Volumetric Analysis

For each reconstructed brain, we extracted volume information for each neuropil from label-field data by using the *material statistics* tool in Amira 5.3. All raw data is available in Supplementary Tables S1–S3. We calculated relative volumes by normalization, i.e., the absolute volumes were divided by the total volume of all neuropils of each brain, thus eliminating effects of size differences between individuals and species. To assess the overall investment into each type of neuropil, we summed the values of the right and left hemispheres within each brain.

The comparison of relative volumes between the neuropils of the two moth species was carried out by the Mann-Whitney U test, given that the volume distribution of some neuropils deviated significantly from normal (tested with Shapiro-Wilk normality test). The means and standard deviations of each neuropil were calculated and displayed. For three species comparison between the moths and the Monarch butterfly, we used non-parametric ANOVA (Kruskal-Wallis test) with Dunn's test for multiple comparisons. As the gall-region of the LX was not segmented separately in the Monarch butterfly, and the strap-region of the AOTU was not found in the two moths, we combined the gall with the LAL in the moth species and included the strap with the AOTU-lower unit in the Monarch butterfly for the three-species comparison. All the statistical analyses above were performed in Graphpad-Prism 6.0 software.

To investigate whether differences in neuropil volume resulted from true differences in the size of the neuropils of

interest (i.e., grade shifts), rather than apparent differences in relative size caused by non-isometric scaling, we carried out standardized major axis regression analysis on all neuropils (Warton et al., 2006; Ott and Rogers, 2010), first between the two moth species and second between all three species. We used the SMATR v.3 package for R, as described by Warton et al. (2012). This method assumes an allometric relationship of the form $y = a * x^b$, which translates to the linear relationship $\log(y) = \log(x) * b + \log(a)$. In cases where we did not find differences in allometric scaling between species (equal slopes b), we could test for differences in the y-axis intercept, or elevation ($\log(a)$), called a grade shift. All neuropils examined fulfilled this criterion. If grade shifts exist, they indicate a true difference in neuropil volume across species (Ott and Rogers, 2010). The extent of the shift in elevation was quantified as the grade shift index (GSI) as described by Ott and Rogers (2010). Additionally we tested if the scaling relationship of a neuropil (using the common slope of the examined species) was different from isometric scaling (i.e., the neuropil scales at the same rate as the overall neuropils). The difference in slope from isometric scaling is defined as the slope index (SI).

Neuron Registration

Neurons reconstructed from individual brains were mapped into the standard atlas following the method described in detail in el Jundi et al. (2009a), applied according to Heinze et al. (2013). In short, we first reconstructed the neuropils innervated by the neuron of interest based on the background fluorescence in the image stack containing the neuron. These were then affinely and elastically registered onto the standard atlas. The resulting transformation parameters were then applied to the neuron reconstruction itself and yielded a neuron that was matched to the reference frame of the standard atlas, as well as locally adjusted in shape to compensate for any distortions present in the individual brain.

Naming of neuropils follows the naming scheme developed by the Brain Name Working Group (Ito et al., 2014) and differ in some neuropils from the names used by Heinze et al. (2013) in the Monarch butterfly. All neuropil orientations are stated according to body axis (not neuraxis).

RESULTS

Proposed Migration-Relevant Neuropils in Noctuid Moths

The Bogong and Turnip moth's counterparts of the Monarch butterfly's "compass neuropils" also consist of the four compartments of the CX, the three compartments of the LX, and one large and several small compartments of the AOTU (**Figures 1**, **2**). The CX can be divided into the upper and lower division of the central body (CBU and CBL), the paired NO, and the posteriorly located PB. The overall shape of these neuropils resembles that of other lepidopteran insects: the PB is discontinuous across the midline, the CBL has an elongated, straight shape, located anteriorly of the much larger CBU, and the NO are small, ventrally located structures consisting of two major subunits, one large and one small (**Figures 1**, **2**). Whereas horizontal layers are clearly visible in the CBU (three major layers from dorsal to ventral; **Figures 1F,F′**, **2K–M**),

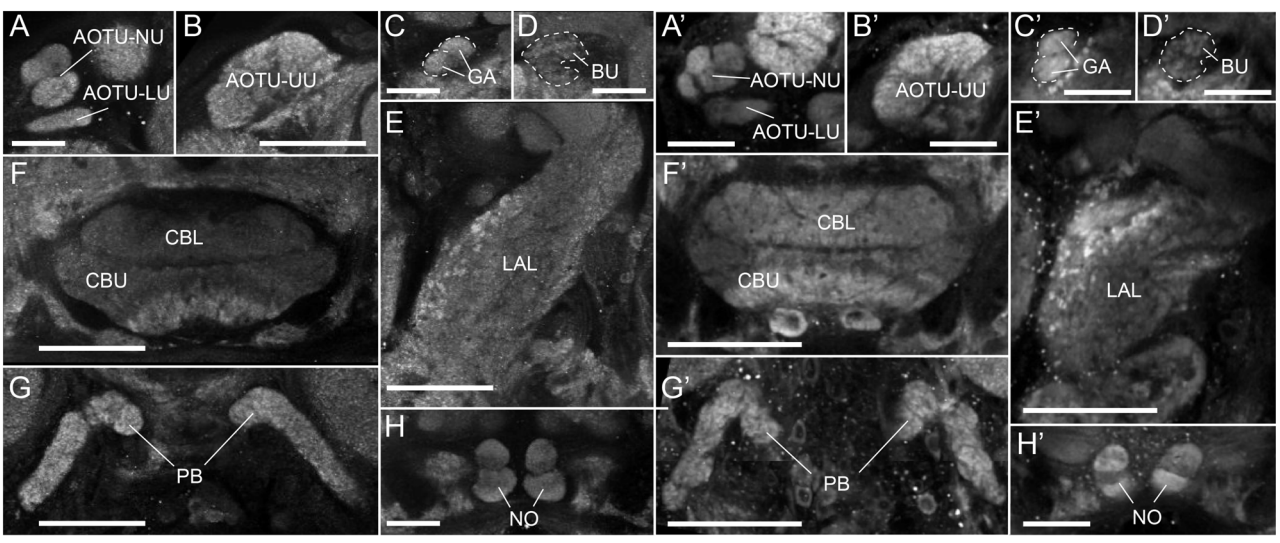

FIGURE 1 | The anatomy of proposed navigation-relevant neuropils in two species of noctuid moths. **(A–H)** Single confocal sections (frontal orientation) of an anti-synapsin labeled Bogong moth brain, scanned directly from whole-mount preparation. **(A)** Lower unit complex (LUC) of the anterior optic tubercle (AOTU) consisting of lower unit (LU) and nodular unit (NU). **(B)** Upper unit of the AOTU (UU). **(C)** The gall (GA) of the lateral complex (LX). **(D)** The bulb (BU) of the LX. **(E)** The lateral accessory lobe (LAL) or the LX. **(F)** The upper and lower divisions of the central body (CBU, CBL) of the central complex (CX). **(G)** The protocerebral bridge (PB) of the CX. **(H)** The noduli (NO) of the CX. **(A′–H′)** As **(A–H)**, but for the Turnip moth. **(G′)** is a maximal intensity projection of three individual images. Scale bars: **(A,C,D,H)** 50 μm; **(B,E,F,G)** 100 μm.

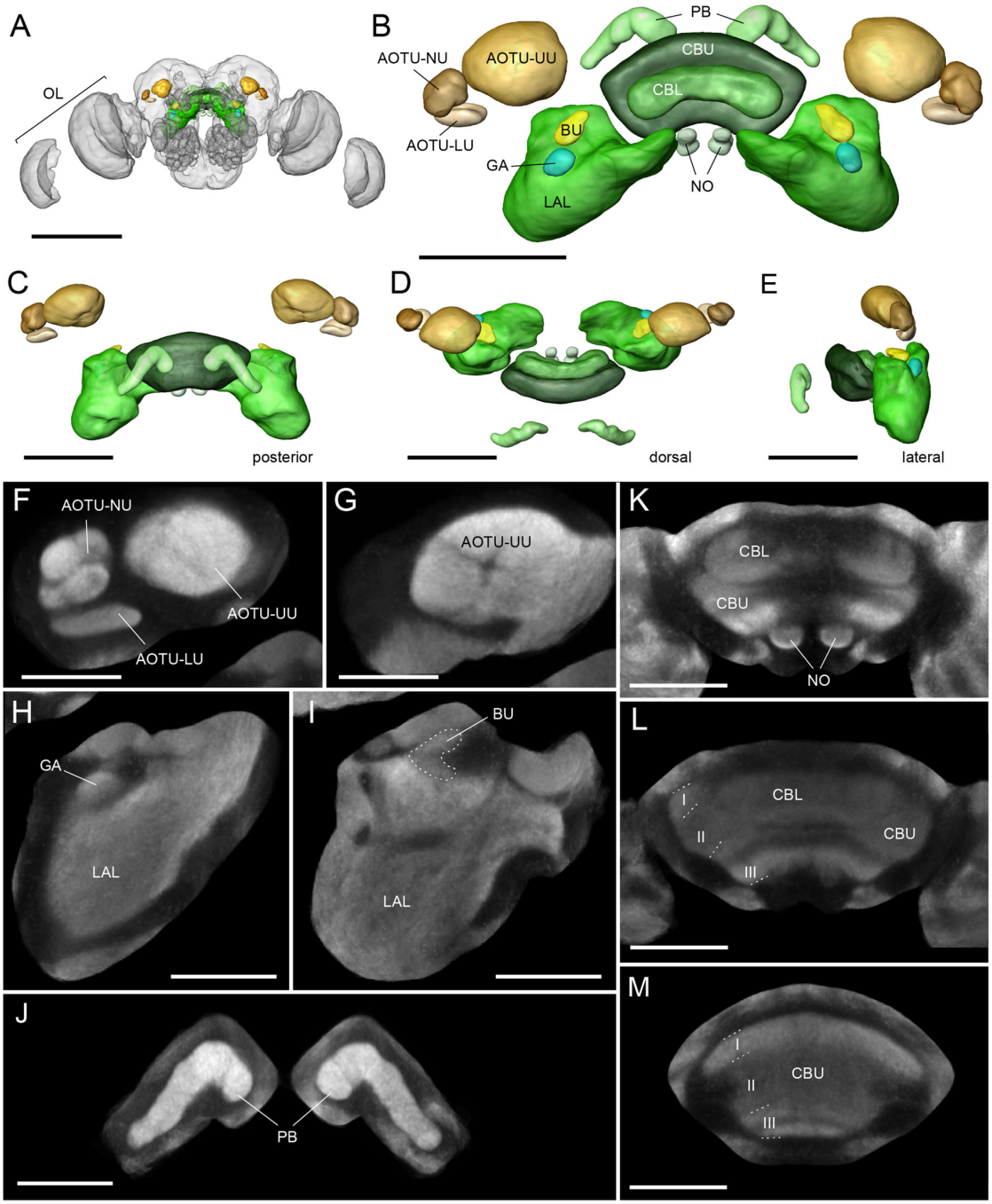

FIGURE 2 | The standardized average-shape Bogong moth "compass neuropils". **(A)** Anterior view of the Bogong moth brain with regions of interest highlighted in color. **(B)** Anterior view of the finalized standard atlas. Shown are surface renderings of average-shape label-fields. **(C–E)** As for **(A)** but posterior view **(C)** dorsal view **(D)**, and lateral view **(E)**. **(F–L)** Single optical sections of the averaged confocal data stack resulting from the standardization protocol. **(F)** Lower unit complex of the AOTU with lower unit (LU) and nodular unit (NU), shown with upper unit of the AOTU (AOTU-UU). **(G)** More posterior level of the AOTU-UU. **(H,I)** Different levels of the lateral complex showing the lateral accessory lobes (LAL), gall (GA) and bulb (BU). The BU is outlined with a dashed line. **(J–M)** Different levels of the central complex showing the lower division of the central body (CBL), upper division of the central body (CBU), noduli (NO) and the protocerebral bridge (PB). Scale bars: **(A)** 500 μm; **(B–D)** 200 μm; **(F,G)** 80 μm; **(J–M)** 100 μm. OL, optic lobe.

the columnar neuroarchitecture typical for the insect CX is not pronounced on the level of neuropils in the Bogong moth.

The LX are located anterior-ventrally on either side of the CX and consist of the large LAL (**Figures 1E,E′**) and two small neuropils, the bulb (BU; **Figures 1D,D′**) and the gall

(GA; **Figures 1C,C′**). In the Monarch butterfly these small regions had been originally named the lateral triangle and the anterior loblet (Heinze and Reppert, 2012). Typical for the LAL, the boundaries of this region are highly defined only on its anterior and medial side. Dorsally, ventrally and laterally it merges with the surrounding neuropil regions. These boundaries have hence been defined in accordance with criteria used in the Monarch butterfly, *Drosophila* and the dung-beetle. The gall on the other hand is clearly visible as a small structure on the anterior face of the LAL, just posterior of the antennal lobe. It consists of two fused ellipsoids of smooth, even appearance in synapsin-labeled preparations (**Figures 1C,C′**). Immediately dorsal of the gall lies the bulb. This neuropil consists of many small microglomeruli (**Figures 1D,D′**) and, due to their irregular spatial arrangement, the overall neuropil shape and volume are comparably variable across individuals. The bulbs are nevertheless well-defined by providing a cap-like end to the isthmus tracts leaving the CBL on either side, while laterally and dorsally bordering the mushroom body lobes (**Figures 1D,D′**).

The AOTU consists of the large upper unit (AOTU-UU) as well as the much smaller lower unit complex (LUC), which can be divided into the lower unit (AOTU-LU) and the nodular unit (AOTU-NU; **Figures 1A,A′**, **2F**). The latter can be further divided into four glomerular sub-compartments. While the small subunits are highly defined and can be easily separated from other brain regions, the upper unit merges medially with the surrounding superior protocerebrum, but can nevertheless be distinguished by its brighter synapsin labeling (**Figures 1B,B′**, **2G**).

Average-Shape Atlases of Migration-Relevant Neuropils

To generate a baseline for future anatomical work on the neural circuits underlying the Bogong moth's migratory behavior, we have used the ISA protocol (ISA), implemented through the CMTK toolkit, to generate a standardized, shape averaged version of the Bogong and Turnip moth's counterparts of the Monarch butterfly "compass neuropils" (**Figure 2**). These standards are based on 12 individual brains each and now provide a reference atlas for registration of anatomical data from any individual of both species. At a voxel-size of $1 \times 1 \times 1\ \mu m$, the resolution of this atlas is equivalent to that of the Monarch butterfly and exceeds that of all other species in which brain atlases have been published, with the exception of *Drosophila*. To illustrate the functionality as standardized Bogong moth reference neuropils, we have registered three intracellularly filled neurons into this standard atlas, generating a starting point for collecting an increasing amount of anatomical data (**Figure 3**). These neurons included two columnar neurons of the CX (CPU1-neurons), which are well described in other insects (e.g., Monarch butterfly; **Figures 3C,D**; Heinze et al., 2013; locusts, el Jundi et al., 2009a), as well as a type of CX neuron described here for the first time. This cell (TL-(GA-BU-POTU)) innervates the CBL, the gall, the bulbs and the posterior optic tubercle (the latter is not part of the standard atlas due to its high variability in size, shape and location; **Figures 3A,B**), i.e., most compass-related regions of the insect CX. This broad innervation pattern combined with an unpronounced anatomical polarity (no clear input and output regions based on morphological criteria) suggests a modulatory role for this neuron within the compass circuit.

The same 12 randomly selected brains also provide a representative sample of neuropil volumes for quantitative analysis (**Figures 4B–D**). Both absolute and relative volumes (fractions of the overall volume of all compass neuropils) were calculated to serve as a basis for quantitative, interspecies comparisons. So as not to overestimate the relative investment into unpaired neuropils (CBU and CBL), we summed the right and left hemispheres of all paired brain areas for all volume calculations, similar to previous work (**Tables 1, 2**). In the following we compare the neuropil volumes of the Bogong moth to the Turnip moth and to reanalyzed, previously published data from the diurnal migratory Monarch butterfly (Heinze et al., 2013).

Comparison between Bogong Moth and Turnip Moth

All neuropils found in the Bogong moth were also identified in the brain of the Turnip moth. Moreover, the overall shape of all regions resembled that of the Bogong moth closely and no principal differences were obvious despite the difference in behavioral strategy (**Figures 4F–I**). The total absolute size of the Turnip moth's combined compass neuropils was approximately 20% smaller than in the Bogong moth, in line with its smaller body size (**Figure 4B**; $p < 0.001$; unpaired, two-tailed *t*-test). To quantitatively compare individual neuropils of the two species, we performed two types of analyses. First, we compared relative volumes of all neuropils, and second, we carried out standardized major axis regression analysis. The first method has previous been used in many species and is thus aimed at providing a basis for direct comparison of the presented data with those studies. The second analysis yields a more robust estimate of true difference between species, as it does not assume isometric scaling of all included neuropils. It is therefore a more rigorous basis for drawing functional conclusions.

When normalized to overall size, the relative volumes between the two species matched remarkably well for all parts of the CX (no significant differences, Mann-Whitney U test). The data for the LX also revealed no differences for the LAL and the BU, while showing a small, but weakly significant ($p = 0.039$) volume increase in the Turnip moth's gall region. However, in contrast, all neuropils of the AOTU showed a consistent trend towards smaller size in the Turnip moth (between 7%–25%). Of these, only the small subunits (lower and nodular unit) were significantly smaller ($p < 0.001$), whereas the upper unit just missed significance ($p = 0.068$; **Figures 4C–E**).

To examine whether these differences in relative volume are truly independent of overall size, we analyzed the detailed allometric relationships of all involved neuropils (using standardized major axis regression analysis in R; **Figure 5**). When plotting the absolute volume of each region against the total remaining volume of the compass neuropils, all regions

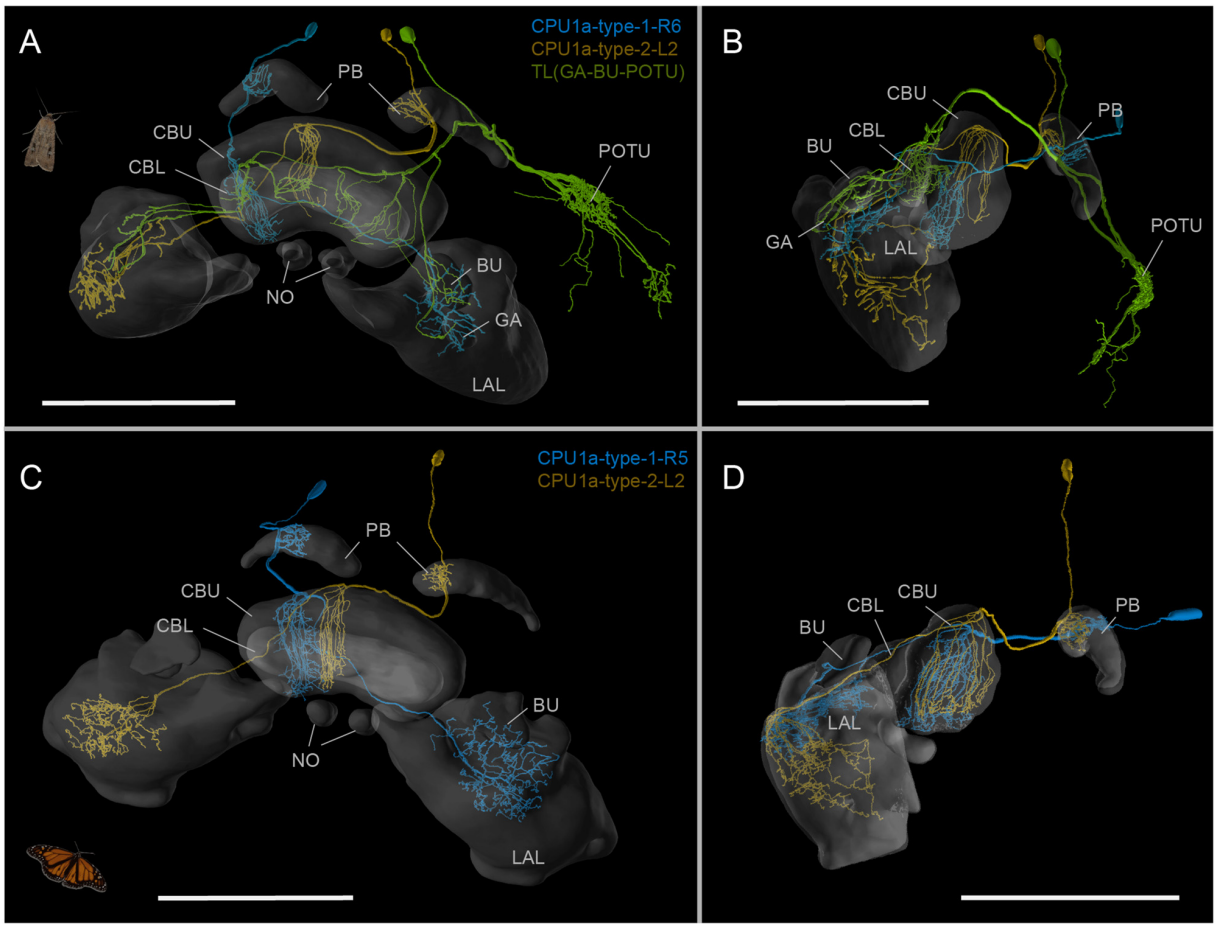

FIGURE 3 | The Bogong moth standard atlas as reference frame for neuron morphologies. **(A,B)** Three intracellularly injected and reconstructed neurons from the CX, mapped into the standard atlas by elastic registration. The TL-(GA-BU-POTU)-neuron is reported here for the first time. Oblique frontal view **(A)**; lateral view **(B)**. **(C,D)** Neuron of the same types as the cells with identical color in **(A)** (two types of CPU1a-neurons), but from the Monarch butterfly, registered into the standard atlas of the Monarch butterfly compass neuropils. Note the high degree of similarity between the species. Oblique frontal view **(C)**; lateral view **(D)**. Data from Heinze et al. (2013). Scale bars: 200 μm; Abbreviations: CBL, lower division of the central body; CBU, upper division of the central body; BU, bulb; LAL, lateral accessory lobe; GA, gall; PB, protocerebral bridge; NO, noduli; POTU, posterior optic tubercle. Images obtained at www.insectbraindb.org.

showed identical slopes between both species (a common slope described the data best). In about half the cases this slope was not significantly different from the expected isometric relationship, in which the neuropil volume would increase at the same rate as the total volume (**Figure 5F**). Highly significant exceptions were the AOTU-LU and the bulbs, while the PB, NO and the gall showed a weakly significant deviation. In all cases the neuropils showed disproportionately large size increases, i.e., the individual volume increased faster in size than the total volume. This finding is of key importance when interpreting the results of the relative volume analysis, which due to the normalization to overall volume, assumes isometry for all neuropils.

When analyzing the vertical displacement of the regression lines between both species (the grade-shift, expressed as the GSI), the AOTU-NU and the gall yielded significant differences, with the AOTU-NU being larger in the Bogong moth and the gall being larger in the Turnip moth, in line with the simple analysis of mean relative volumes (**Figures 5B–E**). Moreover, the LAL and the PB also showed a significant GSI towards larger volumes in the Turnip moth, that were obscured in the earlier analysis. Interestingly, the highly significant difference found in the AOTU-LU for the mean volumes was not confirmed in the more detailed analysis. This is because the simple analysis assumes an isometric scaling of the neuropils. Given that the AOTU-LU volume increases faster than expected with larger brains, and the Bogong moth brain is generally larger than the Turnip moth brain, the difference in relative volume is best explained by a shift of the neuropil volumes along the same regression line.

Comparison to the Migratory Monarch Butterfly

If the differences found between the two moth species are required for a migratory lifestyle, they should also be reflected in

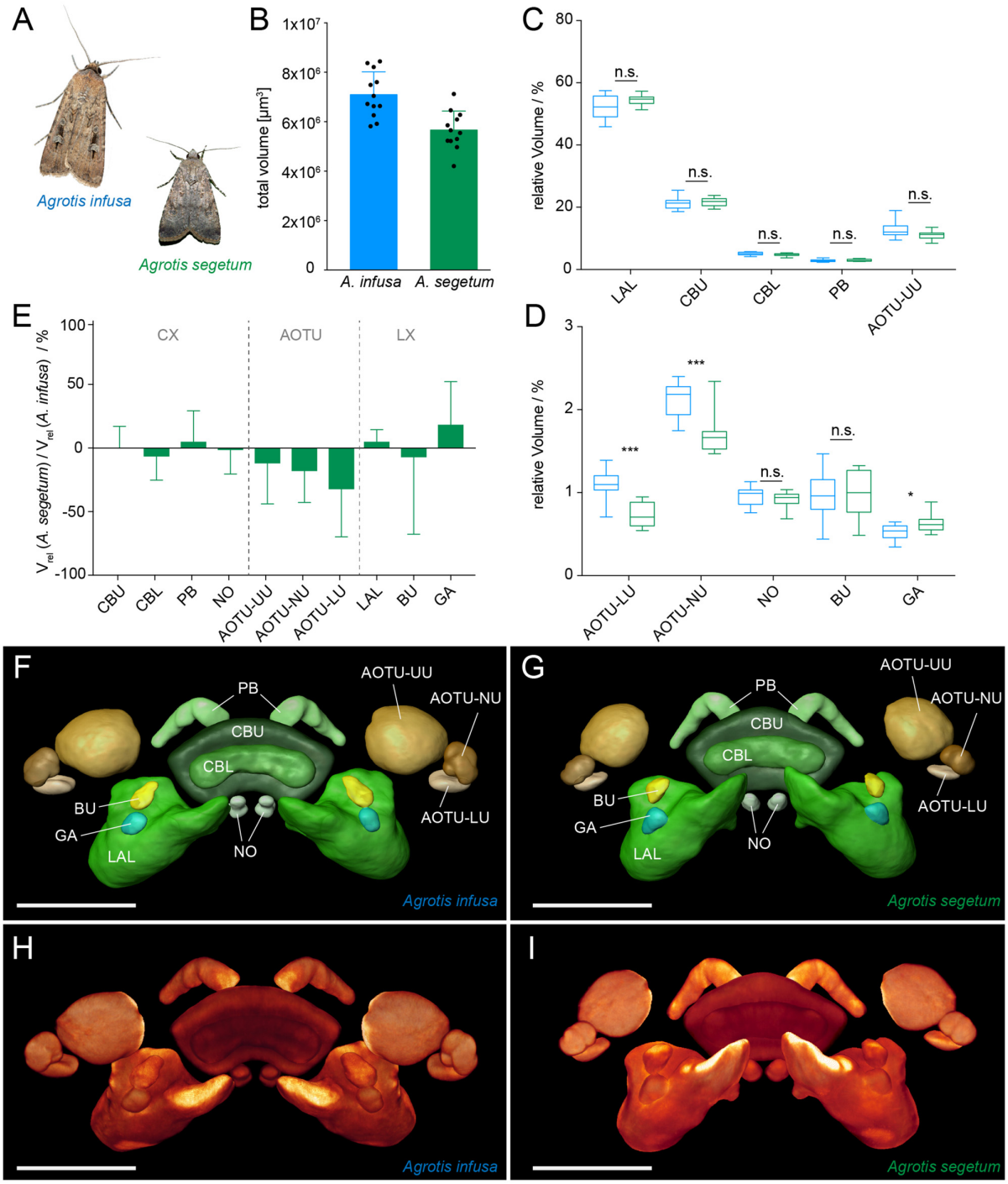

FIGURE 4 | Comparison of migration-relevant neuropils between the migratory Bogong moth (*Agrotis infusa*) and the non-migratory Turnip moth (*A. segetum*). **(A)** Photographs of both species (Bogong moth photo courtesy of Ajay Narendra); wingspan: 40–50 mm (*A. infusa*), 32–42 mm (*A. segetum*). **(B)** Total volume of the combined compass neuropils of both species. Individual data points are shown together with mean and standard deviation. **(C,D)** Box plots of relative volumes of each examined neuropil (normalized to the total volume); whiskers: data range; box: 25% and 75% percentiles; line: median. Bogong moth, blue; Turnip moth, green. **(C)** Large neuropils; **(D)** small neuropils. Asterisks indicate significance levels resulting from Mann-Whitney U test. **(E)** Ratio of neuropil volumes between Turnip moth and Bogong moth. Values smaller than one indicate larger volumes in the Bogong moth, while values larger than one indicate larger volumes in the Turnip moth. Error bars are summed relative standard deviations of corresponding neuropils from both species. **(F,G)** Surface rendering of standardized label-fields of average-shape atlases of the Bogong moth **(F)** and the Turnip moth **(G)**. **(H,I)** Direct volume rendering of image stack resulting from the standardization protocol. **(H)** Bogong moth; **(I)** Turnip moth. Scale bars: 200 µm. Abbreviations: AOTU, anterior optic tubercle; UU, upper unit; LU, lower unit; NU, nodular unit; CBL, lower division of the central body; CBU, upper division of the central body; BU, bulb; LAL, lateral accessory lobe; GA, gall; PB protocerebral bridge; NO, noduli.

TABLE 1 | Volumes of neuropils of Bogong moth (*Agrotis infusa*).

	Mean absolute volume/μm^3	SD/± μm^3	Mean relative volume/%	Relative SD/±%
CBU	1.51×10^6	1.71×10^5	21.43	10.0
CBL	3.59×10^5	4.59×10^4	5.08	9.4
PB	2.03×10^5	4.00×10^4	2.85	13.3
NO	6.80×10^4	1.33×10^4	0.96	12.0
LAL	3.71×10^6	5.39×10^5	52.25	6.9
BU	7.06×10^4	2.58×10^4	0.99	30.4
GA	3.78×10^4	9.10×10^3	0.53	17.6
AOTU-UU	9.07×10^5	2.60×10^5	12.69	19.1
AOTU-NU	1.51×10^5	2.49×10^4	2.12	10.0
AOTU-LU	7.88×10^4	2.15×10^4	1.10	17.0

TABLE 2 | Volumes of neuropils of Turnip moth (*Agrotis segetum*).

	Mean absolute volume/μm^3	SD/± μm^3	Mean relative volume/%	Relative SD/±%
CBU	1.16×10^6	1.52×10^5	21.05	6.13
CBL	2.57×10^5	4.94×10^4	4.65	13.12
PB	1.65×10^5	3.46×10^4	2.99	14.06
NO	5.27×10^4	4.24×10^3	0.96	4.85
LAL	2.98×10^6	2.65×10^5	54.30	4.52
BU	5.48×10^4	1.04×10^4	1.01	24.10
GA	3.33×10^4	3.78×10^3	0.61	14.16
AOTU-UU	6.55×10^5	4.93×10^4	11.97	5.98
AOTU-NU	9.69×10^4	1.04×10^4	1.77	10.87
AOTU-LU	3.79×10^4	1.14×10^4	0.69	25.70

migratory species that are only distantly related to the two moths. To address this hypothesis, we compared our data to previously published data on the migratory Monarch butterfly (Heinze et al., 2013), which had been generated using identical methods (**Figures 6**, **7**). Given that the overall size of the Monarch butterfly is greater than the Bogong moth, the larger total volume of the neuropils (*ca.* 20%) is not unexpected (**Figures 6A,B**). After normalizing each individual neuropil to the total volume of all combined regions, we compared these relative volumes across all three species (non parametric ANOVA (Kruskal-Wallis test, with Dunn's test for multiple comparisons)). As the gall region of the LX had not been reconstructed separately from the LAL in the Monarch butterfly, we needed to combine the LAL and the gall in all three species to be able to carry out direct comparisons. Similarly, the strap region of the Monarch butterfly AOTU had to be combined with the AOTU-LU, as the strap does not exist in moths. In summary, whereas neuropils between the two moth species showed only one significant difference in the ANOVA analysis comparing all three species (AOTU-LU), all neuropils of the Monarch butterfly were significantly different from at least one of the two moths. In seven out of nine cases, the Monarch butterfly neuropils were significantly different in volume from both moths (**Figures 6C–F**). When compared to the Bogong moth, all components of the CX as well as the small subunits of the AOTU were smaller in the Monarch butterfly, whereas the upper unit of the AOTU and the bulb of the LX were significantly larger. The differences were generally more pronounced compared to the differences between the Bogong moth and the Turnip moth, with e.g., the upper unit of the AOTU being more than twice the relative size in the Monarch butterfly and all compartments of the CX being 50% smaller (**Figure 6F**).

More detailed analyses using standardized major axis regression analysis largely confirmed that differences were most pronounced between the Monarch butterfly and either moth species and were comparably modest between the two moths (**Figure 7**). All neuropils followed a consistent slope for linear regression analysis, which was significantly different from the expected isometric relationship in the same cases as when comparing only both moth species. This indicates that the steeper than expected scaling of the AOTU-LU, bulbs, PB and NO is a characteristic inherent to those brain areas across the species we investigated (**Figure 7F**). Highly significant grade shifts were found for all neuropils of the CX and the AOTU ($p < 0.001$), while in the LX only the LAL (plus gall) showed a weakly significant volume decrease in the Monarch butterfly ($p = 0.013$). Consistent with simple comparisons of relative volumes, the GSI indicated larger volumes in the Monarch butterfly for the upper unit of the AOTU, and smaller volumes for all other significantly different neuropils (**Figure 7E**).

DISCUSSION

In this article we have examined the effects of navigational strategy on the morphology of central brain neuropils implicated in navigation across three lepidopteran insects. We used two closely related moths, the migratory Bogong moth and the non-migratory Turnip moth, and compared our results to the migratory Monarch butterfly by reanalyzing previously published data from Heinze et al. (2013). In summary, both qualitative and quantitative analysis revealed that the brain regions we examined are highly conserved in overall shape and relative volumes. Between the two moths, clear differences were

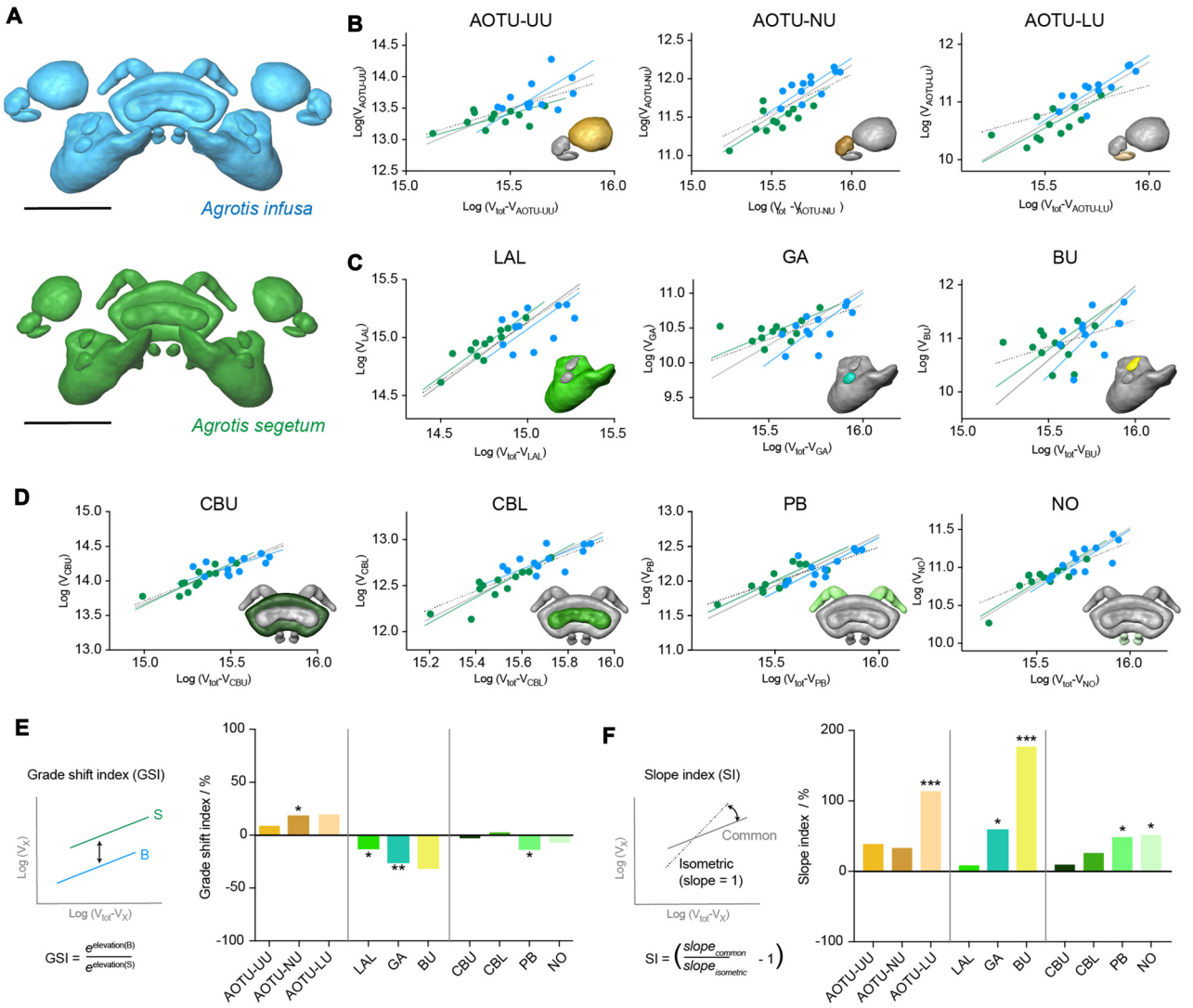

FIGURE 5 | Results from standardized major axis regression analysis comparing the Bogong moth and the Turnip moth compass neuropils. **(A)** Surface rendering of neuropils in each species. **(B–D)** Regression analysis data; colors matching neuropil color in **(A)**. For each neuropil individual data-points are shown together with the individual regression line of each species, the best-fit common regression line (gray) and the isometric expectation (dotted). The inset depicts the respective neuropil for each graph highlighted in color. **(B)** Neuropils of the AOTU. **(C)** Neuropils of the LX. **(D)** Neuropils of the CX. **(E)** Analysis of grade shift indices (GSI) of all neuropils. Positive values indicate a shift towards bigger volumes in the Bogong moth, while negative values indicate smaller volumes in the Bogong moth. Left: schematic illustration and formula of how the GSI is calculated. Asterisks indicate significance level of GSI. **(F)** Analysis of slope index (SI) for all neuropils. Values larger than zero indicate steeper than isometric scaling. Asterisks illustrate significant deviations from isometric scaling. Left: schematic illustration and formula of how the SI is calculated. Scale bars: 200 μm. Abbreviations: AOTU, anterior optic tubercle; UU, upper unit; LU, lower unit; NU, nodular unit; CBL, lower division of the central body; CBU, upper division of the central body; BU, bulb; LAL, lateral accessory lobe; GA, gall; PB protocerebral bridge; NO, noduli.

found in the most peripheral region, the AOTU, in regions of the LX and in the PB of the CX. Between the moths and the Monarch butterfly, larger differences in relative volumes were observed in nearly all regions, none of which however reflected migratory lifestyle when examined across all three species. This suggests that, at least for lepidopteran insects, long-distance migratory behavior cannot be easily predicted from brain structure alone, despite the defining role of this behavior for a species' natural history.

The Compass Neuropils Are Highly Conserved Across Species

When we compared the overall layout of the average-shape neuropils, they struck us as highly similar between all three species. First, all major components of the CX, the LX and the AOTU were identified in both moths and in the Monarch butterfly and, second, their spatial arrangement was largely identical. Neither finding is unexpected, despite the fact that considerable variability regarding the relative

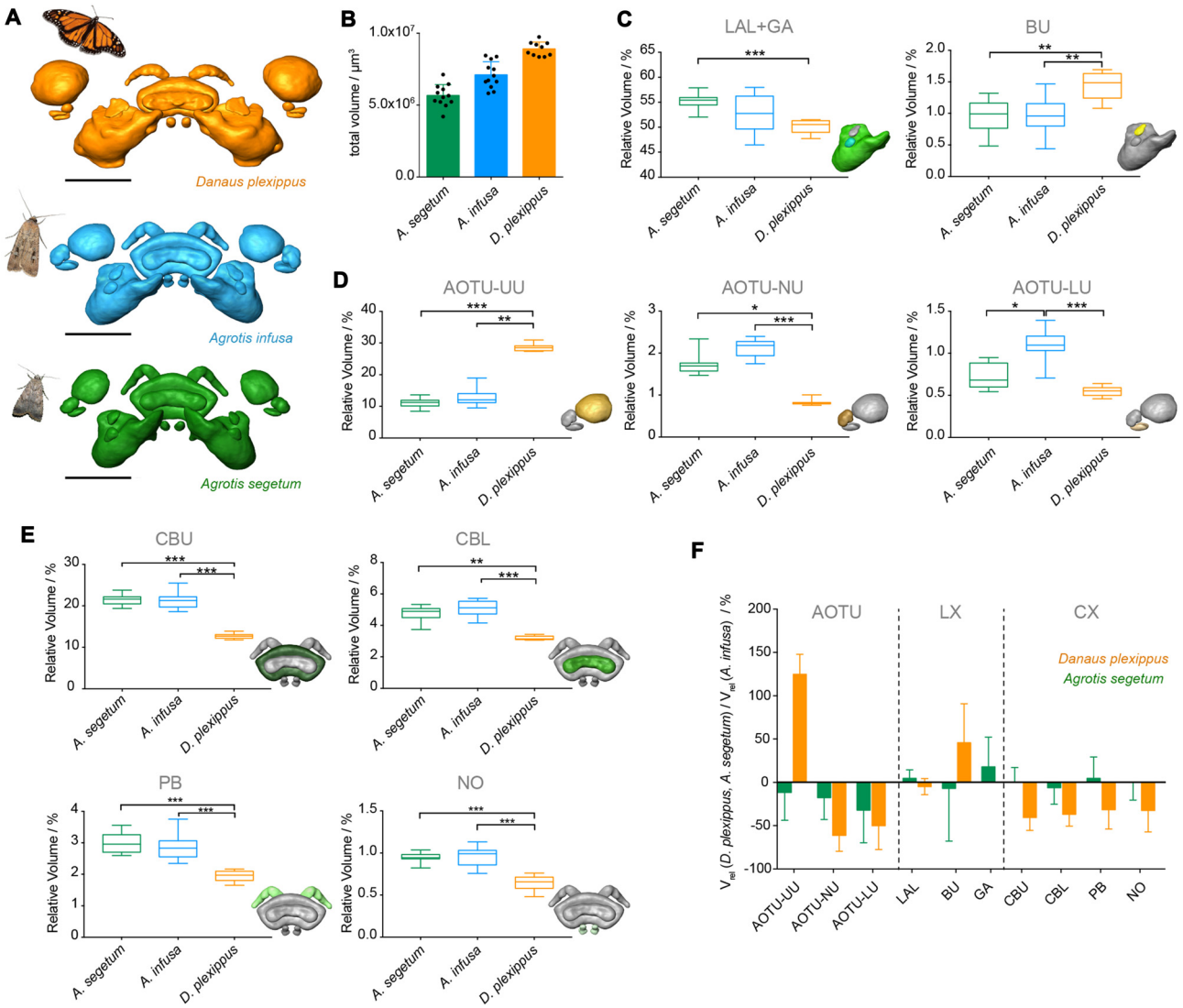

FIGURE 6 | Comparison of compass neuropils between migratory and non-migratory moths (Bogong moth, *A. infusa*; Turnip moth, *A. segetum*) and the migratory Monarch butterfly (*Danaus plexippus*). **(A)** Surface rendering of neuropils in each species (shown in correct relative size), shown with image of each species. **(B)** Total volumes of the combined compass neuropils. Individual data points are shown together with mean and standard deviation. **(C–E)** Box plots of relative volumes of each examined neuropil (normalized to the total volume) whiskers: data range; box: 25% and 75% percentiles; line: median. Bogong moth, blue; Turnip moth, green; Monarch butterfly, orange. The inset depicts the respective neuropil for each graph highlighted in color. Asterisks indicate significance levels resulting from ANOVA analysis (with Dunn's test for multiple comparisons). **(C)** LX neuropils. **(D)** AOTU neuropils. **(E)** CX neuropils. **(F)** Ratio of neuropil volumes between Turnip moth and Bogong moth (green) and the Monarch butterfly and the Bogong moth. Values smaller than one indicate larger volumes in the Bogong moth, while values larger than one indicate smaller volumes in the Bogong moth. Error bars are summed relative standard deviations of corresponding neuropils from both species. Scale bars: 200 µm. Abbreviations: AOTU, anterior optic tubercle; UU, upper unit; LU, lower unit; NU, nodular unit; CBL, lower division of the central body; CBU, upper division of the central body; BU, bulb; LAL, lateral accessory lobe; GA, gall; PB protocerebral bridge; NO, noduli.

positioning of those brain areas exists across insects (Heinze and Homberg, 2008; Heinze and Reppert, 2012; Ito et al., 2014; Immonen et al., 2017). This is because this variability largely underlies constraints during brain development (Wegerhoff and Breidbach, 1992; Huetteroth et al., 2010; Boyan and Reichert, 2011) and all three species examined are lepidopteran insects. Thus the relative positioning of the regions under consideration was expected to reflect the highly similar overall brain morphology.

The CX is involved in a multitude of functions that are relevant across all insects. These include locomotor control (Strauss, 2002; Martin et al., 2015), spatial memory (Ofstad et al., 2011; Kuntz et al., 2017), representation of body orientation (Heinze and Homberg, 2007; Seelig and Jayaraman, 2015; Varga and Ritzmann, 2016), and multisensory integration (Homberg, 1994; Ritzmann et al., 2008; Seelig and Jayaraman, 2015). As these functions are important independent of behavioral strategy, sensory environment, and evolutionary history, the

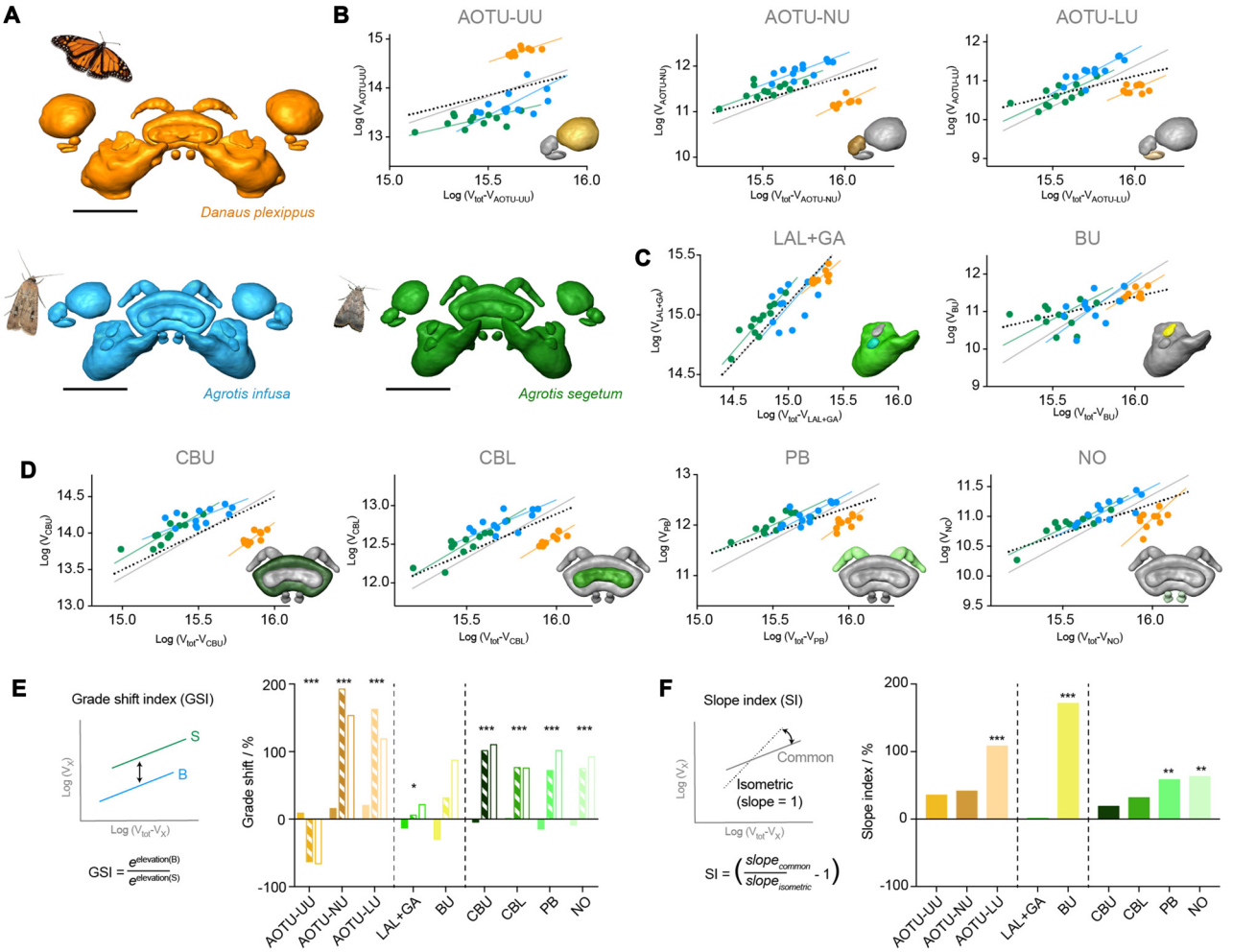

FIGURE 7 | Results from standardized major axis regression analysis comparing the Bogong moth, the Turnip moth and the Monarch butterfly compass neuropils. **(A)** Surface rendering of neuropils in each species (shown in correct relative size), shown with image of each species. **(B–D)** Regression analysis data; colors matching neuropil color in **(A)**. For each neuropil individual data-points are shown together with each species' individual regression line, the best-fit common regression line (gray) and the isometric expectation (dotted). The inset depicts the respective neuropil for each graph highlighted in color. **(B)** Neuropils of the AOTU. **(C)** Neuropils of the LX. **(D)** Neuropils of the CX. **(E)** Analysis of GSI of all neuropils. Solid bars: Bogong moth—Turnip moth comparison (values > 0: Bogong moth bigger; values < 0: Bogong moth smaller); hatched bars: Bogong moth—Monarch butterfly comparison (values > 0: Bogong moth bigger; values < 0: Bogong moth smaller); open bars: Turnip moth—Monarch butterfly comparison (values > 0: Turnip moth bigger; values < 0: Turnip moth smaller). Left: schematic illustration and formula of how the GSI is calculated. Asterisks indicate significance level of GSI. **(F)** Analysis of SI for all neuropils. Values larger than zero indicate steeper than isometric scaling. Asterisks illustrate significance level of deviations from isometric scaling. Left: schematic illustration and formula of how the SI is calculated. Scale bars: 200 μm. Abbreviations: AOTU, anterior optic tubercle; UU, upper unit; LU, lower unit; NU, nodular unit; CBL, lower division of the central body; CBU, upper division of the central body; BU, bulb; LAL, lateral accessory lobe; GA, gall; PB protocerebral bridge; NO, noduli.

underlying neural pathways and circuits are expected to exist in similar form across all insects. Even though some of the identified functions, e.g., involvement in grasshopper singing behavior (Kunst et al., 2011; Balvantray Bhavsar et al., 2017), might be specific to certain species, the fundamental nature of most CX functions demands a high level of structural conservation, which we confirmed in the current work.

Similarly, the LX serves as a crucial input and output relay to and from the CX and has been implicated in generating premotor control signals (Homberg, 1994; Namiki et al., 2014; Namiki and Kanzaki, 2016b). Both roles suggest that the LX regions are indispensable for any insect, despite the fact that they have received little attention so far. This lack of attention is likely due to the fact that the LX components are comparably difficult to identify due to their diffuse boundaries with neighboring neuropils (Heinze and Homberg, 2008; Heinze and Reppert, 2012; Ito et al., 2014; Immonen et al., 2017).

Finally, the AOTU has also been revealed in all insects examined so far, albeit with considerably more variability between species (Homberg et al., 2003; el Jundi et al., 2009b; Mota et al., 2011; Heinze and Reppert, 2012; Pfeiffer and Kinoshita, 2012; Zeller et al., 2015; Immonen et al., 2017). Specifically, the LUC, i.e., the combination of all small AOTU

subunits, varies significantly both in numbers of subunits as well as in shape. AOTU function has been most thoroughly characterized in the context of processing visual compass cues, in particular polarized light, in the desert locust (Pfeiffer et al., 2005; Pfeiffer and Homberg, 2007; el Jundi and Homberg, 2012) and the Monarch butterfly (Heinze and Reppert, 2011). Neurons of the AOTU-LUC feed visual input to the bulbs of the LX via two parallel pathways and provide the basis for head-direction encoding in the CX (Pfeiffer et al., 2005; Pfeiffer and Kinoshita, 2012; Heinze et al., 2013; Held et al., 2016). Recently, in *Drosophila*, a highly similar arrangement has been revealed, both anatomically and functionally, albeit with visual landmark information being encoded rather than skylight compass cues (Seelig and Jayaraman, 2013; Omoto et al., 2017). Therefore, one key role of the AOTU-LUC appears to be to relay and probably preprocess visual information essential to encode body orientation, a function that is fundamental to all oriented behavior, again in principle demanding a high degree of conservation. Nevertheless, the variability in this region suggests that the number of parallel pathways, and relative investment into each of them, depends on the nature of the visual information used by each species, allowing variations of a general scheme. Overall, these functional considerations suggest that differences reflecting the sensory environment (e.g., nocturnal vs. diurnal lifestyle) are likely to be found in the more peripheral AOTU, while adaptations to behavioral demands are more likely to be found in the CX and LX, which are more closely associated with motor control.

Qualitative Difference between Species

If migratory behavior required large-scale, dedicated specializations of the brain, such features would become apparent by comparing the gross morphology of migratory vs. non migratory species' brains. Across the three analyzed species any such qualitative differences were scarce. While none were identified between the Bogong moth and the Turnip moth, the Monarch butterfly neuropils, in comparison, showed three unique features setting them apart from their moth counterparts. First, the AOTU-LUC consisted of three rather than two sub-regions, the lower unit, the nodular unit and the strap, with the strap being unique to the Monarch butterfly (Heinze and Reppert, 2012). Second, the shape and intrinsic composition of the nodular unit was different in the moths compared to the Monarch butterfly. Even though the strap has been identified in other species of butterfly (Montgomery and Ott, 2014; Montgomery et al., 2016), its specific functional role remains unknown. The same applies to the nodular unit, which is present in all lepidopteran insects examined (el Jundi et al., 2009b; Heinze and Reppert, 2012; Montgomery and Ott, 2014; Montgomery et al., 2016). In the Monarch butterfly it contains a subset of polarization-sensitive TuLAL1a neurons, demonstrating that the AOTU-NU is at least partly involved in compass information processing (Heinze and Reppert, 2011; Heinze et al., 2013). Third, the LX-gall had a different appearance in the Monarch butterfly. Even though this region was not separately segmented in that species, Heinze and Reppert (2012) showed that the Monarch butterfly gall (then called anterior loblet) is a single, disc-shaped region occupying the anterior-most part of the LX. It is characterized by very brightly stained micro-glomeruli of dense synapsin-ir. In contrast, the gall of the moths we examined had a uniform appearance after synapsin-labeling and consists of two fused, yet distinct parts, a dorsal and a ventral bulb (not segmented separately). This is equivalent to the structure of this area in *Drosophila* (Ito et al., 2014) as well as in dung beetles (Immonen et al., 2017). Nothing is known about the function of this neuropil, other than that it is targeted by CL1 neurons (wedge/E-PG neurons in *Drosophila*), which are key components in the representation of body orientation and encoding of sky compass cues across insects (Heinze and Reppert, 2011; Heinze et al., 2013; Seelig and Jayaraman, 2015; Wolff et al., 2015). This suggests that they constitute part of an output pathway from the internal compass that might play a role in guiding behavior. In summary, all three differences suggest that no fundamentally different brain composition is required to mediate the ability for migratory behavior and the identified features likely reflect phylogenetic differences between moths and butterflies.

Quantitative Differences between Species

Quantitative differences between neuropils in the three species were much more prominent than qualitative differences and were identified with respect to relative neuropil volumes (fractions of total volume) and grade shifts after major axis regression analysis.

Relative volume analysis has been used in many previous studies across many insect species (e.g., el Jundi et al., 2009b; Wei et al., 2010), which are thus directly comparable to our results. Yet, this analysis assumes isometric scaling of all neuropils, an assumption that is consistently not met by several neuropils examined in the current study. As major axis regression analysis does not make this assumption, the results based on this method are more robust and thus provide the basis for all conclusions of this work. Besides providing continuity to previous anatomical work in insects, we note that including the partly contradictory results of both methods side by side illustrates the need for caution when interpreting volumetric differences between brain regions across insects, both in previous and future studies. This is particularly the case when rigorous major axis regressions cannot be performed, e.g., due to low numbers of available individuals, and when effects are small.

In the current work, quantitative differences between the three species were widespread. Most dramatically, the AOTU upper unit was more than twice as large in the Monarch butterfly. This region is involved in color processing in bees (Mota et al., 2013) and contains a visual input pathway to the LAL, parallel to the sky-compass pathway, in locusts (Pfeiffer et al., 2005) and bees (Mota et al., 2011; Pfeiffer and Kinoshita, 2012). Its large size is characteristic for butterflies (Heinze and Reppert, 2012; Montgomery and Ott, 2014; Montgomery et al., 2016) and, together with the highly developed color-vision ability in these insects, suggests that it is essential for visually guided flower foraging. Consistent with this idea, the more olfactory driven nocturnal moths possess a smaller version of this neuropil. In the remaining regions, all components of the CX and the

AOTU-LUC subunits were substantially larger in the moths, suggesting that the relative investment in those areas is higher in the moth species investigated compared to the Monarch butterfly. This effect was consistent even when the large AOTU upper unit was excluded from the analysis (Supplementary Figure S1) and does thus not merely result from a distorting effect of this unusually large region in the Monarch butterfly. However, it remains unclear whether the "compass neuropils" as a functional unit might occupy a different proportion of the central brain in moths vs. butterflies.

Between the two moth species, only two quantitative differences were consistently found: the nodular unit of the AOTU was larger in the Bogong moth, while the gall of the LX was smaller in the Bogong moth. A similar difference was identified for parts of the AOTU between two hawkmoth species, one diurnal and one nocturnal (Stöckl et al., 2016a). Here, the AOTU-LU was larger in the nocturnal species, while the upper unit was larger in the diurnal species. Similarly, comparison of individual brains of a diurnal and nocturnal dung beetle revealed larger subunits of the LUC in the nocturnal species (Immonen et al., 2017). The nocturnal dung beetle species relies more heavily on polarized light (el Jundi et al., 2015), which could explain the need for more neurons that process this information and relay it to the LX. This in turn likely leads to a size-increase of the AOTU subunit that contains these cells. Following this line of argument, we predict that the nodular unit contains more neurons in the migratory Bogong moth, which implies that this area processes information crucially needed by this species. This is supported by the finding that in Monarch butterflies at least parts of this region contain neurons relaying visual compass information to the LX-bulbs (Heinze and Reppert, 2011; Heinze et al., 2013). In contrast, comparison of the same regions between migratory and non-migratory Monarch butterflies showed no differences in the small AOTU subunits, while revealing a decrease in the AOTU upper unit and a significant increase in the volume of the PB in experienced migrants (Heinze et al., 2013). This means that, overall, no differences were consistent across species that can be correlated with migratory behavior. Whether the smaller size of the gall in migratory Bogong moths in comparison to the Turnip moth indicates that the output pathway mediated via this region is less important for migratory behavior in general, cannot be solved at this point, as this region was not analyzed separately in the Monarch butterfly (Heinze et al., 2013).

Potential Effects Due to Plasticity

One potentially confounding factor of the presented analysis is the different origin of used individuals: Bogong moths were wild-caught after their spring migration, Turnip moths were laboratory-raised, while Monarch butterflies had been freshly eclosed individuals (Heinze et al., 2013). Monarch butterflies were therefore age-matched, while individuals of both moth species were of unknown age, with potentially widely variable origin populations in case of the Bogong moth (Warrant et al., 2016). The consistent age of all Monarch butterfly individuals likely explains the considerably lower variability in the data for this species compared to the moths. Accordingly, the highest variability was found in the Bogong moth data, consistent with the least controlled sampling. The question therefore arises whether the species can be directly compared without taking into account age and experience effects of each population.

Age and experience indeed significantly influence volumes of brain regions in lepidopteran insects, including in the Monarch butterfly (Heinze et al., 2013). The most profound effects were found in *Heliconius* butterflies and were associated with the mushroom bodies. These structures showed remarkably large volume increases in wild-caught, experienced butterflies compared to young individuals or old individuals raised in captivity (Montgomery et al., 2016). Comparing old and young Monarch butterflies, a similar increase in overall neuropil volume was reported for the compass neuropils (Heinze et al., 2013), while grade shifts associated with extensive migratory experience were only found for the PB (larger) and the AOTU upper unit (smaller). These small changes in neuropil volume are the only experience-dependent changes reported for components of the "compass neuropils" to date. If similar effects exist in the examined moth species, they are expected to specifically have affected the Bogong moth brains (experienced individuals), likely amplifying any innate differences. As no large differences were revealed between the two moth species, effects due to migratory experience have most likely not been obscured by the differences in sampling. In fact, the only differences found between migratory Bogong moths and non-migratory Turnip moths were opposite to what would have been expected from comparing migratory and non-migratory Monarch butterflies (smaller PB and larger AOTU in migratory Bogong moths). Whether the sampling of the Bogong moth during their aestivating state, i.e., a state of dormancy, could explain these opposite than expected effects remains an open question. However, as the aestivation state is embedded between two migratory episodes during a Bogong moth's life, any volume change associated with migration would have to be reversible between spring migrants, aestivating state and fall migrants, a degree of plasticity that has to date not been observed in insects, but which nevertheless provides an interesting subject for future studies.

What Does It Take to Migrate?

Migrating over thousands of kilometers over unfamiliar terrain, equipped with a brain the size of a grain of rice seems a daunting endeavor. The question arises how the brain, in particular that of an insect, has to adapt in order to allow these journeys to be successful. In other words, what are the fundamental properties of a brain needed to guide migration? And why is there no strong evidence reflecting that behavior at the level of neuropil structure?

The challenges are both sensory and motor in nature. The brain has to ensure that the available information is used to extract a compass bearing as reliably as needed, while the motor control circuits have to ensure that the correct compass heading is faithfully maintained. If either one of those circuits, or the feedback between them, fails, the animal will not reach its goal and perish. In this respect, mistakes are much more devastating during migration than they are during opportunistic foraging. Given this strong selective pressure, migratory species can be

expected to have invested in neural circuitry that allows their brains to perform course control more reliably than species that can get by with making more mistakes. However, other than being optimized for reliability, the basic circuits likely do not need to be fundamentally altered, as all animals need to compare their desired heading with their current heading and compensate any mismatch with steering movements. The only difference in migrants is that the desired heading is constant over time and does not change with each new situation.

How are the control circuits made sufficiently reliable to avoid failure over thousands of kilometers of travel? On the sensory side, migrants should rely on multiple sources of compass information that are integrated into a coherent estimate of current heading within a global reference frame. For different visual compass cues this integration has been shown physiologically in locusts (Kinoshita et al., 2007; Pfeiffer and Homberg, 2007; el Jundi et al., 2014) and Monarch butterflies (Heinze and Reppert, 2011). Beyond integrating several sources of information, it is also important how this information is processed. While this clearly asks for more physiological experiments, anatomical data also can provide first hints. Reliability can be achieved by more neurons carrying compass signals to the central steering control, in order to allow averaging and eliminating noise, or by more reliable synapses in the compass pathway. This would be in line with our finding that the small subunits of the AOTU, which provide links between the optic lobe and the CX, are larger in the Bogong moth, potentially housing more neurons or larger synapses.

Once a multisensory reference frame is established, we can expect further differences between migratory and non-migratory species. Even though a reference frame is useful for, and potentially required by, all species, migrants should have a reference frame that is either fixed, or regularly recalibrated. The systematic E-vector representation in the locust PB, found over many individuals, suggests a fixed reference frame for that species (Heinze and Homberg, 2007), whereas the changing offset between anatomy and physiology of the landmark-based head direction signal in *Drosophila* (Seelig and Jayaraman, 2015) indicates a flexible reference frame.

On the motor output side, similar arguments to those we made for the sensory inputs also apply and these narrow down the candidate regions housing migration-specific adaptations to the two output areas of the CX: the LAL and the gall (Heinze and Homberg, 2008; Heinze et al., 2013; Wolff et al., 2015). Whereas CX-activity directly modulates turning reflexes in walking cockroaches (Martin et al., 2015), nothing is known about the anatomical substrate of the neurons involved or whether similar direct coupling happens during flight behavior. It therefore remains to be shown which output pathway contains migration relevant adaptations. The smaller gall-volume we found in the Bogong moth might suggest that the gall-output pathway is less relevant for migration than for opportunistic foraging.

Finally, how is the intended heading fixed neurally? Unfortunately, we currently don't know how any intended heading is encoded in an insect brain. Yet it is difficult to imagine that a fixed migratory bearing requires more neural capacity than a flexible one. Thus, these differences are unlikely to be found at the level of neuropils, but rather at the level of circuit connectivity.

The Standard Atlases as Basis for Comparative Circuit Analysis

As the neural underpinnings of migration are likely found at the level of neurons and neural circuits, we have generated the average atlases of the two moth species not only for direct shape and volume comparisons, but to provide a tool to perform efficient circuit analysis. By registration of individually dye injected neurons from intracellular recordings into a common reference frame, these atlases will allow us to map, collect and directly compare neurons between the two species. Differences in the sizes of arborization fields, fiber paths, degree of neural overlap, and likely pathways of information flow can be examined in detail using this tool, similar to what has already been achieved for the desert locust (el Jundi et al., 2009a) and the Monarch butterfly (Heinze et al., 2013).

CONCLUSION

In summary, our anatomical comparison of the regions likely to be involved in guiding compass navigation in migratory Bogong moths has revealed no major qualitative differences between migratory species and non-migratory species. This strongly suggests that the adaptations necessary to ensure successful migratory behavior are manifested at the level of neural circuits and will only be accessible via detailed physiological investigations. The current study aids this endeavor in two ways. First, the identified differences in neuropil volume in the nodular unit of the AOTU, the PB and the gall region of the LX, indicate promising target areas for electrophysiology both on the input and on the output side of the likely control circuits. Second, our new average-shape standard atlas provides an anatomical reference frame in which to embed all functional data obtained from the brain of the remarkable Bogong moth.

ETHICS STATEMENT

All animal procedures were in compliance with the guidelines of the European Union (Directive 86/609/EEc). Approval of the study by an ethics committee was dispensable, because all experiments were on insects.

AUTHOR CONTRIBUTIONS

LV and SH designed the study, performed histological experiments, wrote the manuscript and designed figures. LV carried out 3D-reconstructions and data analysis. AKA carried out electrophysiology, histology, reconstruction and registration of single neurons. KP and BT wrote standardization routines and performed brain atlas generation. EW and KG established Bogong moth field sites, captured moths and co-designed the study. All authors critically read the article and contributed to its final version.

ACKNOWLEDGMENTS

We thank Anna Stöckl, Kristina Brauburger and David Dreyer for help with Bogong moth collection, and Erling Jirle for maintaining the *A. segetum* colony. For help with statistical analysis in R we are grateful to James Foster. We appreciate the help of the MaRC2 team at the IT-center of the University of Marburg with compiling the CMTK binaries and using the HPC Linux cluster. The work was supported by a junior project grant from the Swedish Research Council (Vetenskapsrådet, 2012–2213) to SH and a grant (FA9550-14-1-0242) from the United States Air Force Office of Scientific Research (AFOSR) to EW and SH.

SUPPLEMENTARY MATERIAL

The Supplementary Material for this article can be found online at: http://journal.frontiersin.org/article/10.3389/fnbeh.2017.00158/full#supplementary-material

REFERENCES

Balvantray Bhavsar, M., Stumpner, A., and Heinrich, R. (2017). Brain regions for sound processing and song release in a small grasshopper. *J. Insect Physiol.* 99, 15–24. doi: 10.1016/j.jinsphys.2017.03.006

Boyan, G. S., and Reichert, H. (2011). Mechanisms for complexity in the brain: generating the insect central complex. *Trends Neurosci.* 34, 247–257. doi: 10.1016/j.tins.2011.02.002

Brandt, R., Rohlfing, T., Rybak, J., Krofczik, S., Maye, A., Westerhoff, M., et al. (2005). Three-dimensional average-shape atlas of the honeybee brain and its applications. *J. Comp. Neurol.* 492, 1–19. doi: 10.1002/cne.20644

Dingle, H. (1972). Migration strategies of insects. *Science* 175, 1327–1335. doi: 10.1126/science.175.4028.1327

el Jundi, B., and Heinze, S. (in press). "Three-dimensional atlases of insect brains," in *Neurohistology and Imaging: Basic Techniques*, eds R. Pelc, R. Doucette and W. Walz (New York, NY: Springer, Human Press).

el Jundi, B., and Homberg, U. (2012). Receptive field properties and intensity-response functions of polarization-sensitive neurons of the optic tubercle in gregarious and solitarious locusts. *J. Neurophysiol.* 108, 1695–1710. doi: 10.1152/jn.01023.2011

el Jundi, B., Heinze, S., Lenschow, C., Kurylas, A., Rohlfing, T., and Homberg, U. (2009a). The locust standard brain: a 3D standard of the central complex as a platform for neural network analysis. *Front. Syst. Neurosci.* 3:21. doi: 10.3389/neuro.06.021.2009

el Jundi, B., Huetteroth, W., Kurylas, A. E., and Schachtner, J. (2009b). Anisometric brain dimorphism revisited: implementation of a volumetric 3D standard brain in *Manduca sexta*. *J. Comp. Neurol.* 517, 210–225. doi: 10.1002/cne.22150

el Jundi, B., Pfeiffer, K., Heinze, S., and Homberg, U. (2014). Integration of polarization and chromatic cues in the insect sky compass. *J. Comp. Physiol. A Neuroethol. Sens. Neural Behav. Physiol.* 200, 575–589. doi: 10.1007/s00359-014-0890-6

el Jundi, B., Warrant, E. J., Byrne, M. J., Khaldy, L., Baird, E., Smolka, J., et al. (2015). Neural coding underlying the cue preference for celestial orientation. *Proc. Natl. Acad. Sci. U S A* 112, 11395–11400. doi: 10.1073/pnas.1501272112

Esbjerg, P., and Sigsgaard, L. (2014). Phenology and pest status of *Agrotis segetum* in a changing climate. *Crop Prot.* 62, 64–71. doi: 10.1016/j.cropro.2014.04.003

Evers, J. F., Schmitt, S., Sibila, M., and Duch, C. (2005). Progress in functional neuroanatomy: precise automatic geometric reconstruction of neuronal morphology from confocal image stacks. *J. Neurophysiol.* 93, 2331–2342. doi: 10.1152/jn.00761.2004

Fahrbach, S. E. (2006). Structure of the mushroom bodies of the insect brain. *Annu. Rev. Entomol.* 51, 209–232. doi: 10.1146/annurev.ento.51.110104.150954

Farris, S. M., Robinson, G. E., and Fahrbach, S. E. (2001). Experience- and age-related outgrowth of intrinsic neurons in the mushroom bodies of the adult worker honeybee. *J. Neurosci.* 21, 6395–6404.

Groh, C., Lu, Z., Meinertzhagen, I. A., and Rössler, W. (2012). Age-related plasticity in the synaptic ultrastructure of neurons in the mushroom body calyx of the adult honeybee *Apis mellifera*. *J. Comp. Neurol.* 520, 3509–3527. doi: 10.1002/cne.23102

Gronenberg, W., Ash, L. E., and Tibbetts, E. A. (2008). Correlation between facial pattern recognition and brain composition in paper wasps. *Brain Behav. Evol.* 71, 1–14. doi: 10.1159/000108607

Gronenberg, W., and Couvillon, M. J. (2010). Brain composition and olfactory learning in honey bees. *Neurobiol. Learn. Mem.* 93, 435–443. doi: 10.1016/j.nlm.2010.01.001

Gronenberg, W., and Hölldobler, B. (1999). Morphologic representation of visual and antennal information in the ant brain. *J. Comp. Neurol.* 412, 229–240. doi: 10.1002/(sici)1096-9861(19990920)412:2<229::aid-cne4>3.0.co;2-e

Guerra, P. A., and Reppert, S. M. (2015). Sensory basis of lepidopteran migration: focus on the monarch butterfly. *Curr. Opin. Neurobiol.* 34C, 20–28. doi: 10.1016/j.conb.2015.01.009

Guo, J., Fu, X., Wu, X., Zhao, X., and Wu, K. (2015). Annual migration of *Agrotis segetum* (Lepidoptera: Noctuidae): observed on a small isolated island in northern china. *PLoS One* 10:e0131639. doi: 10.1371/journal.pone.0131639

Heinze, S., Florman, J., Asokaraj, S., el Jundi, B., and Reppert, S. M. (2013). Anatomical basis of sun compass navigation II: the neuronal composition of the central complex of the monarch butterfly. *J. Comp. Neurol.* 521, 267–298. doi: 10.1002/cne.23214

Heinze, S., and Homberg, U. (2007). Maplike representation of celestial E-vector orientations in the brain of an insect. *Science* 315, 995–997. doi: 10.1515/nf-2007-0205

Heinze, S., and Homberg, U. (2008). Neuroarchitecture of the central complex of the desert locust: intrinsic and columnar neurons. *J. Comp. Neurol.* 511, 454–478. doi: 10.1002/cne.21842

Heinze, S., and Reppert, S. M. (2011). Sun compass integration of skylight cues in migratory monarch butterflies. *Neuron* 69, 345–358. doi: 10.1016/j.neuron.2010.12.025

Heinze, S., and Reppert, S. M. (2012). Anatomical basis of sun compass navigation I: the general layout of the monarch butterfly brain. *J. Comp. Neurol.* 520, 1599–1628. doi: 10.1002/cne.23054

Heinze, S., and Warrant, E. J. (2016). Bogong moths. *Curr. Biol.* 26, R263–R265. doi: 10.1016/j.cub.2015.12.022

Held, M., Berz, A., Hensgen, R., Muenz, T. S., Scholl, C., Rössler, W., et al. (2016). Microglomerular synaptic complexes in the sky-compass network of the honeybee connect parallel pathways from the anterior optic tubercle to the central complex. *Front. Behav. Neurosci.* 10:186. doi: 10.3389/fnbeh.2016.00186

Homberg, U. (1994). Flight-correlated activity changes in neurons of the lateral accessory lobes in the brain of the locust *Schistocerca gregaria*. *J. Comp. Physiol. A* 175, 597–610. doi: 10.1007/bf00199481

Homberg, U. (2008). Evolution of the central complex in the arthropod brain with respect to the visual system. *Arthropod Struct. Dev.* 37, 347–362. doi: 10.1016/j.asd.2008.01.008

Homberg, U., Hofer, S., Pfeiffer, K., and Gebhardt, S. (2003). Organization and neural connections of the anterior optic tubercle in the brain of the locust, *Schistocerca gregaria*. *J. Comp. Neurol.* 462, 415–430. doi: 10.1002/cne.10771

Hourcade, B., Muenz, T. S., Sandoz, J.-C., Rössler, W., and Devaud, J.-M. (2010). Long-term memory leads to synaptic reorganization in the mushroom bodies: a memory trace in the insect brain? *J. Neurosci.* 30, 6461–6465. doi: 10.1523/JNEUROSCI.0841-10.2010

Huetteroth, W., el Jundi, B., el Jundi, S., and Schachtner, J. (2010). 3D-reconstructions and virtual 4D-visualization to study metamorphic brain development in the sphinx moth *Manduca sexta*. *Front. Syst. Neurosci.* 4:7. doi: 10.3389/fnsys.2010.00007

Immonen, E.-V., Dacke, M., Heinze, S., and el Jundi, B. (2017). Anatomical organization of the brain of a diurnal and a nocturnal dung beetle. *J. Comp. Neurol.* 525, 1879–1908. doi: 10.1002/cne.24169

Ito, K., Shinomiya, K., Ito, M., Armstrong, J. D., Boyan, G., Hartenstein, V., et al. (2014). A systematic nomenclature for the insect brain. *Neuron* 81, 755–765. doi: 10.1016/j.neuron.2013.12.017

Kinoshita, M., Pfeiffer, K., and Homberg, U. (2007). Spectral properties of identified polarized-light sensitive interneurons in the brain of the desert locust *Schistocerca gregaria*. *J. Exp. Biol.* 210, 1350–1361. doi: 10.1242/jeb.02744

Klagges, B., Heimbeck, G., Godenschwege, T. A., Hofbauer, A., Pflugfelder, G. O., Reifegerste, R., et al. (1996). Invertebrate synapsins: a single gene codes for several isoforms in *Drosophila*. *J. Neurosci.* 16, 3154–3165.

Kondoh, Y., Kaneshiro, K. Y., Kimura, K.-I., and Yamamoto, D. (2003). Evolution of sexual dimorphism in the olfactory brain of Hawaiian *Drosophila*. *Proc. Biol. Soc.* 270, 1005–1013. doi: 10.1098/rspb.2003.2331

Kunst, M., Pförtner, R., Aschenbrenner, K., and Heinrich, R. (2011). Neurochemical architecture of the central complex related to its function in the control of grasshopper acoustic communication. *PLoS One* 6:e25613. doi: 10.1371/journal.pone.0025613

Kuntz, S., Poeck, B., and Strauss, R. (2017). Visual working memory requires permissive and instructive NO/cGMP signaling at presynapses in the *Drosophila* central brain. *Curr. Biol.* 27, 613–623. doi: 10.1016/j.cub.2016.12.056

Kurylas, A. E., Rohlfing, T., Krofczik, S., Jenett, A., and Homberg, U. (2008). Standardized atlas of the brain of the desert locust, *Schistocerca gregaria*. *Cell Tissue Res.* 333, 125–145. doi: 10.1007/s00441-008-0620-x

Kvello, P., Løfaldli, B. B., Rybak, J., Menzel, R., and Mustaparta, H. (2009). Digital, three-dimensional average shaped atlas of the *Heliothis virescens* brain with integrated gustatory and olfactory neurons. *Front. Syst. Neurosci.* 3:14. doi: 10.3389/neuro.06.014.2009

Laughlin, S. B. (2001). Energy as a constraint on the coding and processing of sensory information. *Curr. Opin. Neurobiol.* 11, 475–480. doi: 10.1016/s0959-4388(00)00237-3

Martin, J., Guo, P., Mu, L., Harley, C. M., and Ritzmann, R. E. (2015). Central-complex control of movement in the freely walking cockroach. *Curr. Biol.* 25, 2795–2803. doi: 10.1016/j.cub.2015.09.044

Merlin, C., Heinze, S., and Reppert, S. M. (2012). Unraveling navigational strategies in migratory insects. *Curr. Opin. Neurobiol.* 22, 353–361. doi: 10.1016/j.conb.2011.11.009

Montgomery, S. H., Merrill, R. M., and Ott, S. R. (2016). Brain composition in Heliconius butterflies, posteclosion growth and experience-dependent neuropil plasticity. *J. Comp. Neurol.* 524, 1747–1769. doi: 10.1002/cne.23993

Montgomery, S. H., and Ott, S. R. (2014). Brain composition in *Godyris zavaleta*, a diurnal butterfly, reflects an increased reliance on olfactory information. *J. Comp. Neurol.* 523, 869–891. doi: 10.1002/cne.23711

Mota, T., Gronenberg, W., Giurfa, M., and Sandoz, J.-C. (2013). Chromatic processing in the anterior optic tubercle of the honey bee brain. *J. Neurosci.* 33, 4–16. doi: 10.1523/JNEUROSCI.1412-12.2013

Mota, T., Yamagata, N., Giurfa, M., Gronenberg, W., and Sandoz, J.-C. (2011). Neural organization and visual processing in the anterior optic tubercle of the honeybee brain. *J. Neurosci.* 31, 11443–11456. doi: 10.1523/JNEUROSCI.0995-11.2011

Namiki, S., Iwabuchi, S., Pansopha Kono, P., and Kanzaki, R. (2014). Information flow through neural circuits for pheromone orientation. *Nat. Comm.* 5:5919. doi: 10.1038/ncomms6919

Namiki, S., and Kanzaki, R. (2016a). Comparative Neuroanatomy of the lateral accessory lobe in the insect brain. *Front. Physiol.* 7:244. doi: 10.3389/fphys.2016.00244

Namiki, S., and Kanzaki, R. (2016b). The neurobiological basis of orientation in insects: insights from the silkmoth mating dance. *Curr. Opin. Insect Sci.* 15, 16–26. doi: 10.1016/j.cois.2016.02.009

Niven, J. E., and Laughlin, S. B. (2008). Energy limitation as a selective pressure on the evolution of sensory systems. *J. Exp. Biol.* 211, 1792–1804. doi: 10.1242/jeb.017574

O'Donnell, S., Clifford, M. R., DeLeon, S., Papa, C., Zahedi, N., and Bulova, S. J. (2013). Brain size and visual environment predict species differences in paper wasp sensory processing brain regions (hymenoptera: vespidae, polistinae). *Brain Behav. Evol.* 82, 177–184. doi: 10.1159/000354968

Ofstad, T. A., Zuker, C. S., and Reiser, M. B. (2011). Visual place learning in *Drosophila melanogaster*. *Nature* 474, 204–207. doi: 10.1038/nature10131

Omoto, J. J., Keles, M. F., Nguyen, B.-C. M., Bolanos, C., Lovick, J. K., Frye, M. A., et al. (2017). Visual input to the *Drosophila* central complex by developmentally and functionally distinct neuronal populations. *Curr. Biol.* 27, 1098–1110. doi: 10.1016/j.cub.2017.02.063

Ott, S. R. (2008). Confocal microscopy in large insect brains: zinc-formaldehyde fixation improves synapsin immunostaining and preservation of morphology in whole-mounts. *J. Neurosci. Methods* 172, 220–230. doi: 10.1016/j.jneumeth.2008.04.031

Ott, S. R., and Rogers, S. M. (2010). Gregarious desert locusts have substantially larger brains with altered proportions compared with the solitarious phase. *Proc. Biol. Sci.* 277, 3087–3096. doi: 10.1098/rspb.2010.0694

Pfeiffer, K., and Homberg, U. (2007). Coding of azimuthal directions via time-compensated combination of celestial compass cues. *Curr. Biol.* 17, 960–965. doi: 10.1016/j.cub.2007.04.059

Pfeiffer, K., and Homberg, U. (2014). Organization and functional roles of the central complex in the insect brain. *Annu. Rev. Entomol.* 59, 165–184. doi: 10.1146/annurev-ento-011613-162031

Pfeiffer, K., and Kinoshita, M. (2012). Segregation of visual inputs from different regions of the compound eye in two parallel pathways through the anterior optic tubercle of the bumblebee (*Bombus ignitus*). *J. Comp. Neurol.* 520, 212–229. doi: 10.1002/cne.22776

Pfeiffer, K., Kinoshita, M., and Homberg, U. (2005). Polarization-sensitive and light-sensitive neurons in two parallel pathways passing through the anterior optic tubercle in the locust brain. *J. Neurophysiol.* 94, 3903–3915. doi: 10.1152/jn.00276.2005

Reppert, S. M., Guerra, P. A., and Merlin, C. (2016). Neurobiology of monarch butterfly migration. *Annu. Rev. Entomol.* 61, 25–42. doi: 10.1146/annurev-ento-010814-020855

Ritzmann, R. E., Ridgel, A. L., and Pollack, A. J. (2008). Multi-unit recording of antennal mechano-sensitive units in the central complex of the cockroach, *Blaberus discoidalis*. *J. Comp. Physiol. A Neuroethol. Sens. Neural Behav. Physiol.* 194, 341–360. doi: 10.1007/s00359-007-0310-2

Riveros, A. J., and Gronenberg, W. (2010). Brain allometry and neural plasticity in the bumblebee *Bombus occidentalis*. *Brain Behav. Evol.* 75, 138–148. doi: 10.1159/000306506

Rohlfing, T., Brandt, R., Maurer, C. R. Jr., and Menzel, R. (2001). "Bee brains, B-splines and computational democracy: generating an average shape atlas," in *Proceedings of IEEE Workshop on Mathematical Methods in Biomedical Image Analysis*, (Los Alamitos, CA: IEEE Computer Society), 187–194. doi: 10.1109/MMBIA.2001.991733

Rohlfing, T., and Maurer, C. R. Jr. (2007). Shape-based averaging. *IEEE Trans. Image Process.* 16, 153–161. doi: 10.1109/tip.2006.884936

Schmitt, S., Evers, J. F., Duch, C., Scholz, M., and Obermayer, K. (2004). New methods for the computer-assisted 3-D reconstruction of neurons from confocal image stacks. *Neuroimage* 23, 1283–1298. doi: 10.1016/j.neuroimage.2004.06.047

Seelig, J. D., and Jayaraman, V. (2013). Feature detection and orientation tuning in the *Drosophila* central complex. *Nature* 503, 262–266. doi: 10.1038/nature12601

Seelig, J. D., and Jayaraman, V. (2015). Neural dynamics for landmark orientation and angular path integration. *Nature* 521, 186–191. doi: 10.1038/nature14446

Stöckl, A. L., and Heinze, S. (2015). A clearer view of the insect brain—combining bleaching with standard whole-mount immunocytochemistry allows confocal imaging of pigment-covered brain areas for 3D reconstruction. *Front. Neuroanat.* 9:121. doi: 10.3389/fnana.2015.00121

Stöckl, A., Heinze, S., Charalabidis, A., el Jundi, B., Warrant, E. J., and Kelber, A. (2016a). Differential investment in visual and olfactory brain areas reflects behavioural choices in hawk moths. *Sci. Rep.* 6:26041. doi: 10.1038/srep26041

Stöckl, A. L., Ribi, W. A., and Warrant, E. J. (2016b). Adaptations for nocturnal and diurnal vision in the hawkmoth lamina. *J. Comp. Neurol.* 524, 160–175. doi: 10.1002/cne.23832

Strauss, R. (2002). The central complex and the genetic dissection of locomotor behaviour. *Curr. Opin. Neurobiol.* 12, 633–638. doi: 10.1016/s0959-4388(02)00385-9

Varga, A. G., and Ritzmann, R. E. (2016). Cellular basis of head direction and contextual cues in the insect brain. *Curr. Biol.* 26, 1816–1828. doi: 10.1016/j.cub.2016.05.037

Warrant, E. J., Frost, B., Green, K., Mouritsen, H., Dreyer, D., Adden, A., et al. (2016). The australian bogong moth agrotis infusa: a long-distance nocturnal navigator. *Front. Behav. Neurosci.* 10:77. doi: 10.3389/fnbeh.2016.00077

Warton, D. I., Duursma, R. A., Falster, D. S., and Taskinen, S. (2012). smatr 3- an R package for estimation and inference about allometric lines. *Methods Ecol. Evol.* 3, 257–259. doi: 10.1111/j.2041-210x.2011.00153.x

Warton, D. I., Wright, I. J., Falster, D. S., and Westoby, M. (2006). Bivariate line-fitting methods for allometry. *Biol. Rev.* 81, 259–291. doi: 10.1017/s1464793106007007

Wegerhoff, R., and Breidbach, O. (1992). Structure and development of the larval central complex in a holometabolous insect, the beetle *Tenebrio molitor*. *Cell Tissue Res.* 268, 341–358. doi: 10.1007/bf00318803

Wei, H., el Jundi, B., Homberg, U., and Stengl, M. (2010). Implementation of pigment-dispersing factor-immunoreactive neurons in a standardized atlas of the brain of the cockroach *Leucophaea maderae*. *J. Comp. Neurol.* 518, 4113–4133. doi: 10.1002/cne.22494

Wolff, T., Iyer, N. A., and Rubin, G. M. (2015). Neuroarchitecture and neuroanatomy of the *Drosophila* central complex: a GAL4-based dissection of protocerebral bridge neurons and circuits. *J. Comp. Neurol.* 523, 997–1037. doi: 10.1002/cne.23705

Zeller, M., Held, M., Bender, J., Berz, A., Heinloth, T., Hellfritz, T., et al. (2015). Transmedulla neurons in the sky compass network of the honeybee (*Apis mellifera*) are a possible site of circadian input. *PLoS One* 10:e0143244. doi: 10.1371/journal.pone.0143244

Zhan, S., Merlin, C., Boore, J. L., and Reppert, S. M. (2011). The monarch butterfly genome yields insights into long-distance migration. *Cell* 147, 1171–1185. doi: 10.1016/j.cell.2011.09.052

Conflict of Interest Statement: The authors declare that the research was conducted in the absence of any commercial or financial relationships that could be construed as a potential conflict of interest.

frontiers in Behavioral Neuroscience

ORIGINAL RESEARCH
published: 14 November 2017
doi: 10.3389/fnbeh.2017.00226

The Role of Celestial Compass Information in *Cataglyphis* Ants during Learning Walks and for Neuroplasticity in the Central Complex and Mushroom Bodies

Robin Grob[1]*†, *Pauline N. Fleischmann*[1]*†, *Kornelia Grübel*[1], *Rüdiger Wehner*[2] *and Wolfgang Rössler*[1]

[1]*Behavioral Physiology and Sociobiology (Zoology II), Biozentrum, University of Würzburg, Würzburg, Germany,* [2]*Brain Research Institute, University of Zürich, Zürich, Switzerland*

OPEN ACCESS

Edited by:
Stanley Heinze,
Lund University, Sweden

Reviewed by:
Anna Lisa Stöckl,
Aalto University School of Science, Finland
Ajay Narendra,
Macquarie University, Australia

***Correspondence:**
Robin Grob
robin.grob@uni-wuerzburg.de
Pauline N. Fleischmann
pauline.fleischmann@uni-wuerzburg.de

†These authors have contributed equally to this work.

Received: *01 September 2017*
Accepted: *30 October 2017*
Published: *14 November 2017*

Citation:
Grob R, Fleischmann PN, Grübel K, Wehner R and Rössler W (2017) The Role of Celestial Compass Information in Cataglyphis Ants during Learning Walks and for Neuroplasticity in the Central Complex and Mushroom Bodies. Front. Behav. Neurosci. 11:226. doi: 10.3389/fnbeh.2017.00226

Central place foragers are faced with the challenge to learn the position of their nest entrance in its surroundings, in order to find their way back home every time they go out to search for food. To acquire navigational information at the beginning of their foraging career, *Cataglyphis noda* performs learning walks during the transition from interior worker to forager. These small loops around the nest entrance are repeatedly interrupted by strikingly accurate back turns during which the ants stop and precisely gaze back to the nest entrance—presumably to learn the landmark panorama of the nest surroundings. However, as at this point the complete navigational toolkit is not yet available, the ants are in need of a reference system for the compass component of the path integrator to align their nest entrance-directed gazes. In order to find this directional reference system, we systematically manipulated the skylight information received by ants during learning walks in their natural habitat, as it has been previously suggested that the celestial compass, as part of the path integrator, might provide such a reference system. High-speed video analyses of distinct learning walk elements revealed that even exclusion from the skylight polarization pattern, UV-light spectrum and the position of the sun did not alter the accuracy of the look back to the nest behavior. We therefore conclude that *C. noda* uses a different reference system to initially align their gaze directions. However, a comparison of neuroanatomical changes in the central complex and the mushroom bodies before and after learning walks revealed that exposure to UV light together with a naturally changing polarization pattern was essential to induce neuroplasticity in these high-order sensory integration centers of the ant brain. This suggests a crucial role of celestial information, in particular a changing polarization pattern, in initially calibrating the celestial compass system.

Keywords: look-back behavior, desert ants, vector navigation, sky-compass pathway, memory, central complex, mushroom body, visual orientation

INTRODUCTION

Before starting their foraging career central place foragers, like bees, wasps and ants, have to acquire knowledge about the position of their nest in its surroundings and need to calibrate their navigational toolkit (Collett et al., 2013; Fleischmann et al., 2016). In order to do so, they perform learning flights or walks. Studies of this early learning behavior in bees (Opfinger, 1931; Hempel de Ibarra et al., 2009; Philippides et al., 2013; Degen et al., 2015), wasps (Zeil et al., 1996; Stürzl et al., 2016) and ants (Wehner et al., 2004; Fleischmann et al., 2016, 2017) revealed striking parallels in the general sequence of this behavior (Zeil, 2012). When leaving the nest entrance for the first time honeybees (Lehrer, 1993), bumblebees (Hempel de Ibarra et al., 2009; Collett et al., 2013; Philippides et al., 2013) and wasps (Zeil et al., 1996; Stürzl et al., 2016) turn back immediately towards their nest entrance and look back before flying in multiple arcs parallel to the nest entrance. As walking insects do not walk sideways, ants perform repeated turns during their learning walk loops and make stops to look back towards their nest entrance (Wehner et al., 2004; Fleischmann et al., 2017). During these looks back the animals most probably learn the landmark panorama (honeybees: Opfinger, 1931; Lehrer, 1993; bumblebees: Collett et al., 2013; ants: Fleischmann et al., 2016, 2017). Over time the arcs or loops increase in size, and novices move farther away from the nest entrance, while still looking back towards it (Zeil et al., 1996; Wehner et al., 2004; Philippides et al., 2013; Fleischmann et al., 2016). Likewise, experienced foragers perform a learning behavior that includes looks back to the nest, e.g., when experienced animals had difficulties pinpointing their nest (Zeil, 1993; Zeil et al., 1996) or when the nest surrounding had changed drastically (Müller and Wehner, 2010; Narendra and Ramirez-Esquivel, 2017).

However, to determine the direction of the nest entrance from various positions in space, the animals need some kind of reference system. It has been previously proposed, that this system could be part of the path integrator (Graham et al., 2010; Müller and Wehner, 2010), which integrates information about the walked directions (compass) and the distance covered (odometer) into a vector pointing towards the starting point. In *Cataglyphis* ants the path integrator is the main navigational tool (Müller and Wehner, 1988). The ants use an odometer (Wittlinger et al., 2006) and optic flow (Pfeffer and Wittlinger, 2016) to determine the distance covered. By integrating the odometer information with information about the walked directions, for which the ants use the celestial compass (Müller and Wehner, 1988; Wehner et al., 1996; Wehner, 2003), they determine a vector pointing homewards. The celestial compass mainly relies on information about the position of the sun and the skylight polarization pattern in the UV-spectrum (Duelli and Wehner, 1973). This suggests that the skylight polarization pattern only in the UV-spectrum could provide a suitable reference system for the compass information of the path integrator to align gaze directions during learning walks.

The polarization direction of the UV-skylight is detected by specialized ommatidia in the dorsal rim area of the compound eye (Labhart and Meyer, 1999). The information is transferred by neurons forming the anterior optical tract (AOT) via several stages into the central complex (CX; Schmitt et al., 2016). In the CX polarization of the skylight is represented in a map-like pattern (Heinze and Homberg, 2007; Homberg et al., 2011; Heinze and Reppert, 2012). The CX was also shown to be involved in several tasks closely linked to orientation and navigation (Pfeiffer and Homberg, 2014; Fiore et al., 2017). In *Drosophila* the CX is additionally involved in landmark memory (Neuser et al., 2008), landmark orientation and angular path integration (Seelig and Jayaraman, 2015). Another prominent neuronal pathway in bees and ants, the anterior superior optical tract (asot), transfers visual information into the visual subregions of the mushroom bodies (MB; Gronenberg, 2001; Yilmaz et al., 2016). The MBs are centers for sensory integration, learning and memory. They undergo substantial neuronal changes when exposed first time to light (*Drosophila*: Barth and Heisenberg, 1997; *Apis*: Scholl et al., 2014; *Cataglyphis*: Seid and Wehner, 2009; Stieb et al., 2010, 2012) and during the formation of long-term memory (*Acromyrmex*: Falibene et al., 2015; *Apis*: Hourcade et al., 2010).

The duration of learning walk behaviors lasts for up to 3 days (Wehner et al., 2004; Stieb et al., 2012; Fleischmann et al., 2016). This correlates with the time needed for stable long-term memory formation (Menzel, 2001; Hourcade et al., 2010; Falibene et al., 2015; Scholl et al., 2015) and the time needed to induce neuronal changes in the visual subregions of the MBs after exposure to light pulses in *Cataglyphis fortis* (Stieb et al., 2010, 2012). Therefore, learning walks are perfectly suited to study brain-behavior-environment interactions. In this study, we restricted the input into the sky-compass of *Cataglyphis noda* during their early learning walks to ask, which reference system the ants use during this early learning phase to align their gaze directions. Ants that participated in the behavioral field experiments were subsequently used for neuroanatomical analyses. This allowed us to look at the interaction between the learning-walk behavior, the received information during these walks, as well as changes in the neuronal architecture in the terminal stages of two visual pathways, the CX and the MBs. The results suggest that natural skylight polarization information with the UV part of the light spectrum present induce structural changes in the CX and the MBs indicating their role in the initial calibration of visual pathways processing celestial information. However, exclusion of sky-compass information did not prevent *C. noda* from looking back towards their nest entrance suggesting, that celestial cues do not serve as the initial reference system for compass information during learning walks.

MATERIALS AND METHODS

Animals

Experiments were conducted with *C. noda* (Brullé 1832) (**Figure 1A**) in Schinias National Park, Marathonas, Greece from June–August 2016. A colony with a nest entrance in the middle

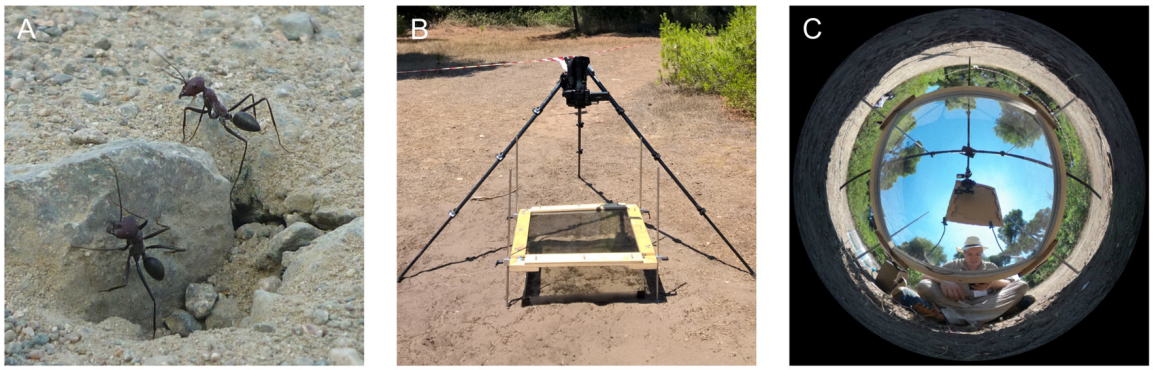

FIGURE 1 | Experimental setup for skylight manipulation experiments. **(A)** Unmarked *C. noda* ants at the nest entrance. **(B)** 30 cm above the nest entrance, a filter was placed in order to alter the skylight information. Learning walks were recorded with a high-speed 4K-camera. In addition, a HD-camcorder recorded the nest entrance for the whole day. **(C)** Panoramic image of the UV-block with sunshade setup (UVBS). The observer was located in the south to trigger the high-speed recording and to prevent unmarked ants from leaving the area covered by the filter through the opening in the fence, which was located in the south-west.

of a small clearing in the pine forest of the national park (38°08'N 24°01'E) was used for the experiments. In order to make sure that only novices (ants performing learning walks for the first time) were used, all ants leaving the nest were marked on at least three consecutive days before the experiment using car paint (Motip Lackstift Acryl, MOTIP DUPLI GmbH, Haßmersheim, Germany). Unmarked ants can then be considered to be naïve, as it was shown in previous studies (Fleischmann et al., 2016, 2017). The animals were allowed to perform learning walks for three consecutive days within an arena (60 cm × 60 cm) restricted by a transparent plastic fence. Only marked foragers were allowed to leave the restricted area through a small exit in the fence.

Manipulation of the Skylight

To manipulate the skylight the ants perceived during their learning walks, different filter systems (60 cm × 60 cm; **Table 1**) were placed 30 cm above the nest entrance from the third day of marking. Thereby, ants that did not leave the nest, but stayed inside of the nest entrance area would only perceive the altered skylight. The ants could still encounter the landmark panorama in the setup. As a control for the setup, a UV-permeable plexiglass was installed above the arena that did not alter the skylight perceived by the ants (UV100). To alter the skylight polarization pattern to an artificial, fixated one, a linear polarization filter was used. To test whether

TABLE 1 | Groups and filter systems used for skylight manipulation.

Group	Icon	Conditions	Analyses
DD	■	Interior workers that had not yet performed learning walks (excavated in the dark using red light);	Neuroanatomy
UV-Block with sunshade (UVBS)		Three days of learning walks under a UV-light impermeable filter (Plexiglas (Gallery) 0A570 GT, Evonik Performance Materials GmbH, Essen, Germany) blocking 99.7% of the light below 420 nm with a sunshade, to additionally disguise the position of the sun;	Neuroanatomy Gaze direction
Diffusor (Dif)		Three days of learning walks under a diffusor that lets UV-light pass (Plexiglas (GS) 2458 SC, Evonik Performance Materials GmbH, Essen, Germany), but diffuses any polarization pattern in the skylight;	Neuroanatomy
Polarization filter (P)		Three days of learning walks under a polarization filter (OUV6060-C—HNP'B replacement, Knight Optical Ltd., Harrietsham, United Kingdom) that lets UV-light pass, but provides an artificial linear, fixed polarization pattern;	Neuroanatomy Gaze direction
UV100	□	Three days of learning walks under a UV-light permeable Plexiglas (Plexiglas (GS) 2458, Evonik Performance Materials GmbH, Essen, Germany), as a control for the setup;	Neuroanatomy Gaze direction
No filter	N	Three days of learning walks under natural conditions, as a control for the experiment;	Gaze direction

the full light spectrum without a polarization pattern had an influence on the ants' behavioral development, a UV-permeable plexiglass that diffused the skylight was installed. The skylight polarization pattern and the position of the sun was blocked using a UV-impermeable plexiglass with a sunshade (UVBS; **Figures 1B,C**). On the second day of marking a camera set-up was placed north to the nest entrance. Two cameras were installed: a 4K-camcorder (HC-X1000, Panasonic Corporation, Kadoma, Japan) that recorded learning walks of novices at 50 fps, and a Full-HD camcorder (HDR-CX330E, Sony Corporation, Minato, Japan) that recorded the nest area at 25 fps for the entire day. Every time an unmarked ant left the nest entrance, an observer positioned south of the experimental setup triggered recordings of the 4K-camcoder using the Panasonic Image App (Version 10.9.2, Panasonic Corporation, Kadoma, Japan) on a Sony Xperia Z1 smartphone (Sony Corporation, Minato, Japan). Since it was not possible to film through the diffusor (Dif), only observational data is available for this experimental trial.

Neuroanatomical Procedures

Anti-Synapsin Immunolabeling

On the third day of recording, novices that performed wide range learning walks reaching up the fence were captured under the filter setup and kept in the dark until the next day. This ensured, that the ants had performed several learning walks under the altered skylight conditions and that their brains had enough time to undergo structural changes (Stieb et al., 2012; Fleischmann et al., 2016, 2017; Schmitt et al., 2016). In addition, interior workers (DD) were collected from another nest in which, similar to the experimental nest, all ants leaving the nest were marked over three consecutive days. In order to get interior workers that had never seen daylight before, the nest was excavated in the night using red light. All ants were kept in a dark box until the next day.

To analyze neuroanatomical changes in the CX and MBs (all neuroanatomical nomenclature after Ito et al., 2014), the brains were stained using a primary antibody to synapsin (SYNORF1, kindly provided by E. Buchner, University of Würzburg, Germany) and a secondary antibody coupled to AlexaFluor 568 (A12380, Molecular Probes, Eugene, OR, USA) dye.

The ants were cooled down in a freezer and decapitated in the dark. Immediately afterwards the brains were carefully dissected and fixated in 4% formaldehyde in phosphate-buffered saline (PBS) for 1 day. The brains were then rinsed three times in PBS for 10 min, followed by one rinse in 2% Triton-X 100 solution in PBS and two rinses in 0.5% Triton-X solution, for 10 min each, to permeabilize cell membranes for antibody application on whole mount brains. To block unspecific binding sites, the brains were then incubated for 1 h at room temperature on a shaker in a 0.5% Triton-X 100 solution in PBS with 2% of Normal Goat Serum (NGS, Jackson ImmunoResearch Laboratories). Afterwards, the brains were incubated for 3 days in the refrigerator (∼4°) on a shaker with the primary anti-synapsin antibody from mouse. A solution with 2% antibody, 2% NGS and 0.5% Triton-X 100 in PBS was used. After incubation the brains were rinsed five times for 10 min each in PBS. Then the secondary antibody, an anti-mouse antibody from goat with an Alexa Fluor 568 dye (4% in PBS with 1% NGS), was incubated for 2 days in the refrigerator on a shaker. The brains were then rinsed again three times in PBS for 10 min each, before they were dehydrated using an ethanol serial dilution. For that, they were rinsed for 10 min in every step: 30%, 50%, 70%, 90%, 95% ethanol in water and two times in 100% ethanol. The dehydrated brains were then cleared in methyl salicylate (M-2047; Sigma-Aldrich, Steinheim, Germany).

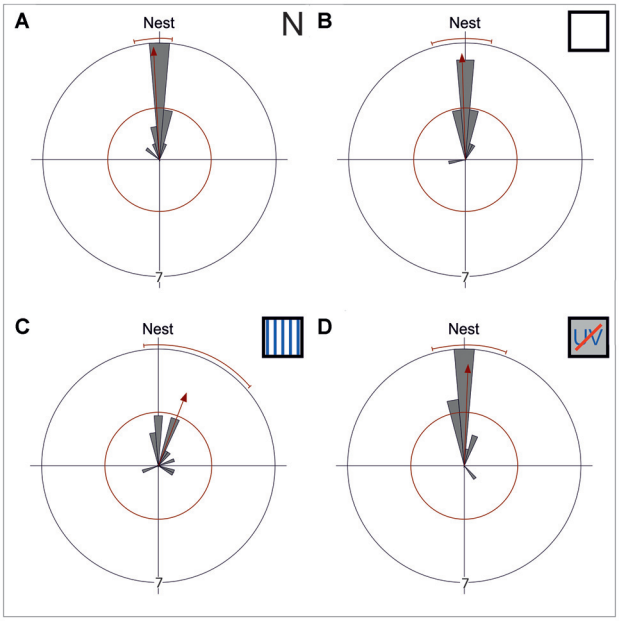

FIGURE 2 | Gaze directions during the longest stopping phases under different skylight conditions. Data are shown in gray and the corresponding statistics in red. The bins of the circular histogram include 10 degrees. The red circle indicates the critical value $\alpha = 0.05$ of the Rayleigh uniformity test. The red arrow indicates the r-vector pointing towards the mean direction. If the length of the vector exceeds the red circle the data is directed ($p < 0.05$). When the data is directed, a red line indicates the 95% confidence interval. If the expected direction (Nest ≙ 180°) lies within the confidence intervals limits, the data is directed towards the nest entrance. The outer circle indicates tic 7. Each data point is contributed by one back turn of one ant. **(A)** The mean gaze direction of the longest stopping phase in pirouettes during learning walks under natural/no filter conditions (N) is directed towards the nest entrance ($n = 15$). **(B)** The same is true for the mean gaze direction of the longest stopping phase under control conditions (UV100; $n = 15$) and **(C)** under an artificial, fixed polarization pattern (P; $n = 14$). **(D)** Even when excluded from all celestial information (UVBS; $n = 15$) the ants were able to gaze towards the nest entrance during the longest stopping phases. The mean angle and the angular variance did not differ between the four groups. For statistical details see text.

Anterograde Tracings of Neuronal Projections from the Medulla

To determine the neuronal projections via the asot in *C. noda*, projection neurons of the dorsal and ventral medulla (ME) were fluorescently stained in ants reared in laboratory colonies. The tracings of neuronal projections from the ME were performed

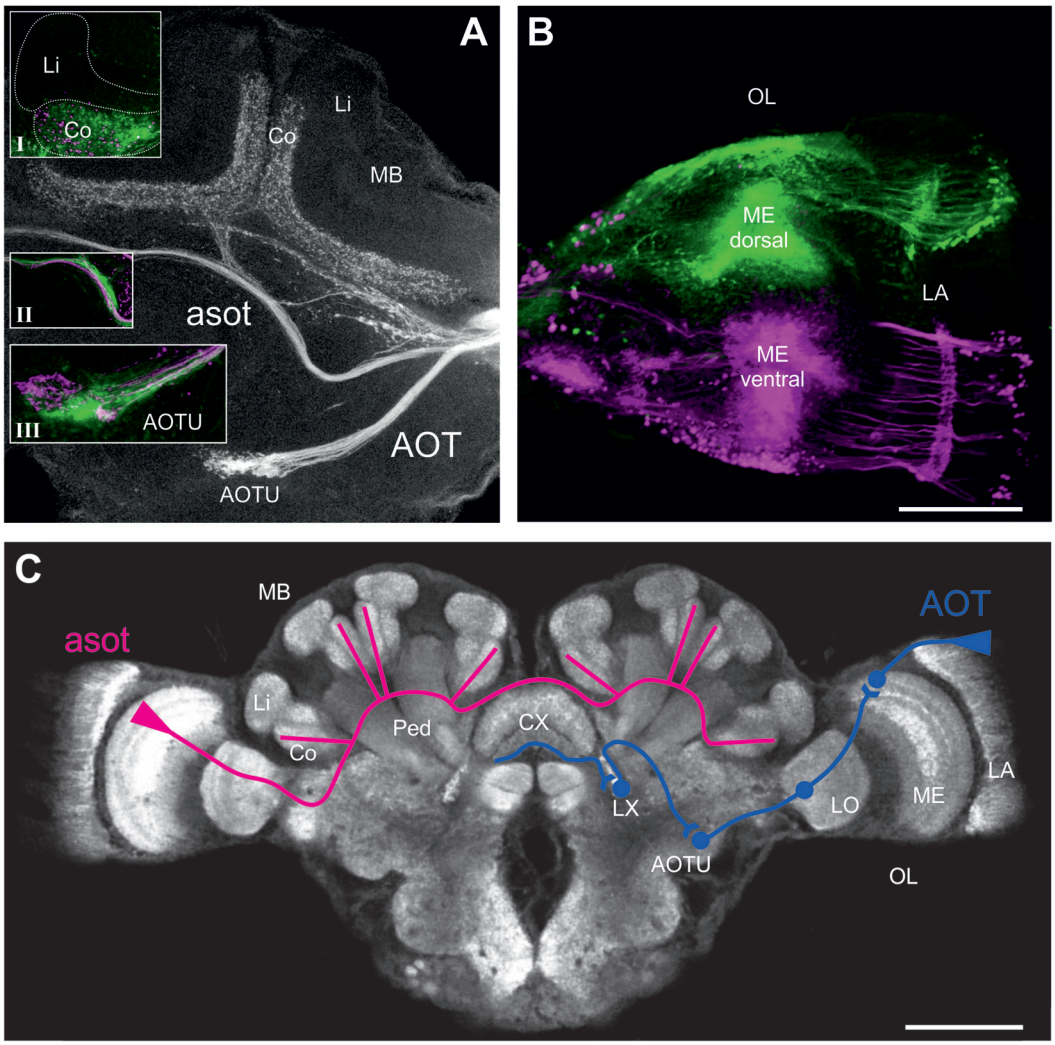

FIGURE 3 | Neuronal projections from the medualla (ME) via the anterior optical tract (AOT) and the anterior superior optic tract (asot) in the *Cataglyphis noda* brain. Anterograde tracings from focal dye injections the dorsal and ventral medulla (ME; microruby in magenta, Alexa 488 dextran in green, see under **B**): **(A)** Axon bundles from projection neurons in the medulla run anterior above the peduncle (Ped) and the central complex (CX) into the visual subregion of the mushroom body (MB) collar (Co) on both sides of the brain. Axonal projections from both the dorsal and the ventral ME run along the asot (inset **II**) into the Co. The most prominent input in the MB-calyx Co was found in injections into the dorsal ME (green) compared to those in the ventral ME (magenta) (inset **I**). Axonal projection from the ME also run into the anterior optical tubercle (AOTU) along the AOT. Z-projection from a stack of 27 images, 10x objective, 5 μm step size. Insets were taken with a 20x objective, 5 μm step size. **(B)** In the dorsal ME Dextran AlexaFloun488 (green) was injected using a glass capillary. In the ventral ME Dextran Tetramethylrhodamine (micro-Ruby) (magenta) was injected using a glass capillary. Images taken with a 10x objective, step size of 10 μm, stack of 19 images, zoom 2.65. The scale bar in **(B)**, also valid for **(A)**, is 100 μm. **(C)** Schematic depiction of the tracing of the asot (magenta) and the AOT (blue). The asot, as seen in the tracings in **(A)**, runs from the ME anterior above the peduncle and the CX into Co. The AOT (information combined with the one from Schmitt et al., 2016) runs from the dorsal rim of the lamina (LA) to the dorsal rim of the ME, and from there via the LO to the AOTU to be relayed further to the lateral complex (LX). The anterior CX pathway terminates in the lower half of the ellipsoid body (EB) of the CX (Schmitt et al., 2016). The confocal scan of the *C. noda* brain shows an anti-synapsin labeled brain, similar to the staining procedure used for the neuroanatomical analyses. The scale bar is 200 μm.

using similar methods as described in detail in Yilmaz et al. (2016). Ants were cooled and fixed with clay. A small window was cut in the head capsule, and the brain was rinsed with cooled ant ringer solution. Using a thin glass capillary, dextran tetramethylrhodamine (micro-Ruby, D-7162, Molecular Probes, Eugene, OR, USA) and Dextran AlexaFluor488 (D-22910, Molecular Probes, Eugene, OR, USA) were focally inserted in the dorsal and ventral medulla. The brain was then rinsed with ringer solution and the head capsule was covered with a thin piece of Parafilm to prevent the brain from drying out. The dyes were allowed to be transported by incubating the ants for 3 h at room temperature in a dark box with high humidity. Afterwards, the brains were dissected in cooled ringer solution and fixated in 4% formaldehyde in PBS overnight. The brains were rinsed five times in PBS for 10 min each before they were dehydrated using an ethanol serial dilution. For that, they were rinsed for 10 min, each

step: 30%, 50%, 70%, 90%, 95% in water, and two times 100% ethanol. The dehydrated brains were then cleared and mounted in methyl salicylate. Finally, the brains were digitized in the confocal laser scanning microscope (see below) using a 20×- or 10×-objective and step sizes of 5 μm or 10 μm.

Data Analyses

High-Speed Video Analyses

The 4K-videos obtained from the experiments were converted into image stacks using the Free Video to JPG Converter (v. 5.0.99 build 823, DVDVideoSoft, DIGITAL WAVE LTD., London, UK). Subsequently, the pirouettes (tight back turns Fleischmann et al., 2017) performed by novices were analyzed frame by frame using the MATLAB (2015a, The MathWorks Inc., Natick, MA, USA) application DIGILITE (Jan Hemmi and Robert Parker, The Australian National University, Canberra, Australia). For this, the positions of the mandibles and the thorax were marked manually in each frame. Additionally, the position of the nest entrance and the north direction were marked. With these coordinates the gaze direction relative to the nest entrance of the ants during their back-turns was determined. The direction of the nest entrance was defined as 180°. Stopping phases during the pirouettes were defined as in Fleischmann et al. (2017), and the longest of these stopping phases was used to test the directedness of the back turns.

Neuroanatomical Analyses

For microscopic analyses, the brains that had been dissected and histochemically treated in our field laboratory were transferred to the University of Würzburg using a refrigerator unit (∼4°C). A confocal laser scanning microscope (Leica TCS SP2, Leica Microsystems GmbH, Wetzlar, Germany) was used for scanning the brains as image stacks at a step size of 5 μm. We used the 10×-objective for overviews with 2.5 optical zoom NA imm (for CX), the 20×-objective with 2.7 optical zoom NA imm for the MB calyx, and the 63×-objective with 2.0 optical zoom NA imm for detailed scans in the lip (Li) and collar (Co) of the MB calyx. Subsequently, the volumes of the different components of the CX (fan-shaped body (FB), ellipsoid body (EB), protocerebral bridge (PB), noduli (No)) and of the MB calyx (Li, Co) were analyzed using the 3D-reconstruction software Amira (Amira 6.0.0, FEI Company, Hilsboro, OR, USA). In addition, synaptic complexes (microglomeruli, MG) were quantified in the visual and olfactory subregions of the MB calyx (Li, Co) using a modified version of the protocol by Groh et al. (2012; for further details, see Rössler et al., 2017). The CX, MB and other major neuropils were easily distinguishable in anti-synapsin labeled whole mount brains (**Figure 3C**), and based on tracings (Yilmaz et al., 2016, **Figures 3A,B** for *C. noda*). MB-calyx MG were quantified by counting the anti-synapsin labeled synaptic boutons in a defined volume of 1000 μm^3. The MG density was then calculated by averaging multiple volumes of interest in the two subregions (three in the Co, four in the Li) as numbers of MG per μm^3 following the protocol by Groh et al. (2012) and Muenz et al. (2015). From these numbers the total number of MG per calyx subdivisions was estimated by multiplying the MG densities by the volume of the corresponding neuropil. The ants used in this experiment had a median thorax length of 4.24 mm, ranging from 3.18 mm to 5.58 mm. Thorax length correlates with body size (Vowles, 1954) and, therefore, also with total brain size (Wehner et al., 2007). Since we did not find a correlation between thorax length and the analyzed neuropils of interest (Spearman roh test ($\alpha = 0.05$): CX: $n_{CX} = 45$, $p_{CX} = 0.545$, $r_{CX} = 0.093$; MB: $n_{MB} = 43$, $p_{MB} = 0.058$, $r_{MB} = 0.291$), absolute volumes and MG numbers were used in this study. These results are coherent with results obtained using head width as a measure for body size in *C. fortis* (Stieb et al., 2010). As no major group-specific differences in thorax lengths were apparent (Supplementary Figure S1), comparisons were made without corrections for group bias in overall brain size.

Statistical Analyses

The gaze directions were grouped into 10°-bins as previously done by Fleischmann et al. (2017). The circular statistical software Oriana (Kovach Computing Services, Anglesey, UK) was used to check with the Rayleigh test whether the data was randomly distributed. If the gaze directions were directed ($\alpha = 0.05$), we calculated the 95% confidence interval to check whether the expected direction (nest entrance: 180°) was within the limits. The mean angle and the angular variance were compared between the groups using a Mardia-Watson-Wheeler multisample test ($\alpha = 0.05$).

In the neuroanatomical studies, the volume between the different groups (DD, UVBS, Dif, P, UV100) within each neuropil (CX, Co, Li) was compared using the Kruskal-Wallis-test ($\alpha = 0.05$). In cases when a difference between the groups occurred, a *post hoc* pairwise comparison between DD and the other groups was performed using a Mann-Whitney U-test with Bonferroni correction. A critical value of $\alpha = 0.05$ was used (after Bonferroni correction: $\alpha = 0.0125$).

RESULTS

Gaze Direction Analyses and Behavioral Observations Under Different Skylight Conditions

While initially leaving their nest under natural conditions (N), *C. noda* walked in small loops around their nest entrance, similar as shown earlier (Fleischmann et al., 2017). These learning walks were repeatedly interrupted by characteristic turns, so called voltes and pirouettes. During the latter, the ants performed multiple stopping phases ($n = 15$, 4 ± 1.75, median ± IQR) with the longest stopping phases directed towards the nest entrance (Rayleigh Uniformity Test: $Z_0 = 13.856$, $n = 15$, $p < 0.001$; 95% Confidence Interval (−/+) 167.9°/186.0°; Mean: 177.0°; **Figure 2A**). The gaze direction during the longest stopping phases was directed towards the nest entrance when the experimental setup was installed using a UV-light

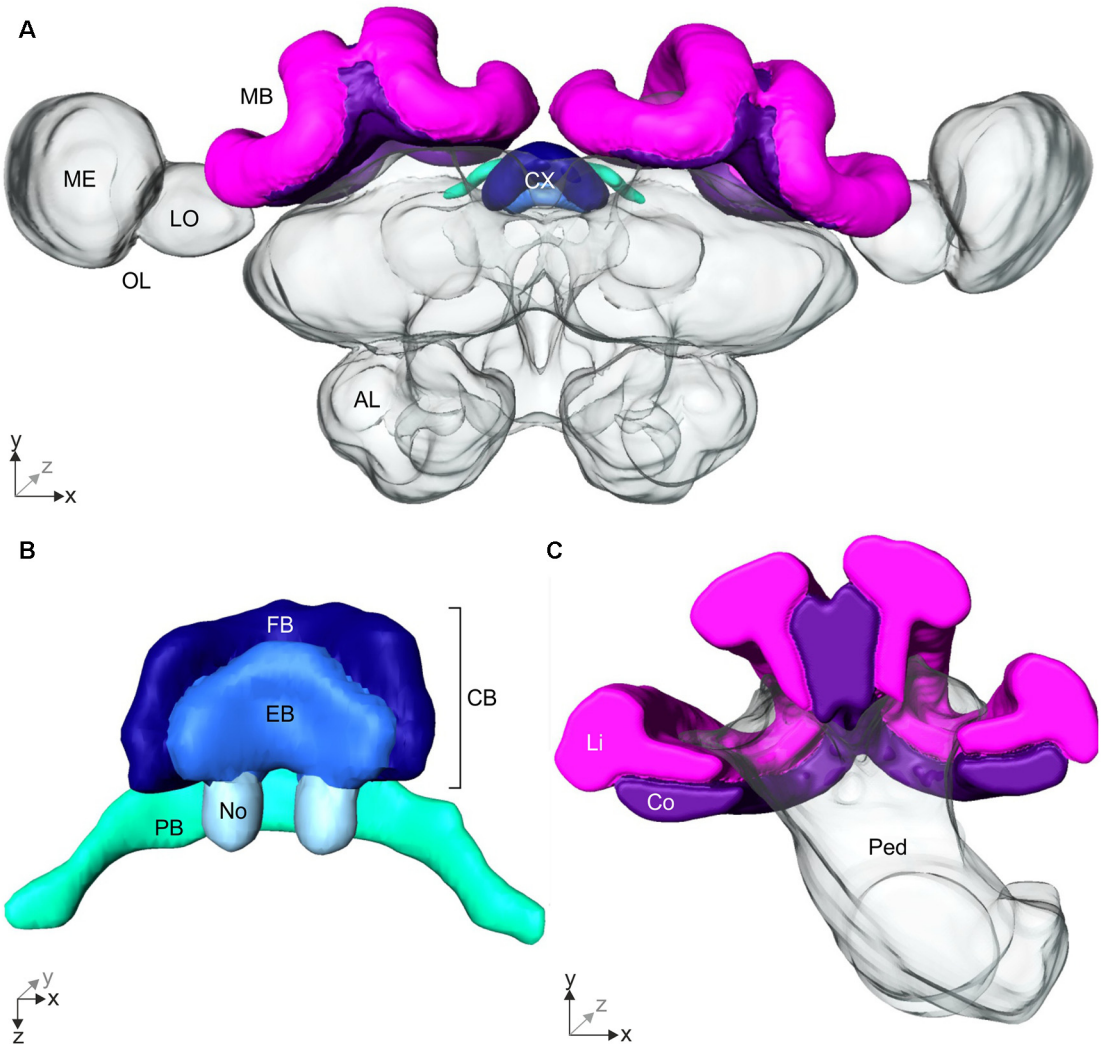

FIGURE 4 | 3D-reconstruction of the *Cataglyphis noda* brain. With the 3D-reconstruction software Amira the neuropils of the *C. noda* brain were manually reconstructed from the image stack obtained by the confocal laser scanning microscope. **(A)** 3D-reconstruction of a whole *C. noda* brain. To analyze the influence of celestial information during learning walks on neuroplasticity, the terminal stages of two visual pathways were reconstructed. The AOT transfers visual information, including polarization information, into the central complex (CX, shades of blue). The CX is located at the midline of the ant brain. Via the asot visual information is transferred to the mushroom body calyces (MB, magenta). Additionally, antennal lobes (AL), and optical lobes (OL) with the medulla (ME) and lobula (LO) are labeled. **(B)** The CX comprises several neuropils: The central body (CB, dark and light blue) is located most anterior. It consists of the large fan-shaped body (FB, dark blue) and the smaller ellipsoid body (EB, light blue), which is covered by the FB dorsally. Behind the CB, two globular neuropils, the noduli (No, pale blue) are located. Dorsally to that and slightly detached from the CB, the protocerebral bridge (PB, green) spans in a bridge-like shape between the mushroom bodies (MB). **(C)** The MB calyx includes the visual input region, the collar (Co, violet) and the olfactory input region, the lip (Li, magenta). They are located at the dorsal rim of the peduncle (Ped). Scale bars, **(A)** 200 μm; **(B,C)** 100 μm.

permeable filter as a control (UV100; Rayleigh Uniformity Test: $Z_0 = 12.306$, $n = 15$, $p < 0.001$; 95% Confidence Interval (−/+) 163.9°/192.55°; Mean: 178.2°; **Figure 2B**). When the natural skylight polarization pattern was altered to a linear one that did not change over the day (P) the overall structure of the walks remained unchanged and the gazes during the longest stopping phases were clearly directed towards the nest entrance (Rayleigh Uniformity Test: $Z_0 = 6.189$, $n = 14$, $p = 0.001$; 95% Confidence Interval (−/+) 173.1°/229.1; Mean: 201.1°; **Figure 2C**). One analyzed pirouette under P did not contain a stopping phase and therefore was not included in the circular statistics. After the learning walks had taken place for several days under this fixed polarization pattern, the polarization filter was rotated by either by 90° or in two steps of 45°. From visual observations we noticed that the sudden changes in the polarization pattern above the nest entrance seemed to increase the number of naïve ants performing learning walks shortly after the change took place (experimental day with stationary linear polarization pattern number of learning walks: $n = 71$ vs. experimental day with stepwise rotated (45°

every hour) linear polarization pattern number of learning walks: $n = 277$). When learning walks were performed under a diffused polarization pattern (Dif) no apparent changes in learning walk patterns compared to natural conditions could be observed. For the Dif conditions, further quantitative video analyses were not possible since we could not record through the diffusor. Nevertheless, more than 100 pirouettes, all directed towards the nest entrance, were observed during the three experimental days. However, even learning walks that were performed under the exclusion of any sky compass information by blocking UV-light, which is necessary for the ants to perceive the polarization pattern (Duelli and Wehner, 1973), and, at the same time, by excluding the position of the sun by using a sunshade (UVBS) were not altered in their overall structure compared to learning walks under natural conditions. The longest stopping phase of pirouettes under UVBS conditions was directed towards the nest entrance (Rayleigh Uniformity Test: $Z_0 = 11.406$, $n = 15$, $p < 0.001$; 95% Confidence Interval (−/+) 166.4°/200.0°; Mean: 183.2°; **Figure 2D**). The mean angle or the angular variance did not differ between all experimental groups (Mardia-Watson-Wheeler multi sample test: $W = 6.124$; $n_N = 15$; $n_{UV100} = 15$; $n_P = 14$; $n_{UVBS} = 15$; $p = 0.375$).

The AOT and asot in the *Cataglyphis* Brain

To investigate visual pathways to high-order integration centers in *C. noda* brains, we performed focal dye injections and anterograde neuronal tracings of neuronal projections from the dorsal and ventral medulla (ME; **Figure 3B**). This clearly revealed neuronal projections via the asot and via the AOT (**Figure 3A**). From 16 dye injected brains, three were successfully double stained (dorsal and ventral ME), three showed tracings from the dorsal ME only, and two from the ventral ME only. In all tracings, the asot projected from the ME anteriorly above the peduncle and the central complex (CX), bilaterally into the collar (Co) of the medial and lateral branches of the MBs (**Figures 3A,C**). Visual inspection of all tracings indicated that axonal projections via the asot from the dorsal ME were more prominent compared to the sparser projections and terminal branches from the ventral ME in the MB Co ($n = 8$; **Figure 3A**, inset I).

All tracings from the dorsal and ventral ME revealed projections to the anterior optic tubercle (AOTU) via the AOT (**Figures 3A,C**). The AOT was previously described in detail for *C. fortis* (Schmitt et al., 2016) by tracing projections only from the dorsal rim area of the lamina LA and ME. From there further stages are the lobula (LO), the AOTU, the lateral complex (LX) and finally the lower half of the EB of the CX (**Figure 3C**; for locust: Homberg et al., 2011; for *C. fortis*: Schmitt et al., 2016). Interestingly, our differential tracings from the dorsal and ventral ME revealed a clear pattern in the AOTU with a clear separation of ventral and dorsal projections in the upper unit of the AOTU and a mixed pattern in the lower part of the AOTU (**Figure 3A**, inset III).

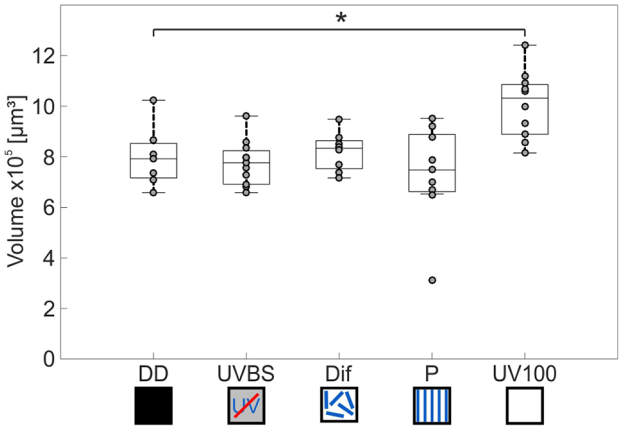

FIGURE 5 | Volume changes of the CX after 3 days of learning walks dependent on celestial information. The central line of each boxplot depicts the median of the data. The upper and lower limits of the boxes show the 25th and 75th percentiles, while the whiskers extend to the extreme data points without outliers. All data points (including outliers) are plotted as gray circles. A difference between the groups can be found using a Kruskal–Wallis test. With the Mann-Whitney U-test with a Bonferroni correction the data was *post hoc* compared to the DD group. The asterisk indicates that data is significantly different (after correction $p < 0.0125$) from the DD group. The central complex shows a volume increase compared to interior workers (DD; $n = 7$) only if the ants perceived the UV mediated natural polarization pattern that changes over the day (UV100; $n = 10$). If the polarization pattern was altered, either by diffusion (Dif; $n = 8$) or by a linear polarization filter (P; $n = 9$), no change in the volume of the CX occurred compared to DD. Similarly, when ants were excluded from any celestial information (UVBS; $n = 11$), no volume increase occurred. For statistical details and further explanations, see text.

Influence of Manipulated Skylight Input during Learning Walks on Neuronal Plasticity in the CX and MB

We investigated the influence of skylight manipulations during learning walks on neuronal changes in the terminal stages of the AOT and asot. The brains of ants that had participated in the behavior tests and had performed several days of learning walks under normal or altered skylight conditions were analyzed using 3D-reconstructions of the CX and MB (**Figure 4**), and quantifications of synaptic complexes in the MB. For comparison, brains of ants that had not yet performed learning walks (DD) were analyzed.

Volumetric Changes in the CX

The AOT transfers visual information into the CX (**Figure 3C**). The CX comprises several neuropils (**Figure 4B**): The central body (CB) is located most anterior and consists of the large FB and the smaller EB, which is covered by the FB dorsally. Behind the CB, two globular neuropils, the No, are located. Dorsally to that and slightly detached from the CB, the PB spans in a bridge-like shape between the MBs (**Figure 4B**). Comparing the CX of the ants that had previously participated in the behavioral studies (DD, UVBS, Dif, P, UV100), showed a statistically significant difference between their CX volumes (Kruskal–Wallis test: CX Volume: $\chi^2_4 = 16.38$; $n = 45$; $p = 0.0046$; **Figure 5**). Compared to the CX of interior workers (DD) the CX

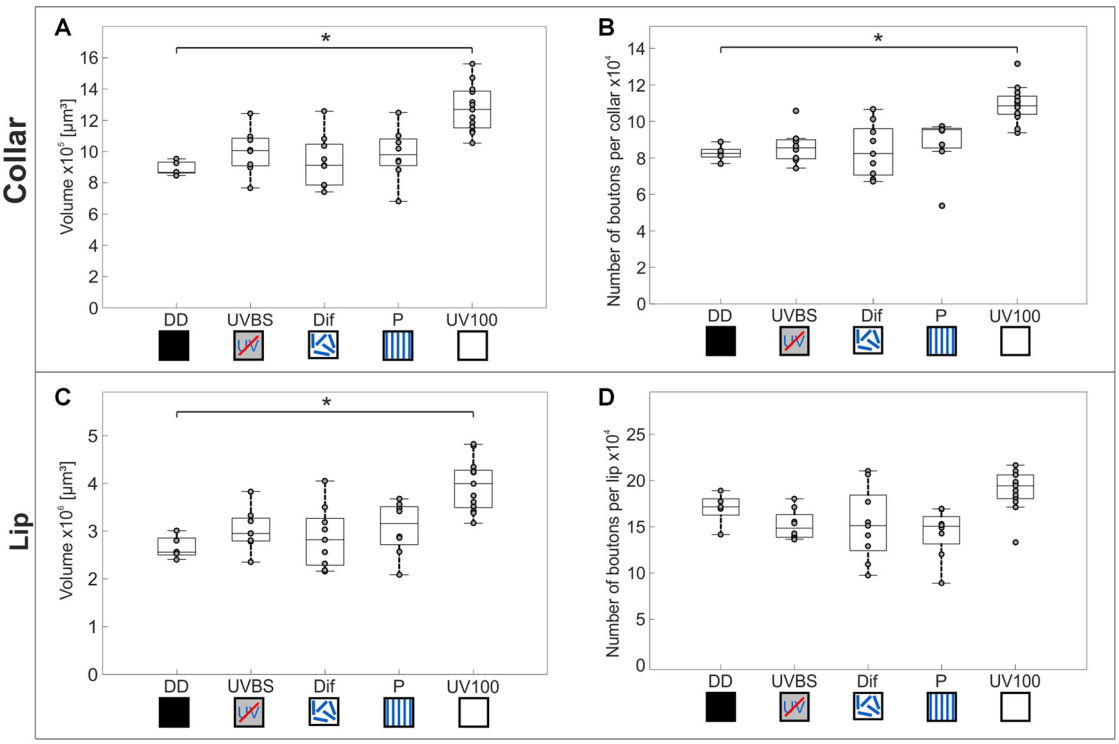

FIGURE 6 | Volume changes and changes in numbers of synaptic complexes in MB calyx subdivisions. The central line of each boxplot depicts the median of the data. The upper and lower limits of the boxes show the 25th and 75th percentiles, while the whiskers extend to the extreme data points without outliners. All data points (including outliers) are plotted as gray circles. To find a difference between the groups, a Kruskal–Wallis test was used ($\alpha = 0.05$). With the Mann-Whitney U-test with a Bonferroni correction the data was *post hoc* compared to the DD group if the Kruskal–Wallis test indicated a difference. The asterisk indicates data significantly different (after correction $p < 0.0125$) from the DD group. **(A)** In the MB-calyx Co, a significant volume increase compared to DD ($n = 5$) occurred only when the learning walks were conducted under the natural UV mediated changing polarization pattern (UV100; $n = 13$). **(B)** Similarly, the total number of synaptic boutons per calyx in the Co only increased when the learning walks were performed under UV100 compared to DD. **(C)** In the MB-calyx Li, a volume increase occurred only under UV100 conditions compared to DD, similar to the conditions in the Co. **(D)** However, in the Li no change in the total number of synaptic boutons per calyx occurred under any conditions. No significant differences in the MB occurred between DD and UVBS ($n = 8$), Dif ($n = 9$), or P ($n = 8$). For statistical details and further explanations, see text.

in brains of *C. noda* that had performed several learning walks under a naturally changing polarization pattern (UV100) showed a volumetric increase (Mann-Whitney U-test with Bonferroni correction: DD vs. UV100, $Z_4 = -2.6837$; $n_{DD} = 7$; $n_{UV100} = 10$; $p = 0.0073$). The volumetric increase in the CX was absent compared to DD when the ants performed their learning walks under restricted skylight conditions including an artificially fixed linear polarization pattern (P) (Mann-Whitney U-test with Bonferroni correction: DD vs. P, $Z_3 = 0.4234$; $n_{DD} = 7$; $n_P = 9$; $p = 0.6720$), a diffused polarization pattern (Dif) (Mann-Whitney U-test with Bonferroni correction: DD vs. Dif, $Z_2 = -0.7522$; $n_{DD} = 7$; $n_{Dif} = 8$; $p = 0.4519$), and without polarization pattern and information about the position of the sun (UVBS; Mann-Whitney U-test with Bonferroni correction: DD vs. UVBS, $Z_1 = 0.5434$; $n_{DD} = 7$; $n_{UVBS} = 11$; $p = 0.5869$). The same statistical relationships were found for the volume of the CB only, which includes the ellipsoid (EB) and the fan-shaped body (FB). When comparing the subunits (EB, FB, PB and No) individually, the same tendency was found, but was not statistically significant.

Volumetric Changes in the MB and Plasticity of Synaptic Complexes

Comparison of the volume and the numbers of synapsin labeled synaptic boutons in the MB calyx Co (**Figure 4C**) revealed a significant difference between the experimental groups of the behavior essay (Kruskal–Wallis test: Co Volume: $\chi^2_4 = 22.43$; $n = 43$; $p = 0.00016$; Co No. Synapses: $\chi^2_4 = 23.06$; $n = 43$; $p = 0.00012$; **Figures 6A,B**). Only ants that had performed several learning walks under a naturally changing skylight polarization pattern (UV100) showed an increase in the volume of the MB calyx Co and the estimated total number of synapses per calyx compared to ants that had not yet performed learning walks (DD; Mann-Whitney U-test with Bonferroni correction: Co Volume: DD vs. UV100, $Z_4 = -3.1543$; $n_{DD} = 5$; $n_{UV100} = 13$; $p = 0.0016$; Co No. Synapses: DD vs. UV100, $Z_4 = -3.1543$; $n_{DD} = 5$; $n_{UV100} = 13$; $p = 0.0016$). All groups that had performed learning walks under restricted skylight conditions did not show a significant increase compared to DD, neither in the volume nor in the total number of MG synaptic complexes per calyx in the MB calyx Co (Mann-Whitney

U-test with Bonferroni correction: CO Volume: DD vs. UVBS, $Z_1 = -1.5370$; $n_{DD} = 5$; $n_{UVBS} = 8$; $p = 0.1243$; DD vs. Dif, $Z_2 = -0.2667$; $n_{DD} = 5$; $n_{Dif} = 9$; $p = 0.7897$; DD vs. P, $Z_3 = -1.5370$; $n_{DD} = 5$; $n_P = 8$; $p = 0.1243$; Co No. Synapses: DD vs. UVBS, $Z_1 = -0.6587$; $n_{DD} = 5$; $n_{UVBS} = 8$; $p = 0.5101$; DD vs. Dif, $Z_2 = 0$; $n_{DD} = 5$; $n_{Dif} = 9$; $p = 1$; DD vs. P, $Z_3 = -1.8298$; $n_{DD} = 5$; $n_P = 8$; $p = 0.0673$). The volume of the Li also differed significantly between groups (Kruskal–Wallis test: Li volume: $\chi^2_4 = 20.08$; $n = 43$; $p = 0.00048$; **Figure 6C**). The volume was increased significantly compared to DD in ants that had performed several learning walks under UV100 conditions (Mann-Whitney U-test with Bonferroni correction: Li Volume: DD vs. UV100, $Z_4 = -3.1543$; $n_{DD} = 5$; $n_{UV100} = 13$; $p = 0.0016$). No difference in the Li volume occurred between DD and the other groups, (Mann-Whitney U-test with Bonferroni correction: Co Volume: DD vs. UVBS, $Z_1 = -1.2443$; $n_{DD} = 5$; $n_{UVBS} = 8$; $p = 0.2134$; DD vs. Dif, $Z_2 = -0.5333$; $n_{DD} = 5$; $n_{Dif} = 9$; $p = 0.7897$; DD vs. P, $Z_3 = -1.5370$; $n_{DD} = 5$; $n_P = 8$; $p = 0.1243$). In contrast to the visual MB subregion (Co), however, there was no significant difference compared to DD based on pair-wise comparison of the total number of MG synaptic complexes per calyx in the MB olfactory Li, despite the groups not coming from the same distribution (Kruskal–Wallis test: Li No. synaptic complexes: $\chi^2_4 = 15.81$; $n = 43$; $p = 0.0033$; Mann-Whitney U-test with Bonferroni correction: Li No. synaptic complexes: DD vs. UVBS, $Z_1 = 1.5370$; $n_{DD} = 5$; $n_{UVBS} = 8$; $p = 0.1243$; DD vs. Dif, $Z_2 = 0.9333$; $n_{DD} = 5$; $n_{Dif} = 9$; $p = 0.3506$; DD vs. P, $Z_3 = 1.9762$; $n_{DD} = 5$; $n_P = 8$; $p = 0.0481$; DD vs. UV100, $Z_4 = -1.9715$; $n_{DD} = 5$; $n_{UV100} = 13$; $p = 0.0487$; **Figure 6D**).

DISCUSSION

Celestial Information Is Not Necessary for the Look Back to the Nest Behavior

In the beginning of their foraging careers, *C. noda* perform learning walks that are repeatedly interrupted by turns with several stopping phases. The longest stopping phases are accurately directed towards the nest entrance (Fleischmann et al., 2017). It has previously been suggested that ants may use path integration information to align their back turns (Graham et al., 2010; Müller and Wehner, 2010). We used this conspicuous feature in the learning walks of *C. noda* as an easily quantifiable behavior readout in skylight manipulation experiments to ask whether celestial cues may serve as a reference system to align gaze direction. Our results demonstrate that neither an artificial (P) nor a diffused (Dif) polarization pattern disturbed the directedness of the longest stopping phases toward the nest entrance. Even with complete exclusion of the polarization pattern and the position of the sun (UVBS), the ants were still able to perform the look back to the nest entrance behavior. This strongly suggests that the celestial compass—providing the directional component of the path integration system during foraging (review: Wehner, 2003)—is not the system of reference used by ants to initially align the gaze direction during naïve learning walks. Our results underline the robustness and importance of the mechanism that is used to align the gaze direction during the longest stopping phases.

Possible Reference Systems for the Look Back to the Nest Behavior

As our results show that the celestial compass does not provide a reference system used during learning walks, other possibilities for the compass component of the path integrator have to be considered. A potential candidate could be the visual landmark panorama. Schultheiss et al. (2016) recently demonstrated that UV-light plays a crucial role for the use of the landmark panorama. However, our results show that *C. noda* was still able to look back to the nest entrance during learning walks under blocked UV-light spectrum (UVBS). Furthermore, the panorama information is not yet known or memorized in ants during naïve (first) learning walks and requires the completion of several learning walks (Fleischmann et al., 2016). The ants might also use nest odors to detect the direction of the nest. *C. fortis* were shown to use olfactory landmark cues near the nest (Steck et al., 2009). However, as the ants conduct their learning walks in increasing distances and in all compass (including upwind) directions away from the nest (Fleischmann et al., 2016), olfactory cues are not reliable during the entire learning walk sequences. The ants also walk cross wind in order to approach odor sources, in particular prey items during foraging (Wolf and Wehner, 2000; Buehlmann et al., 2014). This behavior has not become evident in learning walks, and as the ants perform pirouette-like turns all-around the nest entrance, cross wind orientation seems highly unlikely. Finally, the ants could use intrinsic (idiothetic) orientation mechanisms. Such mechanisms however, would be highly prone to cumulative errors (Müller and Wehner, 1994). An error in the gaze direction during the longest stopping phase of pirouettes would lead to a snapshot taken into the wrong direction. This could easily lead to serious errors in foragers, but also during learning walks with extended lengths. A more promising candidate for an initial reference system for the compass component of the path integrator during learning walks of *C. noda* is the geomagnetic field. This had already been suggested for the learning flights of bumblebees (Collett et al., 2013). Furthermore, *C. noda* was shown to learn magnetic landmarks (Buehlmann et al., 2012). Although the magnetic field strength, in these experiments, was far above the natural geomagnetic field, it appears likely that the ants possess a magnetic sense that could be used for the initial calibration of navigational information. A potential role of a magnetic sense has also been suggested for other ants (fire ants: Anderson and Vander Meer, 1993; leaf-cutter ants: Banks and Srygley, 2003; wood ants: Çamlitepe and Stradling, 1995; for a review see: Wajnberg et al., 2010). However, so far no use of the geomagnetic field for navigation, in particular as compass information for path integration, has been described in ants, neither for experienced foragers during their foraging runs, nor for learning walks in novices. Therefore, at this

point the question regarding an initial reference system for the alignment of gaze directions to acquire and calibrate navigational information during learning walks has to remain open.

Visual Pathways in the *C. noda* Brain

To be used as navigational information, the visual information perceived by the ants during learning walks needs to be relayed to and processed in higher integration centers of the brain. Using anterograde tracing techniques, two prominent visual pathways become apparent in *C. noda*. Visual information from the ME is transferred bilaterally to the MB collars of the medial and lateral MB calyces, very similar to the projections found in other Hymenoptera (Gronenberg, 2001; Yilmaz et al., 2016). In *Drosophila* only a very small subset of visual neurons transfers information from the OL to the MB calyx (Vogt et al., 2016). This may suggest that this pathway is highly conserved across insects, but the number of neurons and their projection patterns are adapted to the visual ecology of individual species (Groh et al., 2014; Vogt et al., 2016; Yilmaz et al., 2016). One interesting feature in *C. noda* is that axonal projections from the dorsal ME appear more extensive compared to projections from dye injections into the ventral ME. This may indicate that the dorsal retina and celestial view aspects are more prominently represented in the MB calyx Co compared to terrestrial aspects from the lower part of the compound eye. More focal injections, also along the horizontal axis, are needed to further analyze this. In *C. fortis* the AOT was shown to house projections from the dorsal most regions of the medulla indicating that polarization information from the dorsal rim area of the eye is transferred via this pathway to the AOTU and the LX into the lower half of the EB of the CX (Schmitt et al., 2016), similar to the conditions found in locusts (Homberg et al., 2011). Our results show that also the ventral region of the medulla is relayed to the upper and lower part of the AOTU. Next we tested whether the high-order sensory integration centers (MB, CX) express neuroplasticity related to the quality of celestial information experienced during learning walks.

Natural Polarization Pattern Is Necessary for a Volume Increase in the CX

Although our manipulations of celestial information did not significantly alter the learning walk behavior, the restriction of skylight information interfered with neuroanatomical changes in the CX. A volume increase in the CX as compared to DD occurred only when the learning walks had been conducted under the full spectrum including UV-light and the naturally changing polarization pattern. Exposure to the full light spectrum including UV-light with an artificial, fixed polarization pattern (P) or without a usable polarization pattern (Dif) did not lead to a CX volume increase. In contrast, a volume increase in the CB of *Drosophila* occurs after the flies were exposed to UV-light (Barth and Heisenberg, 1997). However, in that case *Drosophila* did not perceive a natural light and polarization pattern. In *C. noda* the exclusion of UV-light, and thereby the reception of the polarization pattern during learning walks, prevented volumetric chances of the CX. It is not possible with the methods available to count synapses within subunits of the CX. Therefore, we only analyzed volumetric changes in the CX. Previous studies on large synaptic complexes (giant synapses, GS) in the lateral complex (LX) along the sky-compass pathway of *C. fortis* revealed a significant increase of GS numbers depending on exposure to the UV part of the light spectrum (Schmitt et al., 2016). Therefore, it seems likely that the volume increase in the CX is also due to an increase in the number of synapses along this pathway. This increase was found to be significant in the CB units, i.e., the input region of the CX. Within the CX, in particular the PB, the skylight polarization direction is represented in a map-like manner (Pfeiffer and Homberg, 2014), and it has been shown through computational investigation that the CX is able to store spatial information (Fiore et al., 2017). Whether the neuroanatomical changes we found in the CX are triggered by appropriate sensory exposure or following the formation of spatial memory is an interesting question that needs to be investigated in a more focused approach. The CX is also involved in higher order control of movement of the limbs (Strauss, 2002; Martin et al., 2015), landmark orientation, and angular path integration (Seelig and Jayaraman, 2015). All this makes the CX a well suited neuropil to link polarization information to other stimuli mediating directional information important for navigation, for example other terrestrial reference systems.

Sensory Experience of a Natural Polarization Pattern Is Necessary for an Increase in the Number of Synaptic Complexes in the Visual Subregions of the MB Calyx

Similar to the results just described for the CX it was only under exposure to the naturally changing UV polarization pattern that a volume increase was found in the MB-calyx of ants that had performed their learning walks. Kühn-Bühlmann and Wehner (2006) had previously shown an increase in the MB volume of experienced (aged) foragers compared to dark reared ants of age-controlled *Cataglyphis bicolor*. In our study, we focused on the transition phase between interior worker (DD) and forager. Our data suggests that a volume increase in the MBs occurs already during learning walks and that it is dependent on the presence of the natural polarization pattern (UV100). A net increase of MB synaptic complexes was found only in the visual input region. As the MB is a higher order integration center involved in learning and memory, this may indicate that the increase in MG numbers is related to visual experience. Computer simulations by Ardin et al. (2015) suggest that the large synaptic capacity of visual subregions in ant MBs are well suited for the storage of visual snapshots underling the potential role of the MBs for learning and memorizing panoramic landmark cues during learning walks. Studies by Stieb et al. (2010, 2012) have shown that the MB Co expresses light-induced and age-dependent changes in MG numbers in *C. fortis*. Stieb et al. (2010) also

showed a volume increase in the Co after exposure to full spectrum light accompanied by a decrease in MG densities. Furthermore, studies in the honeybee (Hourcade et al., 2010) and leafcutter ants (Falibene et al., 2015) showed that the formation of stable long-term olfactory memory leads to an increase in the density and number of MG in the Li. In contrast to the laboratory and partly restrained conditions in these experiments, the ants used in our study were allowed to perform their natural behaviors in their natural habitat under natural or altered skylight conditions. Therefore, a mix of both effects—the first exposure to light and long-term memory formation following learning, might be expected in our experimental ants. As UV-light is crucial for learning terrestrial landmarks (Schultheiss et al., 2016), an increase in synaptic complexes could be expected in the presence of UV-light, even without a naturally changing polarization pattern (Dif). Our data shows that a volume increase in the Co was absent in ants that had performed their learning walks under the full light spectrum, but without a usable polarization pattern (Dif) or with an artificial, fixed polarization pattern (P). Only when ants perceived a full spectrum including UV light together with a naturally changing polarization pattern, an increase in the volume and number of MG occurred in the MB calyx Co. No such effect was seen in MB collar MG of honeybees after a fine color discrimination task (Sommerlandt et al., 2016) indicating that only certain parameter combinations may lead to measurable effects of structural synaptic plasticity. The increase in the estimated MG numbers in the MB-calyx Co indicates an outgrowth of new presynapses during learning walks under natural skylight—a process similar to what has been observed after the formation of long-term memory (Hourcade et al., 2010; Falibene et al., 2015).

Due to the prominent role of path integration, *Cataglyphis* have to calibrate their internal skylight compass to the solar ephemeris (the season- and place-specific course of the sun over the day) at the beginning of their foraging career (Wehner and Müller, 1993). A panoramic- and celestial snapshot based mechanisms based on long-term memory in the visual MBs might play a role in this initial calibration. Similarly, short term learning of celestial snapshots was recently suggested for sky-compass orientation in dung beetles (el Jundi et al., 2016). When the skylight polarization pattern, however, does not change over the day (P), is diffused (Dif), or is not available (UVBS), it would not make sense to take and store celestial snapshots. To store new celestial information and thereby fine tune an internal template of the solar ephemeris function makes only sense if the polarization pattern changes compared to a fixed reference system. This hypothesis is also backed up by our observation that the number of learning walks drastically increased when the linear polarization filter was rotated. Analyzing neuroanatomical changes in ants that have performed learning walks under such a systematically changed artificial polarization pattern would allow for a deeper insight into the correlation shown so far.

The present study represents a first step of probing potential effects of learning walks on neuroplasticity. We started this combined field and laboratory study by focusing on the terminal projection areas of two prominent visual pathways in the CX and MB. To obtain a more comprehensive understanding of the total extent of learning-walk induced neuroplasticity, future investigations will have to include more extensive neuroanatomical analyses of all major brain neuropils, for example analyzing their volume relationships, synapse densities (whenever feasible), also in relation to overall brain volumes—for example like it was done in recent volumetric analyses of brains in migratory and solitary locusts, or migratory and non-migratory moths (Ott and Rogers, 2010; de Vries et al., 2017). In the same line, as previous work in *Camponotus* ants (Yilmaz et al., 2016) and in *Drosophila* (Barth and Heisenberg, 1997) show that the optic lobes undergo plastic changes after artificial light exposure, future studies on learning-walk induced neuroplasticity in *Cataglyphis* ants should include neuropils peripheral to the CX and MB, like the optic lobes, the AOTU and the lateral complex.

CONCLUSION

Neither the polarization pattern, or other information from UV-light input, nor the position of the sun are necessary for *C. noda* to align their gaze directions during the longest stopping phase of pirouettes in learning walks. Thus, the celestial compass as part of the path integrator does not provide the ants with the reference system needed during naïve learning walks. However, although not being necessary for the accuracy of the look-back behavior, we show that proper perception of the natural polarization pattern that changes over the day is important for triggering neuroanatomical changes in the CX and MB calyx that take place during learning walks. In the MB-calyx Co, this volume increase is linked to an increase in the number of MG synaptic complexes indicating that plasticity related processes are triggered when the ants are confronted with a naturally perceived polarization pattern that changes over the day.

ETHICS STATEMENT

This study was carried out in accordance with the Greek and German laws.

AUTHOR CONTRIBUTIONS

RG, PNF, RW, WR conceived the study. WR and RW led the study. RG, PNF and KG collected and analyzed the data. RG and PNF drafted and WR and RW revised the manuscript. All authors approved the final version of the manuscript for submission.

FUNDING

This study was supported by the Deutsche Forschungsgemeinschaft (DFG), Collaborative Research Center SFB1047 "Insect Timing" (Project B6 to WR and RW). This publication was funded by the DFG and the University of Würzburg in the funding program Open Access Publishing.

ACKNOWLEDGMENTS

We want to thank Greek government and the management board of the Schinias National Park for permission to perform our research in the Schinias National Park in Marathon. We especially want to thank Maria Trivourea and Olga Papigioti for their support in the field and Christos Georgiadis for his help with administrative issues. We thank the teams of the field season Greece 2016 and the team that excavated the animals in the middle of the night for the neuroanatomical study group DD. Furthermore, we thank Bernhard Ronacher who supported our research in Greece by lending us his VW bus, and Jochen Zeil for providing us with the MATLAB application Digilite and for his help in data analyses.

SUPPLEMENTARY MATERIAL

The Supplementary Material for this article can be found online at: https://www.frontiersin.org/articles/10.3389/fnbeh.2017.00226/full#supplementary-material

REFERENCES

Anderson, J. B., and Vander Meer, R. K. (1993). Magnetic orientation in the fire ant, *Solenopsis invicta*. *Naturwissenschaften* 80, 568–570. doi: 10.1007/bf01149274

Ardin, P., Mangan, M., Wystrach, A., and Webb, B. (2015). How variation in head pitch could affect image matching algorithms for ant navigation. *J. Comp. Physiol. A Neuroethol. Sens. Neural Behav. Physiol.* 201, 585–597. doi: 10.1007/s00359-015-1005-8

Banks, A. N., and Srygley, R. B. (2003). Orientation by magnetic field in leaf-cutter ants, *Atta colombica* (Hymenoptera: Formicidae). *Ethology* 109, 835–846. doi: 10.1046/j.0179-1613.2003.00927.x

Barth, M., and Heisenberg, M. (1997). Vision affects mushroom bodies and central complex in *Drosophila melanogaster*. *Learn. Mem.* 4, 219–229. doi: 10.1101/lm.4.2.219

Buehlmann, C., Graham, P., Hansson, B. S., and Knaden, M. (2014). Desert ants locate food by combining high sensitivity to food odors with extensive crosswind runs. *Curr. Biol.* 24, 960–964. doi: 10.1016/j.cub.2014.02.056

Buehlmann, C., Hansson, B. S., and Knaden, M. (2012). Desert ants learn vibration and magnetic landmarks. *PLoS One* 7:e33117. doi: 10.1371/journal.pone.0033117

Çamlitepe, Y., and Stradling, D. J. (1995). Wood ants orient to magnetic fields. *Proc. R. Soc.* 261, 37–41. doi: 10.1098/rspb.1995.0114

Collett, T. S., Hempel de Ibarra, N., Riabinina, O., and Philippides, A. (2013). Coordinating compass-based and nest-based flight directions during bumblebee learning and return flights. *J. Exp. Biol.* 216, 1105–1113. doi: 10.1242/jeb.081463

Degen, J., Kirbach, A., Reiter, L., Lehmann, K., Norton, P., Storms, M., et al. (2015). Exploratory behaviour of honeybees during orientation flights. *Anim. Behav.* 102, 45–57. doi: 10.1016/j.anbehav.2014.12.030

de Vries, L., Pfeiffer, K., Trebels, B., Adden, A. K., Green, K., Warrant, E., et al. (2017). Comparison of navigation-related brain regions in migratory versus non-migratory noctuid moths. *Front. Behav. Neurosci.* 11:158. doi: 10.3389/fnbeh.2017.00158

Duelli, P., and Wehner, R. (1973). The spectral sensitivity of polarized light orientation in *Cataglyphis bicolor* (Formicidae, Hymenoptera). *J. Comp. Physiol.* 86, 37–53.doi: 10.1007/BF00694476

el Jundi, B., Foster, J. J. J., Khaldy, L., Byrne, M. J. J., Dacke, M., and Baird, E. (2016). A snapshot-based mechanism for celestial orientation. *Curr. Biol.* 26, 1456–1462. doi: 10.1016/j.cub.2016.03.030

Falibene, A., Roces, F., and Rössler, W. (2015). Long-term avoidance memory formation is associated with a transient increase in mushroom body synaptic complexes in leaf-cutting ants. *Front. Behav. Neurosci.* 9:84. doi: 10.3389/fnbeh.2015.00084

Fiore, V. G., Kottler, B., Gu, X., and Hirth, F. (2017). *In silico* interrogation of insect central complex suggests computational roles for the ellipsoid body in spatial navigation. *Front. Behav. Neurosci.* 11:142. doi: 10.3389/fnbeh.2017.00142

Fleischmann, P. N., Christian, M., Müller, V. L., Rössler, W., and Wehner, R. (2016). Ontogeny of learning walks and the acquisition of landmark information in desert ants, *Cataglyphis fortis*. *J. Exp. Biol.* 219, 3137–3145. doi: 10.1242/jeb.140459

Fleischmann, P. N., Grob, R., Wehner, R., and Rössler, W. (2017). Species-specific differences in the fine structure of learning walk elements in *Cataglyphis* ants. *J. Exp. Biol.* 220, 2426–2435. doi: 10.1242/jeb.158147

Graham, P., Philippides, A., and Baddeley, B. (2010). Animal cognition: multi-modal interactions in ant learning. *Curr. Biol.* 20, R639–R640. doi: 10.1016/j.cub.2010.06.018

Groh, C., Kelber, C., Grübel, K., and Rössler, W. (2014). Density of mushroom body synaptic complexes limits intraspecies brain miniaturization in highly polymorphic leaf-cutting ant workers. *Proc. Biol. Sci.* 281:20140432. doi: 10.1098/rspb.2014.0432

Groh, C., Lu, Z., Meinertzhagen, I. A., and Rössler, W. (2012). Age-related plasticity in the synaptic ultrastructure of neurons in the mushroom body calyx of the adult honeybee *Apis mellifera*. *J. Comp. Neurol.* 520, 3509–3527. doi: 10.1002/cne.23102

Gronenberg, W. (2001). Subdivisions of hymenopteran mushroom body calyces by their afferent supply. *J. Comp. Neurol.* 435, 474–489. doi: 10.1002/cne.1045

Heinze, S., and Homberg, U. (2007). Maplike representation of celestial E-vector orientations in the brain of an insect. *Science* 315, 995–997. doi: 10.1126/science.1135531

Heinze, S., and Reppert, S. M. (2012). Anatomical basis of sun compass navigation I: the general layout of the monarch butterfly brain. *J. Comp. Neurol.* 520, 1599–1628. doi: 10.1002/cne.23054

Hempel de Ibarra, N., Philippides, A., Riabinina, O., and Collett, T. S. (2009). Preferred viewing directions of bumblebees (*Bombus terrestris* L.) when learning and approaching their nest site. *J. Exp. Biol.* 212, 3193–3204. doi: 10.1242/jeb.029751

Homberg, U., Heinze, S., Pfeiffer, K., Kinoshita, M., and el Jundi, B. (2011). Central neural coding of sky polarization in insects. *Philos. Trans. R. Soc. Lond. B Biol. Sci.* 366, 680–687. doi: 10.1098/rstb.2010.0199

Hourcade, B., Muenz, T. S., Sandoz, J.-C., Rössler, W., and Devaud, J.-M. (2010). Long-term memory leads to synaptic reorganization in the mushroom bodies: a memory trace in the insect brain? *J. Neurosci.* 30, 6461–6465. doi: 10.1523/jneurosci.0841-10.2010

Ito, K., Shinomiya, K., Ito, M., Armstrong, J. D., Boyan, G., Hartenstein, V., et al. (2014). A systematic nomenclature for the insect brain. *Neuron* 81, 755–765. doi: 10.1016/j.neuron.2013.12.017

Kühn-Bühlmann, S., and Wehner, R. (2006). Age-dependent and task-related volume changes in the mushroom bodies of visually guided desert ants, *Cataglyphis bicolor*. *J. Neurobiol.* 66, 511–521. doi: 10.1002/neu.20235

Labhart, T., and Meyer, E. P. (1999). Detectors for polarized skylight in insects: a survey of ommatidial specializations in the dorsal rim area of the compound eye. *Microsc. Res. Tech.* 47, 368–379. doi: 10.1002/(sici)1097-0029(19991215)47:6<368::aid-jemt2>3.0.co;2-q

Lehrer, M. (1993). Why do bees turn back and look? *J. Comp. Physiol. A* 172, 549–563. doi: 10.1007/bf00213678

Martin, J. P., Guo, P., Mu, L., Harley, C. M., and Ritzmann, R. E. (2015). Central-complex control of movement in the freely walking cockroach. *Curr. Biol.* 25, 2795–2803. doi: 10.1016/j.cub.2015.09.044

Menzel, R. (2001). Searching for the memory trace in a mini-brain, the honeybee. *Learn. Mem.* 8, 53–62. doi: 10.1101/lm.38801

Muenz, T. S., Groh, C., Maisonnasse, A., Le Conte, Y., Plettner, E., and Rössler, W. (2015). Neuronal plasticity in the mushroom body calyx during

adult maturation in the honeybee and possible pheromonal influences. *Dev. Neurobiol.* 75, 1368–1384. doi: 10.1002/dneu.22290

Müller, M., and Wehner, R. (1988). Path integration in desert ants, *Cataglyphis fortis*. *Proc. Natl. Acad. Sci. U S A* 85, 5287–5290. doi: 10.1073/pnas.85.14.5287

Müller, M., and Wehner, R. (1994). The hidden spiral: systematic search and path integration in desert ants, *Cataglyphis fortis*. *J. Comp. Physiol. A* 175, 525–530. doi: 10.1007/bf00199474

Müller, M., and Wehner, R. (2010). Path integration provides a scaffold for landmark learning in desert ants. *Curr. Biol.* 20, 1368–1371. doi: 10.1016/j.cub.2010.06.035

Narendra, A., and Ramirez-Esquivel, F. (2017). Subtle changes in the landmark panorama disrupt visual navigation in a nocturnal bull ant. *Philos. Trans. R. Soc. B Biol. Sci.* 372:20160068. doi: 10.1098/rstb.2016.0068

Neuser, K., Triphan, T., Mronz, M., Poeck, B., and Strauss, R. (2008). Analysis of a spatial orientation memory in *Drosophila*. *Nature* 453, 1244–1247. doi: 10.1038/nature07003

Opfinger, E. (1931). Über die Orientierung der Biene an der Futterquelle—die Bedeutung von Anflug und Orientierungsflug für den Lernvorgang bei Farb-, Form- und Ortsdressuren. *Z. Vgl. Physiol.* 15, 431–487. doi: 10.1007/BF00338108

Ott, S. R., and Rogers, S. M. (2010). Gregarious desert locusts have substantially larger brains with altered proportions compared with the solitarious phase. *Proc. Biol. Sci.* 277, 3087–3096. doi: 10.1098/rspb.2010.0694

Pfeiffer, K., and Homberg, U. (2014). Organization and functional roles of the central complex in the insect brain. *Annu. Rev. Entomol.* 59, 165–184. doi: 10.1146/annurev-ento-011613-162031

Pfeffer, S. E., and Wittlinger, M. (2016). Optic flowodometry operates independently of stride integration in carried ants. *Science* 353, 1155–1157. doi: 10.1126/science.aaf9754

Philippides, A., de Ibarra, N. H., Riabinina, O., and Collett, T. S. (2013). Bumblebee calligraphy: the design and control of flight motifs in the learning and return flights of *Bombus terrestris*. *J. Exp. Biol.* 216, 1093–1104. doi: 10.1242/jeb.081455

Rössler, W., Spaethe, J., and Groh, C. (2017). Pitfalls of using confocal-microscopy based automated quantification of synaptic complexes in honeybee mushroom bodies (response to Peng and Yang 2016). *Sci. Rep.* 7:9786. doi: 10.1038/s41598-017-09967-8

Schmitt, F., Stieb, S. M., Wehner, R., and Rössler, W. (2016). Experience-related reorganization of giant synapses in the lateral complex: potential role in plasticity of the sky-compass pathway in the desert ant *Cataglyphis fortis*. *Dev. Neurobiol.* 76, 390–404. doi: 10.1002/dneu.22322

Scholl, C., Kübert, N., Muenz, T. S., and Rössler, W. (2015). CaMKII knockdown affects both early and late phases of olfactory long-term memory in the honeybee. *J. Exp. Biol.* 218, 3788–3796. doi: 10.1242/jeb.124859

Scholl, C., Wang, Y., Krischke, M., Mueller, M. J., Amdam, G. V., and Rössler, W. (2014). Light exposure leads to reorganization of microglomeruli in the mushroom bodies and influences juvenile hormone levels in the honeybee. *Dev. Neurobiol.* 74, 1141–1153. doi: 10.1002/dneu.22195

Schultheiss, P., Wystrach, A., Schwarz, S., Tack, A., Delor, J., Nooten, S. S., et al. (2016). Crucial role of ultraviolet light for desert ants in determining direction from the terrestrial panorama. *Anim. Behav.* 115, 19–28. doi: 10.1016/j.anbehav.2016.02.027

Seelig, J. D., and Jayaraman, V. (2015). Neural dynamics for landmark orientation and angular path integration. *Nature* 521, 186–191. doi: 10.1038/nature14446

Seid, M. A., and Wehner, R. (2009). Delayed axonal pruning in the ant brain: a study of developmental trajectories. *Dev. Neurobiol.* 69, 350–364. doi: 10.1002/dneu.20709

Sommerlandt, F. M. J., Spaethe, J., Rössler, W., and Dyer, A. G. (2016). Does fine color discrimination learning in free-flying honeybees change mushroom-body calyx neuroarchitecture? *PLoS One* 11:e0164386. doi: 10.1371/journal.pone.0164386

Steck, K., Hansson, B. S., and Knaden, M. (2009). Smells like home: desert ants, *Cataglyphis fortis*, use olfactory landmarks to pinpoint the nest. *Front. Zool.* 6:5. doi: 10.1186/1742-9994-6-5

Stieb, S. M., Hellwig, A., Wehner, R., and Rössler, W. (2012). Visual experience affects both behavioral and neuronal aspects in the individual life history of the desert ant *Cataglyphis fortis*. *Dev. Neurobiol.* 72, 729–742. doi: 10.1002/dneu.20982

Stieb, S. M., Muenz, T. S., Wehner, R., and Rössler, W. (2010). Visual experience and age affect synaptic organization in the mushroom bodies of the desert ant *Cataglyphis fortis*. *Dev. Neurobiol.* 70, 408–423. doi: 10.1002/dneu.20785

Strauss, R. (2002). The central complex and the genetic dissection of locomotor behaviour. *Curr. Opin. Neurobiol.* 12, 633–638. doi: 10.1016/s0959-4388(02)00385-9

Stürzl, W., Zeil, J., Boeddeker, N., and Hemmi, J. M. (2016). How wasps acquire and use views for homing. *Curr. Biol.* 26, 470–482. doi: 10.1016/j.cub.2015.12.052

Vogt, K., Aso, Y., Hige, T., Knapek, S., Ichinose, T., Friedrich, A. B., et al. (2016). Direct neural pathways convey distinct visual information to *Drosophila* mushroom bodies. *Elife* 5:e14009. doi: 10.7554/eLife.14009

Vowles, D. M. (1954). The orientation of ants. I. The substitution of stimuli. *J. Exp. Biol.* 31, 341–355.

Wajnberg, E., Acosta-Avalos, D., Alves, O. C., de Oliveira, J. F., Srygley, R. B., and Esquivel, D. M. S. (2010). Magnetoreception in eusocial insects: an update. *J. R. Soc. Interface* 7, S207–S225. doi: 10.1098/rsif.2009.0526.focus

Wehner, R. (2003). Desert ant navigation: how miniature brains solve complex tasks. *J. Comp. Physiol. A* 189, 579–588. doi: 10.1007/s00359-003-0431-1

Wehner, R., Fukushi, T., and Isler, K. (2007). On being small: brain allometry in ants. *Brain Behav. Evol.* 69, 220–228. doi: 10.1159/000097057

Wehner, R., Meier, C., and Zollikofer, C. (2004). The ontogeny of foraging behaviour in desert ants, *Cataglyphis bicolor*. *Ecol. Entomol.* 29, 240–250. doi: 10.1111/j.0307-6946.2004.00591.x

Wehner, R., Michel, B., and Antonsen, P. (1996). Visual navigation in insects: coupling of egocentric and geocentric information. *J. Exp. Biol.* 199, 129–140.

Wehner, R., and Müller, M. (1993). How do ants acquire their celestial ephemeris function? *Naturwissenschaften* 80, 331–333. doi: 10.1007/bf01141909

Wittlinger, M., Wehner, R., and Wolf, H. (2006). The ant odometer: stepping on stilts and stumps. *Science* 312, 1965–1967. doi: 10.1126/science.1126912

Wolf, H., and Wehner, R. (2000). Pinpointing food sources: olfactory and anemotactic orientation in desert ants, *Cataglyphis fortis*. *J. Exp. Biol.* 868, 857–868.

Yilmaz, A., Lindenberg, A., Albert, S., Grübel, K., Spaethe, J., Rössler, W., et al. (2016). Age-related and light-induced plasticity in opsin gene expression and in primary and secondary visual centers of the nectar-feeding ant *Camponotus rufipes*. *Dev. Neurobiol.* 76, 1041–1057. doi: 10.1002/dneu.22374

Zeil, J. (1993). Orientation flights of solitary wasps (Cerceris; Sphecidae; Hymenoptera). *J. Comp. Physiol. A* 172, 189–205. doi: 10.1007/bf00189396

Zeil, J. (2012). Visual homing: an insect perspective. *Curr. Opin. Neurobiol.* 22, 285–293. doi: 10.1016/j.conb.2011.12.008

Zeil, J., Kelber, A., and Voss, R. (1996). Structure and function of learning flights in bees and wasps. *J. Exp. Biol.* 252, 245–252.

Conflict of Interest Statement: The authors declare that the research was conducted in the absence of any commercial or financial relationships that could be construed as a potential conflict of interest.

frontiers in Behavioral Neuroscience

ORIGINAL RESEARCH
published: 30 May 2017
doi: 10.3389/fnbeh.2017.00098

Different Roles for Honey Bee Mushroom Bodies and Central Complex in Visual Learning of Colored Lights in an Aversive Conditioning Assay

Jenny A. Plath[1,2†], *Brian V. Entler*[1,3†], *Nicholas H. Kirkerud*[2,4], *Ulrike Schlegel*[2,5], *C. Giovanni Galizia*[2] *and Andrew B. Barron*[1*]

[1] Department of Biological Sciences, Macquarie University, Sydney, NSW, Australia, [2] Department of Biology, University of Konstanz, Konstanz, Germany, [3] Department of Biology, University of Scranton, Scranton, PA, United States, [4] International Max-Planck Research School for Organismal Biology, University of Konstanz, Konstanz, Germany, [5] Department of Biosciences, University of Oslo, Oslo, Norway

The honey bee is an excellent visual learner, but we know little about how and why it performs so well, or how visual information is learned by the bee brain. Here we examined the different roles of two key integrative regions of the brain in visual learning: the mushroom bodies and the central complex. We tested bees' learning performance in a new assay of color learning that used electric shock as punishment. In this assay a light field was paired with electric shock. The other half of the conditioning chamber was illuminated with light of a different wavelength and not paired with shocks. The unrestrained bee could run away from the light stimulus and thereby associate one wavelength with punishment, and the other with safety. We compared learning performance of bees in which either the central complex or mushroom bodies had been transiently inactivated by microinjection of the reversible anesthetic procaine. Control bees learned to escape the shock-paired light field and to spend more time in the safe light field after a few trials. When ventral lobe neurons of the mushroom bodies were silenced, bees were no longer able to associate one light field with shock. By contrast, silencing of one collar region of the mushroom body calyx did not alter behavior in the learning assay in comparison to control treatment. Bees with silenced central complex neurons did not leave the shock-paired light field in the middle trials of training, even after a few seconds of being shocked. We discussed how mushroom bodies and the central complex both contribute to aversive visual learning with an operant component.

Keywords: visual learning, operant learning, mushroom bodies, central complex, honey bees, procaine

OPEN ACCESS

Edited by:
Keram Pfeiffer,
University of Würzburg, Germany

Reviewed by:
Etsuro Ito,
Waseda University, Japan
Jean-René Martin,
Neurosciences Institute Paris-Saclay (NeuroPSI), France

***Correspondence:**
Andrew B. Barron
andrew.barron@mq.edu.au

[†] *These authors have contributed equally to this work.*

Received: *12 March 2017*
Accepted: *09 May 2017*
Published: *30 May 2017*

Citation:
Plath JA, Entler BV, Kirkerud NH, Schlegel U, Galizia CG and Barron AB (2017) Different Roles for Honey Bee Mushroom Bodies and Central Complex in Visual Learning of Colored Lights in an Aversive Conditioning Assay. Front. Behav. Neurosci. 11:98. doi: 10.3389/fnbeh.2017.00098

INTRODUCTION

Learning of a predictive relationship between a stimulus or an action and a certain outcome is essential for an animal's survival. Honey bees are excellent learners, quickly forming association between stimuli of different sensory modalities and meaningful appetitive and aversive stimuli (Giurfa, 2007). Over the past decades, research has been dedicated to uncover the neural

mechanisms and processes underlying learning in bees, and honey bees have been established as a powerful model to investigate learning and memory (Menzel, 1999, 2001, 2012; Giurfa, 2003, 2007). Learning assays are typically performed with free-flying bees as well as harnessed bees (Menzel, 1999, 2001; Giurfa, 2003, 2007; Menzel, 2012). Free-flying bees readily learn olfactory as well as visual stimuli. Appetitive learning and memory dynamics have been studied extensively using odors and colors or shapes paired with sucrose rewards.

Harnessed bees have been used in the proboscis extension response (PER) assay, in which the conditioned stimulus (CS) is paired with a sucrose reward (unconditioned stimulus: US) which leads to an extension of the proboscis (Bitterman et al., 1983; Felsenberg et al., 2011; Giurfa and Sandoz, 2012). Olfactory conditioning is easily studied with this assay since 50–60% of the trained bees already respond to an odor after one CS-US pairing (Bitterman et al., 1983; Felsenberg et al., 2011). It has proven difficult, however, to achieve successful conditioning of color stimuli with rewards or punishment in harnessed honey bees. Differential conditioning with a reward-paired color stimulus and a non-rewarded color stimulus resulted in moderate learning rates when the antennae were ablated (Kuwabara, 1957; Hori et al., 2006, 2007; Niggebrugge et al., 2009), when the bee was able to turn her head easily (Dobrin and Fahrbach, 2012) or when the color stimulus was combined with movement (Balamurali et al., 2015). Colored light, however, has been used successfully as a context for olfactory learning in PER when presented as an occasion-setter (Mota et al., 2011) or in a reinstatement paradigm (Plath et al., 2012). The difficulty in establishing robust visual learning in the PER assay has inhibited functional analyses of roles of different brain regions in visual learning in bees.

Here we used a recently developed aversive visual conditioning assay: the Automated Performance Index System (APIS) (Kirkerud et al., 2017) to analyze the roles of central processing regions of the bee brain in visual learning. This system was an adapted version of the one used for aversive olfactory conditioning (Kirkerud et al., 2013; Schott et al., 2015; Wehmann et al., 2015). In the APIS assay bees are able to move freely in a conditioning chamber, which is equipped with LEDs to provide visual stimuli of different wavelengths and intensities. Visual stimuli can be paired with low voltage electric shocks. Tracking of the animal's position is fully automated thanks to infrared sensors in the chamber. The chamber can be used to investigate differential learning presenting light in half of the chamber and light with different properties in the other half. One light field is paired with electric shock, so that the bee needs to cross over to the other half of the chamber to avoid being shocked. The assay has been extensively tested with different light stimuli including light of different wavelengths and intensities (Kirkerud et al., 2017). Bees easily learn to associate 465 nm light (blue for humans) and 590 nm light (yellow for humans) but not 525 nm light (green for humans; in the following, we use the human colors instead of the wavelengths for simplicity) with the aversive shock stimulus. In this study, we paired blue light with shocks in one half of the chamber and illuminated the "safe" part of the chamber with green light. Bees can be treated pharmacologically and then their behavior can be assessed in the APIS chamber. Here, we investigated the role the mushroom bodies (MBs) and the central complex (CX) in visual learning.

MBs and the CX are considered the main integrative centers in the insect brain, and both regions could be involved in learning an appropriate behavioral response to a visual stimulus. We investigated the behavioral consequence of silencing of the input region of the MBs, the collar region in the mushroom body calyces (MBC), and the vertical lobes (VL) as the output region of the MBs. The collar region receives direct visual input from the lobula and medulla in honey bees (Ehmer and Gronenberg, 2002; Gronenberg and Lopez-Riquelme, 2004). A recent study has found two types of Kenyon cells in the fruit fly MBC that respond to either light intensity or wavelength (color) information relayed from the optic neuropils (Vogt et al., 2016). Interestingly, in flies both types of neurons are required for learning and memory in an aversive differential conditioning, either testing different intensities or different wavelengths. The output of the collar region in the mushroom bodies terminates in an inner layer of the vertical lobes in honey bees (Strausfeld, 2002). It has been repeatedly shown that the vertical lobes play a crucial role for different forms of olfactory learning and memory formation in honey bees (Menzel, 1999, 2012) and fruit flies (Heisenberg, 2003; Keene and Waddell, 2007; Busto et al., 2010; Davis, 2011), but visual learning has only been investigated sparsely so far.

The CX comprises a group of unpaired neuropils in the center of the insect brain. One important role of the CX is generation of motor outputs according to processed internal and external stimuli (Pfeiffer and Homberg, 2014; Plath and Barron, 2015). The CX is essential for the initiation and termination of walking, turning and climbing behavior in fruit flies (Strauss and Heisenberg, 1993; Martin et al., 1999; Strauss, 2002; Poeck et al., 2008; Triphan et al., 2010), cockroaches (Guo and Ritzmann, 2013; Guo et al., 2014; Martin et al., 2015) and crickets (Kai and Okada, 2013) and is considered as site for action selection and goal-directed behavior (Libersat and Gal, 2013; Strausfeld and Hirth, 2013; Barron et al., 2015; Fiore et al., 2015; Barron and Klein, 2016). A role of the CX in visual learning of patterns and spatial features has been shown in various behavioral assays using fruit flies (Liu et al., 2006; Neuser et al., 2008; Wang et al., 2008; Pan et al., 2009; Hou et al., 2011; Ofstad et al., 2011; Kuntz et al., 2012, 2017).

In this study, we used the transient and local anesthetic procaine to selectively silence neural activity in these three brain regions. Procaine is a reversible blocker of voltage-gated Na^+- and other voltage-gated channels to a lesser degree and has been established as a means to study olfactory learning and memory in honey bees (Muller et al., 2003; Devaud et al., 2007, 2015). Procaine has also been utilized to show that silencing the central body reduces spontaneous walking and optomotor responses (Kathman et al., 2014; Kaiser and Libersat, 2015). Our expectation was that mushroom bodies are needed for this form of visual conditioning with a strong operant component. This allowed the bee to learn from consequences of her behavior and not only from a stimulus-stimulus pairing. Interrupting processing in the collar region and blocking the further processing in the output regions of the mushroom bodies could lead to an impairment in performance in aversive

visual learning which can be measured in the APIS assay. We hypothesized further that learning of the stimulus-shock pairing would remain intact when the central complex was anesthetized but the reaction of running away from the stimulus would be impaired. We discuss how our results will contribute to uncovering mechanisms underlying visual learning in insects.

MATERIALS AND METHODS

Animals and Surgical Procedure

For all experiments, honey bees were collected from two established queen-right colonies at Macquarie University in Sydney, Australia. Foragers were collected at the hive entrance while leaving for a foraging bout. Bees were immobilized on ice and harnessed in PER tubes (Bitterman et al., 1983; Felsenberg et al., 2011). To prepare the animals for injections, the bee's neck was filled with soft dental wax to prevent movement of the head. A stripe of wax was positioned loosely over the antennae to prevent their movement during the operation.

For MBC injections, we entered through the ocellar tract. The lens of the median ocellus was carefully pushed outwards with the tip of a micro-scalpel and a small incision was made into the neurilemma sheath covering the brain to ease entering of the micropipette.

To access the brain for intracerebral injections (VL and CX), a window was cut into the head capsule with three cuts: One above the antennal stems (dorsal), one below the median ocellus (ventral), and one at the border of the right eye (Devaud et al., 2007). The created flap was opened and held in place with soft dental wax. The glands and trachea above the brain were carefully moved aside and a small incision was made into the neurilemma above the target structure to enable a smooth entry of the micropipette during injections. After injections the flap was carefully released to close the window and sealed with a drop of eicosane (Sigma-Aldrich Australia) melted at ∼35°C). For detailed demonstration of the procedure please refer to Søvik et al. (2016).

Injections

In the following study four different treatment groups were compared: procaine-injected animals (procaine/proc), saline-injected animals (vehicle/veh), animals that underwent the operation and injection procedure without having any solution injected into the brain (sham), and non-treated animals (NT), which were directly transferred to the chamber after catching.

To locally and temporarily inhibit neural activity, the drug procaine was used. In the honey bee procaine reduces Na^+- and K^+-currents and spiking activity in mushroom body neurons (Devaud et al., 2007). Procaine HCl (Sigma-Aldrich Australia) was dissolved in physiological saline (7.54 g/L NaCl, 0.448 g/L KCl, 0.872 g/L $MgCl_2 \times 6\ H_20$, 0.735 g/L $CaCl_2 \times 2H_20$, 54.72 g/L Sucrose, 4.95 g/L D-glucose, and 2.38 g/L HEPES, pH = 6.7, 500 mOsm, Sigma-Aldrich Australia, see Burger et al., 2013) as a stock solution of 40% (w/v). On the day of the experiment, the solution was diluted with additional saline to create a 20% (w/v) procaine solution. Physiological saline was also used as a control solution. To identify the injection site afterwards, both solutions contained 0.5 mg/ml dextran Alexa fluor 546 or dextran Alexa fluor 568 (10.000 MW, Molecular probes by Life technologies, Carlsbad, CA, USA). Microinjections were performed with a microinjector (Eppendorf, Hamburg, Germany) and an electronic micromanipulator (Luigs & Neumann Feinmechanik und Elektrotechnik, Ratingen, Germany). Micropipettes were pulled from glass capillaries (World Precisions Instruments, Sarasota, FL, USA) using an electrode puller (Scientific & Research Instruments, Karnataka, India). The tips were broken to an outer diameter of 10–15 μm. The injection volume was adjusted and rechecked both before and after every animal by measuring a droplet injected into mineral oil.

Injections into the MBC occurred via the ocellar tract of the median ocellus. The micropipette was brought to the opening of the removed lens and then finely adjusted until the micropipette was just above the incision made earlier. The micropipette was then inserted to a maximum injection depth of ∼215 μm and a volume of ∼2 nL was injected. The micropipette was removed and the bee was quickly transferred into the conditioning chamber (**Figure 1A**).

To target the center of the VL, ∼1 nL of solution was injected into each lobe at a depth of ∼60 μm and at an angle of 68–70° relative to the brain surface. A stereomicroscope fluorescent adapter was then used to visualize the injection site (Green- Light and Filter Set; NIGHTSEA, Lexington, MA, USA). Successful injections were identified by spreading of the fluorescent dye throughout the VL. To target the CX, ∼0.5 nL of solution was injected at a depth of ∼330 μm and at an angle of 68–75° relative to the brain surface; entering at the midline between the VLs. Successful injections were identified using laser scanning confocal microscopy (see below).

Behavioral Assay

Honey bees were conditioned in the APIS chamber, designed and manufactured at the University of Konstanz, Germany with an aversive visual conditioning paradigm established in (Kirkerud et al., 2017). Tracking of the bee and delivery of stimuli in APIS are fully automated which eliminates human error or bias. Due to the design of the chamber, bees can only move in almost straight lines, either toward or away from a stimulus, and any turn made by the animal is tracked as a complete reversal by the sensors. Shock and light stimuli were controlled with a script loaded into the system software. The program utilizes sensor feedback to determine the bee's location and initiates stimuli at specified time points. The operation of the chamber and the assay used are similar to methods used earlier in flies (Zars et al., 2000; Claridge-Chang et al., 2009).

Following injection, the bee was quickly placed into the chamber and allowed to acclimate for 15 min while freely moving around in the dark. The conditioning protocol consisted of one unreinforced preference test followed by nine reinforced training trials (**Figure 1B**), and ending with four unreinforced test trials (**Figure 1C**). In each trial, a blue light field (λ^B = 465 nm, Luminous intensity: 105 mcd) was switched on in the half of the chamber where the bee was situated and a green light field (λ^G = 525 nm, Luminous intensity: 119 mcd) illuminated the

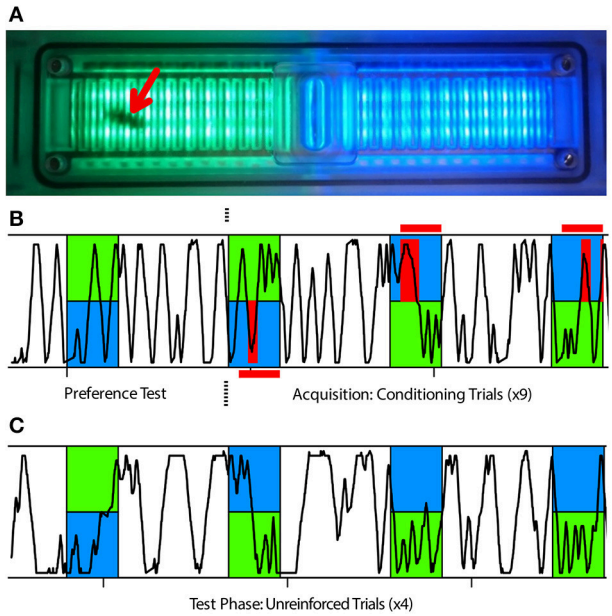

FIGURE 1 | APIS learning assay used in this study. (A) The APIS chamber can be illuminated with two different light fields of varying wavelengths and intensities; in this case light appearing green to humans and light appearing blue to humans. The chamber is equipped with an electrifiable grid to deliver 10 V shocks to the bee's feet and with infrared sensors to automatically track the bee's movement. A bee in the chamber (red arrow) could only move in a straight line, either toward or away from a stimulus, and turns were scored as a reversal of direction as detected by the infrared sensors. **(B,C)** Typical running trace of a bee in the chamber. Blue and green indicate illumination wavelength and red indicates when shocks were available (red horizontal bars) or delivered (red vertical bars) to the bee. Blue light was always illuminating the half of the chamber in which the bee was located at light-onset. **(B)** After an acclimatization period of 15 min post-injection, the bee was exposed to 14 s of both green and blue illumination as a preference test. The bee was then subjected to nine conditioning trials in which, after 3 s of illumination, the bee experienced shocks on the blue side for another 11 s, but not on the green side. **(C)** Subsequently, the bee was tested four times with 14 s of illumination without shocks to determine the post-training response to blue and green light fields.

opposite half. All trials lasted 14 s and were presented at regular intervals of 44 s (from onset to onset). For the training trials, electric shock pulses (10 V, 4 Hz, 100 ms) were activated 3 s after light onset. These shock pulses were delivered to the feet of the bee through the metal grid as long as movement sensors on the blue side were triggered. This meant that the bee could either escape the shocks by crossing from the shock-predicting blue side to the safe green side or potentially avoid them completely by escaping within 3 s and remain on the green side until the end of the trial. Since bees were always located on the blue half at trial onset (Figure S3), there was an inherent bias in the calculated preference toward this side. Once the behavioral assay was complete, the bee was quickly placed onto ice and anesthetized for dissection.

Histology and Imaging

Once anesthetized, the bee's head capsule was opened and the brain was removed in 0.1 M PBS (Sigma-Aldrich Australia) using forceps and a fresh breaker-blade piece. Whole brains were fixed in 4% paraformaldehyde (Electron Microscopy Sciences, Hattfield, PA, USA) in 0.1 M PBS overnight in a chilled room (16°C). Brains were then washed in 0.1 M PBS (3 × 10 min) at room temperature (22°C) and stored in the fridge (4°C). Samples were either washed daily with fresh 0.1 M PBS or they were processed immediately for histology.

Whole brains were incubated in 250 µL DAPI (2 µg/ml, Sigma-Aldrich Australia) in 0.1 M PBS and 0.2% Triton-X 100 (Sigma-Aldrich Australia) overnight. Brains were then washed in 0.1 M PBS (3 × 10 min) followed by an ethanol dehydration series (i.e., 50, 70, 90, 98, 100, 100% 10–30 min each step) and cleared in methylsalicylate (Sigma-Aldrich Australia).

Brains were then mounted on previously prepared slides with a cavity well. Wells were created with glass cover slips (Marienfeld-Superior, Lauda-Koeningshofen, Germany) and custom made aluminum slides (manufactured at the University of Konstanz, Germany) secured together using DPX mounting medium (Sigma-Aldrich Australia). Cleared brains were mounted in the well using DPX mounting medium and sealed with another cover slip.

Samples were imaged (4.77 µm slice) using an Olympus Fluoview inverted confocal microscope (FV-1000 IX81) located at Macquarie University in Sydney, Australia. DAPI staining and auto-fluorescence of the tissue was used to identify the neuropils and determine the location of the injection site marked by the Alexa dye (**Figure 2**).

All injections in the CX group were located in the central body (**Figures 2E,F**). One injection in the vehicle group (**Figure 2E**, red dot with black border), and one injection in the procaine group (**Figure 2F**, red dot with black border), was located at the border of the lower division of the central body and some dye was also found in the noduli; indicating that those areas were possibly affected as well. Since the performance in APIS was very similar for both injection sites, results were presented for all combined CX injections.

Data Analysis

The data was analyzed and graphed using R 3.3.2 (R Core Team, Vienna, Austria) and RStudio 1.0.136 (RStudio Inc., Boston, MA, USA) with a custom written script. As a measurement for learning, the Performance Index (PI) was calculated: difference between time spent on the green side of the chamber and time spent on the blue (shocked) side of the chamber divided by the total trial time:

$$PI = \frac{t\,(green) - t\,(blue)}{t\,(green) + t\,(blue)}$$

This resulted in a variable ranging from −1 to 1, where positive values indicate that the bee spent more time on the safe side than on the shocked side, negative values the opposite. A bee that had learnt to associate the blue light with shock would run away from the blue side shortly after light-onset and avoid returning to the blue side. As a consequence, the relative time spent on the green side increased leading to higher PI-values (**Figure 3A**). A bee that had not learnt, spent equal amounts of time on each side

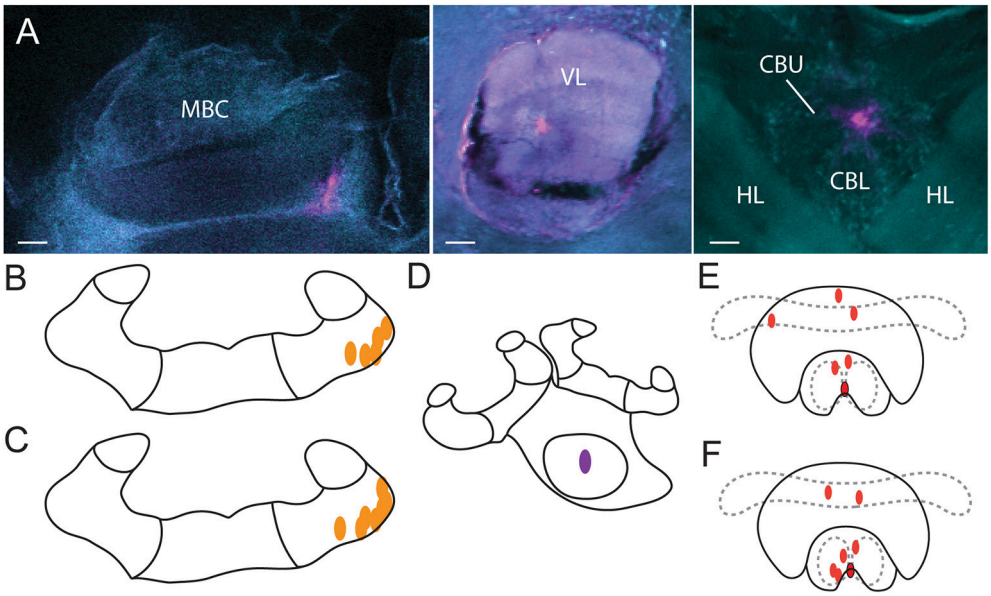

FIGURE 2 | Injection sites. (A) Alexa dye injections are shown in magenta (false color) in the MBC (left), VL (middle) and the CX (right). A DAPI-counterstain and auto-fluorescence of the brain tissue (false colored in cyan) allowed us to identify brain neuropils. Orientation of all three scans was aligned with rostral (neuraxis) facing upwards. Injections of vehicle **(B)** and of procaine solution **(C)** into the MBC as identified by the CLSM scans. Injections into the VL **(D)** were identified visually with fluorescent light and were all located in the center. Injections of vehicle **(E)** and of procaine solution **(F)** into the central body (red dots) and injections located at the border of the lower division of the central body with spread into the noduli (red dots with black border). MBC, mushroom body calyces; VL, ventral lobes; HL, horizontal lobes; CBU, upper division of the central body; CBL lower division of the central body; Scale bar = 30 μm.

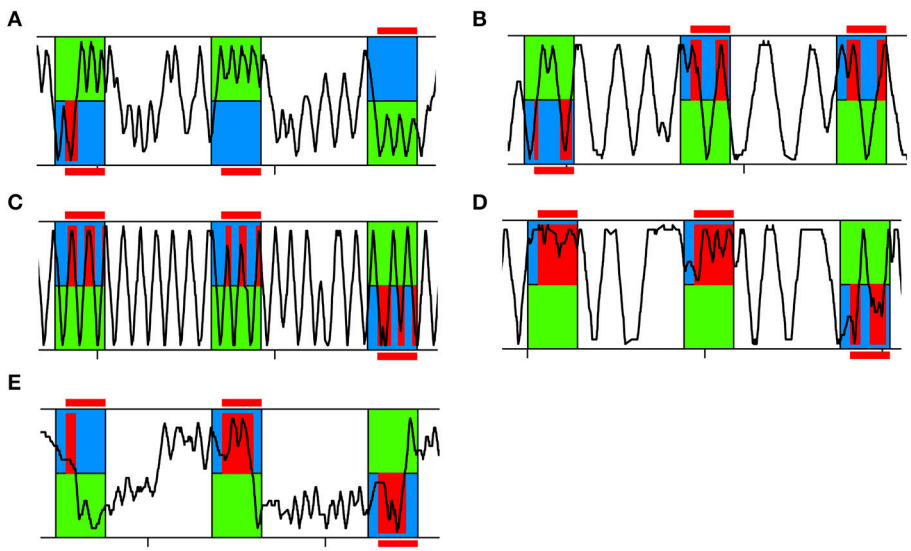

FIGURE 3 | Representative running traces of individual bees in APIS. Three training trials are shown. The bee was exposed to 14 s of blue and green light fields. After a 3 s delay the bee experienced shock when located on the blue side (red). **(A)** Typical running trace of a bee spending more time on the green side than on the blue side, thus achieving high Performance Indices (PIs). **(B)** Typical running trace of a bee spending more time on the blue side than on the green side, thus achieving low PIs. **(C)** Typical running trace of a bee with an equal number of reversals on the green and blue side, thus achieving a Reversing Difference close to zero. **(D)** Representative running trace of a bee reversing more often on the blue side than on the green side, thus achieving a negative Reversing Difference. **(E)** Typical running trace of a slowly responding bee taking a long time to cross over to the green side at the beginning of each trial and after light-onset, thus achieving a high Crossing Latency.

or more time on the blue side. A bee that had not learnt, would be expected to have lower PI-values (**Figure 3B**).

To investigate the movement pattern of the bee in more detail we further analyzed how many reversals of direction were performed in the chamber. We analyzed the total number of reversals per trial and the Reversing Difference: number of reversals performed on the blue side subtracted from the number of reversals performed on the green side of the chamber divided by the total number of reversals:

$$Reversing\ Difference = \frac{reversals\,(green) - reversals\,(blue)}{reversals\,(green) + reversals\,(blue)}$$

A bee that had learnt to avoid returning to the blue side typically ran back and forth on the green side (**Figure 3A**). If a bee had not learnt to avoid the blue side, we found two patterns: either she was running back and forth in the whole chamber (**Figure 3C**) or she was running back and forth on the blue side (**Figure 3D**). In the former case, the number of reversals performed would be equal for both sides (Reversing Difference close to zero). In the latter case, the number of reversals performed was higher on the blue side than on the green side (negative Reversing Difference).

As another parameter for learning performance as well as to evaluate the reaction to the shock-paired light, we analyzed how fast an animal would cross over to the green side after light-onset (Crossing Latency). If the bee managed to cross over under 3 s, she could completely avoid being shocked due to the delay of the shock-onset after light-onset, assuming she would not then return to the blue side (**Figure 3A**, second and third trial shown). If Crossing Latency was higher than 3 s she would experience shocks on the blue side (**Figure 3E**).

For statistical analysis of PI, Speed, Reversing Difference, Crossing Latency and Position in Chamber (at light-onset), the calculated data were fitted to linear mixed models with trial and treatment (procaine, vehicle, sham, NT) as fixed effects and bee identity as a random effect to correct for repeated measurements in the training, as well as the test phase (lme function in the R nlme package, Pinheiro et al., 2016). For statistical analysis of Reverses per Trial the calculated data were fitted to generalized linear mixed models (Poisson distribution) with trial and treatment (procaine, vehicle, sham, NT) as fixed effects and bee identity as a random effect to correct for repeated measurements in the training, as well as the test phase (glmer function in the R lme4 package, Bates et al., 2015). Statistical differences were determined *post-hoc* with the Tukey's range test using the R multcomp package (Hothorn et al., 2008). Since bees with lower speeds could not perform well in this assay in which performance is based on movement, animals with lower speeds than 2.1 cm/s were excluded from the analysis (Figure S1).

RESULTS

Control Animals Learned to Remain on the Green Side

In this study, we investigated color learning and how the animal's behavior in response to a learned stimulus changed. We first studied the behavior of the non-treated (NT) and sham-treated control groups. NT and sham-treated bees both developed a preference for the safe green side after few trials of color-shock conditioning (**Figure 4**). For both control groups PIs increased over the course of training (**Figure 4A**). PIs corresponded to around 39% of the first trial spent on the green side which increased to 61% (NT) and 72% (sham) in last trial. Increase of PIs from the first to the last trial was significant for both, NT animals (paired t-test, df $= 25$, $t = -2.682$, $p = 0.013$) and for sham-treated animals (paired t-test, df $= 39$, $t = -5.4861$, $p < 0.001$). In the test phase both groups continued to spend more time on the green side (**Figure 4A**).

We further explored how running and reversing in the chamber changed in response to the first light-shock pairing. Sham-treated animals were slower than NT-animals in the training but not in the test phase (**Figure 4B**). After five conditioning trials both groups performed on average three to five more reversals on the green side (**Figure 4C**). The total number of reversals performed in the chamber remained constant in that period (Figure S2A). Both groups crossed over to the green side after 2 to 4 s into the trial (**Figure 4D**). In the last training trial 20 out of 26 NT-animals and 21 out of 40 sham-treated animals crossed over under 3 s (data not shown). Taken together, after learning to associate blue light with shock the control bees ran away from the blue side before or shortly after shock-onset and thereafter ran back and forth on the green side.

Procaine Injections into the MBC Did Not Impair Performance in the Visual Learning Paradigm

We then examined how silencing of neurons of a collar region in the MBC with procaine injections changed the bees' behavior in the APIS assay (**Figure 5**). Procaine- and vehicle-injected animals were compared to sham-treated animals which were operated on in the same way. Overall, we observed no impairment of the bees' performance in the learning assay due to the injections. All bees were able to avoid the blue side after a few trials and moved normally. Curiously, we found a difference between PIs for all three groups in the preference test (**Figure 5A**). However, this did not seem to have an effect on the training where all groups performed similarly. Neither speed (**Figure 5B**), Reversing Differences (**Figure 5C**), Reversals per Trial (Figure S2B) or Crossing Latencies (**Figure 5D**) after the second trial were affected by injections (Table S1).

Procaine and Vehicle Injections into the VLs Impaired Performance in the Visual Learning Assay

Next, we investigated which role the VL as part of the MB output played in visual learning (**Figure 6**). Surprisingly, injections into the VL with either, procaine or vehicle solution resulted in impairment of color learning. Both groups achieved mean PI-values around zero, indicating that they spent equal amount of

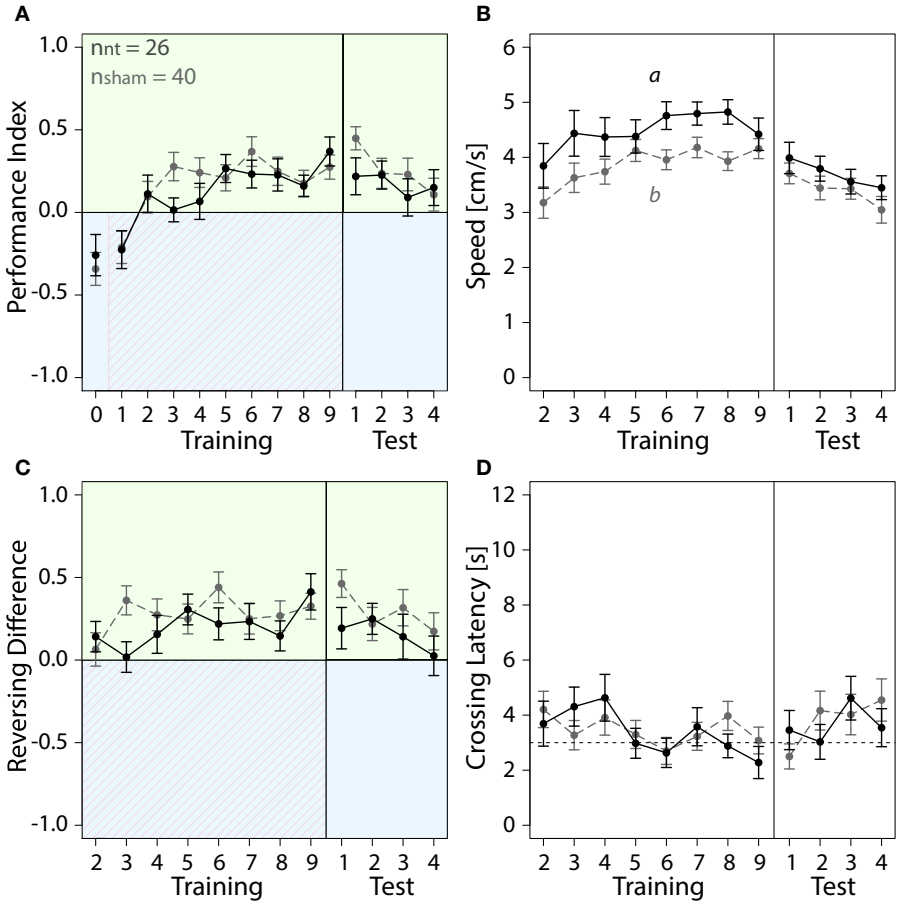

FIGURE 4 | With training, bees of sham and NT control groups learned to spend more time on the safe green side than the shocked blue side. Means ± SEM are plotted for all variables. Non-treated animals (NT) are shown in black, sham-treated animals (sham) in gray. No effect of the different injection methods used for the different regions on any of the four variables shown was found (ANOVA, $p > 0.05$). Sham-treated animals were therefore pooled into one group to compare with NT animals. Significant treatment effects determined with an LMM ($p < 0.05$, Table S1) are indicated with letters a and b. Bees were subjected to one preference test (0) nine training trials and four test trials. Control animals spent more time on the green side and avoided the shock-paired blue side (shocked period indicated by red diagonal lines) after a few trials. **(A)** No effect of treatment on Performance Index was found in training or in the test phase (Table S1). **(B)** An LMM indicated a significant effect of treatment on speed (Table S1). After one conditioning trial, speed was lower in sham-treated animals than in NT-animals in the training (*post-hoc* Tukey HSD, $z = -2.188$, $p = 0.03$), but no significant effect of treatment on speed was found in the test phase (Table S1) **(C)** Number of reversals on the green side was higher after one conditioning trial. No significant effect of treatment was found in training or in the test phase (Table S1). **(D)** Crossing Latency approached the 3-s threshold (horizontal dashed line) over the course of training, which corresponds to the delay between light-onset and shock-onset. **(A)** No significant effect of treatment on Crossing Latency was found for training or in the test phase (Table S1).

time on both sides (**Figure 6A**). This was not the case in sham-treated animals, which preferred the safe green side after two trials. Thus injection of the vehicle (with or without procaine), but not the insertion of the micropipette itself impaired learning of the light-shock pairing. Lower PIs in vehicle and procaine groups were not the result of impaired locomotion, since speed (**Figure 6B**) was not affected by treatment (Table S1). Furthermore, vehicle and procaine groups with injections into the VLs showed equal number of turns on the green side as on the blue side (**Figure 6C**), while Reversals per Trial (Figure S2C) remained unaffected. This indicated that the bees were either running back and forth from one side of the chamber to the other or were spending equal amounts of time running back and forth on each side. However, Crossing Latencies (**Figure 6D**) were found not to be significantly different (Table S1). Thus, vehicle- and procaine-treated bees ran away from the shocks after a similar delay as sham-treated bees in most trials.

Procaine Injections into the CX Changed Behavioral Responses in the Visual Learning Paradigm

Lastly, we explored how an animal's performance in the APIS-chamber was changed by silencing neural activity in the CX with procaine (**Figure 7**). Procaine-treated animals did not show a preference for the green side in the middle trials of the training. Rather, they remained on the shock-paired blue side longer than vehicle- and sham-treated animals. PIs were lower in procaine-treated animals in the training (**Figure 7A**). In fact, these bees

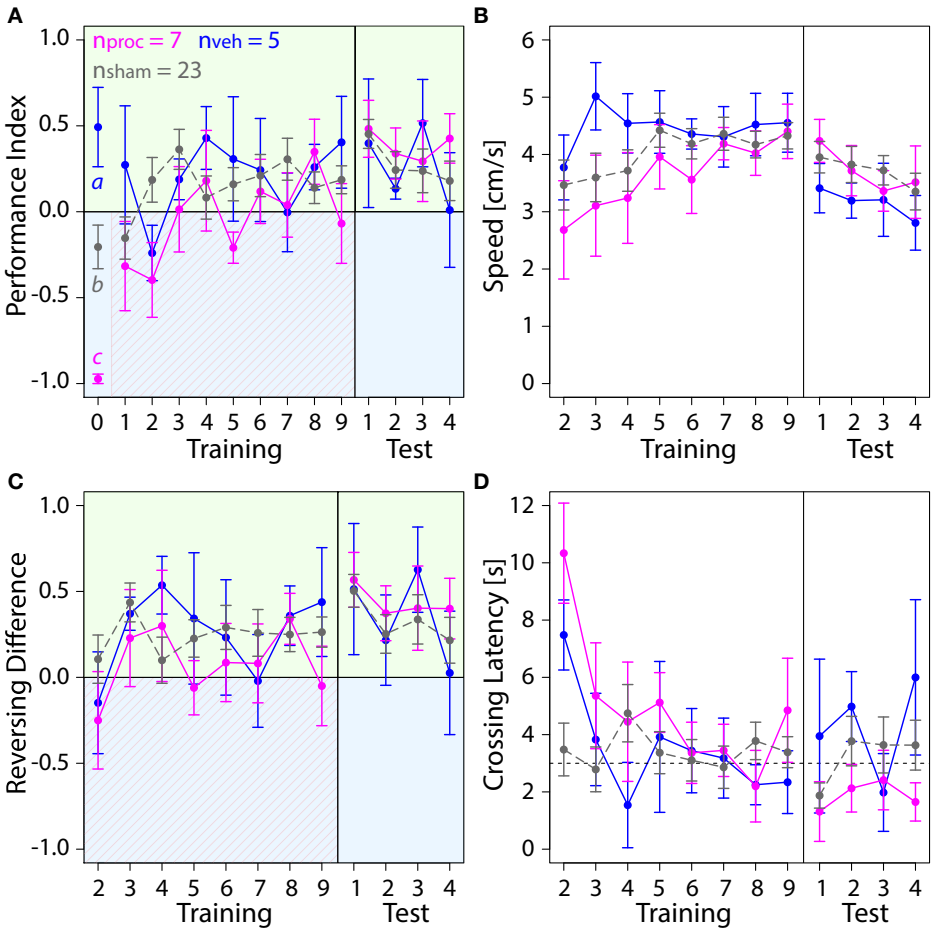

FIGURE 5 | Comparison of behavior in the APIS assay for bees injected with the vehicle (blue) or procaine solution (magenta) into the MBC, or sham-treated bees (gray). All groups learned to spend more time on the green side. Means ± SEM are plotted for all variables. Significant treatment effects determined with an LMM ($p < 0.05$, Table S1) are indicated with letters a, b, and c. Bees were subjected to one preference test (0) nine training trials and four test trials. **(A)** An LMM indicated an effect of treatment on Performance Index (PI) in the preference test (Table S1). Treatment comparison with a Tukey HSD *post-hoc* test revealed differences in PIs of vehicle and sham groups ($z = 2.631$, $p = 0.02$), PIs of procaine and sham groups ($z = -3.310$, $p = 0.003$) and PIs of procaine and vehicle groups ($z = -4.657$, $p < 0.001$). An LMM indicated a significant difference between PIs of procaine and sham groups in training (Table S1), but a Tukey *post-hoc* test, which corrects for multiple testing indicated no difference between PIs of these groups ($z = 2.080$, $p = 0.09$). No effect of treatment on PIs was found for the test phase (LMM, Table S1). All bees spent more time on the green side and avoided the shock-paired blue side (shocks indicated by diagonal lines) after a few trials. **(B)** Speed did not differ between experimental groups (LMM, Table S1). **(C)** Number of reversals on the green side was higher after one conditioning trial. No effect of treatment on Reversing Differences was found in training or in the test phase (Table S1). **(D)** Crossing Latency approached the 3-s threshold (horizontal dashed line) over the course of training, which corresponds to the delay between light-onset and shock-onset. No significant effect of treatment on Crossing Latency was found for training or in the test phase (Table S1).

spent 60–70% of the trial duration on the blue side in the middle of the training. Hence, the animals either did not leave the blue side or returned to the blue side more often. This behavior was not due to an impairment in locomotion since we found no differences in speed (**Figure 7B**) in the training (Table S1). However, toward the end of the training and in the test phase procaine-treated bees preferred the green side and PIs were similar to those found for vehicle- or sham-treated bees. We further explored if the ability to reverse in the chamber might have been affected. Procaine-treated bees did not reverse in the chamber less often than vehicle- or sham-treated bees (Figure S2D) (Table S1). But they performed on average three to four more reversals on the blue side than on the green side in the middle trials of training (**Figure 7C**). In contrast, vehicle- and sham-treated bees performed on average three to five more reversals on the green side in the same trials. Additionally, Crossing Latency was found to be on average 6 to 8 s in the middle trials for procaine-treated bees (**Figure 7D**). This was about twice as long as Crossing Latencies found for vehicle-treated and sham-treated bees and around 40–60% of the trial duration. Thus, procaine-treated bees did not leave the blue side even when the shocks were delivered for more than 3 s. Differences in Crossing Latencies were not due to different starting positions at light-onset in the training (Figure S3D) (Table S1).

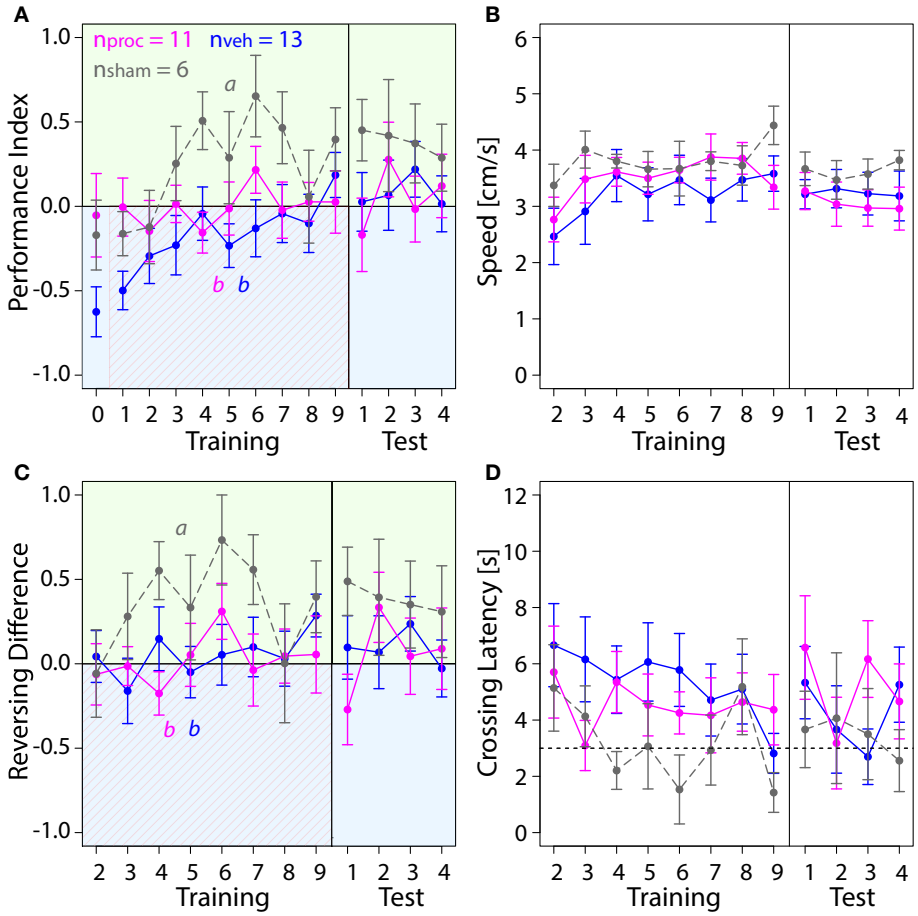

FIGURE 6 | Comparison of behavior in APIS for bees injected with vehicle (blue) or procaine solution (magenta) into the VLs, or sham-treated bees (gray). Learning to differentiate the shock-paired blue side and the safe green side was impaired in procaine and vehicle groups. Means ± SEM are plotted for all variables. Significant treatment effects determined with an LMM ($p < 0.05$) are indicated with letters a and b. Bees were subjected to one preference test (0) nine training trials and four test trials. **(A)** An LMM indicated an effect of treatment on Performance Index (PI) in the training but not in the test phase (Table S1). Treatment comparison with a Tukey HSD *post-hoc* test showed differences in PIs of vehicle and sham groups ($z = -4.217$, $p < 0.001$) and PIs of procaine and sham groups ($z = -2.638$, $p = 0.02$). **(B)** Speed did not differ between experimental groups (LMM, Table S1). **(C)** Reversing Differences were affected by treatment in the training but not in the test phase (LMM, Table S1). Treatment comparison with a Tukey HSD *post-hoc* test showed differences in Reversing Difference of vehicle and sham groups ($z = -3.107$, $p = 0.005$) and Revering Differences of procaine and sham groups ($z = -3.567$, $p = 0.001$). **(D)** Crossing Latency approached the 3-s threshold (horizontal dashed line) over the course of training, which corresponds to the delay between light-onset and shock-onset. No significant effect of treatment on Crossing Latency was found for training or in the test phase (Table S1).

DISCUSSION

About a decade ago the MBs were believed to process mainly olfactory information to generate meaningful associations to other stimuli. The CX was believed to primarily process visual and spatial information. Amongst other recent studies this study has shown this division might not necessarily be so clear. Our data indicate that the VLs as part of the MB output as well as the CX are involved in differential visual learning in the APIS assay.

Mushroom Body Function Was Required for Visual Learning with a Choice Component

Control bees escaped the shock-paired light field and avoided returning to it after only a few conditioning trials (**Figure 4**). These results were congruent with data obtained from untreated forager bees conditioned in the same assay in Konstanz, Germany (Kirkerud et al., 2017), and confirms the robustness of the paradigm across continents. While the operation and injection is an invasive procedure, we found that sham-treated animals recovered well and showed no deficits in learning performance compared to NT animals. In contrast, bees with silenced VLs escaped the shock-paired light field but failed to remain in the safe light field (**Figure 6**). Instead, they ran back and forth in the chamber resulting in lower PIs. This behavior indicated that they most likely failed to associate one light field with danger and the other light field with safety. We found a similar behavior in bees injected with the vehicle only. A similar phenomenon was found when injections of PBS into the MB lobes led to a reduced performance in olfactory reversal learning in comparison to injections into the calyces (Boitard et al., 2015). However, no effect of the vehicle was found when observing neural activity

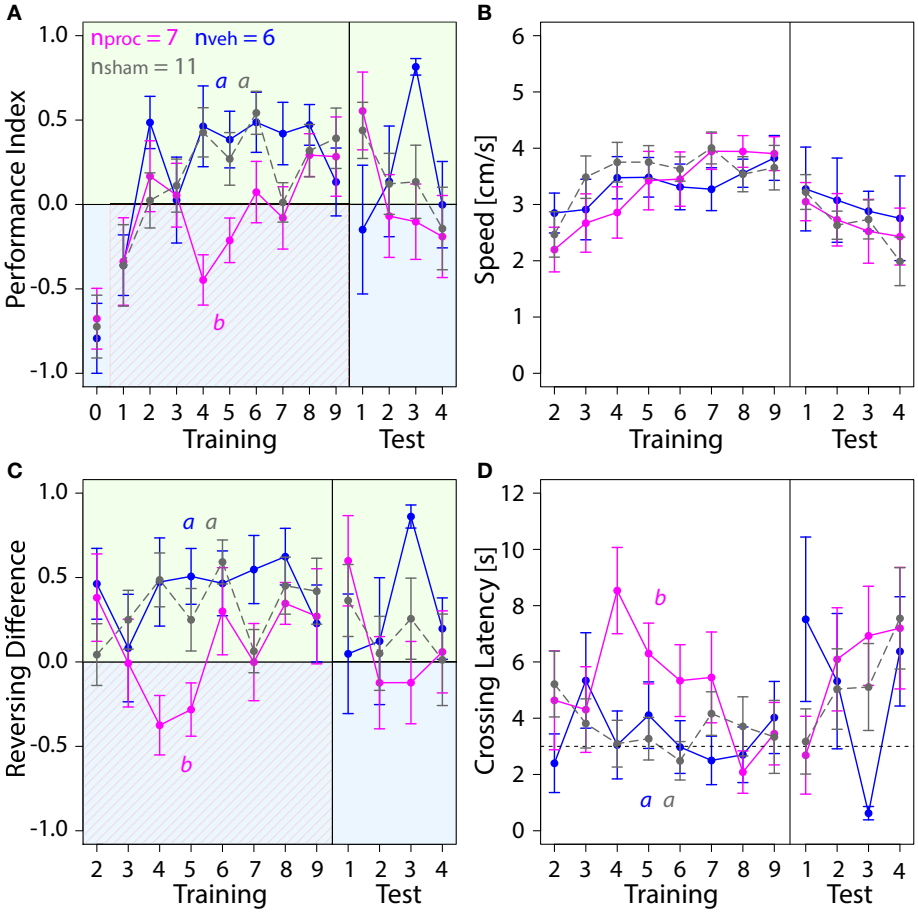

FIGURE 7 | Comparison of behavior in APIS for bees injected with vehicle (blue) or procaine solution (magenta) into the CX, or sham-treated bees (gray). Bees injected with procaine into the CX did not run away from the shock-paired blue side. Means ± SEM are plotted for all variables. Significant treatment effects determined with an LMM ($p < 0.05$, Table S1) are indicated with letters a and b. Bees were subjected to one preference test (0) nine training trials and four test trials. **(A)** Performance Indices (PIs) were affected by treatment in the training but not in the test phase (LMM, Table S1). Treatment comparison with a Tukey HSD *post-hoc* test showed differences in PIs of procaine and sham groups ($z = -2.512$, $p = 0.03$) and PIs of procaine and vehicle groups ($z = -3.052$, $p = 0.006$). **(B)** Speed did not differ between experimental groups (LMM, Table S1). **(C)** An LMM indicated an effect of treatment on Reversing Differences in the training but not in the test phase (Table S1). Treatment comparison with a Tukey HSD *post-hoc* test revealed differences in Reversing Difference of procaine and sham groups ($z = -2.629$, $p = 0.02$) and Reversing Differences of procaine and vehicle groups ($z = -2.995$, $p = 0.008$). **(D)** In vehicle and sham groups Crossing Latency approached the 3-s threshold (horizontal dashed line) over the course of training, which corresponds to the delay between light-onset and shock-onset. An LMM revealed an effect of treatment on Crossing Latency in the training but not in the test phase (Table S1). Treatment comparison with a Tukey HSD *post-hoc* test showed differences in Crossing Latencies of procaine and sham groups ($z = 2.467$, $p = 0.04$) and Crossing Latencies of procaine and vehicle groups ($z = 2.532$, $p = 0.03$).

changes due to injections using calcium imaging (Girardin et al., 2013).

When targeting one collar region of the MBC with procaine we found no deficits in performance (**Figure 5**). But since the honey bee collar region receives color input (Ehmer and Gronenberg, 2002; Gronenberg and Lopez-Riquelme, 2004) and the VLs were clearly involved in visual learning in APIS, it is possible that silencing neurons in only one of the eight collar regions in all MBCs might not have been sufficient to impair performance in the APIS assay. Further studies impacting all collar regions are necessary to clarify, but technically this would be extremely tricky to do.

In freely moving fruit flies, MB function was required for a visual paradigm with color stimuli and aversive reinforcement (Vogt et al., 2014, 2016). Similar to the paradigm presented here, blue and green light fields were presented simultaneously rather than sequentially. These findings stand in contrast to other studies implicating no involvement of the MBs in visual learning. Mutant flies (*Drosophila melanogaster*) with severely underdeveloped MBs and interrupted MB input were either conditioned by being shaken while illuminated with one color (Heisenberg et al., 1985) or trained with heat stimuli in a differential visual assay while being tethered in a flight simulator (Wolf et al., 1998). In both cases, mutant flies showed no learning deficits. In the latter case the fly was able to terminate the heat stimulus by turning left or right until the adjacent 90°-quadrant of the arena was faced and the arena was then illuminated with light of a different color. This suggests that the MBs are involved

in color learning which includes a choice situation rather than learning of sequentially presented color stimuli in a differential paradigm. Indeed, it has been shown that MBs are required to make a choice of responding to conflicting information of color and shape or color and position based on saliency (Tang and Guo, 2001; Zhang et al., 2007).

In both, bees and flies the dominant input to the MBs is olfactory, but it appears that MBs are also crucial for learning of visual information in bees in a binary-choice assay. Strausfeld (2012) and Farris (2015) argue that processing of visual information in the MB in insects is largely driven by the ecological relevance in the animal's life and the nature of visual input received. Large MBs with developed calyces are therefore not limited to species which rely predominately on olfactory information to navigate in their environment. They can also be found in aquatic beetle species which navigate mainly by vision (Lin and Strausfeld, 2012). It remains to be investigated if the MBs play a role in visual learning in other insect orders as well.

Silencing Neurons in the Central Complex Affected the Behavioral Response

We also found that silencing of neurons in the CX led to a change in behavior (**Figure 7**). Procaine-treated bees spent more time in the safe light field than on the shock-paired light field in the second and third trials and in the end of the training. This indicates, that learning of the light-shock pairing might still have been present. In the middle of the training period, however, procaine-treated bees remained on the shock-paired side of the chamber even after several seconds of shocks being delivered. This was not a result of an impaired ability to initiate reversals or an inability to walk in a straight line (Figure S2D). Nor was it caused by a major deficit in locomotion since speed was not found to be affected by procaine-injections, and rather bees appeared unable to execute an avoidance of the shocked light field.

But why was the effect not visible in the first learning trials? It seems very unlikely that procaine was only active in the middle trials of the training. Cockroaches with central bodies silenced by procaine showed deficits in locomotion and optomotor responses immediately after injections (Kathman et al., 2014; Kaiser and Libersat, 2015). Another explanation is that the response in the first trials might have mainly been driven by a direct reaction to the shocks, resulting in a short-lasting reflex-like escape maneuver. Initial responses to the shock could have been initiated by more direct and faster-processing "escape-pathways" generating a quick behavioral response to an obnoxious stimulus without involving the CX. Various escape reactions in insects have been proposed that bypass the higher processing centers of the brain (Horridge, 1962; Card, 2012). Is it possible that silencing of the CX only interfered with coordinating a motor response to a learned visual stimulus, but not an escape response from an aversive stimulus? In this case, a learned response to the blue light field would have been impaired but not the response to the shock itself. Toward the end of the training the procaine-effect seemed to have worn off, since the bees rapidly increased the proportion of time spent on the safe green side.

The CX has been implicated as the site to generate goal-directed behavior and to modulate movement in insects (Strausfeld and Hirth, 2013; Barron et al., 2015; Plath and Barron, 2015). Various studies have shown that the CX is crucial for spatial orientation memory (Neuser et al., 2008; Kuntz et al., 2012, 2017), visual pattern memory (Liu et al., 2006; Hou et al., 2011) and visual place learning (Ofstad et al., 2011) in fruit flies. A recent study has shown that a group of neurons in the ellipsoid body (part of the CX in the fruit fly) represents the orientation of the animals in relation to a visual stimulus (Seelig and Jayaraman, 2015). Taken together, the CX clearly has a role in visual learning and memory involving spatial orientation of the cues in fruit flies and possibly in other insects. We propose that the CX might also initiate the appropriate responses to learned stimuli which are processed by the MBs such as color stimuli.

Information about a Learned Stimulus Might Be Conveyed Indirectly to the Central Complex

Taken together, we showed that both, the MBs and the CX contributed to the behavioral response to a learned light stimulus. We propose the MBs integrated the coinciding shock and light information and the CX initiated the escape from the light field. We summarized the information flow between the different

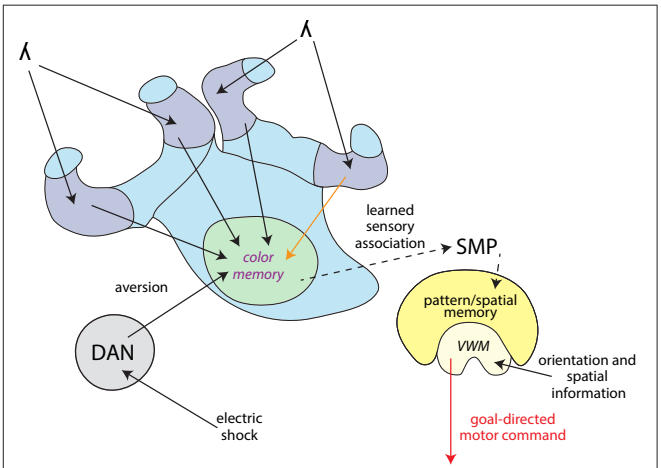

FIGURE 8 | Information flow model for differential color learning in a binary choice assay. Information about the light wavelength (λ) enters the collar region (dark blue) of the MBC from the optic neuropils. Visual information is passed on from the collar region to the VL (light green) via Kenyon cells. This process was partially disrupted by a procaine injection into one collar region (orange arrow). Electric shock information is passed on from the ventral nerve cord to dopaminergic neurons (DAN, gray) which modulate MB output. In the VL wavelength information is associated with aversion and most likely color memories are formed here. This process was disrupted by procaine-injections into the VL (marked in purple). Information about the learned sensory association might be passed on indirectly to the CX (yellow) via the superior medial protocerebrum (SMP). The CX receives orientation and spatial information and processes how the animal is orientated in relation to its environment using visual working memory (VWM). The CX initiates a goal-directed motor response, possibly modified in regards to the learned sensory association. This process was disrupted by procaine-injections into the CX (red arrow).

brain regions with the addition of other findings from different insect orders (**Figure 8**). To integrate coinciding shock and light information, both stimuli need to be received by the MBs. In the fruit fly γ lobe (part of the VL), a descending Kenyon cell carrying olfactory information forms synapses along the axon with a set of MB output neurons. Dopaminergic neurons modulate these individual compartments in relation to the internal state of the animal (Cohn et al., 2015). In flies, a group of these dopaminergic neurons (PPL1 cluster) carry information of aversive stimuli such as electric shocks (Waddell, 2013; Kaun and Rothenfluh, 2017). It needs to be studied, however, if this process is also found in other insect orders. In fruit flies, olfactory short-term memory is formed in the γ lobes which transitions into long-term memory to α and β lobes via the α' and β' lobes. Kenyon cells which convey wavelength and intensity information to the collar (Vogt et al., 2016) descend into the γ lobes in fruit flies. It remains to be investigated where exactly visual memories relating to color information are formed and where they transition from short-term to long-term memories.

A great question remains, whether there is a connection between the MBs and the CX. A direct connection between the MBs and the CX has not been found so far, with the exception of a single neuron recently discovered in the monarch butterfly (Heinze et al., 2013). An indirect connection could be found in the superior medial protocerebrum (Strausfeld and Hirth, 2013), which comprises outputs from the MBs carrying visual information in fruit flies (Ito et al., 1998) as a well as inputs to the upper division of the central body found in different insects (Strausfeld and Hirth, 2013; Pfeiffer and Homberg, 2014). It is therefore possible that information about the learned sensory association generated by the MBs is passed on indirectly to the CX in order to produce the conditioned response. Evidence for a connection between the MBs and CX manifesting in behavior was found when a sensory preconditioning paradigm involving cross-modal stimuli was investigated (Zhang et al., 2013). Here, an olfactory stimulus and a visual stimulus based on elevation were pre-conditioned. Then one stimulus was paired with reinforcement. A subsequent test of the other stimulus produced a response, even though it was never reinforced. Tested individually, blocking part of the MBs abolished olfactory memory and blocking part of the ellipsoid body (part of the CX in the fruit fly) abolished visual elevation memory. Remarkably, when the olfactory stimulus was reinforced after pre-conditioning and MBs were blocked, animals responded to the visual elevation stimulus. Thus, an association of the two CSs must have occurred in the pre-conditioning.

To explore the connection between the MBs and the CX will be a challenge in the future. The vast knowledge gained about learning and memory in the honey bee field in combination with pharmacological techniques (Felsenberg et al., 2011; Søvik et al., 2016) and assays such as APIS could provide a powerful tool to uncover how the different brain regions interact.

AUTHOR CONTRIBUTIONS

All authors (JP, BE, NK, US, CG, and AB) contributed substantially to the design and conception of the experiments, analysis and interpretation of the data and revision of the manuscript. JP, BE, and US contributed to acquisition and analysis of the data. JP and NK contributed to R analysis and statistical analysis of the data. JP and BE drafted the manuscript.

ACKNOWLEDGMENTS

We thank Marcus JA Plath for creating graphical elements for **Figures 2**, **8**. This work was supported by an Australian Research Council Future Fellowship (Grant no FT140100452) awarded to AB and by funds provided from the Federal Ministry of Food, Agriculture and Consumer Protection (BMELV) to CG based on a decision of the Parliament of the Federal Republic of Germany via the Federal Office for Agriculture and Food (BE) under the innovation support program. JP was supported by an iMQRES scholarship awarded by Macquarie University and by a DAAD Doktorandenstipendium awarded by the German Academic Exchange service. BE was supported by a Fulbright Postgraduate Scholarship awarded by the Australian-American Fulbright Commission.

SUPPLEMENTARY MATERIAL

The Supplementary Material for this article can be found online at: http://journal.frontiersin.org/article/10.3389/fnbeh.2017.00098/full#supplementary-material

REFERENCES

Balamurali, G. S., Somanathan, H., and Hempel de Ibarra, N. (2015). Motion cues improve the performance of harnessed bees in a colour learning task. *J. Comp. Physiol. A Neuroethol. Sens. Neural Behav. Physiol.* 201, 505–511. doi: 10.1007/s00359-015-0994-7

Barron, A. B., Gurney, K. N., Meah, L. F., Vasilaki, E., and Marshall, J. A. (2015). Decision-making and action selection in insects: inspiration from vertebrate-based theories. *Front. Behav. Neurosci.* 9:216. doi: 10.3389/fnbeh.2015.00216

Barron, A. B., and Klein, C. (2016). What insects can tell us about the origins of consciousness. *Proc. Natl. Acad. Sci. U.S.A.* 113, 4900–4908. doi: 10.1073/pnas.1520084113

Bates, D., Maechler, M., Bolker, B., and Walker, S. (2015). Fitting linear mixed-effects models using lme4. *J. Stat. Softw.* 67, 1–48. doi: 10.18637/jss.v067.i01

Bitterman, M. E., Menzel, R., Fietz, A., and Schafer, S. (1983). Classical conditioning of proboscis extension in honeybees (*Apis mellifera*). *J. Comp. Psychol.* 97, 107–119. doi: 10.1037/0735-7036.97.2.107

Boitard, C., Devaud, J. M., Isabel, G., and Giurfa, M. (2015). GABAergic feedback signaling into the calyces of the mushroom bodies enables olfactory reversal learning in honey bees. *Front. Behav. Neurosci.* 9:198. doi: 10.3389/fnbeh.2015.00198

Burger, H., Ayasse, M., Dotterl, S., Kreissl, S., and Galizia, C. G. (2013). Perception of floral volatiles involved in host-plant finding behaviour: comparison of a bee specialist and generalist. *J. Comp. Physiol. A Neuroethol. Sens. Neural Behav. Physiol.* 199, 751–761. doi: 10.1007/s00359-013-0835-5

Busto, G. U., Cervantes-Sandoval, I., and Davis, R. L. (2010). Olfactory learning in Drosophila. *Physiology* 25, 338–346. doi: 10.1152/physiol.00026.2010

Card, G. M. (2012). Escape behaviors in insects. *Curr. Opin. Neurobiol.* 22, 180–186. doi: 10.1016/j.conb.2011.12.009

Claridge-Chang, A., Roorda, R. D., Vrontou, E., Sjulson, L., Li, H., Hirsh, J., et al. (2009). Writing memories with light-addressable reinforcement circuitry. *Cell* 139, 405–415. doi: 10.1016/j.cell.2009.08.034

Cohn, R., Morantte, I., and Ruta, V. (2015). Coordinated and compartmentalized neuromodulation shapes sensory processing in Drosophila. *Cell* 163, 1742–1755. doi: 10.1016/j.cell.2015.11.019

Davis, R. L. (2011). Traces of Drosophila memory. *Neuron* 70, 8–19. doi: 10.1016/j.neuron.2011.03.012

Devaud, J. M., Blunk, A., Podufall, J., Giurfa, M., and Grunewald, B. (2007). Using local anaesthetics to block neuronal activity and map specific learning tasks to the mushroom bodies of an insect brain. *Eur. J. Neurosci.* 26, 3193–3206. doi: 10.1111/j.1460-9568.2007.05904.x

Devaud, J. M., Papouin, T., Carcaud, J., Sandoz, J. C., Grunewald, B., and Giurfa, M. (2015). Neural substrate for higher-order learning in an insect: mushroom bodies are necessary for configural discriminations. *Proc. Natl. Acad. Sci. U.S.A.* 112, E5854–E5862. doi: 10.1073/pnas.1508422112

Dobrin, S. E., and Fahrbach, S. E. (2012). Visual associative learning in restrained honey bees with intact antennae. *PLoS ONE* 7:e37666. doi: 10.1371/journal.pone.0037666

Ehmer, B., and Gronenberg, W. (2002). Segregation of visual input to the mushroom bodies in the honeybee (*Apis mellifera*). *J. Comp. Neurol.* 451, 362–373. doi: 10.1002/cne.10355

Farris, S. M. (2015). Evolution of brain elaboration. *Philos. Trans. R. Soc. Lond. B. Biol. Sci.* 370:20150054. doi: 10.1098/rstb.2015.0054

Felsenberg, J., Gehring, K. B., Antemann, V., and Eisenhardt, D. (2011). Behavioural pharmacology in classical conditioning of the proboscis extension response in honeybees (*Apis mellifera*). *J. Vis. Exp.* e2282. doi: 10.3791/2282

Fiore, V. G., Dolan, R. J., Strausfeld, N. J., and Hirth, F. (2015). Evolutionarily conserved mechanisms for the selection and maintenance of behavioural activity. *Philos. Trans. R. Soc. Lond. B. Biol. Sci.* 370:2015.0053. doi: 10.1098/rstb.2015.0053

Girardin, C. C., Kreissl, S., and Galizia, C. G. (2013). Inhibitory connections in the honeybee antennal lobe are spatially patchy. *J. Neurophysiol.* 109, 332–343. doi: 10.1152/jn.01085.2011

Giurfa, M. (2003). Cognitive neuroethology: dissecting non-elemental learning in a honeybee brain. *Curr. Opin. Neurobiol.* 13, 726–735. doi: 10.1016/j.conb.2003.10.015

Giurfa, M. (2007). Behavioral and neural analysis of associative learning in the honeybee: a taste from the magic well. *J. Comp. Physiol. A. Neuroethol. Sens. Neural Behav. Physiol.* 193, 801–824. doi: 10.1007/s00359-007-0235-9

Giurfa, M., and Sandoz, J. C. (2012). Invertebrate learning and memory: fifty years of olfactory conditioning of the proboscis extension response in honeybees. *Learn. Mem.* 19, 54–66. doi: 10.1101/lm.024711.111

Gronenberg, W., and Lopez-Riquelme, G. O. (2004). Multisensory convergence in the mushroom bodies of ants and bees. *Acta Biol. Hung.* 55, 31–37. doi: 10.1556/ABiol.55.2004.1-4.5

Guo, P., Pollack, A. J., Varga, A. G., Martin, J. P., and Ritzmann, R. E. (2014). Extracellular wire tetrode recording in brain of freely walking insects. *J. Vis. Exp.* 86:e51337. doi: 10.3791/51337

Guo, P., and Ritzmann, R. E. (2013). Neural activity in the central complex of the cockroach brain is linked to turning behaviors. *J. Exp. Biol.* 216, 992–1002. doi: 10.1242/jeb.080473

Heinze, S., Florman, J., Asokaraj, S., El Jundi, B., and Reppert, S. M. (2013). Anatomical basis of sun compass navigation II: the neuronal composition of the central complex of the monarch butterfly. *J. Comp. Neurol.* 521, 267–298. doi: 10.1002/cne.23214

Heisenberg, M. (2003). Mushroom body memoir: from maps to models. *Nat. Rev. Neurosci.* 4, 266–275. doi: 10.1038/nrn1074

Heisenberg, M., Borst, A., Wagner, S., and Byers, D. (1985). Drosophila mushroom body mutants are deficient in olfactory learning. *J. Neurogenet.* 2, 1–30. doi: 10.3109/01677068509100140

Hori, S., Takeuchi, H., Arikawa, K., Kinoshita, M., Ichikawa, N., Sasaki, M., et al. (2006). Associative visual learning, color discrimination, and chromatic adaptation in the harnessed honeybee *Apis mellifera* L. *J. Comp. Physiol. A Neuroethol. Sens. Neural Behav. Physiol.* 192, 691–700. doi: 10.1007/s00359-005-0091-4

Hori, S., Takeuchi, H., and Kubo, T. (2007). Associative learning and discrimination of motion cues in the harnessed honeybee *Apis mellifera* L. *J. Comp. Physiol. A Neuroethol. Sens. Neural Behav. Physiol.* 193, 825–833. doi: 10.1007/s00359-007-0234-x

Horridge, G. A. (1962). Learning of leg position by the ventral nerve cord in headless insects. *Proc. R. Soc. Lond. Ser. B. Biol. Sci.* 157, 33–52. doi: 10.1098/rspb.1962.0061

Hothorn, T., Bretz, F., and Westfall, P. (2008). Simultaneous inference in general parametric models. *Biom. J.* 50, 346–363. doi: 10.1002/bimj.200810425

Hou, Q., Jiang, H., Zhang, X., Guo, C., Huang, B., Wang, P., et al. (2011). Nitric oxide metabolism controlled by formaldehyde dehydrogenase (fdh, homolog of mammalian GSNOR) plays a crucial role in visual pattern memory in Drosophila. *Nitric Oxide* 24, 17–24. doi: 10.1016/j.niox.2010.09.007

Ito, K., Suzuki, K., Estes, P., Ramaswami, M., Yamamoto, D., and Strausfeld, N. J. (1998). The organization of extrinsic neurons and their implications in the functional roles of the mushroom bodies in *Drosophila melanogaster* Meigen. *Learn. Mem.* 5, 52–77.

Kai, K., and Okada, J. (2013). Characterization of locomotor-related spike activity in protocerebrum of freely walking cricket. *Zool. Sci.* 30, 591–601. doi: 10.2108/zsj.30.591

Kaiser, M., and Libersat, F. (2015). The role of the cerebral ganglia in the venom-induced behavioral manipulation of cockroaches stung by the parasitoid jewel wasp. *J. Exp. Biol.* 218, 1022–1027. doi: 10.1242/jeb.116491

Kathman, N. D., Kesavan, M., and Ritzmann, R. E. (2014). Encoding wide-field motion and direction in the central complex of the cockroach Blaberus discoidalis. *J. Exp. Biol.* 217, 4079–4090. doi: 10.1242/jeb.112391

Kaun, K. R., and Rothenfluh, A. (2017). Dopaminergic rules of engagement for memory in Drosophila. *Curr. Opin. Neurobiol.* 43, 56–62. doi: 10.1016/j.conb.2016.12.011

Keene, A. C., and Waddell, S. (2007). Drosophila olfactory memory: single genes to complex neural circuits. *Nat. Rev. Neurosci.* 8, 341–354. doi: 10.1038/nrn2098

Kirkerud, N. H., Schlegel, U., and Galizia, C. G. (2017). Aversive learning of colored lights in walking honeybees. *Front. Behav. Neurosci.* doi: 10.3389/fnbeh.2017.00094

Kirkerud, N. H., Wehmann, H. N., Galizia, C. G., and Gustav, D. (2013). APIS-a novel approach for conditioning honey bees. *Front. Behav. Neurosci.* 7:29. doi: 10.3389/fnbeh.2013.00029

Kuntz, S., Poeck, B., Sokolowski, M. B., and Strauss, R. (2012). The visual orientation memory of Drosophila requires Foraging (PKG) upstream of Ignorant (RSK2) in ring neurons of the central complex. *Learn. Mem.* 19, 337–340. doi: 10.1101/lm.026369.112

Kuntz, S., Poeck, B., and Strauss, R. (2017). Visual working memory requires permissive and instructive NO/cGMP signaling at presynapses in the Drosophila central brain. *Curr. Biol.* 6, 613–623. doi: 10.1016/j.cub.2016.12.056

Kuwabara, M. (1957). Bildung des bedingten reflexes von pavlovs typus bei der honigbiene, Apis mellifica. *J. Fac. Sci. Hokkaido Univ. Ser. VI Zool.* 13, 458–464.

Libersat, F., and Gal, R. (2013). What can parasitoid wasps teach us about decision-making in insects? *J. Exp. Biol.* 216, 47–55. doi: 10.1242/jeb.073999

Lin, C., and Strausfeld, N. J. (2012). Visual inputs to the mushroom body calyces of the whirligig beetle Dineutus sublineatus: modality switching in an insect. *J. Comp. Neurol.* 520, 2562–2574. doi: 10.1002/cne.23092

Liu, G., Seiler, H., Wen, A., Zars, T., Ito, K., Wolf, R., et al. (2006). Distinct memory traces for two visual features in the Drosophila brain. *Nature* 439, 551–556. doi: 10.1038/nature04381

Martin, J. P., Guo, P., Mu, L., Harley, C. M., and Ritzmann, R. E. (2015). Central-complex control of movement in the freely walking cockroach. *Curr. Biol.* 25, 2795–2803. doi: 10.1016/j.cub.2015.09.044

Martin, J. R., Raabe, T., and Heisenberg, M. (1999). Central complex substructures are required for the maintenance of locomotor activity in *Drosophila melanogaster*. *J. Comp. Physiol. A.* 185, 277–288. doi: 10.1007/s003590050387

Menzel, R. (1999). Memory dynamics in the honeybee. *J. Comp. Physiol. A.* 185, 323–340. doi: 10.1007/s003590050392

Menzel, R. (2001). Searching for the memory trace in a mini-brain, the honeybee. *Learn. Mem.* 8, 53–62. doi: 10.1101/lm.38801

Menzel, R. (2012). The honeybee as a model for understanding the basis of cognition. *Nat. Rev. Neurosci.* 13, 758–768. doi: 10.1038/nrn3357

Mota, T., Giurfa, M., and Sandoz, J. C. (2011). Color modulates olfactory learning in honeybees by an occasion-setting mechanism. *Learn. Mem.* 18, 144–155. doi: 10.1101/lm.2073511

Muller, D., Staffelt, D., Fiala, A., and Menzel, R. (2003). Procaine impairs learning and memory consolidation in the honeybee. *Brain Res.* 977, 124–127. doi: 10.1016/S0006-8993(03)02760-4

Neuser, K., Triphan, T., Mronz, M., Poeck, B., and Strauss, R. (2008). Analysis of a spatial orientation memory in Drosophila. *Nature* 453, 1244–1247. doi: 10.1038/nature07003

Niggebrugge, C., Leboulle, G., Menzel, R., Komischke, B., and de Ibarra, N. H. (2009). Fast learning but coarse discrimination of colours in restrained honeybees. *J. Exp. Biol.* 212, 1344–1350. doi: 10.1242/jeb.021881

Ofstad, T. A., Zuker, C. S., and Reiser, M. B. (2011). Visual place learning in *Drosophila melanogaster*. *Nature* 474, 204–207. doi: 10.1038/nature10131

Pan, Y., Zhou, Y., Guo, C., Gong, H., Gong, Z., and Liu, L. (2009). Differential roles of the fan-shaped body and the ellipsoid body in Drosophila visual pattern memory. *Learn. Mem.* 16, 289–295. doi: 10.1101/lm.1331809

Pfeiffer, K., and Homberg, U. (2014). Organization and functional roles of the central complex in the insect brain. *Annu. Rev. Entomol.* 59, 165–184. doi: 10.1146/annurev-ento-011613-162031

Pinheiro, J., Bates, D., DebRoy, S., Sarkar, D., and R Core Team (2016). *Nlme: Linear and Nonlinear Mixed Effects Models*. R package version 3.1–128.

Plath, J. A., and Barron, A. B. (2015). Current progress in understanding the functions of the insect central complex. *Curr. Opin. Insect. Sci.* 12, 11–18. doi: 10.1016/j.cois.2015.08.005

Plath, J. A., Felsenberg, J., and Eisenhardt, D. (2012). Reinstatement in honeybees is context-dependent. *Learn. Mem.* 19, 543–549. doi: 10.1101/lm.026831.112

Poeck, B., Triphan, T., Neuser, K., and Strauss, R. (2008). Locomotor control by the central complex in Drosophila-An analysis of the tay bridge mutant. *Dev. Neurobiol.* 68, 1046–1058. doi: 10.1002/dneu.20643

Schott, M., Klein, B., and Vilcinskas, A. (2015). Detection of illicit drugs by trained honeybees (*Apis mellifera*). *PLoS ONE* 10:e0128528. doi: 10.1371/journal.pone.0128528

Seelig, J. D., and Jayaraman, V. (2015). Neural dynamics for landmark orientation and angular path integration. *Nature* 521, 186–191. doi: 10.1038/nature14446

Søvik, E., Plath, J. A., Devaud, J. M., and Barron, A. B. (2016). Neuropharmacological manipulation of restrained and free-flying honey bees, *Apis mellifera*. *J. Vis. Exp.* e54695. doi: 10.3791/54695

Strausfeld, N. J. (2002). Organization of the honey bee mushroom body: representation of the calyx within the vertical and gamma lobes. *J. Comp. Neurol.* 450, 4–33. doi: 10.1002/cne.10285

Strausfeld, N. J. (2012). *Arthropod Brains: Evolution, Functional Elegance, and Historical Significance*. Cambridge, MA: Harvard University Press.

Strausfeld, N. J., and Hirth, F. (2013). Deep homology of arthropod central complex and vertebrate basal ganglia. *Science* 340, 157–161. doi: 10.1126/science.1231828

Strauss, R. (2002). The central complex and the genetic dissection of locomotor behaviour. *Curr. Opin. Neurobiol.* 12, 633–638. doi: 10.1016/S0959-4388(02)00385-9

Strauss, R., and Heisenberg, M. (1993). A higher control center of locomotor behavior in the Drosophila brain. *J. Neurosci.* 13, 152–1861.

Tang, S., and Guo, A. (2001). Choice behavior of Drosophila facing contradictory visual cues. *Science* 294, 1543–1547. doi: 10.1126/science.1058237

Triphan, T., Poeck, B., Neuser, K., and Strauss, R. (2010). Visual targeting of motor actions in climbing Drosophila. *Curr. Biol.* 20, 663–668. doi: 10.1016/j.cub.2010.02.055

Vogt, K., Aso, Y., Hige, T., Knapek, S., Ichinose, T., Friedrich, A. B., et al. (2016). Direct neural pathways convey distinct visual information to Drosophila mushroom bodies. *Elife* 5:e14009. doi: 10.7554/eLife.14009

Vogt, K., Schnaitmann, C., Dylla, K. V., Knapek, S., Aso, Y., Rubin, G. M., et al. (2014). Shared mushroom body circuits underlie visual and olfactory memories in Drosophila. *Elife* 3:e02395. doi: 10.7554/eLife.02395

Waddell, S. (2013). Reinforcement signalling in Drosophila; dopamine does it all after all. *Curr. Opin. Neurobiol.* 23, 324–329. doi: 10.1016/j.conb.2013.01.005

Wang, Z., Pan, Y., Li, W., Jiang, H., Chatzimanolis, L., Chang, J., et al. (2008). Visual pattern memory requires foraging function in the central complex of Drosophila. *Learn. Mem.* 15, 133–142. doi: 10.1101/lm.873008

Wehmann, H. N., Gustav, D., Kirkerud, N. H., and Galizia, C. G. (2015). The sound and the fury–bees hiss when expecting danger. *PLoS ONE* 10:e0118708. doi: 10.1371/journal.pone.0118708

Wolf, R., Wittig, T., Liu, L., Wustmann, G., Eyding, D., and Heisenberg, M. (1998). Drosophila mushroom bodies are dispensable for visual, tactile, and motor learning. *Learn. Mem.* 5, 166–178.

Zars, T., Wolf, R., Davis, R., and Heisenberg, M. (2000). Tissue-specific expression of a type I adenylyl cyclase rescues the rutabaga mutant memory defect: in search of the engram. *Learn. Mem.* 7, 18–31. doi: 10.1101/lm.7.1.18

Zhang, K., Guo, J. Z., Peng, Y., Xi, W., and Guo, A. (2007). Dopamine-mushroom body circuit regulates saliency-based decision-making in Drosophila. *Science* 316, 1901–1904. doi: 10.1126/science.1137357

Zhang, X., Ren, Q., and Guo, A. (2013). Parallel pathways for cross-modal memory retrieval in Drosophila. *J. Neurosci.* 33, 8784–8793. doi: 10.1523/JNEUROSCI.4631-12.2013

Conflict of Interest Statement: The authors declare that the research was conducted in the absence of any commercial or financial relationships that could be construed as a potential conflict of interest.

frontiers in Behavioral Neuroscience

ORIGINAL RESEARCH
published: 07 October 2016
doi: 10.3389/fnbeh.2016.00186

Microglomerular Synaptic Complexes in the Sky-Compass Network of the Honeybee Connect Parallel Pathways from the Anterior Optic Tubercle to the Central Complex

*Martina Held[1], Annuska Berz[1], Ronja Hensgen[1], Thomas S. Muenz[2], Christina Scholl[2], Wolfgang Rössler[2], Uwe Homberg[1] and Keram Pfeiffer[1]**

[1] Department of Biology, Animal Physiology, Philipps-University Marburg, Marburg, Germany, [2] Biozentrum, Behavioral Physiology and Sociobiology (Zoology II), University of Würzburg, Würzburg, Germany

While the ability of honeybees to navigate relying on sky-compass information has been investigated in a large number of behavioral studies, the underlying neuronal system has so far received less attention. The sky-compass pathway has recently been described from its input region, the dorsal rim area (DRA) of the compound eye, to the anterior optic tubercle (AOTU). The aim of this study is to reveal the connection from the AOTU to the central complex (CX). For this purpose, we investigated the anatomy of large microglomerular synaptic complexes in the medial and lateral bulbs (MBUs/LBUs) of the lateral complex (LX). The synaptic complexes are formed by tubercle-lateral accessory lobe neuron 1 (TuLAL1) neurons of the AOTU and GABAergic tangential neurons of the central body's (CB) lower division (TL neurons). Both TuLAL1 and TL neurons strongly resemble neurons forming these complexes in other insect species. We further investigated the ultrastructure of these synaptic complexes using transmission electron microscopy. We found that single large presynaptic terminals of TuLAL1 neurons enclose many small profiles (SPs) of TL neurons. The synaptic connections between these neurons are established by two types of synapses: divergent dyads and divergent tetrads. Our data support the assumption that these complexes are a highly conserved feature in the insect brain and play an important role in reliable signal transmission within the sky-compass pathway.

Keywords: sky-compass orientation, insect brain, central complex, polarization vision, honeybee, synaptic connections, anterior optic tubercle

OPEN ACCESS

Edited by:
Nuno Sousa,
University of Minho, Portugal

Reviewed by:
Wolf Huetteroth,
University of Konstanz, Germany
Wulfila Gronenberg,
University of Arizona, USA

****Correspondence:***
Keram Pfeiffer
keram.pfeiffer@staff.uni-marburg.de

Received: *01 June 2016*
Accepted: *21 September 2016*
Published: *07 October 2016*

Citation:
Held M, Berz A, Hensgen R, Muenz TS, Scholl C, Rössler W, Homberg U and Pfeiffer K (2016) Microglomerular Synaptic Complexes in the Sky-Compass Network of the Honeybee Connect Parallel Pathways from the Anterior Optic Tubercle to the Central Complex. Front. Behav. Neurosci. 10:186. doi: 10.3389/fnbeh.2016.00186

Abbreviations: AL, antennal lobe; AOT, anterior optic tract; AOTU, anterior optic tubercle; CB, central body; CBL, lower division of the central body; CBU, upper division of the central body; CNS, central nervous system; cV, clear vesicle; CX, central complex; dcV, dense core vesicle; DRA, dorsal rim area; GABA, γ-aminobutyric acid; GS, glia sheath; IT, isthmus tract; KLH, keyhole-limpet hemocyanin; LA, lamina; LBU, lateral bulb; LCA, lateral calyx; LO, lobula; LP, large profile; LUC, lower unit complex of the anterior optic tubercle; LX, lateral complex; M, mitochondrion; MBU, medial bulb; ME, medulla; MEDRA, dorsal rim area of the medulla; N, nucleus; NO, nodulus; NOL, lower division of the nodulus; NOU, upper division of the nodulus; PED, pedunculus; RE, retina; SP, small profile; TL, tangential neuron; TuLAL, tubercle-lateral accessory lobe neuron; UU, upper unit of the anterior optic tubercle; VL, vertical lobe.

INTRODUCTION

Many insects have well developed abilities for orientation and navigation. En route, they rely on different strategies, like landmark navigation or vector integration (reviewed by Wehner, 2003; Menzel et al., 2006; Collett et al., 2013; Srinivasan, 2015). For spatial orientation many insects use sky-compass cues, like the position of the sun, the chromatic gradient and the polarization pattern of the sky (reviewed in Homberg et al., 2011). The ability to navigate in relation to the polarization pattern of the sky was first shown in behavioral studies on honeybees by von Frisch (1949). The neuronal basis and mechanisms underlying sky-compass orientation have been investigated anatomically and physiologically in a most detailed manner in locusts and crickets (reviewed by Homberg et al., 2011), whereas in honeybees, research into this topic is still at the beginning. Recently the sky-compass pathway in the honeybee brain has been described anatomically from the compound eye up to the lateral complex (LX; Zeller et al., 2015). The goal of this study is to investigate the anatomy of this pathway further from the LX into the central complex (CX), a neuropil which, amongst other functions, holds a neuronal representation of space around the animal (reviewed by Pfeiffer and Homberg, 2014).

The sky-compass pathway receives input via a specialized area of the compound eye, the dorsal rim area (DRA). DRA photoreceptors project through the lamina (LA) and terminate in the DRA of the medulla (MEDRA). Transmedulla neurons ramify in the MEDRA. Their fibers run dorsoventrally through the medulla (ME) and enter the lower unit complex (LUC) of the anterior optic tubercle (AOTU) via the anterior optic tract (AOT). From there two types of neuron, tubercle-lateral accessory lobe neuron 1a (TuLAL1a) and TuLAL1b project toward the LX and end in conspicuously large synaptic terminals in the lateral and the medial bulbs (LBUs, MBUs; Mota et al., 2011; Zeller et al., 2015). In the desert locust tangential TL2 and TL3 neurons of the lower division of the central body (CBL) have dendritic branches in the bulbs, forming large synaptic complexes with the terminals of TuLAL1 neurons (Vitzthum et al., 2002; Träger et al., 2008). The boundaries of the bulbs are defined by the presence of these microglomerular synaptic complexes. Locust TL2 and TL3 neurons are immunoreactive with antisera against γ-aminobutyric acid (GABA) and therefore, can be labeled using immunocytochemistry (Homberg et al., 1999). Large synaptic structures in the bulbs, either from TuLAL1 or TL neurons, have been found in other insect species as well, such as the fruit fly *Drosophila melanogaster* (Hanesch et al., 1989; Seelig and Jayaraman, 2013), the moth *Manduca sexta* (Homberg et al., 1990), the cricket *Gryllus bimaculatus* (Sakura et al., 2008), the monarch butterfly *Danaus plexippus* (Heinze and Reppert, 2011), the bumblebee *Bombus ignitus* (Pfeiffer and Kinoshita, 2012), and the desert ant *Cataglyphis fortis* (Schmitt et al., 2016). While in most of these species these neurons are involved in sky-compass vision, in *Drosophila melanogaster* a different function has been found. The dendrites of the equivalent to TL neurons, called ring neurons, represent visual features of the environment with a strong preference for a vertical stripe. The associated microglomeruli in the bulbs are arranged retinotopically and therefore form a spatial map of the visual field of the fly (Seelig and Jayaraman, 2013). Additionally, these neurons have been found to be activated by an optic flow pattern around the yaw axis (Weir and Dickinson, 2015). Thus far the sky-compass pathway of the honeybee has been traced with anatomical methods from the DRA to the bulbs of the LX (Mota et al., 2011; Zeller et al., 2015). The neurons in this pathway share many anatomical features with those of locusts, where electrophysiological studies revealed their sensitivity to polarized and chromatic light stimuli (el Jundi et al., 2014). In this study we investigate the sky-compass pathway in the honeybee from the LUC of the AOTU to the central body (CB). To reveal whether neurons from the LUC are connected to GABA-immunoreactive tangential neurons of the CB as shown in locusts, we analyzed the anatomy and ultrastructure of synaptic complexes in the MBUs and LBUs.

MATERIALS AND METHODS

Animals

Worker honeybees (*Apis mellifera*) were caught at the entrance of the hive, which was maintained at the Department of Biology at the Philipps-University Marburg. Injections and immunostainings were performed in spring and summer, when the colony was outside. The preparations for transmission electron microscopy were made in winter. At this time the hive was kept inside a greenhouse at 25°C, and bees were fed with honey water (20–30% honey) and pollen. Experiments for synapsin/f-actin double labeling for 3D reconstructions were made during the winter season using adult worker bees ("winterbees") from inside a colony maintained at the departmental bee station at the University of Würzburg.

Preparation

Bees were cooled at 4°C until immobilized. For better handling during preparation, the animals were waxed to a holder with dental wax. The cuticle of the frons between the compound eyes, ocelli and labrum was removed. For getting access to the brain, the hypopharyngeal glands and air-sacks as well as the neural sheath were removed.

Extracellular Iontophoretic Dye Injection

Extracellular iontophoretic dye injections were performed to achieve staining of small numbers of neurons (1–20) connecting the AOTU to the bulbs of the LX or the bulbs to the CX. Sharp glass microelectrodes were fabricated by pulling borosilicate capillary tubes (outer diameter 1.5 mm, inner diameter 0.75 mm, Hilgenberg, Malsfeld, Germany) with a Flaming/Brown puller (P97, Sutter instrument, Novato, CA, USA). Electrode tips were filled with 4% Neurobiotin tracer (Vector Laboratories, Burlingame, CA, USA) in 1 M KCl and backed up with 2.5 M KCl. These electrodes had a resistance of 100–200 MΩ in the tissue. Using a micromanipulator an electrode was

positioned in the area of the LUC of the AOTU or the CBL. By applying a pulsed current of 10 nA (1 Hz, 50% duty cycle) for 20–45 min the tracer was ejected from the electrode and entered the neurons in the vicinity of the tip presumably through pores created by an electroporating effect of the electric field. After removing the electrode, brains were dissected from the head capsule and immersed in a fixative containing 4% paraformaldehyde (Sigma-Aldrich, Steinheim, Germany), 0.25% glutaraldehyde (Carl Roth, Karlsruhe, Germany) and 0.25% saturated picric acid in 0.1 M phosphate buffered saline (PBS, pH 7.4) overnight at 4°C. They were then washed with PBS. To detect neurons labeled with Neurobiotin, brains were immersed in a solution containing Cy3-conjugated streptavidin (1:1000, Jackson Immunoresearch Laboratories, West Grove, PA, USA), 0.3% Triton X-100 (TrX; Sigma, Deisenhofen, Germany) and PBS. After incubation at 4°C for 3 days, brains were washed with PBS and 0.3% TrX (PBT) and afterwards with PBS. The brains were then dehydrated in an ascending ethanol series. To increase image quality brains were cleared with methyl salicylate (Merck, Darmstadt, Germany). Finally, the brains were embedded between two cover slips in Permount (Fisher Scientific, Pittsburgh, PA, USA). Eight reinforcement rings (Zweckform, Oberlaindern, Germany) served as spacers to prevent squishing the tissue.

Mass Staining Procedure

For tracing of TuLAL1 neurons, dextran Texas Red crystals (lysine-fixable, 3000 MW, Molecular Probes, Eugene, OR, USA) were inserted into the LUC. To do this, the tip of a sharp glass microcapillary, that was created as described above, was broken to a diameter of about 5–30 μm. The tip was dipped into petroleum jelly and then into the dextran Texas Red to pick up a few tracer crystals. After removing all liquid around the brain with a piece of paper tissue, the microcapillary was manually advanced into the target area. Excess dye was washed off with Ringer solution (130 mM NaCl, 5 mM KCl, 4 mM $MgCl_2$, 15 mM HEPES, 25 mM glucose, 160 mM saccharose, 5 mM $CaCl_2$). To allow for complete uptake and distribution of the tracer in the neurons, the head capsule was covered with tissue paper and the bee was kept overnight at 4°C in a moist chamber. To prevent bleaching of the fluorescent dye all further steps were performed in darkness if possible. After removing the brain from the head capsule it was fixed overnight at 4°C in 4% paraformaldehyde and 0.5% glutaraldehyde in 0.1 M sodium phosphate buffer (NaPi; pH 7.4). The brain was then washed with 0.01 M PBS. After embedding in albumin-gelatin (12% ovalbumin and 4.8% gelatin in demineralized water) and fixation overnight at 4°C with 8% formaldehyde in NaPi, the brain was sectioned at 40 μm in the frontal plane using a vibrating-blade microtome (VT 1000S or VT 1200S; Leica, Wetzlar, Germany).

GABA Immunostaining

To label GABA-immunoreactive neurons, we used two different antisera that were raised against GABA conjugated to keyhole-limpet hemocyanin (KLH) via glutaraldehyde. The first antiserum was raised in guinea pig (ab17413; Lot GR51659; Abcam, Cambridge, UK). According to the manufacturer the specificity of the antiserum was tested on brain slices of rats by preadsorption with 100 nM GABA conjugated to glutaraldehyde, which abolished all staining. Preadsorption with 500 nM of similar conjugates of glutamic acid, glutamate and taurine failed to block staining (product datasheet anti-GABA antibody ab17413). The second antibody was raised in rabbit (# 9/24; kindly provided by Dr. T.G. Kingan). It had been affinity purified against KLH. The specificity of this antiserum was tested on brain sections of the sphinx moth *Manduca sexta*, the honeybee and the desert locust *Schistocerca gregaria*. In *Manduca sexta* liquid-phase preadsorption of the diluted antiserum with GABA-glutaraldehyde-KLH and similar conjugates of L-glutamic acid, β-alanine, L-glutamine and taurine was performed (Hoskins et al., 1986). GABA-glutaraldehyde-KLH blocked immunostaining at a concentration of 24 nM, whereas similar concentrations of the other amino acid conjugates were without effect (Hoskins et al., 1986). Likewise, on brain sections of the honeybee, preadsorption with 1 mM GABA-glutaraldehyde completely blocked labeling (Schäfer and Bicker, 1986), and in the desert locust, preadsorption with 15 nM GABA-glutaraldehyde-bovine serum albumin (BSA) conjugate abolished all staining on brain sections (Homberg et al., 1999).

For double staining of tracer-injected brains with GABA antiserum, gelatin slices were washed with 0.1% TrX in saline substituted Tris-buffer (SST; pH 7.4). Sodium borohydride was used to reduce background autofluorescence caused by Schiff bases that occur during glutaraldehyde fixation (Baschong et al., 1999). Sections were covered for 10 min with 10 mg/ml $NaBH_4$ and 0.1% TrX in NaPi. Deposit was washed out with 0.1% TrX in SST. To block unspecific binding sites the slices were pre-incubated for 1 h at room temperature on a shaker with 10% normal donkey serum (NDS; Dianova, Hamburg, Germany), 0.5% TrX and SST. The primary antibody against GABA was diluted 1:500 in a solution of 1% NDS, 0.02% sodium azide and 0.5% TrX in SST. Slices were incubated overnight at 30°C in an incubator on a shaker. After washing in SST containing 0.1% TrX, sections were treated with the secondary antibody solution. It consisted of Cy2-conjugated donkey anti-guinea pig IgG against the antiserum from Abcam (1:300; Dianova, Hamburg, Germany) and donkey anti-rabbit IgG against the antiserum from Kingan (1:200; Dianova, Hamburg, Germany), 1% NDS and 0.5% TrX in SST. The secondary antiserum was applied for 1 h on a shaker at room temperature. After further washing with 0.1% TrX in SST the sections were mounted on chromalum/gelatin-coated microscope slides, dehydrated in an ascending ethanol series, and embedded in Entellan (Merck, Darmstadt, Germany) under cover slips.

F-actin Staining and Immunolabeling for Synapsin

To obtain an overview of all synaptic complexes in the bulbs of the LX, we performed double labeling for the vesicle-associated protein synapsin and filamentous actin (see Groh et al., 2004; Schmitt et al., 2016). Brains were dissected

from the head capsule and immediately fixed with ice-cold 4% paraformaldehyde (methanol free, 28908, Fischer Scientific, Schwerte, Germany) in PBS overnight at 4°C. After washing with PBS, brains were embedded in 5% low-melting point agarose (Agarose II, no. 210–815, Amresco, Solon, OH, USA), adjusted to a frontal plane and sectioned at 100 μm thickness using a vibrating-blade microtome (VT 1000S; Leica, Wetzlar, Germany). Preincubation was performed using 0.2% TrX in PBS containing 2% normal goat serum (NGS, 005-000-121, Jackson ImmunoResearch Laboratories, West Grove, PA, USA) for 1 h at room temperature. To visualize f-actin, sections were incubated with 0.2 units Alexa Fluor 488 conjugated phalloidin (A12379, Molecular Probes, Eugene, OR, USA) in 0.2% TrX and 2% NGS in PBS for 3 days at 4°C. For the additional labeling of synapsin, a monoclonal antibody raised against the *Drosophila* synaptic-vesicle-associated protein synapsin I (SYNORF1, kindly provided by E. Buchner, University of Würzburg, Germany) was added (1:50). SYNORF1 in honeybee tissue has been characterized by Pasch et al. (2011). Sections were washed several times in PBS, before incubated in Alexa Fluor 568 conjugated goat anti-mouse (1:250, A11004, Molecular Probes, Eugene, OR, USA) in PBS with 1% NGS for 2 h at room temperature. After washing with PBS, sections were transferred into 60% glycerol in PBS for 30 min. They were then mounted in 80% glycerol in PBS on glass slides covered with cover slips.

Wholemount Preparation for Neuropil Reconstruction

Brains were dissected from the head capsule as described above and fixed with ice-cold 2% paraformaldehyde and 2% glutaraldehyde in PBS for 4 days at 4°C. After several washing steps with PBS the brain tissue was dehydrated in an ascending ethanol series (50%, 70%, 90%, 95% and 3 × 100% for 10 min each) before being cleared in methyl salicylate for 4 days at 4°C. Brains were then mounted in methyl salicylate in custom metal slides covered with cover slips (method adapted from Kuebler et al., 2010).

Transmission Electron Microscopy

To investigate the ultrastructure of synaptic complexes brains were fixed using the high-pressure freezing technique (McDonald, 2007; Müller-Reichert et al., 2007; Rachel et al., 2010; Peschke et al., 2013). Dissected brains were prefixed overnight at 4°C with 4% paraformaldehyde and 2.5% glutaraldehyde in 0.1 M sodium cacodylate buffer (NaCB; pH 7.2). After washing in 0.1 M NaCB, brains were embedded in 7% low-melting point agarose (LM3, AppliChem GmbH, Darmstadt, Germany), and a 200 μm thick slice, containing the area of interest, was cut with a vibratome. These sections were then high-pressure frozen with a Wohlwend HPF Compact 02 (M. Wohlwend, Engineering Office, Sennwald, Switzerland). They were then transferred to an automatic ASF2 freeze substitution unit (Leica Microsystems, Wetzlar, Germany) to replace the water and enhance contrast. For cryo-substitution fixation (CSF) a solution of 0.2% OsO_4, 0.25% uranyl acetate and 5% (vol/vol) H_2O in acetone (A.O.U.H; Walther and Ziegler, 2002; Junglas et al., 2008; Rachel et al., 2010) was added. Freeze-substitution was carried out at −90°C for 46.5 h, −60°C for 8 h, −30°C for 8 h and held at 0°C for 3 h. The heating time between the steps was 1 h. Afterwards, the sections were washed twice with ice-cold acetone (100%) and were then gradually infiltrated with Epon at room temperature, followed by polymerization for 72 h at 60°C. Ultrathin sections (60–80 nm) were cut with an ultramicrotome (Ultracut; Reichert-Labtech, Wolfratshausen, Germany), collected on uncoated copper 400 mesh grids (Plano, Wetzlar, Germany) and contrast enhanced by positive staining with 2% uranyl acetate and lead citrate (Reynolds, 1963).

Image Acquisition and Processing

Images of fluorescent samples were acquired with a confocal laser scanning microscope (CLSM; TCS SP5 and TCS SP2, Leica Microsystems, Wetzlar, Germany). Optical serial sections of an overview of all synaptic complexes in the tracer-injected brains immunostained for GABA were scanned using a 40× objective (HCX PL APO 40×/1.25−0.75 Oil Lbd. bl.; Leica, Bensheim. Germany) at a resolution of 1024 × 1024 pixels and a *z*-stepsize of 1.5 μm. For detailed scans at the same resolution with a *z*-stepsize of 1 μm a 63× objective (HCX PL APO 63×/1.3 GLY CORR CS 21, Leica, Bensheim, Germany) was used. For double labeled synapsin/f-actin preparations, physical sections containing the whole two clusters of synaptic complexes in the bulbs were selected and scanned at a resolution of 1024 × 1024 pixels using a 20× objective (HC PL APO 20×/0.70 Imm, Leica, Bensheim, Germany) and 63× objective (HCX PL APO 63×/1.4−0.6 Oil, Leica, Bensheim, Germany) to obtain image stacks at a *z*-stepsize of 1 μm. Exploiting the increased autofluorescence attributes of the paraformaldehyde/glutaraldehyde-fixed wholemount preparations, these brains were scanned with a 10× objective (HC PL APO 10×/0.4 Imm, Leica, Bensheim, Germany) at a *z*-stepsize of 4 μm in three tiles to create a panoramic overview image stack of the whole brain.

All image stacks were processed with Amira (versions 3.1.1 and 5.3.3; FEI Visualization Sciences Group, Mérignac Cedex, France). Amira was further used for the 3D reconstruction of individual synaptic complexes in the bulbs based on f-actin positive profiles in synapsin/f-actin double labeled preparations and to create a whole brain reconstruction of all major neuropils based on autofluorescence wholemount preparations. To evaluate the spatial distribution and localization of synaptic complexes in the context of the whole brain the synaptic reconstructions were transformed into the whole brain reconstruction using the CX as a landmark for orientation. Volumes of the reconstructed postsynaptic portion of the microglomeruli were calculated using Amira 5.6. The data for the lateral and medial cluster were statistically compared using the Mann-Whitney test (VassarStats[1]).

Transmission electron micrographs were taken using a JEOL JEM-2100 transmission electron microscope (JEOL, Tokio,

[1]http://vassarstats.net/

Japan) at an acceleration voltage of 120 kV. Images were taken with a 2k × 2k pixel CCD-camera F214 and the software EM-Menu 4 (TVIPS, Gauting, Germany). Contrast and brightness were optimized with Adobe Photoshop CC (Adobe Systems, San Jose, CA, USA) software if necessary, and all figures were created with Adobe Illustrator CC.

RESULTS

We investigated the anatomy and ultrastructure of microglomerular synaptic complexes in the bulbs of the LX that connect the AOTU to the CB in the brain of the honeybee *Apis mellifera* (**Figure 1**). We first describe the different neuron types that are involved in these conspicuous connections. Then the general distribution and appearance of the synaptic complexes is shown. Last, we present data on the subcellular organization and show two types of synapses forming cell-cell connections. Positional information within the brain is given with respect to the body axis. For neuropils we followed the terminology suggested by Ito et al. (2014) wherever possible. Additionally, we refer to the entirety of small subunits of the AOTU as "LUC" as suggested by Zeller et al. (2015). The nomenclature of all neurons corresponds to the terminology used in locusts, monarch butterflies and bumblebees (Müller et al., 1997; Homberg et al., 2003; Pfeiffer et al., 2005; Heinze and Reppert, 2011; Pfeiffer and Kinoshita, 2012).

Neurons Innervating the Bulbs

Using extracellular iontophoretic dye injections, we were able to identify and distinguish two subtypes of TuLAL1 neuron connecting the LUC of the AOTU to the bulbs. The bulbs are neuropils located laterally on both sides of the CX. In each hemisphere there are two bulbs: the MBU and LBU. Together with the lateral accessory lobe they form the LX which is closely associated with the CX (Ito et al., 2014). Both subtypes of TuLAL1 neuron had their cell bodies medially to the AOTU and their axons extended around the vertical lobe (VL) of the mushroom body toward the CX. The axons of both subtypes ended in conspicuous large, hat-like terminals. The majority of the injected neurons had only one of those synaptic endings, but in a few cases the axon ended in more than one terminal. In these cases, the terminals were always in close proximity to each other and in the same bulb. The terminals of TuLAL1a neurons were located in the LBU, ventrolaterally to the CB (**Figure 1B**). The second subtype, TuLAL1b neurons, projected to the MBU which lies directly adjacent to the groove formed between the lateral boundary of the lower and upper divisions of the CB (**Figure 1C**). The transmission of information from the bulbs into the CB is assumed to take place in tangential neurons of the type TL2 and TL3, the presumptive equivalent to ring neurons in the fruit fly (*Schistocerca gregaria*: Vitzthum et al., 2002; Träger et al., 2008; *Drosophila melanogaster*: Seelig and Jayaraman, 2013; Wolff et al., 2015). We were able to identify these neuronal cell types in the honeybee brain. They had their cell bodies medially to the AOTU and posteriorly from the somata of TuLAL1 neurons. Their primary neurites ran toward the isthmus tract (IT), where they gave off single large side branches that extended into one of the bulbs and had dense accumulations of protrusions at their tips (**Figures 1D,E** arrowheads). These dendritic side branches were about 20 μm to 50 μm long in TL2 neurons (**Figure 1D**) and invaded the LBU. In contrast, in TL3 neurons they had a stub-like appearance of only a few μm and innervated the MBU (**Figure 1E**). The axons of both types of neuron extended into the CBL, where they branched in all slices of defined layers.

Owing to the close morphological similarity of these four neuron types with equivalent neurons in locusts, monarch butterflies and bumblebees (Müller et al., 1997; Homberg et al., 2003; Pfeiffer et al., 2005; Heinze and Reppert, 2011; Pfeiffer and Kinoshita, 2012), we suppose that these neurons form the large synaptic complexes found in the bulbs. More precisely, TuLAL1a neurons develop synaptic connections with TL2 and TuLAL1b with TL3 neurons (**Figure 1A**).

Appearance of the Microglomerular Synaptic Complexes

To obtain an overview of the synaptic complexes within the bulbs, we performed double labeling experiments using anti-synapsin and f-actin phalloidin staining. Synaptic complexes were clearly visible using this method and arranged in two distinct clusters, one group of synaptic complexes very close to the CBL in the MBU, and another group located more laterally in the LBU (**Figure 2A**). Higher magnification revealed that synapsin-immunoreactivity (IR) was localized within a cup-shaped profile, and dense f-actin phalloidin staining was concentrated inside the halo of synapsin-IR (**Figure 2B**). The anterior-posterior expansion of both clusters becomes obvious in horizontal sections (**Figure 2C**).

Figures 3A,B show a complete 3D reconstruction of the lateral (red) and medial (blue) clusters of one brain hemisphere of synaptic complexes merged into a tissue section of phalloidin-labeled fiber bundles. The total number of synaptic complexes within each of the two clusters was assessed by individual 3D reconstructions of phalloidin-labeled profiles revealing 68 ± 1.9 SD ($n = 4$) complexes in the lateral cluster and 197.5 ± 37.5 SD ($n = 4$) in the medial cluster (**Figures 3C–E**). Because synapsin-positive presynaptic profiles often appeared fused, we used the more distinct phalloidin-labeled profiles to quantify individual synaptic complexes. It cannot be excluded, however, that in some cases, particularly in the medial cluster, more than one phalloidin-labeled profile was associated with one (fused) synapsin-positive complex at this level of resolution. In addition to the total numbers of synaptic complexes defined by phalloidin-labeled clusters, the 3D reconstructions illustrate the position and extension of the two clusters in relation to other brain structures, in particular the CB. Based on the 3D reconstruction of the f-actin positive (postsynaptic) portion of the microglomeruli, we measured their volumes (**Figure 4**). Owing to the rather small size of these structures, compared to the *z*-resolution of the image stacks, these values should be treated with caution and should not be taken as absolute measurements. However, they illustrate the size difference between the elements of the lateral

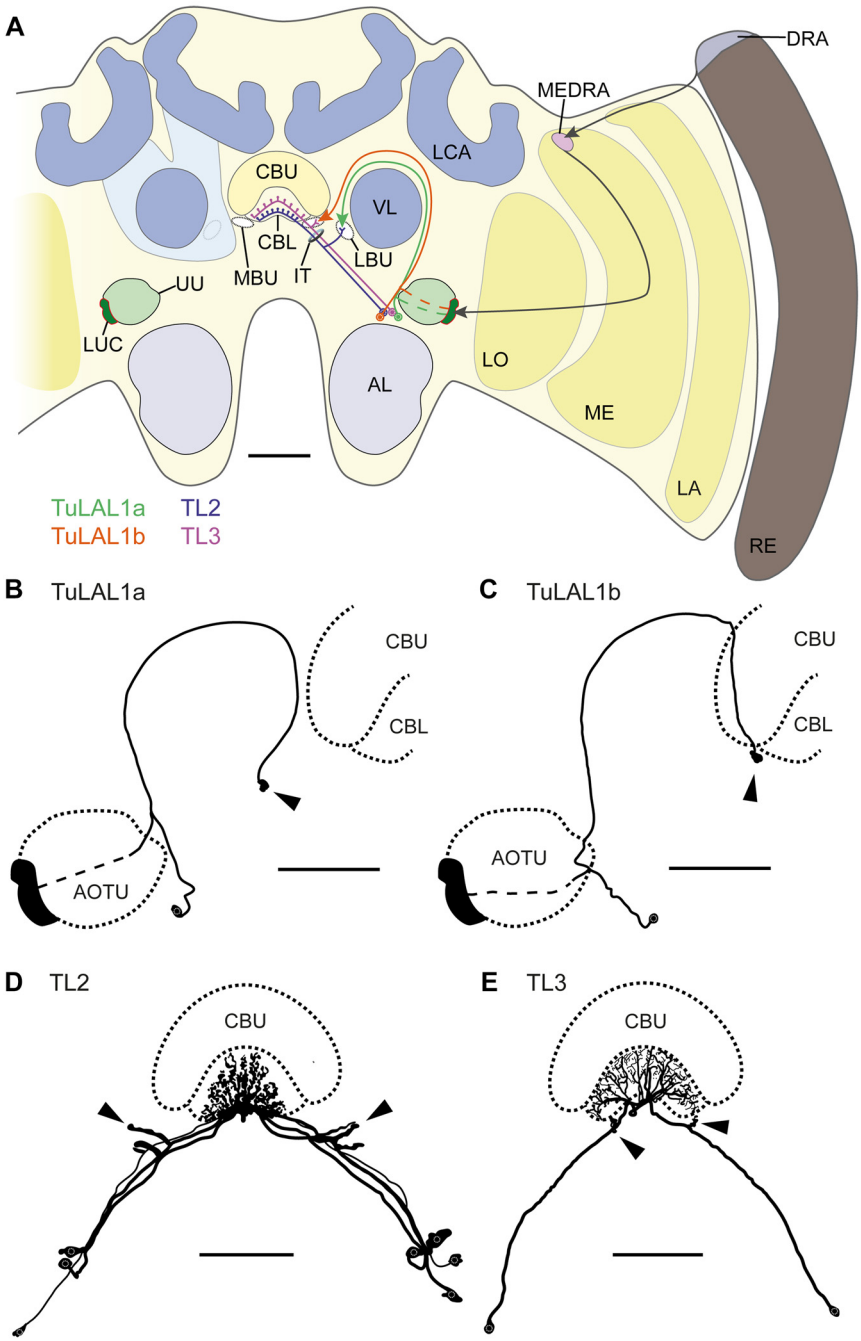

FIGURE 1 | (A) Schematic drawing of the position of the neuron types forming microglomerular synaptic complexes in the medial and lateral bulbs of the honeybee *Apis mellifera*. The connection from the anterior optic tubercle to the central complex (CX) is formed by tubercle-lateral accessory lobe neurons 1a (TuLAL1a; green) and TuLAL1b neurons (orange). Two types of tangential neuron (TL2, blue; TL3, purple) provide input into the lower division of the central body (CBL). **(B–E)** Reconstructed morphologies of neurons labeled by extracellular dye injections. TuLAL1a **(B)** and TuLAL1b **(C)** neurons have their cell bodies medially from the AOTU. The axons of both types run toward the central body (CB), where they end in large terminals (arrowheads). In TuLAL1a neurons these terminals are located in the LBU (**B**, arrowhead), whereas TuLAL1b neurons terminate in the MBU (**C**, arrowhead), close to the CBL. TL neurons have their cell bodies medially to the AOTU and posteriorly to the somata of TuLAL1 neurons. Their primary neurites run toward the isthmus tract (IT), where they give off sidebranches. The sidebranches of TL2 neurons extend into the LBU, and those of TL3 to the MBU (**D,E**, arrowheads). The axons extend from the bulbs further into the CBL, where they branch in all slices but not in all layers. TL2 neurons branch in the dorsal part of the CBL, TL3 neurons in the ventral part. AL, antennal lobe; CBU, upper division of the CB; DRA, dorsal rim area; LA, lamina; LBU, lateral bulb; LCA, lateral calyx; LO, lobula; LUC, lower unit complex of the AOTU; MBU, medial bulb; ME, medulla; MEDRA, dorsal rim area of the medulla; RE, retina; UU, upper unit of the AOTU; VL, vertical lobe. Scale bars: **A** = 200 μm, **B–E** = 100 μm.

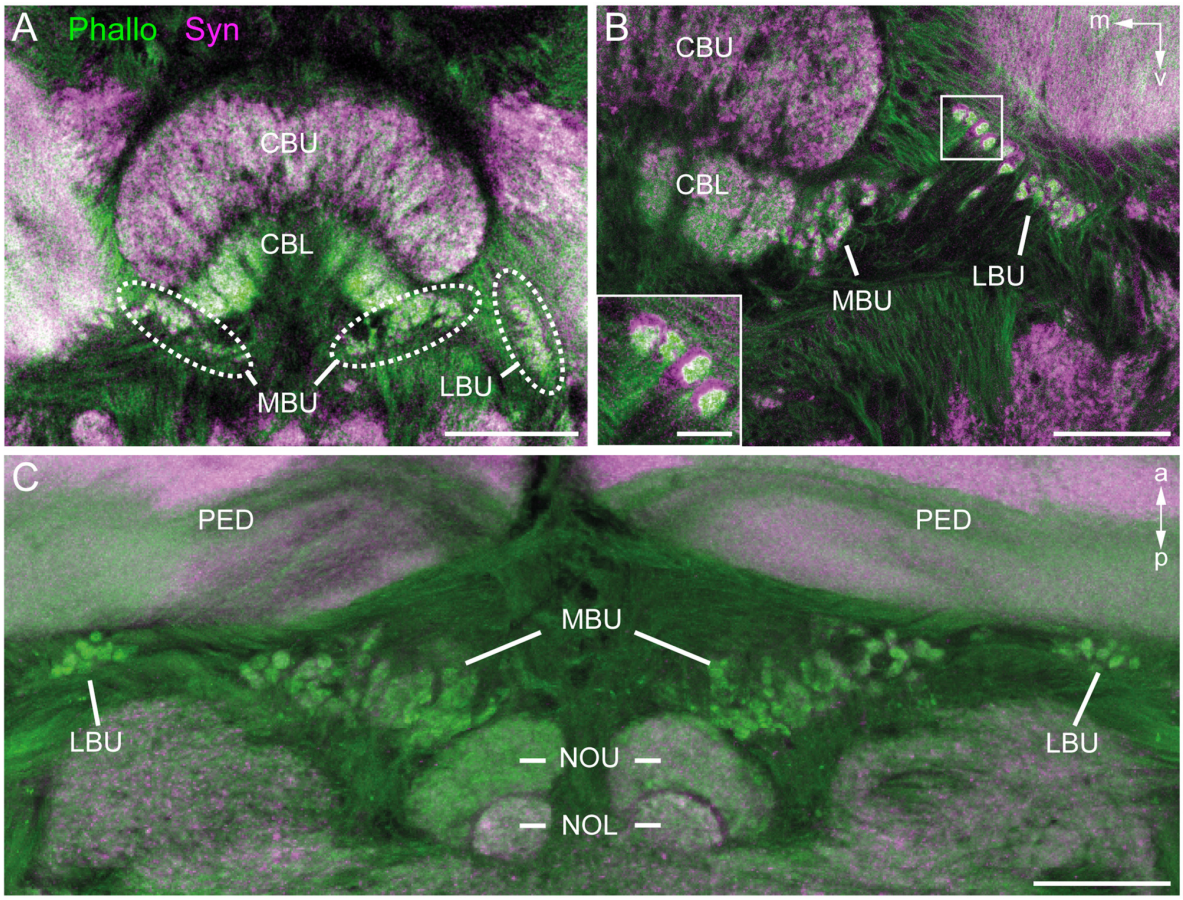

FIGURE 2 | Anti-synapsin (Syn, magenta) and f-actin phalloidin (Phallo, green) staining of the microglomerular synaptic complexes. (A) Frontal sections show that the synaptic complexes are arranged in two clusters: one in the MBU close to the connection of the CBL and the upper division (CBU). The second cluster is located in the LBU. **(B)** At higher magnification of both clusters the distribution of the anti-synapsin and f-actin phalloidin staining reveals a synapsin-positive cup-shaped structure with an f-actin containing profile in the center. **(C)** In horizontal sections the distribution in the anterior-posterior axis becomes apparent. The synaptic complexes in both bulbs appear posterior to the pedunculi (PED). Those of the MBU extend posterior to the upper division of the noduli (NOU). a, anterior; m, medial; NOL, lower division of the noduli; p, posterior; v, ventral. Scale bars: **A** = 100 μm, **B,C** = 50 μm, inset in **B** = 10 μm.

and the medial cluster as well as the distribution of volumes within the clusters. The median volume of the postsynaptic elements from four brains in the medial cluster was 33 μm^3, whereas it was 79 μm^3 in the lateral cluster. This difference was statistically significant (Mann-Whitney test, $P < 0.0001$, $U = 157060.5$, $z = -13.39$, $N_{medial} = 772$, $N_{lateral} = 262$). The total volume of all postsynaptic elements was 8485 μm^3 in the medial cluster and 6244 μm^3 in the lateral cluster (median values, $n = 4$).

To investigate whether the synaptic complexes are formed by TuLAL1a/b and TL2/3 neurons we performed double label experiments. In *Schistocerca gregaria*, TL2 and TL3 tangential neurons of the CB are GABA-immunoreactive (Homberg et al., 1999; Träger et al., 2008). In honeybees immunostaining for GABA also labels putative tangential neurons in the CBL (Schäfer and Bicker, 1986). Immunofluorescent labeling for GABA confirmed the data of Schäfer and Bicker (1986) and revealed a subdivision of terminals of the labeled TL neurons lateral to the CB into two larger medial groups and two smaller lateral groups (**Figure 5A**). It also confirmed that branching of these neurons in the CB is restricted to the CBL. The few fibers stained in the upper division of the central body (CBU) likely belong to TU1 and TU2 neurons as described in *Schistocerca gregaria* (Homberg et al., 1999). To analyze whether the TL neurons are candidates for postsynaptic partners of TuLAL1 neurons, we stained TuLAL1 neurons through tracer injection into the LUC of the AOTU, followed by marking of TL neurons through GABA immunofluorescence labeling. Terminals of TuLAL1 neurons were large hat-like structures with an uneven surface (**Figures 5B,C**). Close inspection of single complexes in double labeled samples revealed a distinct pattern: hat-like terminals from TuLAL1 neurons partly enclosed the terminals of side branches of TL neurons (**Figures 5B,C**).

Ultrastructure and Synaptic Connections

To investigate the synaptic connectivity between TuLAL1 and TL neurons, we studied the microglomeruli at the ultrastructural

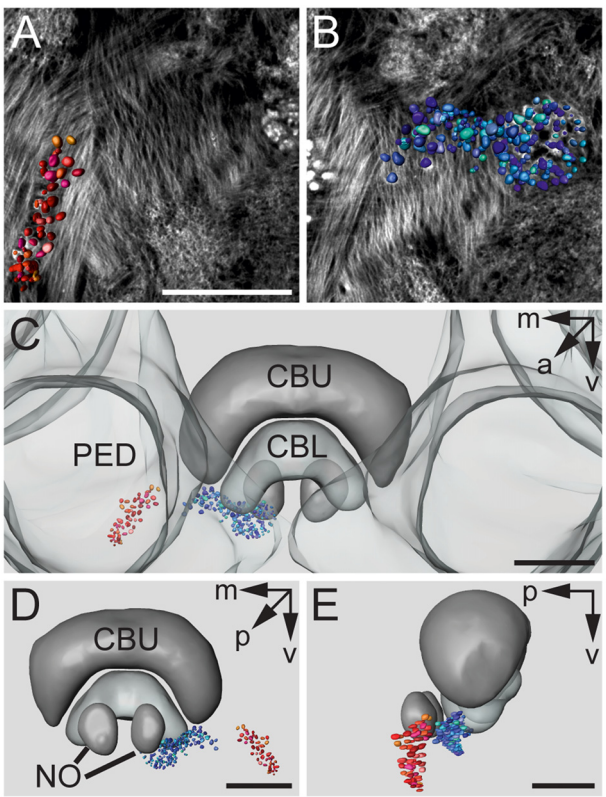

FIGURE 3 | 3D reconstructions of f-actin phalloidin labeled microglomerular synaptic complexes. (A) Reconstruction of the cluster (red) in the LBU. **(B)** Reconstruction of the synaptic complexes in the MBU (blue). **(C)** 3D reconstruction of the microglomerular synaptic complexes and their spatial distribution in relation to the PED and the CBU and CBL. **(D)** View from posterior reveals the distribution of the clusters in relation to the CB and the noduli (NO). **(E)** Sagittal view shows the location of the clusters in anterior-posterior axis extending to the NO. Scale bars: **A,B** = 50 μm, **C–E** = 70 μm.

level. Transmission electron micrographs showed that the synaptic complexes have a diameter of up to 8 μm and are partly enwrapped by layers of glia (**Figures 6A,B**). Therefore, individual synaptic complexes were clearly distinguishable from one another. Each microglomerular complex consisted of a single large cup-shaped profile, apparently from a TuLAL1 neuron, enclosing numerous small profiles (SPs), apparently originating from TL neurons. The large profiles (LPs) of TuLAL1 neurons were less electron dense than the small central profiles. They contained many mitochondria and two types of vesicle, numerous clear vesicles (cVs) with a diameter of 20–60 nm and a small number of dense core vesicles (dcVs) with a diameter of 50–80 nm (**Figure 6**). The bulk of vesicles was concentrated close to the internal membrane of the cup-shaped LP. The synaptic endings of the TL neurons formed many SP surrounded by the single LP. Apparently, one or a few processes from TL neurons enter the microglomerulus and give rise to a dense bush of ramifications in the center (**Figure 6**). These profiles also contained some mitochondria but additional organelles were difficult to distinguish. All synaptic connections were made at the inside of the complexes; we never found active zones at the exterior membrane of the LP.

Synaptic release sites were identified based on their electron dense ultrastructural specializations as described previously in other studies (Gray, 1959; Uchizono, 1965; Aghajanian and Bloom, 1967; Colonnier, 1968; Mayhew, 1996; Watson and Schürmann, 2002). The synapses we found were only formed between LPs and SPs, no synaptic connections were found between SPs. The electron dense synaptic release sites enabled us to identify the LPs of TuLAL1 neurons as presynaptic terminals. They included transmitter-containing vesicles and a number of mitochondria as described above. Additionally, an electron-dense membrane structure was present as transmitter release site. The associated membranes of the small postsynaptic profiles of TL neurons showed an electron-dense thickening, implying postsynaptic densities. Another feature of synaptic sites was a cleft of diverse thickness between the pre- and postsynaptic membranes. We were able to distinguish two types of synapses. The more frequent type was a divergent dyad where one presynaptic profile (**Figure 7A**, LP) was connected to two postsynaptic partners (**Figure 7A**, arrowheads). Due to the triangular arrangement and the preserved membranes the synaptic cleft was well defined. The presynaptic membranes showed aggregations of cVs in the vicinity of the electron-dense region. All involved postsynaptic profiles showed characteristic electron-dense membrane regions. The inside of the postsynaptic profiles was devoid of synaptic vesicles but contained mitochondria. The second type of synapse was a divergent tetrad, where the presynaptic profile (**Figure 7B**, LP) formed one synapse with four postsynaptic profiles (**Figure 7B**, arrowheads). The structure was nearly the same as in dyads: the presynaptic membrane showed an electron-dense fusion region with adjacent cVs, and a visible thickening of the postsynaptic membranes.

DISCUSSION

We characterized the anatomy and ultrastructure of microglomerular synaptic complexes in the bulbs of the honeybee brain. These complexes have been investigated previously in the sky-compass pathway of the locust *Schistocerca gregaria* (Träger et al., 2008) and in the brain of the desert ant *Cataglyphis fortis* (Schmitt et al., 2016), and therefore, seem to be a highly conserved feature of the insect brain. The sky-compass pathway in locusts originates in specialized photoreceptors of the DRA of the compound eye and runs through the ME toward the LUC of the AOTU and from there to the LX and into the CB (reviewed by Pfeiffer and Homberg, 2014). This pathway has been characterized anatomically in the honeybee from the DRA to the LX, and the involved neurons strongly resemble those described in the locust (Zeller et al., 2015). In this study, we focused on the synaptic contacts in the bulbs of the LX, connecting the LUC of the AOTU to the CBL. In the locust (Träger et al., 2008) and desert ant (Schmitt et al., 2016) these microglomeruli have a remarkable size and structure. Therefore,

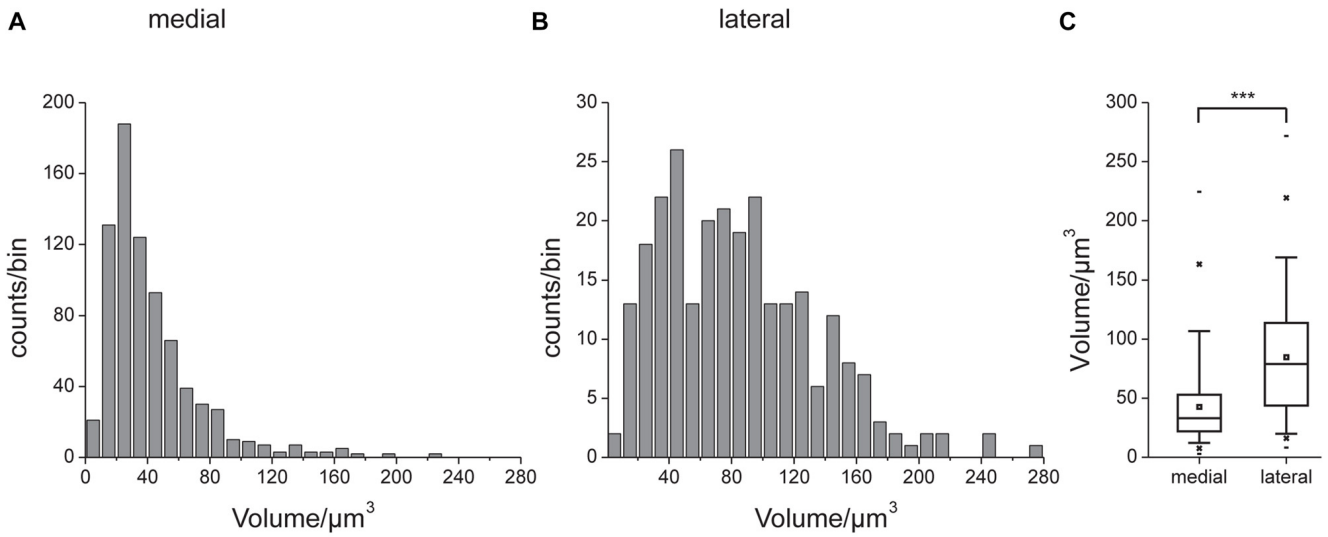

FIGURE 4 | Volumes of the reconstructed f-actin positive postsynaptic portion of the microglomeruli. Unilateral data from four brains. Histograms of data from the medial **(A)** and lateral **(B)** cluster. Note different scaling in **(A,B)**. **(C)** Comparison of volume data. Box: 25th, 50th and 75th percentile, small square: average, whiskers: 5th and 95th percentile, cross: 1st and 99th percentile, dash: minimum and maximum value. The median microglomerulus volume in the medial cluster was 33 μm^3, whereas it was 79 μm^3 in the lateral cluster. This difference was statistically significant (indicated by ***, Mann-Whitney test, $P < 0.0001$, $U = 157060.5$, $z = -13.39$, $n = 4$, $N_{medial} = 772$, $N_{lateral} = 262$).

they are likely to play an important role in the processing of visual information, like sky-compass cues or visual detection, by providing proper visual input into the CX.

Structure of the Microglomeruli of the LX Compared to Other Species

The large microglomerular synaptic complexes in *Apis mellifera* are located in the MBU and LBU of the LX. Each synaptic complex consists of one large presynaptic terminal formed by a TuLAL1a or TuLAL1b projection neuron from the LUC of the AOTU (Zeller et al., 2015). These terminals have been mentioned in a previous study (Mota et al., 2011) but have not been investigated in bees any further. The TuLAL1 neurons are connected to GABA-immunoreactive TL2 and TL3 tangential neurons of the CBL. Those TL neurons have conspicuous dendritic endings with single bushy structures at the tip of a stalk. At the ultrastructural level these endings appear as SP that are enclosed by a single LP of a TuLAL1 neuron. The large presynaptic terminals contain two types of vesicles: cVs and dcVs, but no information exists on their transmitter content. Single complexes are enclosed by glia cells. This glia can be referred to as astrocyte-like, as described in the fruit fly (Awasaki et al., 2008). It is the only known type of glia located within neuropils and associated with synaptic connections. Its function is likely the support of neurons, which in our case is very crucial considering the size and the amount of mitochondria in pre- and postsynaptic profiles. Additionally, this type of glia probably takes part in the modulation of neural connections (Awasaki et al., 2008; Edwards and Meinertzhagen, 2010).

Homologs of the involved neuron types were characterized anatomically and physiologically in many other insect species and, therefore, seem to be highly conserved. In the fruit fly *Drosophila melanogaster* GABAergic ring neurons of the ellipsoid body are homologous to TL neurons in honeybees. They form microglomeruli in the bulbs and connect them to the ellipsoid body, the equivalent of the CBL in the honeybee (Hanesch et al., 1989). Calcium-imaging experiments in tethered fruit flies showed that these microglomeruli are sensitive to visual features with an orientation tuning to vertical stripes (Seelig and Jayaraman, 2013; Weir and Dickinson, 2015). In the cricket *Gryllus bimaculatus* compass-neuron like cells (homologs of TL2 neurons in other species) that connect the LX with the CBL are sensitive to polarized light (Sakura et al., 2008). In the monarch butterfly (*Danaus plexippus*) there is only one cluster, the LBU, but different subtypes of TuLAL1 neuron ramify in spatially segregated areas. That is suggestive for a similar connectivity specificity as in honeybees. Colabeling of TL3- and TuLAL1 neurons revealed spatial proximity of large terminals of TuLAL1 neurons and profiles of TL3 neurons (Heinze and Reppert, 2011, 2012; Heinze et al., 2013). In the bumblebee *Bombus ignitus* TuLAL1a/b neurons share a very similar anatomy to the two cell types shown here (Pfeiffer and Kinoshita, 2012).

Although in all of these species one or both types of TuLAL1- and TL neuron have been described morphologically and partly investigated physiologically, the synaptic complexes they form have been explored only in desert ants and desert locusts. In the desert ant *Cataglyphis fortis* the microglomerular synaptic complexes are clustered in a single bulb (LBU; Schmitt et al., 2016) whereas in honeybees we found two clusters, one in the

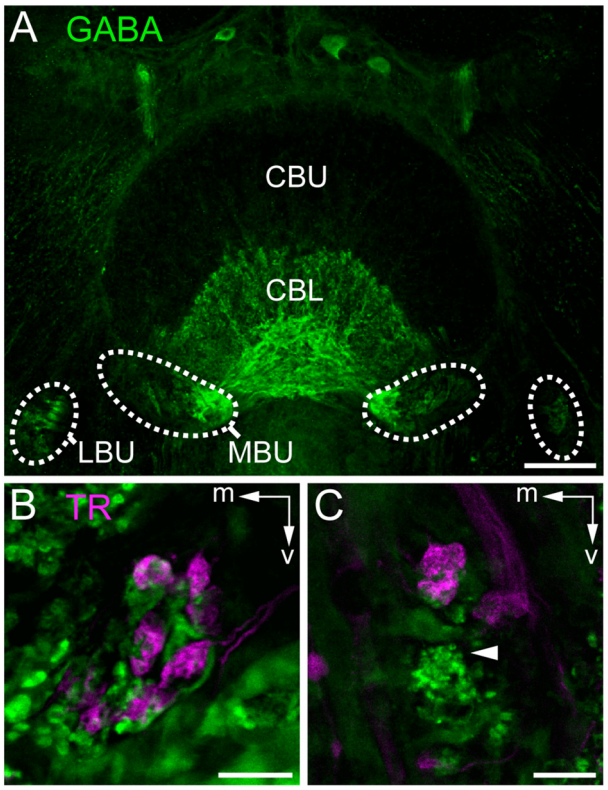

FIGURE 5 | Staining of neurons contributing to terminals in the bulbs. **(A)** Immunostaining for γ-aminobutyric acid (GABA; green) using the antibody from Abcam. GABA-immunoreactive TL neurons branch in the LBUs and the larger MBUs. The neurons have dense ramifications in the CBL whereas the upper division (CBU) is barely stained. **(B,C)** Double labeling by injection of dextran Texas Red into the AOTU, labeling TuLAL1 neurons (magenta) and immunostaining for GABA (green) with the antibody of Kingan, labeling TL neurons, reveals the structure of microglomerular synaptic complexes. **(B)** In the MBU TL3 neurons form complexes with large terminals of TuLAL1b neurons. The TuLAL1b neuron terminals are located on top of the TL neuron branches. **(C)** In the LBU the complexes have a similar structure. Here, GABA immunostaining exposes a bushy structure at the tip of the extension of a TL neuron (arrowhead). Scale bars: **A** = 50 μm, **B,C** = 10 μm.

LBU and the other one in the MBU. Although the general anatomy appears very similar in honeybees and ants, a closer look reveals some distinct differences. In honeybees the complexes have a diameter of up to 8 μm compared to only 5 μm in ants (Schmitt et al., 2016). Likewise, the presynaptic terminals appear larger and swollen whereas in ants they have the shape of a thin cup. Another difference between the two species lies in the vesicle pool within the presynaptic terminals. In ants the LP is densely packed with cVs and only a few dcVs and mitochondria are visible (Schmitt et al., 2016). In the honeybee a higher number of mitochondria and dcVs, but fewer cVs were found. The reason for the differences in the vesicle stock is currently unknown, fixation artifacts seem unlikely due to the high-quality conservation of the tissue.

Microglomerular synaptic complexes of the bulbs in the desert locust *Schistocerca gregaria* share a similar distribution, anatomy and ultrastructure to those in honeybees (Träger et al., 2008). However, one difference arises again in the vesicle stock. In locusts the presynaptic terminal is filled with cVs throughout the profile like in ants, whereas in honeybees vesicles are concentrated near synaptic release sites. Electrophysiological and anatomical studies in locusts showed that these synaptic complexes are part of the sky-compass pathway (Vitzthum et al., 2002; Pfeiffer et al., 2005; Träger et al., 2008). Taken together, the pathway described by Zeller et al. (2015) and the anatomical similarity to locusts shown here strongly suggest that the complexes are part of the sky-compass pathway in honeybees as well.

Synaptic Complexes in Other Species

In insects, neuromuscular junctions are monads, and most chemical synaptic connections in the central nervous system (CNS) are dyads (Wernitznig et al., 2015). In the visual system, more complex multi-contact synapses have been described in the optic lobes, more precisely in the LA, of muscomorph flies (Shaw and Meinertzhagen, 1986; Meinertzhagen and O'Neil, 1991) and locusts (Wernitznig et al., 2015). In both taxa, photoreceptor neurons provide input to LA monopolar cells via triads and tetrads. At a later stage of visual processing, multi-contact synapses have been mentioned in the calyces of honeybees and in the microglomerular synaptic complexes in the bulbs of the desert locust *Schistocerca gregaria* and in the desert ant *Cataglyphis fortis*. In ants the synaptic connection is formed by triads, tetrads and only a few dyads (Schmitt et al., 2016). Our data revealed a slightly different synaptic formation in the honeybee, with connections being formed by dyads and tetrads. By contrast in locusts the synaptic connections within the microglomerular complexes consists solely of regular ribbons of dyads (Träger et al., 2008). Neither in ants nor in honeybees synapses in the microglomerular complexes are arranged in such a distinguishable and regular manner.

Microglomeruli containing multi-contact synapses also occur in the calyces of the mushroom bodies of insects that are regarded as high-order sensory integration centers. The organization of microglomerular complexes in the calyces is reversed compared to those in the bulbs. In the mushroom body, a microglomerulus consists of one central presynaptic bouton that is surrounded by many postsynaptic profiles belonging to several Kenyon cells (Trujillo-Cenóz and Melamed, 1962; Schürmann, 1974; Ganeshina and Menzel, 2001; Groh and Rössler, 2011). In the complexes in the bulbs of the honeybee it is so far not known if the postsynaptic profiles are related to one or various neurons in one microglomerulus. The calycal microglomerular complexes are smaller than those in the bulbs. In the bulbs of the bee, complexes have a diameter of approximately 8 μm, whereas the size of the microglomeruli in the calyx of honeybees reaches only 2–3 μm (Ganeshina and Menzel, 2001). The synaptic connections in the calyx of honeybees are formed by dyads, triads and tetrads (Groh et al., 2012). In the calycal microglomeruli of fruit flies the number of postsynaptic profiles within one synapse can differ between 1

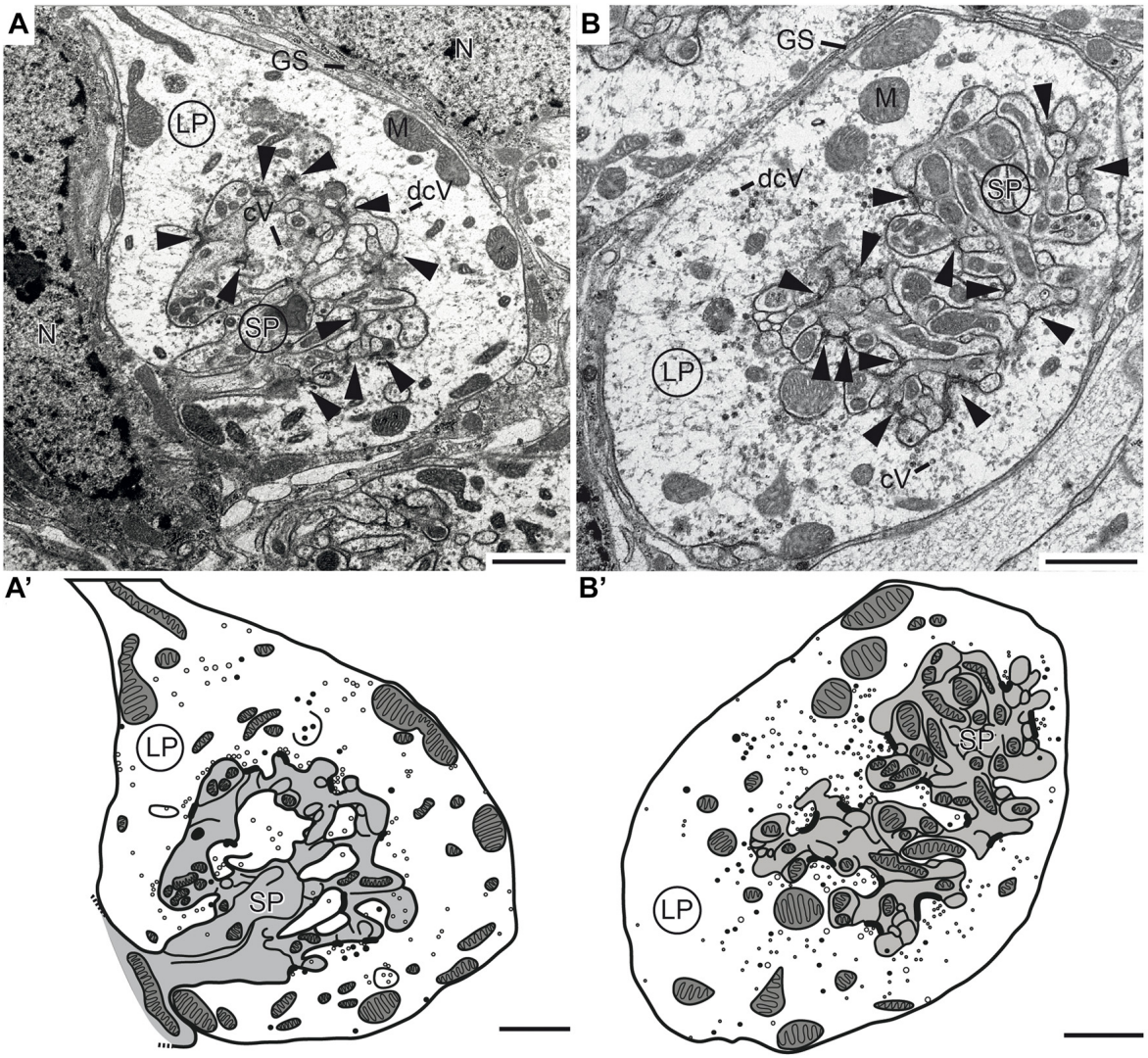

FIGURE 6 | Transmission electron micrographs showing the ultrastructure of microglomerular synaptic complexes in the LBU (A,A') and the MBU (B,B') of the lateral complex (LX). (A) The complex consists of one large profile (LP) enclosing many small profiles (SPs). The LP contains clear vesicles (cVs), some large dense core vesicles (dcVs) and many mitochondria (M) and forms numerous synaptic connections with the SP (arrowheads). A glial sheath (GS) is wrapped around the complex. It is located in proximity to two nuclei of other cells (N). **(A')** Drawing of the complex in **(A)** shows the borders of the profiles, organelles and synaptic connections. All parts of the LP are shown in white and the SP in gray. **(B,B')** The structure of the complex in the LBU is similar to the one in the MBU: one LP encloses many SP. Scale bars = 1 μm.

and 14 (Butcher et al., 2012). Similar to the synaptic complexes in the bulbs, the postsynaptic elements of mushroom body microglomeruli contain high concentrations of motile f-actin (Groh and Rössler, 2011).

Microglomerular synaptic complexes do not only occur in insects. Two well studied types of giant axosomatic synapses in the mammalian CNS, more precisely in the auditory pathway, are the endbulb and the calyx of Held. The presynaptic calyx of Held, probably the largest synaptic terminal in the mammalian CNS, envelopes the soma of a principal cell (Walmsley et al., 1998; review von Gersdorff and Borst, 2002; Schneggenburger and Forsythe, 2006; Rodríguez-Contreras et al., 2008). EM studies in rats showed that one calyx contains about 550 active zones (Sätzler et al., 2002). In comparison, a small glomerulus in the LX of locusts had around 150 active zones (Träger et al., 2008).

Functional Implications of Microglomerular Synaptic Complexes

Indications for the functional implication of these complexes exist so far only for ring neurons, the *Drosophila melanogaster* equivalent to honeybee TL neurons. There, activity patterns of the dendrites in the bulbs, triggered by a vertical stipe, suggest a retinotopic arrangement and therefore a representative map of the visual surrounding (Seelig and Jayaraman, 2013).

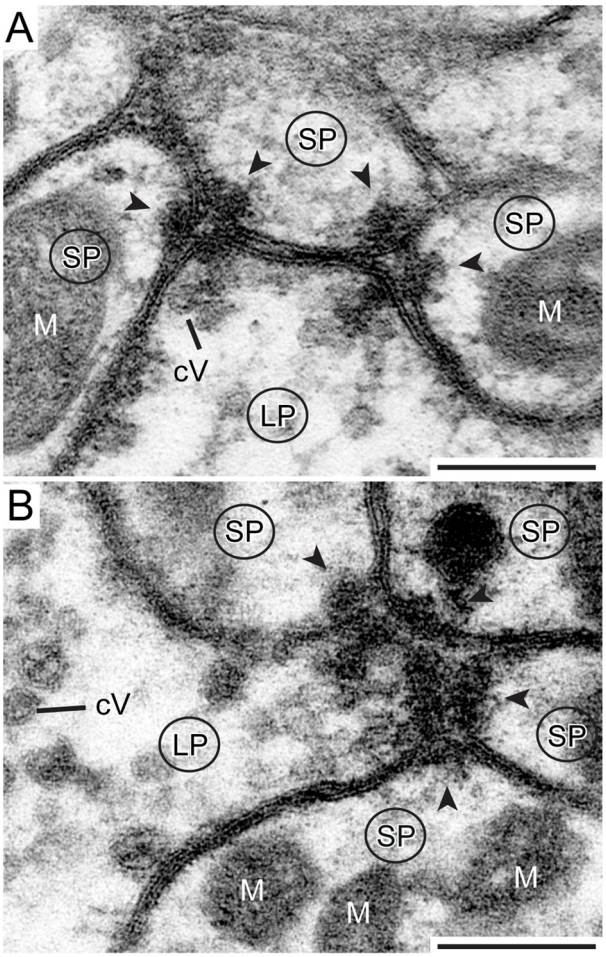

FIGURE 7 | Detailed view of two types of synapse. (A) One presynaptic LP of a TuLAL1 neuron (LP) gives input into three small postsynaptic profiles (SP) of a TL neuron via two divergent dyads. The structure of both dyads is similar: some small cVs are near an electron dense stalk-like structure at the presynaptic membrane. The synaptic cleft between the pre- and postsynaptic membranes has a triangular structure. In both postsynaptic profiles the membranes form electron dense foldings due to transmitter receptors (arrowheads) and contain mitochondria (M). **(B)** One presynaptic terminal (LP) and four postsynaptic profiles (SP) forming a divergent tetrad. Many small cVs are concentrated at the presynaptic membrane. Scale bars = 200 nm.

While the anatomical data presented in this study provide no direct insight into the physiology of the synaptic complexes of the LX, their structural characteristics allows for some speculations concerning functionality. First, their striking size is remarkable and to our knowledge unique within the insect brain. We assume that the organization and ultrastructure of the complexes leads to a fast and reliable signal transmission. The composition of one large presynaptic terminal enclosing the postsynaptic profiles with all active zones in the center might indicate a low-noise signal transmission. Additionally, the astrocyte-like glial layers around the synaptic complexes likely support reliable transmission. In *Drosophila* astrocyte-like glia is important to clear the synaptic cleft from neurotransmitters and their enzymatic breakdown products (reviewed in Freeman, 2015). In honeybees acetylcholinesterase has been detected in the microglomerular synaptic complexes in the bulbs (Kreissl and Bicker, 1989), suggesting that acetylcholine is likely to act as a transmitter there. NADPH diaphorase labeling in locusts, suggesting nitric oxide synthase activity, revealed staining in TL2 neurons and the LBUs, suggesting the presence of nitric oxide (Kurylas et al., 2005). Nitric oxide is known to function as a retrograde messenger in sensory processing in the nervous system. Since it is gaseous it can pass membranes and diffuse into the surrounding tissue without synaptic release (Dawson and Synder, 1994; Müller, 1997; Bicker, 2001). Therefore, the glia sheaths (GS) around the single complexes might work as diffusion barrier for NO as well as transmitters between adjacent complexes like the ensheathing glia around individual neuropils.

Electrophysiological data of the calyx of Held showed that one single action potential in the presynaptic profile leads to rapid depolarization of the postsynaptic profiles. This on the other hand ensures not only a rapid transmission but also the retention of the timing of signals (Schneggenburger and Forsythe, 2006). Given that the organization of the calyces of Held is comparable to the synaptic complexes in the LX of honeybees, the same principle for fast transmission could be valid here as well. The divergent multi-contact synapses support this assumption, as the transmitter release from one presynaptic membrane simultaneously addresses two or four postsynaptic partners. This could lead to a depolarization of the postsynaptic neuron above threshold by only one presynaptic action potential. So far we could not determine the ratio between the involved pre- and postsynaptic neurons. Whether this ratio is 1:1 as in the calyx of Held, divergent as in locusts, or convergent might be addressed in further studies.

Why do honeybees need such large complexes promoting reliable signal transmission? A closer look at the localization might give some indications. These microglomerular complexes are part of the visual pathway. The preservation of timing is a crucial feature in most sensory pathways to maintain all information of a stimulus. The calyces of Held are part of a pathway for sound-source localization based on time delays, where signal timing is absolutely essential. Another example for the importance of timing for an efficient signal processing is the dual olfactory pathway of the honeybee, where the responses within and between the two tracts reveal an odor-dependent latency (Brill et al., 2013, 2015). Studies on experience-related plasticity of the synaptic complexes in the LX of the desert ant (Schmitt et al., 2016) revealed that the number of synaptic complexes increases upon first exposure to light. The relatively high variation in the total number of synaptic complexes we found in the honeybee may arise from different levels of visual experience in the samples of winter bees used for the present study.

Taken together, the anatomical formation, compared to well-known features of other synaptic complexes, strongly suggests that the microglomerular synaptic complexes in the LX of

honeybees and other insects are essential for reliable signal transmission in the sky-compass pathway. It seems plausible that transmission speed and input timing is crucial in a sophisticated visual task like navigation and orientation during flight. However, future neurophysiological experiments on the neurons described here and their synaptic complexes are needed to better understand the properties of signal transmission at this specific point of the visual neuronal system.

AUTHOR CONTRIBUTIONS

KP, UH and WR designed the study. MH, AB, CS and RH acquired the data. MH and TSM analyzed and interpreted the data and drafted the manuscript. All authors revised the manuscript critically for important intellectual content, approved the final version to be published and are accountable for all aspects of the work.

FUNDING

Funding was provided by the German Research Foundation (DFG) through grant number PF 714/4-1 to KP, and through the Collaborative Research Center SFB 1047 "Insect Timing" (Project B6, WR).

ACKNOWLEDGMENTS

We thank Drs. Andreas Klingl and Kathrin Bolte for their support concerning TEM, Dr. Uwe Maier for access to the microscope, and Drs. Timothy Kingan and Erich Buchner for gifts of antibodies. We greatly appreciate Dr. Ian Meinertzhagen's helpful comments on the TEM data. We are grateful to Eric Auffenberg for his contribution to Figure 2C, Joss von Hadeln for help with Amira, Jutta Seyfarth for expert bee keeping and to Martina Kern for technical assistance.

REFERENCES

Aghajanian, G. K., and Bloom, F. E. (1967). The formation of synaptic junctions in developing rat brain: a quantitative electron microscopic study. *Brain Res.* 6, 716–727. doi: 10.1016/0006-8993(67)90128-x

Awasaki, T., Lai, S. L., Ito, K., and Lee, T. (2008). Organization and postembryonic development of glia cells in the adult central brain of *Drosophila*. *J. Neurosci.* 28, 13742–13753. doi: 10.1523/jneurosci.4844-08.2008

Baschong, W., Duerrenberger, M., Mandinova, A., and Suetterlin, R. (1999). Three dimensional visualization of the cytoskeleton by confocal laser scanning microscopy. *Methods Enzymol.* 307, 173–189. doi: 10.1016/S0076-6879(99)07013-5

Bicker, G. (2001). Sources and targets of nitric oxide signaling in insect nervous systems. *Cell Tissue Res.* 303, 137–146. doi: 10.1007/s004410000321

Brill, M. F., Meyer, A., and Rössler, W. (2015). It takes two—coincidence coding within the dual olfactory pathway of the honeybee. *Front. Physiol.* 6:208. doi: 10.3389/fphys.2015.00208

Brill, M. F., Rosenbaum, T., Reus, I., Kleineidam, C. J., Nawrot, M. P., and Rössler, W. (2013). Parallel processing via a dual olfactory pathway in the honeybee. *J. Neurosci.* 33, 2443–2456. doi: 10.1523/jneurosci.4268-12.2013

Butcher, N. J., Friedrich, A. B., Lu, Z., Tanimoto, H., and Meinertzhagen, I. A. (2012). Different classes of input and output neurons reveal new features in microglomeruli of the adult *Drosophila* mushroom body calyx. *J. Comp. Neurol.* 520, 2185–2201. doi: 10.1002/cne.23037

Collett, M., Chittka, L., and Collett, T. S. (2013). Spatial memory in insect navigation. *Curr. Biol.* 23, R789–R800. doi: 10.1016/j.cub.2013.07.020

Colonnier, M. (1968). Synaptic patterns on different cell types in the different laminae of the cat visual cortex. An electron microscope study. *Brain Res.* 9, 268–287. doi: 10.1016/0006-8993(68)90234-5

Dawson, T. M., and Synder, S. H. (1994). Gases as biological messengers: nitric oxide and carbon monoxide in the brain. *J. Neurosci.* 14, 5147–5159.

Edwards, T., and Meinertzhagen, I. A. (2010). The functional organization of glia in the adult brain of *Drosophila* and other insects. *Prog. Neurobiol.* 90, 471–497. doi: 10.1016/j.pneurobio.2010.01.001

el Jundi, B., Pfeiffer, K., Heinze, S., and Homberg, U. (2014). Integration of polarization and chromatic cues in the insect sky compass. *J. Comp. Physiol. A Neuroethol. Sens. Neural Behav. Physiol.* 200, 575–589. doi: 10.1007/s00359-014-0890-6

Freeman, M. R. (2015). *Drosophila* central nervous system glia. *Cold Spring Harb. Perspect. Biol.* 7:a020552. doi: 10.1101/cshperspect.a020552

Ganeshina, O., and Menzel, R. (2001). GABA-immunoreactive neurons in the mushroom bodies of the honeybee: an electron microscopic study. *J. Comp. Neurol.* 437, 335–349. doi: 10.1002/cne.1287

Gray, E. G. (1959). Axosomatic and axodendritic synapses in the cerebral cortex: an electron microscopy study. *J. Anat.* 93, 420–433.

Groh, C., Lu, Z., Meinertzhagen, I. A., and Rössler, W. (2012). Age-related plasticity in the synaptic ultrastructure of neurons in the mushroom body calyx of the honeybee *Apis mellifera*. *J. Comp. Neurol.* 520, 3509–3527. doi: 10.1002/cne.23102

Groh, C., and Rössler, W. (2011). Comparison of microglomerular structures in the mushroom body calyx of neopteran insects. *Arthropod Struct. Dev.* 40, 358–367. doi: 10.1016/j.asd.2010.12.002

Groh, C., Tautz, J., and Rössler, W. (2004). Synaptic organization in the adult honey bee brain is influenced by brood-temperature control during pupal development. *Proc. Natl. Acad. Sci. U S A* 101, 4268–4273. doi: 10.1073/pnas.0400773101

Hanesch, U., Fischbach, K.-F., and Heisenberg, M. (1989). Neuronal architecture of the central complex in *Drosophila melanogaster*. *Cell Tissue Res.* 257, 343–366. doi: 10.1007/bf00261838

Heinze, S., and Reppert, S. M. (2011). Sun compass integration of skylight cues in migratory monarch butterflies. *Neuron* 69, 345–358. doi: 10.1016/j.neuron.2010.12.025

Heinze, S., and Reppert, S. M. (2012). Anatomical basis of sun compass navigation I: the general layout of the monarch butterfly brain. *J. Comp. Neurol.* 520, 1599–1628. doi: 10.1002/cne.23054

Heinze, S., Florman, J., Asokaraj, S., el Jundi, B., and Reppert, S. M. (2013). Anatomical basis of sun compass navigation II: the neuronal composition of the central complex of the monarch butterfly. *J. Comp. Neurol.* 521, 267–298. doi: 10.1002/cne.23259

Homberg, U., Heinze, S., Pfeiffer, K., Kinoshita, M., and el Jundi, B. (2011). Central neural coding of sky polarization in insects. *Philos. Trans. R. Soc. Lond. B Biol. Sci.* 366, 680–687. doi: 10.1098/rstb.2010.0199

Homberg, U., Hofer, S., Pfeiffer, K., and Gebhardt, S. (2003). Organization and neural connections of the anterior optic tubercle in the brain of the locust, *Schistocerca gregaria*. *J. Comp. Neurol.* 462, 415–430. doi: 10.1002/cne.10771

Homberg, U., Kingan, T. G., and Hildebrand, J.G. (1990). Distribution of FMRFamide-like immunoreactivity in the brain and suboesophageal ganglion of the sphinx moth Manduca sexta and colocalization with SCP_B^-, BPP^- and GABA-like immunoreactivity. *Cell Tissue Res.* 259, 401–19. doi: 10.1007/bf01740767

Homberg, U., Vitzthum, H., Müller, M., and Binkle, U. (1999). Immunocytochemistry of GABA in the central complex of the locust *Schistocerca gregaria*: identification of immunoreactive neurons and colocalization with neuropeptides. *J. Comp. Neurol.* 409, 495–507. doi: 10.1002/(SICI)1096-9861(19990705)409:3<495::AID-CNE12>3.0.CO;2-F

Hoskins, S. G., Homberg, U., Kingan, T. G., Christensen, T. A., and Hildebrand, J. G. (1986). Immunocytochemistry of GABA in the antennal lobes of the sphinx moth *Manduca sexta*. *Cell Tissue Res.* 244, 243–252. doi: 10.1007/bf00219199

Ito, K., Shinomiya, K., Ito, M., Armstrong, J. D., Boyan, G., Hartenstein, V., et al. (2014). A systematic nomenclature for the insect brain. *Neuron* 81, 755–765. doi: 10.1016/j.neuron.2013.12.017

Junglas, B., Briegel, A., Burghardt, T., Walther, P., Wirth, R., Huber, H., et al. (2008). *Ignicoccus hospitalis* and *Nanoarchaeum equitas*: ultrastructure, cell-cell interaction and 3D reconstruction from serial sections of freeze-substituted cells and by electron cryotomography. *Arch. Microbiol.* 190, 395–408. doi: 10.1007/s00203-008-0402-6

Kreissl, S., and Bicker, G. (1989). Histochemistry of acetylcholinesterase and immunocytochemistry of an acetylcholine receptor-like antigen in the brain of the honeybee. *J. Comp. Neurol.* 286, 71–84. doi: 10.1002/cne.902860105

Kuebler, L. S., Kelber, C., and Kleineidam, C. J. (2010). Distinct antennal lobe phenotypes in the leaf-cutting ant (*Atta vollenweideri*). *J. Comp. Neurol.* 518, 352–365. doi: 10.1002/cne.22217

Kurylas, A. E., Ott, S. R., Schachtner, J., Elphick, M. R., Williams, L., and Homberg, U. (2005). Localization of nitric oxide synthase in the central complex and surrounding midbrain neuropils of the locust *Schistocerca gregaria*. *J. Comp. Neurol.* 484, 206–223. doi: 10.1002/cne.20467

Mayhew, T. M. (1996). How to count synapses unbiasedly and efficiently at the ultrastructural level: proposal for a standard sampling and counting protocol. *J. Neurocytol.* 25, 793–804. doi: 10.1007/bf02284842

McDonald, K. (2007). Cryopreparation methods for electron microscopy of selected systems. *Methods Cell Biol.* 79, 23–56. doi: 10.1016/s0091-679x(06)79002-1

Meinertzhagen, I. A., and O'Neil, S. D. (1991). Synaptic organization of columnar elements in the lamina of the wild type in *Drosophila melanogaster*. *J. Comp. Neurol.* 305, 232–263. doi: 10.1002/cne.903050206

Menzel, R., De Marco, R. J., and Greggers, U. (2006). Spatial memory, navigation and dance behavior in *Apis mellifera*. *J. Comp. Physiol. A Neuroethol. Sens. Neural Behav. Physiol.* 192, 889–903. doi: 10.1007/s00359-006-0136-3

Mota, T., Yamagata, N., Giurfa, M., Gronenberg, W., and Sandoz, J. C. (2011). Neural organization and visual processing in the anterior optic tubercle of the honeybee brain. *J. Neurosci.* 31, 11443–11456. doi: 10.1523/jneurosci.0995-11.2011

Müller, U. (1997). The nitric oxide system in insects. *Prog. Neurobiol.* 51, 363–381. doi: 10.1016/s0301-0082(96)00067-6

Müller, M., Homberg, U., and Kühn, A. (1997). Neuroarchitecture of the lower division of the central body in the brain of the locust (*Schistocerca gregaria*). *Cell Tissue Res.* 288, 159–176. doi: 10.1007/s004410050803

Müller-Reichert, T., Srayko, M., Hyman, A., O'Toole, E. T., and McDonald, K. (2007). Correlative light and electron microscopy of early *Caenorhabditis elegans* embryos in mitosis. *Methods Cell Biol.* 79, 101–119. doi: 10.1016/s0091-679x(06)79004-5

Pasch, E., Muenz, T. S., and Rössler, W. (2011). CaMKII is differentially localized in synaptic regions of Kenyon cells within the mushroom bodies of the honeybee brain. *J. Comp. Neurol.* 519, 3700–3712. doi: 10.1002/cne.22683

Peschke, M., Moog, D., Klingl, A., Maier, U. G., and Hempel, F. (2013). Evidence for glycoprotein transport into complex plastids. *Proc. Natl. Acad. Sci. U S A* 110, 10860–10865. doi: 10.1073/pnas.1301945110

Pfeiffer, K., and Homberg, U. (2014). Organization and functional roles of the central complex in the insect brain. *Annu. Rev. Entomol.* 59, 165–184. doi: 10.1146/annurev-ento-011613-162031

Pfeiffer, K., and Kinoshita, M. (2012). Segregation of visual inputs from different regions of the compound eye in two parallel pathways through the anterior optic tubercle of the bumblebee (*Bombus ignitus*). *J. Comp. Neurol.* 520, 212–229. doi: 10.1002/cne.23016

Pfeiffer, K., Kinoshita, M., and Homberg, U. (2005). Polarization-sensitive and light-sensitive neurons in two parallel pathways passing through the anterior optic tubercle in the locust brain. *J. Neurophysiol.* 94, 3903–3915. doi: 10.1152/jn.00276.2005

Rachel, R., Meyer, C., Klingl, A., Gürster, S., Heimerl, T., Wasserburger, N., et al. (2010). Analysis of the ultrastructure of archaea by electron microscopy. *Methods Cell Biol.* 96, 47–69. doi: 10.1016/s0091-679x(10)96003-2

Reynolds, E. S. (1963). The use of lead citrate at high pH as an electron-opaque stain in electron microscopy. *J. Cell Biol.* 17, 208–213. doi: 10.1083/jcb.17.1.208

Rodríguez-Contreras, A., van Hoeven, J. S. S., Habets, R. L. P., Locher, H., and Borst, J. G. G. (2008). Dynamic development of the calyx of Held synapse. *Proc. Natl. Acad. Sci. U S A* 105, 5603–5608. doi: 10.1073/pnas.0801395105

Sakura, M., Lambrinos, D., and Labhart, T. (2008). Polarized skylight navigation in insects: model and electrophysiology of e-vector coding by neurons in the central complex. *J. Neurophysiol.* 99, 667–682. doi: 10.1152/jn.00784.2007

Sätzler, K., Söhl, L. F., Bollmann, J. H., Borst, J. G. G., Frotscher, M., Sakmann, B., et al. (2002). Three-dimensional reconstruction of a calyx of Held and its postsynaptic principal neuron in the medial nucleus of the trapezoid body. *J. Neurosci.* 22, 10567–10579.

Schäfer, S., and Bicker, G. (1986). Distribution of GABA-like immunoreactivity in the brain of the honeybee. *J. Comp. Neurol.* 246, 287–300. doi: 10.1002/cne.902460302

Schmitt, F., Stieb, S. M., Wehner, R., and Rössler, W. (2016). Experience-related reorganization of giant synapses in the lateral complex: potential role in plasticity of the sky-compass pathway in the desert ant *Cataglyphis fortis* . *Dev. Neurobiol.* 76, 390–404. doi: 10.1002/dneu.22322

Schneggenburger, R., and Forsythe, I. D. (2006). The calyx of Held. *Cell Tissue Res.* 326, 311–337. doi: 10.1007/s00441-006-0272-7

Schürmann, F. W. (1974). Bemerkungen zur Funktion der Corpora Pedunculata im Gehirn der Insekten aus morphologischer Sicht. *Exp. Brain Res.* 19, 406–432. doi: 10.1007/bf00234464

Seelig, J. D., and Jayaraman, V. (2013). Feature detection and orientation tuning in the *Drosophila* central complex. *Nature* 503, 262–266. doi: 10.1038/nature12601

Shaw, S. R., and Meinertzhagen, I. A. (1986). Evolutionary progression at synaptic connections made by identified homologous neurons. *Proc. Natl. Acad. Sci. U S A* 83, 7961–7965. doi: 10.1073/pnas.83.20.7961

Srinivasan, M. V. (2015). Where paths meet and cross: navigation by path integration in the desert ant and the honeybee. *J. Comp. Physiol. A Neuroethol. Sens. Neural Behav. Physiol.* 201, 533–546. doi: 10.1007/s00359-015-1000-0

Träger, U., Wagner, R., Bausenwein, B., and Homberg, U. (2008). A novel type of microglomerular synaptic complex in the polarization vision pathway of the locust brain. *J. Comp. Neurol.* 506, 288–300. doi: 10.1002/cne.21512

Trujillo-Cenóz, O., and Melamed, J. (1962). Electron microscope observations on the calyces of the insect brain. *J. Ultrastruct. Res.* 7, 389–398. doi: 10.1016/s0022-5320(62)90035-7

Uchizono, K. (1965). Characteristics of excitatory and inhibitory synapses of the central nervous system. *Nature* 207, 642–643. doi: 10.1038/207642a0

Vitzthum, H., Müller, M., and Homberg, U. (2002). Neurons of the central complex of the locust *Schistocerca gregaria* are sensitive to polarized light. *J. Neurosci.* 22, 1114–1125.

von Frisch, K. (1949). Die Polarisation des Himmelslichtes als orientierender Faktor bei den Tänzen der Bienen. *Experientia* 5, 142–148. doi: 10.1007/bf02174424

von Gersdorff, H., and Borst, J. G. G. (2002). Short-term plasticity at the calyx of Held. *Nat. Rev. Neurosci.* 3, 53–64. doi: 10.1038/nrn705

Walmsley, B., Alvarez, F. J., and Fyffe, R. E. W. (1998). Diversity of structure and function at mammalian central synapses. *Trends Neurosci.* 21, 81–88. doi: 10.1016/s0166-2236(97)01170-3

Walther, P., and Ziegler, A. (2002). Freeze substitution of high-pressure frozen samples: the visibility of biological membranes is improved when the substitution medium contains water. *J. Microsc.* 208, 3–10. doi: 10.1046/j.1365-2818.2002.01064.x

Watson, A. H. D., and Schürmann, F. W. (2002). Synaptic structure, distribution and circuitry in the central nervous system of the locust

and related insects. *Microsc. Res. Tech.* 56, 210–226. doi: 10.1002/jemt.10031

Wehner, R. (2003). Desert ant navigation: how miniature brains solve complex tasks. *J. Comp. Physiol. A Neuroethol. Sens. Neural Behav. Physiol.* 189, 579–588. doi: 10.1007/s00359-003-0431-1

Weir, P. T., and Dickinson, M. H. (2015). Functional divisions for visual processing in the central brain of flying *Drosophila*. *Proc. Natl. Acad. Sci. U S A* 112, E5523–E5532. doi: 10.1073/pnas.1514415112

Wernitznig, S., Rind, F. C., Pölt, P., Zankel, A., Pritz, E., Kolb, D., et al. (2015). Synaptic connections of first-stage visual neurons in the locust *Schistocerca gregaria* extend evolution of tetrad synapses back 200 million years. *J. Comp. Neurol.* 523, 298–312. doi: 10.1002/cne.23682

Wolff, T., Iyer, N. A., and Rubin, G. M. (2015). Neuroarchitecture and neuroanatomy of the *Drosophila* central complex: a GAL4-based dissection of protocerebral bridge neurons and circuits. *J. Comp. Neurol.* 523, 997–1037. doi: 10.1002/cne.23705

Zeller, M., Held, M., Bender, J., Berz, A., Heinloth, T., Hellfritz, T., et al. (2015). Transmedulla neurons in the sky compass network of the honeybee (*Apis mellifera*) are a possible site of circadian input. *PLoS One* 10:e0143244. doi: 10.1371/journal.pone.0143244

Conflict of Interest Statement: The authors declare that the research was conducted in the absence of any commercial or financial relationships that could be construed as a potential conflict of interest.

frontiers in Behavioral Neuroscience

ORIGINAL RESEARCH
published: 06 December 2016
doi: 10.3389/fnbeh.2016.00230

Ultrastructure of GABA- and Tachykinin-Immunoreactive Neurons in the Lower Division of the Central Body of the Desert Locust

Uwe Homberg[1]* *and Monika Müller*[2]

[1] *Faculty of Biology, Animal Physiology, Philipps-Universität, Marburg, Germany,* [2] *Institute for Zoology, University of Regensburg, Regensburg, Germany*

The central complex, a group of neuropils spanning the midline of the insect brain, plays a key role in spatial orientation and navigation. In the desert locust and other species, many neurons of the central complex are sensitive to the oscillation plane of polarized light above the animal and are likely involved in the coding of compass directions derived from the polarization pattern of the sky. Polarized light signals enter the locust central complex primarily through two types of γ-aminobutyric acid (GABA)-immunoreactive tangential neurons, termed TL2 and TL3 that innervate specific layers of the lower division of the central body (CBL). Candidate postsynaptic partners are columnar neurons (CL1) connecting the CBL to the protocerebral bridge (PB). Subsets of CL1 neurons are immunoreactive to antisera against locustatachykinin (LomTK). To better understand the synaptic connectivities of tangential and columnar neurons in the CBL, we studied its ultrastructural organization in the desert locust, both with conventional electron microscopy and in preparations immunolabeled for GABA or LomTK. Neuronal profiles in the CBL were rich in mitochondria and vesicles. Three types of vesicles were distinguished: small clear vesicles with diameters of 20–40 nm, dark dense-core vesicles (diameter 70–120 nm), and granular dense-core vesicles (diameter 70–80 nm). Neurons were connected via divergent dyads and, less frequently, through convergent dyads. GABA-immunoreactive neurons contained small clear vesicles and small numbers of dark dense core vesicles. They had both pre- and postsynaptic contacts but output synapses were observed more frequently than input synapses. LomTK immunostaining was concentrated on large granular vesicles; neurons had pre- and postsynaptic connections often with neurons assumed to be GABAergic. The data suggest that GABA-immunoreactive tangential neurons provide signals to postsynaptic neurons in the CBL, including LomTK-immunolabeled CL1 neurons, but in addition also receive input from LomTK-labeled neurons. Both types of neuron are additionally involved in local circuits with other constituents of the CBL.

Keywords: insect brain, central complex, γ-aminobutyric acid, locustatachykinin, synaptic organization, desert locust

OPEN ACCESS

Edited by:
Stanley Heinze,
Lund University, Sweden

Reviewed by:
Etsuro Ito,
Waseda University, Japan
Ian A. Meinertzhagen,
Dalhousie University, Canada

***Correspondence:**
Uwe Homberg
homberg@biologie.uni-marburg.de

Received: *21 October 2016*
Accepted: *22 November 2016*
Published: *06 December 2016*

Citation:
Homberg U and Müller M (2016) Ultrastructure of GABA- and Tachykinin-Immunoreactive Neurons in the Lower Division of the Central Body of the Desert Locust. Front. Behav. Neurosci. 10:230. doi: 10.3389/fnbeh.2016.00230

INTRODUCTION

The central complex comprises a group of neuropils in the insect brain that extend across the brain midline. Prominent subdivisions are the protocerebral bridge (PB), the upper (CBU) and lower (CBL) divisions of the central body, also termed fan-shaped body and ellipsoid body, respectively, and a pair of globular noduli (**Figure 1A**; Ito et al., 2014; Pfeiffer and Homberg, 2014). The PB, the CBL and the CBU are subdivided into linear arrangements of 16 slices (in *Drosophila* 18), and numerous sets of columnar neurons provide intricate chiasmal connections between the slices of the different subcompartments (**Figure 1A**; Heinze and Homberg, 2008; Wolff et al., 2015). Convergent evidence from studies in flies, beetles, the monarch butterfly, the desert locust, the honeybee, and the field cricket point to a role for the central complex in spatial orientation. In fruit flies, the central complex is involved in spatial working memory and place learning (Neuser et al., 2008; Ofstad et al., 2011). Calcium imaging in tethered walking *Drosophila* revealed a 360° representation of headings in columnar neurons of the ellipsoid body (Seelig and Jayaraman, 2015). Likewise, extracellular recordings from central-complex neurons of the discoid cockroach demonstrated head-direction coding (Varga and Ritzmann, 2016). In dung beetles, the field cricket, the desert locust and the monarch butterfly, neurons of the central complex are sensitive to the plane of dorsally presented polarized light and likely signal compass directions provided by the polarization pattern of the blue sky (Homberg et al., 2011; Heinze, 2014; el Jundi et al., 2015). In the desert locust zenithal *E*-vectors are topographically represented in the slices of the PB, indicating a compass-like representation of celestial directions (Heinze and Homberg, 2007).

Photoreceptors in a specialized dorsal rim area of the compound eye are sensitive to the oscillation plane of celestial polarized light (Labhart and Meyer, 1999; Schmeling et al., 2014, 2015). Signals are transferred via a specific pathway to the CBL (Homberg et al., 2003; Pfeiffer and Kinoshita, 2012; Held et al., 2016; Schmitt et al., 2016). In the desert locust, three types of tangential neuron to the CBL, termed TL1, TL2, and TL3 neurons provide polarization signals to the central complex (Vitzthum et al., 2002; Heinze et al., 2009). Two of these cell types, TL2 and TL3, comprising as many as 100 bilateral pairs of neurons, are immunoreactive to antisera against γ-aminobutyric acid (GABA; **Figures 1B,E**; Homberg et al., 1999). The neurons receive massive dendritic input in microglomerular synaptic complexes from presynaptic projection neurons of the anterior optic tubercles (Träger et al., 2007). Heinze and Homberg (2009) suggested that TL neurons synapse upon certain types of columnar neurons (CL neurons, **Figure 1D**) in the CBL, which would carry the polarization signal to the PB, but synaptic connectivities in the CBL have so far only been inferred from the light microscopic appearances of terminal arborizations of neurons in the CBL. A subpopulation of CL neurons of the locust is immunoreactive to antisera against the neuropeptide locustatachykinin (LomTK; **Figure 1C**; Vitzthum and Homberg, 1998). To further elucidate the synaptic organization at the input stage to the polarization vision network in the central complex, we investigated the ultrastructural organization of the CBL in the desert locust and analyzed the connectivities of GABA- and LomTK-immunoreactive neurons.

MATERIALS AND METHODS

Animals

Experiments were performed on adult locusts, *Schistocerca gregaria*, obtained from crowded colonies at the University of Regensburg. Animals were reared under 12L:12D photoperiod, and a temperature of 34°C during the light phase and 27°C during the dark phase. Experiments were performed on sexually mature adult males and females. Prior to dissection animals were immobilized by cooling to 4°C.

Conventional Electron Microscopy

For routine electron microscopy, dissected brains were fixed for 4 h or overnight in freshly prepared fixative containing 2% paraformaldehyde/2.5% glutaraldehyde in sodium cacodylate buffer (0.1 M, pH 7.2), and 2% sucrose. After rinsing in sodium cacodylate buffer, brains were postfixed in osmium tetroxide (1% in sodium cacodylate buffer) for 1 h, dehydrated in an ethanol series and embedded in Epon 812 (Serva, Heidelberg, Germany) or Durcupan (Fluka, Buchs, Switzerland). Ultrathin sections (∼70 nm in thickness, gray to silver interference colors) were cut in a frontal plane on an ultramicrotome (Ultracut E, Reichert, Vienna, Austria) and collected on copper slot grids coated with pioloform (Plano, Marburg, Germany). Sections were contrasted with 2% uranyl acetate (15 min) followed by lead citrate (5 min; Venable and Coggeshall, 1965).

GABA Immunolabeling, Preembedding Technique

GABA immunolabeling on ultrathin sections was performed following the preembedding technique and the postembedding technique (immunogold technique). Two antisera against GABA were employed. Anti-GABA antiserum I was raised in rabbit against conjugates of GABA and keyhole limpet hemocyanin (#9/24, provided by Dr. T.G. Kingan). The antiserum has been widely used to study GABA immunostaining at the light microscopic level in insect nervous systems (Hoskins et al., 1986; Homberg et al., 1987, 1999). The anti-GABA antiserum II (#4 TB) was provided by Dr. H. Dircksen. The antiserum was raised in rabbits against GABA-glutaraldehyde conjugates as described by Seguela et al. (1984). In the locust brain and central complex both antisera revealed virtually identical immunolabeling patterns (Homberg et al., 1999). They provided dense immunostaining throughout the CBL (**Figure 1B**) resulting from immunolabeled TL2 and TL3 neurons, whereas TL1 neurons were immunonegative (Homberg et al., 1999). Preadsorption of the diluted antiserum I with 15 nM GABA-BSA (bovine serum albumin), and the diluted antiserum II with 20 μM GABA-glutaraldehyde conjugate abolished all immunolabeling on 30-μm microtome sections

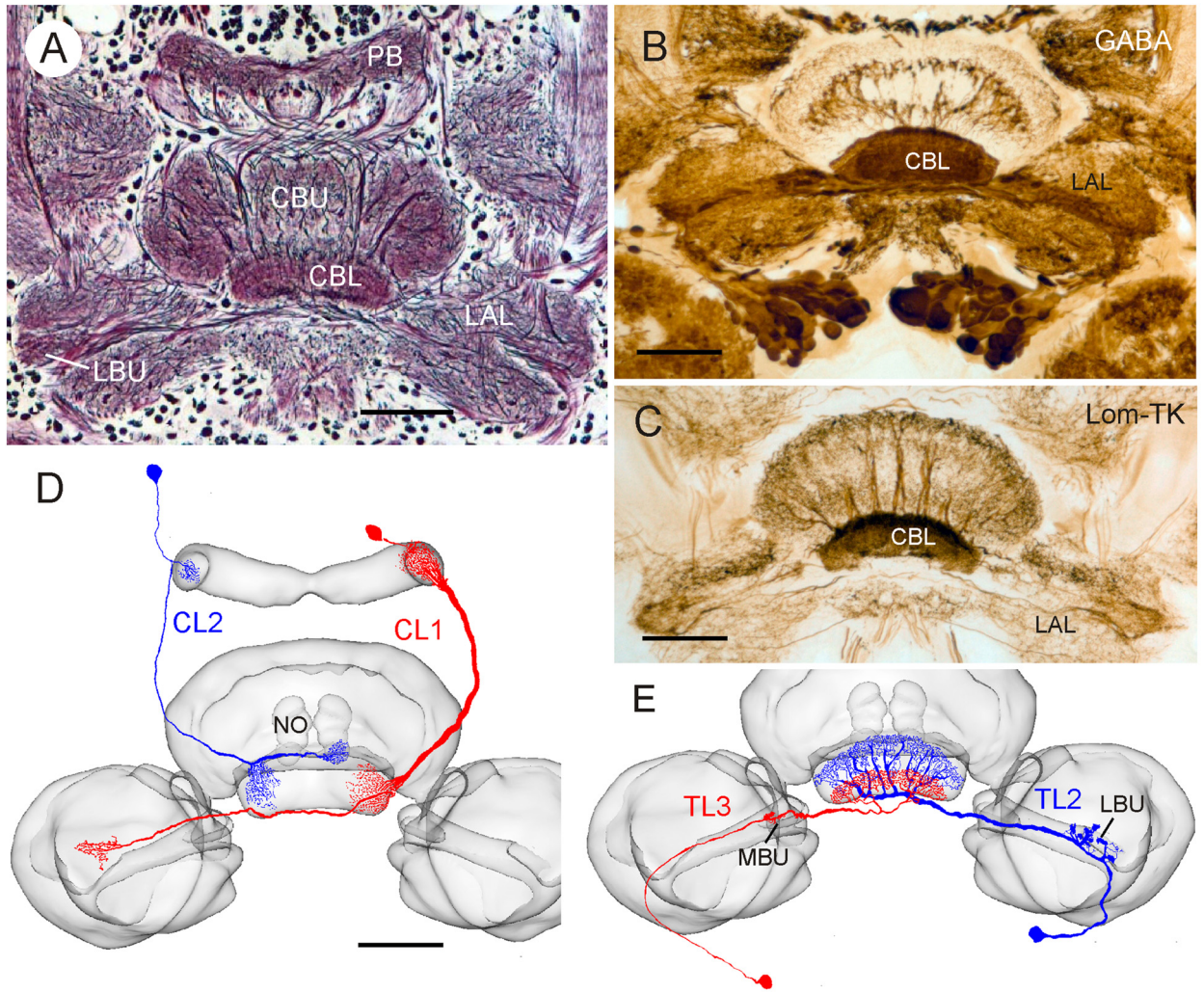

FIGURE 1 | Anatomical and neurochemical organization of the lower division of the locust central body (CBL). (A) Frontal Bodian-stained paraffin section through the central complex and lateral complexes. CBL, lower division of the central body; CBU, upper division of the central body; LAL, lateral accessory lobe, LBU, lateral bulb; PB, protocerebral bridge. **(B)** Frontal Vibratome section illustrating dense γ-aminobutyric acid (GABA) immunolabeling in the CBL, revealed by the peroxidase-antiperoxidase (PAP) technique as described by Homberg et al. (1999). **(C)** Immunostaining of the CBL on frontal Vibratome section using an antiserum against locustatachykinin II (LomTK II); PAP technique as described by Vitzthum and Homberg (1998). **(D,E)** Two types of columnar **(D)** and tangential **(E)** neuron innervating the CBL. Frontal camera lucida reconstructions of Neurobiotin- or Lucifer Yellow-labeled neurons were projected onto the standard locust central complex (el Jundi et al., 2010). **(D)** Columnar neuron 1 and 2 (CL1, CL2). NO, nodulus. **(E)** Tangential neuron 2 and 3 (TL2, TL3). MBU, medial bulb. Scale bars: 100 μm.

(Homberg et al., 1999). The GABA antiserum II has, in addition, been used in immunogold labeling of ultrathin sections of the locust brain (Träger et al., 2007). Here, omission of the primary antiserum abolished all staining, and preadsorption of the diluted antiserum with 20 μM GABA-glutaraldehyde conjugate again resulted in complete loss of immunostaining (Träger et al., 2007).

For preembedding immunolabeling, brains were dissected and immersed for 45 min in fixative containing 2.5% glutaraldehyde in 0.1 M sodium phosphate buffer (pH 7.4). Brains were then embedded in gelatin/albumin. Frontal sections at 20 μm were cut with a Vibratome (Technical Products, St. Louis, MO, USA) and collected in cell culture plates. GABA immunostaining was performed on the free floating sections following the peroxidase-antiperoxidase (PAP) technique of Sternberger (1979). To reduce background staining, the sections were preincubated for 1 h in 10 mM phosphate buffered saline (PBS) containing 0.01% Triton X-100 (TrX) and 10% normal goat serum (NGS). Incubation in anti-GABA antiserum I, diluted 1:4000 or antiserum II, diluted 1:20,000 in 10 mM PBS, 0.01% Triton X-100 and 1% NGS was performed overnight at 4°C. Following rinses in 10 mM PBS, 0.01% TrX and 1% NGS, the sections were incubated for 2 h in secondary antiserum, goat anti-rabbit (1:80 in 10 mM PBS, 0.01% TrX and 1% NGS; Sigma, Deisenhofen, Germany). Afterwards, the sections were rinsed again and incubated for 2 h in rabbit PAP complex

(1:100 in 10 mM PBS, 0.01% TrX and 1% NGS; Dakopatts, Hamburg, Germany). Subsequently the sections were rinsed 3 × 10 min in 0.05 M Tris/HCl (pH 7.4) and stained in 0.02% 3,3-diaminobenzidine tetrahydrochloride (Sigma) in 0.05 M Tris/HCl. The redox reaction was started by adding 10 µl H_2O_2 (30% solution) per 50 ml solution. The development of the brown reaction product was controlled visually and stopped by rinses in 0.05 M Tris/HCl.

For ultrastructural analysis, the sections were transferred to 10 mM phosphate buffer (pH 7.4) and postfixed for 20–30 min in 1% OsO_4 in phosphate buffer. Following rinses in phosphate buffer, the sections were dehydrated in an ascending ethanol series and embedded in Epon 812 as described above. The sections were attached to an Epon block, sectioned with an Ultracut microtome and contrasted as described above.

GABA Immunolabeling, Postembedding Technique

For immunogold labeling (postembedding staining), brains were dissected and fixed as described for conventional electron microscopy. Brains were embedded in Araldite epoxy resin (EMS, Washington, PA, USA). Ultrathin sections were collected on coated nickel slot grids. Prior to immunolabeling, ultrathin sections were incubated for 1 h on drops of a 25% aqueous solution of sodium metaperiodate. After thorough washing in distilled water and 0.5 M HCl, grids were incubated in PBS containing 0.01% TrX for 15 min and subsequently for 30 min in incubation buffer (0.01 M sodium phosphate buffer, pH 7.4, containing 0.5 M NaCl, 0.75% fish gelatin, 0.1% ovalbumin, and 0.01% Tween 20). The sections were exposed to the anti-GABA antiserum I (1:6000), or anti-GABA antiserum II (1:2000–1:6000) in incubation buffer for at least 15 h at 4°C and were afterwards washed thoroughly in PBS. Finally, the grids were transferred for 4 h at room temperature to a solution of 10-nm gold-labeled goat-anti-rabbit antibody (Auro Probe EM GAR G10, Amersham, Braunschweig, Germany) diluted 1:40 in incubation buffer. Preparations were then washed in PBS and distilled water and were contrasted with uranyl acetate (8 min) and lead citrate (2 min). In control experiments, substitution of the primary antibody solution with incubation buffer resulted in complete lack of gold labeling. Preadsorption of the GABA antiserum with 20 µM GABA-glutaraldehyde conjugate, prepared as described by Ottersen et al. (1986), abolished all immunostaining.

LomTK Immunolabeling, Postembedding Technique

Brains were dissected and fixed as described for conventional electron microscopy. After postfixation in OsO_4 and dehydration as described above they were embedded in Epon 812 or Durcupan. Immunolabeling was performed as described for GABA-immunogold staining. The anti-LomTK II antiserum (kindly provided by Dr. Hans Agricola, Jena) was used at a concentration of 1:1000. The antiserum has been used to analyze LomTK immunostaining on Vibratome sections of the locust central complex at the light microscopic level (Vitzthum and Homberg, 1998). In that study, preadsorption of the primary antiserum with 10 µM LomTK II abolished all staining.

Data Evaluation and Statistics

Ultrathin sections were examined and photographed with a transmission electron microscope (EM 109 and EM10C, Zeiss, Oberkochen, Germany). Photomicrographs (Agfa Scientia EM film) from selected sections were scanned at 2400 dpi (CanoScan 9000F MarkII, Canon, Tokyo, Japan) and processed further with Adobe Photoshop CS3 and CorelDRAW X3.

GABA-labeled immunogold sections were evaluated statistically. The mean labeling density of gold particles (GPs) over selected profiles was determined in 4–8 consecutive ultrathin sections and compared against GP levels in adjacent, presumably unlabeled profiles of similar size and organelle composition (Watson, 1988; Watson et al., 2000; Träger et al., 2007). Profiles were accepted as GABA-immunoreactive, if they had a significantly higher GP concentration than an adjacent reference profile (t-test, $p < 0.05$); when tested against two adjacent profiles, one-way ANOVA with Tukey-HSD multiple range test was performed ($p < 0.05$).

RESULTS

The anatomical organization and patterns of GABA- and LomTK immunostaining in the lower division of the locust central body (CBL) are shown in **Figure 1**. All layers of the CBL exhibit dense GABA immunolabeling (**Figure 1B**). Homberg et al. (1999) showed that two types of tangential neuron, termed TL2 and TL3 (**Figure 1E**) are GABA-immunoreactive. TL2 and TL3 neurons have ramifications in microglomeruli of the lateral (TL2), resp. medial bulb (MBU; TL3). They connect the bulbs to all layers of the CBL, but individual neurons of both types only invade specific layers of the CBL. In addition, two major types of columnar neuron with ramifications in the CBL, termed CL1 and CL2 have been identified (**Figure 1D**; Müller et al., 1997). Both types of CL neuron provide connections between slices of the CBL and the PB (**Figure 1D**). Whereas most types of CL1 neurons have additional ramifications in small areas of the lateral accessory lobe (LAL), likely homologous to the gall in *Drosophila*, TL2 neurons have fine projections in the lower unit of a nodulus (**Figure 1D**). Vitzthum and Homberg (1998) showed that two subtypes of CL1 neurons exhibit immunostaining with antisera against LomTK resulting in dense immunolabeling of the CBL (**Figure 1C**).

Ultrastructural Organization of the CBL

At the ultrastructural level, neuronal profiles of different size, shape and organelle composition could be distinguished in the CBL. Glial processes were interspersed between neuronal profiles, and especially large neuronal fibers were surrounded by glia (**Figure 2**). Although no precise measurements were done, in all sections studied the proportion of glia in the neuropil was considerably lower than that of neuronal profiles. The CBL as a whole was largely surrounded by a glial sheath

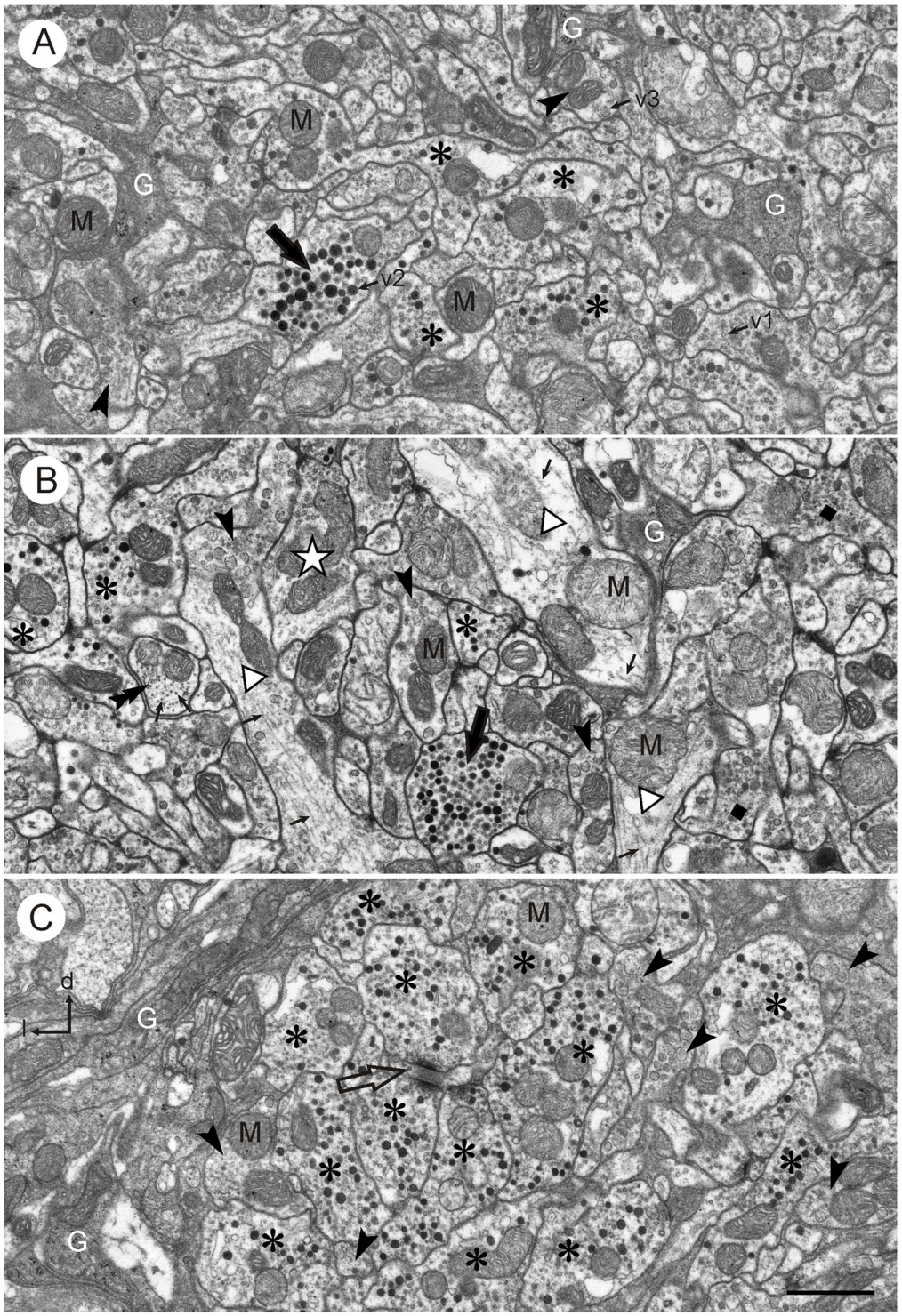

FIGURE 2 | Ultrastructure of the CBL. (A,B) Central neuropil area from two different brains. The CBL consists of densely packed neuronal processes containing mitochondria (M) and numerous vesicles (small arrows; v1: small clear vesicles; v2: large dense core vesicles, v3: large granular vesicles). Glial processes (G) extend between the neuronal profiles. Neuronal profiles differ with respect to vesicle composition. Profiles with small clear vesicles and dark dense core vesicles (asterisks) and profiles with large granular vesicles (arrowheads) occur frequently. Profiles with numerous dense core vesicles (large black arrows) and profiles with small clear and granular vesicles (dark squares in **B**) occur more rarely. The white star in **(B)** marks a profile which contains only clear vesicles. Three large neuronal

(*Continued*)

FIGURE 2 | Continued
processes in (**B**; open triangles) contain only few vesicles but numerous microtubules (small arrows). The double arrow in **(B)** points to a cross-sectioned fiber which contains no vesicles but numerous cross-sectioned microtubules. **(C)** Section from the left dorsal margin of the CBL, same brain as **(B)**. It shows an accumulation of profiles with small clear and large dense core vesicles (asterisks). Two of these profiles make output synapses onto a smaller third profile (open arrow). Near this cluster of profiles are some processes with large granular vesicles (arrowheads). The dorso-lateral margin of the CBL is covered with layers of glial processes (G). l, left; d, dorsal. Scale bar in **(C)**: 1 μm (applies to **A–C**).

against adjacent neuropils (**Figure 2C**) but along its dorsal face, a glial boundary against the adjacent CBU was only partially present.

Neuronal profiles in the CBL were rich in mitochondria and contained numerous vesicles. Three main types of vesicles could be distinguished: (1) small, clear vesicles (**Figures 2A–C**, **3**); they had a circular or ovoid form and a size of 20–40 nm; (2) dense-core vesicles filled with homogeneous electron dense material; they usually had a spheroidal form and a size of 70–120 nm, but some profiles also contained elongated ovoid dense core vesicles (**Figure 3A**); and (3) dense-core vesicles filled with granular material (**Figures 2**, **3C**). In most cases their membranes were ruptured, but when intact they had diameters of 70–80 nm (**Figures 2**, **3C**). Their content was granular and more lightly stained than that of type 2 dense core vesicles. All numbers for vesicle sizes are based on uncorrected measurements of vesicle profiles taken from the sections and may, thus, slightly underestimate the true range of diameters, because profiles sectioned peripherally are likely included in these numbers. The distinction of three vesicle types is based on obvious differences in size and electron density, but it is likely that further subtypes may be distinguished based on statistical evaluation of size and shape. Especially the small clear vesicles appeared to be rather pleomorphic and indistinct in some profiles, whereas in others they were more distinct and uniform in size and shape. Likewise, the granular content of type 3 vesicles may be further differentiated based on electron density and granular appearance.

Many neuronal profiles of the CBL contained two different types of vesicles. Based on vesicle composition, the following types of profiles, resp. neurons could be distinguished:

1. Profiles with many small clear vesicles of pleomorphic appearance and usually smaller numbers of dense core vesicles (**Figures 2**, **3A,D**). These profiles occurred most frequently in the CBL. **Figure 2C** shows a section through the left dorsal margin of the CBL with numerous profiles of this type.
2. Profiles with granular dense-core vesicles. These profiles were again abundant in the CBL (**Figures 2A–C**, **3A–C**).
3. Profiles densely filled with dark dense core vesicles of spheroidal or ovoid shape (**Figures 2A,B**, **3A**). These profiles usually also contained small clear vesicles (**Figure 3A**). These profiles occurred regularly but more rarely than the previous two types.
4. Profiles with small clear vesicles and granular vesicles (**Figure 2B**). These profiles were found rarely.

In some cases, sectioned profiles only showed small clear vesicles (e.g., **Figure 1B**). In adjacent sections, however, other types of vesicles were usually seen in addition in these profiles. Therefore, it remains unclear whether profiles exist that contain exclusively small clear vesicles. Some profiles did not contain vesicles. Those profiles were either very small (0.03–0.05 μm^2) or quite large. The large profiles contained microtubules, suggesting that they were larger neurites or axonal profiles. **Figure 2B** shows several large profiles which in large parts do not contain vesicles but microtubules. Those profiles were probably neural fibers extending to terminal, vesicle containing ramifications.

Synaptic Contacts in the CBL

Synaptic contacts in the CBL were identified according to established criteria for insect nervous tissue, such as a presynaptic zone with accumulation of synaptic vesicles and electron dense material at the presynaptic membrane; a synaptic cleft, characterized by electron dense material in an enlarged intercellular space between pre- and postsynaptic membrane; and more or less prominent accumulation of electron dense material along the postsynaptic membrane (Steiger, 1967; Boeckh et al., 1970; Schürmann and Wechsler, 1970; Dowling and Chappell, 1972; Goodman et al., 1979; Tolbert and Hildebrand, 1981; Watson and Burrows, 1982). In the CBL, synaptic contacts between profiles were abundant. With few exceptions (see below) three profiles contributed to a synaptic figure. In most cases (type I synapse), one presynaptic profile was opposite two postsynaptic profiles. This configuration, a synaptic dyad, has been described in many studies before Westfall (1987). At the contact area of the three profiles, accumulation of electron dense material occurred along the presynaptic profile, opposite from the two postsynaptic profiles (**Figures 2B**, **3A–C**). This aggregation had a round to triangular shape and was usually surrounded by small clear vesicles. Dense core vesicles were never observed near this area. The intercellular cleft between the three profiles was enlarged and filled with moderately electron dense material. Accumulation of electron dense material along the postsynaptic membranes was sparser or completely absent (**Figures 3B**, **4A–C**).

In addition to type I synaptic profiles, numerous synapses were found in which two profiles with presynaptic structures were opposed to one postsynaptic profile (type II synapse; **Figures 3C**, **4B,C**). In both of these synaptic configurations, the presynaptic characters were observed across two or more ultrathin sections. Therefore, the round or triangularly shaped presynaptic density rather has the three-dimensional form of an elongated bar which is typical for locust central synapses (Watson and Schürmann, 2002). In some cases, these densities were sectioned longitudinally, revealing their bar-shaped form (**Figures 3D**, **4D**). The elongated presynaptic densities were associated with clear, translucent vesicles along their entire length. It is possible that the synapses in **Figure 4D** were monadic, consisting of one presynaptic and one postsynaptic profile, but in this case, the adjacent critical section, which would have revealed whether a third profile is present, was not available. Therefore, the existence of monadic synapses

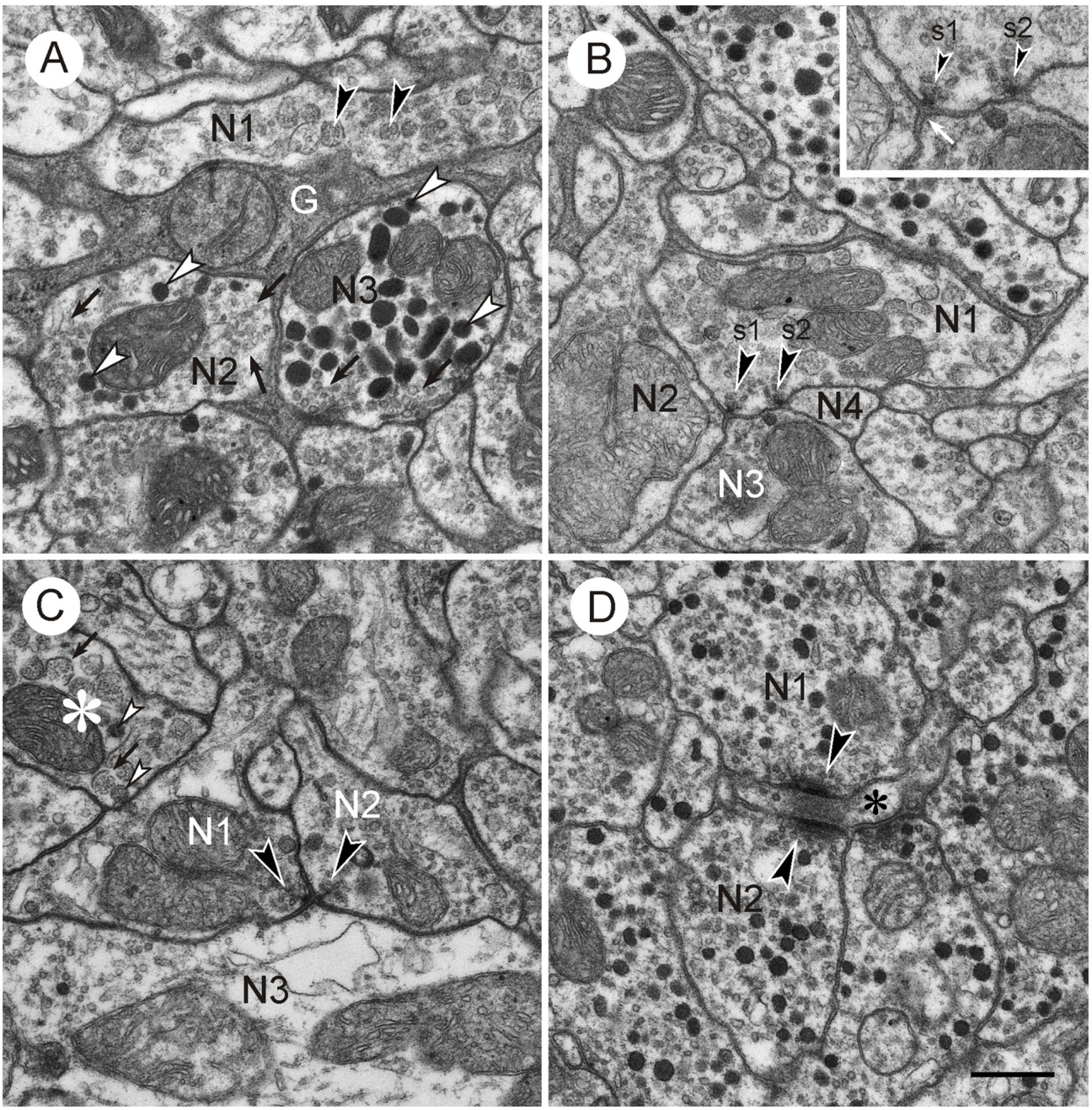

FIGURE 3 | Vesicles and synapses of neuronal profiles in the CBL. Details from frontal ultrathin sections through the CBL. **(A)** Central neuropil area showing neuronal profiles with different vesicle content (N1–N3) and processes from a glial cell (G). N1, neuronal profile with large granular vesicles (arrowheads); N2, neuronal profile with small clear pleomorphic vesicles and large dense core vesicles; N3, profile with circular small clear vesicles (arrows) and large ovoid dense core vesicles (white arrowheads). Note the different appearance of the small vesicles in N2 and N3. **(B)** Central neuropil area. Neuronal profile with large granular vesicles (N1) and two dyadic output synapses (s1, s2, arrowheads). Both synapses are of type I, i.e., one presynaptic profile (N1) faces two postsynaptic profiles (N2 and N3, resp. N3 and N4). Inset shows synaptic profiles at higher magnification (45,000×). Both synapses show a presynaptic membrane density (arrowheads) surrounded by synaptic vesicles. The intercellular space in enlarged at the active zone. The postsynaptic membrane only shows minor accumulation of electron dense material (white arrow). **(C)** Type II synapse. Two presynaptic profiles (N1,N2) with small clear synaptic vesicles and large granular vesicles face a postsynaptic profile with small clear and large dense core vesicles. Arrowheads point to presynaptic densities with accumulations of clear synaptic vesicles. The asterisk marks a profile with large granular vesicles. The membrane of most vesicles is broken (arrows). These have a lighter granular content than intact vesicles (white arrowheads). **(D)** Magnified detail from **Figure 2C**. Profiles N1 and N2 with small clear and dark dense core vesicles are presynaptic to a third small profile (asterisk). In adjacent sections, this profile contained large granular vesicles. Presynaptic structures consist of a bar-shaped density surrounded by small clear vesicles. The synapses may be monadic or dyadic. Scale bar in **(D)**: 0.5 μm (applies to **A–D**).

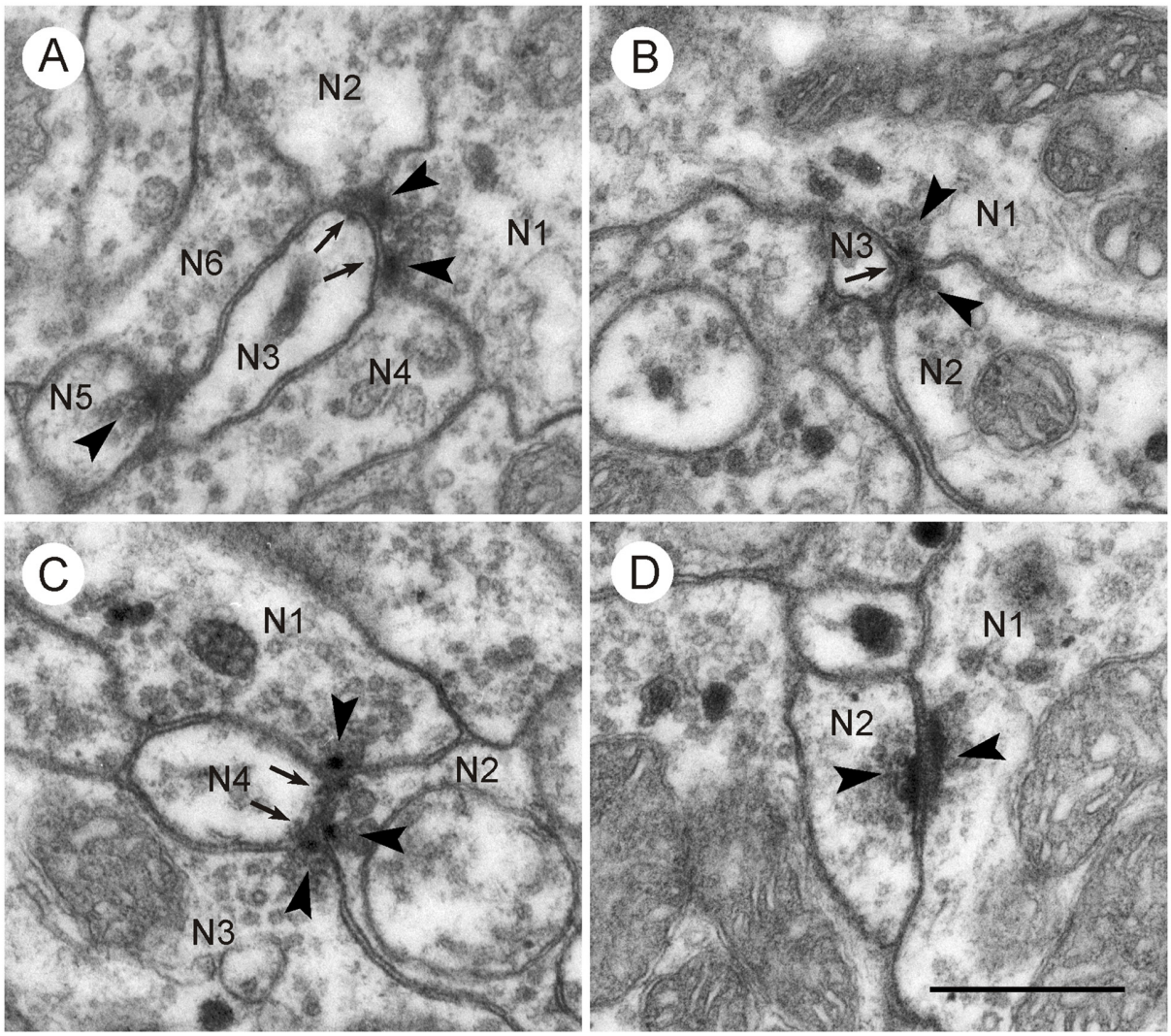

FIGURE 4 | Synaptic contacts in the CBL. Details from frontal sections through the CBL from a brain embedded in Durcupan. **(A)** Type I synapses. N1 is presynaptic to N2/N3 and to N3/N4. N5 is also presynaptic to N3 and N6. Arrowheads point to synaptic densities and vesicles. Arrows point to indistinct postsynaptic densities in N3. **(B)** Type II synapse. The profiles N1 and N2 show typical presynaptic characters (arrowheads). They face a third postsynaptic profile, N3. Arrows point to postsynaptic densities in N3. **(C)** Type I and type II synapse. Profile N4 receives triple synaptic input via a type I synapse (N1 presynaptic to N2 and N4) and a type II synapse (N2 and N2 presynaptic to N4). Arrowheads point to presynaptic specializations, arrow to minor postsynaptic density. **(D)** Two profiles (N1,N2) with bar-shaped presynaptic densities (arrowheads) facing each other. It may be a type II synapse which has been sectioned such that only the two presynaptic profiles are visible. Scale bar in **(D)**: 0.5 μm (applies to **A–D**).

cannot be excluded in the CBL, but the large majority of synaptic profiles had a dyadic symmetry when cut in cross section. Besides the described types of synapses, no evidence for other mechanisms of neuronal communication was found, such as exocytosis of dense core vesicles or structures suggesting electrical synapses.

Ultrastructure of GABA-Immunoreactive Profiles

Both pre- and postembedding techniques yielded specific immunolabeling of neuronal profiles in the CBL and were used for analyzing synaptic connections. Control sections without primary antiserum were free of immunostaining. Owing to slight differences in GP densities, the GABA antiserum II resulted in superior immunogold labeling. Here, an antiserum dilution of 1:2000 yielded best staining quality and was used in most preparations evaluated in detail (**Figures 5**, **7**). In areas outside the CBL, immunolabeled processes could be easily identified because they were surrounded by numerous unlabeled profiles. In the CBL, however, profiles with high GP densities were abundant, which made it more difficult to differentiate them from unlabeled neurons. We, therefore, evaluated GP densities in presumably immunolabeled profiles over 4–8 consecutive

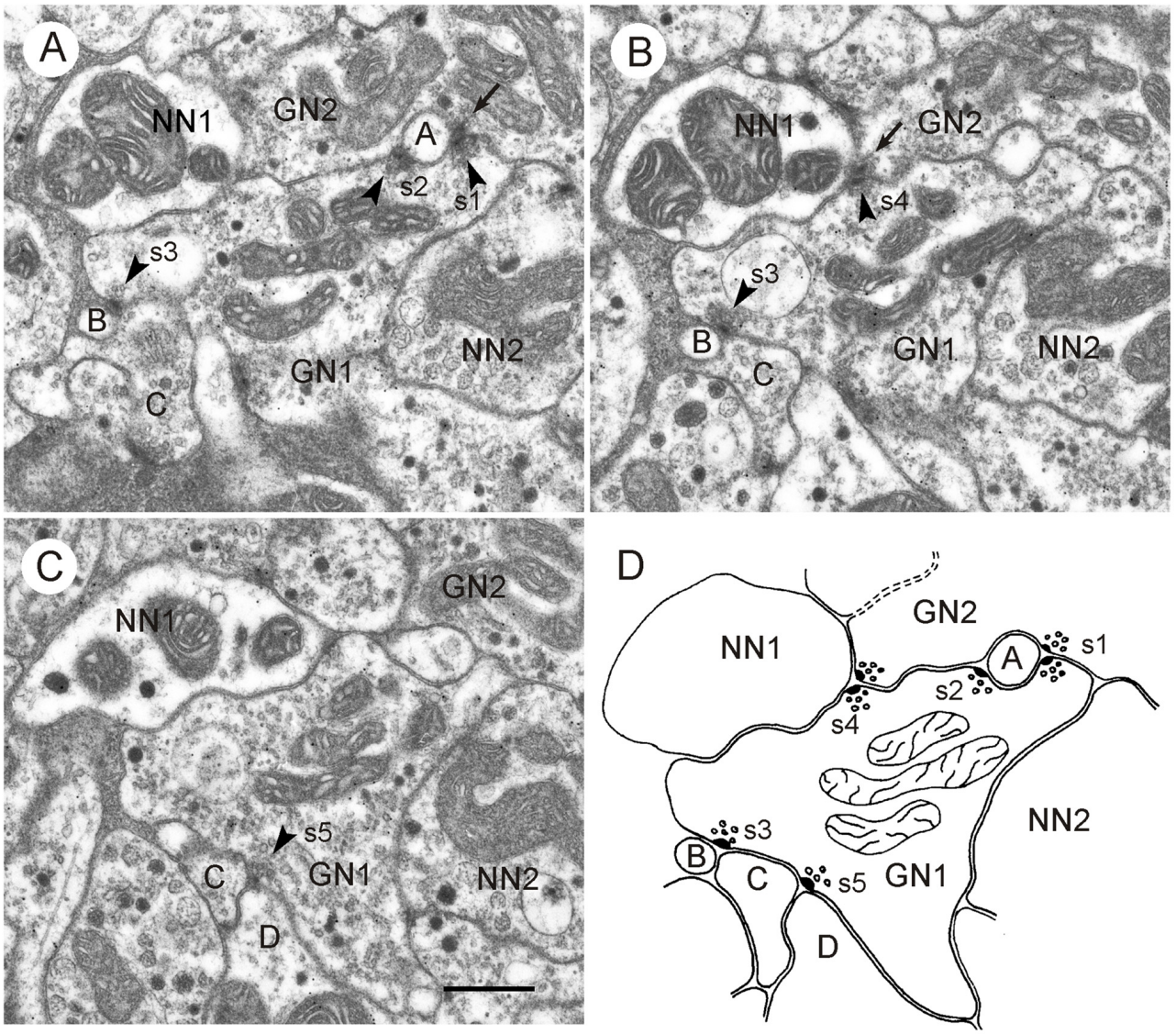

FIGURE 5 | GABA-immunoreactive neuron with output synapses. (A–C) Details from section three **(A)**, five **(B)** and eight **(C)** out of eight consecutive immunogold-labeled sections through the CBL. The GABA-immunoreactive profile (GN1) makes five output synapses (s1-s5) to neighboring profiles (**A–D**, NN1). Arrowheads point to presynaptic densities. Two of these synapses (s1 in **A** and s4 in **B**) are of type II, i.e., the presynaptic profile (GN1) and a second presynaptic profile (GN2) face one postsynaptic profile (A and NN1). GN2 is like GN1 GABA-immunolabeled. The postsynaptic profile NN1 of s4 was not immunolabeled; it contains a few dense core vesicles. Whether profile A is GABA-immunolabeled or not, could not be determined. Output synapses s2, s3 and s5 are of type I. In synaptic profile s2, **(A)** GN1 is presynaptic to profile A and to the second GABA-immunolabeled profile GN2. In synaptic profiles s3 **(A,B)** and s5 **(C)** GN1 is presynaptic to profiles B and C (s3), resp. profiles C and D (s5). To the right of GN1, an unlabeled profile (NN2) contains granular vesicles. The mean gold particle (GP) densities ($n = 8$) were 13.0 ± 4.1 GP/μm^2 (GN1), 8.0 ± 2.5 GP/μm^2 (GN2) 1.8 ± 1.4 GP/μm^2 (NN1), and 1.2 ± 0.9 GP/μm^2 (NN2). The GP densities in GN1 and GN2 were significantly different from those in NN1 and NN2 (one-way ANOVA, Tukey-HSD, $p < 0.05$). **(D)** Schematic diagram illustrating synaptic contacts of GN1 in the eight sections. Scale bar in **(C)**: 0.5 μm (applies to **A–D**).

sections against neighboring, presumably unlabeled profiles of similar size. Profiles were accepted as GABA-immunoreactive, if GP densities were significantly different ($p < 0.05$) from those of neighboring presumably unlabeled profiles. In total, five analyzed profiles were evaluated. They had GP densities ranging from 8.0 ± 2.5 GP/μm^2 to 18.4 ± 12.7 GP/μm^2. Adjacent immunonegative profiles had GP densities ranging from 1.2 ± 0.9 GP/μm^2 to 1.8 ± 1.4 GP/μm^2. The ratio of GP densities between unlabeled and labeled profiles ranged from 1:6 to 1:11. Profiles that could neither be assigned as GABA-labeled nor unlabeled, e.g., because of small profile area, were termed "non-classified".

In contrast to the immunogold technique, GABA antiserum I was superior in the preembedding technique and was used

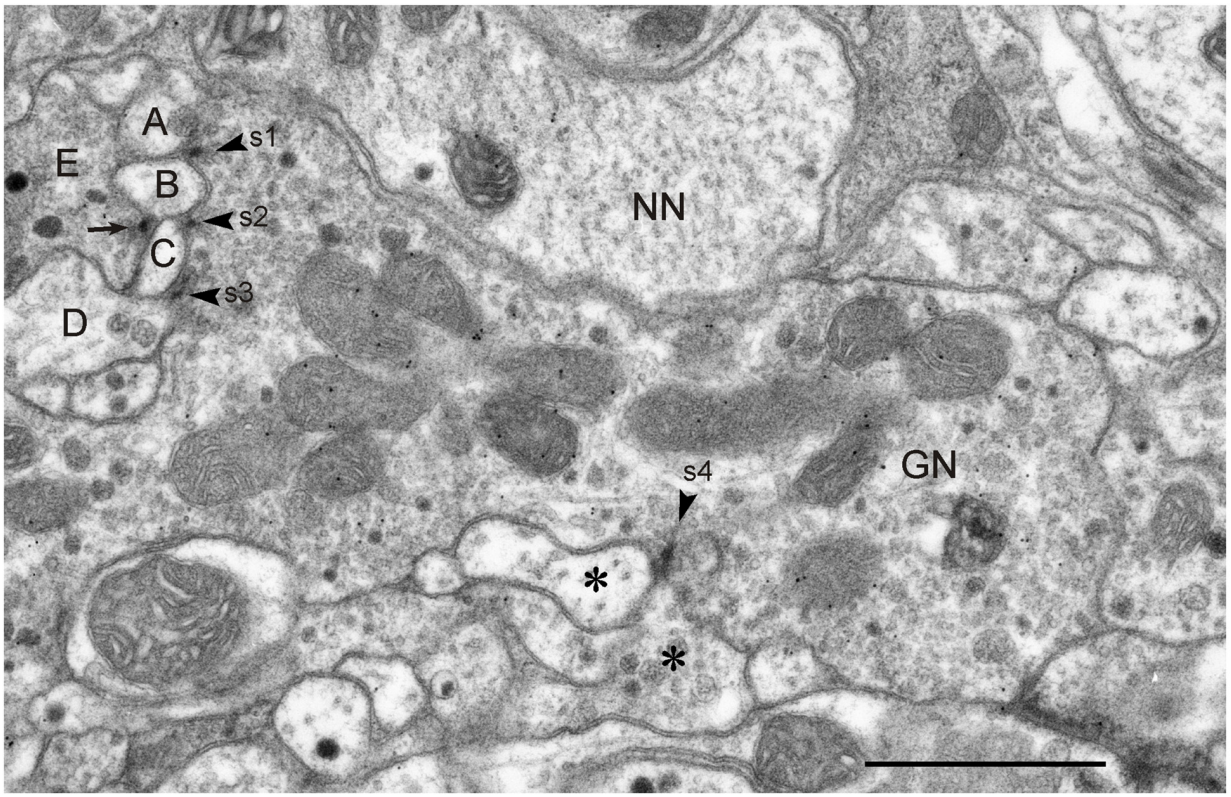

FIGURE 6 | GABA-immunoreactive neuron with output synapses. Details from one out of four consecutive immunogold-labeled sections through the CBL near its dorsal boundary with the CBU. Dilution of the GABA antiserum 1:4000. The GABA-immunoreactive neuron (GN) makes four output synapses (s1-s4) with non-classified small profiles (A–D; asterisks) surrounding GN. Arrowheads point to presynaptic densities. All synapses are of type I. The small profiles B and C receive dual synaptic input. Both profiles are, in addition, postsynaptic to another probably also GABA-immunolabeled profile E. Arrow points to presynaptic density. One of the postsynaptic profiles at s3 and s4, respectively, contains granular dense core vesicles (D, right asterisk). The mean GP densities (n = 4) were 10.1 ± 4.0 GP/μm^2 (GN), 1.3 ± 0.7 GP/μm^2 for the profile NN, and 0.8 ± 0.7 GP/μm^2 for a second unlabeled profile (not shown). The GP density in GN was significantly different from those of the two other profiles (one-way ANOVA, Tukey-HSD, $p < 0.05$). Scale bar: 1 μm.

for detailed evaluation of immunolabeling (**Figures 8**, **9**). In preembedding GABA immunostaining, only low concentrations of Triton X-100 were used to achieve satisfactory preservation of ultrastructure. As a consequence, antisera penetration was impaired and therefore, only a small region below the surface of the Vibratome section was immunostained. Here, GABA-immunolabeled profiles could be easily distinguished from unlabeled neurons, based on the electron-dense diaminobenzidine precipitate.

Both staining techniques showed that GABA-immunolabeled profiles in the CBL were highly abundant. Although the numbers of labeled vs. unlabeled profiles were not evaluated quantitatively, we estimate that about 50% of all neuronal profiles in the CBL showed GABA immunostaining. In total, six profiles were identified as GABA-immunolabeled with the postembedding technique (**Figures 5**–**7**), and four using the preembedding technique (**Figures 8**, **9**). These profiles had a size ranging from 0.3 μm^2 (**Figure 8B**, GN1) to 5.6 μm^2 (**Figure 6**). Prominent organelles were mitochondria and numerous vesicles. All GABA-immunolabeled profiles contained two different vesicle types, small clear vesicles and large dense core vesicles (**Figures 5**–**7**). The number of clear vesicles usually considerably exceeded that of the dense core vesicles (**Figures 5**–**7**). The clear vesicles were of pleomorphic appearance and were often indistinct, especially in comparison to small clear vesicles in profiles with numerous dense core vesicles. In addition, the content of the dense core vesicles in GABA-immunoreactive profiles was slightly less electron dense compared to dense core vesicles in profiles with numerous dense core vesicles. Profiles with large granular vesicles (**Figures 5**–**7**) and one profile with numerous dark dense core vesicles (not shown) were unlabeled.

Synaptic Contacts of GABA-Immunolabeled Profiles in the CBL

GABA-immunolabeled profiles in the CBL had both input and output synapses with neighboring profiles. Nine of the 12 evaluated profiles had output synapses (**Figures 5**–**9**), four profiles received synaptic input (**Figures 5**, **7**, **9**). Two profiles had input and output synapses (**Figures 5**, **7**). In total, 19 output synapses and six input synapses were found.

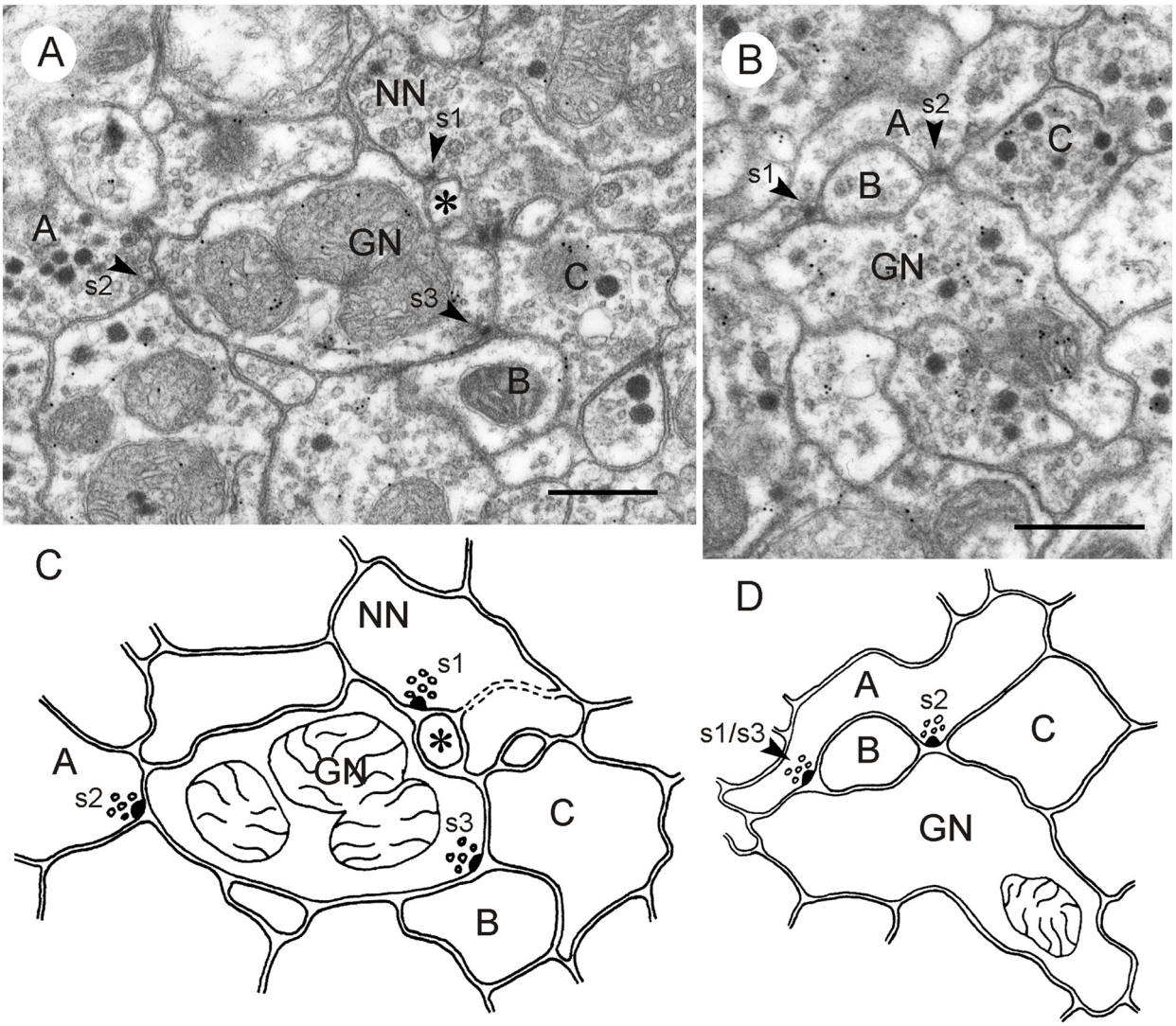

FIGURE 7 | GABA-immunoreactive neurons with input and output synapses. (A,C) Section five out of five consecutive immunogold-labeled sections through the CBL **(A)** and corresponding schematic diagram of synaptic contacts **(C)**. A neuron with granular vesicles (NN) makes an input synapse of type I (s1, arrowhead) with the GABA-immunoreactive neuron and a second small profile (asterisk). Although NN had a relatively small diameter, it is most likely not immunolabeled because it contained no GP in any of the five sections. NN receives a second synaptic input from a profile with small clear and dark dense core vesicles (s2, arrowhead); its immunostaining could not be determined. Finally, GN is presynaptic to two other profiles (s3, B, C), illustrating serially synaptic connections of GN. The mean GP densities (n = 5) were 13.3 ± 6.0 GP/μm^2 (GN), and for a second profile not shown 1.6 ± 1.4 GP/μm^2. The GP densities in GN were significantly different from those of the second profile (t-test, p = 0.0031). **(B)** Section two out of five consecutive immunogold-labeled sections through the CBL. The GABA-immunoreactive profile receives dual synaptic input (s1, s2 arrowheads). In synapse s1, profile A is presynaptic to GN and a non-classified profile B (type I synapse). Synapse s2 might be a triadic synapse with one non-classified presynaptic profile (A) facing three postsynaptic profiles (GN, B, C). In the first section of this series, however (not shown), only profiles B and GN seemed to be postsynaptic to A. The mean GP densities (n = 5) were 18.4 ± 12.7 GP/μm^2 (GN), and for a second profile with granular vesicles and small clear vesicles not shown 1.6 ± 1.5 GP/μm^2. The large standard deviation of GP density of GN resulted from very low GP densities on one out of the five sections. Perhaps this section was not sufficiently exposed to the primary or secondary antibody (e.g., by an air bubble between section and incubation medium). The GP densities in GN were significantly different from those of the second profile (t-test, p = 0.02). **(D)** Schematic diagram of synaptic contacts of the series in **(B)**. Synapse s3 occurred on section 5 of the series at the same site as synapse s1, but with two sections (3 and 4) in between without synaptic contact. Scale bars: 0.5 μm.

Output Synapses

Three profiles contributed to all types of output synapses. In most cases the GABA-immunoreactive profile was presynaptic to two postsynaptic profiles (type I synapse; n = 13; **Figures 5–8**). In addition, configurations with one presynaptic GABA-immunostained profile, another unlabeled presynaptic profile, and a third unlabeled postsynaptic profile occurred (type II synapse; n = 6; **Figures 5**, **9**). In both types of

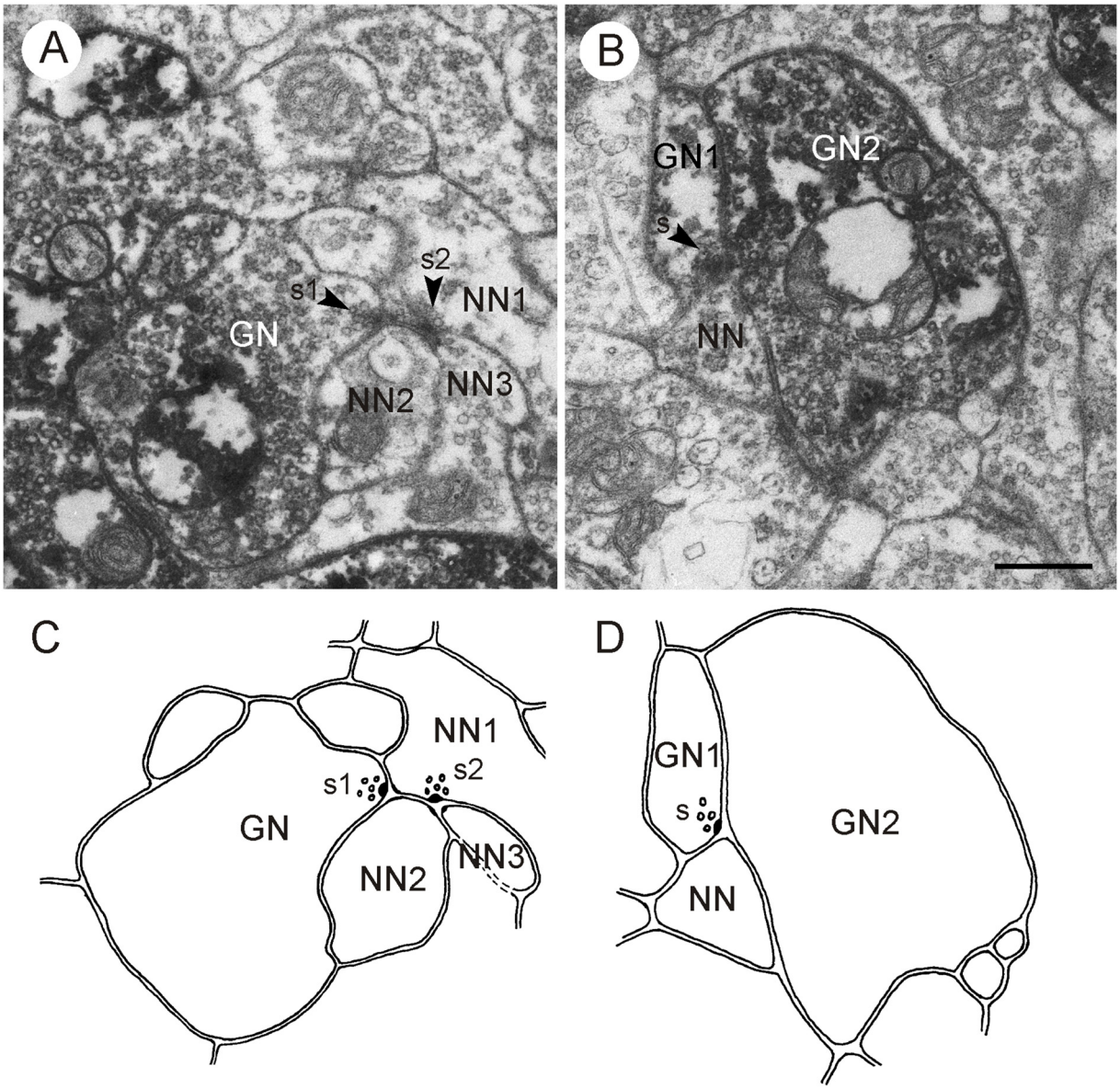

FIGURE 8 | GABA-immunoreactive neurons contributing to type I synapses; postembedding technique. (A,C) Second out of two consecutive sections through the CBL **(A)** and corresponding schematic diagram of synaptic contacts **(C)**. A GABA-immunoreactive profile (GN) is presynaptic (s1, arrowhead) to two postsynaptic profiles (NN1,NN2). NN1 is, in addition, presynaptic (s2, arrowhead) to NN2 and a third unlabeled profile (NN3), illustrating serial connectivity. **(B,D)** Second out of two consecutive sections through the CBL **(B)** and corresponding schematic diagram of synaptic contacts **(D)**. A GABA-immunoreactive profile (GN1) is presynaptic (s, arrowhead) to a second GABA-labeled profile (GN2) and an unlabeled profile (NN). Scale bar in **(B)**: 0.5 μm (applies to **A–D**).

synapse, the postsynaptic profiles were usually much smaller than the presynaptic GABA-immunoreactive profiles (**Figures 5**, **6**, **8**). Their immunolabeling (GABA-positive or -negative) could, therefore, not be determined unequivocally in the immunogold preparations. Throughout the series of sections, however, most of these profiles had no or only one or two GPs, suggesting that they were not GABA-immunolabeled. **Figure 8A** shows a GABA-immunostained profile obtained by the preembedding technique which makes an output synapse with two clearly unlabeled profiles. Postsynaptic profiles often contained small clear vesicles, a few dark dense core vesicles or both (**Figures 5**–**7**). Very small profiles contained no vesicles at all (profile A in **Figure 6**). In two cases, postsynaptic profiles had large granular vesicles (**Figure 6**). In type II synapses, the second presynaptic profile was also GABA-immunoreactive in one case (**Figure 5**); in another case, the second presynaptic profile was not GABA-labeled (**Figure 9A**).

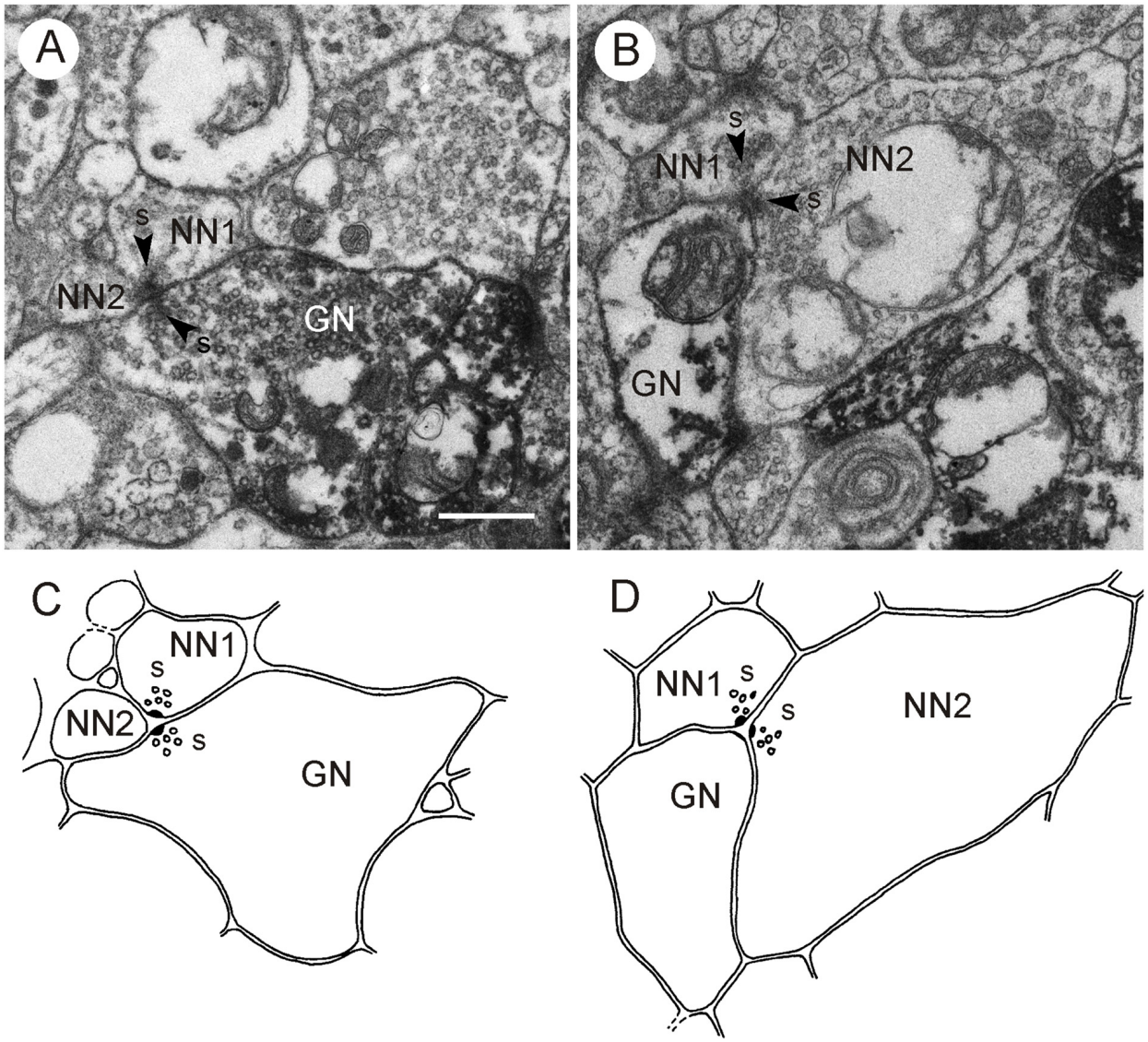

FIGURE 9 | GABA-immunoreactive neurons contributing to type II synapses; postembedding technique. (A,C) Second out of two consecutive sections through the CBL **(A)** and corresponding schematic diagram of synaptic contacts **(C)**. A GABA-immunoreactive neuron (GN) and an unlabeled neuron (NN1) are presynaptic (s, arrowhead) to a second unlabeled profile (NN2). **(B,D)** Second out of two consecutive sections through the CBL **(B)** and corresponding schematic diagram of synaptic contacts **(D)**. A GABA-immunoreactive profile (GN) is postsynaptic to two unlabeled profiles (NN1, NN2) with presynaptic specializations (s, arrowheads). Scale bar in **(A)**: 0.5 μm (applies to **A–D**).

Three out of the eight identified GABA-immunoreactive profiles had conspicuously many output synapses (n = 4, resp. 5; **Figures 5**, **6**). In all of these cases the neuron profile occupied a rather large area (up to 5.6 μm^2), and these profiles had numerous vesicles and mitochondria. The postsynaptic profiles were largely small (<0.02 μm^2) and arranged around the GABA-immunoreactive profile (**Figures 5**, **6**). Some of these postsynaptic profiles received dual synaptic input from the same GABA-immunoreactive profile (profiles A and C in **Figure 5**; profiles B and C in **Figure 6**). One of the input synapses of profile A in **Figure 5** is a type II synapse. In this case the second presynaptic profile is also GABA-immunoreactive. These configurations suggest that the small postsynaptic profiles in the CBL received massive GABAergic input.

Two instances showed a serial synaptic configuration in which a GABA-immunolabeled neuron contributed an output synapse (**Figure 8A**). The GABA-immmunolabeled profile in **Figure 8** was presynaptic to two unlabeled profiles (NN1, NN2), and NN1 was itself presynaptic to NN2 and a third unlabeled profile NN3. A similar connectivity was found in another preparation (not shown).

Input Synapses

Only five of the 12 evaluated GABA-immunolabeled profiles were postsynaptic to other profiles. **Figures 7B,D** shows an immunolabeled profile which receives triple synaptic input (s1–s3) from a non-classified profile with small clear vesicles and a few dense core vesicles. Two of these synaptic profiles (s1 and s3) had identical postsynaptic partners B and GN. The GABA-immunoreactive profile of **Figure 7A,C** received input via type I synapses from two different profiles. One of these profiles (NN, synapse s1) contained large granular vesicles. Although its cross sectional area was smaller than 0.5 μm^2 it was most probably not GABA-immunoreactive, because it had no GP in any of the examined sections and many other profiles with similar vesicle content were shown to be immunonegative. The second presynaptic profile (A, synapse s2) contained dense core vesicles and small clear vesicles. Its immunolabeling could not be classified. The postsynaptic GABA-immunoreactive profile was itself presynaptic to two other non-classified profiles (C and D), illustrating serial synaptic contacts with the GABA-immunostained neuron being pre- and postsynaptic to surrounding profiles. In two type I synapses, GABA-immunoreactive profiles (GN2 in **Figure 5** and GN2 in **Figure 8B**) received synaptic input from another GABA-immunostained profile (GN1 in **Figures 5**, **8B**), which was also presynaptic to a third profile, which in **Figure 8B** was not GABA-immunolabeled. **Figures 9B,D**, finally shows a type II synapse with two non-immunolabeled neurons being presynaptic to a GABA-immunolabeled profile.

LomTK Immunostaining

In contrast to GABA immunolabeling, immunogold staining for LomTK II revealed a strong association of GPs with a particular type of vesicle, large granular dense core vesicles (**Figures 10**, **11**). This is particularly obvious in larger fibers, where granular dense core vesicles occurred more rarely (**Figure 10B**). In fact, granular vesicle containing profiles that were not immunostained were observed only very rarely. Based on GP density, immunolabeled profiles could be easily distinguished from unlabeled profiles, which rendered statistical analysis unnecessary (**Figures 10**, **11**). Profiles with numerous dark dense core vesicles were unlabeled (**Figure 10A**). Likewise, profiles with dense core vesicles and pleomorphic clear vesicles were unlabeled except for two very rare cases, in which the GPs were found on dense core vesicles, but not on the clear vesicles (**Figure 11C**). Omission of the primary antiserum abolished all immunogold labeling on the sections.

LomTK-immunolabeled profiles had pre- and postsynaptic contacts with adjacent profiles. Small immunolabeled profiles were often surrounded by presynaptic profiles with pleomorphic clear and dense core vesicles which made both type I and type II synapses onto the LomTK profiles (**Figure 10C,D**). Output synapses more often occurred in larger profiles, again with postsynaptic partners that could often be identified as profiles with pleomorphic small clear vesicles and some large dense core vesicles. In several cases, output synapses had a monadic appearance, but adjacent sections for closer inspection were not available in those cases. In contrast to GABA-immunostained profiles, input and output synapses were never found together in the same profile. Likewise, synaptic contacts between two LomTK-immunolabeled profiles were not found.

DISCUSSION

The CBL in the insect brain is a major site of bilateral convergence of visual pathways from the two compound eyes (Homberg et al., 2011; Pfeiffer and Homberg, 2014). In the monarch butterfly, the field cricket, two species of dung beetle and the desert locust, neurons connecting the bulbs to the CBL, termed TL neurons, are sensitive to the plane of zenithal polarized light and constitute the principal input for sky compass signaling in the central complex (Vitzthum et al., 2002; Sakura et al., 2008; Heinze and Reppert, 2011; el Jundi et al., 2015). In the fly *Drosophila*, homologous neurons to the ellipsoid body are sensitive to the azimuth of a vertical light bar, and likely provide spatial landmark information for head direction coding in the central complex (Seelig and Jayaraman, 2013, 2015). In locusts and probably other species as well, two subtypes of TL neurons (TL2, TL3, **Figure 1C**) are GABA-immunoreactive suggesting that they signal through synaptic inhibition (Homberg et al., 1999). Candidate postsynaptic partners of TL neurons are columnar neurons (CL neurons) that occur in sets of 16 individuals and connect the CBL to the slices of the PB (**Figure 1D**). Two sets of CL1 neurons are LomTK-immunoreactive (Vitzthum and Homberg, 1998). How these different cell types are interconnected is unknown. The present study shows that the CBL in the desert locust is a neuropil of rich synaptic connectivities. Neuronal profiles differing distinctly in vesicle composition could be distinguished. Two types of synaptic contacts occur, convergent (type I) and divergent (type II) dyadic contacts. Both GABA- and LomTK-immunolabeled profiles show characteristic ultrastructures. GABA-immunostained neurons contain small clear and large dense core vesicles. They make predominantly output synapses to unlabeled profiles but, in addition, also receive synaptic input. LomTK immunostaining, in contrast, is largely confined to profiles with granular dense-core vesicles. LomTK-immunolabeled neurons make input and output synapses with unlabeled profiles, often those presumed to be GABAergic. The data support synaptic transmission from TL2/3 neurons to columnar CL1 neurons but suggest that CL1 neurons may also signal from the PB to the CBL. Both TL and CL neurons may, furthermore, be involved in local interactions in the CBL.

Neuronal Organization and Ultrastructure of the CBL

The lower division of the locust central body is composed of the processes of at least seven types of tangential neuron and two types of columnar neuron (Müller et al., 1997; Heinze and Homberg, 2008; Bockhorst and Homberg, 2015). Tangential neurons, termed TL1–6 and TLU1 ramify in distinct areas of the lateral complex and target certain (TL2, TL3, TL4) or all

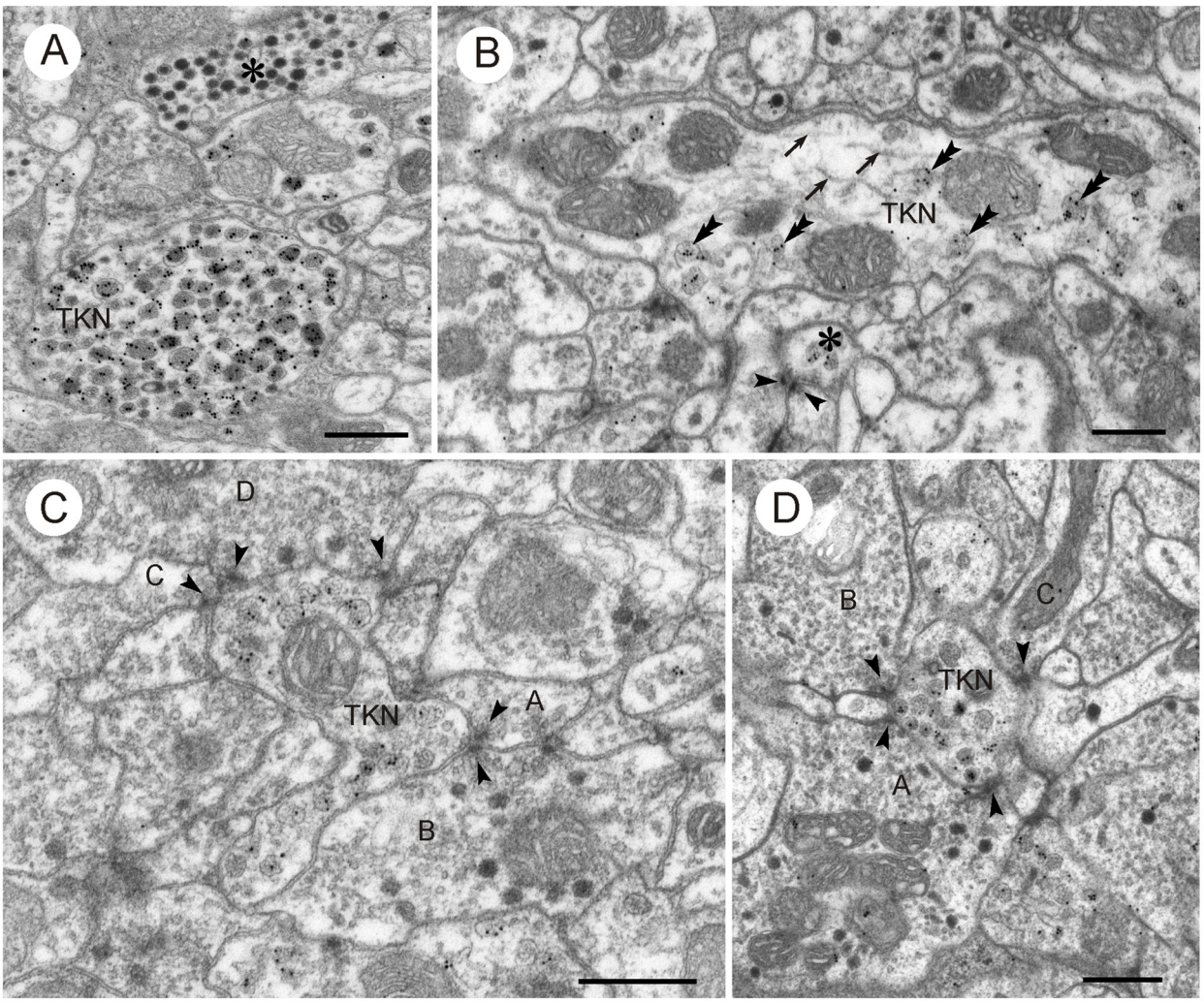

FIGURE 10 | LomTK II-immunoreactive neurons in the CBL. (A) GPs are associated with granular dense core vesicles within a profile (TKN), but not with dark dense core vesicles in another profile (asterisk). **(B)** A larger fiber contains numerous microtubules (arrows), mitochondria (M) and a few granular vesicles. GPs are found almost exclusively on the granular vesicles (double arrowheads). A second small LomTK-labeled profile receives input from two neurons via a type II dyad. Arrowheads point to presynaptic densities. **(C,D)** Small LomTK-labeled profiles (TKN) receive numerous input synapses (type I and type II dyads) from unlabeled profiles (A–D in **C**, A–C in **D**). Arrowheads point to presynaptic densities. All of the presynaptic profiles contain small pleomorphic clear vesicles and in some of these (B,D in **C**; A,B in **D**) dark dense core vesicles are also present. Scale bars: 0.5 μm.

layers (TL1, TL5, TL6, TLU1) of the CBL. Columnar neurons (CL1a-d, CL2) occur as systems of 16 neurons with ramifications in columnar domains of the lower division and projections to the PB, noduli (CL2) or LAL (CL1a, b, d). Similar cell types have been found in other insect species, notably, the monarch butterfly (Heinze et al., 2013) and the fruit fly *Drosophila* (Hanesch et al., 1989; Martín-Peña et al., 2014; Wolff et al., 2015). In sections largely from the center of the CBL, three types of vesicle could be distinguished in neuronal profiles, small clear vesicles, large dark dense core vesicles and large granular dense core vesicles. While clear vesicles have been associated with classical transmitters such as glutamate, GABA or acetylcholine, dense core vesicles have been shown to contain neuropeptides or biogenic amines (reviewed by Watson and Schürmann, 2002). Dyadic synaptic contacts as found here are the most common synaptic configurations in the nervous system of locusts (Schürmann and Wechsler, 1970; Leitch and Laurent, 1996; Watson and Schürmann, 2002; Träger et al., 2007) and other insect species (e.g., Tolbert and Hildebrand, 1981; Boeckh and Tolbert, 1993; Reischig and Stengl, 2003). In the CBL of *Drosophila* and the honeybee, in contrast, single (monadic) synapses were reported most frequently (Martín-Peña et al., 2014). These authors also found multiple synapses with two active zones in close proximity and coincident synapses with two presynaptic profiles facing a single postsynaptic profile. The latter type synapse probably corresponds to the type II (convergent) dyads found here. Convergent dyads are less common than type I (divergent) dyads, but have also been reported in other areas

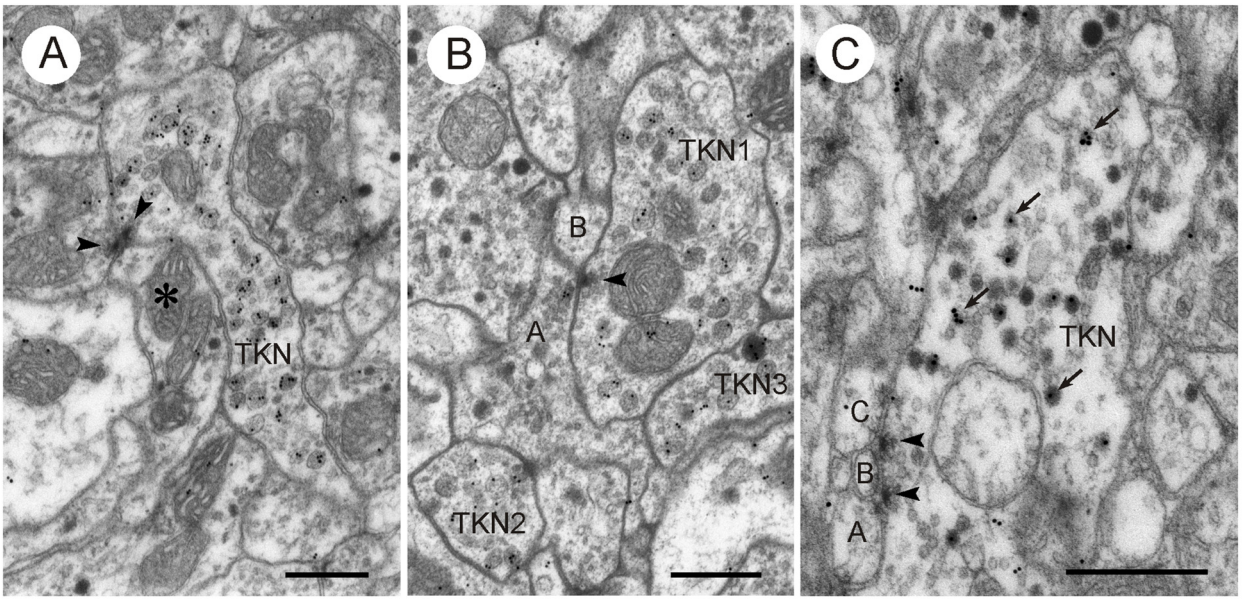

FIGURE 11 | LomTK II-immunoreactive neurons in the CBL. (A,B) Profiles with LomTK-immunolabeled granular dense-core vesicles (TKN) making output synapses. **(A)** The immunolabeled profile is one of two presynaptic elements in a type II dyadic connection with a profile containing pleomorphic clear and a few dense core vesicles (asterisk). Arrowheads point to presynaptic densities. **(B)** Synaptic connection of an immunolabeled profile (TKN1) with one or two postsynaptic elements (A,B). Profile A contains pleomorphic clear and dark dense core vesicles. Arrowhead points to synaptic density. Two other profiles are LomTK-immunolabeled (TKN2, TKN3). **(C)** Profile (TKN) with small clear and large dark dense core vesicles. GPs are associated with the dense core vesicles (arrows). The profile makes two type I output synapses with three unclassified small profiles (A–C). Arrowheads point to presynaptic densities. Scale bars: 0.5 μm.

of the locust brain (Schürmann and Wechsler, 1970; Goodman et al., 1979; Leitch and Laurent, 1996). Martín-Peña et al. (2014) interpret these as coincidence detectors, possibly involved in learning and memory or decision making, but further studies are clearly required to substantiate these claims.

GABA-Immunoreactive Neurons

The ultrastructure of GABA-immunoreactive neurons has been investigated in the brain and ventral nerve cord of various insect species (locust: Watson, 1988, 1990; Watson and Laurent, 1990; Leitch and Laurent, 1996; honeybee: Ganeshina and Menzel, 2001; cockroach: Distler, 1990; Malun, 1991). In all of these studies, GABA-immunolabeled profiles were characterized by the presence of numerous small pleomorphic clear vesicles and, often, smaller numbers of large dense core vesicles. The abundance of GABA-immunolabeled profiles in the locust CBL corresponds well with the dense innervation by an estimated number of about 100 bilateral pairs of TL neurons, which were identified as TL2, TL3 and TL4 (Homberg et al., 1999). The presence of large dense core vesicles in GABA-immunostained profiles suggests that these neurons contain peptide- or amine-cotransmitters. Candidate neuropeptides are peptides related to Dip-allatostatin, FMRFamide and orcokinin in TL4 neurons and LomTK II and orcokinin in TL2 neurons (Homberg et al., 1999; Hofer et al., 2005). A small subset of TL2 neurons, moreover, shows NADPH-diaphorase activity and may therefore release the gaseous transmitter nitric oxide (Kurylas et al., 2005). The high incidence of profiles with small clear vesicles and large dense core vesicles near the dorsal rim of the CBL, corresponding to the dorsalmost layer 1 (**Figure 2C**) likely relates to prominent immunostaining of TL4 neurons that exclusively innervate this layer for GABA, Dip-allatostatin, FMRFamide and orcokinin (Homberg et al., 1999; Hofer et al., 2005).

LomTK Immunolabeling

At the light microscopic level, LomTK immunostaining in the CBL could be assigned to two sets of 16 CL1 neurons, corresponding to two neurons per slice of the CBL, and to two bilateral pairs of TL2 neurons (Vitzthum and Homberg, 1998). Double immunolabeling showed that the two TL2 neurons contain colocalized LomTK- and GABA-immunoreactivities (Vitzthum and Homberg, 1998). The ultrastructural data correspond well to the light-microscopic identification of immunolabeled neurons. LomTK immunogold labeling was highly concentrated on granular dense core vesicles, which suggests that profiles containing granular vesicles are those of the immunostained CL1 neurons. The much rarer finding of GP association with dark dense core vesicles in profiles with dense core and small clear vesicles (**Figure 11C**) is consistent with those profiles originating from the two LomTK/GABA-immunolabeled TL2 neurons. The regular presence of classical dyadic synapses in LomTK-labeled profiles suggests that, in addition to LomTK, these neurons also contain a classical neurotransmitter. So far, the ultrastructure of tachykinin-containing neurons has only rarely been investigated in the nervous system. In the vertebrate dorsal horn, tachykinin

immunoreactivity is associated with large dense core vesicles (Merighi et al., 1991; Salio et al., 2001), and except for an early study on the locust brain (Benedeczky et al., 1982), no ultrastructural studies have been performed in invertebrates.

Synaptic Connectivities and Functional Implications

Ultrathin sections of the CBL showed frequent synaptic contacts between different profiles usually in the form of divergent and, less frequently, convergent dyads. GABA-immunolabeled profiles had a higher number of output synapses compared to input synapses, suggesting that TL2, TL3 and TL4 neurons largely provide synaptic input to the CBL. This is consistent with the study of Träger et al. (2007), showing that TL2 and TL3 neurons have exclusively input synapses in the medial and lateral bulbs (LBUs; see **Figure 1E**). Output synapses in the CBL are made with a variety of profiles, including those containing large dense granular vesicles, presumed to originate from LomTK-labeled CL1 neurons. Other profiles may be those of CL2 neurons or LomTK-negative CL1 neurons. Synaptic contacts are also made between GABA-immunolabeled profiles suggesting lateral mutual inhibitions perhaps serving a role in shaping their tuning to polarized light. In addition, GABA-immunolabeled profiles also receive synaptic input in the CBL and often, output and input synapses were observed on the same profile. This suggests local interactions with unknown synaptic partners, possibly columnar neurons or TL1, TL5 or TL6 tangential neurons.

In LomTK-immunoreactive profiles, both input and output synapses were observed. Often, small LomTK-labeled profiles received numerous input synapses from surrounding profiles that often had the appearance of GABA-labeled ones, characterized by pleomorphic clear vesicles and small numbers of large dense core vesicles (**Figures 10C,D**). Here, the LomTK-immunolabeled CL1 neurons possibly receive synaptic input from polarized-light sensitive TL neurons. Output synapses in LomTK profiles occured usually individually and never together with input synapses on the same profile. This could mean that two different sets of LomTK-labeled profiles exist, one with output synapses and one with input synapses in the CBL, or that in the same neuron, input and output synapses as spatially segregated. Light microscopic observations, indeed, suggested that the tree of ramifications of CL1a neurons in the CBL is spatially organized into a core of stout varicose processes covering a single slice surrounded by a peripheral area of finer processes in adjacent slices (Heinze and Homberg, 2008). An ultrastructural analysis of single dye filled CL1 neurons might help to solve this question and bring more light into the synaptic connectivities of CL1 neurons in the CBL.

The present study supports electrophysiological data showing that CL1 neurons mainly receive inhibitory synaptic input from presynaptic neurons (Bockhorst and Homberg, 2015), likely to be the GABAergic TL2 and TL3 inputs to the CBL. The interactions between tangential and columnar neurons in the CBL is clearly an important step in shaping the topographic representation of preferred *E*-vector orientations in the slices of the PB, which occurs through neural computations and is not present at the level of TL neurons. An analysis of synaptic partners of individually labeled elements of the CBL is likely to shed further light on the synaptic computations in the CBL that contribute to the unique sensory representation in the PB.

ETHICS STATEMENT

All animal procedures were in compliance with the guidelines of the European Union (Directive 86/609/EEc) and the German Animal Welfare Act. Approval of the study by an ethics committee was dispensable, because all experiments were on insects.

AUTHOR CONTRIBUTIONS

UH and MM conceived the research topic, MM performed most of the experiments, MM and UH evaluated the data, UH wrote the article.

FUNDING

Supported by Deutsche Forschungsgemeinschaft (DFG) grant HO 950/24-1.

ACKNOWLEDGMENTS

We are grateful to Drs. Heinrich Dircksen and Timothy Kingan for donation of anti-GABA antisera, Hans Agricola for the gift of the LomTK II antiserum, and to Gesa Thieß for technical assistance.

REFERENCES

Benedeczky, I., Kiss, J. Z., and Somogyi, P. (1982). Light and electron microscopic localization of substance P-like immunoreactivity in the cerebral ganglion of locust with a monoclonal antibody. *Histochemistry* 75, 123–131. doi: 10.1007/bf00492539

Bockhorst, T., and Homberg, U. (2015). Amplitude and dynamics of polarization-plane signaling in the central complex of the locust brain. *J. Neurophysiol.* 113, 3291–3311. doi: 10.1152/jn.00742.2014

Boeckh, J., Sandri, C., and Akert, K. (1970). Sensorische Eingänge und synaptische Verbindungen im Zentralnervensystem von Insekten. *Z. Zellforsch. Mikrosk. Anat.* 193, 429–446.

Boeckh, J., and Tolbert, L. P. (1993). Synaptic organization and development of the antennal lobe in insects. *Microsc. Res. Tech.* 24, 260–280. doi: 10.1002/jemt.1070240305

Distler, P. (1990). GABA-immunohistochemistry as a label for identifying types of local interneurons and their synaptic contacts in the antennal lobes of the American cockroach. *Histochemistry* 93, 617–626. doi: 10.1007/bf00272204

Dowling, J. E., and Chappell, R. L. (1972). Neural organization of the median ocellus of the dragonfly. II. Synaptic structure. *J. Gen. Physiol.* 60, 148–165. doi: 10.1085/jgp.60.2.148

el Jundi, B., Heinze, S., Lenschow, C., Kurylas, A., Rohlfing, T., and Homberg, U. (2010). The locust standard brain: a 3D standard of the central complex as

a platform for neural network analysis. *Front. Syst. Neurosci.* 3:21. doi: 10.3389/neuro.06.021.2009

el Jundi, B., Warrant, E. J., Byrne, M. J., Khaldy, L., Baird, E., Smolka, J., et al. (2015). Neural coding underlying the cue preference for celestial orientation. *Proc. Natl. Acad. Sci. U S A* 112, 11395–11400. doi: 10.1073/pnas.1501272112

Ganeshina, O., and Menzel, R. (2001). GABA-immunoreactive neurons in the mushroom bodies of the honeybee: an electron microscopic study. *J. Comp. Neurol.* 437, 335–349. doi: 10.1002/cne.1287

Goodman, L. J., Mobbs, P. G., and Kirkham, J. B. (1979). The fine structure of the ocelli of *Schistocerca gregaria*. The neural organization of the synaptic plexus. *Cell Tissue Res.* 196, 487–510. doi: 10.1007/bf00234742

Hanesch, U., Fischbach, K.-F., and Heisenberg, M. (1989). Neuronal architecture of the central complex in *Drosophila melanogaster*. *Cell Tissue Res.* 257, 343–366. doi: 10.1007/bf00261838

Heinze, S. (2014). "Polarized-light processing in insect brains: recent insights from the desert locust, the monarch butterfly, the cricket and the fruit fly," in *Polarized Light and Polarization Vision in Animal Sciences*, ed. G. Horváth (Berlin Heidelberg: Springer), 61–111.

Heinze, S., Florman, J., Asokaraj, S., el Jundi, B., and Reppert, S. M. (2013). Anatomical basis of sun compass navigation II: The neuronal composition of the central complex of the monarch butterfly. *J. Comp. Neurol.* 521, 267–298. doi: 10.1002/cne.23214

Heinze, S., Gotthardt, S., and Homberg, U. (2009). Transformation of polarized light information in the central complex of the locust. *J. Neurosci.* 29, 11783–11793. doi: 10.1523/JNEUROSCI.1870-09.2009

Heinze, S., and Homberg, U. (2007). Maplike representation of celestial *E*-vector orientations in the brain of an insect. *Science* 315, 995–997. doi: 10.1126/science.1135531

Heinze, S., and Homberg, U. (2008). Neuroarchitecture of the central complex of the desert locust: intrinsic and columnar neurons. *J. Comp. Neurol.* 511, 454–478. doi: 10.1002/cne.21842

Heinze, S., and Homberg, U. (2009). Linking the input to the output: new sets of neurons complement the polarization vision network in the locust central complex. *J. Neurosci.* 29, 4911–4921. doi: 10.1523/JNEUROSCI.0332-09.2009

Heinze, S., and Reppert, S. M. (2011). Sun compass integration of skylight cues in migratory monarch butterflies. *Neuron* 69, 345–358. doi: 10.1016/j.neuron.2010.12.025

Held, M., Berz, A., Hensgen, R., Muenz, T., Scholl, C., Rössler, W., et al. (2016). Microglomerular synaptic complexes in the sky-compass network of the honeybee connect parallel pathways from the anterior optic tubercle to the central complex. *Front. Behav. Neurosci.* 10:186. doi: 10.3389/fnbeh.2016.00186

Hofer, S., Dircksen, H., Tollbäck, P., and Homberg, U. (2005). Novel insect orcokinins: characterization and neuronal distribution in the brains of selected dicondylian insects. *J. Comp. Neurol.* 490, 57–71. doi: 10.1002/cne.20650

Homberg, U., Heinze, S., Pfeiffer, K., Kinoshita, M., and el Jundi, B. (2011). Central neural coding of sky polarization in insects. *Philos. Trans. R. Soc. Lond. B Biol. Sci.* 366, 680–687. doi: 10.1098/rstb.2010.0199

Homberg, U., Hofer, S., Pfeiffer, K., and Gebhardt, S. (2003). Organization and neural connections of the anterior optic tubercle in the brain of the locust, *Schistocerca gregaria*. *J. Comp. Neurol.* 462, 415–430. doi: 10.1002/cne.10771

Homberg, U., Kingan, T. G., and Hildebrand, J. G. (1987). Imunocytochemistry of GABA in the brain and suboesophageal ganglion of *Manduca sexta*. *Cell Tissue Res.* 248, 1–24. doi: 10.1007/bf01239957

Homberg, U., Vitzthum, H., Müller, M., and Binkle, U. (1999). Immunocytochemistry of GABA in the central complex of the locust *Schistocerca gregaria*: Identification of immunoreactive neurons and colocalization with neuropeptides. *J. Comp. Neurol.* 409, 495–507. doi: 10.1002/(sici)1096-9861(19990705)409:3<495::AID-CNE12>3.0.CO;2-F

Hoskins, S. G., Homberg, U., Kingan, T. G., Christensen, T. A., and Hildebrand, J. G. (1986). Immunocytochemistry of GABA in the antennal lobes of the sphinx moth *Manduca sexta*. *Cell Tissue Res.* 244, 243–252. doi: 10.1007/bf00219199

Ito, K., Shinomiya, K., Ito, M., Armstrong, J. D., Boyan, G., Hartenstein, V., et al. (2014). A systematic nomenclature for the insect brain. *Neuron* 81, 755–765. doi: 10.1016/j.neuron.2013.12.017

Kurylas, A. E., Ott, S. R., Schachtner, J., Elphick, M. R., Williams, L., and Homberg, U. (2005). Localization of nitric oxide synthase in the central complex and surrounding midbrain neuropils of the locust *Schistocerca gregaria*. *J. Comp. Neurol.* 484, 206–223. doi: 10.1002/cne.20467

Labhart, T., and Meyer, E. (1999). Detectors for polarized skylight in insects: a survey of ommatidial specializations in the dorsal rim area of the compound eye. *Microsc. Res. Tech.* 47, 368–379. doi: 10.1002/(SICI)1097-0029(19991215)47:6<368::AID-JEMT2>3.0.CO;2-Q

Leitch, B., and Laurent, G. (1996). GABAergic synapses in the antennal lobe and mushroom body of the locust olfactory system. *J. Comp. Neurol.* 372, 487–514. doi: 10.1002/(SICI)1096-9861(19960902)372:4<487::AID-CNE1>3.0.CO;2-0

Malun, D. (1991). Synaptic relationships between GABA-immunoreactive neurons and an identified uniglomerular projection neuron in the antennal lobe of *Periplaneta americana*: a double-labeling electron microscopic study. *Histochemistry* 96, 197–207. doi: 10.1007/bf00271538

Martín-Peña, A., Acebes, A., Rodríguez, J.-R., Chevalier, V., Casas-Tinto, S., Triphan, T., et al. (2014). Cell types and coincident synapses in the ellipsoid body of *Drosophila*. *Eur. J. Neurosci.* 39, 1586–1601. doi: 10.1111/ejn.12537

Merighi, A., Polak, J. M., and Theodosis, D. S. (1991). Ultrastructural visualization of glutamate and aspartate immunoreactivities in the rat dorsal horn, with special reference to the co-localization of glutamate, substance P and calcitonin-gene related peptide. *Neuroscience* 40, 67–80. doi: 10.1016/0306-4522(91)90175-n

Müller, M., Homberg, U., and Kühn, A. (1997). Neuroarchitecture of the lower division of the central body in the brain of the locust *Schistocerca gregaria*. *Cell Tissue Res.* 288, 159–176. doi: 10.1007/s004410050803

Neuser, K., Triphan, T., Mronz, M., Poeck, B., and Strauss, R. (2008). Analysis of a spatial orientation memory in *Drosophila*. *Nature* 453, 1244–1247. doi: 10.1038/nature07003

Ofstad, T. A., Zuker, C. S., and Reiser, M. B. (2011). Visual place learning in *Drosophila melanogaster*. *Nature* 474, 204–207. doi: 10.1038/nature10131

Ottersen, O. P., Storm-Mathisen, J., Madsen, S., Skumlien, S., and Strømhang, J. (1986). Evaluation of the immunocytochemical method for amino acids. *Med. Biol.* 64, 147–158.

Pfeiffer, K., and Homberg, U. (2014). Organization and functional roles of the central complex in the insect brain. *Annu. Rev. Entomol.* 59, 165–184. doi: 10.1146/annurev-ento-011613-162031

Pfeiffer, K., and Kinoshita, M. (2012). Segregation of visual inputs from different regions of the compound eye in two parallel pathways through the anterior optic tubercle of the bumblebee (*Bombus ignitus*). *J. Comp. Neurol.* 520, 212–229. doi: 10.1002/cne.22776

Reischig, T., and Stengl, M. (2003). Ultrastructure of pigment-dispersing hormone-immunoreactive neurons in a three-dimensional model of the accessory medulla of the cockroach *Leucophaea maderae*. *Cell Tissue Res.* 314, 421–435. doi: 10.1007/s00441-003-0772-7

Sakura, M., Lambrinos, D., and Labhart, T. (2008). Polarized skylight navigation in insects: model and electrophysiology of e-vector coding by neurons in the central complex. *J. Neurophysiol.* 99, 667–682. doi: 10.1152/jn.00784.2007

Salio, C., Fischer, J., Wijkhuisen, A., Franzoni, M. F., and Conrath, M. (2001). Distribution and ultrastructure of the tachykinin-like immunoreactivity in the frog (*Rana esculenta*) spinal cord, notably, the dorsal horn. *J. Comp. Neurol.* 433, 183–192. doi: 10.1002/cne.1134

Schmeling, F., Tegtmeier, J., Kinoshita, M., and Homberg, U. (2015). Photoreceptor projections and receptive fields in the dorsal rim area and main retina of the locust eye. *J. Comp. Physiol. A Neuroethol. Sens. Neural Behav. Physiol.* 201, 427–440. doi: 10.1007/s00359-015-0990-y

Schmeling, F., Wakakuwa, M., Tegtmeier, J., Kinoshita, M., Bockhorst, T., Arikawa, K., et al. (2014). Opsin expression, physiological characterization and identification of photoreceptor cells in the dorsal rim area and main retina of the desert locust, *Schistocerca gregaria*. *J. Exp. Biol.* 217, 3557–3568. doi: 10.1242/jeb.108514

Schmitt, F., Stieb, S. M., Wehner, R., and Rössler, W. (2016). Experience-related reorganization of giant synapses in the lateral complex: potential role in plasticity of the sky-compass pathway in the desert ant *Cataglyphis fortis*. *Dev. Neurobiol.* 76, 390–404. doi: 10.1002/dneu.22322

Schürmann, F.-W., and Wechsler, W. (1970). Synapsen im Antennenhügel von *Locusta migratoria* (Orthoptera, Insecta). *Z. Zellforsch. Mikrosk. Anat.* 108, 563–581. doi: 10.1007/bf00339659

Seelig, J. D., and Jayaraman, V. (2013). Feature detection and orientation tuning in the *Drosophila* central complex. *Nature* 503, 262–266. doi: 10.1038/nature12601

Seelig, J. D., and Jayaraman, V. (2015). Neural dynamics for landmark orientation and angular path integration. *Nature* 521, 186–191. doi: 10.1038/nature14446

Seguela, P., Geffard, M., Buijs, R. M., and Le Moal, M. (1984). Antibodies against γ-aminobutyric acid: specificity studies and immunocytochemical results. *Proc. Natl. Acad. Sci. U S A* 81, 3888–3892. doi: 10.1073/pnas.81.12.3888

Steiger, U. (1967). Über den Feinbau des Neuropils im Corpus pedunculatum der Waldameise. *Z. Zellforsch. Mikrosk. Anat.* 81, 511–536. doi: 10.1007/bf00541012

Sternberger, L. A. (1979). *Immunocytochemistry*. New York, NY: John Wiley & Sons.

Tolbert, L. P., and Hildebrand, J. G. (1981). Organization and synaptic ultrastructure of glomeruli in the antennal lobes of the moth *Manduca sexta*: a study using thin sections and freeze fracture. *Proc. R. Soc. Lond. B Biol. Sci.* 213, 179–301. doi: 10.1098/rspb.1981.0067

Träger, U., Wagner, R., Bausenwein, B., and Homberg, U. (2007). A novel type of microglomerular synaptic complex in the polarization vision pathway of the locust brain. *J. Comp. Neurol.* 205, 288–300. doi: 10.1002/cne.21512

Varga, A. G., and Ritzmann, R. R. (2016). Cellular basis of head direction and contextual cues in the insect brain. *Curr. Biol.* 26, 1816–1828. doi: 10.1016/j.cub.2016.05.037

Venable, J. H., and Coggeshall, R. (1965). A simplified lead citrate stain for use in electron microscopy. *J. Cell Biol.* 25, 407–408. doi: 10.1083/jcb.25.2.407

Vitzthum, H., and Homberg, U. (1998). Immunocytochemical demonstration of locustatachykinin-related peptides in the central complex of the locust brain. *J. Comp. Neurol.* 390, 455–469. doi: 10.1002/(SICI)1096-9861(19980126)390:4<455::AID-CNE1>3.0.CO;2-#

Vitzthum, H., Müller, M., and Homberg, U. (2002). Neurons of the central complex of the locust *Schistocerca gregaria* are sensitive to polarized light. *J. Neurosci.* 3, 1114–1125.

Watson, A. H. D. (1988). Antibodies against GABA and glutamate label neurons with morphologically distinct synaptic vesicles in the locust central nervous system. *Neuroscience* 26, 33–44. doi: 10.1016/0306-4522(88)90125-x

Watson, A. H. D. (1990). Ultrastructural evidence for GABAergic input onto cercal afferents in the locust (*Locusta migratoria*). *J. Exp. Biol.* 148, 509–515.

Watson, A. H. D., and Burrows, M. (1982). The ultrastructure of identified locust motor neurones and their synaptic relationships. *J. Comp. Neurol.* 205, 383–397. doi: 10.1002/cne.902050407

Watson, A. H. D., Bévengut, M., Pearlstein, E., and Cattaert, D. (2000). GABA and glutamate-like immunoreactivity at synapses on depressor motorneurones of the leg of the crayfish, *Procambarus clarkii*. *J. Comp. Neurol.* 422, 510–520. doi: 10.1002/1096-9861(20000710)422:4<510::AID-CNE3>3.0.CO;2-O

Watson, A. H. D., and Laurent, G. (1990). GABA-like immunoreactivity in a population of locust intersegmental interneurones and their inputs. *J. Comp. Neurol.* 302, 761–767. doi: 10.1002/cne.903020408

Watson, A. H. D., and Schürmann, F.-W. (2002). Synaptic structure, distribution and circuitry in the central nervous system of the locust and related insects. *Microsc. Res. Tech.* 56, 210–226. doi: 10.1002/jemt.10031

Westfall, J. A. (1987). "Ultrastructure of invertebrate synapses," in *Nervous Systems of Invertebrates*, ed. M. A. Ali (New York, NY: Plenum), 3–28.

Wolff, T., Iyer, N. A., and Rubin, G. M. (2015). Neuroarchitecture and neuroanatomy of the *Drosophila* central complex: a GAL4-based dissection of protocerebral bridge neurons and circuits. *J. Comp. Neurol.* 523, 997–1037. doi: 10.1002/cne.23773

Conflict of Interest Statement: The handling Editor declared a past co-authorship based on data generated 7 years ago, though no other collaboration, with one of the authors UH and states that the process nevertheless met the standards of a fair and objective review.

The other author declares that the research was conducted in the absence of any commercial or financial relationships that could be construed as a potential conflict of interest.

frontiers in Behavioral Neuroscience

ORIGINAL RESEARCH
published: 03 August 2017
doi: 10.3389/fnbeh.2017.00142

In silico Interrogation of Insect Central Complex Suggests Computational Roles for the Ellipsoid Body in Spatial Navigation

Vincenzo G. Fiore[1]*, *Benjamin Kottler*[2], *Xiaosi Gu*[1] and *Frank Hirth*[2]*

[1] School of Behavioral and Brain Sciences, University of Texas at Dallas, Dallas, TX, United States, [2] Department of Basic & Clinical Neuroscience, Institute of Psychiatry, Psychology & Neuroscience, King's College London, London, United Kingdom

The central complex in the insect brain is a composite of midline neuropils involved in processing sensory cues and mediating behavioral outputs to orchestrate spatial navigation. Despite recent advances, however, the neural mechanisms underlying sensory integration and motor action selections have remained largely elusive. In particular, it is not yet understood how the central complex exploits sensory inputs to realize motor functions associated with spatial navigation. Here we report an *in silico* interrogation of central complex-mediated spatial navigation with a special emphasis on the ellipsoid body. Based on known connectivity and function, we developed a computational model to test how the local connectome of the central complex can mediate sensorimotor integration to guide different forms of behavioral outputs. Our simulations show integration of multiple sensory sources can be effectively performed in the ellipsoid body. This processed information is used to trigger continuous sequences of action selections resulting in self-motion, obstacle avoidance and the navigation of simulated environments of varying complexity. The motor responses to perceived sensory stimuli can be stored in the neural structure of the central complex to simulate navigation relying on a collective of guidance cues, akin to sensory-driven innate or habitual behaviors. By comparing behaviors under different conditions of accessible sources of input information, we show the simulated insect computes visual inputs and body posture to estimate its position in space. Finally, we tested whether the local connectome of the central complex might also allow the flexibility required to recall an intentional behavioral sequence, among different courses of actions. Our simulations suggest that the central complex can encode combined representations of motor and spatial information to pursue a goal and thus successfully guide orientation behavior. Together, the observed computational features identify central complex circuitry, and especially the ellipsoid body, as a key neural correlate involved in spatial navigation.

Keywords: insect brain, central complex, ellipsoid body, lateral accessory lobes, computational model, spatial navigation, cognitive map

OPEN ACCESS

Edited by:
Stanley Heinze,
Lund University, Sweden

Reviewed by:
Paul Graham,
University of Sussex, United Kingdom
Roy Ritzmann,
Case Western Reserve University, United States

***Correspondence:**
Vincenzo G. Fiore
vincenzo.g.fiore@gmail.com
Frank Hirth
frank.hirth@kcl.ac.uk

Received: *30 April 2017*
Accepted: *18 July 2017*
Published: *03 August 2017*

Citation:
Fiore VG, Kottler B, Gu X and Hirth F (2017) In silico Interrogation of Insect Central Complex Suggests Computational Roles for the Ellipsoid Body in Spatial Navigation. Front. Behav. Neurosci. 11:142. doi: 10.3389/fnbeh.2017.00142

INTRODUCTION

Ambulatory animals are constantly subject to changing stimuli. These include external sensory stimuli, such as light, temperature or food locations; and internal stimuli, such as body posture, position in space, thirst or hunger. Efficient mechanisms to identify, consolidate and recall information and appropriate motor actions are essential for the animal's ability to respond to the external stimuli, avoid obstacles, move away from potential threats or approach hedonic rewards. Accordingly, hunters, foragers or harvesters have evolved neural mechanisms that exploit the integration of changing internal and external stimuli to trigger action sequences in order to drive both goal-driven behaviors and reactive sensory-driven habits. The selection of appropriate motor commands allows the animal to change position in space or to interact with elements in the environment. This self-motion information is then computed jointly with new incoming sensory stimuli to consolidate memory of experienced action-outcome contingencies, in association with allocentric and egocentric representations. Eventually, the association of outcomes with a representation of sensory stimuli, body posture, and actions result in a mental map (Tolman, 1932; Collett et al., 2013), which guides adaptive behavior and is essential for intentional spatial navigation.

Like all ambulatory animals, insects express behaviors that result in intentional spatial navigation. For instance, complex visual features (Neuser et al., 2008; Ofstad et al., 2011) or antennal mechanosensations (Ritzmann et al., 2008; Varga et al., 2017) perceived whilst exploring an arena, can be learned and stored to subsequently recall an action (Neuser et al., 2008; Ofstad et al., 2011). However, it has remained contentious whether insects use spatial representations to guide their navigation (e.g., Cheeseman et al., 2014; Cheung et al., 2014) or rather their orientation behavior relies on a collective of guidance cues (Cruse and Wehner, 2011; Collett et al., 2013) that include neural correlates of head direction (e.g., Varga and Ritzmann, 2016), celestial compass cues (e.g., el Jundi et al., 2015) and configurations of visual stimuli in view-based panoramas (e.g., see Zeil, 2012; Seelig and Jayaraman, 2015; Weir and Dickinson, 2015). A key neural correlate involved in processing these guidance cues and mediating behavioral outputs resulting in spatial navigation is the central complex (CX) (Strausfeld and Hirth, 2013; Pfeiffer and Homberg, 2014; Turner-Evans and Jayaraman, 2016; Webb and Wystrach, 2016).

The CX is a central brain structure composed of midline neuropils comprising the protocerebral bridge (PB), the fan-shaped body (FB), the ellipsoid body (EB), the noduli and the lateral accessory lobes (LAL) (**Figures 1A,B**). Histological (Williams, 1975; Hanesch et al., 1989), immunocytochemical (Hanesch et al., 1989; Renn et al., 1999; Young and Armstrong, 2010; Kahsai and Winther, 2011; Boyan and Liu, 2016), and clonal analyses (Ito and Awasaki, 2008; Ito et al., 2013; Lin et al., 2013; Wolff et al., 2015) reveal the CX organization as a modular system of neuronal layers and columns (**Figure 1C**). Columnar neurons leading to and from the CX connect all its component neuropils (Ito and Awasaki, 2008; Lin et al., 2013; Wolff et al., 2015), which are themselves subdivided into modules. These modules encode spatial information about sensory events (Heinze and Homberg, 2007; Sakura et al., 2008; Heinze and Reppert, 2011; Seelig and Jayaraman, 2013). As shown for the EB, tangential layers of neural processes intersect columnar projections and modulate spatial representations of sensory events across modules (Vitzthum et al., 2002; Heinze and Homberg, 2007; Sakura et al., 2008; Heinze and Reppert, 2011; Rosner and Homberg, 2013). Specific sensory inputs (afferents signaling "**what**" is perceived and its features) are mapped across modules (afferents signaling "**where**" the stimulus is located with respect to the body and the environment), each representing a segment of sensory space (Strausfeld, 2012). These representations are relayed to the EB, which weights them according to input salience and strength of connectivity. Finally, the strength of connectivity can be modulated by dopamine-related learning processes (Waddell, 2013), so that the EB effectively integrates current and previous information about all its incoming sensory inputs. In turn, the EB processes its incoming input to release the inhibition of appropriate premotor programs in the LAL, selecting actions in response to the computed sensory stimuli (Fiore et al., 2015; Kottler et al., 2017).

This proposed model of CX functionality identifies the EB as a key node in mediating sensorimotor integration and action selection for reactive stimulus-responses and goal-directed behavior, thus driving purposeful spatial navigation. In support of this notion, recent studies identified columnar neurons that project from PB to EB where they form wedge-specific arborisations that together cover all layers and modules of the EB, and thus all segments of sensory space represented in the EB (Seelig and Jayaraman, 2015; Wolff et al., 2015; Omoto et al., 2017; **Figure 1D**). These studies propose that visual cues and their positions are represented in the EB relative to the animal's heading. If correct, this hypothesis suggests that columnar wedge-neuron activity encodes an internal compass that combines visual landmarks with self-generated (idiothetic) cues (Heinze, 2015). Despite these advances, the neural mechanisms underlying sensory integration and motor action selections have remained largely elusive. In particular, it is not clear how the CX exploits sensory inputs and encoded head and body orientation to realize motor functions associated with spatial navigation.

We previously proposed that all of these functions may rely on computational processes that can also be found in the vertebrate basal ganglia (Strausfeld and Hirth, 2013). In particular, transient winner-take-all competitions (Rabinovich et al., 2001; Afraimovich et al., 2008) may be a common solution across species for the essential functions of sensory noise suppression, detection and selection of salient inputs weighed by previous experience and sensorimotor integration (Fiore et al., 2015). Here we examine how these functions can be implemented by the CX, as a simulated insect is required to navigate arenas of increasing complexity, to reach two target regions, whilst avoiding obstacles. To solve its task, the simulated insect relies on a heterogeneous set of sensory information about body orientation and visual landmarks, organized in an egocentric representation. These inputs are processed in a bio-constrained neural model (i.e., whose structure is constrained

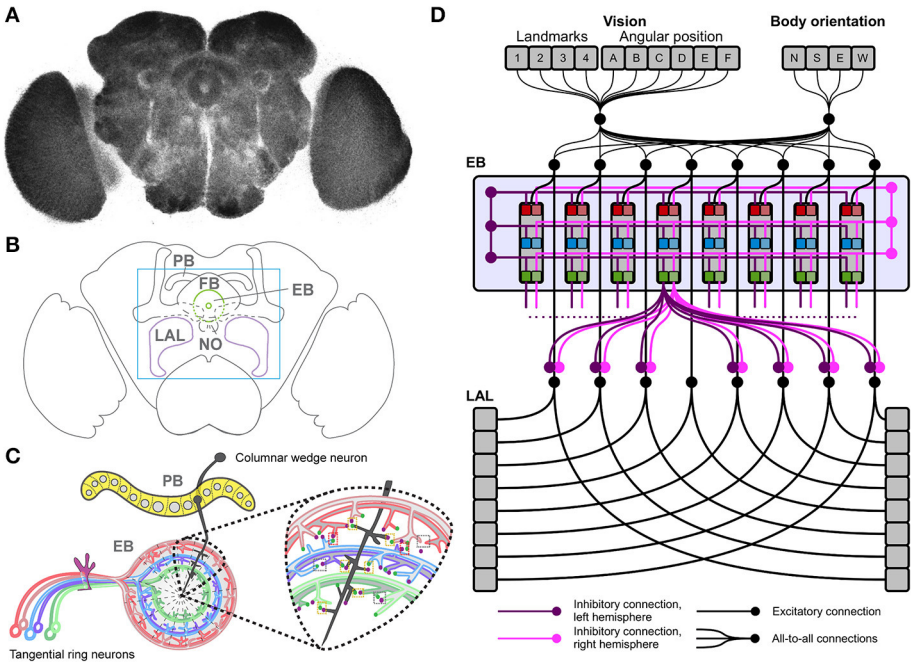

FIGURE 1 | The *Drosophila* central complex and derived architecture of the computational model. **(A)** Confocal image (color inverted) of a dissected adult *Drosophila* brain immuno-labeled with an antibody that specifically recognizes synaptic terminals. **(B)** Cartoon of adult *Drosophila* brain showing central complex neuropils (PB, protocerebral bridge; FB, fan-shaped body; EB, ellipsoid body; NO, noduli; LAL, lateral accessory lobes—mushroom bodies are shown for orientation); box indicates enlarged region in C. **(C)** Schematic summary of PB and EB to show key assumptions of computational model: columnar wedge neurons project to specific EB wedges (here shown for one in black), tangential ring neurons project in a subtype and layer-specific manner into EB ring (colour coded); the model assumes synaptic connections between both neuron types (see enlarged area for one wedge). **(D)** Architecture of the neural model, replicating the local connectome of the central complex in the connections among modules.

by known neuroanatomy) simulating the neural activity of the EB and LAL as parts of the CX. Our model relies on evidence-based assumptions (Ito et al., 2013; Lin et al., 2013; Seelig and Jayaraman, 2015; Wolff et al., 2015; Kottler et al., 2017) that a somatotopic columnar input organization and lateral inhibitions can generate transient winner-take-all competitions. The behavior of the simulated insect shows the activity in the ellipsoid body can integrate and encode inputs from different sensory sources, and successfully rely on visual information and body orientation to correctly estimate its position in space.

MATERIALS AND METHODS

Neural Architecture and Computational Features of the Model

We developed a neural model based on an architecture that replicates known connectivity of the CX, focusing on afferent and efferent EB projections (**Figure 1D**). The model relies on two core features, a loop architecture between EB and LAL, and lateral inhibition among tangential EB ring neurons, both of which are supported by clonal, immunocytological, and functional analyses (Hanesch et al., 1989; Kahsai and Winther, 2011; Lin et al., 2013; Seelig and Jayaraman, 2015; Wolff et al., 2015; Kottler et al., 2017).

The model simulates activity in the modules of EB and LAL in a continuous-time differential equation termed "leaky integrator," which is used to simulate the mean-field activity of an entire pool of neurons (Deco et al., 2008):

$$\tau_g \dot{u}_j = -u_j + b_j + \sum_i w_{ji} y_i \quad (1)$$

$$y_j = \left[\tanh(u_j)\right]^+ \quad (2)$$

Equation (1) defines the activation potential of a generic unit j and Equation (2) defines the final activation of the unit in a positive saturation transfer function. $\sum_i w_{ji} y_i$ represents the overall input reaching unit j from all units i and w_{ji} represents the connection weight between an input unit i and a target unit j. Finally, a bias b_j represents the basal activity of the unit j. The value of this constant is equal to 0 under all conditions, with the exception of those simulating either deactivation or overactivation of the EB, when the value is set < -0.5 for deactivation and >0.5 for overactivation, for all EB units.

The neural architecture of the model was based on the projections of columnar neurons which divide the CX into 8 units/columns per hemisphere; and tangential neurons which in the case of the EB project in a subtype specific manner to generate 3 layers of the EB neuropil (Strausfeld and Hirth, 2013; Pfeiffer and Homberg, 2014; Turner-Evans and Jayaraman, 2016; Webb and Wystrach, 2016). Hence our model consisted of 48 units for the EB (16 modules, also called

wegdes, each subdivided into 3 layers). Furthermore, based on neuroanatomical and functional studies (Williams, 1975; Hanesch et al., 1989; Namiki and Kanzaki, 2016) we assumed 16 units for the LAL (one unit per LAL segment or module, grouped in 8 units per hemisphere). Sensory information was organized in vectors, where elements represented landmark features and their allocentric position, body orientation of the simulated insect and its position in space (see subsections below). All elements in the input sources were connected with all modules in both EB and LAL, allowing for the integration of heterogeneous sensory information. Tangential ring neuron projections (Fiore et al., 2015; Kottler et al., 2017) were modeled following a computationally parsimonious assumption, which assumed symmetric lateral inhibitions within each layer and among all layers of the EB, per hemisphere (**Figure 1D**). Lateral inhibitions among layers and modules/wedges resulted in the competition among inputs and the subsequent selection of the strongest signal among competitors (see also: Kottler et al., 2017). In turn, this competition resulted in a transient winner-takes-all functionality, which replicated the structurally stable dynamics reported for the EB (Seelig and Jayaraman, 2015). This selection process carried out in the EB was biased by the weights of the connections streaming sensory information toward the EB itself. Thus, the behavior of the simulated insect ultimately depended on the configuration of the parameters representing the weights w_{ji} between sensory inputs and EB.

In the model, information processed in the EB (sensory integration and selection) was then streamed to the LAL via inhibitory connections (Fiore et al., 2015; Wolff et al., 2015), conveying EB-mediated selections into premotor outputs. The topology of the inhibitory connections linking EB–LAL has been only partially described in the literature. Thus, we completed the model connectivity relying again on a computationally parsimonious assumption, where all EB modules exerted an off-center gating function toward the two separate layers of the LAL (**Figure 1D**). Layers in the LAL encode premotor commands, which provide essential feedback to the EB in terms of self-motion information (Namiki and Kanzaki, 2016), besides triggering motor selections. In the simulated agent, LAL self-motion information is conveyed via parallel connectivity from both layers in the LAL toward all layers in the EB, completing the EB-LAL-EB loop. Motor selections were modeled in a simple correlation between activity in the eight modules of the two LAL layers and the execution of basic motor commands. For the spatial navigation task, we mapped the actions *move forward*, *turn right* (clock-wise) and *turn left* (counter-clockwise) to the activity of three arbitrary modules (per hemisphere). Activity in the remaining five modules (per hemisphere) was used to trigger a series of actions (e.g., grooming, eating, standing still etc.,) that did not produce any change in terms of the position of the simulated insect in the arena or its body orientation. Although these actions were not relevant in terms of spatial navigation, they were part of the transient competition for motor commands and could be selected in response to any combination of perceived sensory stimuli. Thus, the described configuration of motor commands was meant to illustrate how sensory integration can trigger a sequence of actions—it does not represent the entire repertoire of actions that can be performed by an insect. The specifications of our model are well supported by experimental evidence that identifies key roles for the EB in sensorimotor integration and goal-directed behavioral output (e.g., Martin et al., 1999; Heinze and Homberg, 2007; Neuser et al., 2008; Lebestky et al., 2009; Kong et al., 2010; Ofstad et al., 2011; Seelig and Jayaraman, 2015; Kottler et al., 2017) which are essential for spatial navigation.

Simulated Environment

We tested the navigation behavior of an artificial insect in a simulated environment that allowed manipulation of its complexity and of the source of sensory information available for the orientation of the simulated insect. Three different environments or arenas were used to limit the movements of the simulated insect and to set obstacles between a starting position and a target area. Independent of the complexity of the simulated environment, all arenas/environments were composed of 1600 distinct locations (40×40). In each of the different arenas, external *walls* defined the overall number of locations. The starting position of the simulated insect was randomly selected out of 100 locations (10×10) in the southwest of the arena. Two target areas were defined as squares of 10×10 locations, both of which were placed in the northern part of the arena, thus leading to a considerable distance between the artificial insect's starting location and the target area it had to reach (**Figure 2A**).

The complexity of the simulated environment was modified by introducing three conditions, characterized by an increasing number of obstacles that had to be circumnavigated in order to reach the target areas. Thus, in the environment termed "***open arena***" (**Figure 2A**), the simulated insect was able to change location by freely moving North, East, South or West. If the simulated insect reached any of the arena walls and tried to execute a command to move further, the command was ignored and the agent remained in its position. In the environment termed "***simple maze***" (**Figure 2B**), the arena presented internal obstacles as additional walls. These walls divided the arena in half with the exception of a narrow passage of one sector width (equal to 10 locations), thereby limiting the ability of the simulated insect to cross from South to North and vice versa. In the environment termed "***complex maze***" (**Figure 2C**), additional obstacles were introduced to further limit the movements of the agent, thereby forcing the simulated agent to execute a series of at least five well-timed turns to be able to reach a target area.

Simulated Sensory Information

The simulated insect relied on two sources of sensory information that were made available either in combination or alone.

Self-Motion

To illustrate the anterior-posterior orientation in relation to the arena's polarity (N-E-S-W), the simulated insect was graphically represented in videos and images with two red circles for the eyes (e.g., see **Figure 2D** and **Supplementary Videos**). This "body orientation" was encoded in a four dimensional vector characterized by a binary 0/1 activity. The activity of this

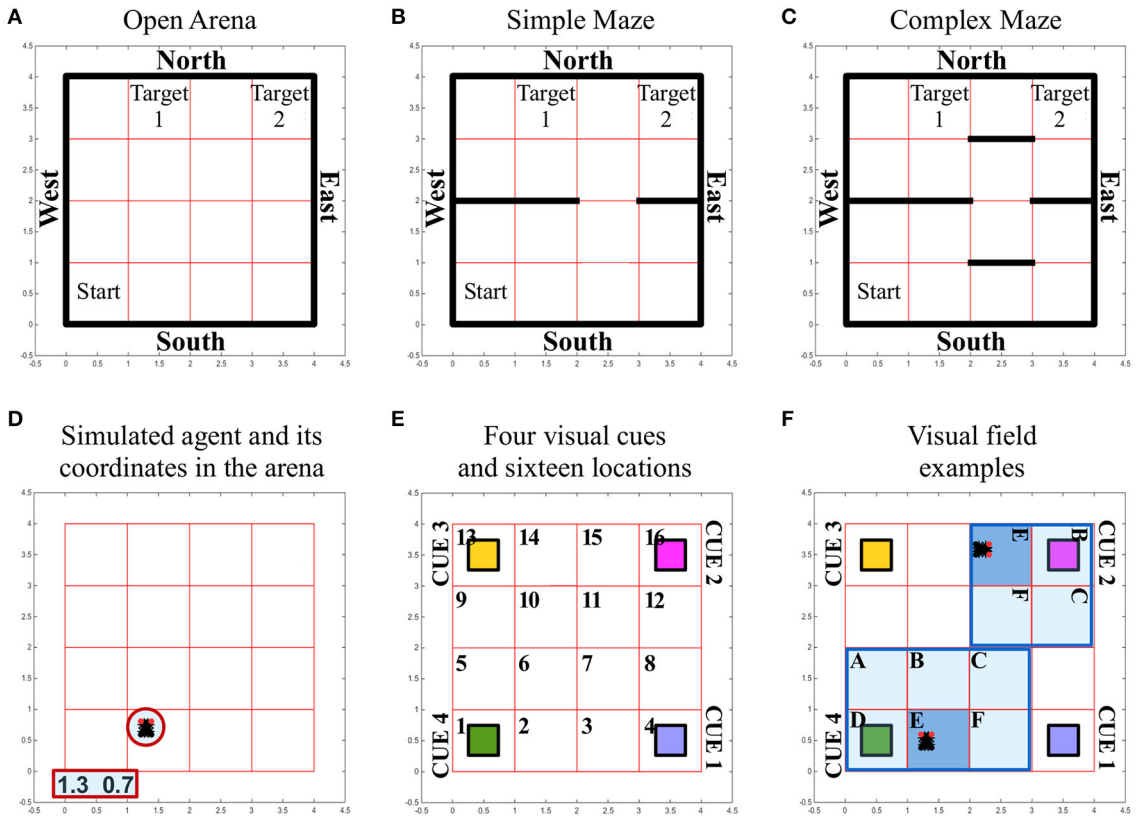

FIGURE 2 | Simulated environment and insect specifics. **(A–C)** Different arenas and corresponding boundaries for the spatial navigation tasks of the simulated insect: open arena **(A)**, simple maze **(B)** and complex maze **(C)**. Under all conditions, arenas are composed of 40 × 40 locations that can be occupied by the simulated insect while it navigates the virtual space. The simulated insect starts each trial in one location, randomly selected among the 100 locations characterizing the south-west sector of the arena, marked as "Start." The simulated insect can navigate the space freely for a limited time of 30 s of simulated time. The simulation is considered successful if the insect reaches any of the locations defining the target areas (marked as "Target 1" and "Target 2"). At each step of the simulation, the insect can select an action that allows it to leave the location it occupies and move into a new location north, south, east or west. These movements are only prevented if the location occupied by the insect is close to a *wall* (marked in black), in which case the action is not executed and the agent keeps its previous position. **(D)** The simulated insect is graphically represented with black segment for its body and two small red circles for its eyes, to indicate the front of the simulated insect. At any time the location occupied by the insect is reported in terms of coordinates, outside the arena. **(E)** Grid organization and perceived landmarks in the arenas. Under all conditions, the arena is divided into 16 sectors composed of 10 × 10 locations. Four, differently colored, visual cues or landmarks are located at the four corners under all conditions. **(F)** Illustration of the way the visual field adapts depending on the position and body orientation of the simulated insect. The agent can perceive a visual landmark, activating the corresponding visual input to a value of 1, only if this is found in the sector the insect is occupying (E, dark blue sector of the visual field). If the landmark is found in a sector on the front-left (A), front (B), front-right (C), left (D), or right (F) of the simulated insect (pale blue sectors of the visual field), the corresponding visual input signal the presence of the cue with a value of 0.5. Angular position units encode, with a 0/1 activity, an egocentric representation of the position of the landmarks with respect to the body of the simulated insect (one unit per each sector in the visual field). In panel (F), we illustrate two arbitrary examples of the egocentric landmark representation in terms of sensory input. In these examples, angular position units would signal the presence of a generic landmark on the left of the body in one case (cue 4 in sector D of the visual field) or in front of the body in the other case (cue 2 in sector B of the visual field). See also related **Supplementary Videos**.

vector changed with the execution of turning behavior and it was propagated toward the CX. Jointly with the vector of activity recorded in the LAL and determining motor selections in the simulated agent, these two signals provided the agent information about self-generated motion and posture.

Vision

Any movement resulting in changing the position of the simulated insect or its body orientation could result in the modification of its visual field. To simulate this dynamic change, we first divided the arenas into 16 sectors of 10 × 10 locations (**Figure 2E**). Second, we defined the visual field as covering the sectors in front and on the side of the insect, in a putative 180° forward-facing arc (**Figure 2F**). If any of the visual cues or landmarks located at the four corners of the arena entered the visual field of the simulated insect, its presence was encoded in two signals, representing objects in terms of "*what*" is perceived, and its angular position, an egocentric "*where*" they are perceived. We simplified the neural representation of the unique visual features of each landmark (i.e., color) by providing a different *visual unit* per each landmark, in a localistic representation. The activity of a visual unit was set to 1 if the corresponding landmark was located in the same sector occupied by the simulated insect. The same value was set to 0.5 when a cue was located anywhere

else in the visual field, therefore responding to the presence of a landmark independently of its position. To spatially represent and differentiate between landmarks located, for instance, on the left rather than on the right of the body, a second source of visual input was conveyed via six *angular position units*. These units encoded, with a binary 0/1 activity, an egocentric representation of the position of the landmarks with respect to the body of the simulated insect (i.e., each unit was active to signal the presence of a landmark located, respectively: left, front-left, front, front-right, right, or in the same sector of the simulated insect body; **Figure 2F**). In contrast to visual units, angular units could not differentiate among landmarks, so that the agent needed to integrate both sources of visual information in order to determine which landmark was visible and where.

Putative Desired Outcomes

We explored whether the modeled CX could store multiple sequences of actions at the same time, and recall the correct one, depending on a desired outcome. Therefore, we provided the modeled CX with two "biases" simulating a physiological assessment of the body status (e.g., representing *hunger* and *thirst*). Under this condition, termed "***intentional spatial navigation,***" each of the two target areas was assumed to satisfy only one of the two desired outcomes: target 1 was associated with bias 1 and target 2 was associated with bias 2. The biases were activated in sequence and maintained active until the end of the trial time or until the appropriate target area was found.

Parameter Estimation

The selection process eventually carried out in the EB is biased by the weights of the connections streaming sensory information toward the EB itself. Thus, the behavior of the simulated insect ultimately depends on the configuration of the parameters representing the weights w_{ji} between sensory inputs and EB. In a real-life experiment, an insect would randomly explore the physical equivalent of the proposed simulated arenas, eventually reaching one of the target areas. In presence of unexpected positive outcomes (e.g., food or water), reinforcement learning processes would occur (Sutton and Barto, 1998), thereby altering the connection weights between sensory regions and the EB (Waddell, 2010, 2013). In the long run this process results in instrumental conditioning, effectively generating and storing motor responses to perceived stimuli in the connection weights that bias the selection process in the EB. For the time being, we did not simulate fast dopamine burst firings in our model, which are essential in regulating the learning process (Schultz, 2002; Waddell, 2010, 2013). Therefore, we tested the simulated insect under the theoretical assumption that it had already completed its training and formed its stimulus-response associations. This assumption entails there are configurations of connection weights w_{ji} that allow the simulated insect to exploit the sensory information and recall a path of motor responses to navigate the arena. We looked for such configurations of parameters relying on a Monte Carlo method for parameter estimation and tested the simulated insect in two million randomly sampled configurations, or behavioral phenotypes, per each condition.

Software

The model, Monte Carlo parameter estimation and simulated interaction between environment and agent were developed and run in MatLab in *ad hoc* libraries.

RESULTS

We exposed the simulated insect to three different arenas of increasing complexity. The sensory inputs conveyed information about visual landmarks and self-motion that changed dynamically, depending on body orientation of the simulated insect and its location in the arena. We hypothesized the simulated insect can rely on the accessible information as guidance cues for both reactive sensory-driven and intentional spatial navigation (**Table 1**). Our model explored two key assumptions:

Columnar Wedge Neurons Integrate Visual Landmarks with Idiothetic Cues

Visual information available to the insect (**Figure 2E**) was simulated by two signals, encoding the perceived object features and egocentric location. Each of the four *visual units* was used to respond to the presence of a specific landmark in the visual field (**Figure 2F**), independently of its egocentric position. Information about the egocentric position of perceived landmarks was conveyed via six (for landmarks located in a sector on the left, right, front-left, front-right or front of the insect body, or in the same sector of the agent) *angular position units*, which could not differentiate among landmarks. Our simulated agent had to integrate both types of visual information jointly with body orientation and self-motion feed-back information to solve the task and accomplish purposeful navigation. This process of sensory integration simulated information encoded in the real PB->EB columnar wedge neuron activity (Seelig and Jayaraman, 2015) that combines visual landmarks with self-generated cues (Heinze, 2015).

Tangential Ring Neurons Mediate Motor Action Selection

In addition to columnar wedge neurons, we included tangential ring neurons of the EB into the model architecture. Based on lineage analyses revealing their terminal arborisations (Ito et al., 2013; Lin et al., 2013; Wolff et al., 2015), we simulated

TABLE 1 | Successful behaviors over attempts ratios.

Available Input sources	Open arena	Simple maze	Complex maze
Vision +	Target 1–6,950:10^6	Target 1–67:10^6	Target 1–0.5:10^6
Body orientation	Target 2–1,335:10^6	Target 2–175:10^6	Target 2–18:10^6
Vision	Target 1–0:10^6	Target 1–0:10^6	Target 1–0:10^6
	Target 2–0:10^6	Target 2–0:10^6	Target 2–0:10^6
Body orientation	Target 1–0:10^6	Target 1–0:10^6	Target 1–0:10^6
	Target 2–0:10^6	Target 2–0:10^6	Target 2–0:10^6

three ring neuron subtypes and layers (R1, R2/4, and R3), each divided into 16 wedges, and implemented connections between columnar wedge and tangential ring neurons in a layer- and wedge-specific pattern in the EB ring neuropil (**Figures 1C,D**). Given the lack of information about EB internal organization or hierarchy among layers, we implemented symmetric lateral inhibitions among ring neurons (Fiore et al., 2015; Kottler et al., 2017). These lateral inhibitions established a competition among incoming inputs, which resulted in the transient selection of salient stimuli (Rabinovich et al., 2001; Afraimovich et al., 2008). This transient winner-takes-all functionality was consistent with the dynamics reported for the EB (e.g., Seelig and Jayaraman, 2015; Kottler et al., 2017). Finally, EB-mediated selections were conveyed into premotor outputs via the inhibitory gating exerted by the EB toward the LAL. The simulated LAL encoded premotor commands that triggered motor activity and provided essential feedback of self-motion information (Namiki and Kanzaki, 2016).

In silico Interrogation of EB-Mediated Spatial Navigation

We applied these assumptions in our model and utilized the *Monte Carlo* method to compute two million randomly generated patterns of parameters or behavioral phenotypes. This allowed us to investigate configurations of parameters that might have enabled the simulated insect to reach the target areas by responding to incoming sensory stimuli, under each condition. We used this sampling to determine a ratio that captures the number of successful navigations per million attempts, per condition. The resulting value thus provides a proxy for the duration of a putative exploration required to successfully find a target area in the arenas. High ratio values correspond to frequent discovery of successful configurations of parameters, or alternative successful paths for the simulated insect, therefore implying a short exploration time. As expected, the resulting ratios suggested that successful spatial navigation is dependent on the complexity of the arena explored and the quality and combination of available sensory sources (**Table 1**).

Sensory-Driven Navigation

Under the condition termed as "open arena" the simulated insect was able to change location by freely moving North, South, East or West. Therefore, the optimal behavior, marking the shortest path between starting location and target area, required only one turn, to the left (**Figure 3A**, see also **Supplementary Videos 1**, **2**). Nonetheless, many other suboptimal behaviors (longer than the shortest path) were still successful, allowing the simulated insect to reach the target area within the time limit, despite the fact they relied on multiple turns and unnecessarily long paths. Information provided by vision and self-motion allowed the algorithm to find 6950 successful behavioral phenotypes per million attempts to reach target area 1 and 1,335 per million attempts to reach target area 2. Neither visual information nor self-motion information, considered separately, proved to be sufficient to solve the task.

In the "simple maze" arena, the internal walls divided the arena in half, with a narrow passage limiting the movements of the simulated insect from its starting point toward both targets. The arena termed "complex maze" introduced further internal walls that required the simulated insect to execute multiple turns to reach the target areas. Independently of the target area, optimal behavior required two turns in the simple maze (**Figure 3B**, see also **Supplementary Videos 3**, **4**) and five turns in the complex maze (**Figure 4**, see also **Supplementary Videos 5**, **6**). These limits significantly reduced the number of suboptimal behaviors that could successfully solve the task, thus diminishing the chances the search algorithm would be able to find solutions via random sampling. Nonetheless, the search algorithm found several successful configurations of parameters under both simple maze and complex maze conditions (**Table 1**). These allowed the simulated insect to use visual cues and body orientation information to trigger the appropriate sequence of actions, resulting in turns and navigation behavior to avoid the obstacles and reach the target areas. Neither of the input sources, considered alone, endowed the search algorithm with a successful behavior (**Table 1**).

Under all conditions of environment complexity, these tests show that the simulated EB was able to correctly estimate the position of the agent in space via the integration of sensory information. This process resulted from the weighed transformation of a flow of sensory inputs in a sequence of selections. By establishing a winner at each step in the competition among received inputs, the EB was then able to gate all but a single motor response. In turn, this clear-cut transition of activities in the LAL (**Figure 5A)** generated the visible spatial navigation of the simulated insect. Interestingly, in the complex maze arena, successful navigation correlated in several instances with periodic oscillations among EB modules (**Figure 4**). These oscillations were favored by the self-motion information conveyed by the body orientation units and premotor activity. Due to these inputs, the execution of turning behavior alters the incoming input and, because it is becoming part of the sensory input, is affecting the execution of future actions. This information loop resulted in oscillatory activity and cycles of motor sequences, thereby defining a cyclic attractor.

Navigation with Altered Activity Levels of EB Layers and Modules

To further explore the role of the EB in spatial navigation, we simulated either the deactivation or the over-activation of EB layers and modules, by manipulating the value of the constant b_j in equation 1. In the first set of manipulations, any decrease in the activity of EB layers resulted in a proportional decrease of the inhibitory gating function toward the LAL. The model was robust to low levels of manipulation ($b_j = -0.5$). In contrast, the more EB modules and layers were artificially impaired in their activity, the higher the chances of simultaneously co-activating multiple modules of the LAL ($b_j < -0.5$). This co-activation was interpreted in the model as the attempt to trigger multiple, conflicting motor outputs, such as "*turn left and right at the same time*" (cf. **Figures 5A,B**).

In the second set of manipulations, we artificially increased the baseline activity of EB layers and modules. This altered

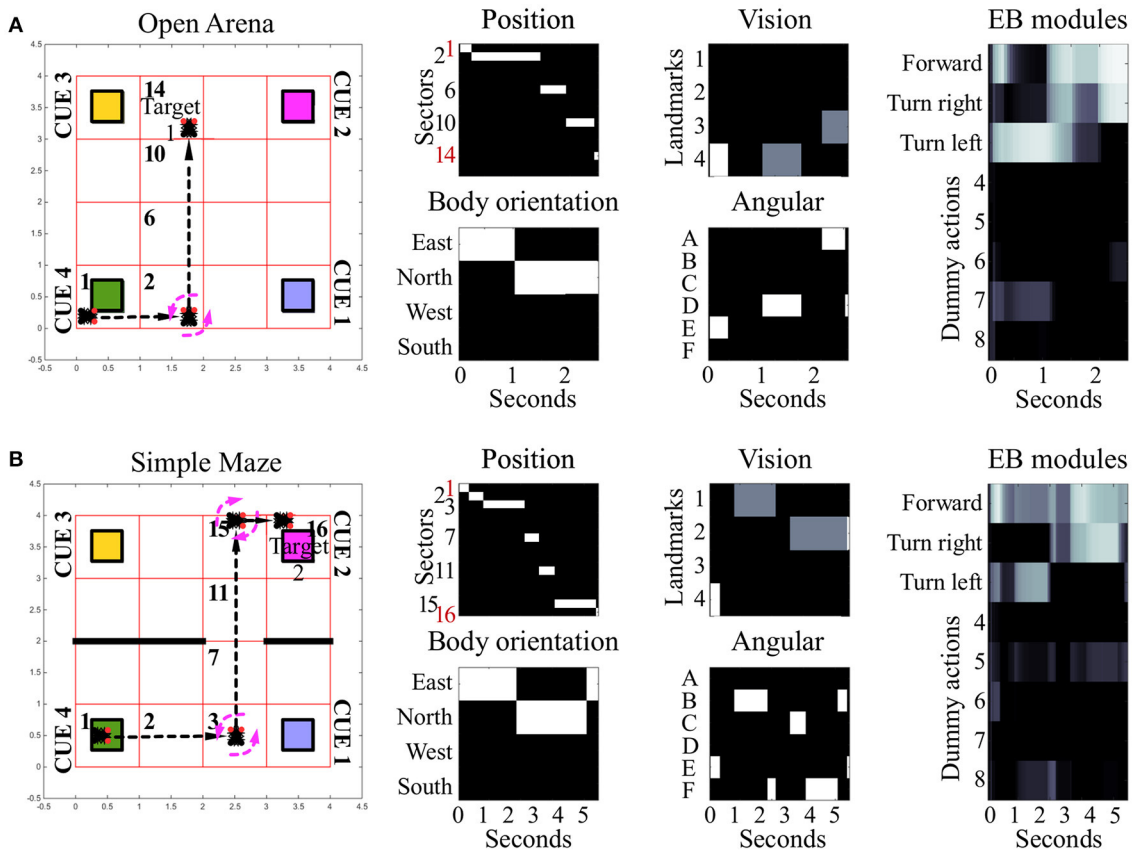

FIGURE 3 | Examples of spatial navigation under the conditions *open arena* and *simple maze*. **(A)** Example of navigation in the open arena, in which the simulated insect walks from its starting position toward the target area 1. In this example the simulated insect starts from sector 1, then turns left whilst in sector 2, and proceeds forward crossing sectors 6 and 10, to reach the target in sector 14 (see also related **Supplementary Videos 1, 2**). **(B)** Example of navigation in the simple maze from starting position toward target area 2. Under this condition, the simulated insect has to move east from its starting position, crossing sector 2, to turn left whilst in sector 3. Then it has to move north, across sectors 7 and 11, before turning right, whilst in sector 15, and complete the path by reaching sector 16 (see also related **Supplementary Videos 3**, **4**). The path of the simulated insect is also represented with a black and white heat-map under the label "Position." This heat-map allows to track the position of the simulated insect at any step of the simulation, where a binary 0/1 activity encodes the presence of the agent in any of the sectors of the arenas (16 units, one per sector). The inputs reaching the EB are reported under the labels: "*body orientation*" (4 units, one per possible direction, binary 0/1 activity), "*vision*" (4 units, one per landmark or visual cue, responding with fixed values of 0, 0.5, or 1, depending on the distance of the landmark), and "*angular*" (6 units, one per egocentric position of any landmark in the visual field, responding with a binary 0/1 activity). Finally, the black and white heat-map, labeled "EB modules," represents the activity of the modules in the EB in a single hemisphere. This heat-map responds with continuous values between 0 and 1 and encodes the average activity across the three layers of the EB ring neuropil. In the simulated EB, the competition among modules triggers the selection of one among eight possible actions via gating of LAL premotor activity. The only actions resulting in changes of the simulated insect position or body orientation are encoded in the first three modules as follows: move forward (module 1), turn left (module 2) and turn right (module 3). The other five actions remain part of the competition in the EB, but represent motor activities (e.g., grooming, eating, standing still etc.,) which do not result in movement in the arena and thus do not change spatial navigation behavior.

the signal to noise ratio in the entire CX, impairing the transient stability of stimulus-driven dynamics characterizing the EB under control conditions. At lower levels of over-activation ($b_j = 0.5$), the simulated insect required more time to change a selected behavior. This effect of over-activation is highlighted by a comparison we established for 50 (randomly selected) configurations of parameters that were found to be successful in reaching either of the two target areas in the open arena, whereby the simulated insect relied on all sensory input sources. These successful configurations were tested again after over-activating one layer in the EB. The comparison showed a significant increase in the simulated time required to reach the target area [4.9 ± 2.3 seconds vs. 3.6 ± 1.3 seconds, $p < 0.001$, $t_{(49)} = -3.58$]. Finally, at high levels of over-activation affecting all EB layers ($0.5 < b_j < 1.0$), the ability of the simulated insect to perform any selection and change it in response to new incoming stimuli was compromised, resulting in irresponsive and unsuccessful navigation behavior (cf. **Figures 5A,C**).

Intentional Spatial Navigation

Under this condition, we tested whether the connectome of the CX, as defined in our model, could account for the flexible selection among different courses of action and navigation paths (e.g., Jourjine et al., 2016). Depending on interoceptive signals (e.g., hunger or thirst), the simulated

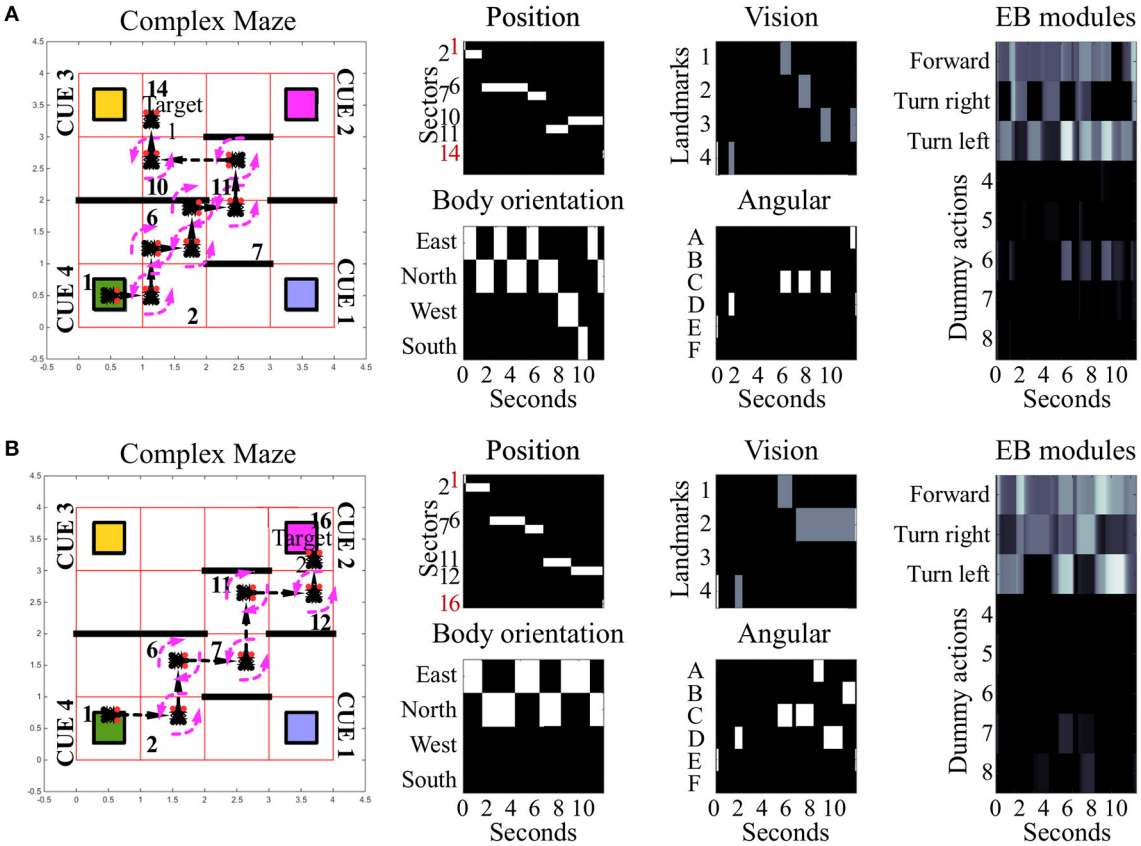

FIGURE 4 | Examples of spatial navigation under the complex maze condition. Both panels illustrate examples of navigation under the complex maze condition (see also related **Supplementary Videos 5**, **6**). **(A)** Motor behavior of the simulated insect, from its starting position toward target area 1. To avoid the obstacles in the arena, the insect turns 7 times and crosses 7 sectors. **(B)** Motor behavior displayed by the simulated insect to reach target area 2. In comparison to **(A)**, the insect reaches its target crossing 5 sectors in total. Under this maze condition, obstacle avoidance requires 5 turns in both versions of the task with the example in **(A)** reporting sub-optimal behavior. In both examples, the path of the simulated insect can be tracked in a black and white heat-map under the label "Position." This heat-map continuously records the position of the agent during the simulation time, responding with a binary 0/1 activity to the presence of the agent in any of the sectors of the arenas (16 units, one per sector). The inputs reaching the EB are reported under the labels: "*body orientation*" (4 units, one per possible direction, binary 0/1 activity), "*vision*" (4 units, one per landmark or visual cue, responding with fixed values of 0, 0.5, or 1, depending on the distance of the landmark), and "*angular*" (6 units, one per egocentric position of any landmark in the visual field, responding with a binary 0/1 activity). Finally the black and white heat-map, labeled "EB modules," represents the activity of the modules in the EB in a single hemisphere. This heat-map responds with continuous values between 0 and 1 and encodes the average activity across the three layers. In the simulated EB, the competition among modules triggers the selection of one among eight possible actions via gating of LAL premotor activity. Activity in the LAL triggers the execution of 8 different actions which can all be selected via the gating function exerted by the EB. Three of these actions result in changes of body orientation or position of the simulated insect and are encoded in the first three modules: move forward (module 1), turn left (module 2) and turn right (module 3). The remaining five actions putatively represent motor activities, such as grooming, eating or standing still which are not graphically represented in terms of behavioral execution.

insect had to decide which of two known repertoires to recall. Each repertoire putatively allowed to reach one of the two desired outcomes (e.g., food or water), each located in a different target area. In comparison with the tests simulating sensory-driven navigation, under this condition, a configuration of parameters or behavioral phenotype was considered successful if it allowed reaching both target area, in a sequence determined by the desired outcome. The search algorithm found a ratio of 90 solutions per million behavioral phenotypes, under the condition of open arena. The simple and complex maze condition provided one and zero solutions per million attempts, respectively (see also **Supplementary Videos 7**, **8**).

DISCUSSION

Previous studies identified the central complex as a key neural correlate involved in processing sensory guidance cues and mediating behavioral outputs that together orchestrate spatial navigation in insects (Strausfeld and Hirth, 2013; Pfeiffer and Homberg, 2014; Turner-Evans and Jayaraman, 2016; Webb and Wystrach, 2016). However, the neural mechanisms underlying sensory integration and motor action selections have remained largely elusive. In particular, it is not yet understood how the CX exploits sensory inputs, including internal representations of head-body orientation, to realize motor functions associated with spatial navigation. Here we presented an *in silico* interrogation of

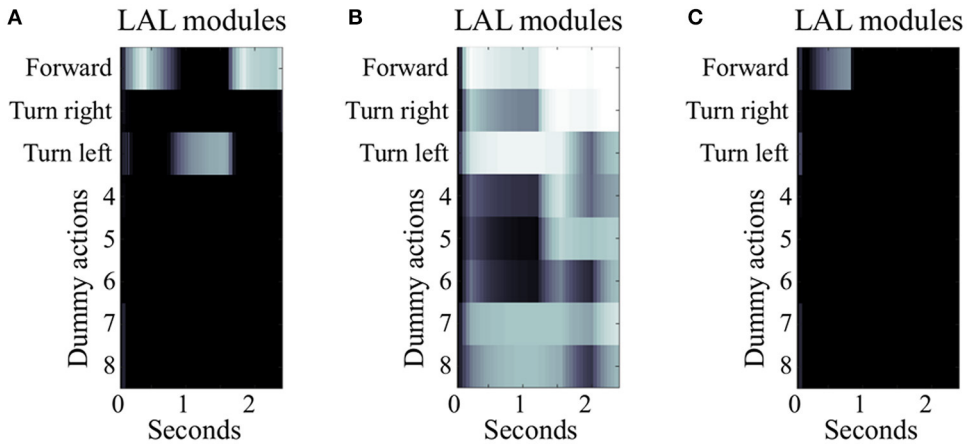

FIGURE 5 | Simulated LAL under different conditions of EB manipulation. The three panels illustrate 2.5 s of simulated activity recorded in the LAL, single hemisphere, under different condition of EB manipulation. **(A)** Under control condition, the heatmap shows differentiated activity in the modules of the LAL, with transient selections due to the gating inhibition performed by the EB. In this example, the simulated insect successfully moves forward, turns left, and moves forward again until it reaches target area 1. **(B)** Under the condition of EB deactivation, the gating function is diminished leading to general overactivation of several modules in the LAL and loss of differentiation in the signal. In this example, the simulated insect is able to perform the initial motor activity, but it stops when the actions "forward" and "turn right" become both strongly active. **(C)** Under the condition of EB overactivation, the gating function exerted by EB on LAL is potentiated. In this example, LAL is only able to trigger one action (move "forward") at the beginning of the simulation, when the visual input is strong enough to overcome the inhibition provided by the EB. As soon as the simulated insect changes its location and the visual input is not accessible, the remaining sensory stimuli are unable to drive any premotor response, leaving the simulated insect motionless.

the computational role the CX can play in sensory integration for motor action selection and spatial navigation. A simulated insect was tasked to navigate a series of environments of increasing complexity, in order to reach either one of two or both target areas in 2-dimensional arenas, whilst avoiding obstacles. The CX, which orchestrated changes in orientation and forward movements of the simulated insect, was characterized by a bio-constrained neural connectome (Fiore et al., 2015; Wolff et al., 2015; Kottler et al., 2017). The simulated insect relied on this structure to process a variety of sensory inputs, store navigation strategies and recall them as either a response to the stimuli perceived or depending on desired outcomes.

The simulations show our model of the CX is compatible with the sensory-driven multi-stable dynamics that characterize the presence of multiple attractor states (Fiore et al., 2015). This key computational feature has been formally described as an essential requirement for action selection across species, as these dynamics allow a neural system to perform a transient winner-take-all competition (Rabinovich et al., 2001; Afraimovich et al., 2008). Such competition, established among weighed sensory inputs, grants the suppression of noise and weak competitors, but does not prevent adaptation, so that the winning signal can change as a function of the sensory input. In the simulations, a continuous stream of sensory inputs is processed in our bio-constrained model of the CX to select sequences of actions resulting in spatial navigation. Furthermore, the simulations show this neural structure integrates multiple sensory sources, simulating how action selection and navigation can be guided by weighed information about polarized light, visual landmarks, view-based panoramas or self-motion and body orientation (Neuser et al., 2008; Ritzmann et al., 2008; Lin et al., 2014; Seelig and Jayaraman, 2015; Varga and Ritzmann, 2016; Omoto et al., 2017).

This process of sensory-driven motor selection is weighed by the columnar formation characterizing the CX, and in particular afferent EB connectivity. In the proposed model, the parameters regulating the weights of EB afferents and associated behavior are fixed and determine reactive responses. These weights could be either genetically determined, identifying innate motor behaviors, or they can be shaped by experience, as found in dopamine-dependent learning processes (Waddell, 2010, 2013; Lin et al., 2014). The latter case entails the insect would be able to form sensory-motor memories about stimulus-response associations, akin to habits.

Finally we tested whether our model could also account for a simplified form of intentional navigation that would overcome the limits posed by reactive sensory-driven navigation. In our test, we show the simulated CX could efficiently store two courses of actions in a single configuration of parameters or behavioral phenotype, each leading to a different target area. This feature allowed the model to arbitrate among different paths and select the sequence of actions that could satisfy a desired outcome. Our computational investigation suggests the CX can form rudimentary representations of space-related action-outcome contingencies and trigger the sequence of movements required to reach a desired position in space. Such a combined representation of motor and spatial information can be exploited to guide navigation and pursue a goal. We argue that the presence of this form of spatial memory can be an indication of a rudimentary mental representation of the environment (Tolman, 1932; Cheeseman et al., 2014).

In our simulations, we assumed that, to produce a simplified motor output, the neural system integrated different sources of information: (1) visual landmarks in the arena and their angular position; (2) body orientation and self-motion. The simulations show none of these input sources was sufficient, if considered

alone, to guide the behavior of the simulated insect toward any of the target areas. Thus, the EB was required to integrate its multisensory inputs to generate a transient selection that would adapt to the continuous change of sensory information. The output of the EB in turn could "gate" the appropriate premotor response in the LAL, generating a sequence of actions in response to this multisensory stream of inputs. Importantly, self-localization in space can be accomplished also by relying on sensory integration of non-visual sources. For instance, antennal mechanosensations, which are also conveyed toward the EB (Ritzmann et al., 2008; Harley and Ritzmann, 2010; Guo and Ritzmann, 2013) can provide information about obstacles and landmarks, where surface features take the place of color or celestial e-vector orientations of polarized light (Heinze and Homberg, 2007). Therefore, these sensory inputs can be exploited also by nocturnal animals to trigger sequences of actions and guide successful spatial navigation (el Jundi et al., 2015).

This hypothesis, assuming multi-stable dynamics for the generation of sequences of actions, may seem at odds with recent findings, which suggest that the EB is characterized by ring attractor dynamics encoding an abstract internal representation of the fly's heading direction (Seelig and Jayaraman, 2015; Kim et al., 2017). Indeed, these studies show visual cues presented to head-fixed *Drosophila* result in a bump-like activity pattern largely confined to one EB module/wedge that can move along the EB and its wedges according to position changes (Seelig and Jayaraman, 2015; Kim et al., 2017). These dynamics have been interpreted as indicative of the presence of a ring attractor, which could be implemented either in specific layers of the EB (e.g., E-PG neurons as suggested by (Kim et al., 2017)) or in the entire neuropil. Different from multi-stable dynamics which are characterized by a finite set of separate stable states, in a ring attractor an infinite set of contiguous stable states respond in the continuum to changes in the input stimuli. These dynamics are reminiscent of those suggested for head direction cells in mammals (Taube, 2007), which encode present head and body direction. Despite compelling data showing how changes in orientation toward visual stimuli are encoded in the EB, the dynamics reported in these studies (Seelig and Jayaraman, 2015; Kim et al., 2017) have also highlighted the presence of clear discontinuity in the state transitions, as a function of the stimulus position (Kim et al., 2017–see their video s9 and related model comparison discussion).

We argue, a different interpretation of these data is supported by both our model and recent computational (Kakaria and de Bivort, 2017; Varga et al., 2017) and functional analyses (Omoto et al., 2017). This interpretation suggests information about body orientation is encoded upstream of the EB wedges and propagated toward the EB as one of several sensory inputs. Importantly, our interpretation does not limit the EB to the representation of head and body orientation, as the ring attractor hypothesis might suggest. The problem with such limitation of EB functions is that the gating exerted on the premotor area of the LAL would be guided by ring attractor dynamics, and would be reduced to the execution of changes of head and body orientation. Such a conclusion would conflict with data showing the important role of the EB in a wide range of motor and cognitive responses to diverse sensory stimuli, including e.g., flying (Weir and Dickinson, 2015), walking (Strauss and Heisenberg, 1993; Kottler et al., 2017), or place learning (Ofstad et al., 2011). All these functions are aided by the presence of a head direction information, as changes of position in space generally take into account the actual body orientation. Nonetheless, these motor and memory functions do not require, nor are limited to, the representation of head and body orientation, as an agent can perform multiple actions (walking, flying, grooming etc.) independently of its body orientation.

Despite the inclusion of several known features characterizing the local connectome of the CX, we acknowledge the presence of important limitations in the proposed model. Several aspects of the neural organization of the EB have not been described in the literature, yet. Details regarding those aspects of the model that come from biological data as stated in the literature as well as limitations in that data set that caused us to make reasonable assumptions can be found in the Methods section. For instance, a plausible hierarchy among EB layers (Fiore et al., 2015) would configure pathways of information processing that would affect the computational functions of the entire CX. Thus, further developments of the model will be necessary to include the micro-organization of the internal structures of the CX. Nonetheless, the dynamics characterizing our model rely on the macro organization of the connectivity among internal structures of the CX and suggest computational roles that account for a wide variety of data and behaviors. In particular, it is the combined effect of columnar input organization and lateral inhibitions that results in the hypothesized transient winner-take-all competitions essential for action selections and their assembly into action sequences. Furthermore, columnar connectivity targeting distinct modules in EB and LAL and associated multi-stability may indicate a hierarchical organization, akin the functional anatomy of the vertebrate basal ganglia (Fiore et al., 2015). In vertebrates, information about head and body orientation is found in the striatum as part of multiple sensory inputs that are computed in this nexus of the basal ganglia (Taube, 2007; Kim et al., 2014; Barter et al., 2015).

Our findings reveal that depleted activity in multiple EB layers and wedges cause conflicting motor output, whereas simultaneous co-activation of multiple EB layers and wedges result in random and ultimately unsuccessful spatial navigation. In the first case, too many conflicting motor commands are selected (*you can't turn left and right at the same time*), and in the second case no motor command is selected, thus causing inaction comparable to indecision or lack of motivation. In both cases, the net result *inaction* is caused by impaired action selection which in turn affects spatial navigation. Our computational data suggest that the functional nexus between wedge-specific columnar PB-EB (Green et al., 2017; Turner-Evans et al., 2017) and EB-LAL (Fiore et al., 2015) feedback loops, together with inhibitory activity from EB ring neurons (Kottler et al., 2017), code for neural mechanisms underlying sensory integration and motor action selection for spatial navigation. This hypothesis is supported by recent studies in *Drosophila* (Green et al., 2017; Turner-Evans et al., 2017) and cockroaches (Martin et al., 2015; Varga and Ritzmann, 2016) and leads to testable predictions, for example that targeted layer and/or wedge-specific activity

manipulations of the EB in *Drosophila* affect goal-directed behavior like turning. It will be interesting to see the outcome of such experiments.

AUTHOR CONTRIBUTIONS

VF and FH conceived and designed the project; BK provided graphical representation of CX; VF performed experiments; VF, BK, XG, and FH analyzed the data. VF and FH prepared the manuscript on which the authors commented.

ACKNOWLEDGMENTS

This work was supported by a faculty startup grant from UT Dallas and the Dallas Foundation to XG and by the UK Medical Research Council (G0701498; MR/L010666/1) and the UK Biotechnology and Biological Sciences Research Council (BB/N001230/1) to FH.

SUPPLEMENTARY MATERIAL

The Supplementary Material for this article can be found online at: http://journal.frontiersin.org/article/10.3389/fnbeh.2017.00142/full#supplementary-material

The videos show examples of simulated successful navigation, under different conditions. In each run, the starting location of the agent is selected randomly within the 100 locations in the South-West sector 1 of the arena. Target locations are found in sectors 14 (Target 1) or 16 (Target 2); the navigation is successful if the agent reaches its designated target within 30 s of simulated time.

Supplementary Video 1 | Agent reaching Target 1 under the condition of open arena.

Supplementary Video 2 | Agent reaching Target 2 under the condition of open arena.

Supplementary Video 3 | An example of successful navigation toward Target 1 under the condition of simple maze.

Supplementary Video 4 | An example of successful navigation toward Target 2 under the condition of simple maze.

Supplementary Video 5 | The behavior of the simulated agent under the condition of complex maze, as it successfully reaches Target 1.

Supplementary Video 6 | The behavior of the simulated agent under the condition of complex maze, as it successfully reaches Target 2.

Supplementary Video 7 | An example of "intentional spatial navigation", defined as the ability of a single phenotype to discriminate between putative goals and to pursue the appropriate course of action. The simulated agent is shown in two consecutive runs as a different goal is activated in each run. The order of the goals is fixed (e.g., hunger first and thirst second) so that the simulated agent is required to pursue Target 1 in the first run and Target 2 in the second run (e.g., food first and water second). The video shows the simulated agent reaching its target sectors in the order defined by its active goals, under the condition of open arena.

Supplementary Video 8 | An example of "intentional spatial navigation," defined as the ability of a single phenotype to discriminate between putative goals and to pursue the appropriate course of action. The simulated agent is shown in two consecutive runs as a different goal is activated in each run. The order of the goals is fixed (e.g., hunger first and thirst second) so that the simulated agent is required to pursue Target 1 in the first run and Target 2 in the second run (e.g., food first and water second). The video shows the simulated agent reaching its target sectors in the order defined by its active goals, under the condition of simple maze.

REFERENCES

Afraimovich, V., Tristan, I., Huerta, R., and Rabinovich, M. I. (2008). Winnerless competition principle and prediction of the transient dynamics in a Lotka-Volterra model. *Chaos* 18:043103. doi: 10.1063/1.2991108

Barter, J. W., Li, S., Sukharnikova, T., Rossi, M. A., Bartholomew, R. A., and Yin, H. H. (2015). Basal ganglia outputs map instantaneous position coordinates during behavior. *J. Neurosci.* 35, 2703–2716. doi: 10.1523/JNEUROSCI.3245-14.2015

Boyan, G. S., and Liu, Y. (2016). Development of the neurochemical architecture of the central complex. *Front. Behav. Neurosci.* 10:167. doi: 10.3389/fnbeh.2016.00167

Cheeseman, J. F., Millar, C. D., Greggers, U., Lehmann, K., Pawley, M. D., Gallistel, C. R., et al. (2014). Way-finding in displaced clock-shifted bees proves bees use a cognitive map. *Proc. Natl. Acad. Sci. U.S.A.* 111, 8949–8954. doi: 10.1073/pnas.1408039111

Cheung, A., Collett, M., Collett, T. S., Dewar, A., Dyer, F., Graham, P., et al. (2014). Still no convincing evidence for cognitive map use by honeybees. *Proc. Natl. Acad. Sci. U.S.A.* 111, E4396–E4397. doi: 10.1073/pnas.1413581111

Collett, M., Chittka, L., and Collett, T. S. (2013). Spatial memory in insect navigation. *Curr. Biol.* 23, R789–R800. doi: 10.1016/j.cub.2013.07.020

Cruse, H., and Wehner, R. (2011). No need for a cognitive map: decentralized memory for insect navigation. *PLoS Comput. Biol.* 7:e1002009. doi: 10.1371/journal.pcbi.1002009

Deco, G., Jirsa, V. K., Robinson, P. A., Breakspear, M., and Friston, K. (2008). The dynamic brain: from spiking neurons to neural masses and cortical fields. *PLoS Comput. Biol.* 4:e1000092. doi: 10.1371/journal.pcbi.1000092

el Jundi, B., Warrant, E. J., Byrne, M. J., Khaldy, L., Baird, E., Smolka, J., et al. (2015). Neural coding underlying the cue preference for celestial orientation. *Proc. Natl. Acad. Sci. U.S.A.* 112, 11395–11400. doi: 10.1073/pnas.1501272112

Fiore, V. G., Dolan, R. J., Strausfeld, N. J., and Hirth, F. (2015). Evolutionarily conserved mechanisms for the selection and maintenance of behavioural activity. *Philos. Trans. R. Soc. Lond. B. Biol. Sci.* 370:20150053. doi: 10.1098/rstb.2015.0053

Green, J., Adachi, A., Shah, K. K., Hirokawa, J. D., Magani, P. S., and Maimon, G. (2017). A neural circuit architecture for angular integration in *Drosophila*. *Nature* 546, 101–106. doi: 10.1038/nature22343

Guo, P., and Ritzmann, R. E. (2013). Neural activity in the central complex of the cockroach brain is linked to turning behaviors. *J. Exp. Biol.* 216(Pt 6), 992–1002. doi: 10.1242/jeb.080473

Hanesch, U., Fischbach, K.-F., and Heisenberg, M. (1989). Neuronal architecture of the central complex in *Drosophila melanogaster*. *Cell Tissue Res.* 257, 343–366. doi: 10.1007/BF00261838

Harley, C. M., and Ritzmann, R. E. (2010). Electrolytic lesions within central complex neuropils of the cockroach brain affect negotiation of barriers. *J. Exp. Biol.* 213(Pt 16), 2851–2864. doi: 10.1242/jeb.042499

Heinze, S. (2015). Neuroethology: unweaving the senses of direction. *Curr. Biol.* 25, R1034–R1037. doi: 10.1016/j.cub.2015.09.003

Heinze, S., and Homberg, U. (2007). Maplike representation of celestial E-vector orientations in the brain of an insect. *Science* 315, 995–997. doi: 10.1126/science.1135531

Heinze, S., and Reppert, S. M. (2011). Sun compass integration of skylight cues in migratory monarch butterflies. *Neuron* 69, 345–358. doi: 10.1016/j.neuron.2010.12.025

Ito, K., and Awasaki, T. (2008). Clonal unit architecture of the adult fly brain. *Adv. Exp. Med. Biol.* 628, 137–158. doi: 10.1007/978-0-387-78261-4_9

Ito, M., Masuda, N., Shinomiya, K., Endo, K., and Ito, K. (2013). Systematic analysis of neural projections reveals clonal composition of the *Drosophila* brain. *Curr. Biol.* 23, 644–655. doi: 10.1016/j.cub.2013.03.015

Jourjine, N., Mullaney, B. C., Mann, K., and Scott, K. (2016). Coupled sensing of hunger and thirst signals balances sugar and water consumption. *Cell* 166, 855–866. doi: 10.1016/j.cell.2016.06.046

Kahsai, L., and Winther, A. M. (2011). Chemical neuroanatomy of the *Drosophila* central complex: distribution of multiple neuropeptides in relation to neurotransmitters. *J. Comp. Neurol.* 519, 290–315. doi: 10.1002/cne.22520

Kakaria, K. S., and de Bivort, B. L. (2017). Ring attractor dynamics emerge from a spiking model of the entire protocerebral bridge. *Front. Behav. Neurosci.* 11:8. doi: 10.3389/fnbeh.2017.00008

Kim, N., Barter, J. W., Sukharnikova, T., and Yin, H. H. (2014). Striatal firing rate reflects head movement velocity. *Eur. J. Neurosci.* 40, 3481–3490. doi: 10.1111/ejn.12722

Kim, S. S., Rouault, H., Druckmann, S., and Jayaraman, V. (2017). Ring attractor dynamics in the *Drosophila* central brain. *Science* 356, 849–853. doi: 10.1126/science.aal4835

Kong, E. C., Woo, K., Li, H., Lebestky, T., Mayer, N., Sniffen, M. R., et al. (2010). A pair of dopamine neurons target the D1-like dopamine receptor DopR in the central complex to promote ethanol-stimulated locomotion in *Drosophila*. *PLoS ONE* 5:e9954. doi: 10.1371/journal.pone.0009954

Kottler, B., Fiore, V. G., Ludlow, Z. N., Buhl, E., Vinatier, G., Faville, R., et al. (2017). A lineage-related reciprocal inhibition circuitry for sensory-motor action selection. *bioRxiv* 100420. doi: 10.1101/100420

Lebestky, T., Chang, J. S., Dankert, H., Zelnik, L., Kim, Y. C., Han, K. A., et al. (2009). Two different forms of arousal in *Drosophila* are oppositely regulated by the dopamine D1 receptor ortholog DopR via distinct neural circuits. *Neuron* 64, 522–536. doi: 10.1016/j.neuron.2009.09.031

Lin, C. Y., Chuang, C. C., Hua, T. E., Chen, C. C., Dickson, B. J., Greenspan, R. J., et al. (2013). A comprehensive wiring diagram of the protocerebral bridge for visual information processing in the *Drosophila* brain. *Cell Rep.* 3, 1739–1753. doi: 10.1016/j.celrep.2013.04.022

Lin, S., Owald, D., Chandra, V., Talbot, C., Huetteroth, W., and Waddell, S. (2014). Neural correlates of water reward in thirsty *Drosophila*. *Nat. Neurosci.* 17, 1536–1542. doi: 10.1038/nn.3827

Martin, J. P., Guo, P., Mu, L., Harley, C. M., and Ritzmann, R. E. (2015). Central-complex control of movement in the freely walking cockroach. *Curr. Biol.* 25, 2795–2803. doi: 10.1016/j.cub.2015.09.044

Martin, J. R., Raabe, T., and Heisenberg, M. (1999). Central complex substructures are required for the maintenance of locomotor activity in *Drosophila melanogaster*. *J. Comp. Physiol. A* 185, 277–288. doi: 10.1007/s003590050387

Namiki, S., and Kanzaki, R. (2016). Comparative neuroanatomy of the lateral accessory lobe in the insect brain. *Front. Physiol.* 7:244. doi: 10.3389/fphys.2016.00244

Neuser, K., Triphan, T., Mronz, M., Poeck, B., and Strauss, R. (2008). Analysis of a spatial orientation memory in *Drosophila*. *Nature* 453, 1244–1247. doi: 10.1038/nature07003

Ofstad, T. A., Zuker, C. S., and Reiser, M. B. (2011). Visual place learning in *Drosophila melanogaster*. *Nature* 474, 204–207. doi: 10.1038/nature10131

Omoto, J. J., Keles, M. F., Nguyen, B. M., Bolanos, C., Lovick, J. K., Frye, M. A., et al. (2017). Visual input to the *Drosophila* central complex by developmentally and functionally distinct neuronal populations. *Curr. Biol.* 27, 1098–1110. doi: 10.1016/j.cub.2017.02.063

Pfeiffer, K., and Homberg, U. (2014). Organization and functional roles of the central complex in the insect brain. *Annu. Rev. Entomol.* 59, 165–184. doi: 10.1146/annurev-ento-011613-162031

Rabinovich, M., Volkovskii, A., Lecanda, P., Huerta, R., Abarbanel, H. D., and Laurent, G. (2001). Dynamical encoding by networks of competing neuron groups: winnerless competition. *Phys. Rev. Lett.* 87:068102. doi: 10.1103/PhysRevLett.87.068102

Renn, S. C., Armstrong, J. D., Yang, M., Wang, Z., An, X., Kaiser, K., et al. (1999). Genetic analysis of the *Drosophila* ellipsoid body neuropil: organization and development of the central complex. *J. Neurobiol.* 41, 189–207. doi: 10.1002/(SICI)1097-4695(19991105)41:2<189::AID-NEU3>3.0.CO;2-Q

Ritzmann, R. E., Ridgel, A. L., and Pollack, A. J. (2008). Multi-unit recording of antennal mechano-sensitive units in the central complex of the cockroach, *Blaberus discoidalis*. *J. Comp. Physiol. A Neuroethol. Sens. Neural Behav. Physiol.* 194, 341–360. doi: 10.1007/s00359-007-0310-2

Rosner, R., and Homberg, U. (2013). Widespread sensitivity to looming stimuli and small moving objects in the central complex of an insect brain. *J. Neurosci.* 33, 8122–8133. doi: 10.1523/JNEUROSCI.5390-12.2013

Sakura, M., Lambrinos, D., and Labhart, T. (2008). Polarized skylight navigation in insects: model and electrophysiology of e-vector coding by neurons in the central complex. *J. Neurophysiol.* 99, 667–682. doi: 10.1152/jn.00784.2007

Schultz, W. (2002). Getting formal with dopamine and reward. *Neuron* 36, 241–263. doi: 10.1016/S0896-6273(02)00967-4

Seelig, J. D., and Jayaraman, V. (2013). Feature detection and orientation tuning in the *Drosophila* central complex. *Nature* 503, 262–266. doi: 10.1038/nature12601

Seelig, J. D., and Jayaraman, V. (2015). Neural dynamics for landmark orientation and angular path integration. *Nature* 521, 186–191. doi: 10.1038/nature14446

Strausfeld, N. (2012). *Arthropod Brains: Evolution, Functional Elegance, and Historical Significance*. Cambridge, MA: Harvard University Press.

Strausfeld, N. J., and Hirth, F. (2013). Deep homology of arthropod central complex and vertebrate basal ganglia. *Science* 340, 157–161. doi: 10.1126/science.1231828

Strauss, R., and Heisenberg, M. (1993). A higher control center of locomotor behavior in the *Drosophila* brain. *J. Neurosci.* 13, 1852–1861.

Sutton, R. S., and Barto, A. G. (1998). *Reinforcement Learning: An Introduction*. Cambridge, MA: MIT Press.

Taube, J. S. (2007). The head direction signal: origins and sensory-motor integration. *Annu. Rev. Neurosci.* 30, 181–207. doi: 10.1146/annurev.neuro.29.051605.112854

Tolman, E. C. (1932). *Purposive Behavior in Animals and Men*. New York, NY: The Century Co.

Turner-Evans, D. B., and Jayaraman, V. (2016). The insect central complex. *Curr. Biol.* 26, R453–R457. doi: 10.1016/j.cub.2016.04.006

Turner-Evans, D., Wegener, S., Rouault, H., Franconville, R., Wolff, T., Seelig, J. D., et al. (2017). Angular velocity integration in a fly heading circuit. *Elife* 6:e23496. doi: 10.7554/eLife.23496

Varga, A. G., Kathman, N. D., Martin, J. P., Guo, P., and Ritzmann, R. E. (2017). Spatial navigation and the central complex: sensory acquisition, orientation, and motor control. *Front. Behav. Neurosci.* 11:4. doi: 10.3389/fnbeh.2017.00004

Varga, A. G., and Ritzmann, R. E. (2016). Cellular basis of head direction and contextual cues in the insect brain. *Curr. Biol.* 26, 1816–1828. doi: 10.1016/j.cub.2016.05.037

Vitzthum, H., Muller, M., and Homberg, U. (2002). Neurons of the central complex of the locust *Schistocerca gregaria* are sensitive to polarized light. *J. Neurosci.* 22, 1114–1125.

Waddell, S. (2010). Dopamine reveals neural circuit mechanisms of fly memory. *Trends Neurosci.* 33, 457–464. doi: 10.1016/j.tins.2010.07.001

Waddell, S. (2013). Reinforcement signalling in Drosophila; dopamine does it all after all. *Curr. Opin. Neurobiol.* 23, 324–329. doi: 10.1016/j.conb.2013.01.005

Webb, B., and Wystrach, A. (2016). Neural mechanisms of insect navigation. *Curr Opin Insect Sci.* 15, 27–39. doi: 10.1016/j.cois.2016.02.011

Weir, P. T., and Dickinson, M. H. (2015). Functional divisions for visual processing in the central brain of flying *Drosophila*. *Proc. Natl. Acad. Sci. U.S.A.* 112, E5523–E5532. doi: 10.1073/pnas.1514415112

Williams, J. L. D. (1975). Anatomical studies of the insect central nervous system: a ground-plan of the midbrain and an introduction to the central complex in the locust, *Schistocerca gregaria* (Orthoptera). *J. Zool.* 176, 67–86. doi: 10.1111/j.1469-7998.1975.tb03188.x

Wolff, T., Iyer, N. A., and Rubin, G. M. (2015). Neuroarchitecture and neuroanatomy of the *Drosophila* central complex: a GAL4-based dissection of protocerebral bridge neurons and circuits. *J. Comp. Neurol.* 523, 997–1037. doi: 10.1002/cne.23705

Young, J. M., and Armstrong, J. D. (2010). Structure of the adult central complex in *Drosophila*: organization of distinct neuronal subsets. *J. Comp. Neurol.* 518, 1500–1524. doi: 10.1002/cne.22284

Zeil, J. (2012). Visual homing: an insect perspective. *Curr. Opin. Neurobiol.* 22, 285–293. doi: 10.1016/j.conb.2011.12.008

Conflict of Interest Statement: BK is co-founder of BFKLab LTD.

The other authors declare that the research was conducted in the absence of any commercial or financial relationships that could be construed as a potential conflict of interest.

frontiers in Behavioral Neuroscience

ORIGINAL RESEARCH
published: 14 February 2017
doi: 10.3389/fnbeh.2017.00008

Ring Attractor Dynamics Emerge from a Spiking Model of the Entire Protocerebral Bridge

*Kyobi S. Kakaria and Benjamin L. de Bivort **

Department of Organismic and Evolutionary Biology, Center for Brain Science, Harvard University, Cambridge, MA, USA

Animal navigation is accomplished by a combination of landmark-following and dead reckoning based on estimates of self motion. Both of these approaches require the encoding of heading information, which can be represented as an allocentric or egocentric azimuthal angle. Recently, Ca^{2+} correlates of landmark position and heading direction, in egocentric coordinates, were observed in the ellipsoid body (EB), a ring-shaped processing unit in the fly central complex (CX; Seelig and Jayaraman, 2015). These correlates displayed key dynamics of so-called ring attractors, namely: (1) responsiveness to the position of external stimuli; (2) persistence in the absence of external stimuli; (3) locking onto a single external stimulus when presented with two competitors; (4) stochastically switching between competitors with low probability; and (5) sliding or jumping between positions when an external stimulus moves. We hypothesized that ring attractor-like activity in the EB arises from reciprocal neuronal connections to a related structure, the protocerebral bridge (PB). Using recent light-microscopy resolution catalogs of neuronal cell types in the PB (Lin et al., 2013; Wolff et al., 2015), we determined a connectivity matrix for the PB-EB circuit. When activity in this network was simulated using a leaky-integrate-and-fire model, we observed patterns of activity that closely resemble the reported Ca^{2+} phenomena. All qualitative ring attractor behaviors were recapitulated in our model, allowing us to predict failure modes of the putative PB-EB ring attractor and the circuit dynamics phenotypes of thermogenetic or optogenetic manipulations. Ring attractor dynamics emerged under a wide variety of parameter configurations, even including non-spiking leaky-integrator implementations. This suggests that the ring-attractor computation is a robust output of this circuit, apparently arising from its high-level network properties (topological configuration, local excitation and long-range inhibition) rather than fine-scale biological detail.

Keywords: central complex, ring attractor, protocerebral bridge, ellipsoid body, fan-shaped body, circuit model, leaky integrate-and-fire model, egocentric navigation

OPEN ACCESS

Edited by:
Keram Pfeiffer,
University of Marburg, Germany

Reviewed by:
Paul Graham,
University of Sussex, UK
Kate Jeffery,
University College London (UCL), UK

Hector Page contributed to the review of Kate Jeffery

****Correspondence:***
Benjamin L. de Bivort
debivort@oeb.harvard.edu

Received: *13 October 2016*
Accepted: *10 January 2017*
Published: *14 February 2017*

Citation:
Kakaria KS and de Bivort BL (2017) Ring Attractor Dynamics Emerge from a Spiking Model of the Entire Protocerebral Bridge. Front. Behav. Neurosci. 11:8. doi: 10.3389/fnbeh.2017.00008

INTRODUCTION

An animal navigating in its environment relies on landmarks to estimate its orientation and position (Collett and Graham, 2004). However, in the absence of visual cues, many animals maintain a representation of their heading and position without landmarks by continuously tracking their own motion to calculate navigation vectors to return to a specific location, a process called

path integration (Etienne and Jeffery, 2004). Numerous studies have identified patterns of neural activity that could represent heading, one of the elements needed for path integration. These studies have further shown that heading representations are tuned by visual information but can be updated in the dark, without any visual feedback (Taube, 2007; Seelig and Jayaraman, 2015; Varga and Ritzmann, 2016), presumably by exploiting self-generated motion cues like efference copy (Kim et al., 2015). By integrating heading and distance traveled, an animal can estimate its current position (McNaughton et al., 2007) and calculate a return vector. Heading estimation requires the tracking of variables in angular coordinates, a computation that can be accomplished by "ring attractor networks" (Skaggs et al., 1995; Zhang, 1996; Solovyeva et al., 2016).

In theoretical models of ring attractor networks, neighboring nodes connect to form a topological ring. The value of an angular variable is encoded in the radial position of a "bump" of neural activity within this ring. This bump arises through the combined dynamics of short range excitation and global or long range inhibition between nodes (Skaggs et al., 1995; Zhang, 1996; Knierim and Zhang, 2012). Asymmetric excitation of adjacent nodes causes the bump to move in the direction of the excitation as its previous position is inhibited. Importantly, these neighboring nodes do not have to be physically adjacent but adjacent only in connectivity. In mammals, ring attractors are thought to explain the dynamics of the head direction (HD) cells, which are primarily found in the thalamus and cortical areas associated with the hippocampus (Taube, 2007). Each HD cell is tuned to a particular head orientation in the horizontal plane and the direction in which the cell fires maximally is referred to as its preferred direction. Activity in topologically neighboring HD cells encodes continuously varying allocentric directions and the motion of the bump through the functionally (though not physically) ring-shaped network of HD cells encodes head orientation. Studying dynamics in mammalian neurons encoding HD is difficult as they are spread across relatively large areas of the brain and not spatially organized according to their preferred directions, making simultaneous monitoring of their activity challenging.

In insects, it was recently shown that a physically ring-shaped concentration of neuronal connections (neuropil) may function as a ring attractor (Seelig and Jayaraman, 2015) within the midline-spanning central complex (CX), of *Drosophila melanogaster*. Specifically, the ellipsoid body (EB) and protocerebral bridge (PB) may contain a neural circuit implementing a ring attractor. The EB neuropil has a closed ring shape in dipteran insects but is split ventrally and therefore roughly linear or bean-shaped in all other insect groups, where it is called the lower division of the central body (Strausfeld, 1976). Due to the evolutionary conservation of morphological cell types in the CX, it likely retains ring-shaped functional connections in all insects (Pfeiffer and Homberg, 2014). Furthermore, the lower division of the central body has been shown to encode the angular position of the sun in locusts, a continuous variable in angular coordinates, suggesting ring-like function without closed ring shape (Heinze and Homberg, 2007; Homberg et al., 2011; Heinze, 2014). In dipterans, the compact size and physical ring shape of this neuropil uniquely facilitates the study of putative ring attractor dynamics in a complete and intact circuit that can be simultaneously imaged in an awake behaving fly (Seelig and Jayaraman, 2015).

In a closed-loop behavioral setup, Ca^{2+} activity in putative dendritic processes of one neuronal population within the EB was shown to encode relative angular position of a vertical stripe on a 2-D light emitting diode screen (Seelig and Jayaraman, 2015). Seelig and Jayaraman (2015) noted several features of their circuit that are typical of ring attractor networks (Haferlach et al., 2007; Knierim and Zhang, 2012; Arena et al., 2013). The Ca^{2+} activity in so-called "wedge neurons" was localized in a single bump at any one time and this bump moved in response to the animal turning on a ball, mimicking a change in heading. Furthermore, the bump exhibited spatial stability. When the fly was stationary for a long period of time, the bump would sometimes fade, but it typically reappeared in the same location when the fly resumed moving. This suggests the bump can be stored in ways other than intracellular Ca^{2+} concentration, such as subthreshold voltages. The bump locked onto a single stripe when two competitor stripes were presented and was observed to jump between identical stripes from time to time. While these bump dynamics were recorded in the context of a closed-loop behavioral assay, causal relationships between the bump, behavior, motor commands and efference copy signals have not yet been identified.

The neurons exhibiting these ring attractor-like dynamics connect two of the neuropil that make up the CX, tiling the EB with dendritic arbors and the PB with presynaptic boutons (**Figure 1**). They are called E-PGs (EB-PB-Gall neurons, called PBG1–8.b-EBw.s-D/Vgall.b in Wolff et al. (2015), EB.w.s or "wedge neurons" in Seelig and Jayaraman (2015) and EIP in Lin et al. (2013); see **Table 1** for all abbreviations), denoting the flow of information within them from the EB to the PB and Gall (a secondary structure immediately outside the CX). The EB and PB are notable for their division into columnar segments, known as glomeruli in the PB and wedges/tiles (Wolff et al., 2015) in the EB. These neuropil contain many different neural cell types beyond those shown by Seelig and Jayaraman (2015) to encode angular position. In the PB, these have been recently characterized at the level of morphology using single-cell stochastic labeling methods (Lin et al., 2013; Wolff et al., 2015). The resulting catalog revealed that of the approximately 18 classes of neurons within the PB, only three reciprocally connected the EB and the PB.

We sought to test the hypothesis that PB neurons have circuit dynamics consistent with a ring attractor, using their connectivity as enumerated in these recent mapping articles. With a leaky integrate-and-fire model and simple connectivity rules, derived from light-microscopy resolution neuronal morphologies, we have found that a simple model recapitulates the bump of Ca^{2+} activity and essentially all of the *in vivo* dynamics previously observed (Seelig and Jayaraman, 2015). Furthermore, we have found that this circuit is robust to variation in synaptic weights, behaving like a ring attractor under a wide variety of parameters, perhaps indicating that computing

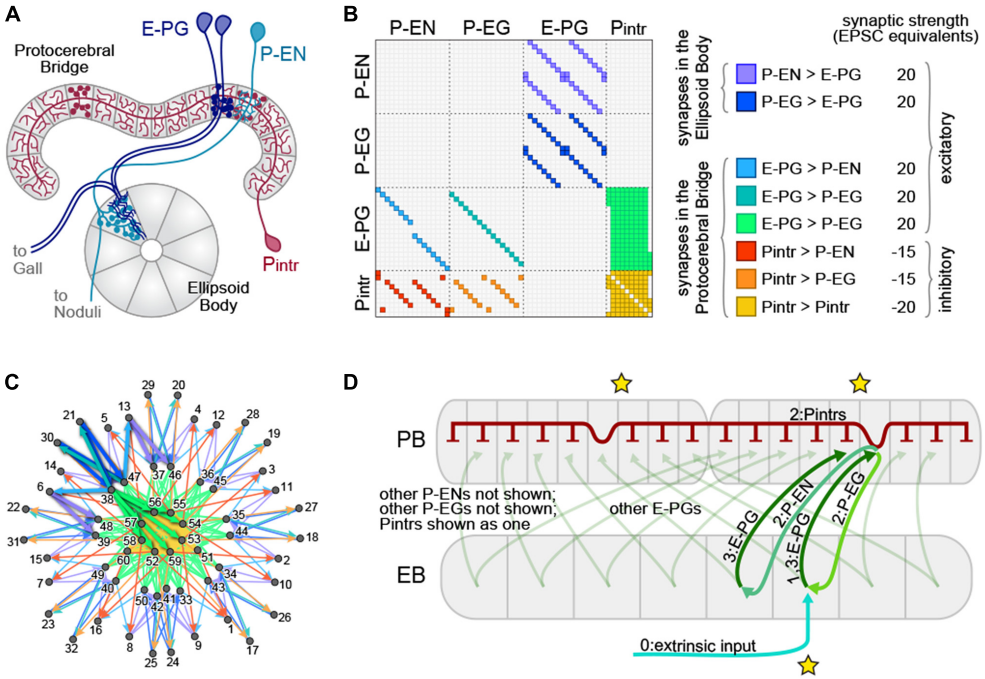

FIGURE 1 | The protocerebral bridge (PB) neural circuit. (A) Diagram of the PB and ellipsoid body (EB), illustrating three out of four modeled neural subtypes, the E-PGs, P-ENs and Pintrs. Not shown are the P-EGs which project from the PB to the EB. Axonal arbors are indicated with circular varicosities/boutons. Dendritic arbors are intricate with fine linear branches. Overlap of an axonal arbor and a dendritic arbor within a single anatomical compartment (gray regions) is sufficient to postulate a synapse between neurons. Neurons with identical morphologies at the level of these anatomical compartments (e.g., the two dark blue E-PGs) are represented in the model as a single neuron. **(B)** Matrix representation of the connectivity of the PB-EB circuit. A filled rectangle in row *i*, column *j* indicates a synapse, with neuron *i* presynaptic and neuron *j* postsynaptic. Different fill colors indicate different synapse classes, whose within-class strengths are shown at right. **(C)** Graph, with node positions determined by a force-directed algorithm of the network with connectivity shown in **(B)**, which forms a ring with bilateral symmetry. Thick edges indicate lateral and reciprocal excitatory loops (local excitation) from neuron 38 (as an example) as well as excitatory connections to inhibitory neurons that target all glomeruli (long-range inhibition). **(D)** Schematic of key circuit motifs in the PB-EB network. Green and blue arrows represent excitatory neurons, red inhibitory neurons. All E-PGs are shown to illustrate the mapping of the EB to each PB hemisphere. Only one P-EG and one P-EN are shown. The pool of Pintrs are represented as a single neuron. Stars indicate the position where the bump will emerge in the EB and the PB hemispheres. Numbers on labels indicate the sequence in which neurons are activated.

TABLE 1 | Abbreviations used herein.

CX	Central Complex
EB	Ellipsoid Body
FB	Fan-shaped Body
PB	Protocerebral Bridge
E-PG	Ellipsoid Body-Protocerebral Bridge-Gall neurons, projecting from the EB to the PB and Gall. Called PBG1–8.b-EBw.s-D/Vgall.b in Wolff et al. (2015) and "wedge neurons" in Seelig and Jayaraman (2015).
P-EG	Protocerebral Bridge-Ellipsoid Body-Gall neurons, projecting from the PB to the EB and Gall. Called PBG1–8.s-EBt.b-D/Vgall.b in Wolff et al. (2015).
P-EN	Protocerebral Bridge-Ellipsoid Body-Noduli neurons, projecting from the PB to the EB and Noduli. Called PBG2–9.s-EBt.b-NO1.b in Wolff et al. (2015).
Pintr	Protocerebral Bridge intrinsic neurons. Comprising PB18.s-GxΔ7Gy.b, PB18.s-9i1i8c.b and PBG6–8.sG9.b in Wolff et al. (2015).
PCA	Principle Components Analysis
HD	Head Direction
PSC	Postsynaptic Current

a ring attractor is the primary evolutionary function of the reciprocal connection between the EB and PB.

MATERIALS AND METHODS

Simulations were run in MATLAB 2015a and 2016a (The MathWorks, Inc., Natick, MA, USA) using custom scripts. All code to recapitulate these results is available at: http://lab.debivort.org/protocerebral-bridge-ring-attractor-model.

Network Construction

To construct a circuit model of the PB, we began with the catalog of morphologically defined cell types in the PB (Wolff et al., 2015). This work enumerates all neuronal cell types within

the PB, characterizing two cells as belonging to the same type if their presynaptic and postsynaptic arbors (as determined by MultiColor FlipOut imaging (Nern et al., 2015)) are in the same neuropil compartments. Compartments are defined as spatially distinct regions of the major glia-ensheathed neuropils of the CX and associated regions. For example, the PB itself contains 18 glomerular compartments and the EB contains 16 wedge and 8 tile compartments. We included in our model: (1) any neuron with postsynaptic processes in the PB and presynaptic processes in other compartments (output neurons), provided there is a PB input neuron with a postsynaptic arbor overlapping the presynaptic arbor of that output neuron; and (2) any neuron with presynaptic processes in the PB and postsynaptic arbors that overlap presynaptic arbors of neurons projecting out of the PB (input neurons; **Figure 1**). This includes all the neuronal cell types cataloged in Wolff et al. (2015) except for five classes of fan-shaped body (FB) projecting neurons (output only) and two classes of PB input neurons from the posterior slope (input only). We assumed that all neurons could be cleanly divided into dendritic and axonal compartments, and that information flows exclusively from the former to the latter.

The broad classes of neurons that met this criterion were the P-ENs (PB output neurons with axons in the EB and noduli), P-EGs (PB output neurons projecting to the EB and Gall), E-PGs (PB input neurons with dendrites in the EB and output to the Gall), and Pintrs (PB intrinsic neurons with both dendritic arbors and presynaptic boutons in the PB). See **Table 1** for abbreviations. P-ENs and P-EGs comprise 16 types each, defined by which PB glomerulus contains their dendrites. E-PGs comprise 18 types, defined by which PB glomerulus contains their axons (unlike "wedge" neurons (Seelig and Jayaraman, 2015) E-PGs also include neurons innervating the first and last glomeruli of the PB G9L and G9R (Wolff et al., 2015)). The Pintrs comprise 10 types, defined by which PB glomerulus contains their axons. If their projections were identical at the level of the 60 types described above, individual neurons were considered identical, and represented by a single neuron in the model. Lastly, we assumed that neurons formed no autapses. The connectivity of the network thus defined is shown in **Figure 1B**. We examined the topological arrangement of this network by using a force-directed algorithm (Fruchterman and Reingold, 1990; Webb and Stone, personal communication) to arrange nodes representing neurons. The connectivity present in this network has a ring-like topology, with bilateral symmetry (**Figure 1C**). From this representation, key circuit motifs can be discerned (**Figure 1D**). Input depolarizing the E-PGs has the potential to: (1) activate a excitatory E-PG/P-EG loop; (2) activate adjacent E-PGs via the P-ENs; and (3) broadly inhibit all PB glomeruli via the pool of Pintrs.

Circuit Physiological Assumptions

Circuit dynamics were implemented using leaky-integrate-and-fire (Stein, 1967) neuronal models, with values for the membrane capacitance, resistance, resting potential, undershoot potential, and postsynaptic current (PSCs) time constants and magnitudes, chosen to reflect generic neuronal properties (Hodgkin and Huxley, 1952). The important free parameters of the model were the strengths and signs of the synapses between each type of neuron. We assume that the strengths of all synapses between two classes of neurons (a "synapse class," e.g., all synapses between P-ENs and E-PGs) were identical.

Strength of synapses was implemented as the number of PSC equivalents per action potential. Excitatory neurons induced positive, depolarizing currents in their postsynaptic partners and inhibitory neurons negative currents. We assumed all neurons were excitatory unless we had evidence otherwise. The Pintrs are glutamatergic (Daniels et al., 2008) and possess connectivity similar to other inhibitory local neurons in spatially compartmentalized neuropils, e.g., the antennal lobe (Chou et al., 2010) and lateral horn (Fişek and Wilson, 2014), therefore we assumed they are inhibitory (Liu and Wilson, 2013).

To deliver inputs to the circuit, we assumed that information first flows into the EB (this assumption has no bearing on our qualitative conclusions). Therefore, for each run of the model, the timing of action potentials in not-explicitly-simulated neurons upstream of the E-PGs was determined. These action potentials induced in the E-PGs excitatory currents with a strength equivalent of one PSC each. We assumed that background activity in these upstream neurons produced a Poisson-process sequence of action potentials with a mean rate of 5 Hz. On top of this, Poisson-process spikes at higher rates (peaking at 120 Hz) in subsets of E-PG types represented sensory-like input into the PB (**Figure 2A**), e.g., the azimuthal angle of light polarization (Heinze, 2014; Bockhorst and Homberg, 2015) or the retinotopic position of a landmark (Seelig and Jayaraman, 2013, 2015).

Circuit Simulations

The circuit network structure was coded from the morphology descriptions in Wolff et al. (2015) per the rules described in the "Results" Section below. Leaky-integrate-and-fire dynamics were used to simulate spiking neurons, and implemented using Euler's method to evaluate the following equation, with $\Delta t = 10^{-4}$ s:

$$dV_\mathrm{i}/dt = \frac{1}{C_\mathrm{m}}\left(\frac{V_0 - V_\mathrm{i}}{R_\mathrm{m}} + I_\mathrm{in} + \sum_{j=1}^{60} M_{\mathrm{j,i}} I_\mathrm{j} + I_\mathrm{ect}\right)$$

where V_i is the membrane voltage of neuron i, I_in is input current from neurons outside the PB-EB circuit (0 in all neurons other than the E-PGs), $M_\mathrm{j,i}$ is the network connectivity matrix with entries equal to the synapse strength (in units of excitatory or inhibitory PSCs), I_j is the output current of other neurons in the PB-EB circuit, and I_ect is simulated ectopic current (such as might be induced by thermogenetic or optogenetic manipulation). We used parameter values that correspond to a generic spiking neuron (Hodgkin and Huxley, 1952), but these values are consistent with various *Drosophila* measurements or measurements of PB neurons in other species. C_m is the

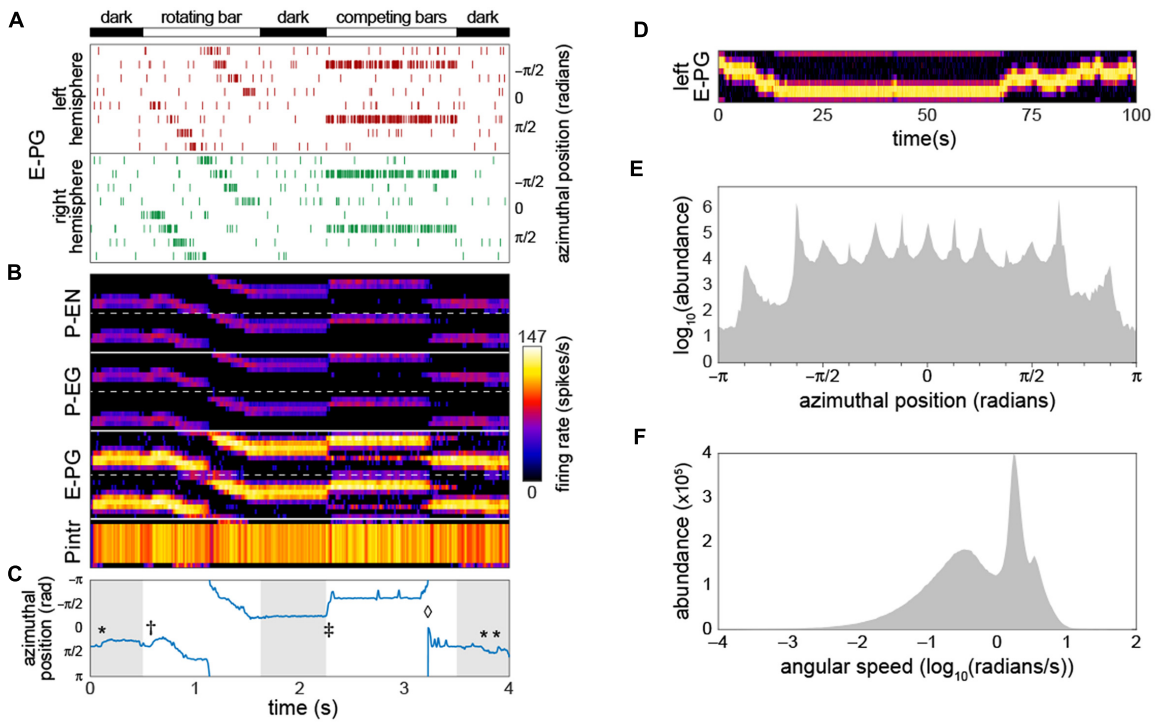

FIGURE 2 | Bump-producing circuit dynamics. (A) Input into the circuit is delivered as action potentials (raster marks) in neurons upstream of the E-PGs, plotted vs. time. Various sensory stimuli can be represented, including rotating bars, and static competitors. In "dark" periods, the only input is Poisson-distributed background activity. Inputs are associated with the eight tiles (Wolff et al., 2015) of the EB, and corresponding azimuthal angles in body coordinates are indicated. **(B)** Activity of all 60 neurons in the circuit vs. time. Plotted heatmap is a Gaussian-convolved raster of action potential times (standard deviation 24 ms). Dotted lines demarcate left from right hemispheres within a neural subtype. **(C)** Position of the bump (centroid of activity in **B**; blue line) vs. time. *Indicates "spontaneous" shifts in the position of the bump in darkness. †Indicates the bump sliding to the position of a bar as soon as it appears, and then following it as it rotates. ‡Indicates the bump jumping to the position of a single competitor when two static competitors appear. ◊Indicates the bump spontaneously switching its position to that of the other competitor. **(D)** Bump behavior in darkness vs. time over a prolonged period in the left hemisphere E-PGs. **(E)** Histogram of bump frame-by-frame centroid position over 383 simulations of 4 s each in darkness. **(F)** Histogram of spontaneous bump angular speed in the same dark simulations.

membrane capacitance (0.002 μF in all neurons, assuming a surface area of 10^{-3}cm^2; Gouwens and Wilson, 2009), V_0 is the resting potential (−52 mV in all neurons; Rohrbough and Broadie, 2002; Sheeba et al., 2008), R_m is the membrane resistance (10 MΩ in all neurons; Gouwens and Wilson, 2009). When a neuron's voltage reached the firing threshold of −45 mV (V_{thr}; Sheeba et al., 2008; Gouwens and Wilson, 2009), a templated action potential trace was inserted into its voltage time series. This trace was defined as follows:

$$V(t) = \begin{cases} V_{thr} + (V_{max} - V_{thr}) \dfrac{\text{Normpdf}(0,1,-1+\frac{t}{t_{AP}/2}) - \alpha}{\beta} & : 0 < t < \frac{t_{AP}}{2} \\ V_{min} + (V_{max} - V_{min}) \dfrac{\sin\left((t - \frac{t_{AP}}{2})\frac{2\pi}{t_{AP}} + \frac{\pi}{2}\right) + \gamma}{\delta} & : \frac{t_{AP}}{2} < t < t_{AP} \end{cases}$$

Where V_{max} is the (purely cosmetic, as it does not affect the circuit dynamics) peak action potential voltage (20 mV; Rohrbough and Broadie, 2002), V_{min} is the spike undershoot voltage (−72 mV; Nagel et al., 2015), t_{AP} is the length of an action potential (2 ms; Gouwens and Wilson, 2009; Gaudry et al., 2013), Normpdf (a, b, c) is the probability density function of a Gaussian with mean a and standard deviation b at c, and α, β, γ and δ are normalization parameters so that the max and min of the Normpdf and sin segments are 1 and 0 respectively prior to scaling by the voltage terms.

The firing of an action potential also triggered the addition of a templated PSC trace to the output current time series of the firing neuron. The PSC trace was defined as follows in terms of t in ms:

$$I(t) = \begin{cases} I_{PSC} \dfrac{\sin(\frac{t\pi}{2} - \frac{\pi}{2}) + \alpha'}{\beta'} & : 0 < t < 2 \\ I_{PSC} \dfrac{2^{-(t-2)/t_{PSC}} + \gamma'}{\delta'} & : 2 < t \leq 2 + 7t_{PSC} \end{cases}$$

Where I_{PSC} is the amplitude of a PSC (5 nA; Gaudry et al., 2013); excitatory and inhibitory PSCs were assumed to have the same magnitude but opposite sign), t_{PSC} is the half-life of PSC decay (5 ms; Gaudry et al., 2013), and α', β', γ' and δ' are normalization parameters so that the max and min of the sin and exponential terms are 1 and 0 respectively prior to scaling by I_{PSC}. PSC traces had a length equal to 2 + 7t_{PSC} ms, corresponding to 2 s of rise time plus 7 times the decay half-life.

Synapse strength parameters were explored manually to identify the baseline configuration in **Figure 1**. Thereafter, parameter exploration was conducted as described in the "Results" Section. The overall magnitude of the synapse strength parameters shown in **Figure 1** was the main free parameter of the model. The average synapse strengths of each synapse class are also free parameters, though we found that adjusting only the strengths of the Pintr > P-EG and Pintr > P-EN synapse classes was sufficient to recapitulate bump dynamics.

Leaky-integrator dynamics were used to simulate non-spiking graded potential neurons, and were implemented using Euler's method to evaluate the following equation, with $\Delta t = 10^{-4}$ s:

$$dV_\mathrm{i}/dt \; = \; \frac{1}{C_\mathrm{m}}\left(\frac{V_0 - V_\mathrm{i}}{R_\mathrm{m}} + I_\mathrm{in} + I_\mathrm{max}\sum_{j=1}^{60} M_\mathrm{j,i}\tanh\left(20 * (V_\mathrm{j} - V_0)\right)\right)$$

Where all variables and constants are as defined above, and I_max is the maximum PSC achievable in a synapse of strength one within the PB-EB circuit. First, the scaling parameter of the current-voltage tanh transfer function (20) was determined empirically. This value yielded dynamics that were the most bump-like, given the synapse strength parameters determined in the leaky-integrate-and-fire model. Then, synapse strength parameters that produced a maximally functional bump were identified by adding Gaussian noise to the baseline synapse strength parameters from the leaky-integrate-and-fire model. This noise had mean of zero and a standard deviation of 100% of the baseline value of each synapse parameter. The dynamics of approximately 200 such random configurations were examined manually, and those producing the best bump-like behavior were then iteratively refined using them as a new baseline, and then adding Gaussian noise with a standard deviation of 10% and then 5% of the respective baseline values. The formula for these dithered synapse strength parameters was (s_k is the strength of synapse class *k*, s'_k is that parameter after dithering):

$$s'_k \; = \; s_k\,(1 + \mathrm{Norm}(0, \sigma))$$

In order to break initial symmetry and allow the bump to move "spontaneously" random Gaussian noise with mean zero and standard deviation of 3×10^{-10}V was added to each neuron in each timestep.

Bump position was estimated and visualized by convolving the action potential rasters of each neuron with a Gaussian kernel with a standard deviation of 24 ms. This approximates a Ca^{2+} signal in these neurons. Bump position was determined by taking the centroid, modulo eight, of this convolved representation for the P-ENs in each hemisphere. The estimated centroid of each hemisphere's P-ENs was averaged to produce the final centroid estimate.

Circuit Dynamics Parameter Sensitivity Analysis

Circuit dynamics were captured for multidimensional analysis by simulating the network for 2 s, with inputs representing a rotating bar and two static competitors (setting parameters *SweepBarBool* and *TwinBarBool* equal to one in PBexperiment.m). Starting from the baseline synapse strength parameters, we added Gaussian noise to each parameter using the dithering formula above. Circuit dynamics during the rotating bar and competitor bar stimuli are particularly diagnostic of bump performance. We trimmed the circuit "Ca^{2+} signal" time series to 200 ms from each of these two stimulus periods, then subsampled the time points 20:1, yielding a final 200 diagnostic time points. Dynamics from 10,000 networks with randomly dithered synapse strength parameters were computed, each yielding a single point in a 12,000 dimensional space representing circuit dynamics (200 diagnostic time points × 60 neurons). In addition, we added points representing the dynamics of networks in which a single synapse class parameter value was swept systematically from $-9x$ to $10x$ its original value. The dynamics from these systematic sweeps were added to the dynamics from the randomly dithered networks and projected into two dimensions using principle components analysis (PCA) for visualization. Clusters of dynamics were enumerated using *k*-means clustering in the original 12,000 dimensional space. Representative dynamics of each cluster were computed by averaging all of the Gaussian-convolved spike rasters receiving each *k*-means cluster label.

RESULTS

Bump Circuit Dynamics

As a starting point for our characterization of circuit dynamics, we assumed, rather arbitrarily, that all synapse classes had a strength of 20 PSCs. With a small amount of manual parameter searching, we found that if the inhibitory synapses between the Pintrs and the P-ENs and those between the Pintrs and P-EGs had strengths of 15, circuit activity recapitulated several key phenomena that have been observed in Ca^{2+} recordings of the E-PGs (**Figures 2B,C**; Movie 1): (1) a stable "bump" of activity appeared at one position in the glomerular axis of the PB and the corresponding EB position, as observed by Seelig and Jayaraman (2015). This bump was almost always distributed over two or three glomeruli (25%–38% of the azimuthal axis), corresponding roughly to the size of the Ca^{2+} bump they imaged (Seelig and Jayaraman, 2015). (2) The bump jumped or slid to the position of a novel sensory cue (i.e., a vertical bar), represented as an increased firing rate in the neurons upstream of a single E-PG. (3) When the position of this input activity moved across adjacent glomeruli (moved in its azimuthal position), the bump followed. (4) When two competing vertical bars were provided in the form of firing-rate-matched activity upstream of two non-adjacent E-PGs, the bump moved to the position of one of the cues. (5) Occasionally, during the presentation of competitor bars, the bump would switch positions from one cue to the other. These characteristics were present for a wide range of synapse strength parameters (see stability analysis below).

As reported by Seelig and Jayaraman (2015), the bump appeared to be fairly stable in the dark (i.e., with only baseline background activity present upstream of the input neurons).

Our baseline synapse strength parameter values yielded a bump "spontaneous drift rate" comparable to those observed *in vivo* (approximately 1 glomeruli/s; **Figure 2D**). We observed that the angular position encoded by the position of the bump had a highly discretized distribution while drifting in the dark (**Figure 2E**); the vast majority of the time, the bump was present in one of 15 azimuthal positions, and among these, $\pm 5\pi/8$ was the most abundant, followed by $\pm\pi/8$. The distribution of bump speed during spontaneous motion (i.e., any motion in the dark) was trimodal (**Figure 2F**). These modes may correspond to staying in position, sliding between adjacent positions, and jumping between non-adjacent positions.

Bump Relation to Action Potentials

The emergence of a bump was remarkably robust, even a single action potential upstream of a single input E-PG was sufficient to induce a bump at the position of that action potential that would persist indefinitely in the absence of further action potentials (**Figures 3A,B**; Movie 1). We observed that occasionally the bump, as encoded by action potentials, would disappear briefly (up to a few tens of milliseconds at a time; **Figures 3C–E**). During these periods, none of the PB neurons would fire any action potentials, even if there were occasional action potentials in the neurons upstream of the E-PGs. This implies that the bump can be "stored" in sub-threshold potentials. These brief disappearances tended to happen when the bump was located at one of the less frequent azimuthal positions (e.g., $\pm 7\pi/8$).

Several sets of neurons appeared to fire synchronously in the circuit (**Figure 3E**), specifically, those Pintrs that have axonal arbors in two PB glomeruli, bilaterally paired P-ENs and P-EGs, and bilaterally paired E-PGs (though this group of neurons is somewhat less synchronous by virtue of their being the input neurons that are stimulated at random times by upstream neurons). Leaky-integrator implementations (without action potentials) of this model could also produce a bump that persisted in the absence of sensory input,

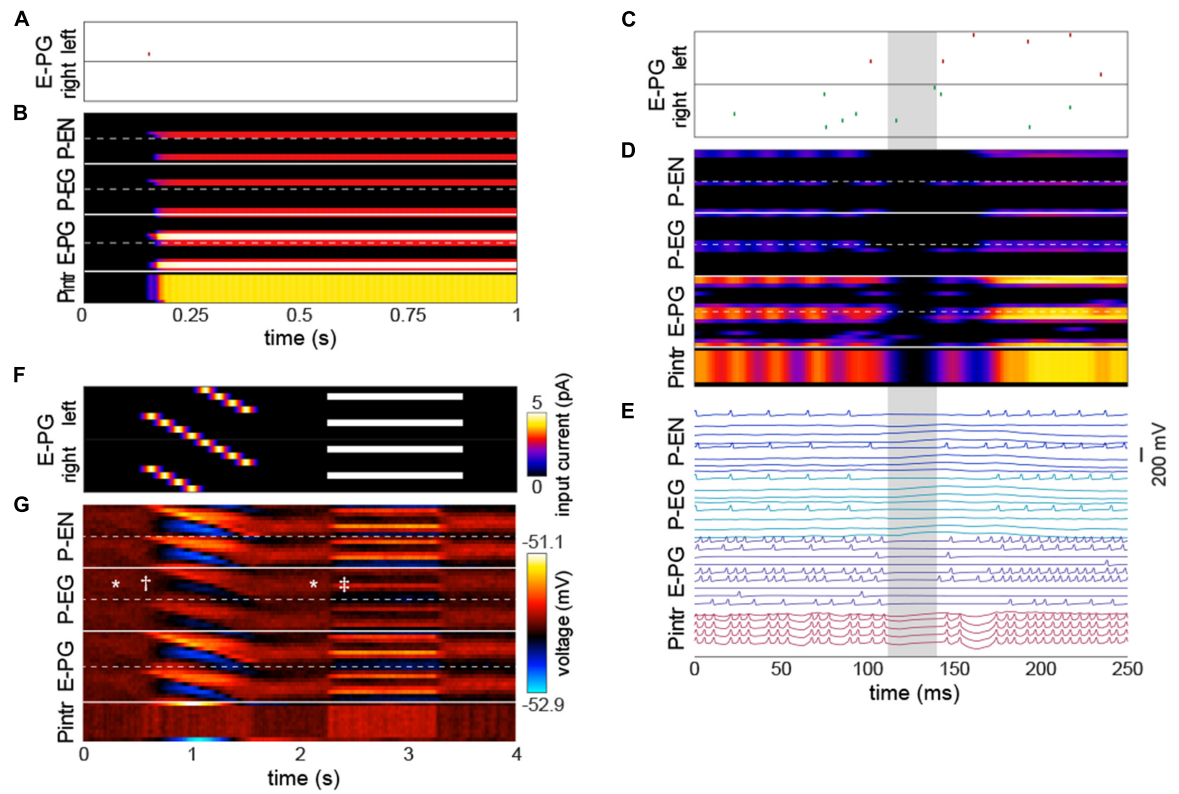

FIGURE 3 | The bump requires action potentials, but can persist momentarily without them. (A,B) Input of a single action potential in an E-PG (red raster mark) is sufficient to induce a stable bump in the circuit. **(B)** Gaussian-convolved raster of neural activity in all neural subtypes (axes and color scale as in **Figure 2B**). **(C)** Circuit input via the E-PGs corresponding to 250 ms of darkness. **(D)** Corresponding dynamics of all neurons in the circuit revealing a ∼20 ms window (shaded gray) in which the bump disappears, i.e., is not represented in action potentials, but reappears in the same position after the window (axes and color scale as in **Figure 2B**). **(E)** Corresponding voltage traces. For clarity, the trace of every other neuron has been removed. **(F)** Depolarizing currents representing input into the E-PGs in a leaky-integrator implementation of the circuit, vs. time. Synapse strength parameters used were those that provided dynamics most closely approximating a bump. **(G)** Corresponding voltages in the entirety of the circuit. Symbols indicate elements of canonical bump phenomenology, as in **Figure 2C**. *Indicates "spontaneous" shifts in the position of the bump in darkness. †Indicates the bump jumping to the position of a bar as soon as it appears, and then following it as it rotates. ‡Indicates the bump jumping to the favoring one of two competitors (the lower competitor, most clearly discernible in the left hemisphere—the top half of each neuron type).

selected between competitor bars or formed a unitary bump after competitors were removed (**Figures 3F,G**). However, the bump in this implementation did not have the same rapid spontaneous bump formation, spatial precision, or strong selectivity between competitors seen in the leaky-integrate-and-fire implementation (though it did have weak selectivity between competitors).

Synapse Strength Parameter Sensitivity

We next examined whether we had serendipitously found the only synapse strength parameters that recapitulated so many experimental bump phenomena or were these dynamics robust to parameter values. We added random, Gaussian-distributed noise (mean = 0, standard deviation = 20% of each parameter's baseline value) to the synapse strength parameters and then stimulated these dithered circuits with inputs of: (1) sequential bursts of activity in adjacent wedges representing a rotating bar; and (2) elevated activity in two non-adjacent glomeruli representing stationary competitor bars (**Figure 4A**). For each of these configurations, the ensuing circuit activity in all neurons during diagnostic periods of this stimulation (200 ms from the rotating bar phase and 200 ms from the beginning of the competitor bars) were treated as points in a high dimensional space of circuit behavior. These points were clustered and averaged within a cluster to provide an exhaustive catalog of the modes of dynamics that this circuit topology can produce (**Figures 4A,B**). Of 15 modes, three feature sets of neurons with essentially no activity (modes 1–3) and five feature sets of seizing neurons (modes 11–15). Two of the remaining modes feature bumps exhibiting all the key properties observed experimentally (i.e., those shown in **Figure 2**): modes 4 and 5, which are distinguished largely by which competitor they select. Two modes have bumps that are stable on too-long timescales and extend over too many adjacent glomeruli, but otherwise show

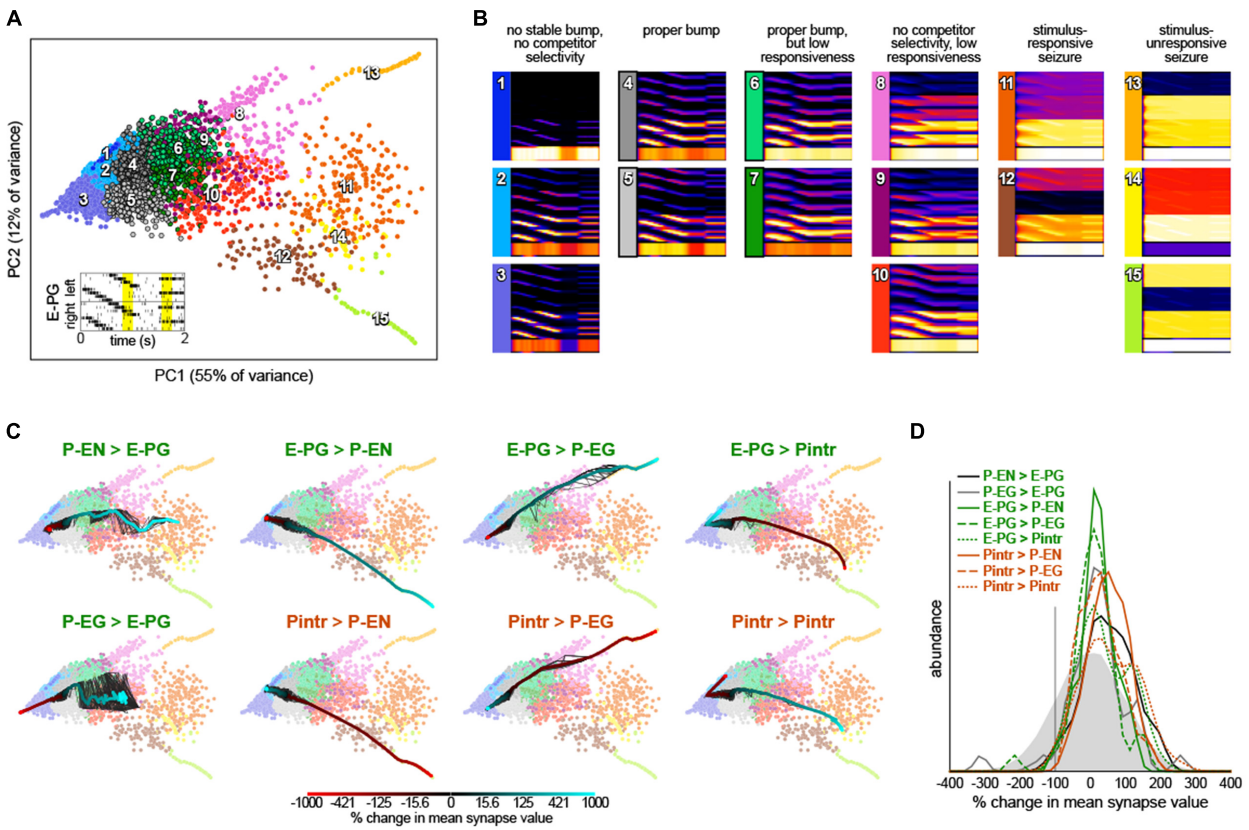

FIGURE 4 | Robustness of bump dynamics. (A) Scatter plot of the first two principal components of circuit dynamics (during the yellow intervals of E-PG stimulation shown in the inset; see "Materials and Methods" Section). Each point represents the dynamics of a circuit with synapse strength parameters equal to either (1) the baseline parameters (**Figure 1B**) plus Gaussian noise with mean = 0 and standard deviation = 20% of baseline value; or (2) the baseline parameters, with one parameter varied adjusted by $-9x$ to $10x$ of its baseline value. Colors indicate 15 *k*-means clusters computed prior to principle components analysis (PCA). Numbers show the approximate cluster centers. **(B)** Mean dynamics of all points within each cluster shown in **(A)**. Each plot is an average of Gaussian-convolved action potentials rasters (as in **Figure 2B**). Numbers and colors correspond to those in **(A). (C)** Systematic variation of each of the eight synapse class strength parameter away from their respective baseline values. Black lines represent 10 different parameter value sweep replicates, and the thick color-mapped line their average, color coded by the shift of each respective parameter. **(D)** Distributions of synapse parameters that support proper bump function. Gaussian noise from the solid gray distribution was sampled and added to each synapse class independently. This was repeated 24,000 times and the resulting circuit dynamics were *k*-means clustered into 400 clusters. Six clusters were identified that had proper bump dynamics comparable to modes 4 and 5 of **(A)**. The distribution of synapse strength parameter offsets represented in these clusters is shown for each synapse class strength parameter.

the key properties (modes 6 and 7). The remaining three modes (8–10) have some key bump properties, but are stable on too-long timescales, are too wide, and fail to select between competitor bars. Thus, it appears that bumps with the properties observed by Seelig and Jayaraman (2015) are a robust output of circuits with this topology under a wide range of synapse strength parameters.

To understand the contribution of each synapse class to circuit function, we systematically varied the strength of each synapse class from $-9x$ to $10x$ its original value (**Figure 4C**). Converting excitatory drive from the PB to the EB into inhibition (by reversing the sign of either the P-EN > E-PG or P-EG > E-PG synapses) eliminated input-independent bump activity in the P-EGs (mode 3). Increasing the strength of that excitatory drive led to too-stable bumps without competitor selectivity (modes 9 and 10) and eventually seizure across the circuit (mode 11). Increasing inhibition of P-ENs (by either reversing the excitatory E-PG > P-EN synapses or amplifying the strength of the inhibitory Pintr > P-EN synapses), not surprisingly, eliminated activity in the P-ENs (mode 1). Conversely, the opposite manipulations resulted in a too-stable bump (mode 10) and eventually seizure of the P-ENs (and E-PGs and Pintrs; modes 12 and 15). Increasing inhibition of P-EGs (by either reversing the excitatory E-PG > P-EG synapses or amplifying the strength of the inhibitory Pintr > P-EG synapses), not surprisingly, eliminated input-independent bump activity in the P-EGs (mode 3). Conversely, the opposite manipulations resulted in a too-stable bump (mode 8) and eventually seizure of the P-EGs (and E-PGs and Pintrs; mode 13). Increasing inhibition of Pintrs (by either reversing the excitatory E-PG > Pintr synapses or amplifying the strength of the inhibitory Pintr > Pintr), resulted in too-stable bumps (mode 7), bumps with no competitor selectivity (mode 10) and eventually seizure in P-ENs, P-EGs, and E-PGs (mode 14). The opposite manipulations eliminated input-independent bump activity in the P-ENs (mode 2) and eventually all activity in P-ENs and P-EGs (mode 1).

This systematic variation of synapse class strength parameter values also provides evidence of the robustness of the bump phenomenon in this circuit. Increasing or decreasing the strength of a synapse class by up to 50% of its baseline value, for example, seldom changes the mode of circuit dynamics (**Figure 4C**). Thus, it seems a sizable parameter subspace around the baseline values can produce bump phenomena. This analysis allows us to assess how much of the parameter space around the baseline produces bumps, not how much of the total space can produce bumps. To discover more distant parameter configurations that might also work, we added a substantial amount of Gaussian noise to all parameters simultaneously (mean = 0, standard deviation = 100% of each parameter's baseline value; this reverses the sign of a parameter 16% of the time). The vast majority of circuits with these more broadly-sampled random parameter configurations seized or were silent in at least one neural subtype but a small portion (∼1.5% of 24,000 random parameter configurations) exhibited correct bump phenomena. These were identified and pooled by *k*-means clustering of circuit dynamics.

The distributions of each parameter within this pool of bump producing circuits are shown in **Figure 4D**. Each parameter can evidently take on a wide range of values, and with the right corresponding changes in other parameters, support bump function. Notably, almost all parameters could even have their sign reversed from excitatory to inhibitory or vice versa, and still contribute to a bump-producing circuit. The exceptions were the Pintr > P-EN and Pintr > P-EG synapses, which could be silenced but not converted into excitatory synapses, and still produce a bump. In general, however, the random noise that was added to the parameters in bump-producing circuits was positive, meaning that excitatory synapses could generally be made more excitatory, and inhibitory synapses more inhibitory, without loss of bump function. Several parameter distributions appeared to be multimodal, notably P-EG > E-PG, E-PG > P-EG, E-PG > Pintr, and Pintr > Pintr, suggesting there may be discrete (or non-linear manifolds of) synapse strength configurations that support bumps.

Prediction of Circuit Manipulation Effects

This framework allowed us to predict the effect of thermogenetic or optogenetic perturbation of neural populations. We computationally injected varying amounts of current into each neural subtype as defined by Wolff et al. (2015), i.e., distinguishing between E-PG and Pintr subtypes (**Figure 5**), and projected the ensuing circuit dynamics into the same space where we defined the dynamics modes (**Figure 4B**). In general, the predicted effects matched the effects of changing the corresponding synapse class parameters. For example, injecting depolarizing current into the P-ENs had the same effect as increasing the strength of the excitatory E-PG > P-EN synapse class (or decreasing the strength of the inhibitory Pintr > P-EN synapse class). Injecting even relatively large (±5 nA) currents into the gall-tip-projecting subset of E-PGs or the P_{6-8}–P_9 subset of Pintrs (Wolff et al., 2015) had little effect, presumably because these neural subtypes are less numerous in our model, represented by only two neurons each.

DISCUSSION

Ring attractor networks are an appealing explanation for the storage and updating of continuous variables in the brain (Skaggs et al., 1995; Zhang, 1996; Taube, 2007; Knierim and Zhang, 2012) and may play a role in visual attention (de Bivort and van Swinderen, 2016). We have shown dynamics consistent with a ring attractor arise in a network of generic spiking neurons with connectivity inferred from light-resolution microscopy and few other assumptions. The neurons in this network represent classes of neurons that are morphologically identical down to the level of independent neuropil subcompartments (glomeruli/wedges) defined in recent efforts to catalog all neurons in the PB of the CX (Wolff et al., 2015).

The model produces a number of key behaviors that are predicted by ring attractor theory (Song and Wang, 2005;

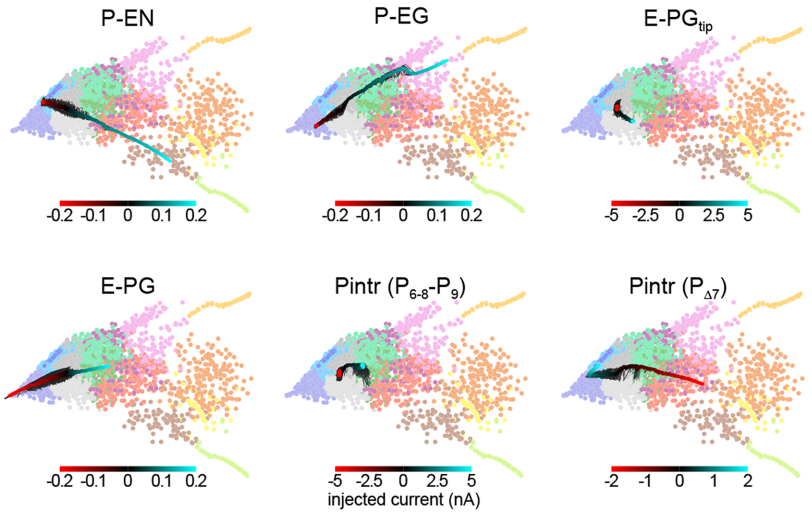

FIGURE 5 | Prediction of circuit dynamics after physiological manipulation of neuronal subtypes. Circuit dynamics projected into two dimensions using the same input stimulus, diagnostic intervals, subsampling and linear projection as **Figure 4B**. Labeled neuronal subtypes were "injected" with ectopic currents as might be brought about by thermogenetic or optogenetic manipulation. Black lines represent 10 different current sweep replicates, and the thick color-mapped line their average. E-PG$_{tip}$ refers to the subset of E-PGs that project to the Gall tip. Pintr (P$_{6-8-9}$) refers to intrinsic PB neurons that project from glomerulus 6–8 to glomerulus 9 and Pintr (P$_{\Delta7}$) to neurons that tile the PB with boutons while projecting dendrites throughout the PB.

Taube, 2007) and observed by Seelig and Jayaraman (2015) by Ca^{2+} activity in the E-PG neurons. In particular, a broad bump of activity (about 90°–120° wide) tracks a simulated cue as it moves. When the cue is removed, the bump persists indefinitely, initially staying in the position of the now-missing cue. In the continued absence of external cues, the bump can "spontaneously" shift in position. These shifts are absent when there is no spike noise in the input neurons (**Figure 3B**). Thus, stochastic fluctuations in circuit input can move the bump, but it is hard to attribute these shifts to specific input spikes, perhaps not surprising considering the interconnected topology of the circuit.

We found that the bump may slide or jump to novel cues, and chooses only a single cue if multiple competitors are provided simultaneously (occasionally spontaneously jumping between them). Furthermore, we found that even when there is a pause in the representation of the bump by action potentials, it will reappear in the same position, as suggested by brief periods of time in which Seelig and Jayaraman (2015) observe the Ca^{2+} bump to disappear and reappear in the same position. These findings suggest the bump is stored in subthreshold voltages.

Interestingly, our model suggests that there are discrete positions in the network in which this bump of activity prefers to reside as it moves through the network. Whether this is true of the circuit *in vivo* is not yet known, but it has been reported that startled cockroaches turn and run at angles that are multimodally distributed (Domenici et al., 2008). The modes of these escape angles are separated by approximately 30°, which is nearly matched by the 13 modes of bump position that we observed (**Figure 2E**). Perhaps discretized bump position tendencies underlie this distribution of escape angles. The origin of these modes surely arises from the discrete segmentation of the PB into nine glomeruli and the EB into 8 tiles/16 wedges. The modes appear to be evenly spaced every 22.5° between ±112.5°. Outside that range, two modes appear at approximately ±152°. The bump dwells in these modes 1–2 orders of magnitude less often than the other modes. Perhaps their spatial irregularity (compared to the other modes) is related to their diminished stability. Furthermore, no mode is present at ±180°, probably due to the broken radial symmetry of the circuit in this position (**Figure 1C**), which is associated with the PB being split into linear segments while the EB has circular topology. The distribution of bump speeds (**Figure 2F**) is also consistent with theoretical work predicting distinct modes of bump motion: sliding between adjacent positions and jumping between non-adjacent positions (Zhang, 1996). In general, sliding motion is induced when a stimulus moves slowly (or stochastic fluctuations increase near to the bump's current position). Conversely, the bump jumps when the stimulus moves rapidly (or stochastic fluctuations increase far from the bump's current position).

Additionally, angular position vectors can be coded not only by which neurons are active, but also by which pairs of neurons have synchronous activity (Ratté et al., 2013). In our circuit, we found that neurons tended to fire synchronously (**Figure 3E**), indicating that perhaps the PB could conceivably participate in a synchrony-based code. However, the sets of neurons observed to fire synchronously, particularly the P-EGs and P-ENs (**Figure 3A**) are predicted by the number of monosynaptic connections each of these neuron classes is from the extrinsic inputs driving the circuit (**Figure 1D**). Thus, the synchrony in the system may be determined by

its topology and not flexible enough to usefully code angular position.

By adding random noise to synapse classes, we determined that a large range of synaptic strength parameters can result in apparently proper ring attractor dynamics (**Figure 4**). Moderate levels of noise in the synaptic strengths within the circuit often still produced dynamics consistent with experimental observations. We were able to characterize potential failure modes of the network, which include absence of action potentials in classes of neurons, an inability to sustain the bump, low responsiveness, low or no competitor selectivity, and/or network seizures.

By systematically varying the values of synapse strength parameters one at a time, we explored the space of failure modes to evaluate the robustness of our model. Our model predicts that perturbing certain synaptic or neuronal classes could have larger impacts on this network than others. In general, neuronal classes with fewer neurons could be perturbed more dramatically before causing a breakdown in bump dynamics. At the same time, all the synaptic or neuronal classes could be dramatically perturbed (or even reversed in sign) and still produce a proper bump, provided appropriate compensatory changes in other classes were made. Going forward, our model may be able to provide a quantitative framework for understanding variability in individual differences in navigation, such as locomotor handedness, a behavior whose variability across individuals is controlled by neurons in the PB (Ayroles et al., 2015; Buchanan et al., 2015). Specifically, we can add noise to individual synapses, reflecting variation from developmental stochasticity and post-developmental plasticity, e.g., by analogy to our synapse class parameter dithering:

$$M'_{\mathrm{j,i}} \;=\; M_{\mathrm{j,i}}\,(1+\mathrm{Norm}(0,\sigma))$$

It is important to consider which assumptions made in this model might not be realistic. The information flow of each neuron class is inferred from the overlap of "dendritic" and "axonal" cellular compartments determined by light-microscopy. Despite being unipolar, neurons in *Drosophila* generally have polarized information flow (Rolls, 2011), however, common axo-axonal, dendro-dendritic and perhaps even dendro-axonal synapses (Schneider-Mizell et al., 2016) paint a more complex picture. Electrical coupling, which can lead to synchronized neuronal firing, is also common in insect neurons (Pereda, 2014), but we have not included any in our model. Furthermore, we have assumed that every neuron has the same integration and firing dynamics despite the fact that the dynamics can vary significantly based on specific ion channel expression levels (Marder, 2011; Berger and Crook, 2015). We also make the assumption that if an axon and dendrite overlap in a compartment then they are connected, but this is not necessarily the case. Neurons that are adjacent with the resolution provided by light microscopy may not come into physical contact (Feinberg et al., 2008). Moreover, axons and dendrites which are in contact do not necessarily form functional synapses (Kasthuri et al., 2015). Due to these caveats, it is remarkable that our model recapitulates so many of the experimental observations of Ca^{2+} of E-PG neurons.

The core computation of this circuit may be robust to many categories of biological detail, emerging instead from high-level connectivity of the sort that can be inferred from light microscopy. Indeed, leaky-integrator implementations of the model simulating graded neurons without action potentials produced passable bumps (**Figures 3F,G**). This suggests that bump dynamics are not only robust to synapse strength parameter variation, but also variation in neuron physiological parameters. However, the leaky-integrator implementation did not exhibit selectivity between competitor stimuli as sharp as the leaky-integrate-and-fire implementation. This suggests that spiking neurons are required to recapitulate experimental Ca^{2+} recordings, while not being required for bump dynamics in general.

Despite the conspicuous ring shape of the EB and its large number of inhibitory neurons with horizontal morphologies spanning all azimuthal positions (Martín-Peña et al., 2014; Kottler et al., 2017), neither of these qualities is necessary to bring about ring attractor-like dynamics in our model. Instead, our model generates global inhibition using intrinsic PB neurons (the PBintrs; **Figure 1**). The EB has been shown to receive spatiotopic information about visual features (Seelig and Jayaraman, 2013) and is involved in visual place learning (Ofstad et al., 2011). These observations suggest that the EB encodes spatial information about landmarks in the environment which could be used to correct accumulated error in the position of a bump. While inhibitory circuitry within the EB is not required for ring attractor dynamics in the PB-EB circuit, we have no evidence that the inhibitory circuitry in the EB does not participate in a ring attractor. It is possible that both the Pintrs in the PB and the ring neurons (Martín-Peña et al., 2014) of the EB implement long-range inhibition for the production of two distinct ring attractors, which could potentially interact to perform more sophisticated computations.

The egocentric heading correlate present in the PB-EB circuit is likely transmitted to other regions of the CX, particularly the FB. This neuropil could be a site of integration of navigational with internal state and sensory information for adaptive decision making. In addition to the PB-EB circuit neurons described here, the PB contains many columnar neurons projecting into the FB that have postsynaptic arbors in individual PB glomeruli and presynaptic boutons in different layers and columns of the FB (Wolff et al., 2015). Thus, it is likely that the FB inherits a bump or vertical band of activity from the PB. The FB is hypothesized to gate the selection of different behaviors in a state-dependent fashion (Weir and Dickinson, 2015) and activation of a single side of the FB induces ipsilateral turning (Guo and Ritzmann, 2013). Horizontal dopaminergic neurons in the FB have been shown to mediate sleep and arousal (Pimentel et al., 2016). The FB receives direct horizontal input from the visual system via the optic glomeruli (Mu et al., 2012) and also from many known modulatory neuropeptidergic neurons (Kahsai and Winther, 2011; Kahsai et al., 2012). The columnar projection neurons coming from the FB likely interact with these horizontal modulatory neurons. Therefore, it is appealing to

hypothesize that the FB contains its own bump, downstream of the PB-EB bump, that it uses to integrate navigational information with neuromodulatory signals encoding internal states and sensory inputs.

AUTHOR CONTRIBUTIONS

BLB conceived of the project. KSK and BLB implemented the model, collected the data, analyzed it and wrote the manuscript.

ACKNOWLEDGMENTS

We thank Tanya Wolff and Vivek Jayaraman for helpful discussions and expert guidance on protocerebral bridge neurobiology. We acknowledge the National Science Foundation Graduate Research Fellowship Program (award number 2013170544) and the Alfred P. Sloan Foundation for funding support. We thank the reviewers for thoughtful feedback that improved the manuscript.

REFERENCES

Arena, P., Maceo, S., and Patane, L. (2013). "A spiking network for spatial memory formation: towards a fly-inspired ellipsoid body model," in *Neural Networks (IJCNN), The 2013 International Joint Conference*, (Dallas, TX).

Ayroles, J. F., Buchanan, S. M., O'Leary, C., Skutt-Kakaria, K., Grenier, J. K., Clark, A. G., et al. (2015). Behavioral idiosyncrasy reveals genetic control of phenotypic variability. *Proc. Natl. Acad. Sci. U S A* 112, 6706–6711. doi: 10.1073/pnas.1503830112

Berger, S. D., and Crook, S. M. (2015). Modeling the influence of ion channels on neuron dynamics in *Drosophila*. *Front. Comput. Neurosci.* 9:139. doi: 10.3389/fncom.2015.00139

de Bivort, B. L., and van Swinderen, B. (2016). Evidence for selective attention in the insect brain. *Curr. Opin. Insect Sci.* 15, 9–15. doi: 10.1016/j.cois.2016.02.007

Bockhorst, T., and Homberg, U. (2015). Amplitude and dynamics of polarization-plane signaling in the central complex of the locust brain. *J. Neurophysiol.* 113, 3291–3311. doi: 10.1152/jn.00742.2014

Buchanan, S. M., Kain, J. S., and de Bivort, B. L. (2015). Neuronal control of locomotor handedness in *Drosophila*. *Proc. Natl. Acad. Sci. U S A* 112, 6700–6705. doi: 10.1073/pnas.1500804112

Chou, Y. H., Spletter, M. L., Yaksi, E., Leong, J. C., Wilson, R. I., and Luo, L. (2010). Diversity and wiring variability of olfactory local interneurons in the *Drosophila* antennal lobe. *Nat. Neurosci.* 13, 439–449. doi: 10.1038/nn.2489

Collett, T. S., and Graham, P. (2004). Animal navigation: path integration, visual landmarks and cognitive maps. *Curr. Biol.* 14, R475–R477. doi: 10.1016/j.cub.2004.06.013

Daniels, R. W., Gelfand, M. V., Collins, C. A., and DiAntonio, A. (2008). Visualizing glutamatergic cell bodies and synapses in *Drosophila* larval and adult CNS. *J. Comp. Neurol.* 508, 131–152. doi: 10.1002/cne.21670

Domenici, P., Booth, D., Blagburn, J. M., and Bacon, J. P. (2008). Cockroaches keep predators guessing by using preferred escape trajectories. *Curr. Biol.* 18, 1792–1796. doi: 10.1016/j.cub.2008.09.062

Etienne, A. S., and Jeffery, K. J. (2004). Path integration in mammals. *Hippocampus* 14, 180–192. doi: 10.1002/hipo.10173

Feinberg, E. H., Vanhoven, M. K., Bendesky, A., Wang, G., Fetter, R. D., Shen, K., et al. (2008). GFP Reconstitution Across Synaptic Partners (GRASP) defines cell contacts and synapses in living nervous systems. *Neuron* 57, 353–363. doi: 10.1016/j.neuron.2007.11.030

Fişek, M., and Wilson, R. I. (2014). Stereotyped connectivity and computations in higher-order olfactory neurons. *Nat. Neurosci.* 17, 280–288. doi: 10.1038/nn.3613

Fruchterman, T. M. J., and Reingold, E. M. (1990). *Graph Drawing by Force-Directed Placement*. Urbana, IL: University of Illinois at Urbana-Champaign.

Gaudry, Q., Hong, E. J., Kain, J., de Bivort, B. L., and Wilson, R. I. (2013). Asymmetric neurotransmitter release enables rapid odour lateralization in *Drosophila*. *Nature* 493, 424–428. doi: 10.1038/nature11747

Gouwens, N. W., and Wilson, R. I. (2009). Signal propagation in *Drosophila* central neurons. *J. Neurosci.* 29, 6239–6249. doi: 10.1523/JNEUROSCI.0764-09.2009

Guo, P., and Ritzmann, R. E. (2013). Neural activity in the central complex of the cockroach brain is linked to turning behaviors. *J. Exp. Biol.* 216, 992–1002. doi: 10.1242/jeb.080473

Haferlach, T., Wessnitzer, J., Mangan, M., and Webb, B. (2007). Evolving a neural model of insect path integration. *Adapt. Behav.* 15, 273–287. doi: 10.1177/1059712307082080

Heinze, S. (2014). "Polarized-light processing in insect brains: recent insights from the desert locust, the monarch butterfly, the cricket and the fruit fly," in *Polarized Light and Polarization Vision in Animal Sciences*, ed. G. Horváth (New York, NY: Springer Berlin Heidelberg), 61–111.

Heinze, S., and Homberg, U. (2007). Maplike representation of celestial E-vector orientations in the brain of an insect. *Science* 315, 995–997. doi: 10.1126/science.1135531

Hodgkin, A. L., and Huxley, A. F. (1952). A quantitative description of membrane current and its application to conduction and excitation in nerve. *J. Physiol.* 117, 500–544. doi: 10.1113/jphysiol.1952.sp004764

Homberg, U., Heinze, S., Pfeiffer, K., Kinoshita, M., and el Jundi, B. (2011). Central neural coding of sky polarization in insects. *Philos. Trans. R. Soc. Lond. B Biol. Sci.* 366, 680–687. doi: 10.1098/rstb.2010.0199

Kahsai, L., Carlsson, M. A., Winther, A. M., and Nässel, D. R. (2012). Distribution of metabotropic receptors of serotonin, dopamine, GABA, glutamate and short neuropeptide F in the central complex of *Drosophila*. *Neuroscience* 208, 11–26. doi: 10.1016/j.neuroscience.2012.02.007

Kahsai, L., and Winther, Å. M. E. (2011). Chemical neuroanatomy of the *Drosophila* central complex: distribution of multiple neuropeptides in relation to neurotransmitters. *J. Comp. Neurol.* 519, 290–315. doi: 10.1002/cne.22520

Kasthuri, N., Hayworth, K. J., Berger, D. R., Schalek, R. L., Conchello, J. A., Knowles-Barley, S., et al. (2015). Saturated reconstruction of a volume of neocortex. *Cell* 162, 648–661. doi: 10.1016/j.cell.2015.06.054

Kim, A. J., Fitzgerald, J. K., and Maimon, G. (2015). Cellular evidence for efference copy in *Drosophila* visuomotor processing. *Nat. Neurosci.* 18, 1247–1255. doi: 10.1038/nn.4083

Knierim, J. J., and Zhang, K. (2012). Attractor dynamics of spatially correlated neural activity in the limbic system. *Annu. Rev. Neurosci.* 35, 267–285. doi: 10.1146/annurev-neuro-062111-150351

Kottler, B., Fiore, V. G., Ludlow, Z. N., Buhl, E., Vinatier, G., Faville, R., et al. (2017). A lineage-related reciprocal inhibition circuitry for sensory-motor action selection. *BioRxiv* doi: 10.1101/100420 [Epub ahead of print].

Lin, C.-Y., Chuang, C.-C., Hua, T.-E., Chen, C.-C., Dickson, B. J., Greenspan, R. J., et al. (2013). A comprehensive wiring diagram of the protocerebral bridge for visual information processing in the *Drosophila* brain. *Cell Rep.* 3, 1739–1753. doi: 10.1016/j.celrep.2013.04.022

Liu, W. W., and Wilson, R. I. (2013). Glutamate is an inhibitory neurotransmitter in the *Drosophila* olfactory system. *Proc. Natl. Acad. Sci. U S A* 110, 10294–10299. doi: 10.1073/pnas.1220560110

Marder, E. (2011). Variability, compensation and modulation in neurons and circuits. *Proc. Natl. Acad. Sci. U S A* 108, 15542–15548. doi: 10.1073/pnas.1010674108

Martín-Peña, A., Acebes, A., Rodríguez, J.-R., Chevalier, V., Casas-Tinto, S., Triphan, T., et al. (2014). Cell types and coincident synapses in the ellipsoid body of *Drosophila*. *Eur. J. Neurosci.* 39, 1586–1601. doi: 10.1111/ejn.12537

McNaughton, B. L., Chen, L. L., and Markus, E. J. (2007). "Dead reckoning," landmark learning and the sense of direction: a neurophysiological and computational hypothesis. *J. Cogn. Neurosci.* 3, 190–202. doi: 10.1162/jocn.1991.3.2.190

Mu, L., Ito, K., Bacon, J. P., and Strausfeld, N. J. (2012). Optic glomeruli and their inputs in *Drosophila* share an organizational ground pattern with the antennal lobes. *J. Neurosci.* 32, 6061–6071. doi: 10.1523/JNEUROSCI.0221-12.2012

Nagel, K. I., Hong, E. J., and Wilson, R. I. (2015). Synaptic and circuit mechanisms promoting broadband transmission of olfactory stimulus dynamics. *Nat. Neurosci.* 18, 56–65. doi: 10.1038/nn.3895

Nern, A., Pfeiffer, B. D., and Rubin, G. M. (2015). Optimized tools for multicolor stochastic labeling reveal diverse stereotyped cell arrangements in the fly visual system. *Proc. Natl. Acad. Sci. U S A* 112, E2967–E2976. doi: 10.1073/pnas.1506763112

Ofstad, T. A., Zuker, C. S., and Reiser, M. B. (2011). Visual place learning in *Drosophila* melanogaster. *Nature* 474, 204–207. doi: 10.1038/nature10131

Pereda, A. E. (2014). Electrical synapses and their functional interactions with chemical synapses. *Nat. Rev. Neurosci.* 15, 250–263. doi: 10.1038/nrn3708

Pfeiffer, K., and Homberg, U. (2014). Organization and functional roles of the central complex in the insect brain. *Annu. Rev. Entomol.* 59, 165–184. doi: 10.1146/annurev-ento-011613-162031

Pimentel, D., Donlea, J. M., Talbot, C. B., Song, S. M., Thurston, A. J. F., and Miesenböck, G. (2016). Operation of a homeostatic sleep switch. *Nature* 536, 333–337. doi: 10.1038/nature19055

Ratté, S., Hong, S., De Schutter, E., and Prescott, S. A. (2013). Impact of neuronal properties on network coding: roles of spike initiation dynamics and robust synchrony transfer. *Neuron* 78, 758–772. doi: 10.1016/j.neuron.2013.05.030

Rohrbough, J., and Broadie, K. (2002). Electrophysiological analysis of synaptic transmission in central neurons of *Drosophila larvae*. *J. Neurophysiol.* 88, 847–860. doi: 10.1152/jn.01010.2001

Rolls, M. M. (2011). Neuronal polarity in *Drosophila*: sorting out axons and dendrites. *Dev. Neurobiol.* 71, 419–429. doi: 10.1002/dneu.20836

Schneider-Mizell, C. M., Gerhard, S., Longair, M., Kazimiers, T., Li, F., Zwart, M. F., et al. (2016). Quantitative neuroanatomy for connectomics in *Drosophila*. *Elife* 5:e12059. doi: 10.7554/eLife.12059

Seelig, J. D., and Jayaraman, V. (2013). Feature detection and orientation tuning in the *Drosophila* central complex. *Nature* 503, 262–266. doi: 10.1038/nature12601

Seelig, J. D., and Jayaraman, V. (2015). Neural dynamics for landmark orientation and angular path integration. *Nature* 521, 186–191. doi: 10.1038/nature14446

Sheeba, V., Gu, H., Sharma, V. K., O'Dowd, D. K., and Holmes, T. C. (2008). Circadian- and light-dependent regulation of resting membrane potential and spontaneous action potential firing of *Drosophila* circadian pacemaker neurons. *J. Neurophysiol.* 99, 976–988. doi: 10.1152/jn.00930.2007

Skaggs, W., Knierim, W., Kudrimoti, H. S., and McNaughton, B. L. (1995). "A model of the neural basis of the rat's sense of direction," in *Advances in Neural Information Processing Systems*, (Vol. 7) eds G. Tesauro, D. S. Touretzky and T. K. Leen, (Cambridge, MA: MIT Press), 173–180.

Solovyeva, K. P., Karandashev, I. M., Zhavoronkov, A., and Dunin-Barkowski, W. L. (2016). Models of innate neural attractors and their applications for neural information processing. *Front. Syst. Neurosci.* 9:178. doi: 10.3389/fnsys.2015.00178

Song, P., and Wang, X.-J. (2005). Angular path integration by moving "hill of activity": A spiking neuron model without recurrent excitation of the head-direction system. *J. Neurosci.* 25, 1002–1014. doi: 10.1523/JNEUROSCI.4172-04.2005

Stein, R. B. (1967). Some models of neuronal variability. *Biophys. J.* 7, 37–68. doi: 10.1016/s0006-3495(67)86574-3

Strausfeld, N. J. (1976). "The primary compartments of the brain," in *Atlas of an Insect Brain*, ed. N. J. Strausfeld (New York, NY: Springer Berlin Heidelberg), 31–40.

Taube, J. S. (2007). The head direction signal: origins and sensory-motor integration. *Annu. Rev. Neurosci.* 30, 181–207. doi: 10.1146/annurev.neuro.29.051605.112854

Varga, A. G., and Ritzmann, R. E. (2016). Cellular basis of head direction and contextual cues in the insect brain. *Curr. Biol.* 26, 1816–1828. doi: 10.1016/j.cub.2016.05.037

Weir, P. T., and Dickinson, M. H. (2015). Functional divisions for visual processing in the central brain of flying *Drosophila*. *Proc. Natl. Acad. Sci. U S A* 112, E5523–E5532. doi: 10.1073/pnas.1514415112

Wolff, T., Iyer, N. A., and Rubin, G. M. (2015). Neuroarchitecture and neuroanatomy of the *Drosophila* central complex: a GAL4-based dissection of protocerebral bridge neurons and circuits. *J. Comp. Neurol.* 523, 997–1037. doi: 10.1002/cne.23705

Zhang, K. (1996). Representation of spatial orientation by the intrinsic dynamics of the head-direction cell ensemble: a theory. *J. Neurosci.* 16, 2112–2126.

Conflict of Interest Statement: The authors declare that the research was conducted in the absence of any commercial or financial relationships that could be construed as a potential conflict of interest.

frontiers in Behavioral Neuroscience

METHODS
published: 30 May 2017
doi: 10.3389/fnbeh.2017.00102

Generating Executable Models of the Drosophila Central Complex

Lev E. Givon[1], *Aurel A. Lazar*[2]* *and Chung-Heng Yeh*[2]

[1] *The Charles Stark Draper Laboratory, Inc., Cambridge, MA, United States,* [2] *Bionet Group, Department of Electrical Engineering, Columbia University, New York, NY, United States*

The central complex (CX) is a set of neuropils in the center of the fly brain that have been implicated as playing an important role in vision-mediated behavior and integration of spatial information with locomotor control. In contrast to currently available data regarding the neural circuitry of neuropils in the fly's vision and olfactory systems, comparable data for the CX neuropils is relatively incomplete; many categories of neurons remain only partly characterized, and the synaptic connectivity between CX neurons has yet to be fully determined. Successful modeling of the information processing functions of the CX neuropils therefore requires a means of easily constructing and testing a range of hypotheses regarding both the high-level structure of their neural circuitry and the properties of their constituent neurons and synapses. To this end, we have created a web application that enables simultaneous graphical querying and construction of executable models of the CX neural circuitry based upon currently available information regarding the geometry and polarity of the arborizations of identified local and projection neurons in the CX. The application's novel functionality is made possible by the Fruit Fly Brain Observatory, a platform for collaborative study and development of fruit fly brain models.

Keywords: central complex, Drosophila, brain emulation, visualization

OPEN ACCESS

Edited by:
Stanley Heinze,
Lund University, Sweden

Reviewed by:
Uwe Homberg,
Philipps University of Marburg, Germany
Barbara Webb,
University of Edinburgh, United Kingdom

***Correspondence:**
Aurel A. Lazar
aurel@ee.columbia.edu

Received: *03 February 2017*
Accepted: *12 May 2017*
Published: *30 May 2017*

Citation:
Givon LE, Lazar AA and Yeh C-H (2017) Generating Executable Models of the Drosophila Central Complex. Front. Behav. Neurosci. 11:102. doi: 10.3389/fnbeh.2017.00102

1. INTRODUCTION

The brain of the fruit fly *Drosophila melanogaster* comprises approximately 50 neuropils. Most of these modules—referred to as local processing units (LPUs) are characterized by unique populations of local neurons; some—called hubs—do not contain any local neurons (Chiang et al., 2011). The central complex (CX) comprises between 2,000 and 5,000 neurons (Strauss, 2014) organized in four neuropils: the protocerebral bridge (PB), fan-shaped body (FB), ellipsoid body (EB), and noduli (NO) (**Figure 1**). Local neurons have been identified in PB and FB, but not in EB or NO (Chiang et al., 2011; Wolff et al., 2015). In contrast to most neuropils in the fly brain, PB, FB, and EB are unpaired; NO comprises 3 paired subunits (Wolff et al., 2015). Accessory brain areas that are connected directly to neuropils in CX include the bulb (BU), crepine (CRE), inferior bridge (IB), lateral accessory lobe (LAL), superior medial protocerebrum (SMP), wedge (WED), and posterior slope (PS) (Lin et al., 2013).

Although, a growing amount of CX structural information is available for several insect species other than the fruit fly such as the monarch butterfly, desert locust, field cricket, and discoid cockroach (Pfeiffer and Homberg, 2014), CX connectome information is currently less complete than that of sensory neuropils such as those in the olfactory and vision systems, the latter of which has recently been mapped in the fly in great detail using electron microscopy (Takemura, 2015). A range of local and projection neurons in CX have been identified and grouped into isomorphic sets

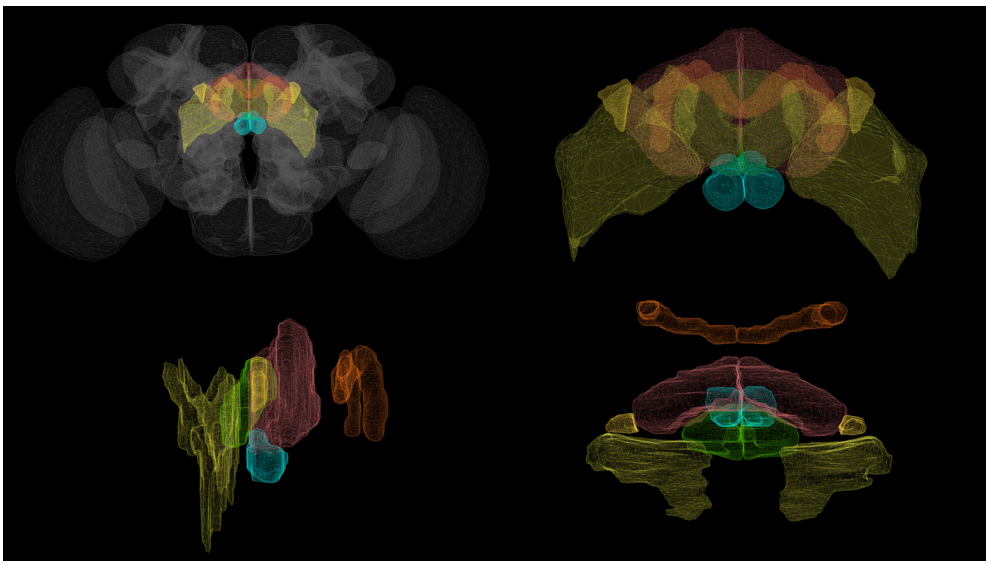

FIGURE 1 | Volumetric rendering of central complex neuropils (PB, FB, EB, NO) and select accessory neuropils (BU, LAL) innervated by CX neurons. (Clockwise from top left: whole brain, front view of the central complex, side view of the central complex, top view of the central complex.) Rendering created with NeuroGFX using volumetric information from the FlyCircuit database (Chiang et al., 2011).

using Golgi staining, genetic tagging techniques, and confocal microscopy (Hanesch et al., 1989; Young and Armstrong, 2010b; Lin et al., 2013; Wolff et al., 2015); however, many other CX neurons have not been systematically characterized and the synaptic connectivity between them remains unknown owing to the limitations of the above optical imaging technologies and the very limited EM-based analysis of CX synapses done to date (for an example of the latter, see Martín-Peña et al., 2014). This ambiguity regarding the structure of the CX neural circuitry compounds the already difficult task of modeling a portion of the brain that does not receive direct sensory input.

Genetic experiments have shown that the CX neuropils play essential roles in a range of important behaviors:

(i) EB appears to be involved in visual place learning (Ofstad et al., 2011; Dewar et al., 2015), short-term orientation memory (Neuser et al., 2008; Seelig and Jayaraman, 2013; Wystrach et al., 2014), angular path integration (Seelig and Jayaraman, 2015), and left-right bargaining (Strauss, 2014);
(ii) FB appears to also play a role in left-right bargaining, as well as visual pattern memory and object recognition (Strauss and Berg, 2010; Strauss, 2014);
(iii) PB plays a role in controlling step length and hence direction of walking (Strauss and Berg, 2010; Strauss, 2014);
(iv) NO neuropils seem to be involved in flight control (Pfeiffer and Homberg, 2014).

While some functional models of the CX neuropils have been presented that attribute high-level functions such as short-term object storage and object recognition to different parts of the circuit (Strauss and Berg, 2010; Strauss, 2014), they do not explicitly show how the CX circuitry explicitly implements the information processing functions associated with the above behaviors or how the various neuropils' individual functions combine to produce more comprehensive behaviors such as long-term motor skill learning or locomotor activity control. In light of the incompleteness of the CX connectome, it is perhaps unsurprising that only a few computational models of the CX neuropils or the entire CX currently exist. A spiking neural network model of spatial memory formation and storage in EB is presented in Arena et al. (2013); while this model can replicate experimental results for specific behaviors using a ring attractor circuit inspired by that of EB, it does not attempt to account for the exact observed biological circuitry or explain how such a model interacts with the other CX neuropils. A model of CX was included in a more comprehensive insect brain simulation described in Arena et al. (2014), but it employs generalized models of the CX neuropils that use artificial behavior selection networks which—although they superficially make use of spiking neuron models— do not employ the observed neural circuitry of the neuropils.

To enable further investigation of the information processing capabilities of the CX neuropils, we need to be able to efficiently generate and evaluate different executable CX models given the limited available connectome data. While a similar approach involving *C. elegans* has been used to generate multiple testable models regarding the neural basis for salt klinotaxis behavior (Izquierdo and Beer, 2013), the greater structural complexity of the fruit fly CX and the need to evaluate the CX models together with models of the neuropils that provide them with input requires

(i) A database-driven approach to generating different models of the CX neural circuitry that incorporate experimentally obtained biological data with hypothetical or algorithmically

inferred structural characteristics that attempt to account for the unknown aspects of the circuitry, and

(ii) A graphical means of interacting with CX models and their outputs that exposes the circuitry at different levels of structural abstraction ranging from individual neurons through families of morphologically similar neurons to circuits comprising multiple neuron families.

To address these requirements, we have developed a web application for simultaneous graphical navigation of the CX and execution of models of its neural circuitry; this application may be accessed at http://fruitflybrain.org/neuroapps/central_complex. In this paper, we first describe the software architecture underlying this application and the unique visualization features of its user interface. We then present a scheme for labeling neurons in terms of their arborization patterns that can be used to algorithmically infer unknown synaptic connectivity in the CX neuropils. Finally, we demonstrate how this software utilizes this scheme to construct executable models comprising several families of neurons in the CX with two examples that, respectively, illustrate model responses to injected input signals and a comparison between the responses of models with circuitry based upon wild type and mutant fly strains.

2. SOFTWARE ARCHITECTURE

The CX web application is built upon several key software components that collectively constitute the **Fruit Fly Brain Observatory**, an open-source platform for the emulation and biological validation of fruit fly brain models in health and disease (Ukani et al., 2016b) (**Figure 2**):

(i) Fly brain circuit models are stored in **NeuroArch**, a graph database designed to facilitate the generation of executable neural circuit models (Givon et al., 2014). NeuroArch provides an extensible data model that unifies the representation of both biological and executable neural circuit data in a single graph. This data model currently supports a range of common point neuron and synapse models such as Leaky Integrate-and-Fire neurons, non-spiking Morris-Lecar neurons, and alpha function synapses. Circuits may be accessed via an object-graph mapping (OGM) interface that enables a range of sophisticated queries to be performed without having to explicitly specify complex query strings. This interface enables implementation of algorithms for inferring executable circuits from incomplete connectome data and sophisticated manipulation of stored neural circuit data to test model hypotheses. NeuroArch's query interface permits all circuit components' parameters to be modified regardless of whether they were algorithmically constructed.

(ii) Fly brain models in NeuroArch may comprise local processing units that potentially contain different modeling components. To fuse these portions into a single executable model regardless of their internal design, the **Neurokernel** package defines a mandatory communication interface for neural circuit models exported by NeuroArch that enables their integration and execution on multiple graphics processing units (GPUs) (Givon and Lazar, 2016). Neurokernel provides support for executing models that utilize a range of neuron and synapse models defined by NeuroArch's current data model. Since Neurokernel's model communication interface is also described in NeuroArch's data model, circuits comprising multiple interconnected neuropils (such as the CX) may be fully specified in NeuroArch and immediately dispatched to Neurokernel for execution.

(iii) **NeuroGFX** provides a reconfigurable graphical interface for navigation, manipulation, and execution of the CX neural circuit; a screenshot of this interface appears in **Figure 3**. (Yeh et al., 2016). Regions of neuropils comprised by and accessory to the central complex may be rendered in 3D. Neurons in the executed CX model may be selected and highlighted in a schematic circuit view; detailed portions of the circuit may also be magnified. The interface also enables multiple selected neuron responses to be concurrently plotted in 2D or 3D. Regions of the CX neuropils innervated by selected neurons may also be highlighted in real time as the model is executed. NeuroGFX's user interface is currently read-only; the capacity to modify stored CX models (via NeuroArch's query interface) will be added in the future.

(iv) In addition to neuropil models exposed through NeuroGFX, the architecture supports development of

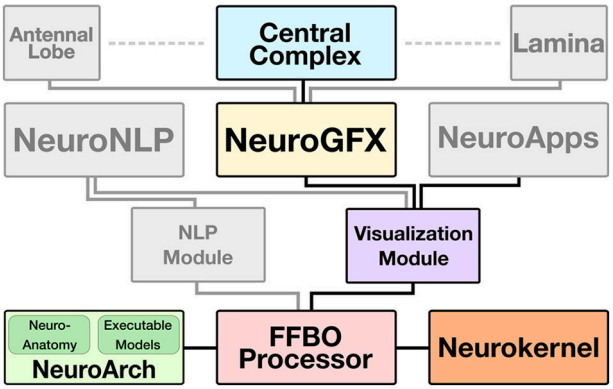

FIGURE 2 | FFBO architecture for support of CX model visualization, manipulation, and execution. Solid lines depict data flow between software components. The **Central Complex Model** and those of other neuropils (e.g., **Antennal Lobe**, **Lamina**) are implemented as software applications that use **NeuroGFX** to support interactive user configuration and launching of model execution. The **Visualization Module** provides low-level routines for 3D rendering of neuropils and neuron morphologies utilized by NeuroGFX and comprehensive models of fly brian subsystems called **NeuroApps**. Neuroanatomy and executable circuit model data is stored in the **NeuroArch** database and efficiently executed by **Neurokernel**. The **FFBO Processor** sets up direct network connections between the other components of the architecture to accelerate data transfer during application execution. The **NLP (Natural Language Processing) Module** provides a high-level query interface to NeuroArch that is exposed to users through the **NeuroNLP** graphical interface.

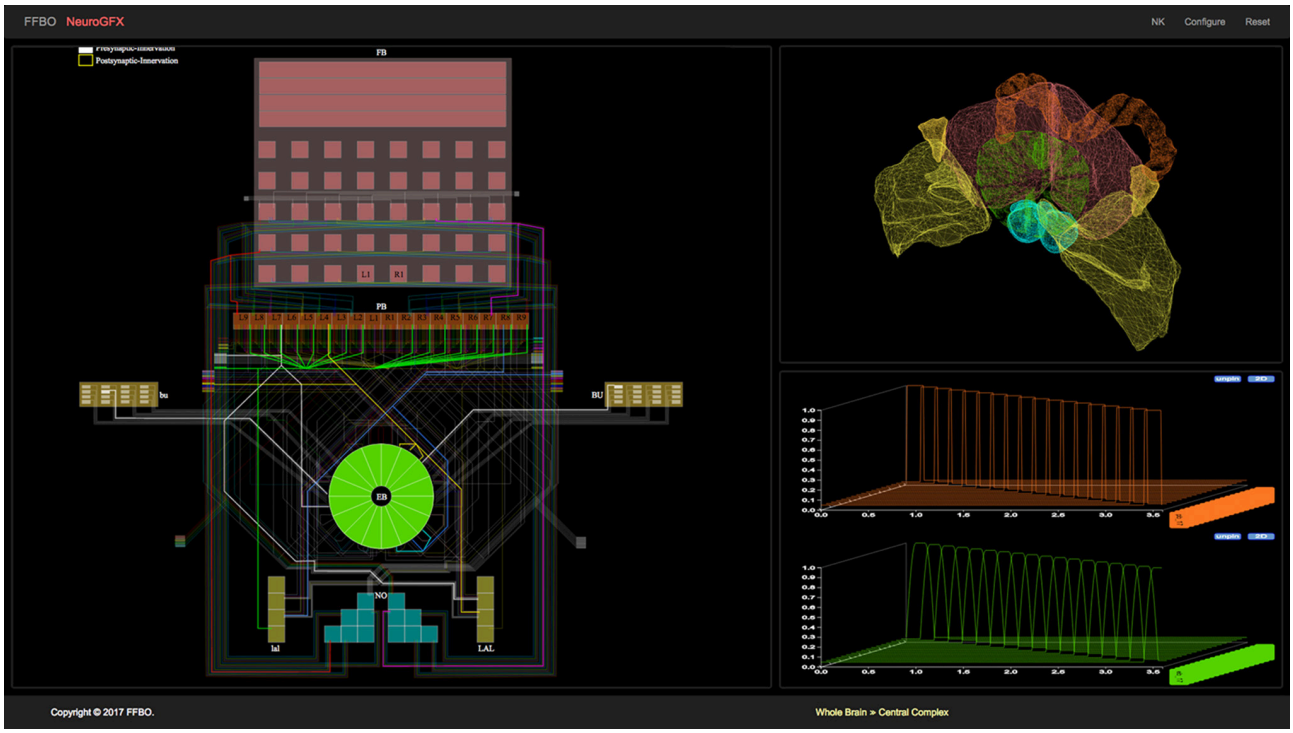

FIGURE 3 | NeuroGFX graphical user interface depicting CX neural circuit, neuropils, and activity of neurons in executed CX model.

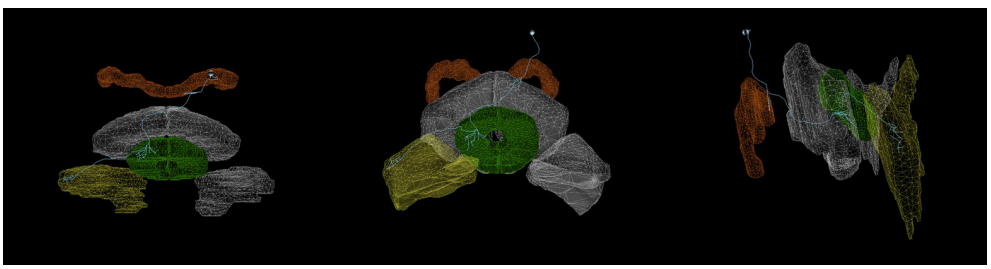

FIGURE 4 | Arborizations of a PB-EB-LAL neuron (Wolff et al., 2015) (light blue) superimposed upon the CX neuropils (from left to right: top view, front view, side view.). Each arborization occupies a specific region of the PB, EB, and LAL neuropils (■PB, ■EB, ■LAL). Rendering created with NeuroGFX using volumetric information of neuropils and skeletonic information of neurons from the FlyCircuit database (Chiang et al., 2011). This neuron is registered in the FlyCircuit database with the indentifier "Gad1-F-400245."

customized graphical applications called **NeuroApps**. These provide access to specialized models of fly brain subsystems such as the vision or olfactory systems for exploring functions associated with models of healthy or diseased neural circuits in these systems.

(v) To provide both NeuroGFX and NeuroApps with the same base set of graphical features, the FFBO architecture provides a **Visualization Module** that contains routines for drawing neuropils and rendering neuron morphologies using WebGL.

(vi) The **Natural Language Interface (NLP) Module** provides a user-friendly way to construct sophisticated queries against NeuroArch in plain English that obviate the need for users to directly interact with NeuroArch's OGM. This functionality is exposed to users through a graphical interface called **NeuroNLP** (Ukani et al., 2016a). NeuroNLP is not currently utilized by the CX model application.

(vii) To accelerate data transmission between the above components and provide the modularity required to build future applications based upon the FFBO platform, the **FFBO Processor** sets up data connections between platform components that need to communication during application execution.

```
⟨label⟩ := ⟨arborization⟩ (⟨hyphen⟩⟨arborization⟩) +
⟨arborization⟩ := ⟨neuropil⟩⟨slash⟩⟨regions⟩⟨slash⟩⟨neurite type⟩
⟨regions⟩ := ⟨region⟩ (⟨bar⟩⟨region⟩) ∗
⟨neuropil⟩ := (BU/bu/CRE/cre/EB/FB/IB/ib/LAL/
    lal/NO/no/PB/PS/ps/SMP/smp/WED/wed)
⟨region⟩ := ⟨tuple2⟩/⟨tuple3⟩/⟨name⟩
⟨tuple2⟩ := ⟨left paren⟩⟨name⟩⟨comma⟩⟨name⟩⟨right paren⟩
⟨tuple3⟩ := ⟨left paren⟩⟨name⟩⟨comma⟩⟨name⟩⟨comma⟩⟨name⟩⟨right paren⟩
⟨name⟩ := LRB/ (⟨side⟩? (⟨integer⟩/⟨range⟩/⟨alpha⟩/⟨list⟩)) /
    (⟨side⟩! (⟨integer⟩/⟨range⟩/⟨alpha⟩/⟨list⟩))
⟨side⟩ := (L/R/LR/RL)
⟨neurite type⟩ := (s/b/bs/sb)
⟨range⟩ := ⟨left bracket⟩⟨integer⟩⟨hyphen⟩⟨integer⟩⟨right bracket⟩
⟨list⟩ := ⟨left bracket⟩⟨alpha⟩ (⟨comma⟩⟨alpha⟩) ∗ ⟨right bracket⟩
⟨integer⟩ := [0 − 9]+
⟨alpha⟩ := [a − z, A − Z, 0 − 9]+
⟨hyphen⟩ := −
⟨bar⟩ := |
⟨slash⟩ := /
⟨comma⟩ := ,
⟨left paren⟩ := (
⟨right paren⟩ := )
⟨left bracket⟩ := [
⟨right bracket⟩ := ]
```

FIGURE 5 | PEG grammar for CX neuron label.

TABLE 1 | Fields in NeuroArch arborization data record.

Field	Data type	Sample values
neurite	set of "b" or "s"	[b], [b, s]
neuropil	string	PB, EB
region	set of strings or tuples	[L1], [(1, R1)]

Region strings or tuples conform to the format described by the grammar in Section 3.1.

TABLE 2 | Assignment of neuron families to neuropils in generated CX model.

Neuropil	Neuron families
BU, bu	*BU-EB*
EB	EB-LAL-PB
FB	*FB local*
PB	PB local, PB-EB-NO, PB-EB-LAL, PB-FB-CRE, PB-FB-NO, PB-FB-LAL, WED-PS-PB, IB-LAL-PS-PB

Arborization data for families in italics is hypothetical.

TABLE 3 | Identified neurons connecting CX and accessory neuropils.

Neuronfamily	Locations of postsynaptic arborizations (dendrites)	Locations of presynaptic arborizations (axons)	References
BU-EB	BU	EB	(Young and Armstrong, 2010b, p. 1509, Table 1)
EB-LAL-PB	EB	EB, LAL, PB	(Lin et al., 2013, Figures 4J–M)
FB local	FB	FB	(Young and Armstrong, 2010a, p. 1439)
IB-LAL-PS-PB	IB, LAL, PS	PB	(Lin et al., 2013, p. 1743, Figure 4A) (Wolff et al., 2015, Figure 3N)
PB local	PB	PB	(Lin et al., 2013, p. 1743),(Wolff et al., 2015, p. 1007)
PB-EB-LAL	PB	EB, LAL	(Lin et al., 2013, Figure 5E)
PB-EB-NO	PB	EB, NO	(Lin et al., 2013, p. 1745, Figure 5G)
PB-FB-CRE	PB	CRE, FB	(Lin et al., 2013, Figure 6F) (Wolff et al., 2015, Figure 3L)
PB-FB-LAL	PB	FB, LAL	(Lin et al., 2013, Figures 6F–H)
PB-FB-LAL-CRE	PB	CRE, FB, LAL	(Wolff et al., 2015, Figure 3M)
PB-FB-NO	PB	FB, NO	(Lin et al., 2013, p. 1746, Figure 5L)
PS-IB-PB	IB, PS	PB	(Wolff et al., 2015, Figures 3S,T)
PS-PB	PS	PB	(Wolff et al., 2015, Figure 3R)
WED-PS-PB	PS, WED	PB	(Lin et al., 2013, p. 1744, Figures 4B,D)

Only neurons whose existence has been confirmed in (Young and Armstrong, 2010b; Lin et al., 2013; Wolff et al., 2015) are listed.

3. CX CIRCUIT REPRESENTATION AND GENERATION

3.1. Arborization-Based Neuron Labeling

Most neurons innervating the various CX and accessory neuropils possess at least two distinct clusters of dendrites (postsynaptic terminals) and/or axons (presynaptic terminals) that occupy geometrically distinct regions of the innervated neuropils (Hanesch et al., 1989). These clusters are referred to as arborizations (**Figure 4**). In the absence of experimental data regarding the actual presence and number of synapses between specific CX neurons, the overlap of presynaptic and postsynaptic arborizations may be used to infer synaptic connectivity and information flow until more detailed connectivity data becomes available. To use arborization data to infer synaptic connectivity, CX neurons with similar morphologies and arborization patterns can be classified and labeled in terms of the latter. If neurotransmitter profiles are ignored and each CX neuron type is assumed to be represented by a single neuron, then each neuron's label unambiguously encodes the geometric regions of its arborizations and whether each arborization contains dendrites, axons, or both.

This neuron labeling scheme can be described in terms of the parsing expression grammar (PEG) depicted in **Figure 5** (Ford, 2004); the grammar may be used to extract the arborizations of a particular neuron for constructing models of the CX circuitry. Note that the grammar includes a special case for handling the string LRB in the ⟨name⟩ rule which corresponds to the left rubus (RB) region of CRE; this is necessary to prevent that string from being incorrectly parsed into LB (a string that does not correspond to any defined region) and RB.

Neuropils are denoted by the abbreviated names mentioned in Section 1; abbreviations corresponding to individual regions

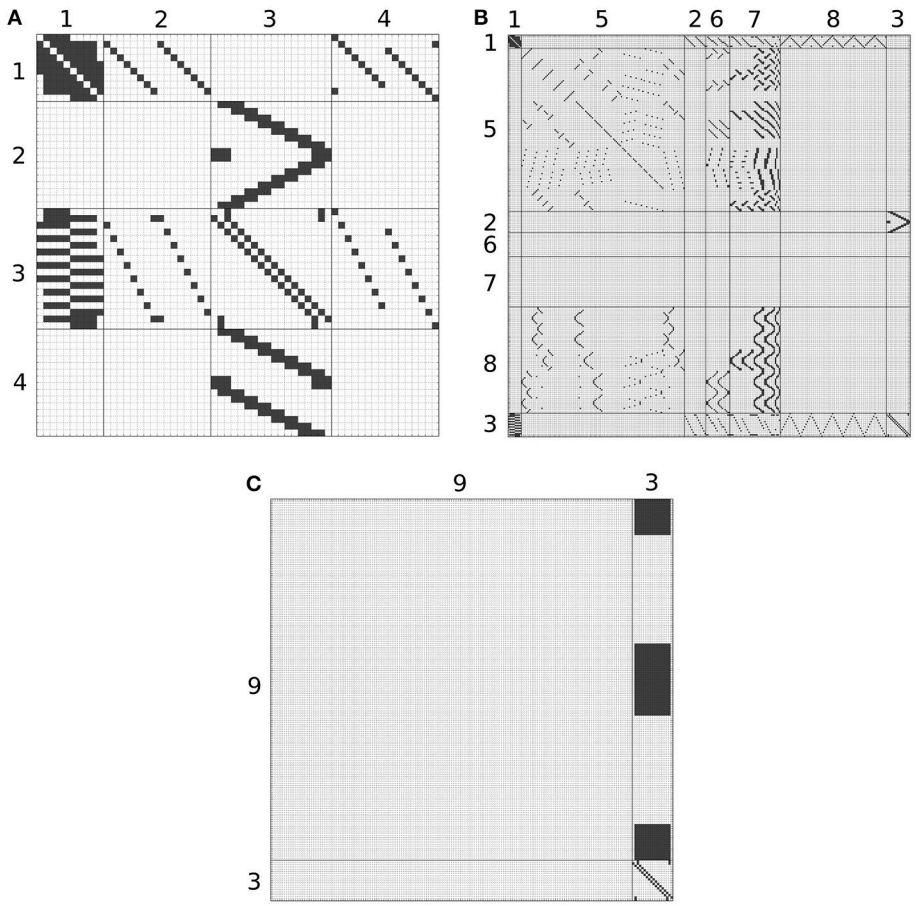

FIGURE 6 | Inferred synapses between PB local (1), PB-EB-LAL (2), EB-LAL-PB (3), PB-EB-NO (4), FB local (5), PB-FB-CRE (6), PB-FB-LAL (7), PB-FB-NO (8), and BU-EB (9) neurons. Rows correspond to presynaptic neurons, while columns correspond to postsynaptic neurons. Owing to its size, the connectivity matrix is depicted as several overlapping matrices **(A–C)**.

within each neuropil are detailed in the Supplementary Material. For neuropils that occur in pairs, upper case denotes the neuropil on the left side of the fly brain (from a dorsal perspective of the fly) while lower case denotes the neuropil on the right side of the fly brain. A neurite's type may be spine (s), bouton (or bleb) (b), or a combination thereof (bs, sb). In the absence of detailed data regarding synapses, information flow polarity is assumed to be reflected by neurite type; spines are assumed to be postsynaptic (and accept input), while boutons are assumed to be presynaptic (and emit output) (Wolff et al., 2015).

3.2. Executable Circuit Generation

To infer the presence of synaptic connections between neurons, each known biological neuron in the CX circuit was loaded into NeuroArch by name. A parser for the grammar described in Section 3.1 was used to extract records containing arborization information from each neuron's name (**Table 1**); these records were reinserted into the NeuroArch database as separate nodes connected to those that represent the original neurons.

After extraction of arborization data, all pairs of neurons in the database were compared to find those pairs with geometrically overlapping arborizations and differing neurite types (i.e., presynaptic vs. postsynaptic). This resulted in the creation of database nodes representing synapses that were connected to the associated biological neuron node pairs in NeuroArch's database.

To illustrate the synapse inference algorithm's operation, consider the neurons EB/([R3,R5],[P,M],[1-4])/s-EB/(R4,[P,M],[1-4])/b-LAL/RDG/b-PB/L3/b and PB/L4/s-EB/2/b-LAL/RVG/b. The former neuron has postsynaptic (spine) arborizations in EB and presynaptic (bouton) arborizations in EB and LAL; the latter has postsynaptic arborizations in PB and presynaptic arborizations in EB and LAL. Since the region EB/(R3,P,[1-4])/s in the former overlaps with region EB/2/b in the latter and the terminal types of the two neurons in the overlapping region differ, the presence of a synapse with information flow from the latter neuron to the former is inferred.

Although, physical overlap of arborizations does not always imply the presence of synapses, the above scheme illustrates how the software platform enables the use of partial structural

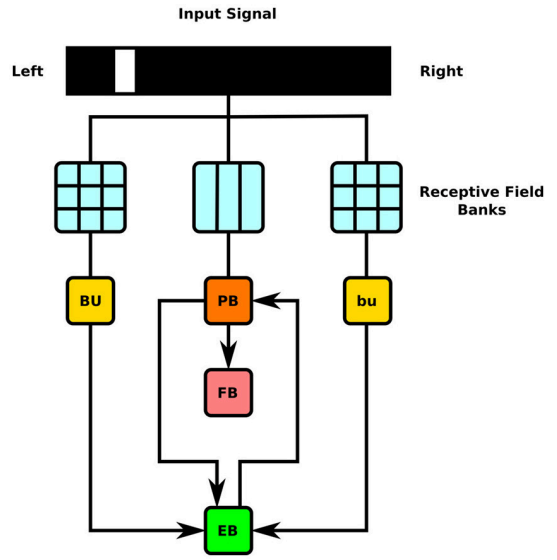

FIGURE 7 | Schematic of information flow in generated CX model. 2D visual signals are passed through rectangular grids of Gaussian receptive fields whose outputs drive BU-EB neurons and through a bank of vertical rectangular receptive fields whose outputs drive neurons that innervate the PB glomeruli. The generated model only comprises neurons that innervate the depicted LPUs (BU, bu, EB, FB, and PB).

information to construct and test CX circuit hypotheses. NeuroArch's data model can be extended to incorporate more detailed neural circuitry when it becomes available, thereby opening the doors to more accurate algorithmic inferences regarding the unknown portions of the CX circuit.

4. RESULTS

4.1. Executable CX Model Response to Visual Input

In light of the current lack of data regarding synapses between the various neurons identified in the central complex neuropils, data regarding the arborizations of these neurons was used to infer the presence or absence of synapses to generate an executable model of the central complex. Local and projection neurons were assigned to neuropils as indicated in **Table 2**. The neuropils in which these neurons arborize and the terminal types of their arborizations is listed in **Table 3**. Further details regarding these neurons is included in the Supplementary Material.

Although, the BU-EB neurons have not been systematically characterized, available information regarding these neurons was used to hypothesize the arborization structure for a total of 80 BU-EB neurons in each hemisphere of the fly brain (Hanesch et al., 1989; Young and Armstrong, 2010b; Seelig and Jayaraman, 2013; Dewar et al., 2015). Likewise, we also hypothesized isomorphic sets of pontine neurons that link regions in FB based upon (Hanesch et al., 1989). The hypothesized arborizations of the BU-EB and pontine neurons were used to assign them names; the latter are detailed in the Supplementary Material. **Figure 6** depicts the inferred synaptic connectivity between PB local, PB local, PB-EB-LAL, EB-LAL-PB, PB-EB-NO, FB local, PB-EB-LAL, PB-FB-CRE, PB-FB-LAL, PB-FB-NO, and BU-EB neurons; the rows of the connectivity matrix correspond to the presynaptic neurons, while the columns correspond to the postsynaptic neurons.

All neurons in the CX circuit were modeled as Leaky Integrate-and-Fire neurons, with the membrane voltage $V_i(t)$ of neuron i described by the differential equation

$$\dot{V}_i(t) = -\frac{V_i(t)}{R_i C_i} + \frac{I_i(t)}{C_i}$$

where R_i and C_i are the neuron's membrane resistance and capacitance and I_i the neuron's total input current. Upon reaching the threshold voltage $V_{t,i}$, each neuron's membrane voltage is reset to $V_{r,i}$. All synapses modeled to produce biexponential alpha function responses to presynaptic spikes; the synaptic conductance $\alpha_i(t) = \bar{g}_i g_i(t)$ response to a spike at $t = t_0$ is described by Ermentrout and Terman (2010)

$$\begin{aligned} \dot{g}_i(t) &= h_i(t)u(t) \\ \dot{h}_i(t) &= -(a_{r,i} + a_{d,i})h_i(t) - a_{r,i}a_{d,i}g_i(t) + \delta(t - t_0)a_{r,i}a_{d,i} \end{aligned}$$

where $\bar{g}_i$ is the maximum conductance of the synapse, $u(t)$ is the Heaviside step function, $\delta(t)$ the Dirac delta function, and $a_{r,i}$ and $a_{d,i}$ are the rise and decay time constants of the synapse's alpha function, respectively. The parameters of synapses between BU-EB neurons and other neurons were configured to exhibit inhibitory behavior; all remaining inferred synapses were configured to be excitatory. In all of the following connectivity matrices, a black square denotes the presence of a connection linking a presynaptic neuron on the y-axis to a postsynaptic neuron on the x-axis.

To test the executability of the generated circuit and its ability to respond to input data, the generated model was driven by a simple visual stimulus consisting of an illuminated vertical bar proceeding horizontally across the 2D visual space. Since the central complex neuropils do not receive direct connections from the vision neuropils, processing of the visual stimulus by the latter was approximated by three banks of receptive fields whose outputs were, respectively provided to BU, bu, and PB as input (**Figure 7**). In light of the reported retinotopy of bulb microglomeruli (Seelig and Jayaraman, 2013), the receptive fields for BU and bu were constructed as evenly spaced 2D grids of 80 circular Gaussians that respectively correspond to one of the microglomeruli in the bulb; each receptive field was connected to one BU-EB neuron such that the 16 neurons in each of the 5 groups of EB ring neurons processed input from a rectangle occupying $\frac{1}{5}$ of the 2D visual space. The azimuthal tracking of visual stimuli by activity in EB (Seelig and Jayaraman, 2015) and the mapping from the linear structure of PB to the circular structure of EB suggested that the PB glomeruli's receptive fields tile the fly's visual field; we therefore assigned 18 vertical rectangular regions with a constant magnitude to the respective glomeruli. Each receptive field was connected to all local and projection neurons that innervated the glomerulus corresponding to the receptive field region. The responses of the neurons in each family to the two input signals are organized in the same order in the respective raster plots. **Figures 8**, **9** depict

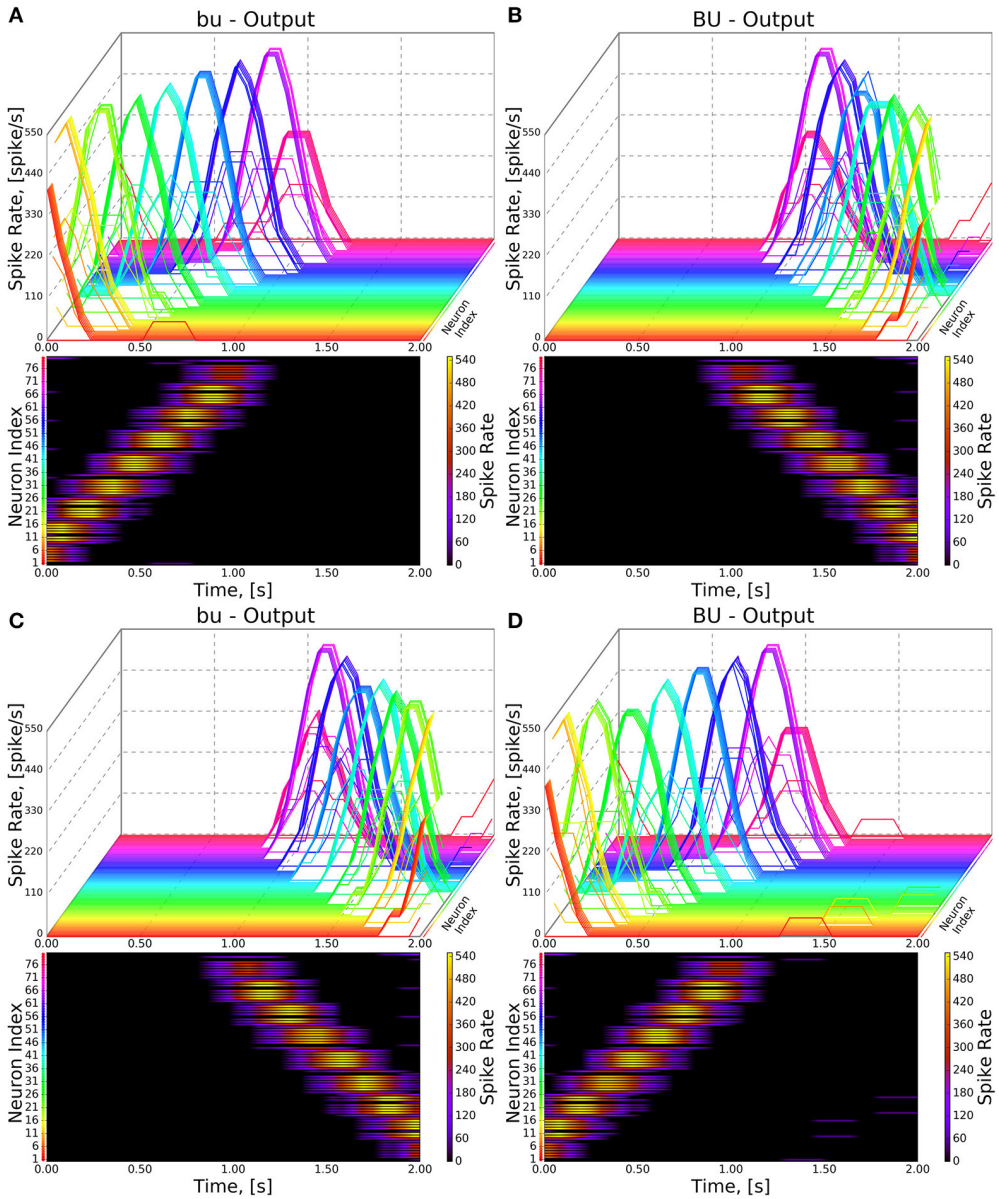

FIGURE 8 | Response of CX projection neurons innervating BU/bu to moving bar input. (Top) The 3D view of the PSTH of a single neuron in the BU/bu family. Each line represents the PSTH of a single neuron. (Bottom) The heatmap view of the PSTH. Neurons are color coded with an one-to-one correspondence to the 3D view. Each row represents the PSTH of a single neuron (indicated by the color dot in front of each row). The PSTH was computed using a 200 ms bin size with a 50 ms sampling interval. **(A,B)** Response of bu/BU neurons to the left-to-right moving bar. **(C,D)** Response of bu/BU neurons to the right-to-left moving bar.

the responses of neurons innervating the PB and BU/bu neuropils to an illuminated vertical bar moving from left to right across a dark background.

4.2. Comparing Normal and Abnormal Neural Circuits

To test hypotheses regarding incompletely characterized parts of the fly brain, one can create models that either attempt to replicate abnormal behaviors or emulate abnormal circuit structures observed in different mutant fly strains. For example, one can attempt to model phenotypes corresponding to mutations that constrict or disrupt connections between the left and right sides of PB such as *no bridge* and *tay bridge* by altering the PB model generation process accordingly. These mutations are known to alter the fly's step length and compromise the fly's directional targeting abilities (Triphan et al., 2010; Strauss, 2014). Since neurons innervating the motor ganglia are known to be postsynaptic to those that innervate LAL, it is reasonable to expect that analogous modifications to the structure of PB may alter the outputs of CX projection neurons that innervate LAL in a manner that reduces their sensitivity to directional visual stimuli.

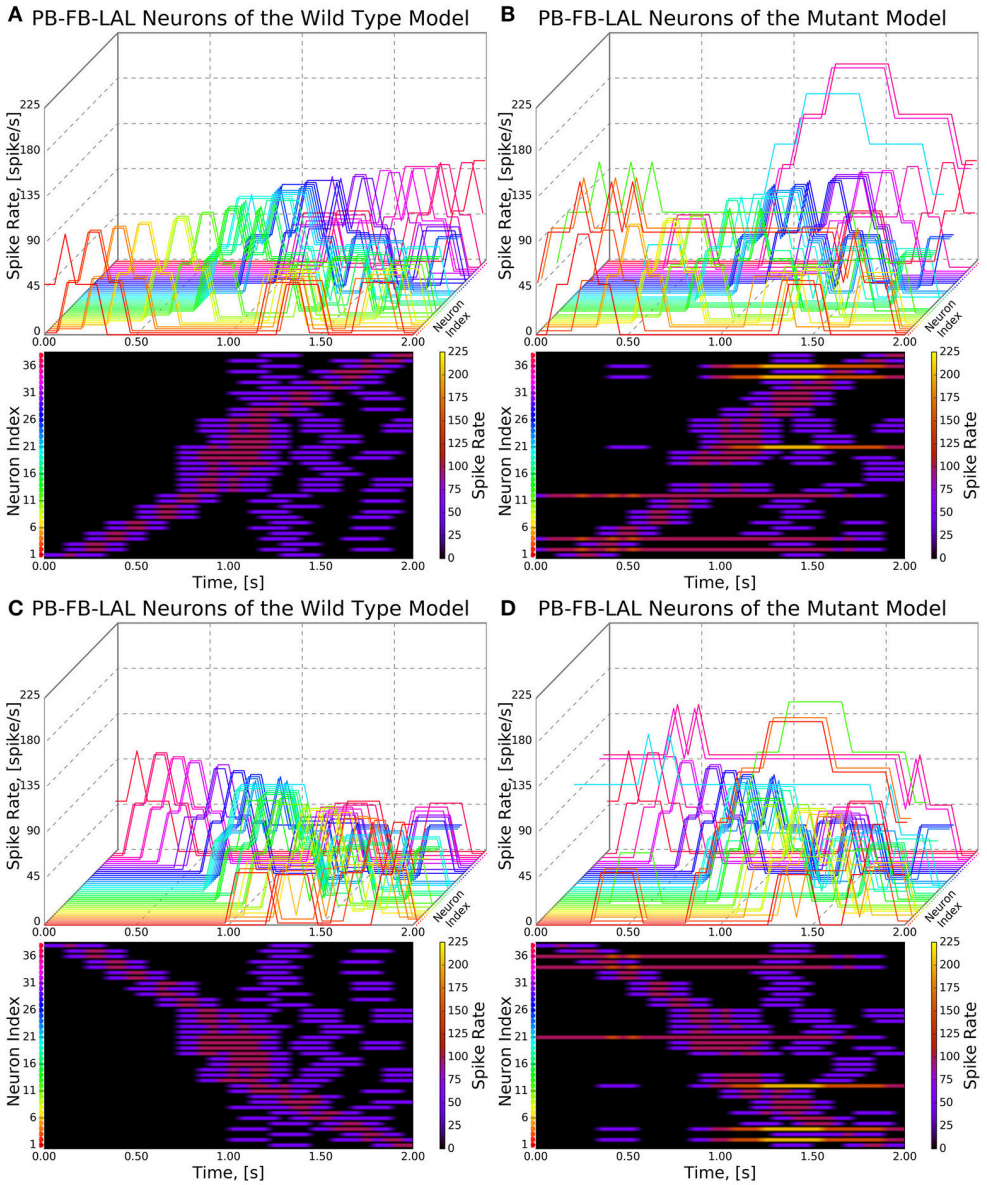

FIGURE 9 | Response of CX projection neurons innervating PB to moving bar input (left to right). (Top) The 3D view of the peristimulus time histogram (PSTH) of a single neuron in the PB-FB-LAL family. Each line represents the PSTH of a single neuron. (Bottom) The heatmap view of the PSTH. Neurons are color coded with an one-to-one correspondence to the 3D view. Each row represents the PSTH of a single neuron (indicated by the color dot in front of each row). The PSTH was computed using a 200 ms bin size with a 50 ms sampling interval. **(A,C)** Response of the neurons in the wild type. **(B,D)** Response of the neurons in the *no bridge* mutant.

We modeled the *no bridge* mutant by positing the development of 16 PB local neurons that only span either the left or right sides of PB in place of the 8 local neurons that normally span the entire neuropil in the wild type fly (**Figure 10**; the hypothesized neurons' names are listed in the Supplementary Material). Although, observations of the *no bridge* mutant suggest that several of the medial glomeruli are not present, this model does not alter any of the other known neurons in CX. The synapse inference algorithm (Section 3.2) was then run on the modified circuits to construct a mutant CX model.

As the inputs to the wild type and mutant models are identical and the BU-EB neurons do not receive any input from other neurons in the generated model, their responses in the mutant model are identical to those in the wild type model (**Figure 8**). The effects of the mutation on the response of the PB-FB-LAL projection neurons can be observed by comparing the mutant model output in **Figure 9B** to **Figure 9A**; in both cases, the PB-FB-LAL neurons along the vertical axes of the PSTH plots are arranged from those that innervate the leftmost glomerulus to the rightmost glomerulus. The PB-FB-LAL neurons in the wild type

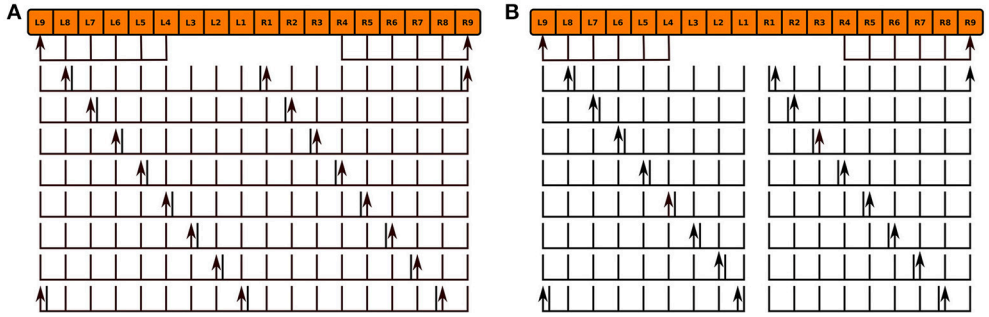

FIGURE 10 | Normal PB local neuron innervation pattern **(A)** and hypothesized abnormal innervation pattern **(B)** in *no bridge* mutant. Arrows and lines respectively mark presynaptic and postsynaptic arborizations within the corresponding glomeruli; the presence of both presynaptic and postsynaptic arborizations within a glomerulus is marked by an adjacent arrow and line.

model exhibit sensitivity to the direction of the visual stimulus across the azimuth. While some of this activity occurs in the mutant model, the mutation causes three PB-FB-LAL neurons on the left and three on the right sides of the fly's brain to produce high activity over abnormally long stretches of time. We posit that the output of these neurons may dominate the inputs to the LAL neuropils and effectively drown out the directionally sensitive responses of the other PB-FB-LAL neurons. This could explain the inability of fly mutants with a laterally interrupted PB to perform the directional targeting necessary to successfully traverse gaps in climbing experiments (Triphan et al., 2010).

5. CONCLUSION

Kakaria and De Bivort (2017) describe a model of the PB and EB circuitry that exhibit ring attractor dynamics similar to those observed in calcium imaging of EB responses to visual landmark stimuli (Seelig and Jayaraman, 2015). While this model comprises the same neuron families as generated model described in Section 4.1, the synaptic connections inferred in **Figure 6** for those neuron families used in both models differ owing to our incorporation of arborization information from both Lin et al. (2013) and Wolff et al. (2015) rather than the latter alone. Our model also incorporates neuron families that innervate FB.

We have demonstrated how NeuroGFX enables the structure of the CX neuropils to be probed simultaneously with execution of neural circuit models inferred from available connectomic data. Although, the NeuroArch component of our software supports extensive customization of supported executable circuit components, the software's current web interface is read-only. We are extending this interface to enable users to directly manipulate the executed circuit by defining new modeling components, loading alternative subcircuits into NeuroArch for evaluation, and modifying the parameters of stored circuit models.

Assessment of CX model accuracy requires a means of analyzing its response to different input signals. Since the CX circuit comprises multiple putative input and output pathways of interest, there is a need to support concurrent injection of inputs and recording of responses from potentially any component in a circuit model. While models of sensory neuropils can be analyzed using prerecorded or generated sensory inputs, similar analysis of non-sensory neuropil models requires the ability to observe their behavior when they receive input from models of sensory neuropils. The communication interface described in Section 2 that Neurokernel and NeuroArch support to enable the integration of models of different neuropils already provides the requisite internal functionality to both inject and record either analog or spike signals into specific model components. We will extend the NeuroGFX interface to enable users to provide prerecorded input signals for injection into the CX circuit and designate which circuit components to stimulate. We also will extend the FFBO component of our software to explicitly support future web applications that let users link CX models to those of other neuropils in the fly's brain.

We aim to incorporate more detailed connectomic data into the application's NeuroArch database; ongoing work by the developers of the FlyCircuit database (Chiang et al., 2011) that utilizes neuron morphology to infer the number of synapses between neurons will enable construction of CX models with more accurate connectivity patterns than those currently inferred from arborization overlap[1].

AUTHOR CONTRIBUTIONS

AL initiated the project and critically reviewed the manuscript text and figures. LG and CY developed the executable CX models. LG developed the NeuroArch/Neurokernel software used for model representation/execution, wrote the manuscript, and prepared the supplementary circuit figures and tables. CY developed the NeuroGFX/FFBO software for CX visualization, prepared the manuscript figures, and reviewed the manuscript.

ACKNOWLEDGMENTS

This research was supported in part by the AFOSR under grant #FA9550-12-10232, in part by the NSF under grant #1544383

[1] C.C. Lo, private communication.

and in part by the Department of Electrical Engineering at Columbia University. A preprint of the manuscript by LG and AL is available on bioRxiv; this preprint is available under a CC-BY 4.0 International license with copyright held by LG and AL.

SUPPLEMENTARY MATERIAL

The Supplementary Material for this article can be found online at: http://journal.frontiersin.org/article/10.3389/fnbeh.2017.00102/full#supplementary-material

REFERENCES

Arena, P., Maceo, S., Patane, L., and Strauss, R. (2013). "A spiking network for spatial memory formation: towards a fly-inspired ellipsoid body model," in *The 2013 International Joint Conference on Neural Networks* (Dallas, TX), 1–6.

Arena, P., Patanè, L., and Termini, P. S. (2014). "A computational model for the insect brain," in *Spatial Temporal Patterns for Action-Oriented Perception in Roving Robots II*, Vol. 21, Cognitive Systems Monographs, eds P. Arena and L. Patanè (Springer International Publishing Switzerland), 43–80.

Chiang, A.-S., Lin, C.-Y., Chuang, C.-C., Chang, H.-M., Hsieh, C.-H., Yeh, C.-W., et al. (2011). Three-dimensional reconstruction of brain-wide wiring networks in *Drosophila* at single-cell resolution. *Curr. Biol.* 21, 1–11. doi: 10.1016/j.cub.2010.11.056

Dewar, A. D. M., Wystrach, A., Graham, P., and Philippides, A. (2015). Navigation-specific neural coding in the visual system of *Drosophila*. *Biosystems* 136, 120–127. doi: 10.1016/j.biosystems.2015.07.008

Ermentrout, G. B., and Terman, D. H. (2010). *Mathematical Foundations of Neuroscience, 1st Edn*. New York, NY: Springer-Verlag.

Ford, B. (2004). "Parsing expression grammars: a recognition-based syntactic foundation," in *ACM SIGPLAN Notices* (New York, NY), 111–122.

Givon, L. E., and Lazar, A. A. (2016). Neurokernel: an open source platform for emulating the fruit fly brain. *PLoS ONE* 11:e0146581. doi: 10.1371/journal.pone.0146581.s001

Givon, L. E., Lazar, A. A., and Ukani, N. H. (2014). Neuroarch: a graph-based platform for constructing and querying models of the fruit fly brain architecture. *Front. Neuroinform.* 2014:42. doi: 10.3389/conf.fninf.2014.18.00042

Hanesch, U., Fischbach, K. F., and Heisenberg, M. (1989). Neuronal architecture of the central complex in *Drosophila melanogaster*. *Cell Tissue Res.* 257, 343–366. doi: 10.1007/BF00261838

Izquierdo, E. J., and Beer, R. D. (2013). Connecting a connectome to behavior: an ensemble of neuroanatomical models of *C. elegans* klinotaxis. *PLoS Comput. Biol.* 9:e1002890. doi: 10.1371/journal.pcbi.1002890

Kakaria, K. S., and De Bivort, B. L. (2017). Ring attractor dynamics emerge from a spiking model of the entire protocerebral bridge. *Front. Behav. Neurosci.* 11:8. doi: 10.3389/fnbeh.2017.00008

Lin, C.-Y., Chuang, C.-C., Hua, T.-E., Chen, C.-C., Dickson, B. J., Greenspan, R. J., et al. (2013). A comprehensive wiring diagram of the protocerebral bridge for visual information processing in the *Drosophila* brain. *Cell Rep.* 3, 1739–1753. doi: 10.1016/j.celrep.2013.04.022

Martín-Peña, A., Acebes, A., Rodríguez, J.-R., Chevalier, V., Casas-Tinto, S., Triphan, T., et al. (2014). Cell types and coincident synapses in the ellipsoid body of *Drosophila*. *Eur. J. Neurosci.* 39, 1586–1601. doi: 10.1111/ejn.12537

Neuser, K., Triphan, T., Mronz, M., Poeck, B., and Strauss, R. (2008). Analysis of a spatial orientation memory in *Drosophila*. *Nature* 453, 1244–1247. doi: 10.1038/nature07003

Ofstad, T. A., Zuker, C. S., and Reiser, M. B. (2011). Visual place learning in *Drosophila melanogaster*. *Nature* 474, 204–207. doi: 10.1038/nature10131

Pfeiffer, K., and Homberg, U. (2014). Organization and functional roles of the central complex in the insect brain. *Annu. Rev. Entomol.* 59, 165–184. doi: 10.1146/annurev-ento-011613-162031

Seelig, J. D., and Jayaraman, V. (2013). Feature detection and orientation tuning in the *Drosophila* central complex. *Nature* 503, 262–266. doi: 10.1038/nature12601

Seelig, J. D., and Jayaraman, V. (2015). Neural dynamics for landmark orientation and angular path integration. *Nature* 521, 186–191. doi: 10.1038/nature14446

Strauss, R. (2014). "Neurobiological models of the central complex and the mushroom bodies," in *Spatial Temporal Patterns for Action-Oriented Perception in Roving Robots II*, eds P. Arena and L. Patanè, Vol. 21 in Cognitive Systems Monographs (Springer International Publishing), 3–41.

Strauss, R., and Berg, C. (2010). "The central control of oriented locomotion in insects - towards a neurobiological model," in *The 2010 International Joint Conference on Neural Networks (IJCNN)* (Barcelona), 1–8.

Takemura, S.-Y. (2015). Connectome of the fly visual circuitry. *Microscopy* 64, 37–44. doi: 10.1093/jmicro/dfu102

Triphan, T., Poeck, B., Neuser, K., and Strauss, R. (2010). Visual targeting of motor actions in climbing drosophila. *Curr. Biol.* 20, 663–668. doi: 10.1016/j.cub.2010.02.055

Ukani, N. H., Tomkins, A., Yeh, C.-H., Bruning, W., Fenichel, A. L., Zhou, Y., et al. (2016a). NeuroNLP: a natural language portal for aggregated fruit fly brain data. *bioRxiv*. doi: 10.1101/092429

Ukani, N. H., Yeh, C.-H., Tomkins, A., Zhou, Y., Florescu, D., Ortiz, C. L., et al. (2016b). The fruit fly brain observatory: from structure to function. *bioRxiv*. doi: 10.1101/092288

Wolff, T., Iyer, N. A., and Rubin, G. M. (2015). Neuroarchitecture and neuroanatomy of the Drosophila central complex: a GAL4-based dissection of protocerebral bridge neurons and circuits. *J. Compar. Neurol.* 523, 997–1037. doi: 10.1002/cne.23705

Wystrach, A., Dewar, A. D., and Graham, P. (2014). Insect vision: emergence of pattern recognition from coarse encoding. *Curr. Biol.* 24, R78–R80. doi: 10.1016/j.cub.2013.11.054

Yeh, C.-H., Zhou, Y., Ukani, N. H., and Lazar, A. A. (2016). NeuroGFX: a graphical functional explorer for fruit fly brain circuits. *bioRxiv*. doi: 10.1101/092437

Young, J., and Armstrong, J. (2010a). Building the central complex in *Drosophila*: the generation and development of distinct neural subsets. *J. Compar. Neurol.* 518, 1525–1541. doi: 10.1002/cne.22285

Young, J., and Armstrong, J. (2010b). Structure of the adult central complex in *Drosophila*: organization of distinct neuronal subsets. *J. Compar. Neurol.* 518, 1500–1524. doi: 10.1002/cne.22284

Conflict of Interest Statement: The authors declare that the research was conducted in the absence of any commercial or financial relationships that could be construed as a potential conflict of interest.

frontiers in Behavioral Neuroscience

REVIEW
published: 24 January 2017
doi: 10.3389/fnbeh.2017.00004

Spatial Navigation and the Central Complex: Sensory Acquisition, Orientation, and Motor Control

Adrienn G. Varga[1], Nicholas D. Kathman[1], Joshua P. Martin[2], Peiyuan Guo[1] and Roy E. Ritzmann[1]**

[1] Department of Biology, Case Western Reserve University, Cleveland, OH, USA, [2] Department of Biology, Colby College, Waterville, ME, USA

Cockroaches are scavengers that forage through dark, maze-like environments. Like other foraging animals, for instance rats, they must continually asses their situation to keep track of targets and negotiate barriers. While navigating a complex environment, all animals need to integrate sensory information in order to produce appropriate motor commands. The integrated sensory cues can be used to provide the animal with an environmental and contextual reference frame for the behavior. To successfully reach a goal location, navigational cues continuously derived from sensory inputs have to be utilized in the spatial guidance of motor commands. The sensory processes, contextual and spatial mechanisms, and motor outputs contributing to navigation have been heavily studied in rats. In contrast, many insect studies focused on the sensory and/or motor components of navigation, and our knowledge of the abstract representation of environmental context and spatial information in the insect brain is relatively limited. Recent reports from several laboratories have explored the role of the central complex (CX), a sensorimotor region of the insect brain, in navigational processes by recording the activity of CX neurons in freely-moving insects and in more constrained, experimenter-controlled situations. The results of these studies indicate that the CX participates in processing the temporal and spatial components of sensory cues, and utilizes these cues in creating an internal representation of orientation and context, while also directing motor control. Although these studies led to a better understanding of the CX's role in insect navigation, there are still major voids in the literature regarding the underlying mechanisms and brain regions involved in spatial navigation. The main goal of this review is to place the above listed findings in the wider context of animal navigation by providing an overview of the neural mechanisms of navigation in rats and summarizing and comparing our current knowledge on the CX's role in insect navigation to these processes. By doing so, we aimed to highlight some of the missing puzzle pieces in insect navigation and provide a different perspective for future directions.

Keywords: central complex, spatial navigation, head direction cells, population code, motor activity, reflex

OPEN ACCESS

Edited by:
Keram Pfeiffer,
University of Marburg, Germany

Reviewed by:
Ansgar Buschges,
University of Cologne, Germany
Basil El Jundi,
Lund University, Sweden

***Correspondence:**
Adrienn G. Varga
agv13@case.edu
Roy E. Ritzmann
roy.ritzmann@case.edu

Received: *28 October 2016*
Accepted: *06 January 2017*
Published: *24 January 2017*

Citation:
Varga AG, Kathman ND, Martin JP, Guo P and Ritzmann RE (2017) Spatial Navigation and the Central Complex: Sensory Acquisition, Orientation, and Motor Control. Front. Behav. Neurosci. 11:4. doi: 10.3389/fnbeh.2017.00004

INTRODUCTION

Insects are by just about any measure the most successful animal group inhabiting almost every conceivable niche on the planet. Behavioral repertoires range from slow walking (e.g., stick insects) to rapid flying (e.g., houseflies). Some species undergo remarkable migrations across entire continents (e.g., monarch butterflies) while others move purposefully within smaller ranges (e.g., dung beetles). Insects are effective predators (e.g., dragonflies and praying mantis), harvesters (e.g., honeybees) and foragers (e.g., cockroaches). Each of these animals must deal with changing environmental and internal conditions. Some dung beetles move only at night while other species are diurnal (el Jundi et al., 2015). Predators may change their stalking behaviors as they become satiated (Holling, 1966; Inoue and Matsura, 1983). The recent explosion of data on the central complex (CX) (Pfeiffer and Homberg, 2014) has documented numerous types of sensory information that converge in these midline neuropils. Moreover, large amounts of neuromodulatory receptors and targets have been identified (Kahsai and Winther, 2011; Boyan and Liu, 2016) and motor control effects demonstrated (Bender et al., 2010; Martin et al., 2015). These studies combine to suggest that the CX plays a pivotal role in guiding appropriate behaviors for each species and adjusting the accompanying movements to match the current context that an individual insect finds itself in at any point in time. In this review, we will primarily focus upon our laboratory's work on the role of CX circuits in controlling navigation in one successful insect, the cockroach *Blaberus discoidalis,* while also discussing relevant findings in other insects. One reason for focusing on cockroaches is that they occupy an ecological niche similar to rat habitats, which are a major model for mammalian navigation. Both rats and cockroaches are scavengers that forage in darkened environments and often navigate in complex, maze-like burrows (Roth and Willis, 1960; Feng and Himsworth, 2014). As they move, they must seek out targets such as food items or potential mates while navigating through complex terrains and avoiding predators (Meyer et al., 1981; Okada and Toh, 1998; Canonge et al., 2009). Whether these shared ecological and behavioral traits similarly influenced the neural mechanisms governing navigation in these distant species, is not known.

In a previous review (Ritzmann et al., 2012), we described movements that the cockroach makes in a large, well-lit arena as they seek out darkened shelters. Because cockroaches have a strong tendency to remain near walls, but greatly prefer the dark, we expected individuals to wall-follow until they detected the dark shelter then move directly toward that part of the arena (Daltorio et al., 2013). The paths that they took did not support that hypothesis. Instead, they appeared to move randomly through the arena but, indeed, did end up in the shelter. A closer analysis of the paths indicated that the cockroaches did take less time to reach the shelter than to reach the same area without a dark shelter present, indicating efficient goal-directed navigation. They also stayed in the darkened shelter for a longer period of time than they did in any comparable region of the arena, suggesting that the seemingly random path was in fact targeting the shelter.

An algorithm, called RAMBLER, simulated the movements of the insect quite well (Daltorio et al., 2013). Under this scheme, a simulated cockroach evaluates whether it is still in contact with the wall and whether it can still see the dark shelter. In live insect observations, cockroaches tend to increase walking speed when they move away from a wall toward the center of the arena (Bender et al., 2011), possibly to reduce the time spent in the open. If the shelter was behind the cockroach, the probability that it would turn increased and the animal tended to turn back to the place where it last detected the shelter. The RAMBLER algorithm captured these properties and implied that some sophisticated decisions might be made in higher centers. Several factors implicated the CX in that role. First, electrolytic lesions in the cockroach CX increased the number of "wrong" turns made while walking on a track (Harley and Ritzmann, 2010). Second, recordings in the CX clearly demonstrated antennal responses that encoded the direction and velocity and antennal deflections (Ritzmann et al., 2008). Finally, CX activity recorded in tethered cockroaches demonstrated increases in firing rate that preceded changes in walking speed, while stimulation through the same electrodes evoked speed changes (Bender et al., 2010). In this review, we will describe findings in our laboratory and others that not only suggest that the CX is involved in this kind of navigation but begin to outline what that role might be.

SENSORY INPUTS TO THE CX

Many different types of sensory information project to the CX and many will undoubtedly be described in detail in other papers in this special issue. Included in this list are polarized light (Heinze and Homberg, 2007; Sakura et al., 2008; Heinze et al., 2009), mechanical deflection of the antenna (Ritzmann et al., 2008) and various forms of non-polarized signals (Heinze and Reppert, 2011; Rosner and Homberg, 2013; Seelig and Jayaraman, 2013; Kathman et al., 2014; Bockhorst and Homberg, 2015). For the goal-directed navigational task outlined above, antennal and visual cues appear to be very important.

Many insects use mechanical cues from antennal contact to guide movements. In stick insects, gap crossing behavior is initiated when the antennae detect a gap in the substrate they are walking on and are further guided by searching front leg movements (Bläesing and Cruse, 2004). Leg movements associated with turning in the stick insect are also guided by antennal contact (Dürr et al., 2001; Dürr and Ebeling, 2005), through descending pathways from the brain to the thoracic ganglia (Ache et al., 2015). The descending pathways bypass higher processing areas such as the CX. Nevertheless, it is reasonable to expect that parallel branches also reach the CX. In cockroach, the antennae clearly are used in initiating climbing behaviors over substantial blocks, since ablation of part or all of the antennae affect the onset time of the climb accordingly (Harley et al., 2009). Lesions in specific regions of the CX compromise either climbing or turning behaviors indicating that the CX plays a role in utilizing mechanosensory information during navigation (Harley and Ritzmann, 2010).

Neurons in the CX of several insects have been shown to respond to visual cues (Ritzmann et al., 2008; Heinze and Reppert, 2011; Rosner and Homberg, 2013). Visual feature detection was demonstrated in *Drosophila* using two-photon calcium imaging of neural activity in genetically-targeted CX populations (Seelig and Jayaraman, 2013). The responses of CX ring neurons resemble those in the mammalian primary visual cortex in that they are retinotopically arranged and have visual fields comprised of excitatory and inhibitory subfields. Moreover, these ring neurons were found to have strong and often direction sensitive responses. In addition to polarized light responses, monarch butterflies, dung beetles and locusts were also shown to be sensitive to non-polarized light stimuli at specific azimuthal orientations (Heinze and Reppert, 2011; el Jundi et al., 2014, 2015). In cockroach, extracellular recordings revealed CX neurons that respond to both antennal stimulation and light changes (Ritzmann et al., 2008). More recently, wide field visual stimuli were further evaluated (Kathman et al., 2014). For these latter studies, cockroaches were restrained in a tube and a 16 channel silicon probe was inserted into the CX in a variety of places in either the fan-shaped body (FB) or the ellipsoid body (EB). Vertically oriented grating patterns with variable direction, speed, and stripe width were projected onto a screen in front of the insect to simulate the yaw rotation, or turning, of the animal. These stimuli produced a wide range of CX responses including phasic and tonic excitation as well as inhibition (**Figure 1**). Phasic responses occurred either at the onset of stimulus presentation or at the termination of the visual stimulus. Tonic responses often were directional (**Figure 2**). That is, some units were excited by left moving grating patterns but either did not respond, responded at significantly lower levels or were inhibited by right moving stimulation. In the same recording both left biased and right biased neurons were found.

The directional responses of tonic CX neurons suggested that turning movements could be controlled at least in part by CX circuitry. Its role in optomotor responses was tested by injecting the local anesthetic, procaine, into the CX (Kathman et al., 2014). The cockroaches were tethered over an air suspended ball and grating patterns moving left or right were projected in front of the animals. As the cockroach walked on the ball its movements were monitored with optical sensors. The pattern of moving stripes readily generated optomotor responses in the direction of the stripes' movement, presumably in an attempt to stabilize the insect's visual field. Procaine is a voltage sensitive K^+ and Na^+ channel blocker (Devaud et al., 2007) that silences action potentials but only for short periods of time. To verify its effect in the CX, we injected procaine into the CX of restrained cockroaches while recording neural activity. Action potentials in the region where procaine was injected were completely silenced for 20 min and returned to baseline firing rates at about 30 min post-injection. Regions outside the CX were unaffected. When procaine was injected into the CX of tethered cockroaches, the optomotor responses decreased significantly then returned following the same time course as that found in silencing CX neurons (**Figure 3**). Similar injections with saline had no effect.

The optomotor observations suggest that CX neurons are involved in guiding movements in response to wide field visual stimuli. Additionally, several studies suggested that visually guided behaviors in the CX are context dependent. For instance, feature detection responses of some EB neurons were diminished in flight, but not during walking (Seelig and Jayaraman, 2013), while a group of FB neurons were shown to be unresponsive

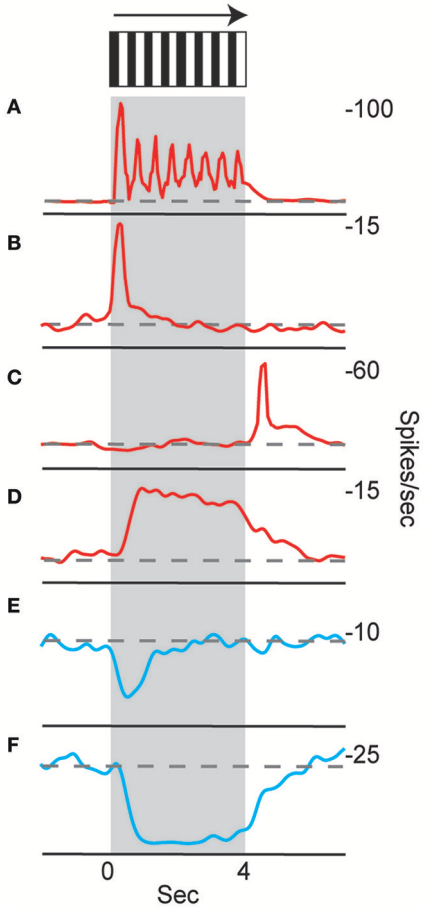

FIGURE 1 | Temporal properties of wide-field motion responses. Six response types were found **(A–F)**. These include **(A)** units with spiking entrained to the temporal frequency of the grating, phasic excitatory responses at the beginning **(B)** and end **(C)** of movement, **(D)** tonic excitatory response lasting the duration of movement, and inhibitory phasic **(E)** and tonic **(F)** responses. Examples of all response types were found for both directions of movement, despite only responses to right movement being shown. Gray block indicates duration of stimulus and dashed line indicates baseline firing rate (Kathman et al., 2014).

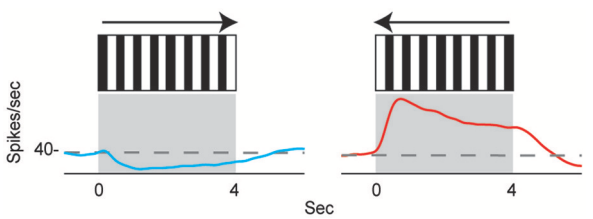

FIGURE 2 | Directional selectivity. Units were directionally selective, often with showing directional opponency, with inhibitory responses to one direction of motion, and excitatory responses to the other (Kathman et al., 2014).

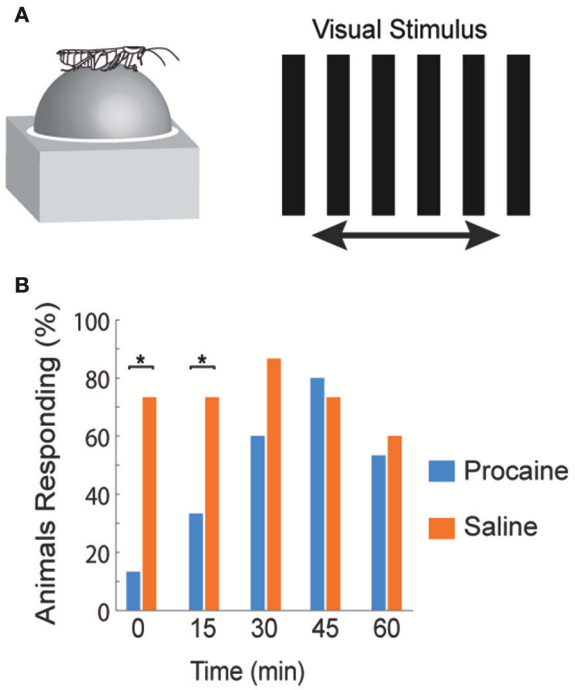

FIGURE 3 | Optomotor response is reduced after reversible chemical ablation in the CX. (A) Turning response of *Blaberus discoidalis* to shifting stripes was measured while the insect was tethered to an air-supported Styrofoam ball. **(B)** Proportions of animals with a successful optomotor response at 15 min time intervals after the injection of procaine (blue) or saline (orange) into the CX. Procaine injected animals were significantly different ($\chi 2$ test, $P < 0.05$) from saline controls at 0 and 15 min (*) and recovered by 30 min (Kathman et al., 2014).

while the fly was quiescent but responded to translational optic flow during flight (Weir et al., 2014). Similar context dependent sensory processes could shape the cockroach's behavior as it moves in the arena and executes turns.

WHAT CAN WE LEARN FROM RAT NAVIGATION STUDIES?

As the cockroach moves through its environment in ways that are similar to the arena experiment described above, information on where it currently is and how it got there play an important role. Yet the neural dynamics underlying such navigational processes in insects are not well understood. On the other hand, several decades of research on mammalian navigation circuits provide us with some basic theories to test. The majority of these studies used rats as a model animal (McNaughton et al., 2006; Jacobs and Menzel, 2014; Geva-Sagiv et al., 2015). The demands of navigation are similar for rats and cockroaches: they are nocturnal, tend to move through restricted corridors and rely heavily on both visual and tactile cues (Feng and Himsworth, 2014). Their similar ecology and foraging behaviors indicate that the two model organisms likely depend on the same sensory cues and similar integration processes to orient themselves, thus we predict that there might be some similarities between the circuits underlying navigation. In this section, we present a simplified outline of rat navigation circuits and a general description of spatial cell types to introduce some of the main concepts that are necessary for navigation—at least in mammals. Considering our limited understanding of associative processes in the insect brain, rather than examining the information flow from sensory perception to motor control, we will restrict this section to the abstract representation of spatial and contextual information in the rat brain, which we will refer back to in the section concerned with the CX's role in navigation.

Spatial navigation in all animals requires the integration of both external and internal sensory information (Geva-Sagiv et al., 2015). External sensory cues - also called allothetic cues - are visual, olfactory, auditory and tactile/mechanosensory information about the environment external to the body. Internal sensory cues—also called idiothetic cues—are derived from self-motion in the form of vestibular cues (or mechanosensory cues), optic flow, proprioceptive feedback and motor efference copy from the limbs. These sensory cues get integrated and compressed to form an inner representation of the environmental and behavioral context. This information can then be used in motor centers to induce and shape optimal motor commands that lead to successful navigation in that particular context (Moser et al., 2008; Hartley et al., 2014; Schiller et al., 2015).

Based on our current understanding of rat navigation, it is thought that the hippocampal formation (including the entorhinal cortex and other parts of the Papez-circuit) and the basal ganglia (specifically the dorsal striatum) in parallel, but differently, process navigational and context-dependent sensory cues to guide behaviors (**Figures 4B,C**). Within both regions, specialized intertwined networks encode the inner representation of the animal's location, head direction, various aspects of movement (e.g., speed, angular velocity) and, if present, navigational task-related rewards (Mizumori et al., 2009; Penner and Mizumori, 2012).

HIPPOCAMPAL FORMATION AND RELATED CIRCUITS

The hippocampal formation is hypothesized to act as a spatial context discriminator in the rat navigation system. Its role in navigation is to compare the current spatial framework to an expected spatial context. The discrimination process requires access to spatial memory and the ability to detect and encode information about novelty. Novelty in the environment induces exploration or goal-directed navigation, because the current spatial context does not match the expected, or the animal has not yet reached the navigational goal. This process not only induces navigation, but also facilitates learning and memory (Paulsen and Moser, 1998). The hippocampal formation needs to continuously integrate sensory information about the environment, sensory information derived from movement and the current motivational state of the animal as a function of space and time, which translates to the current spatial context. This is achieved by hippocampal *place cells*, that each encode a particular *location* in the environment and also information about behavioral context in one signal (O'Keefe and Dostrovsky,

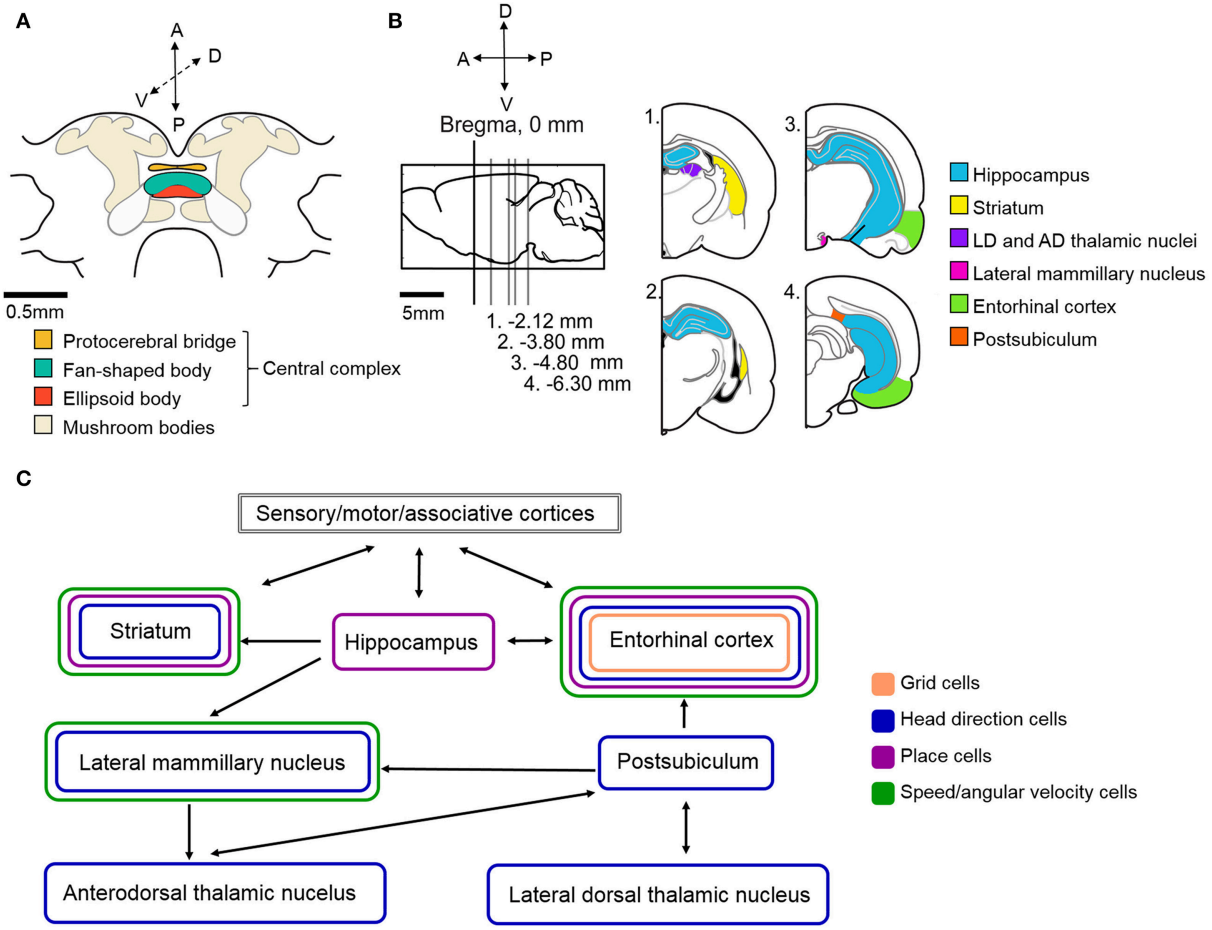

FIGURE 4 | Schematic illustration of the neural circuitry underlying cockroach and rat navigation and context discrimination. (A) Schematic illustration of the cockroach central brain with the potential navigation centers color coded (based upon Mizunami et al., 1998). **(B)** Schematic of a rat brain. Sagittal section where Bregma represents 0 mm (marked by black vertical line). Gray lines indicate the location of sections illustrated in the right side of the panel relative to Bregma. Navigation centers are color coded (all rat brain diagrams were created based upon Paxinos and Watson, 1996) **(C)** Arrows indicate the direction of communication between navigation centers in the rat brain. Brain regions are color coded based on the types of spatial cells that can be found in those locations. The exact roles of the above illustrated structures and the connections within the navigation circuit are described in more detail in the text. Based upon (Taube, 2007; Whitlock et al., 2008; Mizumori et al., 2009; Jankowski et al., 2013).

1971; McNaughton et al., 2006; Yartsev and Ulanovsky, 2013; **Figures 4B,C**). A hippocampal place cell's preferred location, where the cell's activity increases, is called a place field. Place fields are hypothesized to be the result of the specific spatially and temporally relevant organization of the above listed information. In other words, a place cell's place field contains an abstract description of the animal's current spatial context, which includes information about the environment as well as the inner state of the animal (Mizumori et al., 2009; Penner and Mizumori, 2012). Thus, the comparison between the current and expected spatial context may be achieved with the help of place cells in the hippocampus.

The two most critical pieces of information necessary for navigation are *location* and *orientation*. Orientation in mammals is encoded by *head direction cells* located in various parts of the Papez-circuit, including the postsubiculum, entorhinal cortex, anterodorsal thalamic nucleus, the hippocampal CA1 area and the dorsal striatum (Taube et al., 1990a,b; Taube, 2007; Finkelstein et al., 2011; Rubin et al., 2014; **Figures 4B,C**). Each head direction cell is tuned to a single preferred head orientation, thus together the network covers the entire 360° environment like a compass. A head direction cell's firing rate reaches the maximum when the animal faces the cell's preferred direction, and as the animal turns away from that angle, the firing rate drops down to near zero almost linearly. Head direction cell firing rate is independent of the animal's location, the head's pitch or roll within ∼90° of the horizontal plane, as well as any kind of ongoing behavior, which usually includes walking (Taube, 2007). However, head direction cells in some brain areas also encode *angular velocity*, which results in increased firing rates at the preferred angle when the animal quickly turns its head through this angle, and slightly decreased activity when the turn is slow or the animal is stationary (Taube and Burton, 1995). The sensory cues underlying and forming the head direction signal have been studied extensively in rodents (Taube, 2007). In these studies, rats are placed in a darkened arena with a light cue card

placed at some position. Changes in head direction cell preferred angles due to manipulations to the cue card's position suggest that head direction cells establish their preferred orientations primarily based on visual information. Shifting the cue card's position usually leads to corresponding shifts in head direction cell preferred directions, suggesting that the head direction signal may be anchored to visual landmarks (Taube et al., 1990b; Taube and Burton, 1995). The removal of visual landmarks from the environment, or turning off the lights, does not abolish head direction cell firing even when no other allothetic cues (olfactory or tactile) are present, although the preferred angles might drift (Taube et al., 1990b; Goodridge et al., 1998). The directional signal can also be maintained even when the animal is passively rotated around in an arena, indicating that vestibular cues are more critical to the head direction signal than proprioceptive feedback or motor efference copy. The head direction signal is also retained when passive rotations take place in complete darkness, supporting that the head direction system can rely on vestibular inputs when visual landmarks are not available.

Extracellular recordings provide an advantage in these types of studies in that a single electrode can record the activity of multiple cells simultaneously. This technique has been traditionally used in mammalian navigation studies and provided researchers with the opportunity to look at relationships among several head direction cells. The Knierim laboratory provided evidence suggesting that head direction cells, at least within one brain region, might function together as a network (Yoganarasimha et al., 2006). They found that sensory manipulations to the environment, such as landmark removal, result in approximately equal shifts in preferred directions of all recorded cells. However, the amount of the shift is unpredictable, and the neural processes leading to the shift are still not known. Nevertheless, because each cell responds similarly and with equal shifts, we can assume that the specific inputs driving such a change similarly affect all head direction cells in that particular brain region. Thus, head direction cells resemble a coherent neural network where the preferred directions are always a fixed angle apart from each other and perturbations to the environment lead to changes in every individual cell's firing patterns.

The head direction network is a fundamental component in the vertebrate navigation system. Since the two critical pieces of information necessary for navigation are location and orientation, without head direction cells accurate navigation is not possible. Because positional information is independent of orientation, there might not be a direct link between place cells and head direction cells, however to our knowledge, this hypothesis has not been supported or rejected to date.

Another major component of the vertebrate navigation circuits is the grid system (Hafting et al., 2005; Moser et al., 2013; Yartsev and Ulanovsky, 2013; Bush et al., 2015; Rowland et al., 2016). *Grid cells* are principal cells in the medial entorhinal cortex that, similarly to place cells, fire when the animal crosses specific locations within an environment (**Figures 4B,C**). While place cells only have a single place field where they fire, grid cell firing fields are hexagonally arranged and repeat at regular intervals over the entire environment creating a grid-like structure of place fields. This grid-like firing pattern contains complex spatial information, including *location* in the environment, a regular metric of *distance,* movement related information and likely *orientation*. Because grid cells in different layers of the medial entorhinal cortex span multiple scales and orientations (larger/smaller distances in the grid pattern and different orientations based on external cues), combinations of grid cells can provide information about distance and location in any environment (McNaughton et al., 2006; Rowland et al., 2016). The exact source of positional information and thus the relationship between place cells and grid cells is still unknown, however there is physiological evidence supporting interactions between the two populations of spatial cells (Witter and Amaral, 2004; Langston et al., 2010; Wills et al., 2010; Bonnevie et al., 2013). How grid cells might rely on place cells and *vice versa*, is still not clear (Bush et al., 2014; Dordek et al., 2016).

On the other hand, an elegant study from Winter et al. showed that grid cells rely upon head direction cells to encode orientation (Winter et al., 2015). They lesioned the head direction system located in the anterior thalamic nuclei with a reversible lidocaine injection and found that the inactivation of this orientation signal source disrupts grid cell firing. The animals recovered from the lidocaine injections within ∼1.5 h and so did the recorded grid patterns. These data provided the first piece of evidence showing that grid cells receive orientation cues directly from the anterior thalamic head direction network and that the representation of distance, and to some degree, position, is highly dependent on the orientation input from the head direction system.

Another kind of spatial cell located in the entorhinal cortex, *speed cells* (**Figures 4B,C**), are also thought to provide the rat navigation system with continuous updates during navigation (Kropff et al., 2015). Speed cells encode the running speed of the animal at any given moment during locomotion and their firing rates proportionally increase as the animal increases walking/running speed. Speed cells may provide the grid network with information about speed and distance.

Additionally, *border cells or boundary cells* are hypothesized to encode the shape of the environment that navigation takes place in (Barry et al., 2006; Savelli et al., 2008; Solstad et al., 2008; Lever et al., 2009). They do so by significantly increasing (or decreasing) their firing rate next to specific walls and/or corners of the arena. Border cells are located in several brain areas surrounding the hippocampus, including the entorhinal cortex.

SPATIAL CODE IN THE BASAL GANGLIA

Working in parallel with the above described spatial networks, the dorsal striatum of the basal ganglia is thought to assist the navigational system by evaluating the consequences of behaviors in the current navigational context (Schmitzer-Torbert and Redish, 2004; Penner and Mizumori, 2012). As a result of this analysis, planned motor actions can be fine-tuned to appropriately fit the current context. This process, as well as the motor actions approved by the striatum, have spatial components, which suggests that spatial context processing takes place within the striatum. Information about the environment and the animal's position can be derived from preprocessed sensory information that arrives to the striatum from sensory areas, other associative areas and the limbic system (Mcgeorge

and Faull, 1989). Lesion studies showed that impairment of the striatum leads to selective spatial deficits, especially during tasks that require learning (Mizumori et al., 2009). Extracellular recordings in freely behaving animals confirmed that some striatal neurons are sensitive to directional motor components of navigation, such as angular velocity, forward walking speed and navigational context cues, such as a reward's location (Lavoie and Mizumori, 1994; **Figure 4**). The striatum, similarly to the hippocampus, contains *place cells* that encode the inner representation of the animal's position and other context cues in the environment. In addition to place cells, the striatum also contains *head direction cells*, which encode the orientation of the animal (Mizumori et al., 2000; **Figures 4B,C**). Because both place cell and head direction cell responses significantly change in rearranged or novel environments, the spatial code in the striatum is thought to be highly context-dependent. This supports the hypothesis that the striatum evaluates behavioral, or in this case, navigational consequences and selects the motor actions that can potentially lead to the desired consequences in a context-dependent manner.

THE NEURAL SUBSTRATES OF NAVIGATION IN THE CX

To what extent can the principles found in rat systems be applied to insects? Clearly, insects do not have brain systems that are anywhere near as large and sophisticated as those found in mammals (**Figure 4A** shows the schematic of a cockroach brain). Nevertheless, if the mammalian system incorporates critical parts of a navigational system, it is likely that insects, which clearly can perform remarkable navigational feats such as long distance migration by monarch butterflies (Reppert et al., 2010) and foraging by ants (Collett, 2012), have evolved some or all of these solutions. Evidence is accumulating that insects do in fact utilize many of these mechanisms in controlling their movements through complex environments.

A wide range of genetic studies provided evidence for the role of various CX cell types in memory processes with spatial components similar to those observed in the hippocampus. For instance, short-term memory traces for visual pattern elevation and contour orientation were linked to the fruit fly's F5 neurons (dorsal FB neurons) and F1 neurons (ventral FB neurons) respectively (Liu et al., 2006; Pan et al., 2009). Similarly, R2/R4m ring neurons in the EB of flies also serve a role in storing most features of a visual pattern (Pan et al., 2009). Flies with silenced EB ring neurons perform poorly in a detour paradigm (Neuser et al., 2008). In this paradigm, individual flies are placed in the middle of an arena, with similar visual pattern displays on the two opposite sides of the arena, which are removed after the fly crosses the midline. Following the crossing, a distractor target is displayed at a 90° angle compared to the fly's heading. Wild type flies tend to turn toward this new visual target, if it is present for at least 500 ms. When the fly is facing the distractor target, it disappears within 1 s. When wild type flies are left in the arena with no visual targets, they recall their original, pre-distractor heading and start walking in that direction again. Thus, these flies are able to store and recall the position of a former target even though it is no longer present in the environment. Contrary to this, flies with silenced EB ring neurons (R3 and/or R4d) cannot remember their pre-distractor heading, suggesting that these neurons are important components of a spatial working memory circuit (Neuser et al., 2008).

Fruit flies can also perform in a place learning paradigm modeled after the classic Morris water maze, that is most commonly used to study place learning in rodents (Morris, 1981; Morris et al., 1982; Ofstad et al., 2011). The insect version of the maze is a circular arena with heated floor tiles and a single cold tile which serves as a rescue platform, and therefore becomes the animal's goal (Mizunami et al., 1998; Ofstad et al., 2011). When tested in this paradigm, wild type fruit flies quickly learn (one trial, 5 min) to locate the cold tile relative to visual patterns displayed on the arena walls. When the pattern is rotated around, over several trials the flies can learn to associate the cold tile's position with the visual features on the wall. However, individuals with silenced R1 neurons in the EB fail this spatial learning task, even though they can perform normal locomotor and optomotor behaviors, visual pattern discrimination and olfactory learning paradigms. These results indicate that R1 neurons are specifically responsible for some aspect of visually-guided place learning that is independent of basic sensory and locomotor functions (Ofstad et al., 2011).

As described earlier, hippocampal place cells participate in encoding the animal's current and past locations in an environment, thus providing a neural substrate for place learning. Whether any of the above described CX cells have the capacity to integrate environmental and internal context information similarly to place cells, remains to be elucidated. Nevertheless, these genetic studies provide a good starting point for further investigations with different imaging and electrophysiological techniques. In addition to CX circuits, the insect mushroom bodies are also considered an important memory center, which have the potential to contain spatial cells that function similarly to place cells (Mizunami et al., 1998; Heisenberg, 2003). The mushroom bodies do not receive any direct sensory inputs, rather they form a parallel processing loop that receives preprocessed sensory cues, similarly to the hippocampus in the rat brain (Capaldi et al., 1999; Menzel, 2014). It has been suggested many decades ago that the CX and mushroom bodies may play opponent roles in regulating behavior (Huber, 1960). Such parallel processing of sensory information could be the neural substrate of the above described spatial context discrimination (as done by the hippocampus) and evaluation of behavioral consequences in the current spatial context (as done by the dorsal striatum of the basal ganglia). Since in rat systems both the hippocampus and dorsal striatum contain neurons that encode the animal's position, if such cells exist in the insect brain, they could potentially reside in multiple structures as well.

Results from our laboratory indicate that some aspects of movement are also encoded by the CX. Similarly to speed cells in the rat entorhinal cortex, we have reported on single cells in the CX that encoded the speed of locomotion in cockroaches (Bender et al., 2010; Martin et al., 2015). The recorded cells' firing rates strongly correlated with the animal's stepping frequency (Bender

et al., 2010). Electrical stimulation through one of the recording electrodes induced walking in stationary animals and increased walking speed in moving animals, although the extent of the areas affected by this stimulation is not clear (Bender et al., 2010; Martin et al., 2015).

Mechanisms similar to head direction coding have been studied extensively in insects that use a CX-based polarized light compass (Heinze and Homberg, 2007; Heinze and Reppert, 2011; Homberg et al., 2011; Bech et al., 2014; el Jundi et al., 2015; Reppert et al., 2016). Yet, the first study providing physiological evidence for general orientation processes was published recently by Seelig and Jayaraman (Seelig and Jayaraman, 2015). The authors used two-photon Ca^{2+}-imaging to monitor the dendritic responses of a set of 16 columnar neurons that send projections to 16 columns of the EB in the *Drosophila* CX. Unlike some other insects, the fruit fly's EB is ring shaped, or elliptical, so the columns divide it into 16 radial wedges. EB wedge neurons (also called ring neurons) were targeted, because as described earlier, they have previously been shown to process directional visual information and play a role in feature detection (Neuser et al., 2008; Pan et al., 2009; Seelig and Jayaraman, 2013). During the experiments, fruit flies were head-fixed, but they were free to walk on an air-suspended Styrofoam ball in an LED arena. The arena was part of a closed-loop system, where the fly's movements on the ball controlled the position of the projected image on the LED panels. At certain headings relative to the displayed pattern's position, active cells formed a so-called "activity bump," wherein projections going to approximately 5–6 wedges would show increased activity. Whenever the fly changed its heading, the activity bump in the EB rotated as well. Importantly, any kind of visual scenery evoked this specific response, ranging from a single vertical stripe to more complex visual features. This indicates that the neurons were not encoding the visual information itself, but rather the animal's orientation relative to the visual landmark(s). By varying the closed-loop gain that matched the ball's rotational movements to the visual landmark's movements, they observed that CX activity integrated visual cues more heavily, than self-motion cues. Experiments conducted in darkness revealed similar results. The flies were able to maintain the EB wedge neuron activity bumps with no visual cues, but only for a limited period of time. This indicates, that the fly navigation system accumulates error over time when the only updates on the fly's relative orientation come from walking, thus proprioceptive feedback and motor efference copy. This was the first study that provided evidence for the CX's role as a navigation center with a compass-like function that integrates sensory information about the animal's orientation and through unknown downstream targets, guides movements accordingly.

We further extended the results from the fly experiments by adopting some of the classical methods used in rat head direction cell studies and applying them in our experiments on cockroach CX function (Varga and Ritzmann, 2016). We used extracellular recordings to gain insight into how single neurons in the CX might contribute to the head direction signal and to draw more direct comparisons between the neural strategies underlying rodent and insect head direction coding.

Restrained cockroaches with a fixed head-body axis were implanted with a tetrode wire bundle and placed on a computer-controlled platform in the middle of a dark uniform arena with a single, conspicuous visual cue on the wall. We rotated the animals around in 30° increments and analyzed the changes in CX neuron activity displayed during the 10 s immobile periods between the rotational steps. We found that single neurons in both the FB and EB encoded head direction and among all neurons, the entire 360° environment was represented equally. Some of the recorded neurons encoded head direction with similarly narrow tuning as observed in rat head direction cells, while the majority of them were broadly tuned to their preferred angles. These tuning patterns were reminiscent of the tuning characteristics observed in polarized light studies (Heinze et al., 2009). However, unlike those studies, here the landmark cards were blocked from the insects view for some of the angles, suggesting that orientation was being coded rather than a direct response to visual cues.

Through manipulating the visual cue's position in the arena, we established that, similarly to rat head direction cells, some CX neurons are anchored to the visual landmark's position and encode the animal's relative orientation compared to this cue (**Figure 5A**). This result is in accordance with Seelig and Jayaraman's findings where the EB activity bump rotated with the visual landmark (Seelig and Jayaraman, 2015). However, we also recorded from neurons that did not shift their peak firing rates when we shifted the position of the visual landmark (**Figure 5B**), and neurons that encoded two preferred angles after the landmark shift (**Figure 5C**). These results indicate that some cells in the cockroach's CX compass may rely upon movement-derived idiothetic cues (a process called path integration), even when a visual landmark is available to the animal. Visual landmark removal and experiments with head-covered landmark naïve animals revealed similar results. Because of our passive rotation experimental design, we know that these neurons encoded head direction without any access to proprioceptive feedback or motor efference copy. This finding suggests, that insects, similarly to mammals, have access to vestibular-like sensory inputs, which might directly impact neurons in the CX. Such angular velocity signals could potentially originate from the Johnston's organs at the base of the antennae, but physiological evidence supporting this hypothesis remains to be uncovered (Kamikouchi et al., 2009; Yorozu et al., 2009; Matsuo et al., 2014). Interestingly, when compared to fruit flies, cockroaches did not accumulate a lot of error during landmark-deprived trials. This difference between the results of the two studies could stem from the different ecology of the two model animals. Cockroaches are nocturnal animals that have limited access to visual landmarks and might need to rely on idiothetic cues more often than diurnal flies. However, another explanation is that, although the fruit flies in the closed-loop experiments received proprioceptive feedback and motor efference copy from the legs, their heads were fixed therefore they did not have access to vestibular-like inputs unlike the cockroaches in our rotation experiments. Thus, it is possible that, similarly to mammalian navigation systems, insects primarily rely upon vestibular-like cues rather than leg-derived movement information in the dark and other landmark-deprived situations.

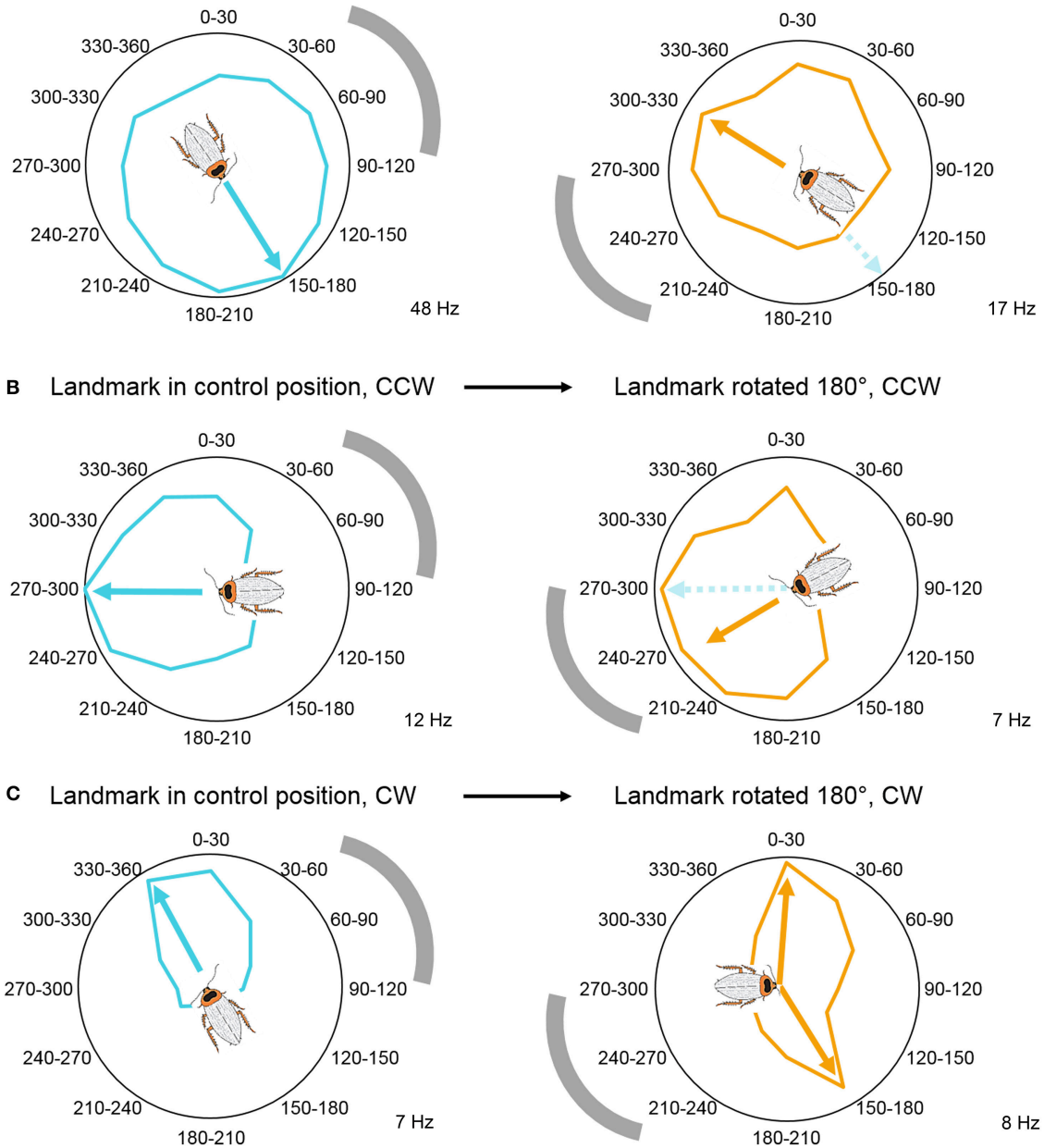

FIGURE 5 | Visual landmark position determines head direction coding. (A) Head direction coding tuned to allothetic cues, wherein angle-modulated units follow the shift in landmark position by shifting their peaks. Example unit's mean firing rate over 6 trials, illustrated in a circular plot. **(B)** Head direction coding tuned to idiothetic cues, wherein angle-modulated units persist to encode the original preferred angle. Example unit's mean firing rate over 4 trials, illustrated in a circular plot. **(C)** Bimodal responses during landmark rotation trials. These units developed a second peak in response to the new landmark position, while the original peak persisted to encode the peak from the control trials. Example unit's mean firing rate over 6 trials, illustrated in a circular plot. Gray arch indicates the position of the visual landmark on the wall of the cylindrical arena. All examples were modulated by head direction, $p < 0.05$ Rayleigh test. The cockroach's preferred direction is marked by arrows and the cartoon cockroach's heading (cyan, preferred direction in control trials; orange, preferred direction in landmark-shifted trials). Maximum average firing rates (Hz) of the example units are marked in the right bottom corner of each panel. Modified with permission from Varga and Ritzmann (2016).

Although these studies provided detailed evidence for orientation coding (not based on specialized sensory cues) in insects, the question whether these cells are "real" head direction cells remains to be addressed. One important characteristic of mammalian head direction cells is that they have the capacity to encode orientation in any environment, completely independent of the animal's *location* in that environment (Taube, 2007). Thus, the above described compass cells will need to be tested in a

range of environments in freely behaving animals to determine the effect of *location,* as well as novelty on the head direction signal.

In addition to the animal's position and head orientation, adaptive navigation also depends on spatial contextual cues, such as a navigational goal, a certain component of a navigational task, or relative movement direction (clockwise vs. counterclockwise; left vs. right). As mentioned earlier, these navigational context cues can be encoded by the dorsal striatum in mammals. The navigation circuits in the striatum then may use these cues to direct and shape motor commands (Mizumori et al., 2009). Additionally, the hippocampal-entorhinal navigation circuits can also encode and utilize such contextual information and use it in spatial memory and context discrimination processes (Penner and Mizumori, 2012). To test whether the CX plays a role in storing spatial contextual information, we rotated the animals in both clockwise and counterclockwise directions in a counterbalanced manner. We found that in addition to the compass cells, both the FB and EB contain neurons that encode the rotation direction history of the animal, by increasing or decreasing their firing rates after the rotations (**Figure 6**). Movement direction is a spatial context cue that is independent of the specific head orientation of the animal. Similarly to mammalian systems, spatial contextual information and head direction may be utilized in spatial memory and in shaping motor commands in downstream circuits.

MOTOR CONTROL FROM THE CX

In order for the information described in the previous sections to guide foraging movements, the CX must be able to produce or influence motor commands. To examine this aspect of behavioral control, we performed a series of experiments that involved multi-unit extracellular recordings in cockroaches that were either tethered or moving free in an arena. These experiments clearly demonstrated motor control properties recorded in the CX.

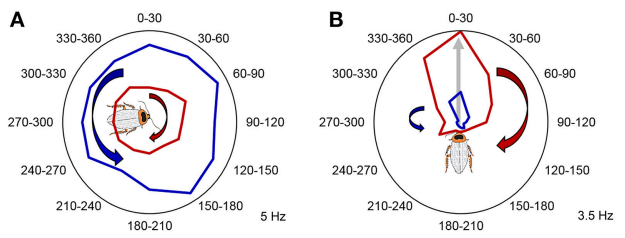

FIGURE 6 | Past rotation direction affects CX unit firing rate during the stationary epochs. (A) Example unit not modulated by angle increased its firing rate following clockwise rotations ($p < 0.05$, two-tailed paired *t*-test). Mean firing rate during counterclockwise rotations is marked with red, while mean firing rate during counterclockwise rotations is marked with blue. **(B)** A representative example of a CX unit that significantly encoded a preferred head direction and increased its relative firing rate during the stationary epochs following clockwise rotations. $P < 0.05$ for both Rayleigh test and two-tailed paired *t*-test. Mean firing rate during clockwise rotations is marked with red, while mean firing rate during counterclockwise rotations is marked with blue. The preferred angle of this unit is indicated by the gray arrow and the cartoon cockroach's heading. Maximum average firing rates (Hz) of the example units are marked in the right bottom corner of each panel. Modified with permission from Varga and Ritzmann (2016).

Our initial recordings were performed in cockroaches tethered over a lightly oiled plate (Bender et al., 2010). In these experiments single tetrodes were constructed out of bundles of fine insulated wires (Guo et al., 2014). The wires were either plated with copper or dipped in a fluorescent dye so that their recording location (but not the individual cells) could be identified histologically after the experiment. Cockroaches walk normally in the oiled plate tether and will spontaneously change walking speed. Plots of walking speed and rate of action potential activity in many CX neurons were strongly correlated. Moreover, delaying the functions that described neural activity increased the correlation with walking speed, suggesting that CX activity changes typically preceded altered walking speed. Also, stimulation through the same electrodes evoked similar increases in step frequency.

Directional turning was examined by placing a wired cockroach on an air-suspended Styrofoam ball (Guo and Ritzmann, 2013). A rod was placed near the cockroach's head. As had been demonstrated earlier, cockroaches will often explore a similar rod with their antennae and turn to examine it further (Okada and Toh, 2000). Before the cockroach turned to the left or right, activity changes were noted in FB recordings (**Figure 7**). This pattern of activity change had a distinctively biased directionality. Recordings made in the left FB found cells that increased activity prior to only left turns, but never found cells that only signaled right turns and vice versa. In addition to these biased responses, cells were also found on both sides of the FB whose activity preceded movement in either direction.

Because the optical sensors that monitored ball movement indicated changes in forward (translational) movement as well as right-left rotational movement, these data could describe two dimensional maps of the movements with which each cell's activity was associated. To generate these maps, we plotted the firing rate for each recorded CX neuron along with forward walking speed and turning. The data were then divided into bins and for each bin the translational and rotational value described a vector (**Figures 8A,B**). At the tip of each vector, we placed a square that was color coded according to the firing rate of that neuron. When this was completed for the vectors describing each bin, the data defined a two dimensional map of the types of movements with which each cell's activity was associated (**Figures 8C,D**).

The resulting maps identified cells in the left FB that were associated with slow left turns (**Figure 9A**) while others were associated with only fast left turns (**Figure 9B**). Neurons were also found associated with fast turns to either direction (**Figure 9C**), but right turn biased cells were only recorded in the right FB and left turn biased cells in the left FB (**Figures 9D,E**). As with the oiled plate experiments, stimulation through the recording electrodes generated turns that were consistent with the recording biases. That is stimulation in the left FB consistently generated left turns while stimulation in the right FB generated right turns.

The observations described above, taken with tethered insects, are very useful, but they represent open loop movements

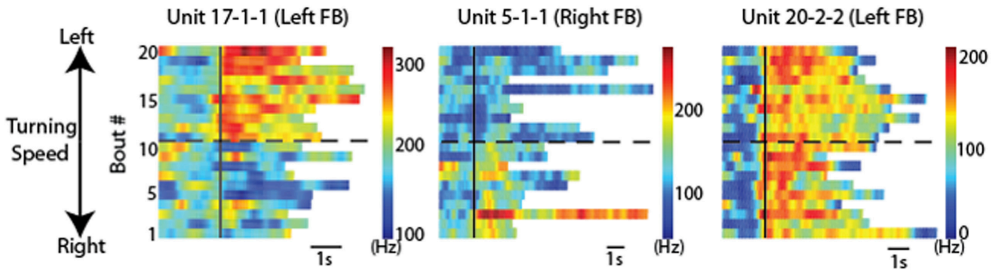

FIGURE 7 | CX units responded to locomotion in a directionally biased manner. Raster plots of 20 bouts of locomotion for three units. Each row is one bout and the color indicates the firing rate. For each graph, the solid black line indicates the start of each bout. Bouts of left turning are above the dashed black line and bouts of right turning are below it. For bouts of left turning, the higher the bout number, the higher the average turning speed. For bouts of right turning, the lower the bout number, the higher the average turning speed. Note the changes of firing rate after locomotion start as a function of locomotion direction. Individual units are named according to preparation, tetrode and unit numbers (e.g., "unit 1-2-3" indicates preparation 1, tetrode 2, unit 3). Reproduced with permission from Guo and Ritzmann (2013).

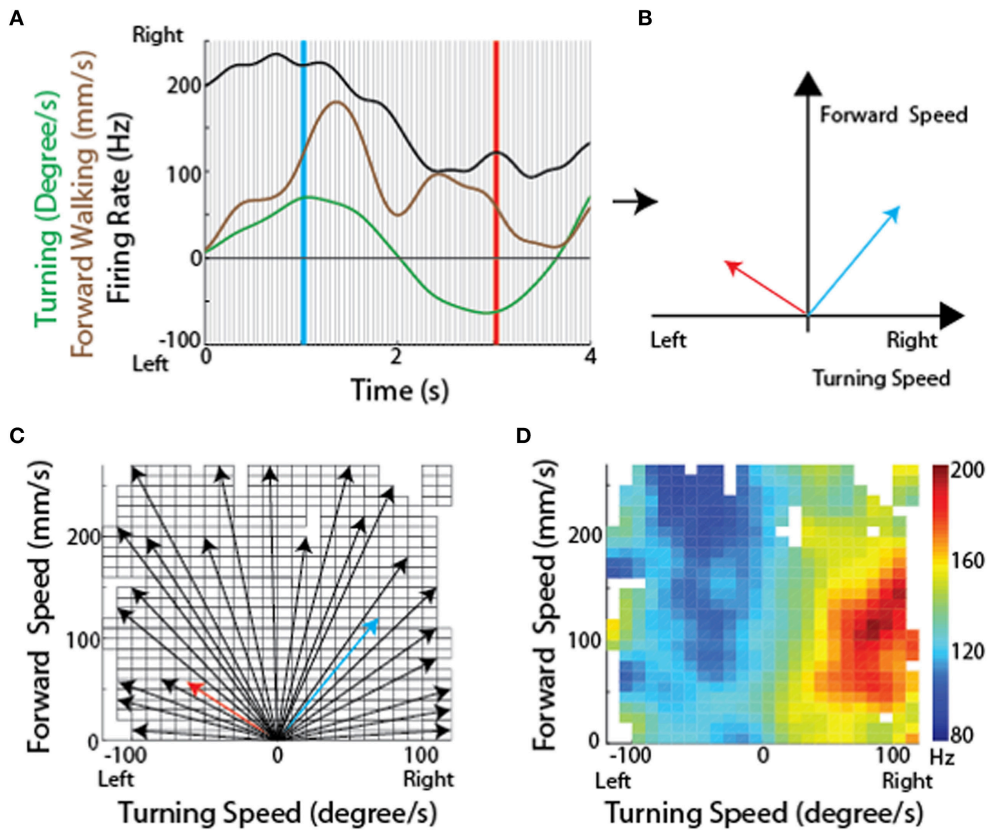

FIGURE 8 | Methodological concept for generating firing rate maps in tethered insects. (A) For every recording session, forward and turning speed as well as spike times of each unit were smoothed using a Gaussian kernel with a standard deviation of 150 ms. Each recording session was divided into non-overlapping 50 ms long sections (between individual gray lines). **(B)** For each divided section, a velocity vector was generated by averaging forward and turning speed within that period. Firing rate for each velocity vector was also calculated. The blue and red vectors were obtained from the blue and red lines, respectively, in **(A)**. **(C)** All velocity vectors were binned into a forward walking speed vs. turning speed graph (10 mm/sec for forward walking speed and 10 deg/sec for turning speed). Only some of the vectors, including the two vectors in B, are shown here. **(D)** A firing rate map was generated by overlaying the averaged firing rate for each bin, obtained by averaging all the firing rates whose corresponding velocity vectors fell into that bin. Reproduced with permission from Guo and Ritzmann (2013).

rather than natural foraging behaviors. To get closer to normal movements, we adapted our recording techniques to allow them to be performed in freely moving cockroaches (**Figure 10A**; Guo et al., 2014; Martin et al., 2015). Here the cockroach's actions were recorded with video cameras and moment-to-moment movements were again separated into forward (translational) and

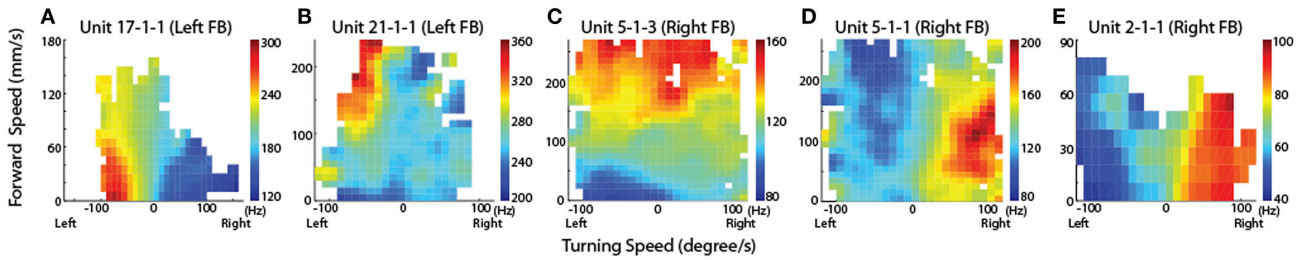

FIGURE 9 | CX units are tuned to self-motion. Firing rate maps for locomotion initiated by antennal contact with the rod for representative CX units. The x-axis is the turning speed and the y-axis is the forward walking speed. Positive turning speed indicates right turning and negative turning speed indicates left turning. CX units showed discrete locomotion-related firing fields, such as left turning irrespective of forward walking speed (**A**, $Z = 3.59$, $P < 0.01$), forward walking to the left (**B**, $Z = 4.08$, $P < 0.01$), forward walking irrespective of turning speed (**C**, $Z = 5.73$, $P < 0.01$), forward walking to the right (**D**, $Z = 6.00$, $P < 0.01$), and right turning irrespective of forward walking speed (**E**, $Z = 2.33$, $P < 0.01$). Reproduced with permission from Guo and Ritzmann (2013).

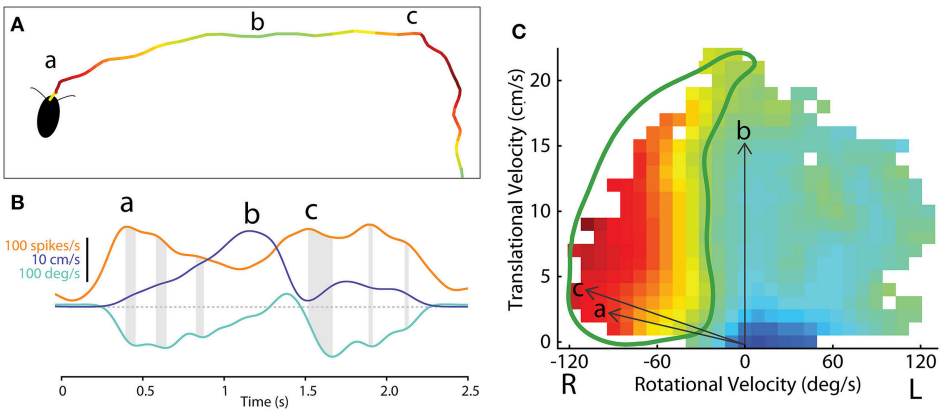

FIGURE 10 | Methodological concept for generating firing rate maps based on locomotor-related activity in the CX of freely-moving cockroach. (A) The path of a cockroach exploring the open arena. Color indicates firing rate of an example central-complex neuron during each segment of movement. **(B)** Smoothed firing rate of a central-complex neuron (orange), translational velocity (purple) and rotational velocity (cyan) of the animal during the bouts indicated at (a) and (b) and (c) in section A. Gray shading indicates the delay between peaks in the firing rate and peak rotational velocity of the resulting movement bout. **(C)** The firing rate for a single neuron is related to direction of movement in a manner similar to that used for tethered experiments (**Figure 8**). Here vectors of translational velocity vs. rotational velocity were created from video data (e.g., vectors a, b and c from time points indicated in **B**). At the tip of each vector a color coded box indicates the firing rate at that point in time. When this is done throughout a bout, a raw map of activity relative to motion is constructed. The firing rate map is then smoothed and gap-filled in 2 dimensions. Contour lines are then constructed from 0 to 100% of the maximum firing rate of this cell (not shown here). The 50% contour (thick, green line) is taken to represent the characteristic activity of the cell relative to movement direction. Adapted with permission from Martin et al. (2015).

left-right (rotational) movements throughout the insect's track. As with the tethered experiments, we could then relate spike frequency of CX neurons to those actions (**Figure 10B**).

These data could then be plotted as two dimensional motor maps as we did in the tethered experiments. We then smoothed and gap filled these maps and plotted contours that encapsulated 0–100% of maximum firing rate. The 50% contour was taken as characteristic for that cell and could then be compared to other neurons in the same and other insects (**Figure 10C**). A plot of all 50% firing contours describes a population code for movement in two dimensions (**Figure 11**). These contours encapsulate the entire set of movements that the cockroach could make in two dimensions. As with the tethered experiments the majority of changes in firing frequency preceded changes in movement. A few effects did follow changes in movement and some cases were recorded where activity changed both before and after a movement was executed.

As with the navigational system study, these data point to yet another similarity between insect and mammalian systems. Population codes for movement have been described in many mammalian motor control systems. Perhaps one of the earliest examples of population codes was demonstrated for arm movements in monkeys (Georgopoulos et al., 1988; Schwartz et al., 1988; Georgopoulos, 1995). In those studies, monkeys were trained to move their arms in three dimensional space from a starting position to a target location while neurons were recorded in the motor cortex. Many of these neurons were found to have a directional bias in that they fired at maximal levels during arm movements in a particular direction with fall-off in other directions. As with the cockroach data, the entire population of preferred directions covered the entire movement space. For any arm movement, a vector sum of the firing rate of 475 cells showing that direction could accurately predict the actual arm movement.

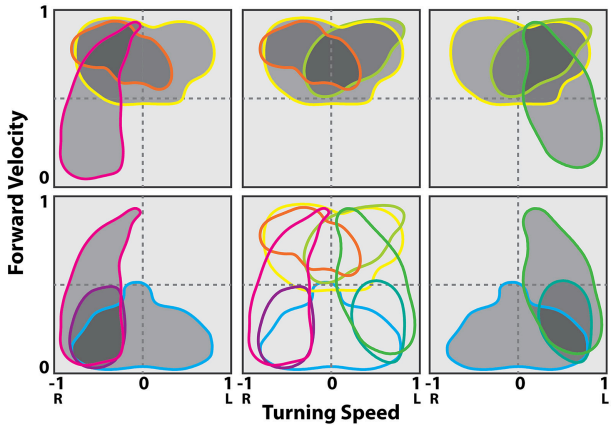

FIGURE 11 | Contour lines in the translational and rotational velocity axes at the 50% of maximum firing rate levels from the firing rate map at the best delay (location of the peak in the stimulus kernel). Cells shown are a representative sampling of cells spanning the range of observed selectivity. Shading indicates groups of cells in a possible population selected for fast turns to the right (gray), fast turns to the left (yellow) and slow turns to the right (cyan). Modified with permission from Martin et al. (2015).

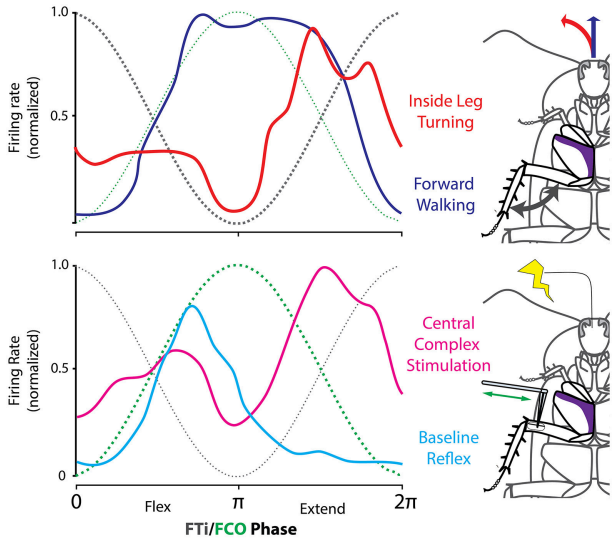

FIGURE 12 | CX stimulation evokes reflex reversal. (Top) The firing rate distribution of Ds neurons as a linear histogram, with the FCo (green) and FTi (black) phase indicated taken during spontaneous forward walking (blue) and turning (red) evoked by stimulation through CX electrodes in a freely moving cockroach. **(Bottom)** Same insect was moved to a preparation dish and the FCo was exposed by dissection. Here Ds activity is shown in response to FCo extension and relaxation with (red) and without (blue) stimulation through the same electrodes in the CX that evoked turning in the top record. Modified with permission from Martin et al. (2015).

How do CX neurons come to affect turning movements? Much of the output from the CX projects to the lateral accessory lobes where they encounter neurons that descend to the thoracic ganglia (Heinze and Homberg, 2008). When the cockroach turns, the motor activity associated with leg movements must change. In particular the middle leg on the inside of the turn switches from extending during stance to extending during swing. That leg then touches down and pulls the body through the turn (Mu and Ritzmann, 2005). In stick insects, walking movements of individual leg joints are coordinated by inter-joint reflexes (Akay et al., 2001, 2004). As the insect turns or walks backward, many of these reflexes reverse (Akay et al., 2007; Hellekes et al., 2012). Similar inter-joint reflexes have been found in cockroach middle legs and reversal of these reflexes occurs when descending activity is removed through bilateral ablation of cervical connectives (Mu and Ritzmann, 2008). These observations suggest that CX circuits could alter leg movements by affecting descending activity which, in turn, orchestrates specific reflex reversals.

To test this hypothesis, we identified a subset of subjects in our arena experiments in which stimulation through the CX tetrodes consistently evoked turning movements in a particular direction. This meant that we could identify the leg that consistently represented the inside leg of turns evoked by CX stimulation in these subjects. In these experiments, we also recorded EMGs from middle leg coxal muscles. As in previous tethered experiments, the slow depressor of the coxa (Ds) changed its firing pattern dramatically when the cockroach transitioned between the patterns associated with forward stepping and to that of inside leg turning (**Figure 12**).

With this in mind, we moved the cockroaches from the arena to a preparation dish with the CX electrodes in place. We then exposed the femoral chordotonal organ (FCo) that monitors femur-tibia joint movements (**Figure 12**). Without CX stimulation, FCo stretch and release generates Ds activity that is consistent with the initial activation seen in forward walking. When FCo stretch and release was repeated in conjunction with CX stimulation, the Ds reflex reversed to follow a pattern very similar to that seen during turning.

Of course, movement in the horizontal plane represents only a portion of the cockroach's, or other insects', foraging behaviors. Cockroaches readily climb over substantial blocks, walk up walls and can even walk inverted along ceilings. Does that pattern of CX motor control change under altered context? To test this we moved cockroaches with the tetrodes in place from the arena to a runway that included a large block. This forced the cockroach to execute climbing movements in order to proceed. We plotted the relationship between step frequency and rate of action potentials for individual CX neurons taken during horizontal walking and climbing. Some of these cells showed no change in this relationship, but others changed dramatically. Some retained their slope but shifted upward. Others altered slope and some were even found to reverse the function so that they decreased activity as step frequency increased. This observation suggests that the population code seen in **Figure 11** for horizontal walking is dynamic in that it can be greatly modified when the cockroach starts to climb. Other behaviors would be expected to generate further alterations in this population code.

CONCLUSIONS

The experiments described here strongly suggest that the CX plays a pivotal role in controlling insect behavior. The specifics of

this role will vary from insect to insect and behavior to behavior. As a result, the effects seen in various insects will vary with the behavioral niches each species inhabits. Thus, migratory insects like monarch butterflies and locusts will tap into polarized light maps to control flight movements as they make long distance flights. Foraging insects, like stick insects and cockroaches will utilize visual and tactile cues to move through their environments toward targets and away from threats. Nocturnal vs. diurnal insects will use appropriate cues to guide their movements (el Jundi et al., 2015). Predatory insects would be expected to use these tools to target prey and guide stalking movements.

Our discussion also demonstrates that many of the properties associated with navigation and motor control in mammals can be found in insect CX data. Whether this is a matter of convergence or, as has been suggested by others, deep homology (Strausfeld and Hirth, 2013), the ramifications are important. At the very least, it suggests that there are neural properties that are essential for effective solutions of navigation and motor control.

AUTHOR CONTRIBUTIONS

AV performed head direction experiments and described head direction work. NK performed visual CX experiments and described CX visual work. JM performed CX motion experiments and described this work. PG performed tethered motion experiments and described this work. RR Oversaw all work as Principle Investigator of Laboratory and oversaw manuscript.

ACKNOWLEDGMENTS

This material is based upon work supported by the National Science Foundation under Grant No. IOS-1120305 and 1557228.

REFERENCES

Ache, J. M., Haupt, S., and Dürr, V. (2015). A direct descending pathway informing locomotor networks about tactile sensor movement. *J. Neurosci.* 35, 4081–4091. doi: 10.1523/JNEUROSCI.3350-14.2015

Akay, T., Bässler, U., Gerharz, P., and Büschges, A. (2001). The role of sensory signals from the insect coxa-trochanteral joint in controlling motor activity of the femur-tibia joint. *J. Neurophysiol.* 85, 594–604.

Akay, T., Haehn, S., Schmitz, J., and Büschges, A. (2004). Signals from load sensors underlie interjoint coordination during stepping movements of the stick insect leg. *J. Neurophysiol.* 92, 42–51. doi: 10.1152/jn.01271.2003

Akay, T., Ludwar, B. C., Goritz, M. L., Schmitz, J., and Büschges, A. (2007). Segment specificity of load signal processing depends on walking direction in the stick insect leg muscle control system. *J. Neurosci.* 27, 3285–3294. doi: 10.1523/JNEUROSCI.5202-06.2007

Barry, C., Lever, C., Hayman, R., Hartley, T., Burton, S., O'Keefe, J., et al. (2006). The boundary vector cell model of place cell firing and spatial memory. *Rev. Neurosci.* 17, 71–97. doi: 10.1515/REVNEURO.2006.17.1-2.71

Bech, M., Homberg, U., and Pfeiffer, K. (2014). Receptive fields of locust brain neurons are matched to polarization patterns of the sky. *Curr. Biol.* 24, 2124–2129. doi: 10.1016/j.cub.2014.07.045

Bender, J. A., Pollack, A. J., and Ritzmann, R. E. (2010). Neural activity in the central complex of the insect brain is linked to locomotor changes. *Curr. Biol.* 20, 921–926. doi: 10.1016/j.cub.2010.03.054

Bender, J. A., Simpson, E. M., Tietz, B. R., Daltorio, K. A., Quinn, R. D., and Ritzmann, R. E. (2011). Kinematic and behavioral evidence for a distinction between trotting and ambling gaits in the cockroach *Blaberus discoidalis*. *J. Exp. Biol.* 214, 2057–2064. doi: 10.1242/jeb.056481

Bläesing, B., and Cruse, H. (2004). Mechanisms of stick insect locomotion in a gap-crossing paradigm. *J. Comp. Physiol. A. Neuroethol. Sens. Neural. Behav. Physiol.* 190, 173–183. doi: 10.1007/s00359-003-0482-3

Bockhorst, T., and Homberg, U. (2015). Amplitude and dynamics of polarization-plane signaling in the central complex of the locust brain. *J. Neurophsyiol.* 113, 3291–3311. doi: 10.1152/jn.00742.2014

Bonnevie, T., Dunn, B., Fyhn, M., Hafting, T., Derdikman, D., Kubie, J. L., et al. (2013). Grid cells require excitatory drive from the hippocampus. *Nat. Neurosci.* 16, 309–317. doi: 10.1038/nn.3311

Boyan, G. S., and Liu, Y. (2016). Development of the neurochemical architecture of the central complex. *Front. Behav. Neurosci.* 10:167. doi: 10.3389/fnbeh.2016.00167

Bush, D., Barry, C., and Burgess, N. (2014). What do grid cells contribute to place cell firing? *Trends Neurosci.* 37, 136–145. doi: 10.1016/j.tins.2013.12.003

Bush, D., Barry, C., Manson, D., and Burgess, N. (2015). Using grid cells for navigation. *Neuron* 87, 507–520. doi: 10.1016/j.neuron.2015.07.006

Canonge, S., Sempo, G., Jeanson, R., Detrain, C., and Deneubourg, J. L. (2009). Self-amplification as a source of interindividual variability: shelter selection in cockroaches. *J. Insect Physiol.* 55, 976–982. doi: 10.1016/j.jinsphys.2009.06.011

Capaldi, E. A., Robinson, G. E. and Fahrbach, S. E. (1999). Neuroethology of spatial learning: the birds and the bees. *Annu. Rev. Psychol.* 50, 651–682. doi: 10.1146/annurev.psych.50.1.651

Collett, M. (2012). How navigational guidance systems are combined in a desert ant. *Curr. Biol.* 22, 927–932. doi: 10.1016/j.cub.2012.03.049

Daltorio, K. A., Tietz, B. R., Bender, J. A., Webster, V. A., Szczecinski, N. S., Branicky, M. S., et al. (2013). A model of exploration and goal-searching in the cockroach, *Blaberus discoidalis*. *Adapt. Behav.* 21, 404–420. doi: 10.1177/1059712313491615

Devaud, J.-M., Blunk, A., Podufall, J., Giurfa, M., and Grünewald, B. (2007). Using local anaesthetics to block neuronal activity and map specific learning tasks to the mushroom bodies of an insect brain. *Eur. J. Neurosci.* 26, 3193–3206. doi: 10.1111/j.1460-9568.2007.05904.x

Dordek, Y., Soudry, D., Meir, R., and Derdikman, D. (2016). Extracting grid cell characteristics from place cell inputs using non-negative principal component analysis. *Elife* 5:e10094. doi: 10.7554/eLife.10094

Dürr, V., and Ebeling, W. (2005). The behavioural transition from straight to curve walking: kinetics of leg movement parameters and the initiation of turning. *J. Exp. Biol.* 208, 2237–2252. doi: 10.1242/jeb.01637

Dürr, V., König, Y., and Kittmann, R. (2001). The antennal motor system of the stick insect *Carausius morosus*: anatomy and antennal movement pattern during walking. *J. Comp. Phsiol. A.* 187, 131–144. doi: 10.1007/s003590100183

el Jundi, B., Pfeiffer, K., Heinze, S., and Homberg, U. (2014). Integration of polarization and chromatic cues in the insect sky compass. *J. Comp. Physiol. A. Neuroethol. Sens. Neural. Behav. Physiol.* 200, 575–589. doi: 10.1007/s00359-014-0890-6

el Jundi, B., Warrant, E. J., Byrne, M. J., Khaldy, L., Baird, E., Smolka, J., et al. (2015). Neural coding underlying the cue preference for celestial orientation. *Proc. Natl. Acad. Sci. U.S.A.* 112, 11395–11400. doi: 10.1073/pnas.1501272112

Feng, A. Y. T., and Himsworth, C. G. (2014). The secret life of the city rat: a review of the ecology of urban Norway and black rats (*Rattus norvegicus* and *Rattus rattus*). *Urban Ecosyst.* 17, 149–162. doi: 10.1007/s11252-013-0305-4

Finkelstein, A., Derdikman, D., Rubin, A., Foerster, J. N., Las, L., and Ulanovsky, N. (2011). Three-dimensional head-direction coding in the bat brain. *Nature* 517, 159–164. doi: 10.1038/nature14031

Georgopoulos, A. P. (1995). Current issues in directional motor control. *Trends Neurosci.* 18, 506–510. doi: 10.1016/0166-2236(95)92775-l

Georgopoulos, A. P., Kettner, R. E., and Schwartz, A. B. (1988). Primate motor cortex and free arm movements to visual targets in three- dimensional space. II. Coding of the direction of movement by a neuronal population. *J. Neurosci.* 8, 2928–2937.

Geva-Sagiv, M., Las, L., Yovel, Y., and Ulanovsky, N. (2015). Spatial cognition in bats and rats: from sensory acquisition to multiscale maps and navigation. *Nat. Rev. Neurosci.* 16, 94–108. doi: 10.1038/nrn3888

Goodridge, J. P., Dudchenko, P. A., Worboys, K. A., Golob, E. J., and Taube, J. S. (1998). Cue control and head direction cells. *Behav. Neurosci.* 112, 749–761. doi: 10.1037/0735-7044.112.4.749

Guo, P., Pollack, A. J., Varga, A. G., Martin, J. P., and Ritzmann, R. E. (2014). Extracellular wire tetrode recording in brain of freely walking insects. *J. Vis. Exp.* 86:e51337. doi: 10.3791/51337

Guo, P., and Ritzmann, R. E. (2013). Neural activity in the central complex of the cockroach brain is linked to turning behaviors. *J. Exp. Biol.* 216, 992–1002. doi: 10.1242/jeb.080473

Hafting, T., Fyhn, M., Molden, S., Moser, M.-B., and Moser, E. I. (2005). Microstructure of a spatial map in the entorhinal cortex. *Nature* 436, 801–806. doi: 10.1038/nature03721

Harley, C. M., English, B. A., and Ritzmann, R. E. (2009). Characterization of obstacle negotiation behaviors in the cockroach, *Blaberus discoidalis*. *J. Exp. Biol.* 212, 1463–1476. doi: 10.1242/jeb.028381

Harley, C. M., and Ritzmann, R. E. (2010). Electrolytic lesions within central complex neuropils of the cockroach brain affect negotiation of barriers. *J. Exp. Biol.* 213, 2851–2864. doi: 10.1242/jeb.042499

Hartley, T., Lever, C., Burgess, N., and O'Keefe, J. (2014). Space in the brain: how the hippocampal formation supports spatial cognition. *Philos. Trans. R. Soc. B.* 369:20120510. doi: 10.1098/rstb.2012.0510

Heinze, S., Gotthardt, S., and Homberg, U. (2009). Transformation of polarized light information in the central complex of the locust. *J. Neuorosci.* 29, 11783–11793. doi: 10.1523/JNEUROSCI.1870-09.2009

Heinze, S., and Homberg, U. (2007). Maplike representation of celestial E-vector orientations in the brain of an insect. *Science* 315, 995–997. doi: 10.1126/science.1135531

Heinze, S., and Homberg, U. (2008). Neuroarchitecture of the central complex of the desert locust: Intrinsic and columnar neurons. *J. Comp. Neurol.* 511, 454–478. doi: 10.1002/cne.21842

Heinze, S., and Reppert, S. M. (2011). Sun compass integration of Skylight cues in migratory monarch butterflies. *Neuron* 69, 345–358. doi: 10.1016/j.neuron.2010.12.025

Heisenberg, M. (2003). Mushroom body memoir: from maps to models. *Nat. Rev. Neurosci.* 4, 266–275. doi: 10.1038/nrn1074

Hellekes, K., Blincow, E., Hoffmann, J., and Büschges, A. (2012). Control of reflex reversal in stick insect walking: effects of intersegmental signals, changes in direction, and optomotor-induced turning. *J. Neurophysiol.* 107, 239–249. doi: 10.1152/jn.00718.2011

Holling, C. S. (1966). The functional response of invertebrate predators to prey density. *Mem. Entomol. Soc. Can.* 98, 5–86. doi: 10.4039/entm9848fv

Homberg, U., Heinze, S., Pfeiffer, K., Kinoshita, M., and el Jundi, B. (2011). Central neural coding of sky polarization in insects. *Philos. Trans. R. Soc. Lond. B.* 366, 680–687. doi: 10.1098/rstb.2010.0199

Huber, F. (1960). Untersuchungen über die funktion des zentralnervensystems und insbesondere des gehirns bei der fortbewegung und lauterzeugung der grillen. *Zeit. Vergleich. Physiol.* 44, 60–132. doi: 10.1007/BF00297863

Inoue, T., and Matsura, T. (1983). Foraging strategy of a mantid, Paratenodera angustipennis S.: Mechanisms of switching tactics between ambush and active search. *Oecologia* 56, 264–271. doi: 10.1007/BF00379700

Jacobs, L., and Menzel, R. (2014). Navigation outside of the box: what the lab can learn from the field and what the field can learn from the lab. *Mov. Ecol.* 2:3. doi: 10.1186/2051-3933-2-3

Jankowski, M. M., Ronnqvist, K. C., Tsanov, M., Vann, S., Wright, N., Erichsen, J., et al. (2013). The anterior thalamus provides a subcortical circuit supporting memory and spatial navigation. *Front. Syst. Neurosci.* 7:45. doi: 10.3389/fnsys.2013.00045

Kahsai, L., and Winther, A. M. E. (2011). Chemical neuroanatomy of the *Drosophila* central complex: distribution of multiple neuropeptides in relation to neurotransmitters. *J. Comp. Neurol.* 519, 290–315. doi: 10.1002/cne.22520

Kamikouchi, A., Inagaki, H. K., Effertz, T., Hendrich, O., Fiala, A., Göpfert, M. C., et al. (2009). The neural basis of *Drosophila* gravity-sensing and hearing. *Nature* 458, 165–171. doi: 10.1038/nature07810

Kathman, N. D., Kesavan, M., and Ritzmann, R. E. (2014). Encoding wide-field motion and direction in the central complex of the cockroach *Blaberus discoidalis*. *J. Exp. Biol.* 217, 4079–4090. doi: 10.1242/jeb.112391

Kropff, E., Carmichael, J. E., Moser, M.-B., and Moser, E. I. (2015). Speed cells in the medial entorhinal cortex. *Nature* 523, 419–424. doi: 10.1038/nature14622

Langston, R. F., Ainge, J. A., Couey, J. J., Canto, C. B., Bjerknes, T. L., Witter, M. P., et al. (2010). Development of the spatial representation system in the rat. *Science* 328, 1576–1580. doi: 10.1126/science.1188210

Lavoie, A. M., and Mizumori, S. J. Y. (1994). Spatial, movement- and reward-sensitive discharge by medial ventral striatum neurons of rats. *Brain Res.* 638, 157–168. doi: 10.1016/0006-8993(94)90645-9

Lever, C., Burton, S., Jeewajee, A., O'Keefe, J., and Burgess, N. (2009). Boundary vector cells in the subiculum of the hippocampal formation. *J. Neuorsci.* 29, 9771–9777. doi: 10.1523/JNEUROSCI.1319-09.2009

Liu, G., Seiler, H., Wen, A., Zars, T., Ito, K., Wolf, R., et al. (2006). Distinct memory traces for two visual features in the *Drosophila* brain. *Nature* 439, 551–556. doi: 10.1038/nature04381

Martin, J. P., Guo, P., Mu, L., Harley, C. M., and Ritzmann, R. E. (2015). Central-complex control of movement in the freely walking cockroach. *Curr. Biol.* 25, 1–9. doi: 10.1016/j.cub.2015.09.044

Matsuo, E., Yamada, D., Ishikawa, Y., Asai, T., Ishimoto, H., and Kamikouchi, A. (2014). Identification of novel vibration- and deflection-sensitive neuronal subgroups in Johnston's organ of the fruit fly. *Front. Physiol.* 5:179. doi: 10.3389/fphys.2014.00179

Mcgeorge, A. J., and Faull, R. L. M. (1989). The organization of the projection from the cerebral cortex to the striatum in the rat. *Neuroscience* 29, 503–537. doi: 10.1016/0306-4522(89)90128-0

McNaughton, B. L., Battaglia, F. P., Jensen, O., Moser, E. I., and Moser, M. B. (2006). Path integration and the neural basis of the "cognitive map." *Nat. Rev. Neurosci.* 7, 663–678. doi: 10.1038/nrn1932

Menzel, R. (2014). The insect mushroom body, an experience-dependent recoding device. *J. Physiol. Paris* 108, 84–95. doi: 10.1016/j.jphysparis.2014.07.004

Meyer, D. J., Margiotta, J. F., and Walcott, B. (1981). The shadow response of the cockroach, Periplaneta americana. *J. Neurobiol.* 12, 93–96. doi: 10.1002/neu.480120109

Mizumori, S. J. Y., Puryear, C. B., and Martig, A. K. (2009). Basal ganglia contributions to adaptive navigation. *Behav. Brain Res.* 199, 32–42. doi: 10.1016/j.bbr.2008.11.014

Mizumori, S. J. Y., Ragozzino, K. E., and Cooper, B. G. (2000). Location and head direction representation in the dorsal striatum of rats. *Psychobiology* 28, 441–462. doi: 10.3758/BF03332003

Mizunami, M., Weibrecht, J. M., and Strausfeld, N. J. (1998). Mushroom bodies of the cockroach: their participation in place memory. *J. Comp. Neurol.* 402, 520–537. doi: 10.1002/(SICI)1096-9861(19981228)402:4<520::AID-CNE6>3.0.CO;2-Ky

Morris, G. M. (1981). Spatial localization does not require the presence of local cues. *Learn. Motiv.* 12, 239–260. doi: 10.1016/0023-9690(81)90020-5

Morris, R. G., Garrud, P., Rawlins, J. N., and O'Keefe, J. (1982). Place navigation impaired in rats with hippocampal lesions. *Nature* 297, 681–683. doi: 10.1038/297681a0

Moser, E. I., Kropff, E., and Moser, M. B. (2008). Place cells, grid cells, and the brain's spatial representation system. *Annu. Rev. Neurosci.* 31, 69–89 doi: 10.1146/annurev.neuro.31.061307.090723

Moser, E. I., Moser, M. B., and Roudi, Y. (2013). Network mechanisms of grid cells. *Philos. Trans. R. Soc. Lond. B. Biol. Sci.* 369:20120511. doi: 10.1098/rstb.2012.0511

Mu, L., and Ritzmann, R. E. (2005). Kinematics and motor activity during tethered walking and turning in the cockroach, *Blaberus discoidalis*. *J. Comp. Physiol. A. Neuroethol. Sens. Neural. Behav. Physiol.* 191, 1037–1054. doi: 10.1007/s00359-005-0029-x

Mu, L., and Ritzmann, R. E. (2008). Interaction between descending input and local thoracic reflexes for joint coordination in cockroach turning: I. Descending influence on thoracic sensory reflexes. *J. Comp. Physiol. A* 194, 283–298. doi: 10.1007/s00359-007-0307-x

Neuser, K., Triphan, T., Mronz, M., Poeck, B., and Strauss, R. (2008). Analysis of a spatial orientation memory in Drosophila. *Nature* 453, 1244–1247. doi: 10.1038/nature07003

Ofstad, T. A., Zuker, C. S., and Reiser, M. B. (2011). Visual place learning in *Drosophila melanogaster*. *Nature* 474, 204–207. doi: 10.1038/nature10131

Okada, J., and Toh, Y. (1998). Shade Response in the escape behavior of the Cockroach, *Periplaneta americana*. *Zool. Sci.* 15, 831–835. doi: 10.2108/zsj.15.831

Okada, J., and Toh, Y. (2000). The role of antennal hair plates in object-guided tactile orientation of the cockroach (*Periplaneta americana*). *J. Comp. Physiol. A. Neuroethol. Sens. Neural. Behav. Physiol.* 186, 849–857. doi: 10.1007/s003590000137

O'Keefe, J., and Dostrovsky, J. (1971). The hippocampus as a spatial map. Preliminary evidence from unit activity in the freely-moving rat. *Brain Res.* 34, 171–175. doi: 10.1016/0006-8993(71)90358-1

Pan, Y., Zhou, Y., Guo, C., Gong, H., Gong, Z., and Liu, L. (2009). Differential roles of the fan-shaped body and the ellipsoid body in *Drosophila* visual pattern memory. *Learn. Mem.* 16, 289–295. doi: 10.1101/lm.1331809

Paulsen, O., and Moser, E. I. (1998). A model of hippocampal memory encoding and rerieval: GABAergic control of synaptic plasticity. *Trends Neurosci.* 21, 273–278. doi: 10.1016/s0166-2236(97)01205-8

Paxinos, G., and Watson, C. (1996). *The Rat Brain in Stereotaxic Coordinates*. San Diego, CA: Academic Press.

Penner, M. R., and Mizumori, S. J. Y. (2012). Neural systems analysis of decision making during goal-directed navigation. *Prog. Neurobiol.* 96, 96–135. doi: 10.1016/j.pneurobio.2011.08.010

Pfeiffer, K., and Homberg, U. (2014). Organization and functional roles of the central complex in the insect brain. *Annu. Rev. Entomol.* 59, 165–184. doi: 10.1146/annurev-ento-011613-162031

Reppert, S. M., Gegear, R. J., and Merlin, C. (2010). Navigational mechanisms of migrating monarch butterflies. *Trends Neurosci.* 33, 399–406. doi: 10.1016/j.tins.2010.04.004

Reppert, S. M., Guerra, P. A., and Merlin, C. (2016). Neurobiology of monarch butterfly migration. *Annu. Rev. Entomol.* 61, 25–42. doi: 10.1146/annurev-ento-010814-020855

Ritzmann, R. E., Harley, C. M., Daltorio, K. A., Tietz, B. R., Pollack, A. J., Bender, J. A., et al. (2012). Deciding which way to go: how do insects alter movements to negotiate barriers? *Front. Neurosci.* 6:97. doi: 10.3389/fnins.2012.00097

Ritzmann, R. E., Ridgel, A. L., and Pollack, A. J. (2008). Multi-unit recording of antennal mechanosensitive units in the central complex of the cockroach, *Blaberus discoidalis*. *J. Comp. Physiol. A. Neuroethol. Sens. Neural. Behav. Physiol.* 194, 341–360. doi: 10.1007/s00359-007-0310-2

Rosner, R., and Homberg, U. (2013). Widespread sensitivity to looming stimuli and small moving objects in the central complex of an insect brain. *J. Neurosci.* 33, 8122–8133. doi: 10.1523/JNEUROSCI.5390-12.2013

Roth, L. M., and Willis, E. R. (1960). The biotic associations of cockroaches. *Smithson Misc. Collect.* 141, 1–470.

Rowland, D. C., Roudi, Y., Moser, M.-B., and Moser, E. I. (2016). Ten years of grid cells. *Ann. Rev. Neurosci.* 39, 19–40. doi: 10.1146/annurev-neuro-070815-013824

Rubin, A., Yartsev, M. M., and Ulanovsky, N. (2014). Encoding of head direction by hippocampal place cells in bats. *J. Neuorsci.* 34, 1067–1080. doi: 10.1523/JNEUROSCI.5393-12.2014

Sakura, M., Lambrinos, D., and Labhart, T. (2008). Polarized skylight navigation in insects: model and electrophysiology of e-vector coding by neurons in the central complex. *J. Neuorophysiol.* 99, 667–682. doi: 10.1152/jn.00784.2007

Savelli, F., Yoganarasimha, D., and Knierim, J. J. (2008). Influence of boundary removal on the spatial representations of the medial entorhinal cortex *Hippocampus* 18, 1270–1282. doi: 10.1002/hipo.20511

Schiller, D., Eichenbaum, H., Buffalo, E. A., Davachi, L., Foster, D. J., Leutgeb, S., et al. (2015). Memory and space: towards an understanding of the cognitive map. *J. Neuorsci.* 35, 13904–13911. doi: 10.1523/JNEUROSCI.2618-15.2015

Schmitzer-Torbert, N., and Redish, A. D. (2004). Neuronal activity in the rodent dorsal striatum in sequential navigation: Separation of spatial and reward responses on the multiple T task. *J. Neurophysiol.* 91, 2259–2272. doi: 10.1152/jn.00687.2003

Schwartz, A. B., Kettner, R. E., and Georgopoulos, A. P. (1988). Primate motor cortex and free arm movements to visual targets in three- dimensional space. I. Relations between single cell discharge and direction of movement. *J. Neurosci.* 8, 2913–2927.

Seelig, J. D., and Jayaraman, V. (2013). Feature detection and orientation tuning in the Drosophila central complex. *Nature* 503, 262–266. doi: 10.1038/nature12601

Seelig, J. D., and Jayaraman, V. (2015). Neural dynamics for landmark orientation and angular path integration. *Nature* 521, 186–191. doi: 10.1038/nature 14446

Solstad, T., Boccara, C. N., Kropff, E., Moser, M.-B., and Moser, E. I. (2008). Representation of geometric borders in the entorhinal cortex. *Science* 322, 1865–1868. doi: 10.1126/science.1166466

Strausfeld, N. J., and Hirth, F. (2013). Deep homology of arthropod central complex and vertebrate basal ganglia. *Science* 340, 157–161. doi: 10.1126/science.1231828

Taube, J. S. (2007). The head direction signal: Origins and sensory-motor integration. *Ann. Rev. Neurosci.* 30, 181–207. doi: 10.1146/annurev.neuro.29.051605.112854

Taube, J. S., and Burton, H. L. (1995). Head direction cell activity monitored in a novel environment and during a cue conflict situation. *J. Neurophysiol.* 74, 1953–1971.

Taube, J. S., Muller, R. U., and Ranck, J. B. (1990a). Head-direction cells recorded from the postsubiculum in freely moving rats. I. Description and quantitative analysis. *J. Neurosci.* 10, 420–435.

Taube, J. S., Muller, R. U., and Ranck, J. B. (1990b). Head-direction cells recorded from the postsubiculum in freely moving rats. II. Effects of environmental manipulations. *J. Neurosci.* 10, 436–447.

Varga, A. G., and Ritzmann, R. E. (2016). Cellular basis of head direction and contextual cues in the insect brain. *Curr. Biol.* 26, 1816–1828. doi: 10.1016/j.cub.2016.05.037

Weir, P., Schnell, B., and Dickinson, M. (2014). Central complex neurons exhibit behaviorally gated responses to visual motion in *Drosophila*. *J. Neurophysiol.* 11, 62–71. doi: 10.1152/jn.00593.2013

Whitlock, J., Sutherland, R., Witter, M., Moser, M., and Moser, E. (2008). Navigating from hippocampus to parietal cortex. *Proc. Natl. Acad. Sci. U.S.A.* 105, 14755–14762. doi: 10.1073/pnas.0804216105

Wills, T. J., Cacucci, F., Burgess, N., and O'Keefe, J. (2010). Development of the hippocampal cognitive map in preweanling rats. *Science* 328, 1573–1576. doi: 10.1126/science.1188224

Winter, S. S., Clark, B. J., and Taube, J. S. (2015). Disruption of the head direction cell network impairs the parahippocampal grid cell signal. *Science* 347, 870–874. doi: 10.1126/science.1259591

Witter, M. P., and Amaral, D. G. (2004). "Hippocampal formation," in *The Rat Nervous System*, ed G. Paxinos (San Diego, CA: Elsevier), 635–704.

Yartsev, M. M., and Ulanovsky, N. (2013). Representation of three-dimensional space in the hippocampus of flying bats. *Science* 340, 367–372. doi: 10.1126/science.1235338

Yoganarasimha, D., Yu, X., and Knierim, J. J. (2006). Head direction cell representations maintain internal coherence during conflicting proximal and distal cue rotations: Comparison with hippocampal place cells. *J. Neurosci.* 26, 622–631. doi: 10.1523/JNEUROSCI.3885-05.2006

Yorozu, S., Wong, A., Fischer, B. J., Dankert, H., Kernan, M. J., Kamikouchi, A., et al. (2009). Distinct sensory representations of wind and near-field sound in the Drosophila brain. *Nature* 458, 201–205. doi: 10.1038/nature 07843

Conflict of Interest Statement: The authors declare that the research was conducted in the absence of any commercial or financial relationships that could be construed as a potential conflict of interest.

Advantages of publishing in Frontiers

OPEN ACCESS
Articles are free to read for greatest visibility and readership

FAST PUBLICATION
Around 90 days from submission to decision

HIGH QUALITY PEER-REVIEW
Rigorous, collaborative, and constructive peer-review

TRANSPARENT PEER-REVIEW
Editors and reviewers acknowledged by name on published articles

Frontiers
Avenue du Tribunal-Fédéral 34
1005 Lausanne | Switzerland

Visit us: www.frontiersin.org
Contact us: info@frontiersin.org | +41 21 510 17 00

REPRODUCIBILITY OF RESEARCH
Support open data and methods to enhance research reproducibility

DIGITAL PUBLISHING
Articles designed for optimal readership across devices

FOLLOW US
@frontiersin

IMPACT METRICS
Advanced article metrics track visibility across digital media

EXTENSIVE PROMOTION
Marketing and promotion of impactful research

LOOP RESEARCH NETWORK
Our network increases your article's readership